

Modeling Report

Bermuda and Climate Change: Impacts from Sea Level Rise and Changing Storm Activity

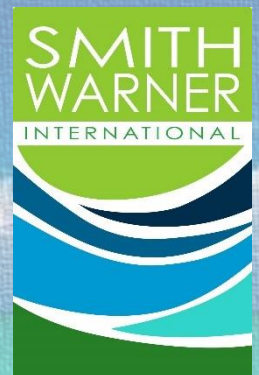
Prepared for:

Ministry of Home Affairs
Department of Planning
Dame Lois Brown-Evans Building, 5th Floor
Court Street
Hamilton, HM12
Bermuda

Submitted by:

Smith Warner International Limited
Unit 13, Seymour Park, 2 Seymour Avenue
Kingston 10, JAMAICA

15 March 2024



Contents

List of Abbreviations	i
Executive Summary.....	ii
Effects of Climate Change on Bermuda	iii
Modeling Approach.....	v
Operational Wave Climate and Climate Change.....	vi
Impacts of Climate Change on the Hurricane Climate	vii
Compound Flooding.....	viii
Predicted Shoreline Change with Sea Level Rise	ix
Climate Change Impact on Fresh Water Lenses.....	x
1 Introduction	1
1.1 Background and Objectives.....	2
1.2 Scope of Work.....	2
1.3 Approach and Methodology.....	3
2 Climate Change Modeling	4
2.1 Description of Datasets Used	4
2.2 Climate Change Analysis	6
2.3 Implications for Coastal Planning.....	10
3 Wave Assessment and Transformation Modeling.....	13
3.1 Summary of Offshore Conditions	13
3.2 Summary of Measured Data	15
3.3 Model Set-Up.....	26
3.4 Model Calibration.....	29
3.5 Day-to-Day Conditions	39
4 Hurricane Risk Assessment.....	61
4.1 Historical Hurricane Activity.....	62
4.2 Storm Tracks of Recent Hurricanes	64
4.3 Deep Water Waves.....	66
4.4 Storm Surge Components.....	67
5 Nearshore Hurricane Waves and Water Levels.....	76
5.1 Present Day Conditions	76
5.2 Hurricane Conditions under the RCP 4.5 and RCP 8.5 Scenarios	80

5.3	Hurricane Conditions under the RCP 4.5 and RCP 8.5 (Consideration for Mesoscale Eddies)	86
5.4	Change in Wind Speeds and Storm Intensity	92
6	Compound Flooding Analysis – Combined Surge and Rainfall effects in Mill Creek/Pembroke Marsh	96
6.1	Description of Model	97
6.2	Rainfall Data	98
6.3	Surge Conditions at Mill Creek	102
6.4	Results	103
6.5	Current Model Limitations	106
7	Beach Erosion Modeling	107
7.1	Historical Erosion Trends	107
7.2	Shoreline Retreat Calculations	108
7.3	Erosion Under Swell Events	112
8	Cliff Erosion Assessment	116
8.1	Cliff Setting	116
8.2	Cliff Erosion Processes	117
8.3	Historical Cliff Erosion Rates	118
8.4	Impacts of sea level rise	119
8.5	Evaluated Sites	120
8.6	Qualitative Comparison	125
8.7	Modified Scape Model	126
8.8	Summary	126
9	Hydrogeologic Assessment	128
10	Next Steps	145
11	Works Cited	146
	Appendix A - Climate Profile and Projections for the Island of Bermuda	
	Appendix B – Description of the Numerical Models	
	Appendix C – Numerical Model Set Up & Validation	
	Appendix D – Measured Data	
	Appendix E – Additional Plots	
	Appendix F – Hydrogeology Modeling Report	

List of Abbreviations

ADCP	Acoustic Doppler Current Profiler
ASTM	American Society for Testing and Materials
AWAC	Acoustic Wave and Current Profiler
BELCO	Bermuda Electric Light Company
BIOS	Bermuda Institute of Ocean Sciences
BOPP	Benthic Ocean Prosperity Programme
BWS	Bermuda Weather Service
CC	Climate Change
CREF	Caribbean Renewable Energy Forum
ECMWF	European Centre for Medium-range Weather Forecast
ERA5	ECMWF re-analysis (Fifth Generation)
GIS	Geographic Information System
GPS	Global Positioning System
LIDAR	Light Detection and Ranging
MSL	Mean Sea Level
NAO	North Atlantic Ocean
NHC	National Hurricane Centre
NOAA	National Oceanic and Atmospheric Administration
SLR	Sea Level Rise
SIDS	Small Island Developing States
SWI	Smith Warner International
TDS	Total Dissolved Solids
UKHO	UK Hydrographic Office

Executive Summary

In 2004, the Government of Bermuda (GoB) assessed Bermuda's vulnerability to coastal erosion. The 2004 study, carried out by Smith Warner International Limited (SWI) identified specific shorelines that were most vulnerable to erosion and storm inundation due to potential wave run-up. Around Bermuda, two types of shorelines were observed: (i) sandy shores/beaches, and (ii) rocky shores, which can be further split into three sub-types: flat rocky, low cliffs, and high cliffs.

A rapidly changing climate necessitated an updated assessment of the risks and vulnerabilities to Bermuda's coastlines, the overall purpose of this collective study. Coastal erosion, through either sandy shores/beaches or coastal cliffs, remains a focal point of the assessment. In addition, the analysis herein considers areas that are vulnerable to flooding from extreme storm events and saltwater intrusion effects from rising sea (and groundwater) levels.

This report presents the data collection, modeling, and associated analysis of various hazards that pose a threat to Bermuda's coastlines. The subsequent (and final) report compiles the collective results of the modeling presented herein into a "Coastal Vulnerability Index" to identify geographical areas that are at present, or will be in the future, at risk from coastal forcing.

This report introduces broad changes expected to impact Bermuda's future climate, based on the latest literature and data at hand. The result of this assessment is then applied to determine the appropriate forcing criteria for detailed modeling, such as sea level rise rates, increases to storm wave heights, changes of hurricane intensity and frequency, and rainfall patterns.

Wave modeling is then introduced, including model setup, data collection, calibration/validation exercise and model runs to compare present to future operational (daily) and yearly (non-hurricane) swell events on Bermuda's coastlines.

Hurricanes are the next focus. Statistics are derived from historical hurricane records and various methodologies are employed to determine the appropriate future hurricane conditions. These conditions are then modeling to identify both storm surge and wave conditions at Bermuda's coastlines.

The Mill Creek/Pembroke Marsh area had been identified for its propensity for flooding from rainfall events. To accurately determine the vulnerability in this low-lying coastal area, a compound modeling approach was employed to incorporate both a hurricane-induced storm surge (from the bay side) with associated rainfall driven flow (from the land side).

The report follows with an assessment of expected erosion of both sandy beach areas and shoreline cliffs based on limited data available.

Finally, a hydrogeological assessment discusses the threats posed by rising sea levels on the hydraulic balance between aquifers and the ocean, which has the potential to threaten various freshwater resources and aquatic ecosystems in Bermuda.

Effects of Climate Change on Bermuda

Climate projections are simulated based on future expectations (scenarios) of the earth’s environment. Conditions will depend on how the global economic and social behaviours trend towards measures for mitigation and adaption. Based on the globe’s ability to adapt and mitigate the amount of greenhouse gas emissions, several scenarios are proposed by the Intergovernmental Panel on Climate Change (IPCC). To refer to these scenarios, representative concentration pathways (RCP) and the shared socio-economic pathways (SSPs) are used. While RCPs consider the effect of the concentration of greenhouse gases in the atmosphere, the SSP combines the social and economic effects on the amount of emission. For this assessment we focussed on SSP2-4.5 and SSP5-8.5.

<i>Shared Socio-economic Pathways (SSPs)</i>	<i>Description</i>	
SSP1-2.6	Sustainability <i>Taking the Green Road</i>	Low challenges to mitigation and adaptation
SSP2-4.5	Middle of the Road	Medium challenges to mitigation and adaptation
SSP4-7.0	Inequality <i>A Road Divided</i>	Low challenges to mitigation, high challenges to adaptation
SSP5-8.5	Fossil-fuelled development <i>Taking the Highway</i>	Major challenges to mitigation, high challenges to adaptation

- SSP2-4.5 is the middle ground where challenges to adapting are of medium difficulty.
- SSP5-8.5 is the worst case. In this scenario the globe accepts the business-as-usual model and greenhouse gas (GHG) emissions are not curbed. Simultaneously, there is high friction to adapt and mitigate the impacts of climate change.

The conditions under the SSP2 4.5 and 8.5 will be used to describe the conditions in the next 20, 50 and 100 years. The following table summarises the historical trends and projections.

Summary of climate change trends and projections for Bermuda

Parameter	Historical Trend	Projection
Temperature	<p>Air temperature varies throughout the year with the highest temperatures from July to September and lowest in January to March. Mean temperature has been increasing between 0.22°C and 0.6°C per decade.</p> <p>Hot days and nights have also been increasing at a rate of 4% and 3% per decade respectively.</p>	<p>Temperature is expected to continuously increase with global warming. In the medium term (2040-2060) the projected annual increase is between 0.6 and 1.7°C for the RCPs. In the long term (2070-2090) the projected annual increase is between 0.6 and 3.2°C for the RCPs.</p> <p>Hot days and nights are increasing and will account for nearly 100% of days by end of century under RCP 8.5.</p> <p>Heatwave durations are increasing and will reach near 60 days by the end of century under RCP 8.5.</p>

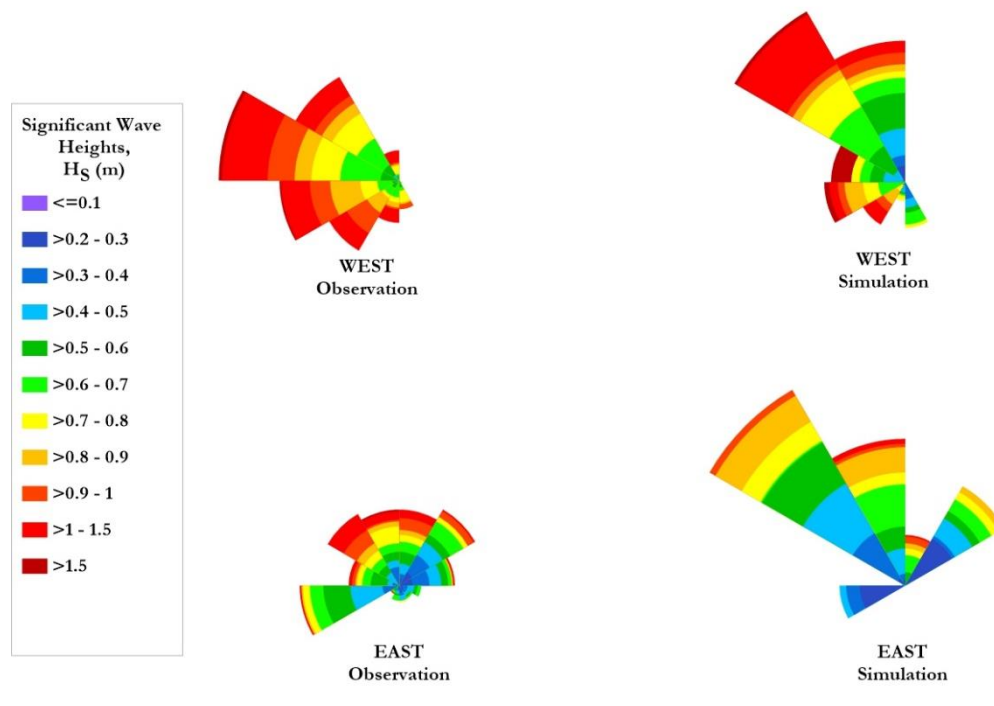
Parameter	Historical Trend	Projection
Rainfall	The island’s climatology exhibits a bimodal rainfall pattern with peaks in January and September, with the September peak receiving more rainfall.	The RCPs suggest no real trend toward the end of the century. In the medium term (2040-2060) mean annual projected change is 4 to 11% over the two RCPs examined. In the long term (2070-2090) mean annual projected change is 3 to 48%. Extreme events will be characterised by significant interannual variability. However, rainfall indices reflect no real overall trends with projected change in consecutive dry days (CDD) (between 0.1 and 0.2 days/decade) and changes in consecutive wet days (CWD) (0 and 0.2 days/decade).
Sea Surface Temperature	SST are highest during August to September and coolest during December to April. SSTs are increasing at a rate of 0.26 °C per decade.	SSTs are projected to increase at a rate of 0.07°C (0.4.3°C) per decade under RCP 2.6 (8.5). In the medium term (2040-2060) monthly projected increase ranges from 0.6 to 1.7°C (1.0 – 2.3°C) for RCP 2.6 (8.5). In the long term (2070-2090) monthly projected increase ranges from 0.8 to 1.7°C (2.5 – 4.0°C) for RCP 2.6 (8.5).
Sea Level Rise	Bermuda lies in an area that has experienced sea level rise of more than 3.84 mm/year.	By 2100, mean SLR is projected to be approximately 0.47m for SSP1-2.6 and between 0.69 and 0.82m for SSP5-8.5. If expert judgement including revised Antarctic ice-sheet contributions are considered, then by 2100 mean SLR for Bermuda is projected to be approximately 1.46m for SSP5-8.5.
Hurricanes	Over the last 4 decades there were 21 storms passing within 50km of Bermuda. Between 5 and 8 storms passed per decade except for 1991 to 2000 when no storms were recorded passing within 50km.	The future will likely be characterized by more intense hurricanes with high winds and greater rainfall. A likely increase in rainfall rate of between 20% and 33% is projected particularly near the hurricane core by the end of the century.

All parameters will affect coastal hazards to varying degrees. However, the effects of sea level rise and changing hurricane conditions will be more profound in coastal areas. In the medium term (up to 2060), a rate of 5.4mm/year and 6.6mm/year will be used for the SSP5 - 4.5 and 8.5 respectively. For the longer-term assessments (beyond 2060), the 7.7mm/year and 10.5mm/year will be used for SSP5 - 4.5 and 8.5 respectively. Under the worst-case scenario (SSP5 – 8.5), in the next 100 years Bermuda could see a total sea level rise of 1.05m. This is compounded by the likelihood of more intense hurricanes affecting the coastal areas of the north Atlantic Ocean.

For sea level rise, the SSC and RCP predictions are similar, hence these terms are applied interchangeably.

Modeling Approach

Baseline coastal zone modeling is needed to gain an understanding of the coastal processes acting along the shorelines of Bermuda. The model's fundamental starting point is the construction of a computational mesh from which spatial variances can be calculated at each simulation time step. MIKE 21 computes the waves and hydrodynamics using a flexible computational mesh. The flexible mesh is ideal for storm surge computations because it allows for the modeling of large complex areas that may require detailed resolutions of smaller features at the same time. The model was set up and calibrated using data collected east and west of the island. All indices used for the model validations were considered acceptable to good for model performance. This statistical method validated the spectral wave model, which was used with confidence to give a realistic representation of the long-term database of day-to-day wave conditions in the nearshore areas. The physical conditions of Bermuda made it difficult to get a good numerical calibration of currents. In general, currents varied widely, which is not easily represented by numerical models.



Summary of significant wave height calibration

Operational Wave Climate and Climate Change

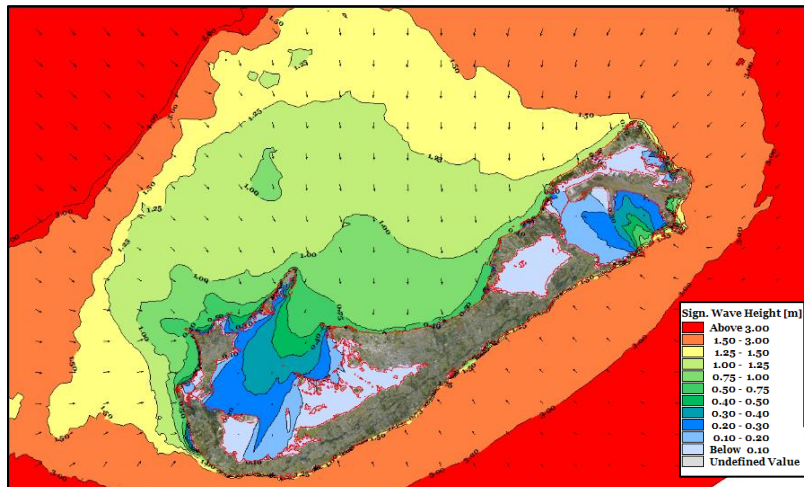
The results show that under present day conditions, wave heights along the south shore average 0.5-0.75m while on the north shore wave heights vary from 0.3-0.5m. The south shoreline is less protected due to substantially fewer outer reef formations. Within enclosed embayments (e.g. Harrison Sound), wave heights are further reduced to less than 0.3m.

Under future climate scenarios, the lagoon in the lee of the reef will see the most impact. This is expected as the effectiveness of the reef to reduce wave heights will be significantly reduced as sea levels rise. For the 100-year horizon, significant wave heights within the lagoon could increase by 0.08m to 0.15m for the RCP 4.5 and RCP 8.5 scenarios, respectively. These values are significant and equate to a 15-20% increase in the significant wave height.

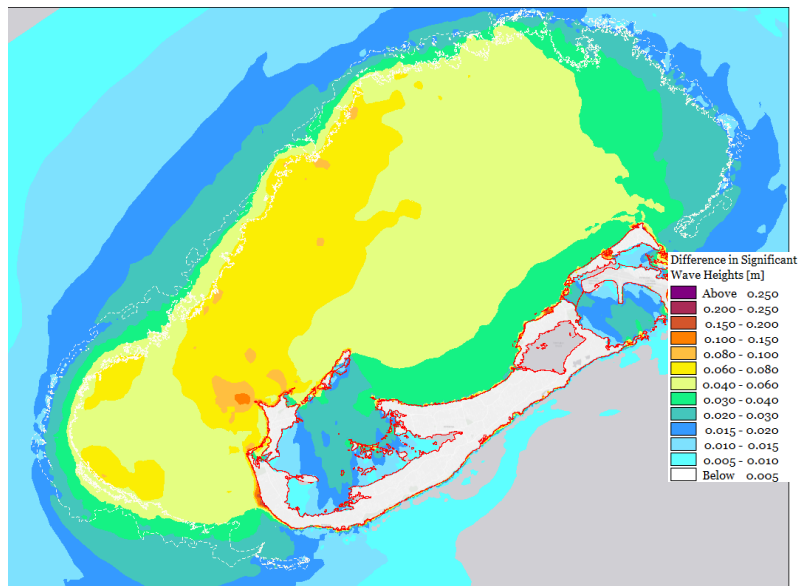
The south coast has less increase in wave energy, likely because the south coast is not as dependent on protection from the reef as is the north coast.

From this assessment we can conclude:

- The western coast (near Dockyards) is at risk of greater wave energy. This has implications for the maritime activities in this area, i.e., more disturbance to cruise ships, shipping, ferries and general navigation in the area.
- Likewise, the north coast areas outside the protection of the sounds will see larger increases in wave energy. Industries such as the power plant could be affected.
- Within the Sounds, wave heights could increase by up to 250%, however, this only reflects a change in wave height of approximately 5mm.



99th percentile significant wave heights (present day conditions)



Increases in 99th percentile significant wave height between present day and SSC 8.5 100 year wave event

- Under statistically significant events, significant wave heights will increase by more than 0.3m and will have implications on sediment movement.

Impacts of Climate Change on the Hurricane Climate

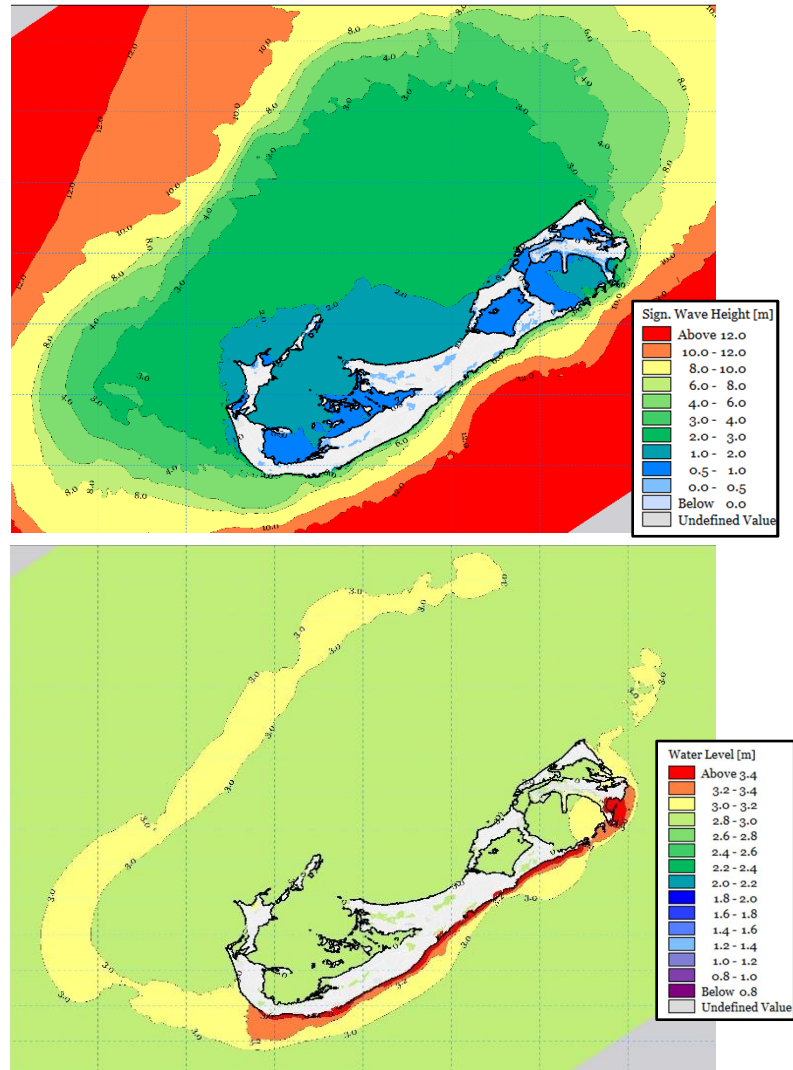
Presently, the reef effectively protects the north shore from hurricane waves. The rim reef at the north reduced wave heights from 10m (offshore) to approximately 2m at the shoreline.

Despite this reduction, waves 1-2m high affect the shoreline of the north coast under the 25-year return period event. Under the 150-year event, wave heights on the north shore are 2-3m with accompanying inundation.

Unlike the north shore, the south shore has significantly less protection from reefs. As a result, wave heights immediately offshore can be 8-10m during a hurricane.

Storm surge is expected to be greater than 1.2m on the north shore while along the south shore, storm surge levels will exceed 1.6m. At these levels, large coastal areas will be under water.

Under future climate change projections, the north shore is more severely impacted as the reef's protection from waves becomes less effective with increased sea levels. Increased storm wave conditions impact the north shore and propagate into the Great Sound area. For example, under the 150-year return period in an RCP 8.5 scenario in the next 100 years, areas previously effectively protected by the reef (the north, north-west and Great Sound) will see increases in wave heights of 10.8% to 20.3%. A similar trend exists for storm surge.



100 year conditions for 150-year storm event under RCP 8.5 scenario

Comparison of points along the Bermudian shoreline (significant wave heights) under the 50-year conditions

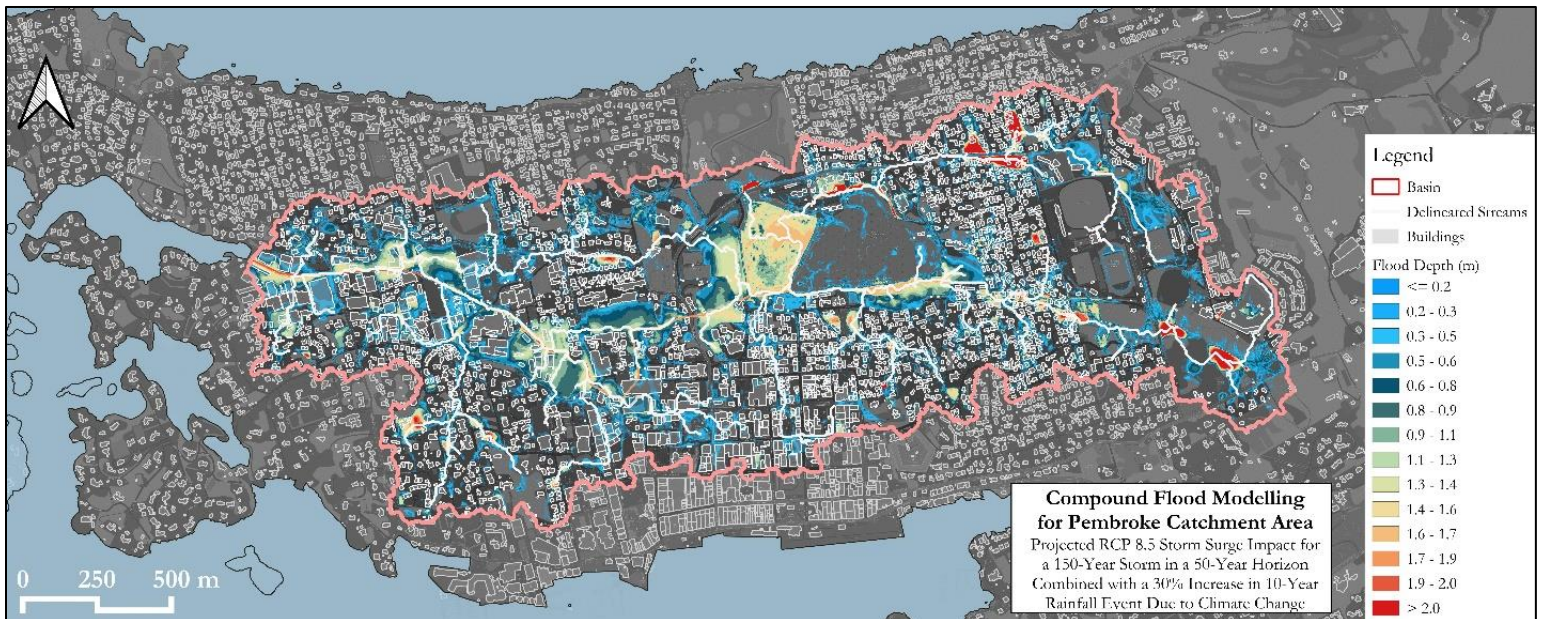
South-west	South	North-east	North	Great Sound	Scenario
2.90m	9.36m	5.21m	1.48m	0.95m	<i>Present</i>
+2.1%	+0.5%	+1%	+0.7%	+2.1%	<i>4.5 20yr</i>
+4.1%	+1.1%	+1.9%	+2%	+3.2%	<i>8.5 20yr</i>
+5.2%	+1.4%	+2.5%	+2.7%	+4.2%	<i>4.5 50yr</i>
+10%	+2.6%	+4.8%	+4.7%	+8.4%	<i>8.5 50yr</i>
+10.7%	+2.7%	+5%	+4.7%	+8.4%	<i>4.5 100yr</i>
+20.3%	+5%	+9.6%	+10.8%	+15.8%	<i>8.5 100yr</i>

Compound Flooding

The compound flood analysis completed for the Mill Creek/Pembroke Marsh area considers the interplay between storm surge and rainfall. The results highlight the catchment area's vulnerability to rainfall-induced flooding due to its low-lying terrain, seaward drainage patterns, and susceptibility to storm surge amplification.

The results offer significant insights into potential flood scenarios, including overflow from the banks and pocket flooding in low-lying areas. Notable findings include water depths ranging from 1.3 to 1.7m along the Pembroke Canal, with areas of concern identified along St. Johns Road and Mill Creek Road. Additionally, the study highlights pocket flooding across the catchment area, impacting residential areas and critical infrastructure.

The analysis identified key flood-prone areas and underscores the importance of considering compound flooding in flood risk assessment and management strategies. However, limitations in the model, such as accounting for all drainage features and the absence of comprehensive data on land use and soil maps, signal the need for future enhancements to improve the accuracy and reliability of flood risk predictions.



50-year Flood depths along Mill Creek/Pembroke Marsh for a 150-year return period event considering the RCP 8.5 scenario

Predicted Shoreline Change with Sea Level Rise

Shoreline retreat related to an increase in local sea level is calculated through the Bruun rule. Within the limitations of this model, the retreat of the sandy shorelines longer than 50m were assessed, with the following key observations:

- Under the RCP 4.5 and 8.5 SLR scenarios, the southern beaches will recede between 10-25m by 2050 and 30-65m by 2100;
- The rate of shoreline retreat for the RCP 4.5 and 8.5 scenarios in 2050 are similar but differ substantially for the 2100 predictions;
- By 2100, Horseshoe Bay retreat is predicted to be up to 60m, and Warwick Long Bay could also retreat by up to 40m. The maximum retreat calculated was 75-85m near the Dockyards on the north-west of Bermuda.

The qualitative comparison of 20 coastal cliff sites around Bermuda was conducted to assess the vulnerability of these cliffs to climate change and increased erosion rates. The assessment involved categorizing the cliffs into two main types based on the presence or absence of a fronting beach. The methodology included on-site visits to visually evaluate present conditions and collect data, such as rock hardness measurements using a Schmidt hammer and observations of geological features like paleosol layers.

Results of the assessment revealed several key findings:

Cliff Types and Beach Presence:

- Cliffs with fronting beaches are predominantly located on the south shore of Bermuda.
- Beaches of sufficient volume can provide natural protection against wave-driven erosion for cliffs with fronting beaches.
- However, it was observed that cliffs fronted by beaches often have a weak rock layer (paleosol) near the cliff base, making them more susceptible to erosion.

Vulnerability to Climate Change and Sea Level Rise:

- As sea levels rise, forecasted increasing wave heights and modeled beach retreat pose significant risks to cliffs, especially those fronted by beaches.
- The presence of weak rock layers near the cliff base exacerbates the vulnerability of these cliffs to erosion under rising sea levels.

Regional Variations in Vulnerability:

- Cliffs with small forecast changes in wave conditions, such as those on the north coast, and headlands plunging directly into deep water, are expected to experience low to moderate increases in future erosion rates.
- The west coast was identified as particularly vulnerable, with the highest modeled increase in day-to-day wave conditions, suggesting a potential moderate acceleration of future cliff retreat rates at those sites. If sea level rise causes waves to interact with a paleosol layer (or other weak layer) that is not currently actively eroded by waves, erosion rates will likely accelerate. The

elevation and locations of the paleosol layers varies along the coastline and are not currently mapped in sufficient detail to allow geographic analysis of this factor but could be a useful focus for future efforts. Additional observations such as high-resolution LiDAR and/or imagery are also needed to develop a detailed inventory of quantitative coastal cliff changes in Bermuda, required to calibrate and develop robust models of coastal cliff evolution under future climate scenarios.

- **Modified SCAPE Model**

Using the modified SCAPE model, which projects future cliff retreat rates based on historical and projected sea level rise along with historical cliff retreat rates, a detailed picture emerges of how coastal erosion might evolve. Specifically, for cliffs that historically retreated at a rate of 33cm/year, under the RCP 8.5 scenario over the next 100 years, this rate is projected to increase to 55cm/year. This trend suggests that areas with higher historical retreat rates will face even more accelerated erosion in the future, especially under the more severe climate change scenarios. This model provides a crucial tool for coastal management, offering insights into potential future changes and the need for adaptive strategies in coastal planning.

Historical Retreat Rate (cm/yr)	Calculated Rate of Change for Cliff Retreat		
	Future Retreat Rate (cm/yr) for RCP 8.5		
	20 Year Horizon	50 Year Horizon	100 Year Horizon
5	7	8	8
10	13	17	17
20	26	33	33
33	44	55	55

Using the modified SCAPE model, which projects future cliff retreat rates based on historical and projected sea level rise along with historical cliff retreat rates, a detailed picture emerges of how coastal erosion might evolve. Specifically, for cliffs that historically retreated at a rate of 33cm/year, under the RCP 8.5 scenario over the next 100 years, this rate is projected to increase to 55cm/year. This trend suggests that areas with higher historical retreat rates will face even more accelerated erosion in the future, especially under the more severe climate change scenarios. This model provides a crucial tool for coastal management, offering insights into potential future changes and the need for adaptive strategies in coastal planning.

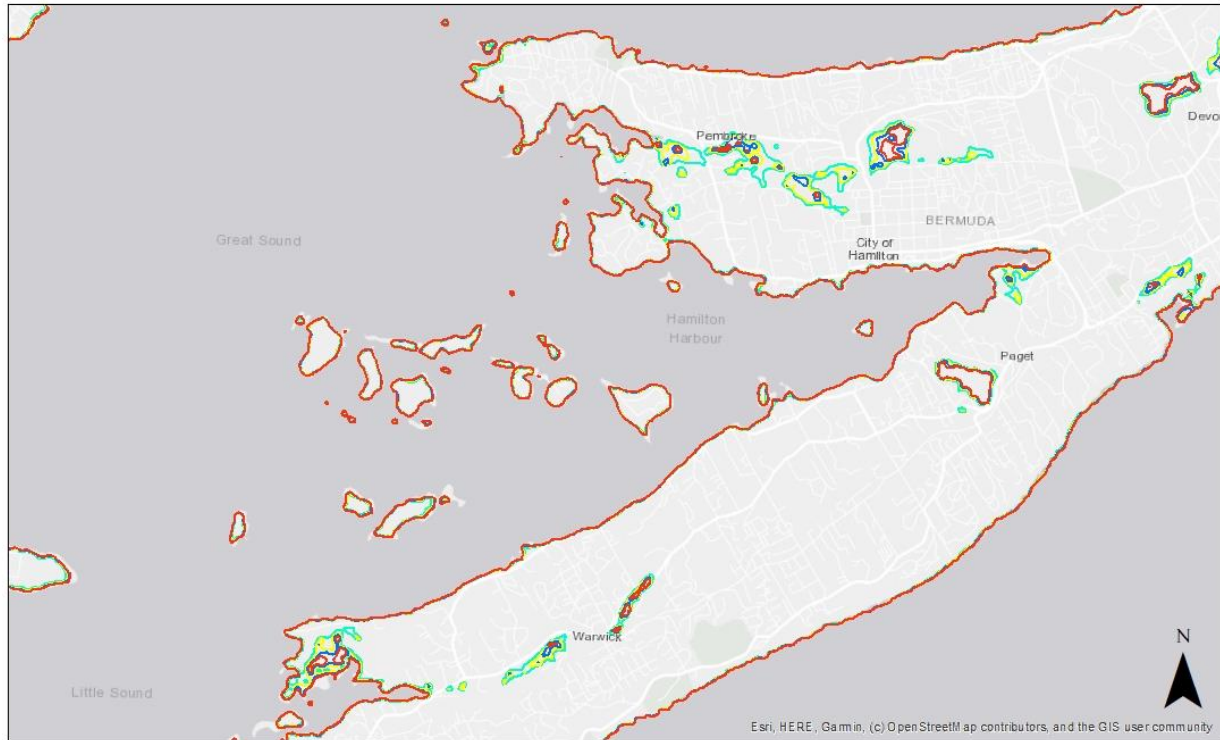
Climate Change Impact on Fresh Water Lenses

Rising sea levels are expected to significantly impact both inland and coastal regions through saltwater intrusion, threatening freshwater resources and ecosystems. This phenomenon occurs as the sea encroaches further inland, mixing saltwater with freshwater aquifers. In Bermuda, the unique geological formation allows freshwater lenses to float atop saline groundwater. These lenses are expected to rise in tandem with sea levels, yet due to the island's steep coastal topography, significant impacts at the surface are anticipated to remain confined near the shorelines for the foreseeable future. The study projects that by 2122, under the RCP 8.5 scenario, sea levels could rise by approximately 1.1m above the current level, leading to increased salinity intrusion into the subsurface. Coastal areas are particularly vulnerable, with estimates suggesting that saline water has already intruded 1.49m above Bermuda Ordinance Datum¹ as of 2022, highlighting the immediacy of the issue.

Several limitations exist within this analysis, including the exclusion of capillary action effects on salt migration in the vadose zone and the assumption of constant recharge and extraction rates, which may not hold true under changing climatic conditions. Moreover, the potential acceleration of sea-level rise and its consequent effects on groundwater systems were not accounted for, indicating that actual impacts could be more severe than predicted. The implications of these findings are profound,

¹ Ordnance datum was set at a mean sea level (msl) of 0.000 m in 1963 from tide gauge records at the Bermuda Biological Station. (Johnson, 1984 cited in Ellison, 1993). Glasspool 2008, gave msl as 0.21 m AOD. Plotting these values on a graph gives a 2022 msl of 0.26m AOD.

suggesting a pressing need for adaptive management strategies to safeguard freshwater resources and maintain ecosystem health. As such, understanding the dynamics of saltwater intrusion is crucial for developing effective responses to mitigate the risks posed by rising sea levels, emphasizing the importance of continued research and monitoring in this field.



BERMUDA - CLIMATE CHANGE STUDY
GREAT SOUND RCP 8.5

LEGEND

- Present Groundwater Elevation 1.49 m Above OD
 - Projected Groundwater Rise 1.98 m Above OD
 - Projected Groundwater Rise 1.68 m Above OD
 - Projected Groundwater Rise 2.42 m Above OD
- 0 0.25 0.5 1 1.5 2 Kilometers

Predicted groundwater rise for the Great Sound area for RCP 8.5

1 Introduction

Bermuda is a British Overseas Territory in the North Atlantic Ocean, with the nearest landmass approximately 1,035km to the west-northwest (Figure 1.1). Because of its isolation, it is vulnerable to severe storms – including both tropical and extratropical storms – from almost any direction. With the general consensus of climate change pointing toward more frequent and higher intensity storms, Bermuda is a target because of its position.

As the ice caps melt and the fetch (area of ocean surface over which the wind blows in an essentially constant direction) increases, the North Atlantic will experience larger waves. This means that, as hurricanes become stronger, the daily wave conditions on Bermuda's shores will be influenced by climate change. Bermuda also faces unique climate change challenges because it's an island: with more than 70% of the people in Small Island Developing States (SIDS) living on the coast, sea level rise (SLR) is an almost existential threat. Ultimately, innovative planning must be implemented to balance the need for continued development in the face of climate change. Herein lies the challenge for Bermuda's Department of Planning and the reason for this project.

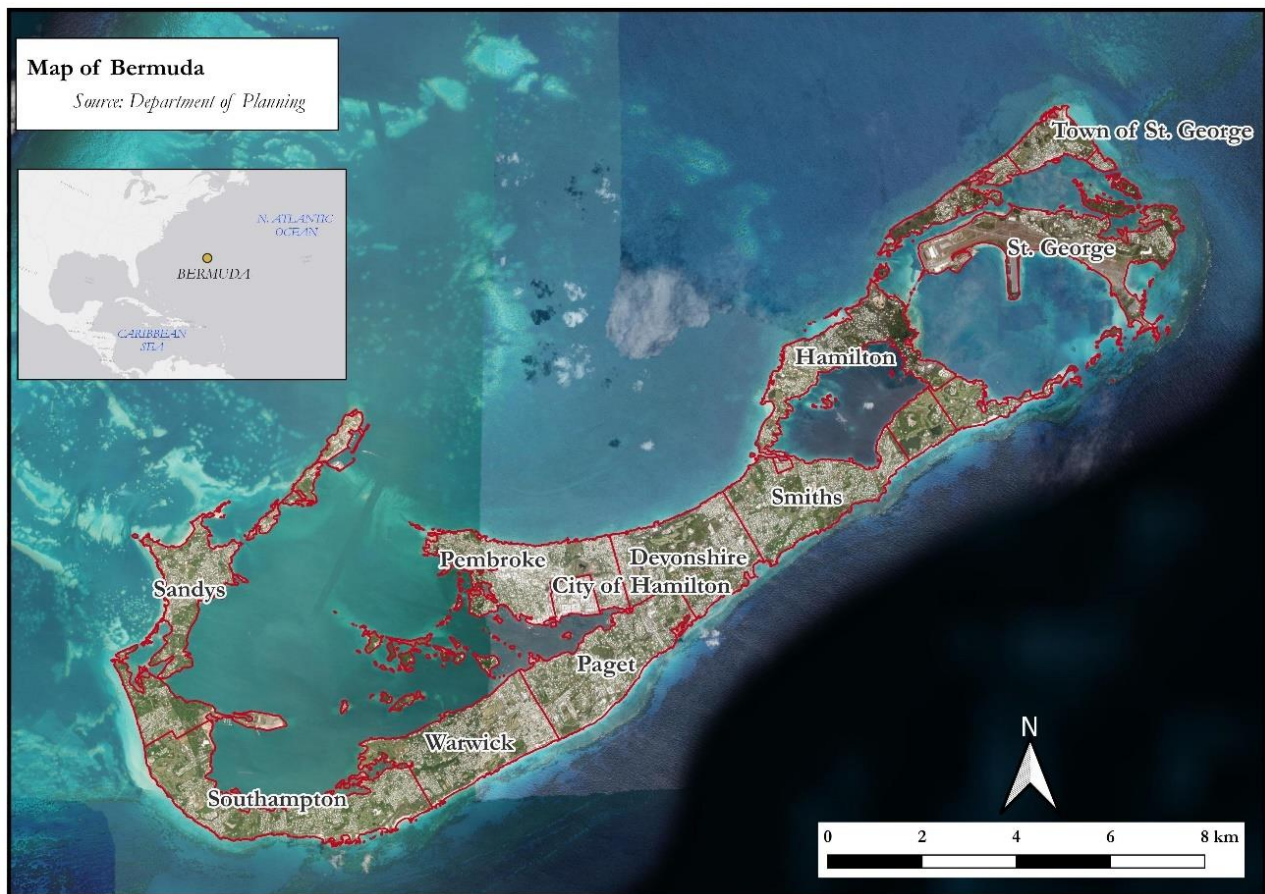


Figure 1.1 Location of Bermuda

This project encompasses the entire island of Bermuda. With a land mass of only 54km² and a population of about 65,000 Bermuda is one of the most densely populated countries on the planet. It also has one of the highest per capita incomes in the world, thanks to an economy based on offshore financial services and tourism. Unfortunately, Bermuda's financial success combined with its limited land space has resulted in significant development pressure, especially along its 291km of shoreline.

1.1 Background and Objectives

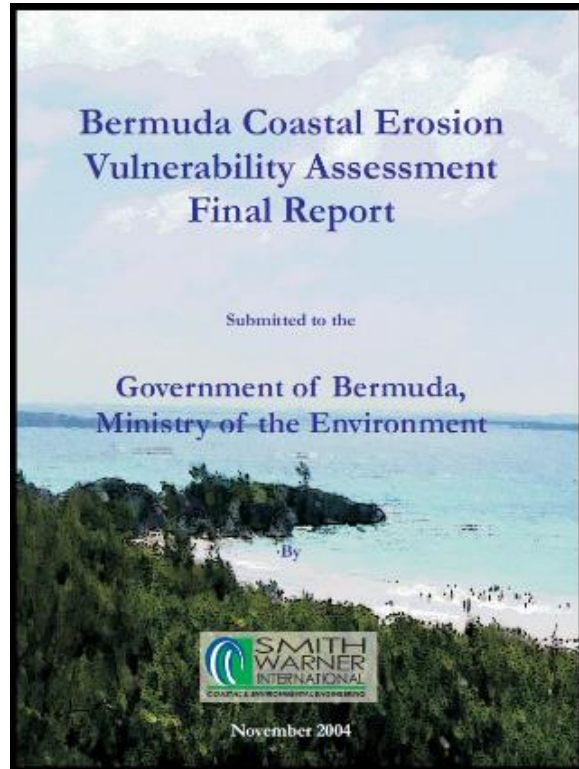
In 2004, the Government of Bermuda (GoB) hired Smith Warner International (SWI) to assess Bermuda's vulnerability to coastal erosion. The 2004 study identified specific shorelines that were most vulnerable to erosion and storm inundation due to potential wave run-up. Around Bermuda, two types of shorelines were observed: (i) sandy shores/beaches, and (ii) rocky shores, which can be further split into three sub-types: flat rocky, low cliffs, and high cliffs.

The 2004 report showed that most significant erosion along the Bermuda coastline is caused by physical forces, particularly wave action. The effects of biological erosion were also visible from *Casuarina sp.* tree roots and boring marine invertebrates.

1.2 Scope of Work

This study is intended to update the 2004 study considering recent projections of sea level rise and other anticipated climate change impacts, and includes the following:

- Current predictions of global warming in the context of sea level rise, combined with expected more severe weather events. The predictions specifically for Bermuda will contain a projection timeline for best- and worst-case climate change scenarios over short-, medium- and long-term time frames.
- Effects of coastal erosion and sea level rise on the mean sea level (MSL) benchmark.
- Identification of Government and critical infrastructure and facilities located at or close to the shoreline that are at risk from erosion or inundation. Undertaking of a vulnerability assessment for major infrastructure i.e., airport, ports, public highways, power plant, subterranean utility cabling, waste (i.e., Tyne's Bay incinerator, sewage management systems, etc.).
- Identification of what effect sea level rise will have on waterways, inshore ponds, marshes, from an ecological perspective.
- Identification of saltwater inundation of agriculture areas (soil salinization), within the context of food security and continued ability to cultivate fields.



- Update coastal erosion and flood inundation projections for the offshore islands, bays, beaches, and dunes, especially during storms and hurricanes.
- Identification of coastal areas prone to hydraulic erosion and / or destabilization of cliff faces or the island's shoreline areas.
- Mapping of projections for inundation island wide, identifying:
 - a) low-lying coastal areas that will be periodically or permanently inundated by seawater, and
 - b) low-lying freshwater resources that could be impacted, i.e., saltwater intrusion into freshwater lens.
- Recommendations for products / construction methods that are effective in controlling or reducing the effects of erosion. e.g., cliffs, beach dunes, including “green” or hybrid approaches.
- Identification of ‘no go’ areas for future development based on predicted flood zones and areas identified as being susceptible to high erosion.
- Identification of critical infrastructure components that will be at risk over the near-, medium- and long-term time frames.

1.3 Approach and Methodology

The project can be divided into three stages.

Stage 1: Project Inception and Baseline Studies,

Stage 2: Numerical Modeling

Stage 3: Vulnerability Assessment to Climate Change.

Stage 1, which was documented in the September 2022 Baseline Conditions Report, described the current conditions determined through site visits, meetings with stakeholders, and an extensive literature review. This report presents the findings of Stage 2, which involved numerical modeling to understand how climate change will affect the baseline conditions. In Stage 3, the modeling data is used to assess the impacts of climate change on the island's vulnerability.

2 Climate Change Modeling

Climate change is a major concern for many regions around the world, especially for small islands. The term climate change describes changes in weather trends occurring at a global scale. Typically, these changes occur over decades with no immediately noticeable effects in many parts of the world. Additionally, the effects of climate change are not all experienced in the same way in different regions. In recent years, there have been quicker changes observed in some weather patterns, impacting particular geographic areas. Some examples of this include rising sea levels, changes in rainfall patterns and even the life cycle of plants changing.

The main source of global climate statistics is the Intergovernmental Panel on Climate Change (IPCC). IPCC was created by the United Nations Environment Programme (UNEP) and the World Meteorological Organization (WMO) in 1988. The IPCC coordinates the activities of scientists and other researchers around the world to prepare projections of future climate changes and associated impacts. The panel's mandate is to prepare assessments of climate change, with the intention of informing realistic response strategies to human-induced climate change.

The IPCC releases assessment reports periodically that describe the current state of science regarding projections of future climate and its impacts. The first four assessment reports were released in 1990, 1995, 2001, and 2007, respectively. The fifth assessment report (AR5) was released in stages between September 2013 and November 2014. The sixth assessment report (AR6) is the most recent and was released in April 2022.

Quantifying the possible impacts of climate change is not easy, and climate scientists around the world rely heavily on climate models.

This climate change assessment for Bermuda was conducted using a combination of literature review, analysis of observed historical climate data as well as climate model outputs. The variables investigated and the associated time periods were subject to data availability and client approval. The final analysis included key climate variables such as temperature, rainfall, wind, as well as sea level rise for mid and end of century timelines. The full *Climate Profile and Projections for the Island of Bermuda* is attached as Appendix A.

2.1 Description of Datasets Used

The analysis characterising the historical and projected climate for the island of Bermuda was based on four data products: (i) station data, (ii) gridded data, (iii) reanalysis data and (iv) simulated outputs.

The projections were derived from simulated outputs from three global climate models namely GFDL-ESM2M, MPI-ESM-MR and HadGEM2-ES, referred to as GFDL, MPI and Had respectively. Table 2-1 summarizes the datasets used, their type, source, and resolution.

Table 2-1 List of datasets used for historical assessment for Bermuda

Variables	Analysis	Source	Dataset	Resolution		Units
				Temporal	Spatial	
Air Temperature Mean, Max & Min	Climatology, Trends & Extremes	Royal Netherlands Meteorological Institute (KNMI)	ERA5 & CRU	Daily	0.50°	°C
Precipitation						mm/day
Sea Surface Temperature	Climatology & Trends	Climate Explorer	NOAA Reynolds OI	Monthly	1.0°	°C
Hurricane	Trends	NOAA	HURDAT2 & IBTrACS			
Sea Level Rise		Copernicus Marine Environment Monitoring Service (CMEMS)	CMEMS		0.25°	

Precipitation and air temperature data for future projections were extracted from the outputs of RegCM, a regional climate model (RCM) from the International Centre for Theoretical Physics (ICTP). These outputs are downscaled values of outputs from the GFDL, MPI and Had General Circulation Models (GCMs), which were configured to run using the representative concentration pathways (RCPs) described by the RCP 2.6 and RCP 8.5 scenarios. The downscaling was done by the Climate Studies Group, Mona (CSGM).

Future projections for sea surface temperatures are from the Had model while information on future hurricanes was extracted from the literature. For sea level rise, published literature and satellite altimetry data were used for historical trends, while for projection trends, results from three climate data sites/tools were used. Table 2-2 presents the datasets used for the climate projection assessment.

Table 2-2 List of datasets used for climate projection assessment for Bermuda

Variables	Analysis	Source	Dataset	Resolution		Units
				Temporal	Spatial	
Air Temperature Mean, Max & Min	Climatology, Trends & Extremes	CSGM	RegCM Downscaled GFDL-ESM2M, MPI-ESM-MR and HadGEM2-ES (RCP 2.6 and RCP8.5)	Daily	0.25°	°C
Precipitation						mm/day
Sea Surface Temperature	Climatology & Trends	KNMI Climate Explorer	HadGEM2-ES (RCP 2.6 and RCP8.5)	Monthly	1.25°	°C
Hurricane	Trends	As reported in the literature.				
Sea Level Rise		As reported in the literature.				

2.2 Climate Change Analysis

2.2.1 Representative Concentration Pathways and Future Horizons

Climate projections are simulated based on future expectations (scenarios) of the earth’s environment. In this regard, future simulations of the Earth’s climate employ one of several standard scenarios used by the IPCC. In this report, the scenarios employed are representative concentration pathways (RCPs). RCPs are factor amalgamated greenhouse gas (GHG) emission scenarios used by the IPCC, which categorize possible future climates of the world. Factors weighed into the scenarios include energy use, economic activity, and land use. There are four (4) defined scenarios, namely RCP 2.6, 4.5, 6 and 8.5, each representing a future subjected to a specific radiative forcing value because of the predicted cumulative GHG emission quantities (Figure 2.1).

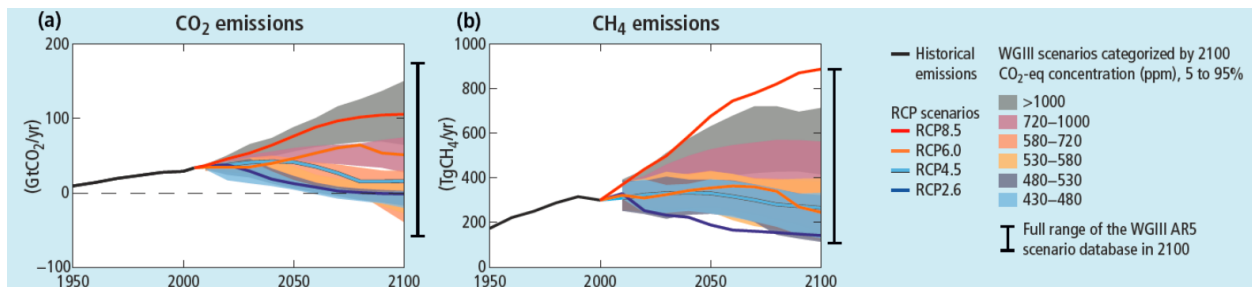


Figure 2.1 RCP projections for CO₂ and methane. The coloured lines show concentrations associated with each of the four RCP scenarios: 8.5, 6.0, 4.5 and 2.6. The shaded areas show the range of concentration projections identified in a survey on which the RCP projections are based. [Source: IPCC, 2014]

Future projections are also presented as Shared Socio-economic Pathways (SSPs), namely, SSP1-2.6, SSP2-4.5, SSP3-7.0, SSP5-8.5. SSPs are a new method of assessing future scenarios which seek to combine the knowledge of the physical sciences of climate change with the societal impacts brought on by the vulnerability caused by climate change. SSPs incorporate adaptation and mitigation research to create more holistic approaches to future projections by combining them with future emission and concentration scenarios with socio-economic development pathways.

Table 2-3 Summary of shared socio-economic pathways

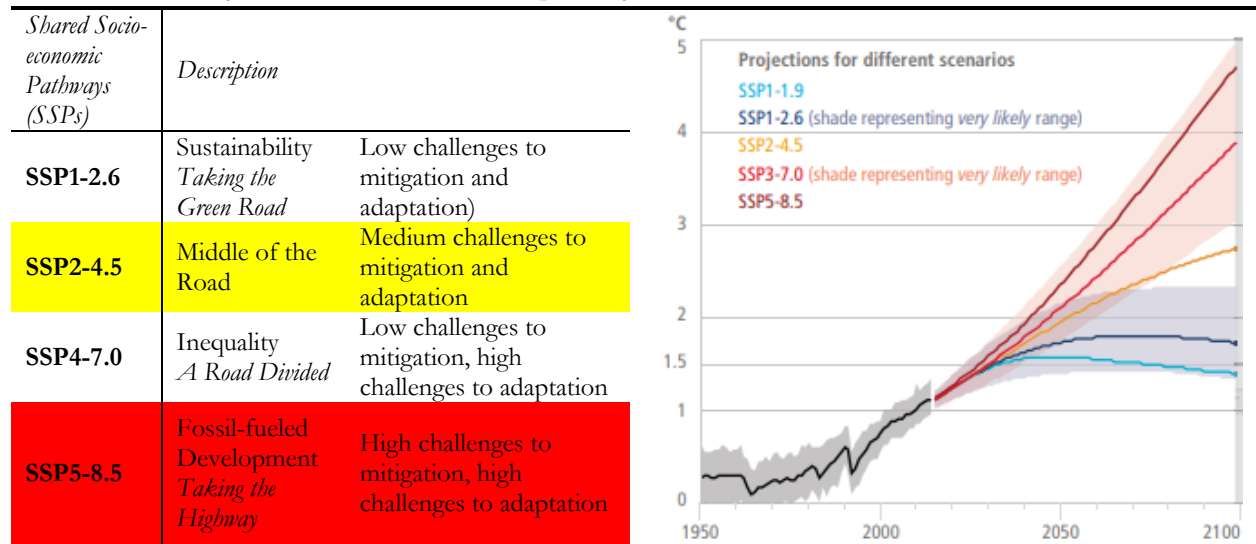


Figure 2.2 describes the RCPs and the projected horizons to be considered in this assessment. The conditions under the RCP 4.5 and 8.5 will be used to describe the conditions in 20, 50, and 100-year horizons.

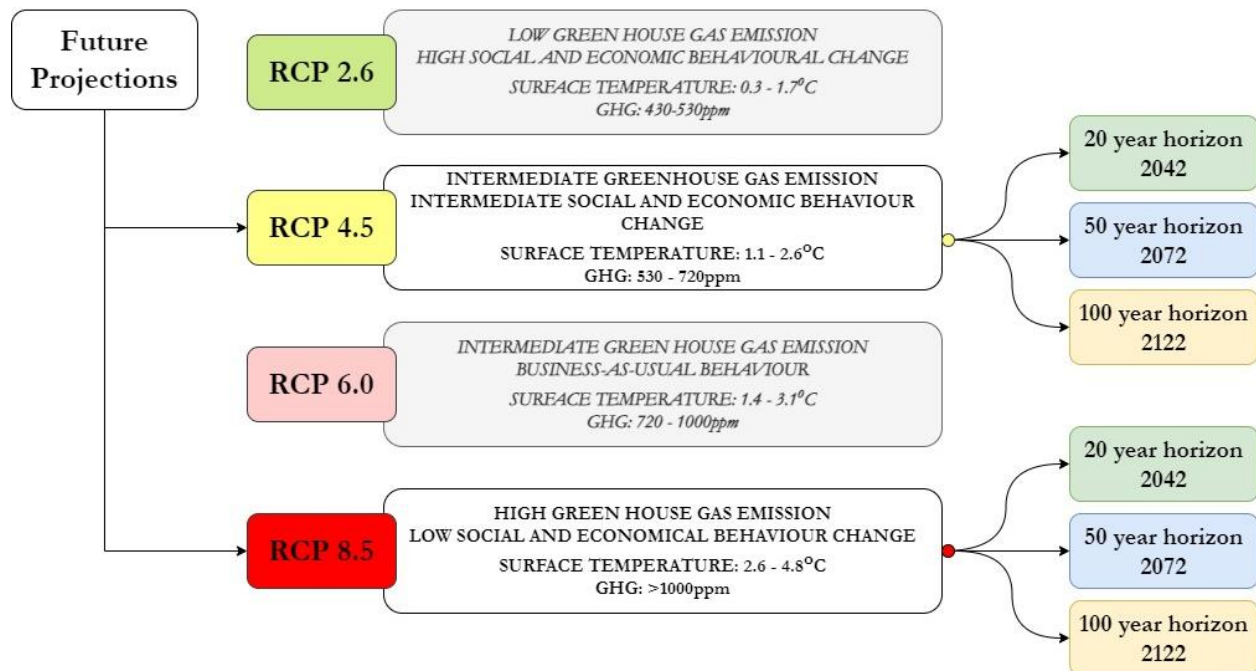


Figure 2.2 Description of the four Representative Concentration Pathway Scenarios

2.2.2 Global Climate Models

Future climates are simulated by global climate models (GCMs). These models are configured using GHG emissions from a specified RCP along with other parameters. GCMs use mathematical equations governing the conservation laws and physical processes to mimic the behaviour of atmospheric motion and their land and ocean interactions. There are numerous GCMs available and are run by various organizations around the world. The skill of individual GCMs varies in performance, with some better suited for specific regions of the globe.

2.2.3 Regional Models

Data output from GCMs are of a coarse resolution, usually greater than 125km. At coarser/lower resolutions, small island states or even local country scales are generally not represented well or identified at all. To have a more accurate representation of smaller regions the output of a GCM can be used as boundary conditions for a regional climate model (RCM), which downscales the GCM to a higher resolution (see Figure 2.3). The higher resolution allows for the study of the influence on dynamics posed by highly variable physical factors; for example, topography, land use and land–sea differences.

The RCM model used in this report is the ICTP RegCM. The RCM domain chosen was centred over the Caribbean Sea, with the domain adopting a horizontal resolution of 0.22 degrees (approximately 25km) with 63 vertical atmosphere levels.

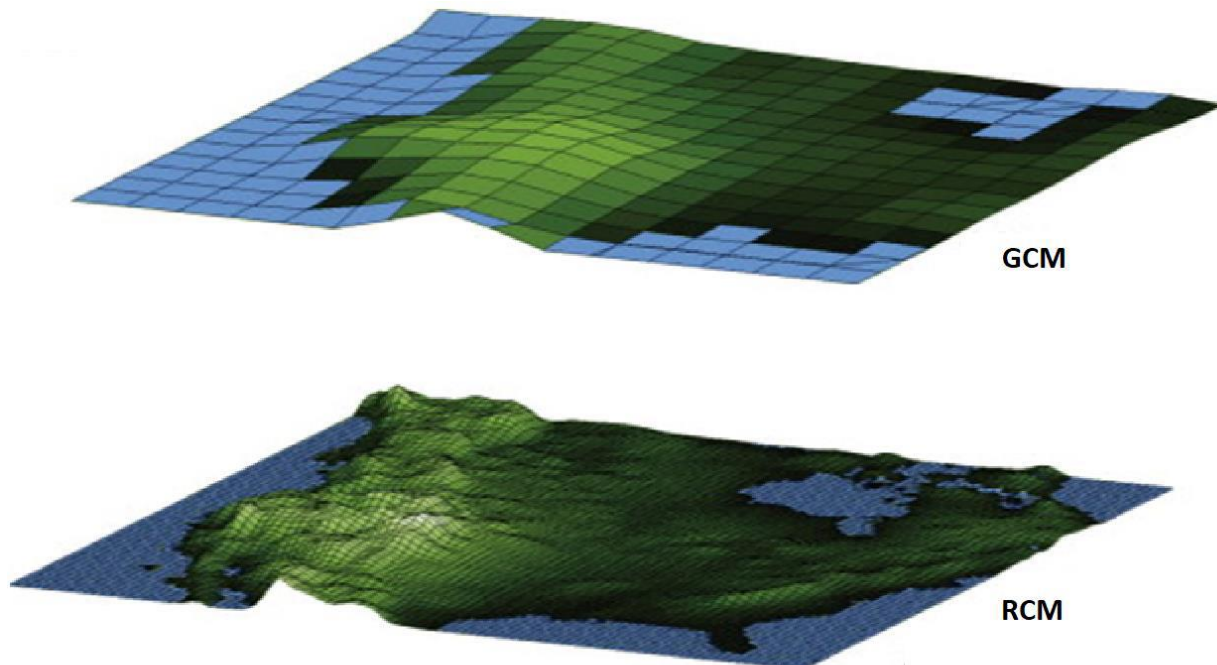


Figure 2.3 Visualization of GCM and RCM Scales

2.2.4 Summary of Climate Analysis

Table 2-4 summarises the parameters considered and changes observed based on historical data as well as climate change models. For all five parameters assessed by the climate change analysis there is evidence that the conditions in Bermuda are changing. The variations noted are driven by global climatic phenomenon and by climate change.

Table 2-4 Summary of climate change trends and projections for Bermuda

Parameter	Historical Trend	Projection
Temperature	<p>Air temperature varies throughout the year with the highest temperatures from July to September and lowest in January to March. Mean temperature has been increasing between 0.22°C and 0.6°C per decade.</p> <p>Hot days and nights have also been increasing at a rate of 4% and 3% per decade respectively.</p>	<p>Temperature is expected to continuously increase with global warming. In the medium term (2040-2060) the projected annual increase is between 0.6 and 1.7 for the RCPs. In the long term (2070-2090) the projected annual increase is between 0.6 and 3.2°C for the RCPs.</p> <p>Hot days and nights are increasing and will account for nearly 100% of days by end of century under RCP 8.5.</p> <p>Heatwave durations are increasing and will reach near 60 days by the end of century under RCP 8.5.</p>
Rainfall	<p>The island’s climatology exhibits a bimodal rainfall pattern with peaks in January and September, with the September peak receiving more rainfall.</p>	<p>The RCPs suggest no real trend toward the end of the century. In the medium term (2040-2060) mean annual projected change is 4 to 11% over the two RCPs examined. In the long term (2070-2090) mean annual projected change is 3 to 48%.</p> <p>Extreme events will be characterised by significant interannual variability. However, rainfall indices reflect no real overall trends with projected change in consecutive dry days (CDD) (between 0.1 and 0.2 days/decade) and changes in consecutive wet days (CWD) (0 and 0.2 days/decade).</p>
Sea Surface Temperature	<p>SST are highest during August to September and coolest during December to April. SSTs are increasing at a rate of 0.26°C per decade.</p>	<p>SSTs are projected to increase at a rate of 0.07°C (0.4.3°C) per decade under RCP 2.6 (8.5). In the medium term (2040-2060) monthly projected increase ranges from 0.6 to 1.7 °C (1.0 – 2.3°C) for RCP 2.6 (8.5). In the long term (2070-2090) monthly projected increase ranges from 0.8 to 1.7°C (2.5 – 4.0°C) for RCP 2.6 (8.5).</p>
Sea Level Rise	<p>Bermuda lies in an area that has experienced sea level rise of more than 3.84mm/year.</p>	<p>By 2100, mean SLR is projected to be approximately 0.47 m for SSP1—2.6 and between 0.69 and 0.82m for SSP5-8.5.</p> <p>If expert judgement including revised Antarctic ice-sheet contributions are considered then by 2100, mean SLR for Bermuda is projected to be approximately 1.46m for SSP5-8.5.</p>
Hurricanes	<p>Over the last 4 decades there were 21 storms passing within 50km of Bermuda. Between 5 and 8 storms passed per decade except for 1991 to 2000 when no storms were recorded passing within 50km.</p>	<p>The future will likely be characterized by more intense hurricanes with high winds and greater rainfall. A likely increase in rainfall rate of between 20% and 33% is projected particularly near the hurricane core by the end of the century.</p>

2.3 Implications for Coastal Planning

The climate change projections for Bermuda have general implications for coastal planning. However, coastal adaptations required to accommodate for the effects of climate change are site specific, depending on the risks for different locations. The main future climate change related risks to be considered in planning will be:

- Temperature rises leading to increased number of heat waves, hot days and hot nights;
- Increased uncertainties related to changes in rainfall and drought patterns;
- Significant increases in sea surface temperatures, which will likely affect marine life;
- Sea level rise;
- Increases in the frequency and/or intensity of extreme meteorological events leading to more frequent flooding occurrences; and
- Increased storm surge and wave action will also lead to coastal erosion.

Going forward this assessment focusses on the climate change effects of sea level rise and changes in hurricane intensity and frequency.

2.3.1 Sea Level Rise

For Bermuda, there is good consensus across the two mapping tools examined about sea level rise (SLR). Though RCPs and SSPs are not directly comparable, by 2050, mean SLR is projected to be 0.23m for RCP4.5 and 0.21m for SSP2-4.5; while by 2100, mean SLR is projected to be 0.53m for RCP4.5 and 0.56m for SSP5-8.5. AR6 (IPCC 2022) suggests that if expert judgement on high impact ice-sheet processes and inputs from a model incorporating marine ice cliff instability are considered, by 2100 SLR may reach up to 1.46m for Bermuda according to SSP5-8.5. These projections are more than estimates of global mean sea level rise by 2100, which are 0.56m for SSP2-4.5 and 0.77m SSP5-8.5.

In Table 2-5 below, the second column shows the multi-model median, column three shows the 66% uncertainty range, and column four shows the 90% uncertainty range. Shown in brackets are sea-level projections including expert judgement revised Antarctic ice-sheet contributions from Bamber et al. (2019).

Table 2-5 Local sea-level projections at St. Georges, Bermuda for RCP4.5 and RCP8.5

Year	Local Sea Level Rise (cm)			
	RCP	Median	Uncertainty Ranges	
			66%	90%
2030	4.5	12	6-19	1-24
	8.5	12 [14]	5-20 [6-22]	0-26 [1-28]
2050	4.5	23	14-34	7-43
	8.5	25 [32]	14-37 [20-46]	7-47 [11-61]
2100	4.5	53	28-82	12-110
	8.5	65 [102]	34-102 [61-160]	14-136 [37-243]

The values specified in Table 2-6 below will be used for informing the conditions in 20 years, 50 years and 100 years. In the medium term (up to 2060), a rate of 5.4mm/year and 6.6mm/year will be used for the RCP 4.5 and 8.5 respectively. For the longer-term assessments (greater than 2060) 7.7mm/year and 10.5mm/year will be used.

Table 2-6 Sea level projections for 5 SSP scenarios, relative to a baseline of 1995-2014, in meters at St. Georges/ Esso Pier (Bermuda)

		SSP1-1.9	SSP1-2.6	SSP2-4.5	SSP3-7.0	SSP5-8.5
Rate (2040-2060)	<i>Mean (mm/yr.)</i>	4.6	4.6	5.4	5.7	6.6
	<i>Rate used for the 20-year horizons</i>					
	<i>Range (mm/yr.)</i>	3.2 - 6.9	2.6 - 7.5	3.8 - 8.1	4.1 - 8.1	4.6 - 9.4
Sea Level Rise Next 20 years	<i>Mean (mm)</i>	92	92	108	114	132
Rate (2080-2100)	<i>Mean (mm/yr.)</i>	4.4	5.6	7.7	9.6	10.5
	<i>Rate used for the 50- and 100-year horizons</i>					
	<i>Range (mm/yr.)</i>	2.2 - 7.4	3.0 - 9.2	3.5 - 13.0	5.2- 15.2	5.2 - 17.7
Sea Level Rise 50 years	<i>Mean (mm)</i>	220	280	385	480	525
100 years	<i>Mean (mm)</i>	440	560	770	960	1050

2.3.2 Storm Surge and Hurricane Wave Impacts

From the available body of literature examined, the following changes related to future intensity and frequency of hurricane occurrences should be noted:

- The number of hurricanes experienced in a given season is likely to decrease or remain unchanged in the future. Zhang, et al. (2019) for instance found an inversely proportional historical relationship between tropical cyclone frequencies and sea surface temperature (SST). That is, tropical cyclone activity decreased with an increase in the warmth of pools in which they form. This is with high confidence (tests of 90-99.9% for the respective pools). Storms in moderate pools (65th-90th percentile) decreased by 0.79 storms/decade and in the warm pools (>90th percentile) by 1.08 storms/decade. The suggestion is that with an increase in future temperatures there may be reduced overall hurricane frequency. These results are echoed in other reports such as the CSGM 2017 report (2017), the IPCC 2012 Special Report on Extremes (IPCC 2012) and Knutson et al. (2013).
- The number of higher category hurricanes are likely to increase in the future. Studies (Bhatia et al., 2018, Bender et al., 2018 and Knutson et al., 2013) have shown an increasing trend in major Atlantic hurricanes. Bhatia et al. (2018) projected a 72.9 and 135.5% increase in category

4 and 5 hurricanes respectively by end of century under RCP 4.5. Bender et al. (2010) and Knutson et al. (2013) presented combined category 4 and 5 percentage increases of 100% and 40% respectively.

- Rainfall rates associated with hurricanes are likely to increase in the future. Warmer temperatures are associated with greater convection and more moisture in the atmosphere. Knutson et al. (2013) indicated a likely increase in rainfall rate of between 20% and 33% particularly near the hurricane core for the late twenty-first century from an ensemble of models run under the SRES A1B scenario and RCP 4.5.
- Maximum wind speeds associated hurricanes are likely to increase in the future as temperature increases (Trepanier 2020). For Bermuda, the rate at which wind speed changes with temperature is between 1 to 1.5 ms⁻¹ per °C. This implies an increase from current wind speed by as much as 1.1ms⁻¹, 2.3ms⁻¹ and 3.5ms⁻¹ in the near-, medium- and long-term future respectively under RCP 8.5.

3 Wave Assessment and Transformation Modeling

To accurately describe Bermuda's wave climate, an assessment of both the operational and hurricane wave climates was performed. This procedure necessitated an examination of the offshore wave conditions. Once the area was understood, a numerical model of the area was created and calibrated using measured data. The wave climate of Bermuda's nearshore was assessed using the knowledge gained from the offshore conditions and the calibrated model. This section of the report presents the findings of this assessment. The mean wave climate and other statistically significant events are discussed as well as how waves will be impacted by climate change.

The operational wave climate at the project site is characterized by (a) day-to-day, relatively calm conditions; and (b) seasonal winter swells (December to May). The day-to-day conditions are primarily generated by the north-east Trade Winds. The swells, however, are generated by north Atlantic cold fronts and these waves approach Bermuda from the north and north-west sectors.

3.1 Summary of Offshore Conditions

For this study, the data used to assess the operational wave climate of Bermuda was procured from the ERA 5 global reanalysis model. Figure 3.1 shows a wave rose plot (wave heights and frequency of occurrence) at each of one of four nodes that bracket the offshore area of Bermuda. The European Centre for Medium-Range Weather Forecasts (ECMWF) produced the ERA5 reanalysis which, once completed, will embody a detailed record of the global atmosphere, land surface and ocean waves from 1950 onwards. Currently, data from 1979 to 2020 is available for use. ECMWF in 2016 implemented significant resolution upgrades and introduced methodology improvements to facilitate high-resolution forecasts (HRES). HRES is now performed using a transform grid with a nominal grid point spacing of 9km (0.08 degrees) and is carried out with IFS (Integrated Forecast System) model cycle CY41r2. ERA5 thus benefits from a decade of developments in model physics, core dynamics and data assimilation. In addition to a significantly enhanced horizontal resolution, ERA5 has hourly output throughout, which is an improvement on most publicly available wave data.

The wave rose shown in Figure 3.1 was developed from nodal information developed at 64°W 33°N. The wave rose may therefore be compared with the ERA5 nodes shown in Figure 3.1. Such a comparison confirms the presence of frequent, but less energetic, waves from the south-east, as well as less frequent, but more energetic waves from the west to north-west sector.

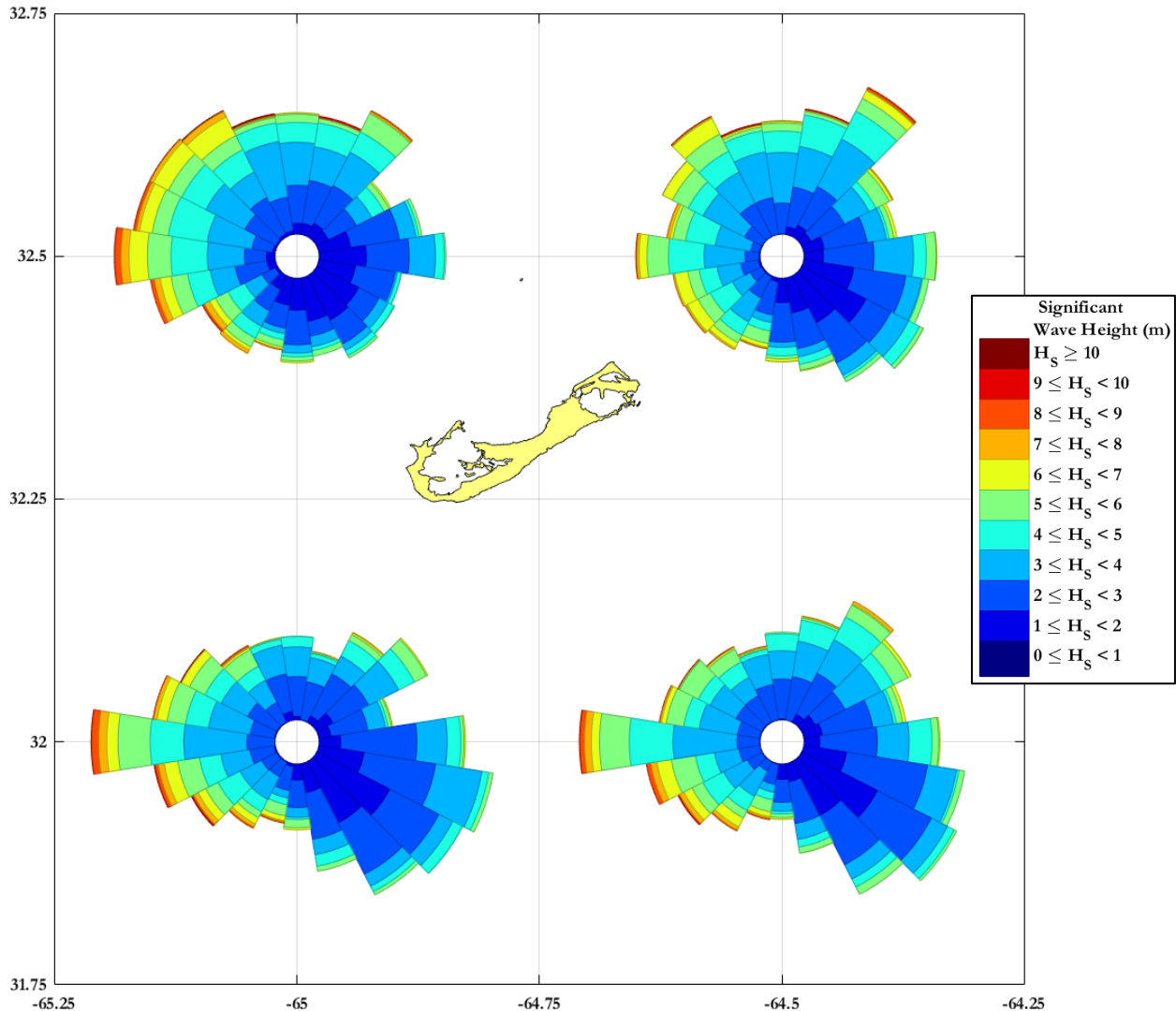


Figure 3.1 Distribution of wave heights from the ERA5 reanalysis (1979 to 2021)

The 43 years of ERA5 wave data were categorized using a frequency analysis of wave height, period, and direction, as well as wind speed and direction. This technique is known as “binning”. This frequency analysis resulted in 700+ different conditions or “events” representing a combination of wave height, peak period, and direction as well as wind speed and direction, each with a specific duration related to the number of occurrences in the 43-year period. Table 3-1 shows a cross tabulation of the significant wave heights, periods and directions. The table shows that:

- Waves come from all directions as shown in the wave roses.
- The most frequent offshore wave height is 0-2m (68.1%), and the most frequent wave periods are 6-8s (56.1%).
- Longer period waves (10-14s) come from the NW to NNE. This is indicative of the north swells originating in the North Atlantic region.

Table 3-1 Cross-tabulation of significant wave height, period and direction

		NNE	NE	ENE	E	ESE	SE	SSE	S	SSW	SW	WSW	W	WNW	NW	NNW	N		
2 - 4s	Hs	0 - 2m																	
	Sum	0.0										0.0			0.0			0.0	
4 - 6s	Hs	0 - 2m	0.4	0.6	0.8	1.0	1.3	1.9	2.2	2.0	2.1	2.5	2.4	1.9	1.1	0.6	0.5	0.4	21.9
		2 - 4m	0.0	0.0	0.0	0.0	0.0	0.0	0.1	0.1	0.2	0.2	0.1	0.1	0.0	0.0	0.0	0.0	0.9
	Sum		0.5	0.7	0.8	1.0	1.3	2.0	2.3	2.1	2.3	2.7	2.6	2.0	1.1	0.6	0.5	0.4	22.8
6 - 8s	Hs	0 - 2m	3.2	3.6	4.0	4.1	3.9	3.6	1.7	1.0	0.9	1.1	1.6	2.1	2.2	2.3	2.8	3.0	41.1
		2 - 4m	1.0	1.0	0.8	0.5	0.3	0.3	0.3	0.4	0.6	1.0	1.5	1.7	1.6	1.5	1.3	1.1	14.8
		4 - 6m	0.0	0.0	0.0	0.0	0.0	0.0	0.0	0.0	0.0	0.0	0.0	0.0	0.0	0.0	0.0	0.0	0.2
	Sum		4.2	4.6	4.8	4.5	4.2	3.9	2.0	1.4	1.5	2.1	3.1	3.9	3.8	3.9	4.1	4.1	56.1
8 - 10s	Hs	0 - 2m	0.8	0.8	0.9	0.4	0.3	0.2	0.1	0.0	0.0	0.0	0.0	0.0	0.1	0.2	0.5	0.6	5.1
		2 - 4m	1.2	0.8	0.5	0.1	0.1	0.1	0.0	0.0	0.0	0.1	0.1	0.5	1.2	2.0	2.7	2.0	11.4
		4 - 6m	0.1	0.0	0.0	0.0	0.0	0.0	0.0	0.0	0.0	0.0	0.1	0.3	0.6	0.5	0.4	0.1	2.2
		6 - 8m	0.0	0.0	0.0	0.0	0.0	0.0	0.0	0.0	0.0	0.0	0.0	0.0	0.0	0.0	0.0	0.0	0.1
		8 - 10m	0.0	0.0	0.0	0.0	0.0	0.0	0.0	0.0	0.0	0.0	0.0	0.0	0.0	0.0	0.0	0.0	0.0
	Sum		2.1	1.7	1.4	0.6	0.3	0.3	0.1	0.1	0.1	0.1	0.3	0.9	1.8	2.7	3.6	2.8	18.8
10 - 12s	Hs	0 - 2m	0.0	0.0	0.0	0.0	0.0	0.0	0.0	0.0	0.0	0.0	0.0	0.0	0.0	0.0	0.0	0.0	0.1
		2 - 4m	0.2	0.2	0.1	0.0	0.0	0.0	0.0	0.0	0.0	0.0	0.0	0.0	0.0	0.1	0.2	0.2	1.1
		4 - 6m	0.1	0.0	0.0	0.0	0.0	0.0	0.0	0.0	0.0	0.0	0.0	0.0	0.1	0.2	0.3	0.1	0.8
		6 - 8m	0.0	0.0	0.0	0.0	0.0	0.0	0.0	0.0	0.0	0.0	0.0	0.0	0.1	0.1	0.1	0.0	0.4
	Sum		0.3	0.2	0.1	0.0	0.0	0.0	0.0	0.0	0.0	0.0	0.0	0.1	0.2	0.5	0.5	0.4	2.4
12 - 14s	Hs	0 - 2m	0.0	0.0	0.0	0.0	0.0	0.0	0.0	0.0	0.0	0.0	0.0	0.0	0.0	0.0	0.0	0.0	0.0
		2 - 4m	0.0	0.0	0.0	0.0	0.0	0.0	0.0	0.0	0.0	0.0	0.0	0.0	0.0	0.0	0.0	0.0	0.0
		4 - 6m	0.0	0.0	0.0	0.0	0.0	0.0	0.0	0.0	0.0	0.0	0.0	0.0	0.0	0.0	0.0	0.0	0.0
		6 - 8m	0.0	0.0	0.0	0.0	0.0	0.0	0.0	0.0	0.0	0.0	0.0	0.0	0.0	0.0	0.0	0.0	0.0
	Sum		0.0	0.0	0.0	0.0	0.0	0.0	0.0	0.0	0.0	0.0	0.0	0.0	0.0	0.0	0.0	0.0	0.0
14 - 16s	Hs	4 - 6m	0.0	0.0	0.0	0.0	0.0	0.0	0.0	0.0	0.0	0.0	0.0	0.0	0.0	0.0	0.0	0.0	0.0
	Sum		0.0	0.0	0.0	0.0	0.0	0.0	0.0	0.0	0.0	0.0	0.0	0.0	0.0	0.0	0.0	0.0	0.0
Total	Hs	0 - 2m	4.5	5.0	5.8	5.5	5.4	5.8	4.0	3.0	3.1	3.6	4.0	4.0	3.4	3.1	3.7	4.1	68.1
		2 - 4m	2.5	2.0	1.4	0.6	0.4	0.4	0.4	0.5	0.8	1.2	1.8	2.3	2.8	3.6	4.2	3.3	28.1
		4 - 6m	0.1	0.1	0.0	0.0	0.0	0.0	0.0	0.0	0.1	0.1	0.4	0.7	0.8	0.7	0.3	0.3	3.3
		6 - 8m	0.0	0.0	0.0	0.0	0.0	0.0	0.0	0.0	0.0	0.0	0.0	0.0	0.1	0.2	0.1	0.0	0.4
	Sum		7.1	7.1	7.2	6.1	5.8	6.2	4.4	3.6	3.9	4.9	5.9	6.8	7.0	7.7	8.6	7.7	100.0

3.2 Summary of Measured Data

Currents were measured under this project using two Teledyne/RDI Acoustic Doppler Current Profilers (ADCP's). Instruments were deployed in varying water depths to get an overall understanding of the wave-induced currents. A description of each deployment and the instruments used is presented below.

An ADCP operates using acoustic signals and determines the current speed and direction by detecting the Doppler shift of reflected acoustic signals, which bounce off tiny particles moving within the water. Using multiple acoustic “pings”, it is possible to divide the water column into distinct layers and simultaneously determine the speed and direction of the water movement within each layer.

In the first deployment, an ADCP was placed west of the island and another placed east of the island, at depths of 14m and 16m respectively. For the second deployment, the “West” recorder was kept in

its original location, while the “East” recorder was moved to the South, in a water depth of 16.1m (Figure 3.2).

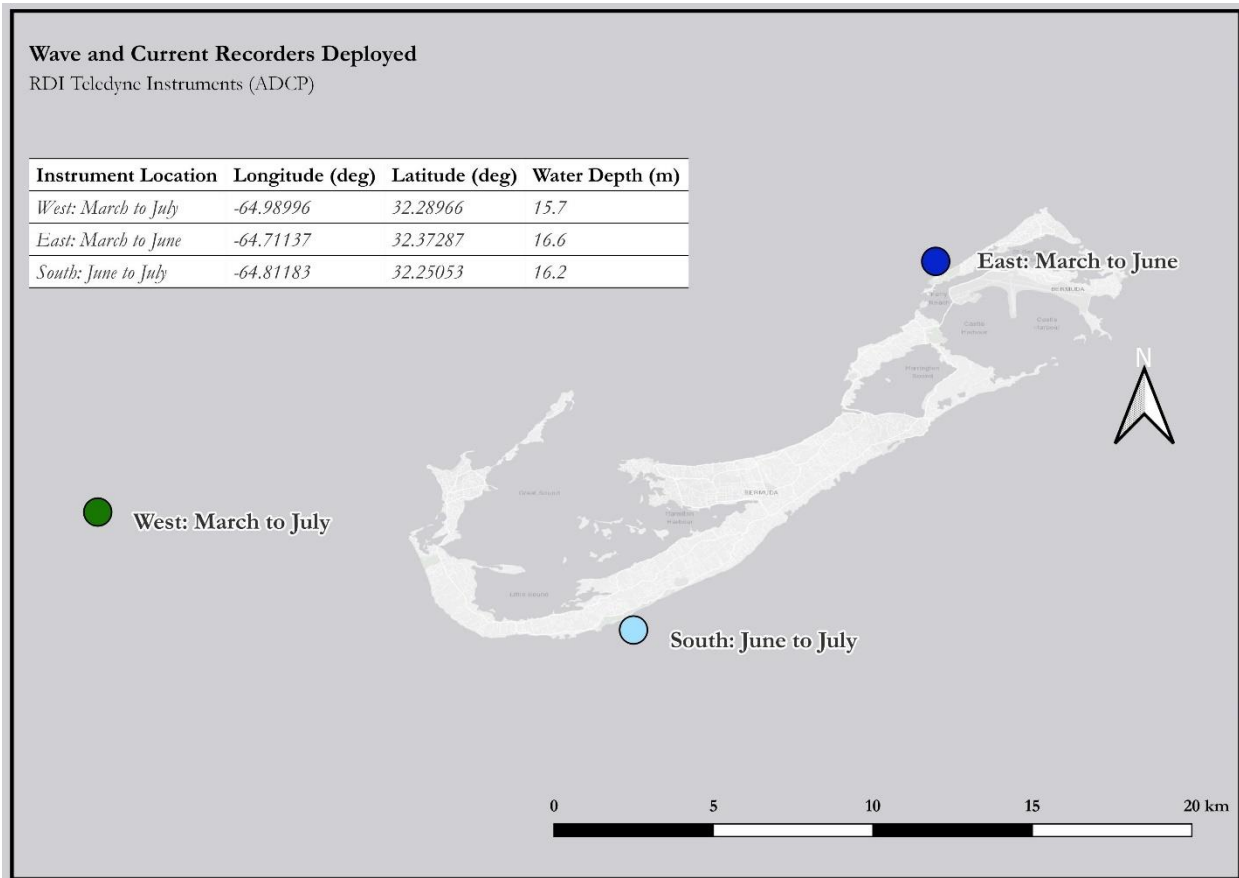


Figure 3.2 Instrument deployment locations

3.2.1 Results of Deployment

Tides and Temperatures

All locations recorded tidal ranges of -0.4m to 0.6m for spring tides and -0.2m to 0.23m for neap tides (Figure 3.3 and Figure 3.4). This is typical for the area and corresponds with data from literature for the area. All locations show a steady increase of the mean sea temperature, with a range of 19.5°C - 25°C. Recordings from the East and South (closer to land) show slightly higher temperatures with an average difference of approximately 0.7°C -1°C.

Figure 3.5 shows temperature data for March 2023 to the end of July 2023 from the Bermuda Weather Service. It confirms the sudden increase in sea surface temperature exhibited in Figure 3.3 and Figure 3.4, with both the sea surface temperature and mean air temperature increasing.

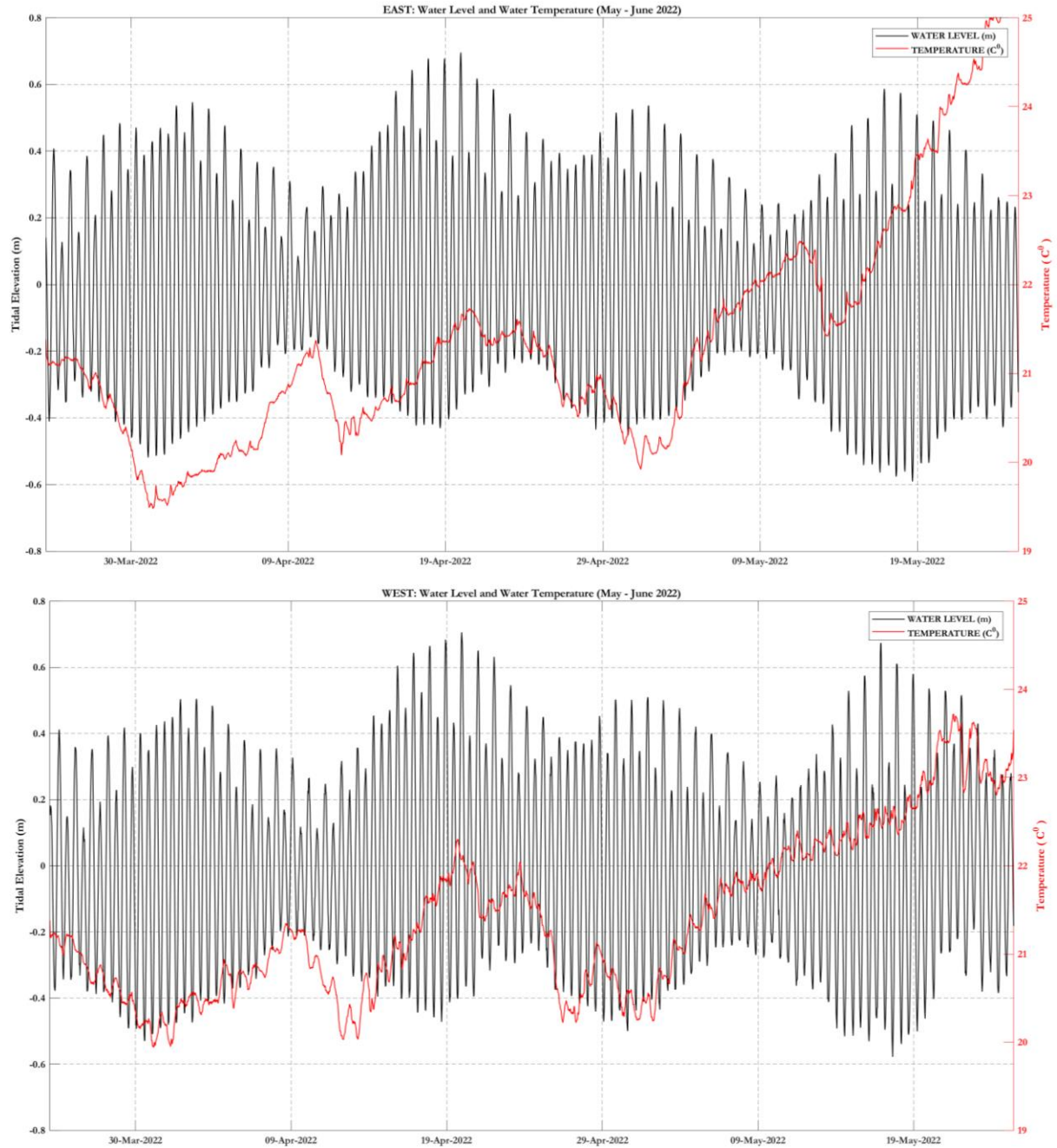


Figure 3.3 Tidal variations and sea temperatures for the East and the West locations

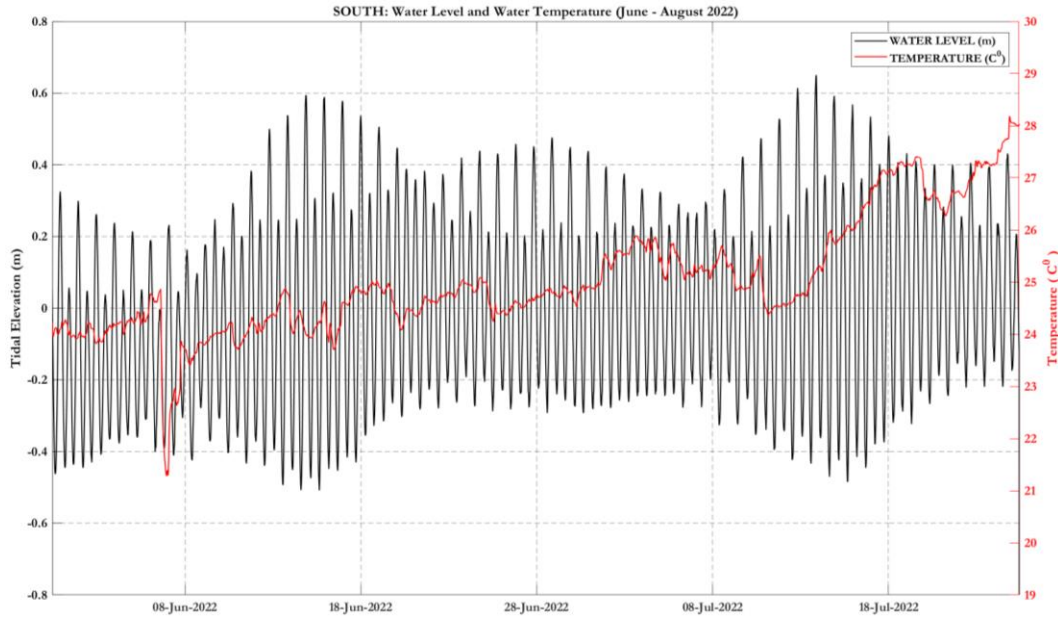


Figure 3.4 Tidal variations and sea temperatures for the South location

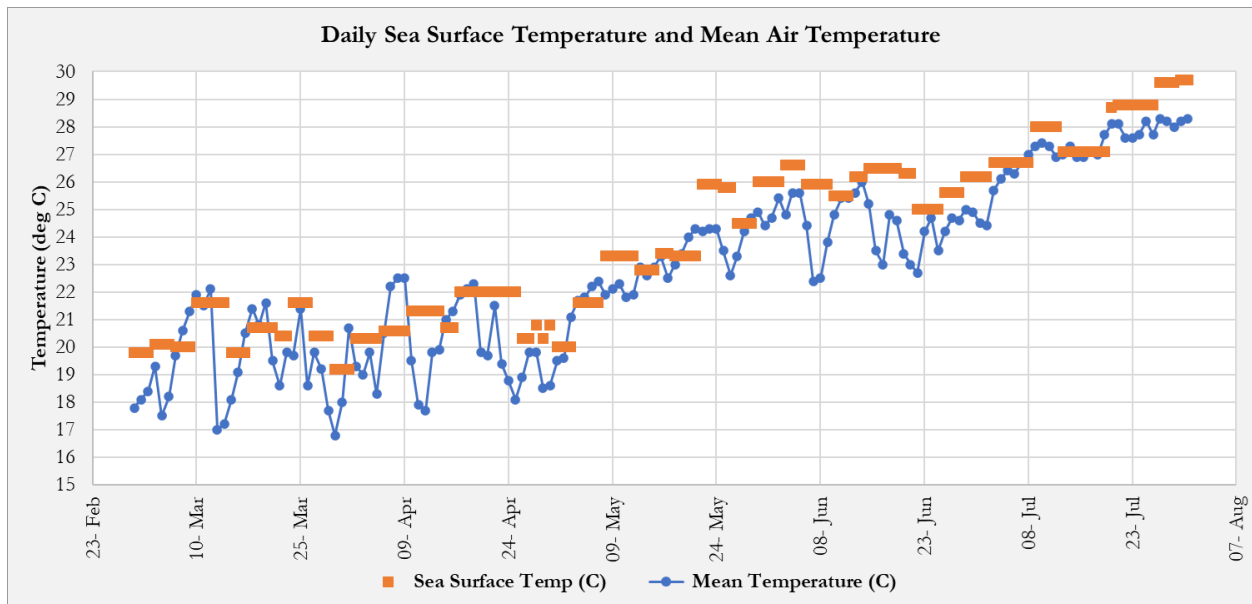


Figure 3.5 Daily sea surface and mean air temperature for Bermuda (Source: Bermuda Weather Service)

Currents

The current measurements indicate that:

- At the East location, currents were primarily shore-parallel along an ENE – WSW axis, with speeds up to 0.2m/s (Figure 3.6 and Figure 3.7). The currents are influenced by tides and show a reversal in direction, with the WSW directed currents somewhat slower (less than 0.15m/s).
- At the South location there is a dominant drift towards the north-east and south-west, with stronger drift towards the north-east (0.18-0.2m/s).
- At the West location there was a broader range of current directions from south to north. The currents have speeds ranging from 0.2 to 0.3m/s. The current directions are also influenced by the tides and reverse when the tides change. The current speed from the north is less than 0.2m/s.

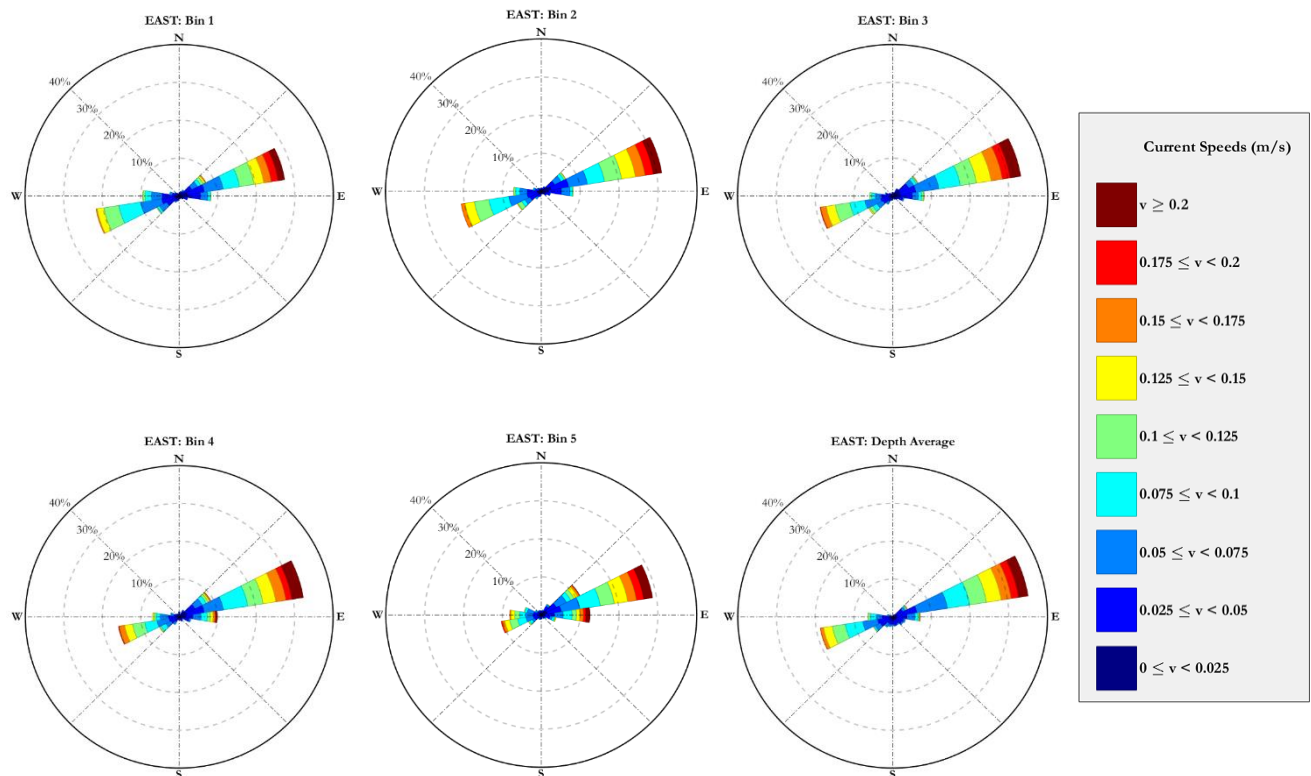


Figure 3.6 Measured current speeds and directions for East location; shown both in varying depth for each bin (bins are 2m deep with Bin 1 just above the sensor) and the depth-averaged throughout the water column

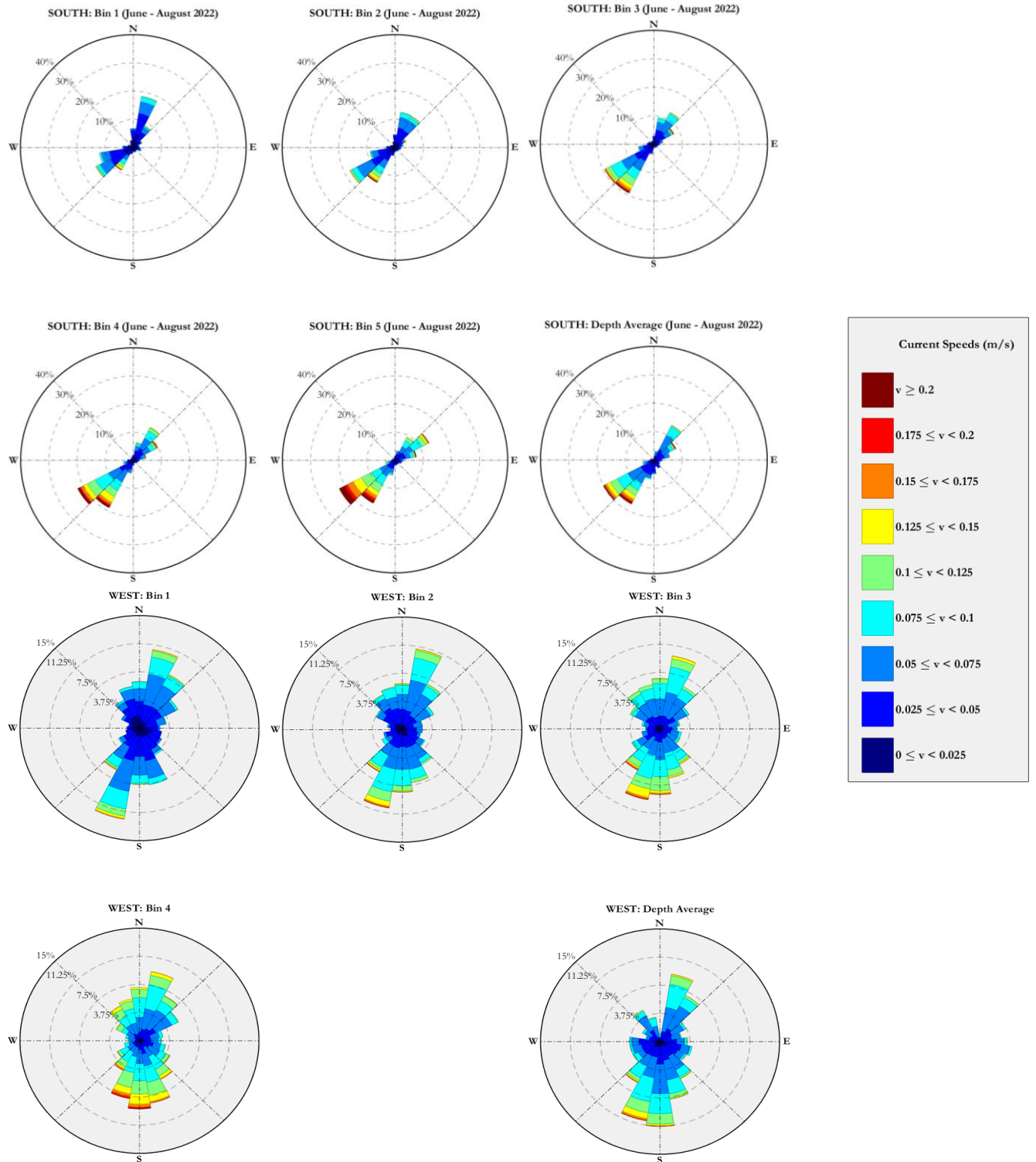


Figure 3.7 Measured current speeds and directions for South and West locations; shown both in varying depth for each bin (bins are 2m deep with Bin 1 just above the sensor) and the depth-averaged throughout the water column

Figure 3.8 shows the three-dimensional distribution of the measured currents within each (vertical) bin and through the water column through U (East-West) and V (North-South) components of velocities. The plots show that for the East instrument there is a narrow band of UV point cluster, which means that most of the currents are flowing in one direction from the NE to the SW.

The red colour in the figure indicates stronger currents coming from the north-east. This would have implications for the flow of sediments or other suspended particles.

The results at the West instrument show a wider shape of the point cluster, which indicates the flow of the current is more multidirectional. This may be due to the influence of the stronger waves that affect this area and which are also multidirectional. Having said that, all figures (West, South and East) have similar shapes for all the bins. This indicates that there is little variation in the currents as one descends through the water column. Ultimately, in terms of numerical modeling requirements, there will be no need to model the hydrodynamics in 3D because the measured data confirms there are no major differences in current patterns with depth throughout the water columns.

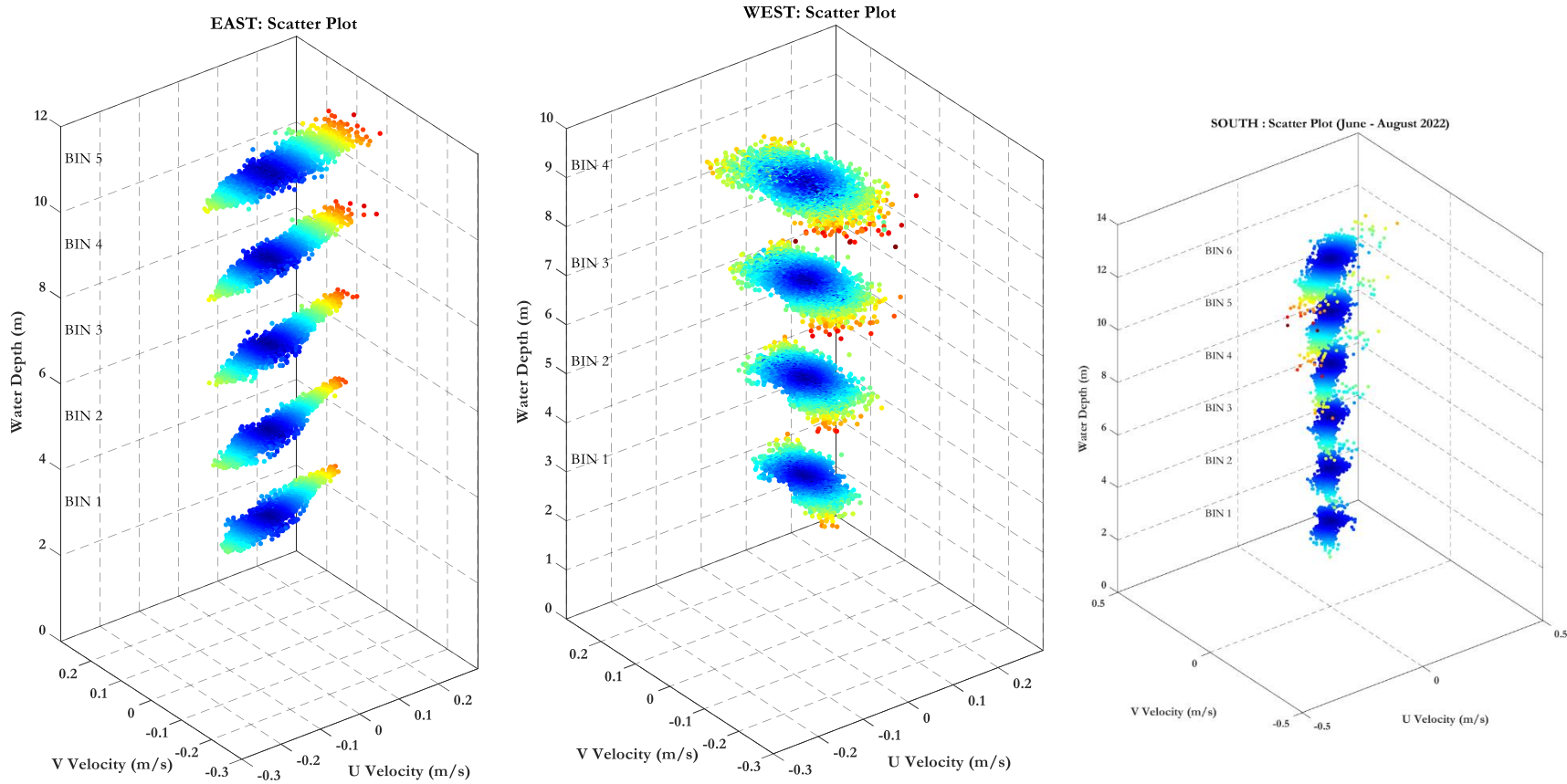


Figure 3.8 U and V Velocities through the Bins for the east (left), the west (middle) and south (right)

Waves

Wave measurements are plotted in Figure 3.9 to Figure 3.11 and indicate that:

- The West instrument shows higher waves, with values up to 2.4m and a mean of approximately 1.2m.
- At the East, the maximum recorded wave height was 1.5m with a mean of approximately 0.7m.
- At the South, the dominant wave direction is from the southeast. The maximum wave height from the south was greater than 2.5m, during the passage of Hurricane Alex in August 2022. The mean wave height for southerly waves was 1.4m.
- During the period of measurement, the dominant wave direction was from the west for both East and West instruments, however for the East instrument, there was also a notable occurrence of waves from the north-east.

It should be noted that the wide spectrum of wave conditions as a result of the influence of the open ocean presented challenges for the calibration of numerical models.

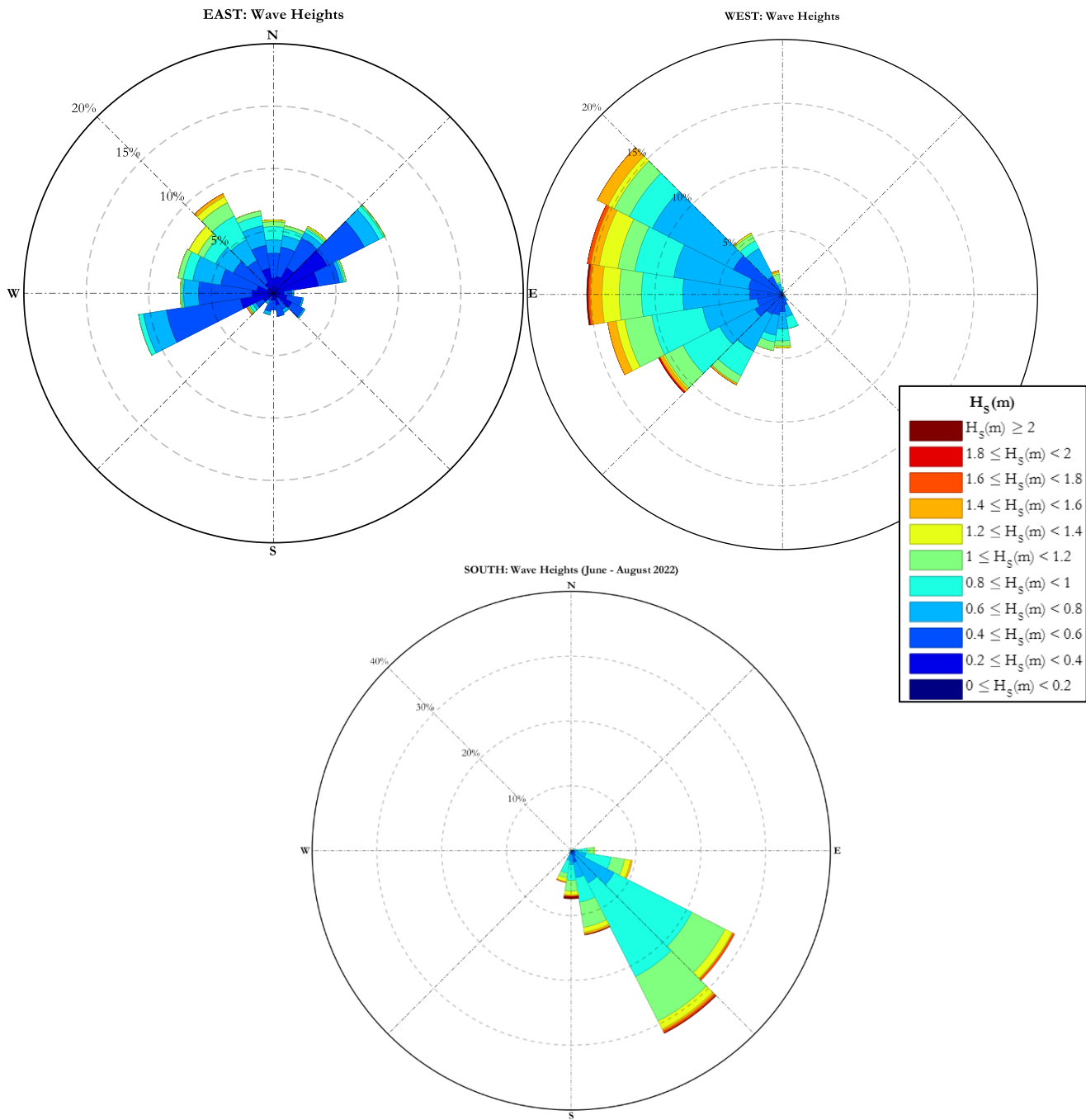


Figure 3.9 Wave roses for recorded wave data

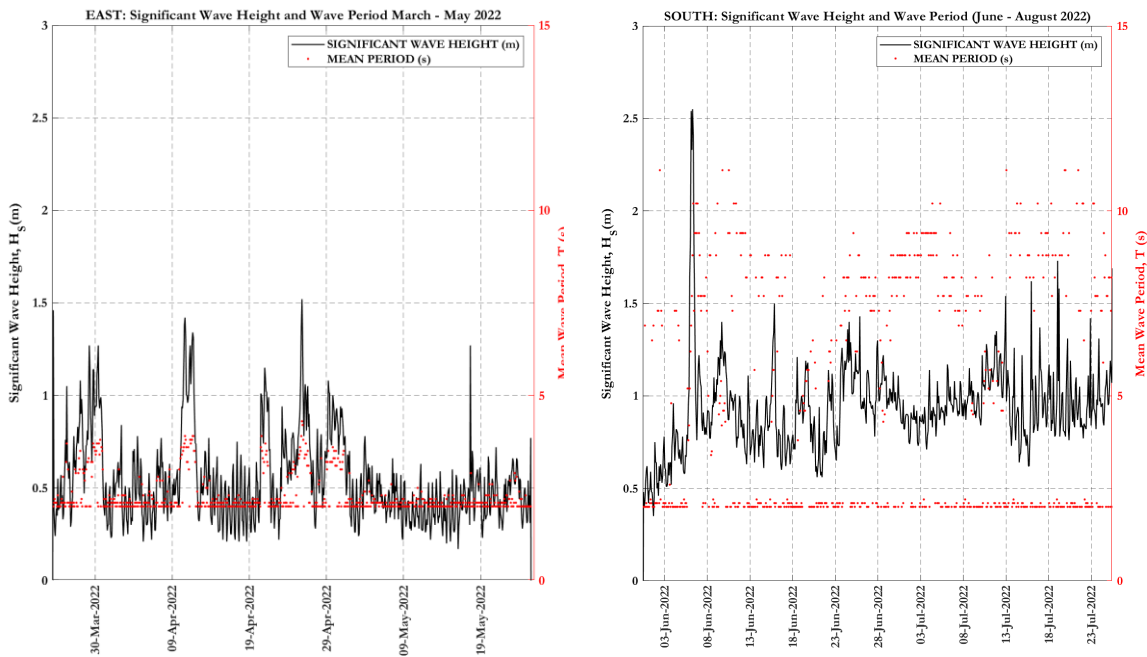


Figure 3.10 Wave heights and periods for East (left) and South (right) instruments

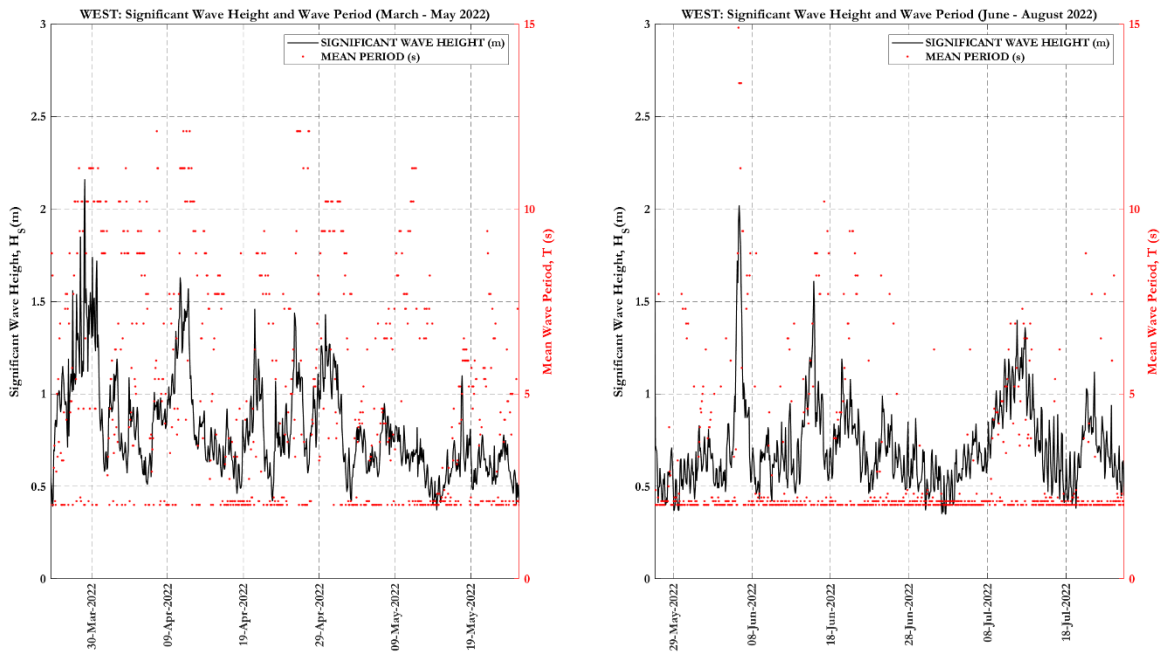


Figure 3.11 Wave heights and periods for West instrument – Deployment 1 and 2

3.3 Model Set-Up

Baseline coastal zone modeling is required to gain an understanding of the coastal processes acting along the Bermuda shoreline. Waves, currents and sediments all interact to affect shoreline morphology, manifested as erosion or accretion.

Coastal hazards include flooding from storm surge due to hurricanes, and shoreline erosion from daily and swell waves. To understand the daily wave climate and storm surge potential of the area, detailed numerical modeling was carried out.

3.3.1 Flexible Mesh Development

The model's fundamental starting point is the construction of a computational mesh from which spatial variances can be calculated at each simulation time step. MIKE 21 computes the waves and hydrodynamics using a flexible computational mesh. The flexible mesh is ideal for storm surge computations because it allows for the modeling of large complex areas that may require detailed resolutions of smaller features at the same time. The mesh, which is primarily governed by water depth, describes the spatial relationship between all the computation points. A detailed description of MIKE 21 is included as Appendix B.

Topography and Bathymetry

The 2019 LiDAR survey provided both bathymetric and topographic data for the model (Figure 3.12). Grid spacing was approximately 12m and the data therefore required several filtering routines to output useable information. The data used in the modeling had a grid spacing of about 3m. The LiDAR data covers from 77m inland down to -46m offshore. The offshore reef platforms are clearly defined and play an important role in dampening the waves.

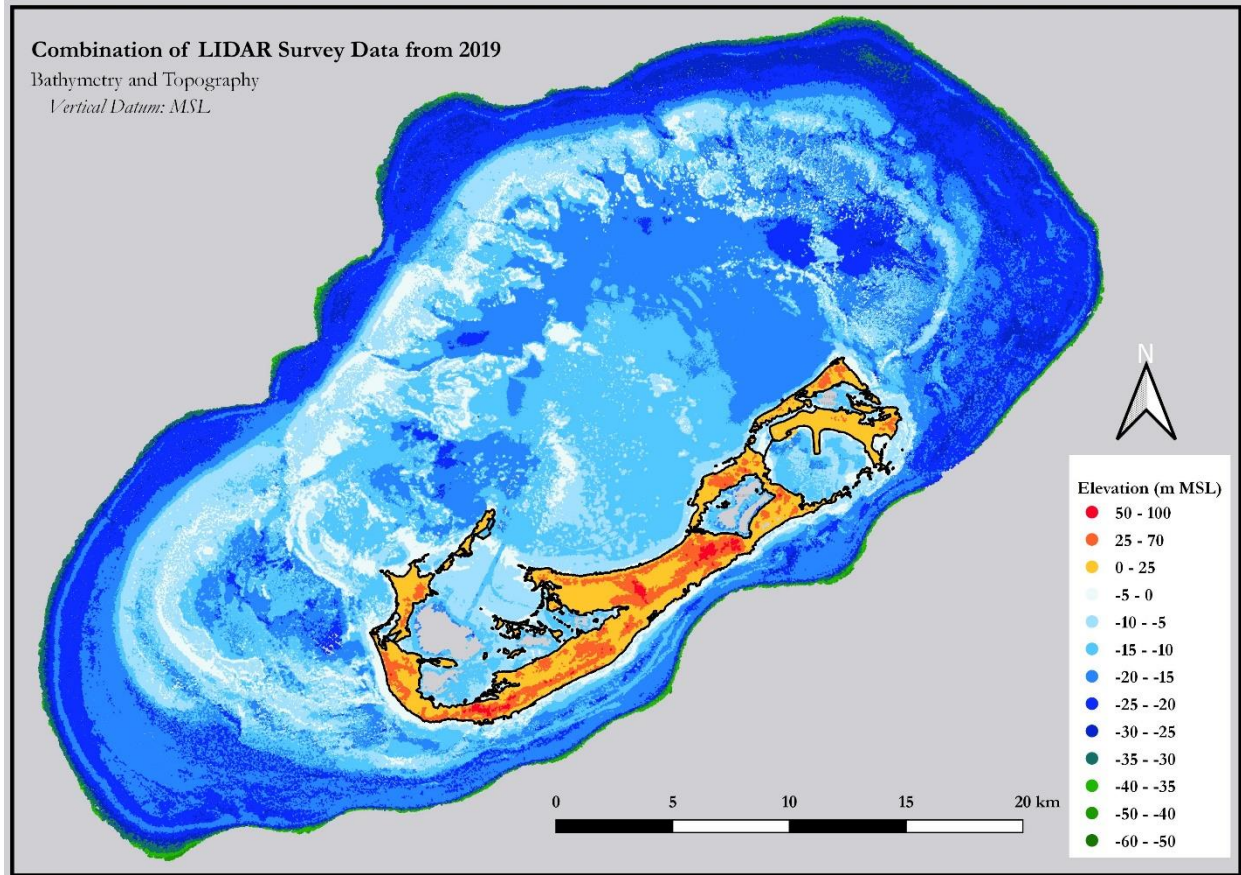


Figure 3.12 2019 LiDAR Data

Figure 3.13 shows the model mesh, with smaller mesh elements in the areas of greater concern – namely shorelines prone to either flooding or erosion. Additionally, smaller elements were used around the areas of significant contour change to adequately resolve wave movements and accurately represent the bathymetry with higher resolution in this area.

Calculations are made at each point in the mesh by solving various mathematical equations. Hydrodynamics are normally governed by two fundamental laws: Conservation of Mass and Conservation of Momentum. Wave effects are computed in a similar way using the Conservation of Wave Action. Wave action is equal to wave energy divided by its angular frequency. The main source of wave energy is from the wind, and wave energy sinks include dissipation through wave breaking, white-capping, and bottom friction. How the wave energy moves is highly dependent on the direction of travel and the water depth contours it encounters on its path to the shoreline or out of the model domain. These various fundamental laws of conservation (mass, momentum, and wave action) can be written as differential equations, which must then be solved using complex numerical methods over the entire computation mesh.

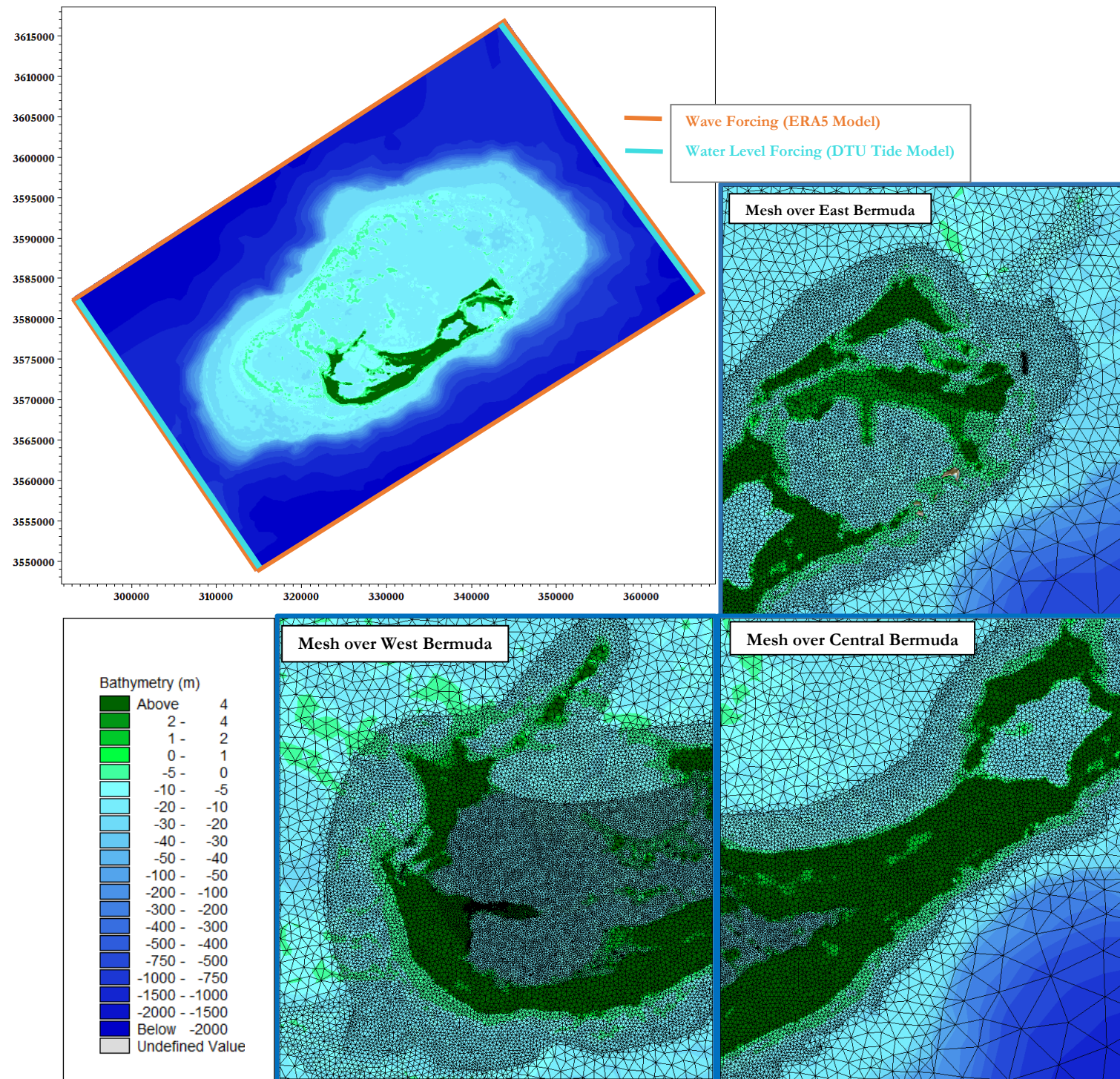


Figure 3.13 Flexible mesh for use in impact modeling

3.3.2 Boundary Conditions

The input boundary values were derived from long-term global or regional databases. Specifically, the offshore wave parameters were derived from the ER5 global wave model and the water level variations were derived from the Denmark Technical University (DTU) global tide model. MIKE 21 uses these input boundary values, which are valid for large areas, and determines the resulting conditions at a specific site.

3.4 Model Calibration

Numerical models were used to develop a working representation of the wave and current environment around Bermuda. An important step in establishing baseline conditions is to validate the numerical model such that the model results match the observed measurements. In general, this validation gives confidence to the comparative results that will subsequently be used to quantify the coastal process at any given location.

The MIKE suite of computer models, created by the Danish Hydraulic Institute (MIKE by DHI, 2016) was used for the analysis. MIKE 21 is a professional engineering software package for the simulation of flows, waves, sediments and ecology in rivers, lakes, estuaries, bays, coastal areas and seas. The spectral wave (SW) module computes the transformation of wind waves as they grow, propagate, and break in the nearshore zone. The hydrodynamic (HD) module computes the currents and water level patterns. Linked together (HD+SW) the modules can be used for storm surge calculations.

The main inputs to the model are:

- The computational grid, which is required to represent the nearshore features at the site under investigation, described above and
- The input boundary values derived from long-term global or regional databases as described above. MIKE 21 uses these input boundary values, which are valid for large areas, and determines the resulting conditions at the specific site.

For the model calibration, the wave and hydrodynamic model were forced with the time series of the ERA 5 deep water wave conditions (significant wave height, peak period, wave direction, wind speed, wind direction) coinciding with the time of instrument measurements (April to May 2022) as well as water level variations from the DTU tide model.

Table 3-2 Summary of instrument data available for calibration

Instrument Name	Location WGS84 UTM - 20N		Deployment Period	
	X	Y	Start Date	End Date
I1 ADCP West Bermuda	-64.988427	32.2895553	1-April-22	1-May-22
I2 ADCP East Bermuda	-64.711317	32.3726829	1-April-22	1-May-22

3.4.1 Model Parameters

The calibration consisted of adjusting various model parameters to minimize the error between the instrument-measured and the model-predicted values until they match with a sufficient degree of accuracy based on acceptable model performance guidelines. The comparison was done for the following parameters:

- Waves – significant wave height, peak wave period, wave direction;
- Currents – speeds, direction, U Velocities, V-Velocities; and
- Tides.

A series of model simulations was carried out to test different model parameters such as directionally decoupled and fully spectral formulation as well as wave dissipation parameters including wave breaking, bottom friction and white capping. The selected model parameters are summarized in Table 3-3 and Table 3-4.

Table 3-3 Spectral wave model parameters

Model Parameters	Selected Values
Wave Equations	Directionally decoupled, quasi-stationary
Spectral Discretization	36 sectors (10° discretization)
Wave Breaking	$\alpha = 1.0$, $\gamma_1 = 0.8$ (depth induced), $\gamma_2 = 1$ (steepness-induced)
Bottom friction	KN = 0.04m
Wind Wave Growth Equation	SPM84

Table 3-4 Hydrodynamic model parameters

Model Parameters	Selected Values
Hydrodynamic Equations	In stationary
Wave Radiation	From spectral wave model
Bed resistance	Varying for various seabed types
Water Level Variations	East and West boundaries varying in time and along line

3.4.2 Operational Wave Model Validation

The wave model validation has two purposes: (i) to assess the adequacy of the MIKE Spectral Wave model as a reliable tool to accurately compute the nearshore wave processes, and (ii) to evaluate the reliability of the long-term wave database, which in turn is used to validate the long-term hydrodynamics (wave-induced currents) at the coastline. The methods are described below.

The model was forced using the time series of ERA5 deep water wave conditions along the numerical model grid boundary. Of note, optimized calibration was achieved with a reduction of the ERA5 input by a factor of 0.6 and inclusion of offshore winds.

The validation methodology includes the following steps:

- (i) Extract the time series of the resulting significant wave heights, peak wave periods and mean wave directions at the physical location of each of the four instruments and coinciding with the same time period of the measurements.
- (ii) Compare the model results to the measured wave data.
- (iii) Calculate the error between the measured and modeling values.
- (iv) Calculate the various parameters listed below to assess whether the model falls within acceptable range of numerical model performance/ standards.
- (v) If not, develop a correlation factor between the model results and instrument measurements and apply where necessary to the long-term offshore wave climate.

The effectiveness of the model was assessed by computing statistical error parameters such as:

- Mean Error (ME) (Measure of general offset between measurements and simulations).
- Mean Absolute Error (MAE) (overall measure of comparison similar to RMSE but puts less emphasis on the largest errors as compared to RMSE where errors are squared).
- Root Mean Square Error (RMSE) (gives a relatively high weightage to large errors).
- Coefficient of Determination (R^2) (statistical measure of how close the data are to the fitted regression line).
- Coefficient of Efficiency (used to assess the predictive power of hydrological models).
- Index of Agreement (used to assess dispersion between model predictions and field recordings. Values closer to 1 indicate a stronger agreement between the two data sets).

The time series comparisons of significant wave heights for the West instrument are presented in Figure 3.14, which shows acceptable comparison between the model-predicted wave heights (red) and instrument-measured values (blue) at the West instrument location.

The statistics indicate that the average of the measured waves at Instrument West is 0.87m and the average modeling wave height is 0.75m, which is a difference of only 0.11m (Mean Error).

The Coefficient of Determination for the wave model is 0.79, which indicates that the model explains about 79% of all the variability of the response data around its mean.

The Index of Agreement is 0.88. Generally, values meaningfully larger than 0.5 are considered to represent good model performance (Willmott et al., 1985)

All indices used for the model validations are considered acceptable for model performance. This statistical method validated the model.

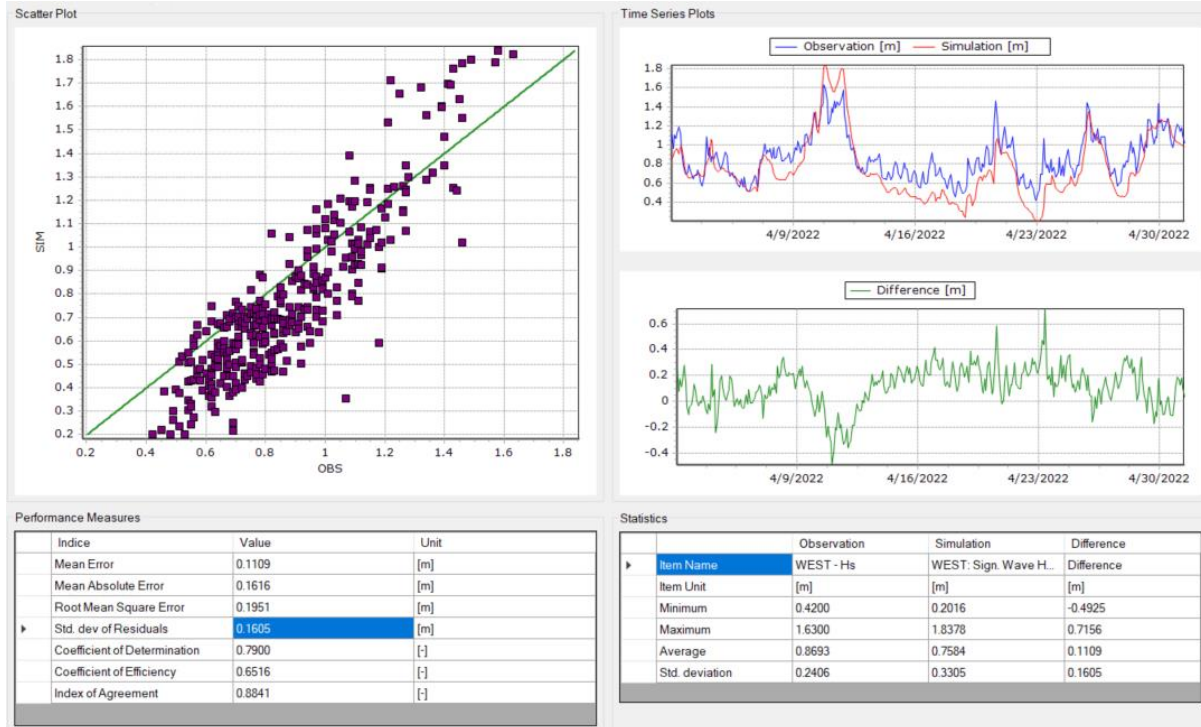


Figure 3.14 AWAC instrument measured wave heights vs modeling predicted wave heights comparison at Instrument West

Figure 3.15 presents a summary graphic of the calibration exercise.

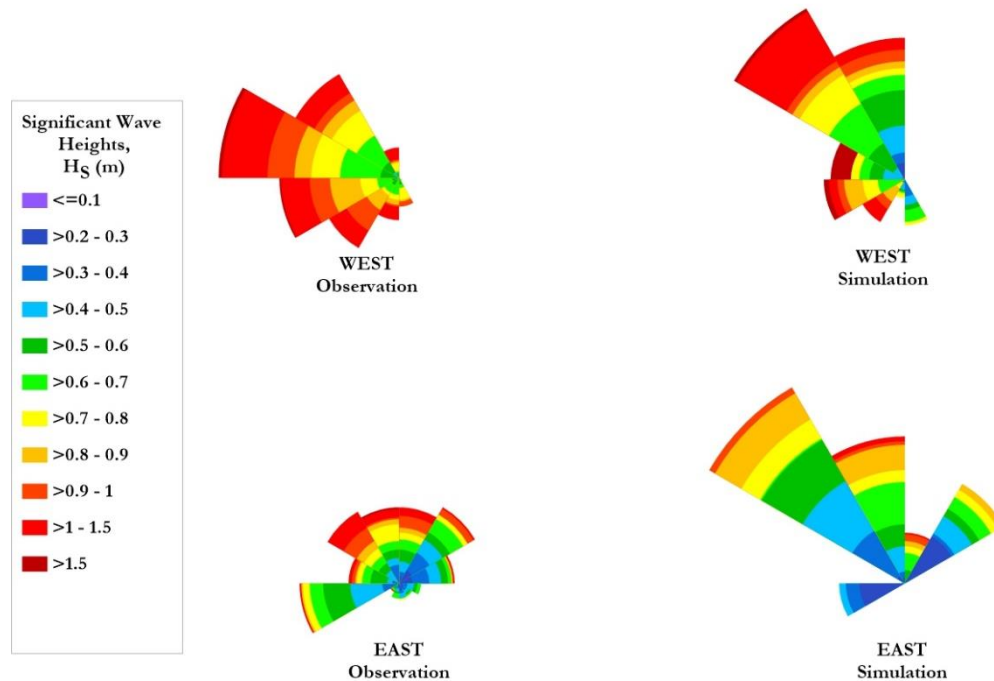


Figure 3.15 Summary of calibration

3.4.3 Operational Hydrodynamic Model Validation

Similar to the nearshore wave processes, it is vital that a detailed model of the operational hydrodynamic climate is established to understand how tidal or wave-induced currents will affect the coastal environment.

As described above, DTU global tide model was used as water level inputs to the model boundaries. The model has been validated at locations in the Caribbean and is generally accepted as sufficiently accurate for investigations of this scope. The validation method is described herein:

- The water level forcing from the DTU model results are extracted at the boundary locations of the hydrodynamic models. Other forcing to the model included wind and wave radiation stress from the ERA5 global wave model, seabed roughness and eddy viscosity.
- The hydrodynamic model computes nearshore currents forced by water level variations from the DTU model. The operational hydrodynamics are then developed and transformed to the nearshore using the hydrodynamic module to produce real-time hydrodynamic variances in current velocities, and surface elevation (HD) coinciding with the time of the measurement period.
- Waves and currents are determined at each simulation time step over the computational mesh.
- The validation compares the various measurements and model-predicted values.

- The error between instrument-measured and model-predicted are calculated and various model parameters are adjusted to minimize model versus measured errors according to the *Foundation of Water Research Guidelines* for assessing hydrodynamic model performance.

The Foundation for Water Research published *A Framework for Marine and Estuarine Model Specifications in the UK* in 1993, which is one of the only documents providing standards for assessing hydrodynamic model performance. These guidelines suggest accuracy levels as follows:

- Water levels to within $\pm 15\%$ during spring tidal ranges and $\pm 20\%$ during neap tidal ranges;
- Current speeds to within $\pm 200\text{mm/s}$ or $\pm 10\text{-}20\%$ of the observed speed; and
- Current directions to within ± 20 degrees.

To quantify the capabilities of the numerical model, the modeling water levels and u and v velocities were compared to the measured water levels and measured u and v velocities. The comparison was evaluated using the root mean square error (RMSE) and the normalized root mean squared error (NRMSE) for the water level.

Table 3-5 indicates the RMSE and NRMSE computed between model-predicted and instrument-measured at the two instrument locations. Overall results indicate that the predicted tides match the measured levels relatively well in terms of both height and phase, with the calculated error levels well within $\pm 20\%$ range indicated in the *Guidelines from the Foundation for Water Research*.

Table 3-5 Calculated errors between model predicted and instrument measured tide heights

Location	Tide Height Comparison					
	RMSE (mm)	Guidelines	Score	NRMSE (%)	Guidelines	Score
I1 West	54.1		Pass	4.67%		Pass
I2 East	67.8	$\pm 150\text{-}200\text{mm}$	Pass	5.62%	$\pm 15\text{-}20\%$	Pass

The results of the RMSE and the NRMSE computed between model predicted (depth averaged) and instrument-measured easting and northing velocities are listed in Table 3-6. Results indicate that the calculated errors are within range of model calibration guidance (within $\pm 0.2\text{m/s}$ or $\pm 10\text{-}20\%$). A typical scatter and progressive vector plot of the measured versus modeling is presented in Figure 3.16 for instrument West and indicates the model reproduces the recorded data in both intensity and direction.



Figure 3.16 ADCP West D1 measured scatter vs modeling scatter u (east-west) and v (north-south) components of the velocities and corresponding progressive vector plot

Table 3-6 Calculated errors from northing and easting velocities between model-predicted and instrument measured at the four locations

I1 (West) AWAC	<i>Easting and Northing Comparison (AWAC West)</i>					
	RMSE (m/s)	Guidelines	Score	NRMSE (%)	Guidelines	Score
Easting (U Vel)	0.07	±0.2 m/s	Pass	38	±10-20%	Fail
Northing (V Vel)	0.12		Pass	36		Fail
I2 (East) AWAC	<i>Easting and Northing Comparison (AWAC East)</i>					
	RMSE (m/s)	Guidelines	Score	NRMSE (%)	Guidelines	Score
Easting (U Vel)	0.08	±0.2 m/s	Pass	41	±10-20%	Fail
Northing (V Vel)	0.04		Pass	24		Pass

Based on the guidelines presented above, the hydrodynamic model was found to meet the minimum standards for model performance. Overall, the validation results were considered satisfactory, and the model considered capable of calculating hydrodynamic parameters with an acceptable level of accuracy.

A detailed description of the model set-up and calibration process is attached as Appendix C and all of the measured data is presented in Appendix D.

3.4.4 Wind Model for Extreme Wave Calculation

Calibration of models for extreme waves, especially those occurring during hurricanes, poses a significant challenge due to the rarity and intensity of such events. The intricate interactions among wind, waves, and coastal structures further complicate the task. Traditional methods rely on historical data, which may not fully capture the spectrum of extreme events because of their infrequency. Moreover, the dynamic nature of hurricanes introduces complexities like rapidly changing wind speeds and directions, storm surges, and wave-breaking patterns. Achieving accurate calibration necessitates sophisticated numerical simulations and high-resolution data assimilation techniques, while inherent uncertainties in predicting extreme events call for a cautious approach emphasizing robustness and resilience in coastal infrastructure design and planning.

Regarding wind models, the SPH73 and SPH84 models are numerical tools commonly used for simulating wind fields, particularly in tropical cyclone contexts. While they share similarities, they have distinct differences in their underlying assumptions. The SPH73 model is based on the Rankine vortex theory, assuming a symmetric wind field, whereas the SPH84 model incorporates additional physics to account for the asymmetric nature of tropical cyclones and environmental factors like ocean surface temperature and terrain. Consequently, SPH84 is preferred for more detailed and accurate simulations, especially in research and engineering applications.

In Bermuda, where the wave models are coupled with wind speeds, careful consideration is given to modeling conditions accurately. Despite SPH84's additional physics, SPH73 has shown to be more effective in certain sound areas within Bermuda, particularly Harrington Sound and Castle Harbour, which are fetch-limited. The figures below illustrate that wave heights in these sounds can increase by

up to 100-150% over SPH84, with Harrington Sound experiencing wave heights 200% higher under SPH73. These findings indicate stronger wave conditions than those predicted by the SPH84 model.

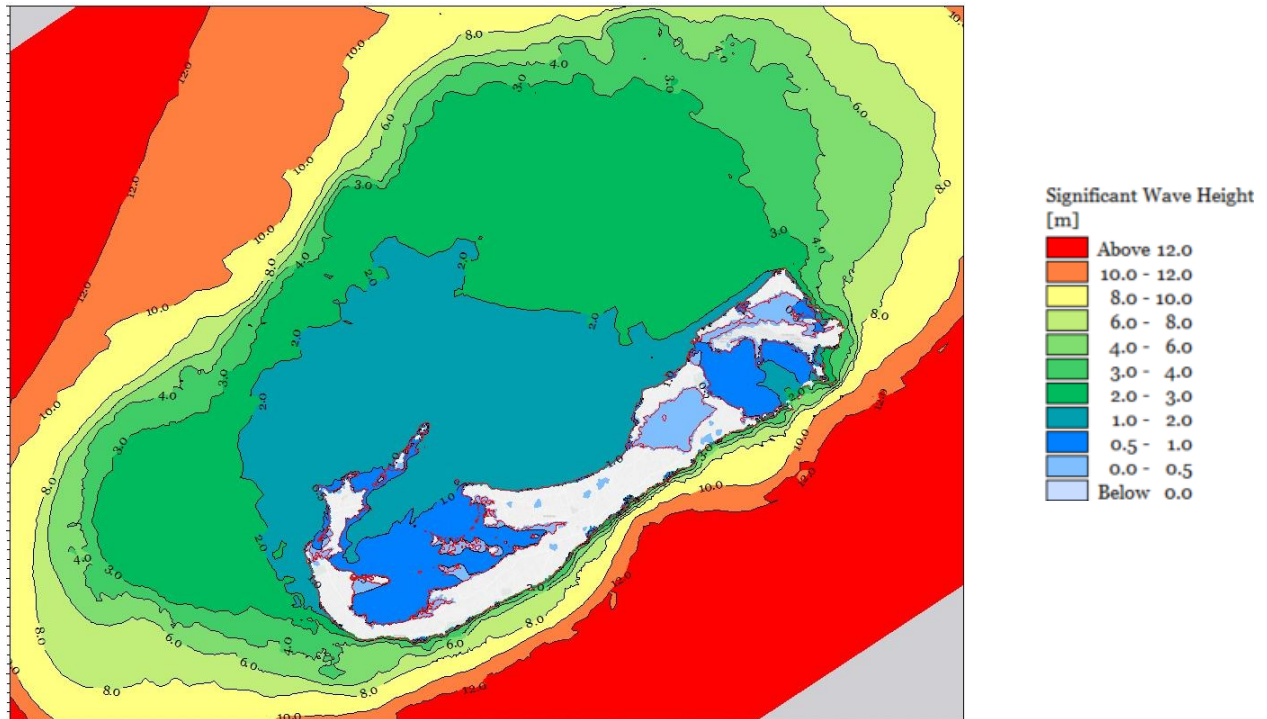


Figure 3.17 Significant Wave Heights in RCP 4.5 20yr Horizon 1 in 150yr Event – SPH84 Wind Model

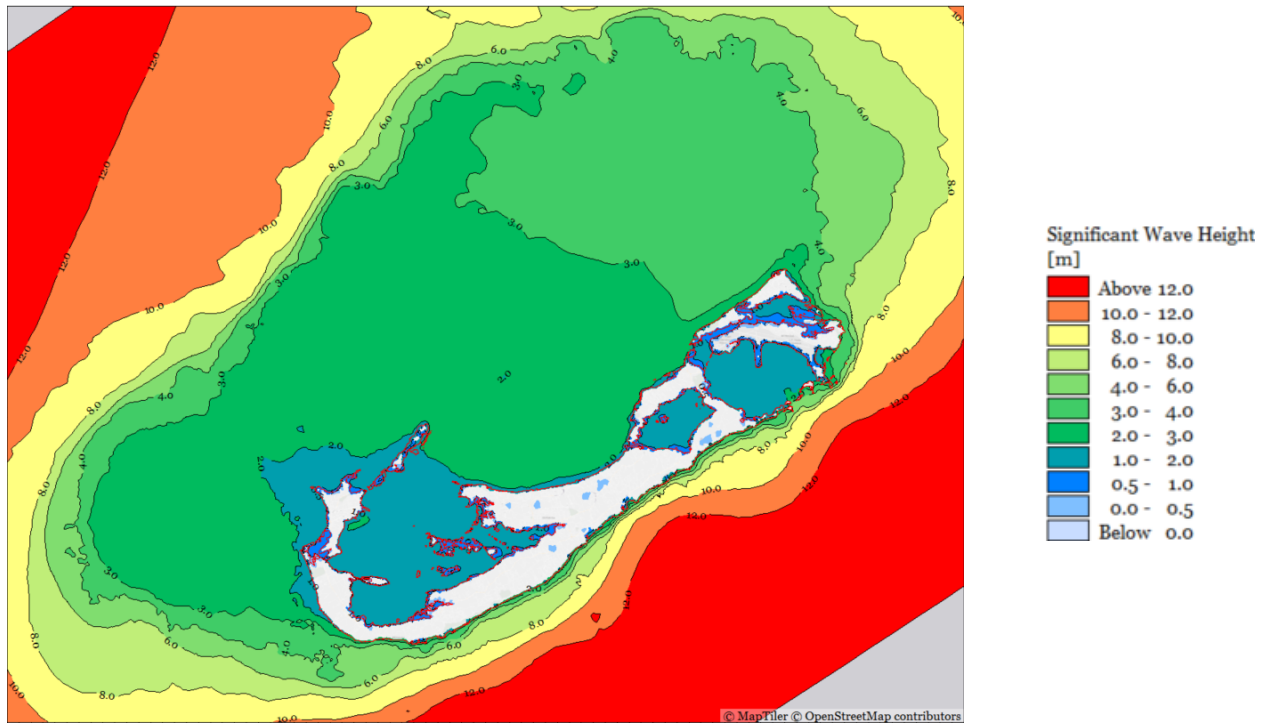


Figure 3.18 Significant Wave Heights in RCP 4.5 20yr Horizon1 in 150yr Event – SPH73 Wind Model

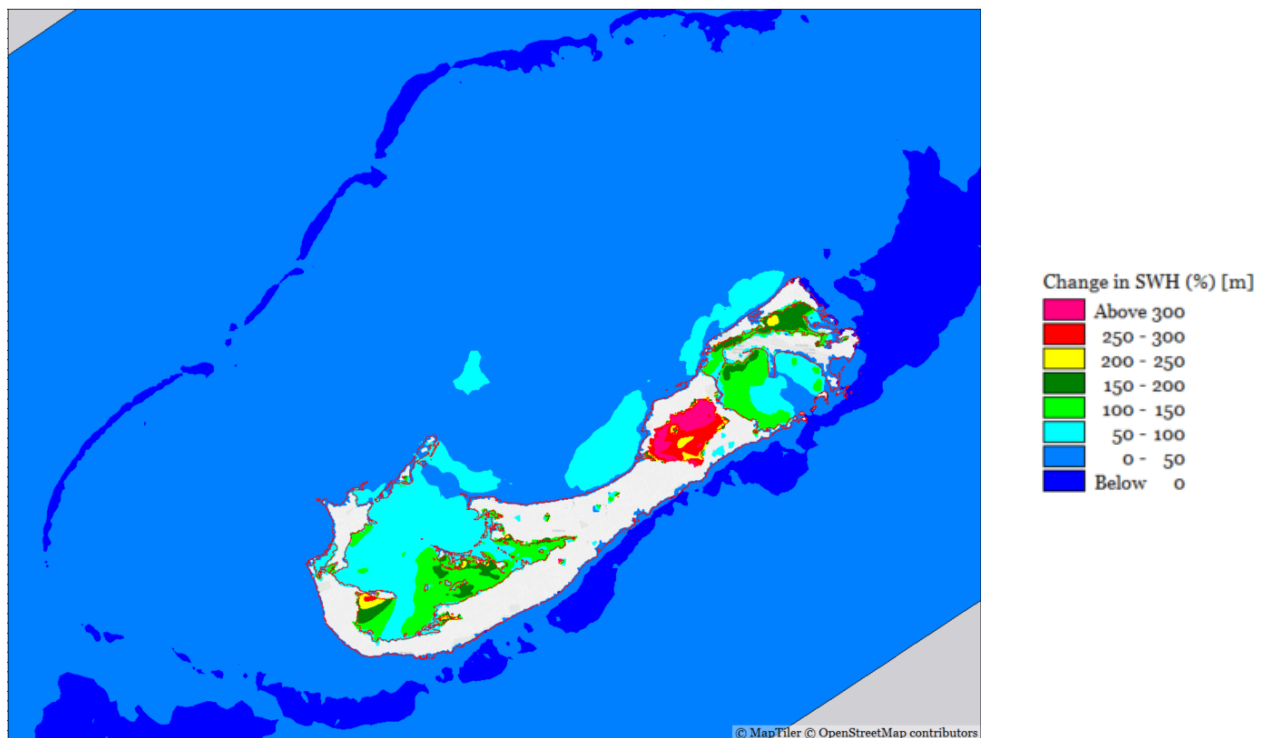


Figure 3.19 Percent Change in Significant Wave Heights for RCP 4.5 20yr Horizon 1 in 150yr Event – $[(SPH73 - SPH84) * 100 / SPH84]$

While no measurements exist for the wave conditions in these Sounds, anecdotal advice and video recording show substantial wave conditions during Hurricane Flora's passing in Harrington Sound, which is more in line with the SPH73 model results. As such the SPH73 model is adopted for hurricane wave model predictions.



Figure 3.20 Wave conditions in Harrington Sound during Hurricane Flora when it was approximately 100 nm NW of Bermuda on September 23, 2022. Waves are seen to overtop the concrete dock, with wave height estimates of approximately 0.6m (2 ft). Image credit: Nick Strong/Mandy Shailer.

3.5 Day-to-Day Conditions

From an examination of the offshore wave database a seasonal variation in the wave conditions was found. It is clear that in general, there is relative calm during the summer months when wave heights in deep water are typically less than 2.0m. By contrast, during the remainder of the year, and particularly in the winter months, wave heights offshore are between 6-8m.

Based on this information, two seasons were derived that appear to characterize the seasonality in wave conditions. The period May-September appears to be dominated by smaller waves from the east-southeast, whereas larger waves from the north-west are more predominant during the winter months (October to April).

3.5.1 Mean Conditions and Statistically Significant Events

The operational wave climate at the project site was assessed using the 43 years of data as described previously. To describe the operational wave climate, two conditions are considered:

1. *Mean Significant Wave Height Condition:* The mean wave condition is the weighted average of the 700+ conditions based on the percentage of time they occur in the record. This condition is an indication of the mean annual wave climate and gives a good estimate of the day-to-day wave conditions that affect the shoreline.
2. *99th Percentile Significant Wave Height Condition:* The 99th percentile wave condition represents the wave condition exceeded only 1% (approximately 4 days per year) of the time within the wave records. This condition is typical for winter storms that affect the north Atlantic Ocean.

The results (Figure 3.21) show that, on average, the mean significant wave heights along the south shore are 0.5-0.75m, and the north shore are 0.3-0.5m. The southern shoreline is more exposed due to limited protection from reef formations. The north shore sees more protection from the rim reef and other reef formations. On average, a mean wave height of 1.25m impacts Bermuda's northern inner reef. As the rim reef and the lagoonal reef structures reduce the wave conditions, waves reaching the shoreline average 0.5m. Within Harrison Sound, the wave conditions are further reduced due to the sheltering provided by the island itself, such that wave heights do not exceed 0.3m on average.

The 99th percentile conditions show wave heights greater than 1.5m along the length of the south shore. On the north shore, the waves are reduced to a similar height as under the mean conditions. Along the north shore outside of the Sound, wave heights under the 99th percentile conditions are less than 0.5m. **The remarkable reduction in wave heights is an indication of the importance of the reef structure offshore.**

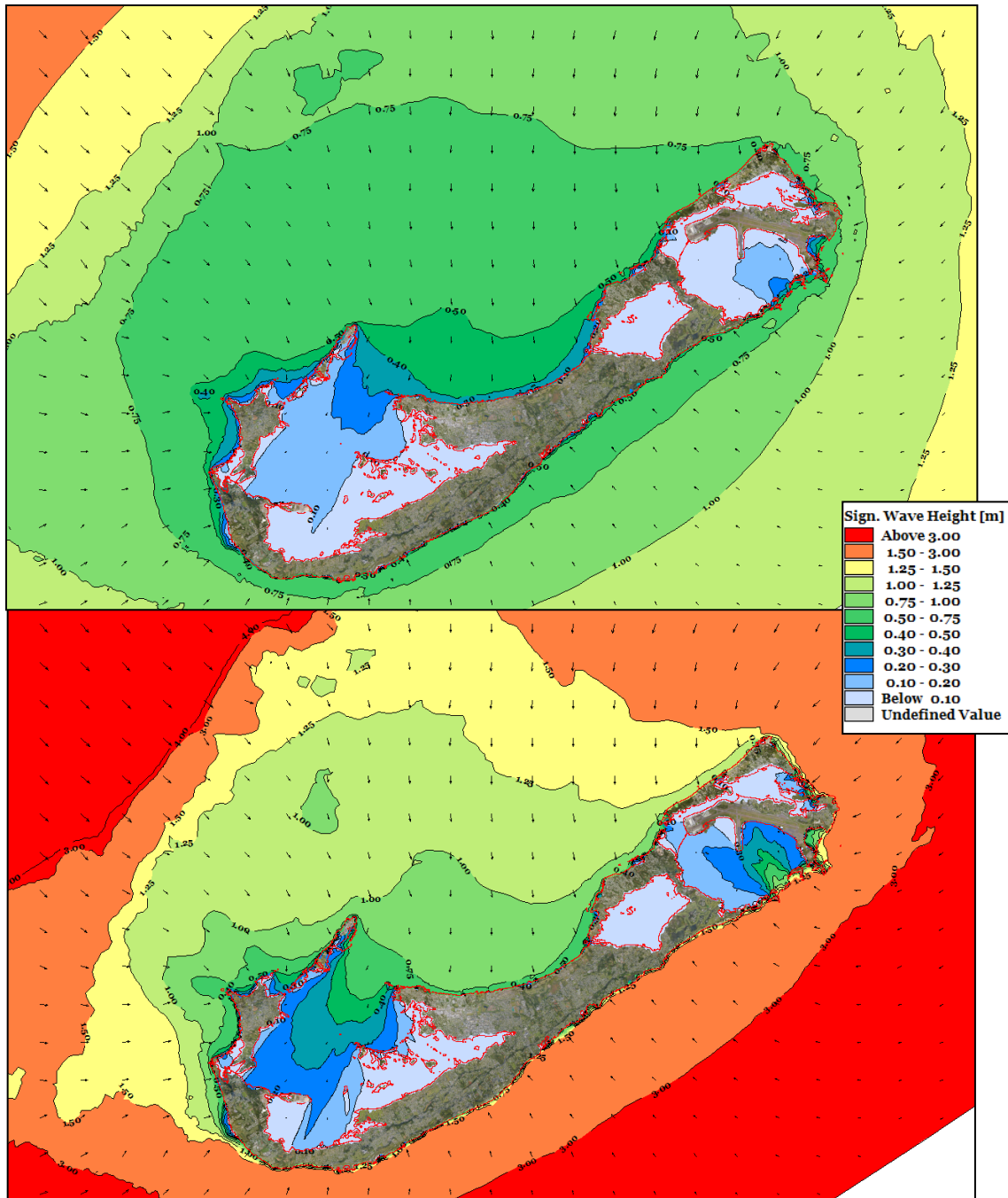


Figure 3.21 (a) Mean and (b) 99th percentile significant wave heights (present day conditions)

Wave roses extracted from the modeling results along the shoreline confirm the gage data, with two distinct seasonal wave climates: (i) relative calm during the summer months when wave heights in deep water are typically less than 2.0m and (ii) during the remainder of the year and particularly in the winter months, wave heights offshore are 6-8m.

Wave conditions in May-September are typically smaller from an east-south-east direction, whereas larger waves from the north-west appear to dominate during the remaining time (October to April).

Figure 3.22 shows wave roses along Bermuda’s shoreline for mean annual wave conditions. The south shore (P3-5) shows two dominant wave directions, namely from the south-east and south-west. The easternmost and westernmost nodes (P6 and P2) at the ends of the island show a wider spectrum of wave directions. The northern points (P1, P7-P9) which are more protected by the reefs, show a more unidirectional wave climate and lower wave energy.

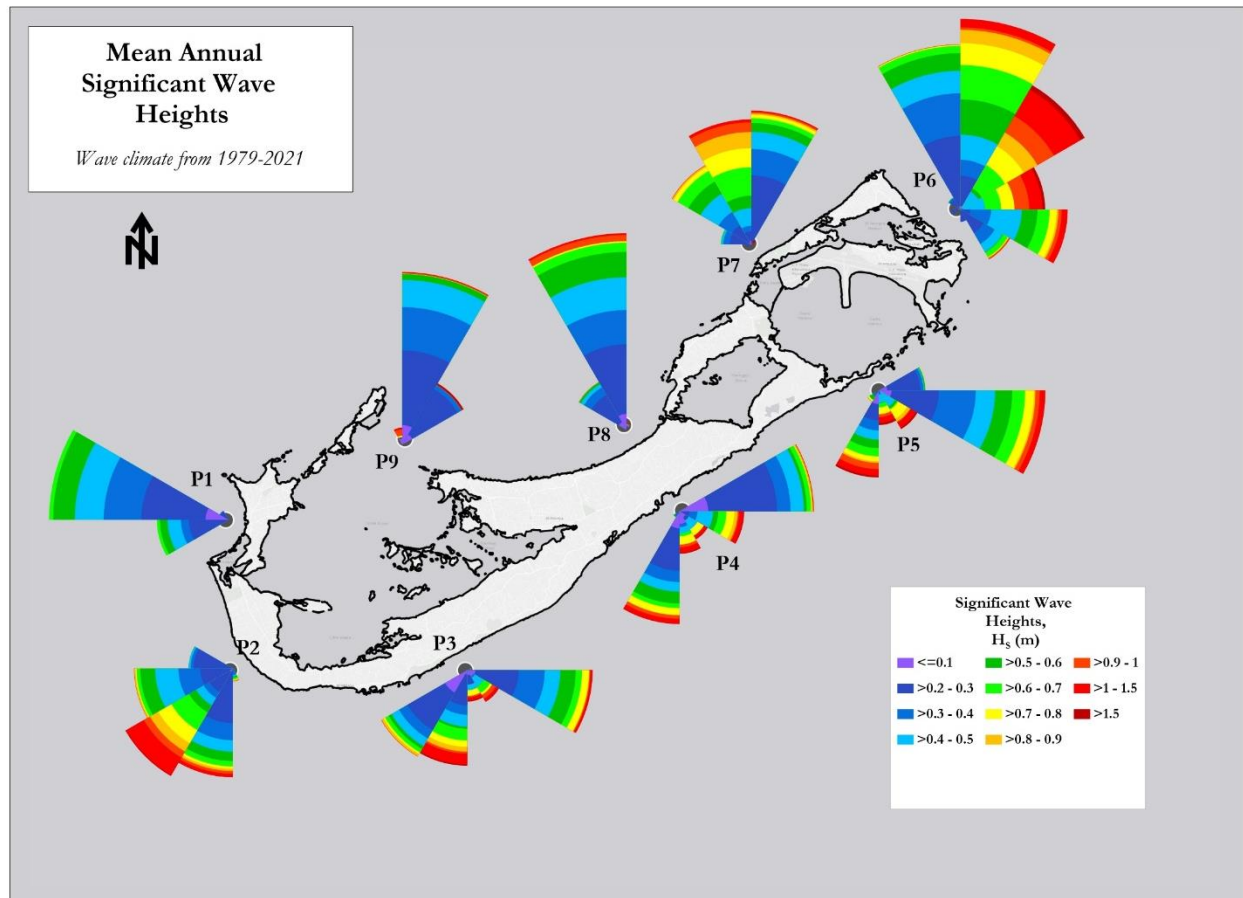


Figure 3.22 Wave roses

Northeast Bermuda

The LF Wade International Airport, the solar farm, and St George’s are located in the northeast part of the island. The modeling of mean wave conditions (Figure 3.23) shows wave heights along this shoreline to the north and south are both between 0.5 and 0.75m. A distinct difference in wave heights is shown for the 99th percentile wave conditions, where the south side of the island is more vulnerable to high-energy waves. The wave energy is seen to propagate through gaps between the smaller islands, causing some disturbance within Castle Harbour.

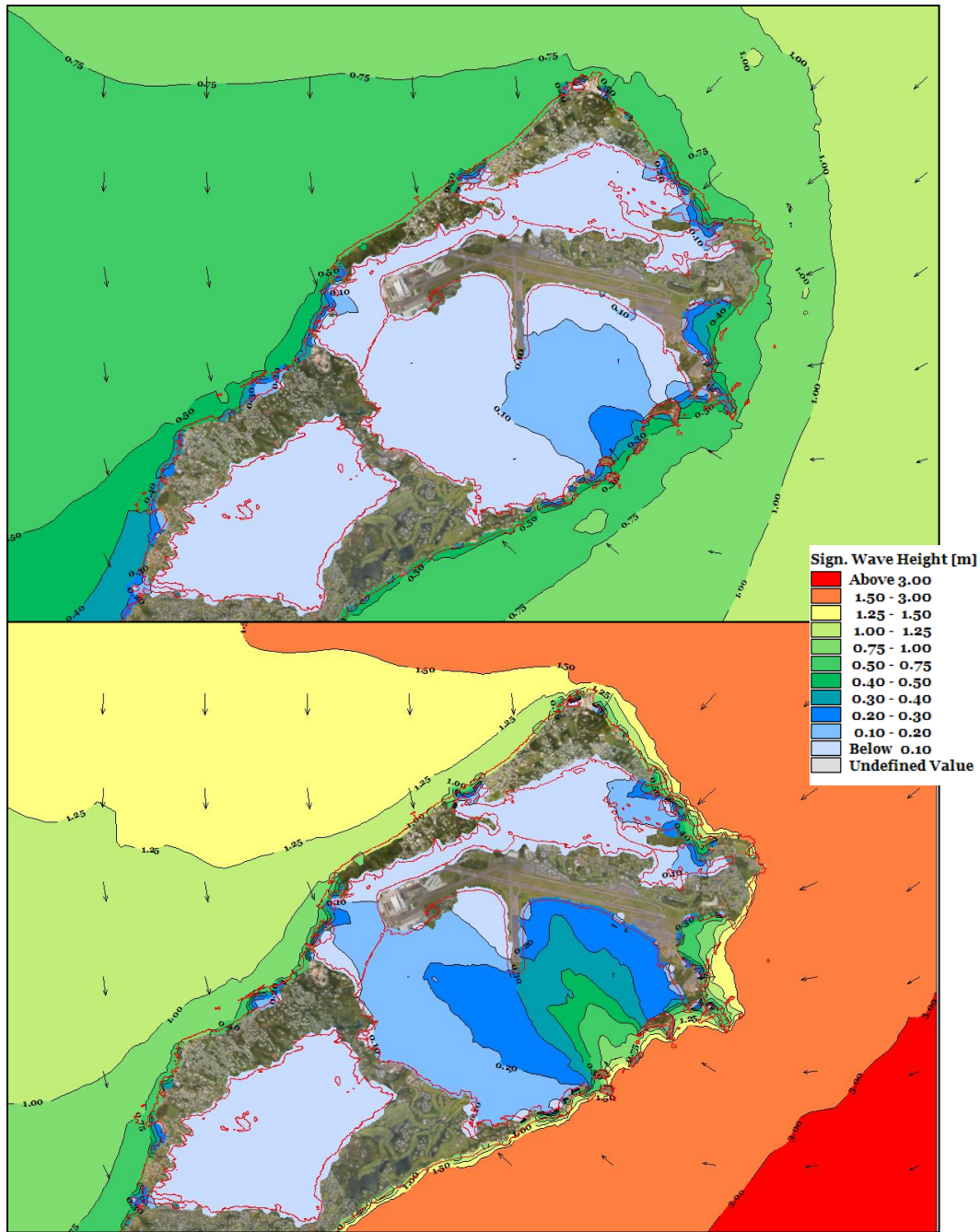


Figure 3.23 North-eastern Bermuda - Mean (top) and 99th percentile (bottom) significant wave heights

Central Bermuda

Within the central part of Bermuda, wave heights are less than 0.4m in exposed locations to the north, and further reduced on entry into Great Sound. The average wave height within the Great Sound is only 0.3m, which makes this waterbody great for marine craft docking. Even in the most extreme conditions, the eastern side of Great Sound experiences little increase in wave energy. Waves from the northeast occasionally affect the western areas of Little Sound. Wave heights can be more than 0.4m under these conditions (Figure 3.24).

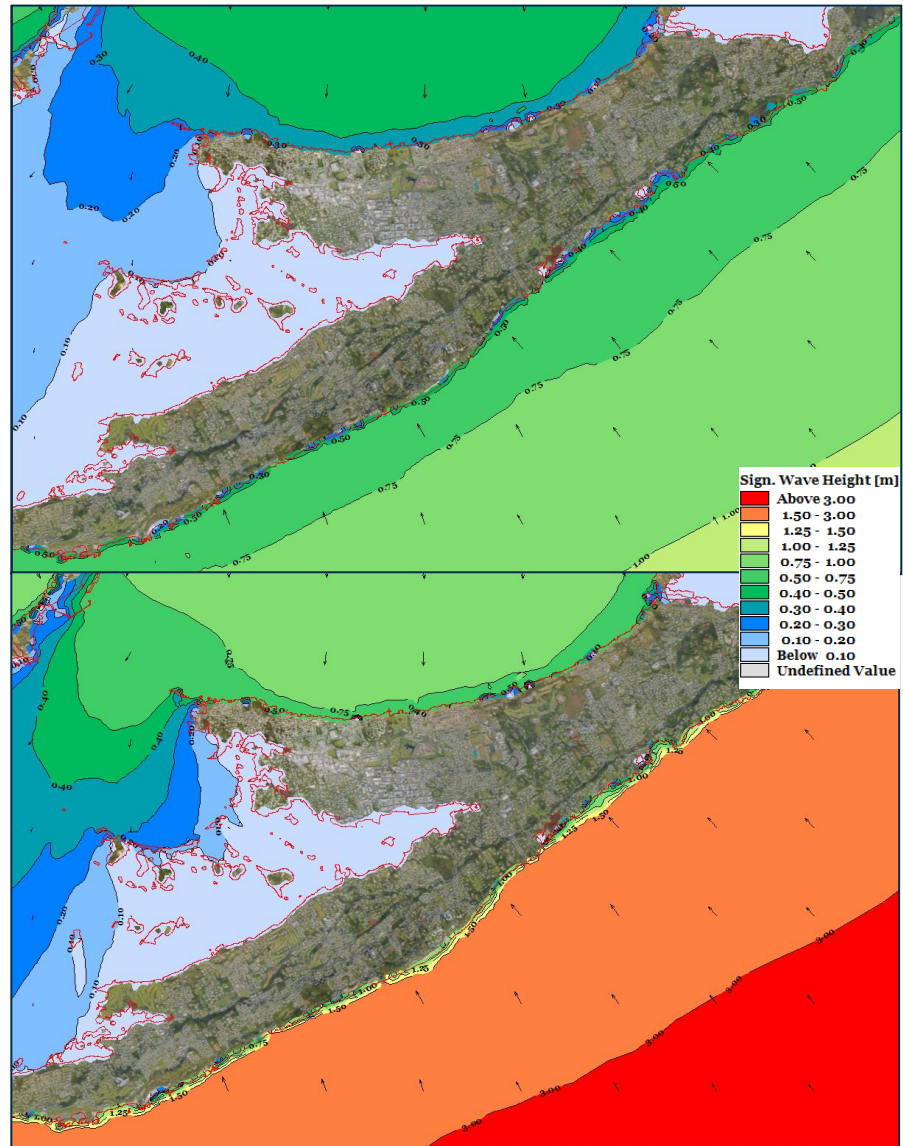


Figure 3.24 Central Bermuda – (a) Mean and (b) 99th percentile significant wave heights

Southwestern Bermuda

The southwest part of Bermuda is characterized by various sandy beaches fronting residential homes. The notable marine infrastructure is located within the Dockyards. The average wave height is less than 0.3m, but wave heights sometimes surpass 0.4m in exposed areas (Figure 3.25). More robust wave conditions and rising sea levels may contribute to higher wave energy within Great Sound in the future.

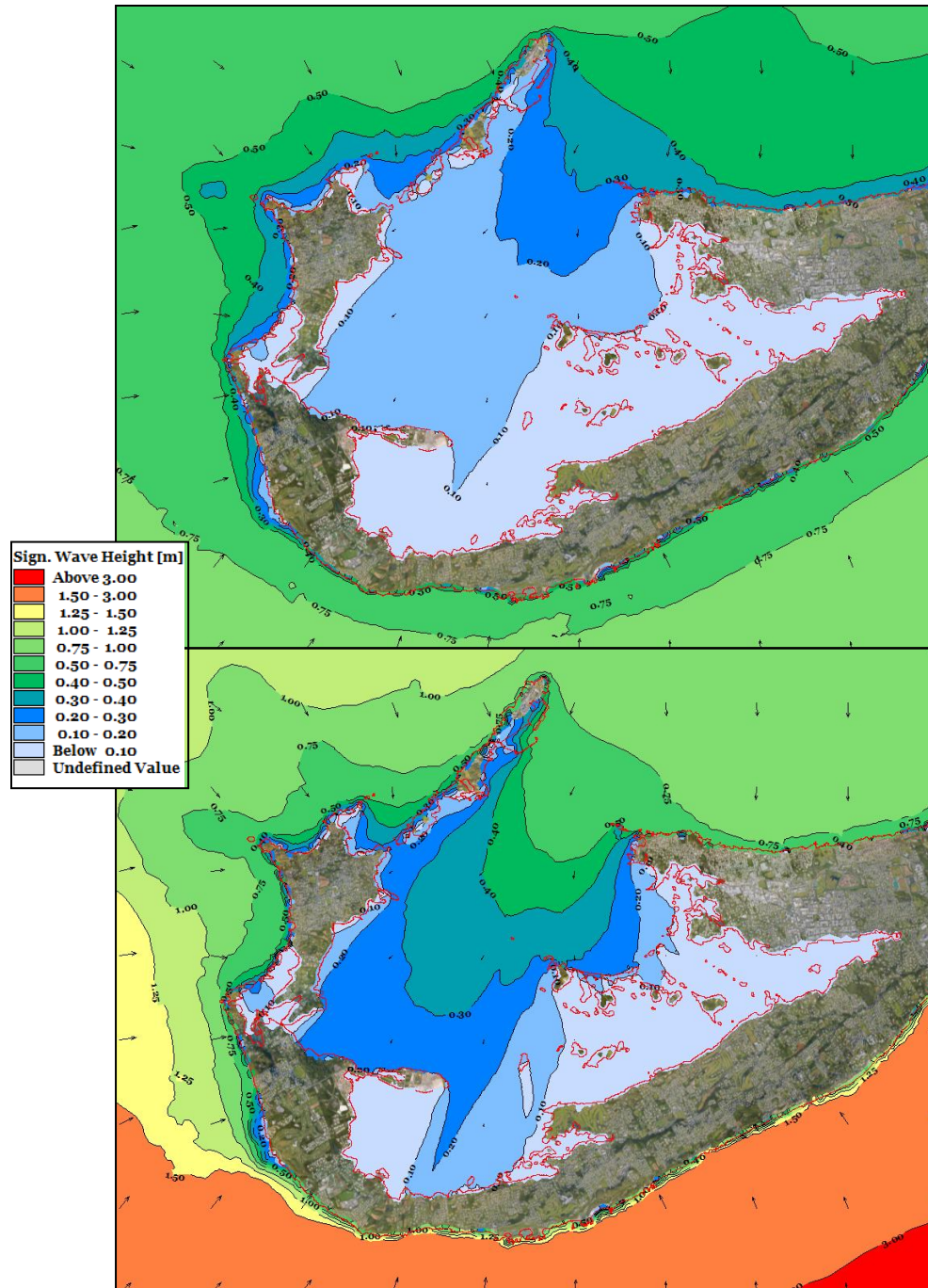


Figure 3.25 Southwestern Bermuda– (a) Mean and (b) 99th percentile significant wave heights

3.5.2 Trends in Significant Wave Heights

Historical Trends in Wave Heights and Storminess

To assess the historical effects of climate change on waves impacting the site, SWI considered the wave heights and periods over the long term ERA5 model records from 1979 to 2021. In general, several research have pointed to an increase in global wave heights due to climate change. From this assessment, the rate of the change of yearly mean, minimum and maximum wave conditions were calculated by linear regression over time. The 43 years of data from the long-term wave reanalysis at four points offshore Bermuda shows decreasing mean wave heights between 1977 and 2021 (Figure 3.26). Lemos et al., 2021 confirms this reduction in wave heights in the North Atlantic Ocean. In fact, the paper presents that historically, the wave heights in the North Atlantic Ocean have declined by between 3-11%, which is likely due a corresponding decrease in wind speeds. This dip in wave activity could now be a function of the North Atlantic Oscillation, discussed below.

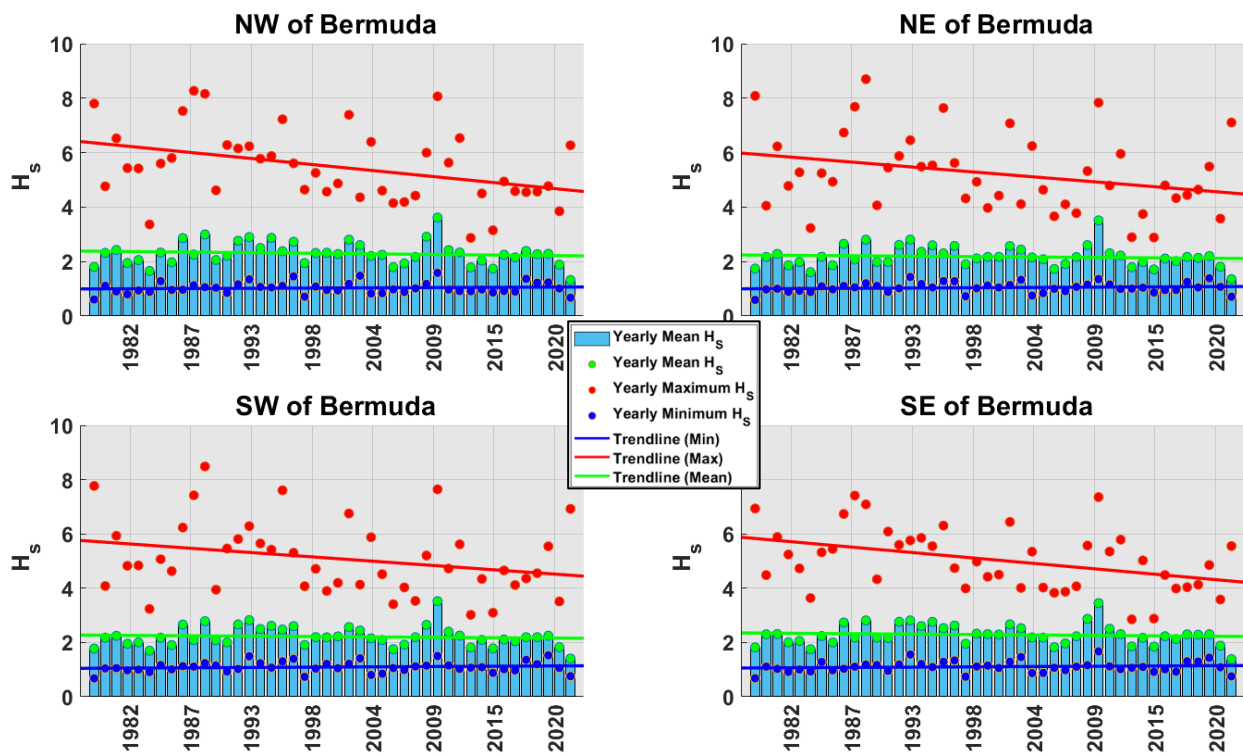


Figure 3.26 Time series showing the change in wave heights offshore Bermuda at four points

The subsequent analysis of historical data aimed to assess changes in storminess over time. Storminess, within this analysis, refers to periods characterized by elevated wave activity, specifically when wave heights surpass the average significant wave heights by a significant margin, typically exceeding two standard deviations. These prolonged periods of intense wave activity are identified through an assessment of wave data, focusing on instances where wave heights remain elevated for durations exceeding six hours. This definition facilitates the identification and analysis of intense wave events, offering insights into the variability and trends in storm events over time.

Upon extraction and analysis of ERA5 data, a declining trendline was observed, accompanied by an oscillating pattern in wave heights recurring approximately every five years. Notably, the results highlighted two years of heightened wave energy (1980/1981 and 2010), during which 8 – 11% of the year exhibited stormy conditions (Figure 3.27). However, in terms of assessing trends, no clear pattern emerged from the data. Overall, this assessment suggests a decrease in storminess over time. In further exploration of any potential oscillation trend, a LOESS² fit was produced for a 5-year moving average, which did not reveal notable periodicity comparable to the North Atlantic oscillation discussed below.

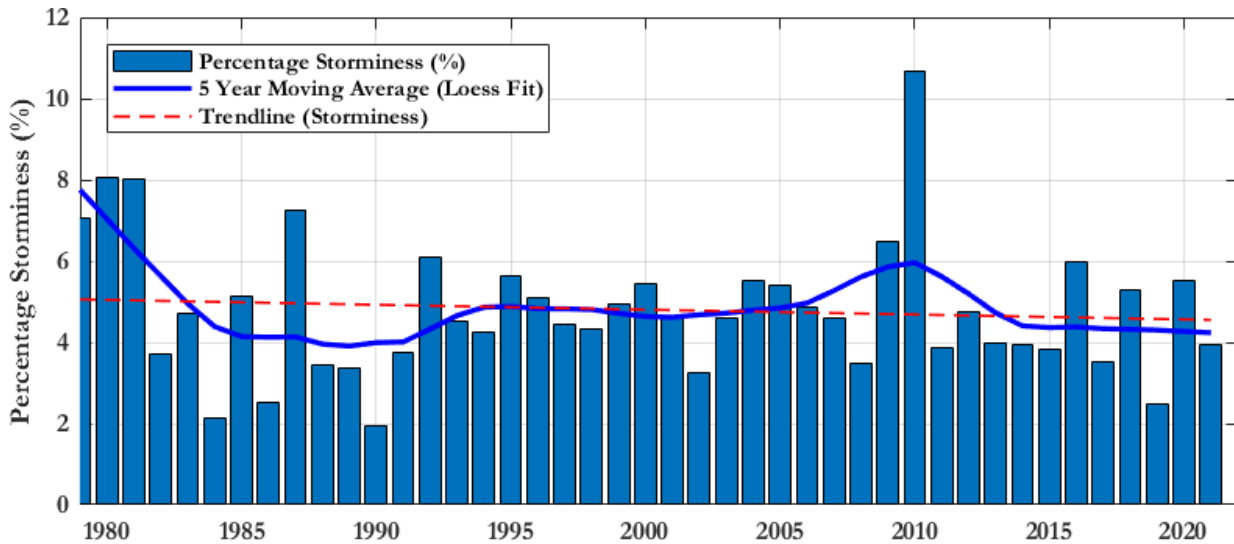


Figure 3.27 Percentage of "Storminess" between 1979 and 2021 based on the extracted ERA5 wave heights

Multi-year and decadal trends in Wave Energy Regional Weather Phenomenon

North Atlantic Oscillation (NAO)

The North Atlantic Oscillation (NAO) is a weather phenomenon over the North Atlantic Ocean with fluctuations in the difference of atmospheric pressure at sea level (SLP) between the Icelandic Low and the Azores High. Through fluctuations in the strength of these adjacent High- and Low-pressure systems, it controls the strength and direction of westerly winds and location of storm tracks across the North Atlantic (Hurrell, 2003).

A 60-year hindcast analysis of the influence of decadal climate variability on long-term trends of North Atlantic wave power (PW), spanning the period 1948–2008, showed PW variations over much of the eastern North Atlantic are strongly influenced by the fluctuating North Atlantic Oscillation (NAO) atmospheric circulation pattern, consistent with previous studies of significant wave height (Bromirski & Cayan, 2015). Increases in wave intensity in the northeast Atlantic were found when both NAO (and an associated Atlantic Oscillation (AO)) were positive. Averaged over the North Atlantic (north of 158N), mean winter wave power, compared with mean pre-1975 levels, increased by about 15% during the NAO positive phase from about 1985–1995, with peak winter wave levels about 30%

² Locally estimated scatterplot smoothing

greater. A positive NAO index also affects sea level rise as regional reduction in atmospheric pressure results in a sea level rise contribution due to the 'inverse barometer effect'.

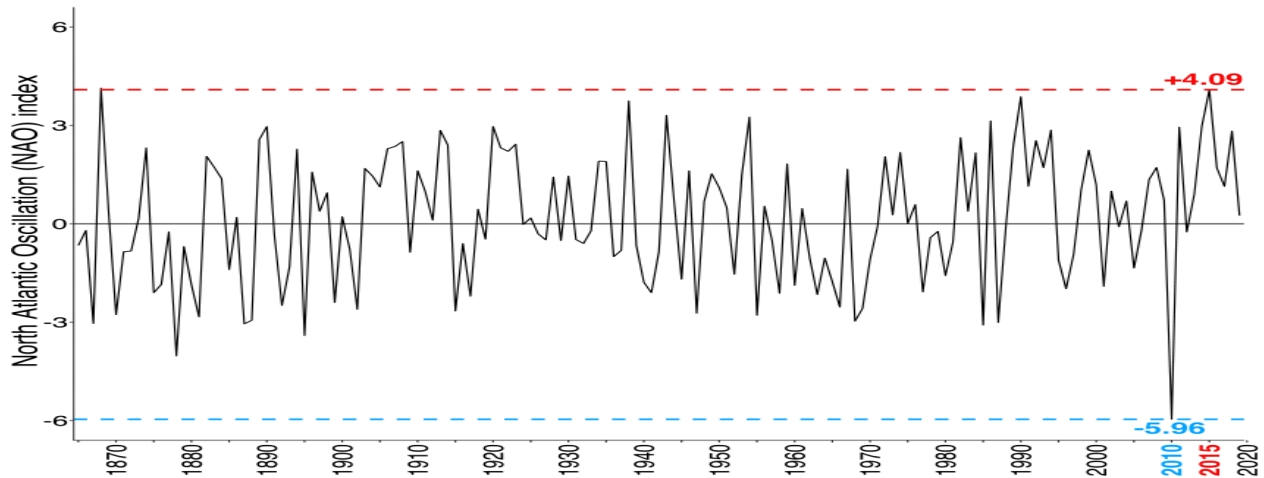


Figure 3.28 Historical annual North Atlantic Oscillation (NAO) index displayed from 1865 to 2020 as computed by Hurrell et al. (2003) and presented in Pereira et al (2020); highlighted is the most negative (2010 in blue) and most positive (2015 in red) phases of NAO index reported in recent decades.

Atlantic Multidecadal Oscillation (AMO)

The Atlantic Multidecadal Oscillation (AMO) also occurs (and affects) North Atlantic waters. The AMO alternates between phases of warm and cool ocean waters in the northern Atlantic, with positive phases having warmer than average sea surface temperatures in the North Atlantic.

AMO has a periodicity of approximately 40-60 years; there are 20-30 years in between an “elevated” and a “depressed” AMO, with the last positive AMO phase commencing around 2000.

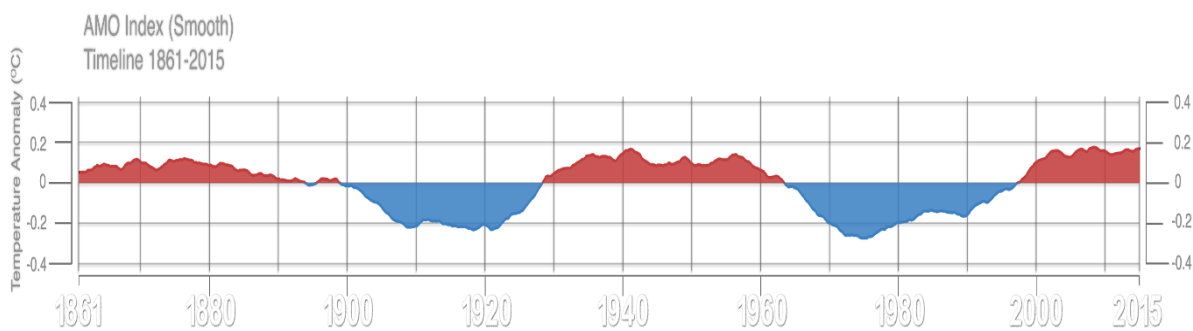


Figure 3.29 Atlantic Multidecadal Oscillation Index 1861-2015 (SVS, 2021)

The AMO appears to affect tropical storm events. Although the limited length of the Atlantic sea surface temperature record prevents scientists from making more definitive statements about the precise nature of the Atlantic Multidecadal Oscillation (AMO), the visual comparison shows a correlation between the various phases of the AMO and average number of tropical storm events, in that the positive phase produces more tropical storms than the negative phase.

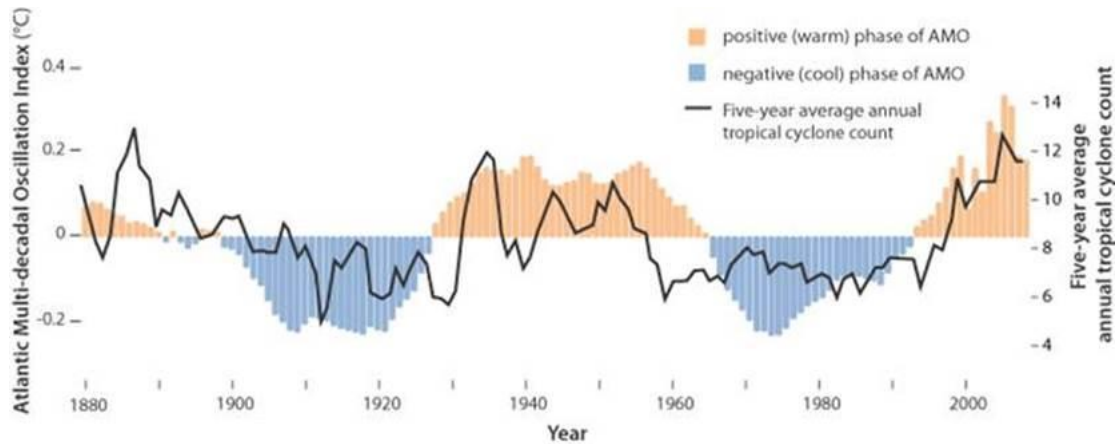


Figure 3.30 The Atlantic Multidecadal Oscillation Index and five-year average counts of tropical cyclones (Graph by LuAnn Dahlman based on data from NOAA and (Landsea, Vecchi, Bengtsson, & Knutson, 2010).

3.5.3 Changes to Significant Wave Heights due to Climate Change

Based on the analyses above, there is no clear increase in wave heights due to changes in the wave energy within the North Atlantic Ocean. Despite multi-year trends in AMO and NOA, the ERA5 database did not show any historical trend of increase that warranted an assessment on how the wave energy in the nearshore of Bermuda will be affected.

This does not change the fact the sea level rise will affect the wave climate in the nearshore regions. SLR will increase the nearshore wave heights by reducing the effectiveness of any bottom features like reefs. As the sea level increases, the water depth increases. Offshore, in deeper waters, the effects of this increase in water depth are not important. However, as you get close to shore, waves begin to feel the friction from the bottom, which causes them to lose energy, slow down, and break. SLR effectively causes the conditions that promote wave breaking to move closer to the shoreline and therefore increase the height of waves that can exist in these areas. Additionally, the more submerged a reef, the less effective it is in wave breaking. SLR will cause more wave energy to be transmitted over the reefs and onto the shoreline.

To quantify this impact in the nearshore, waves were re-modeling to account for the expected increase in mean sea level. The primary impact of an increase in mean sea level is a corresponding increase in wave energy that propagates over the outer reef.

The offshore water levels were increased to account for SLR as shown in Table 3-7.

Table 3-7 Rate of change (mm/yr) and Sea Level Rise (m) used for modeling

Horizon	RCP 4.5		RCP 8.5	
	Rate (mm/yr)	SLR (m)	Rate (mm/yr)	SLR (m)
20yr	5.7	0.114	6.6	0.132
50yr	7.7	0.385	10.5	0.525
100yr	7.7	0.770	10.5	1.05

Figure 3.31 presents mean annual wave heights for select nearshore nodes from various sea level rise projections. Figure 3.32 to Figure 3.35 further document the changes in significant wave heights for various time horizons for both RCP 4.5 and 8.5 scenarios.

The modeling projections show that the lagoon in the lee of the reef will see the most increase in wave heights. This is expected as the effectiveness of the reef will be significantly reduced. The 20-year horizon shows the least increase in the wave heights for both RCP scenarios where, within the lagoon, the wave heights increased 5-10mm. While these are not significant, for the 100-year horizon the significant wave heights increase by 0.08m to 0.15m for the RCP4.5 and RCP8.5 respectively. These values, which account for a 15-20% increase in the significant wave heights, are relatively large.

Waves on the south coast had smaller increases in wave heights. The south coast is more exposed and thus not as dependent on protection from the reef as the north coast.

From this assessment the following can be concluded:

- The western coast (near Dockyards) is at risk of greater wave energy. The water depth in these areas will increase due to the SLR and the reefs would be less effective at reducing the wave conditions. This has implications for the maritime activities in this area: disturbances to cruise ships, shipping, ferries, and general navigation in the area.
- Likewise, the north coast areas outside of the protection of the sounds will see larger increases in wave energy. Here, industries such as the electric generation plant could be affected.
- Within the sounds, wave heights could increase by up to 250%, however, this only reflects a change of approximately 5mm.
- Under statistically significant events, significant wave heights will increase by more than 0.3m. This is a significant amount and will have implications for sediment movement.

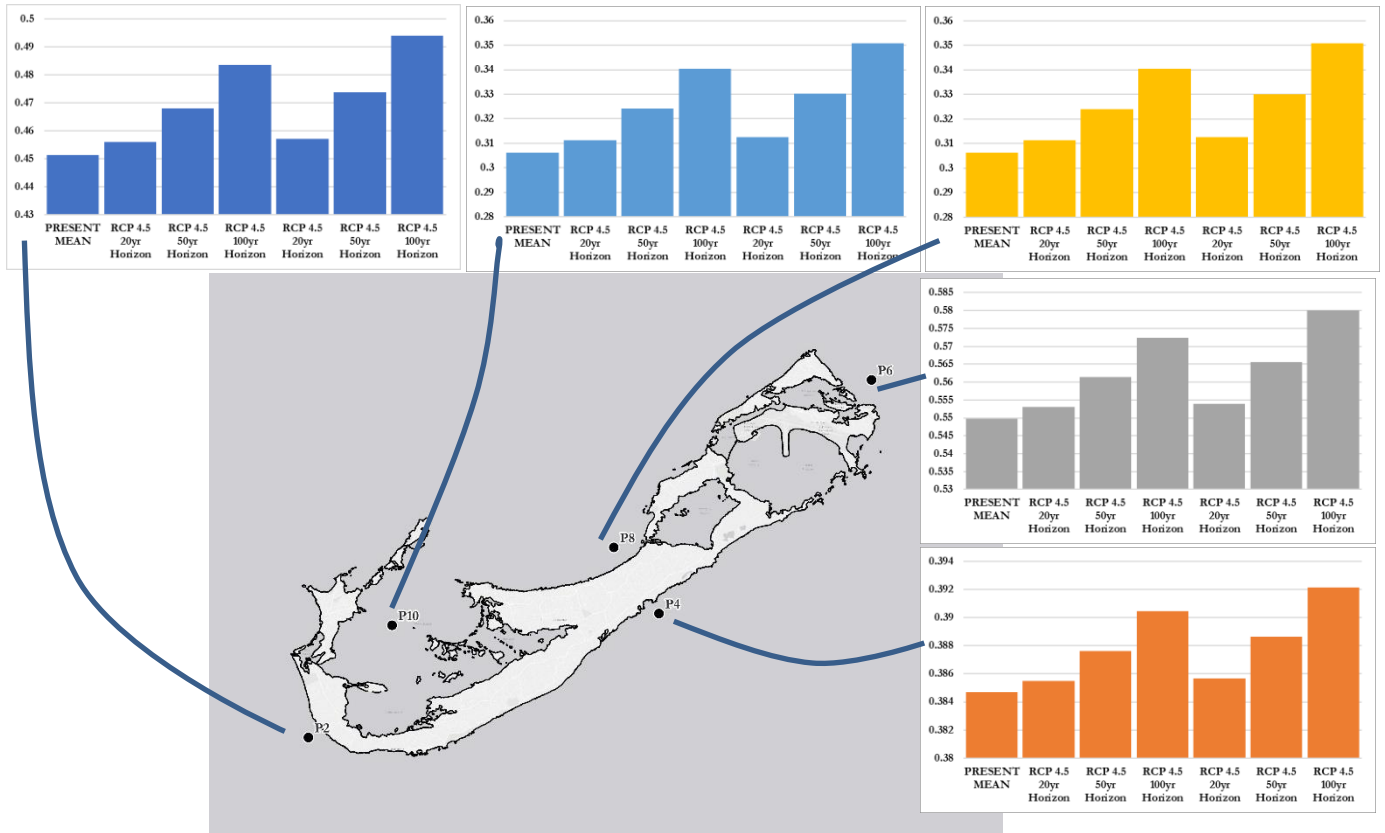


Figure 3.31 Predicted changes in wave heights at five points around Bermuda

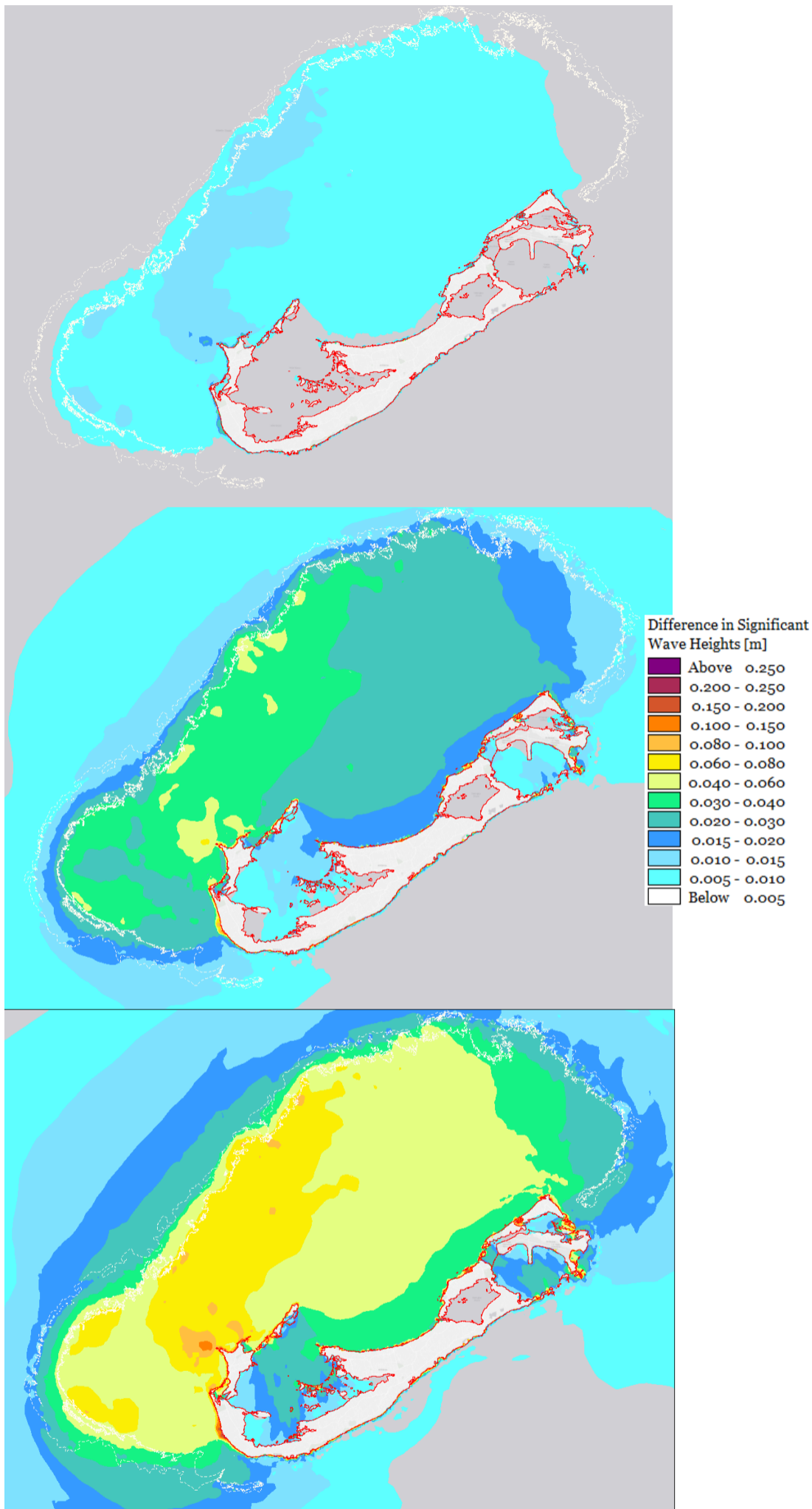


Figure 3.32 Predicted changes in mean wave conditions under the RCP 4.5 for 20-year (top), 50-year (middle) and 100-year (bottom) horizons

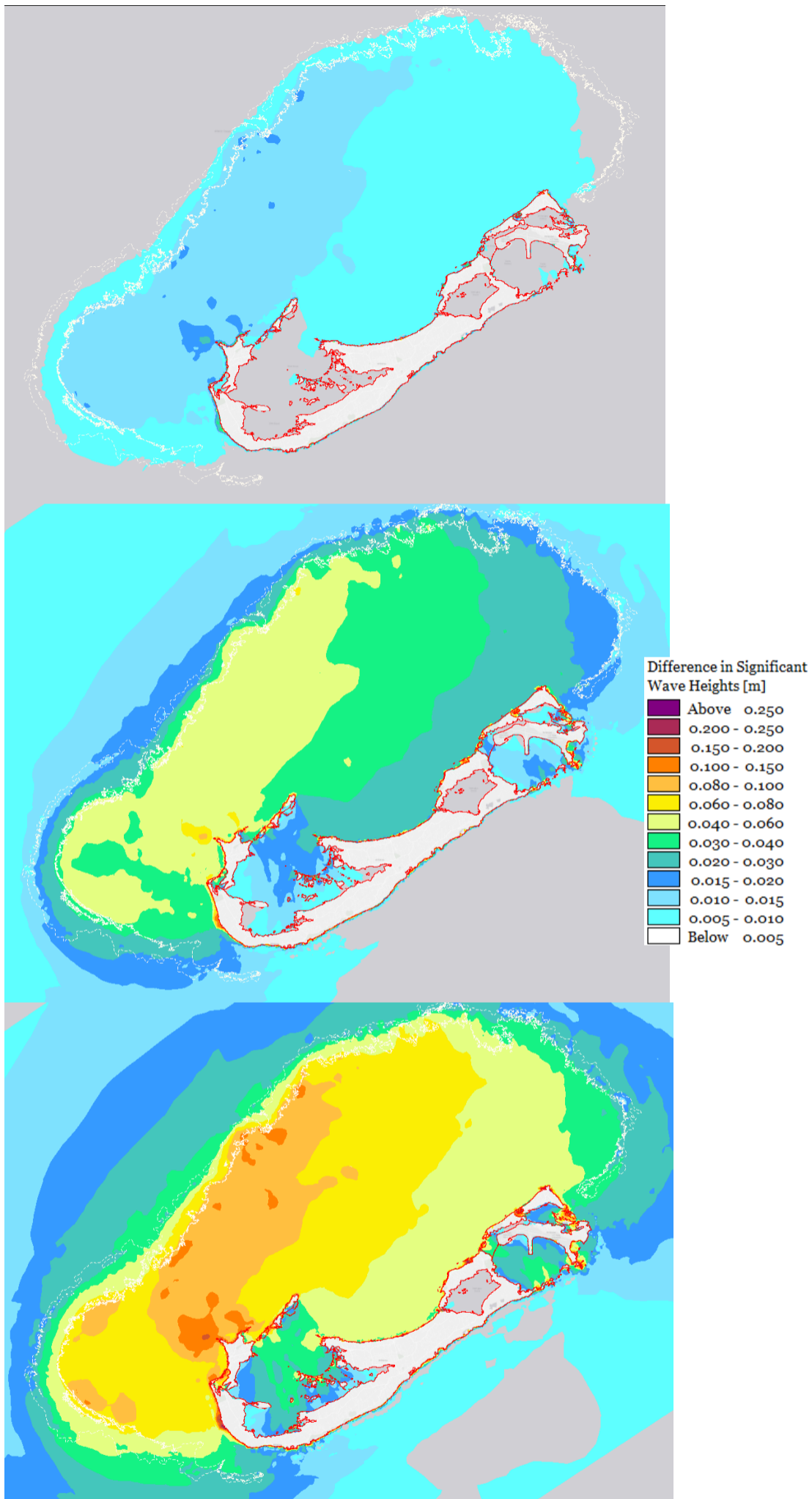


Figure 3.33 Predicted changes in mean wave conditions under the RCP 8.5 for 20-year (top), 50-year (middle) and 100-year (bottom) horizons

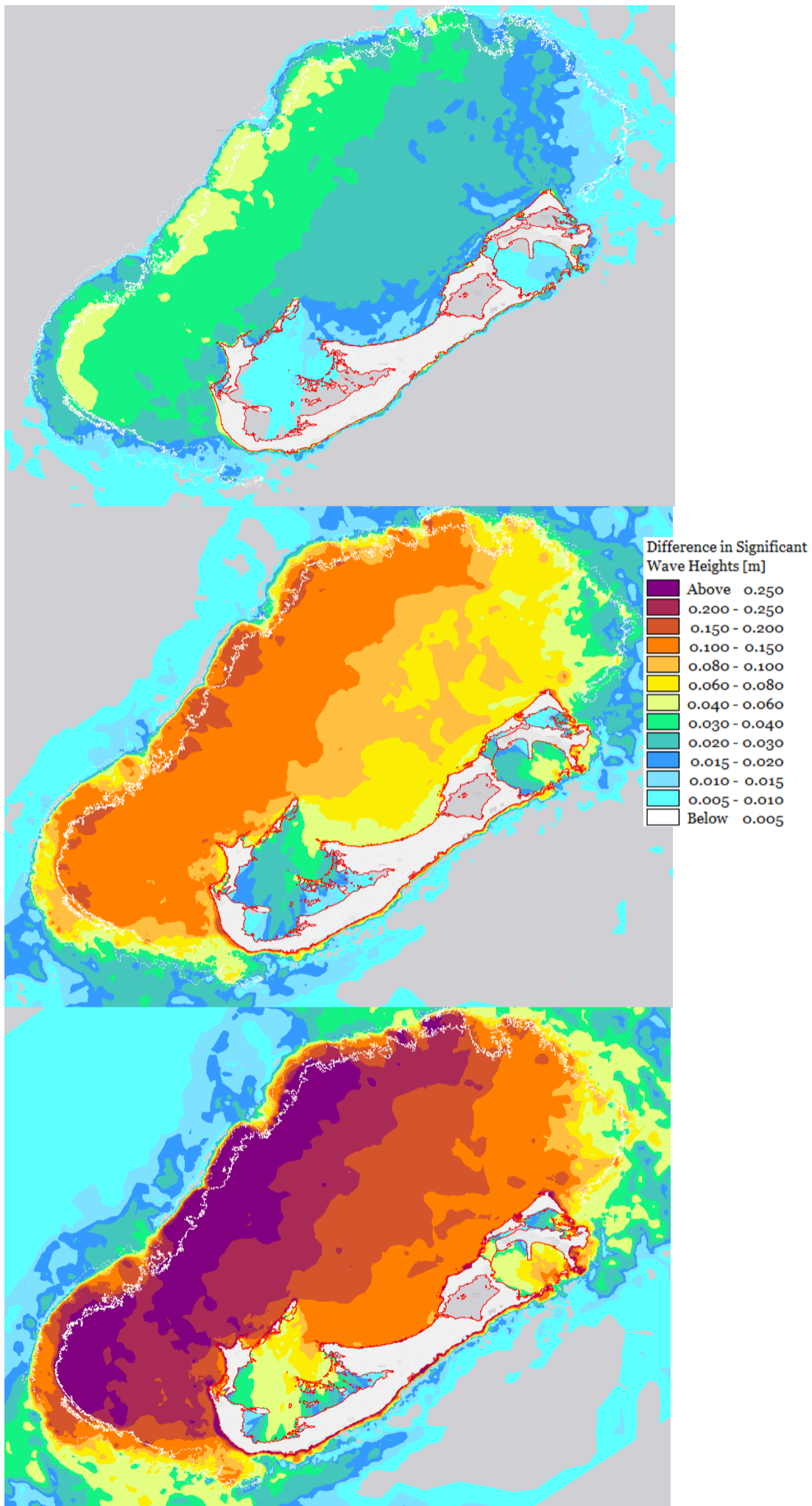


Figure 3.34 Predicted changes in the 99th percentile under the RCP 4.5 for 20-year (top), 50-year (middle), and 100-year (bottom) horizons

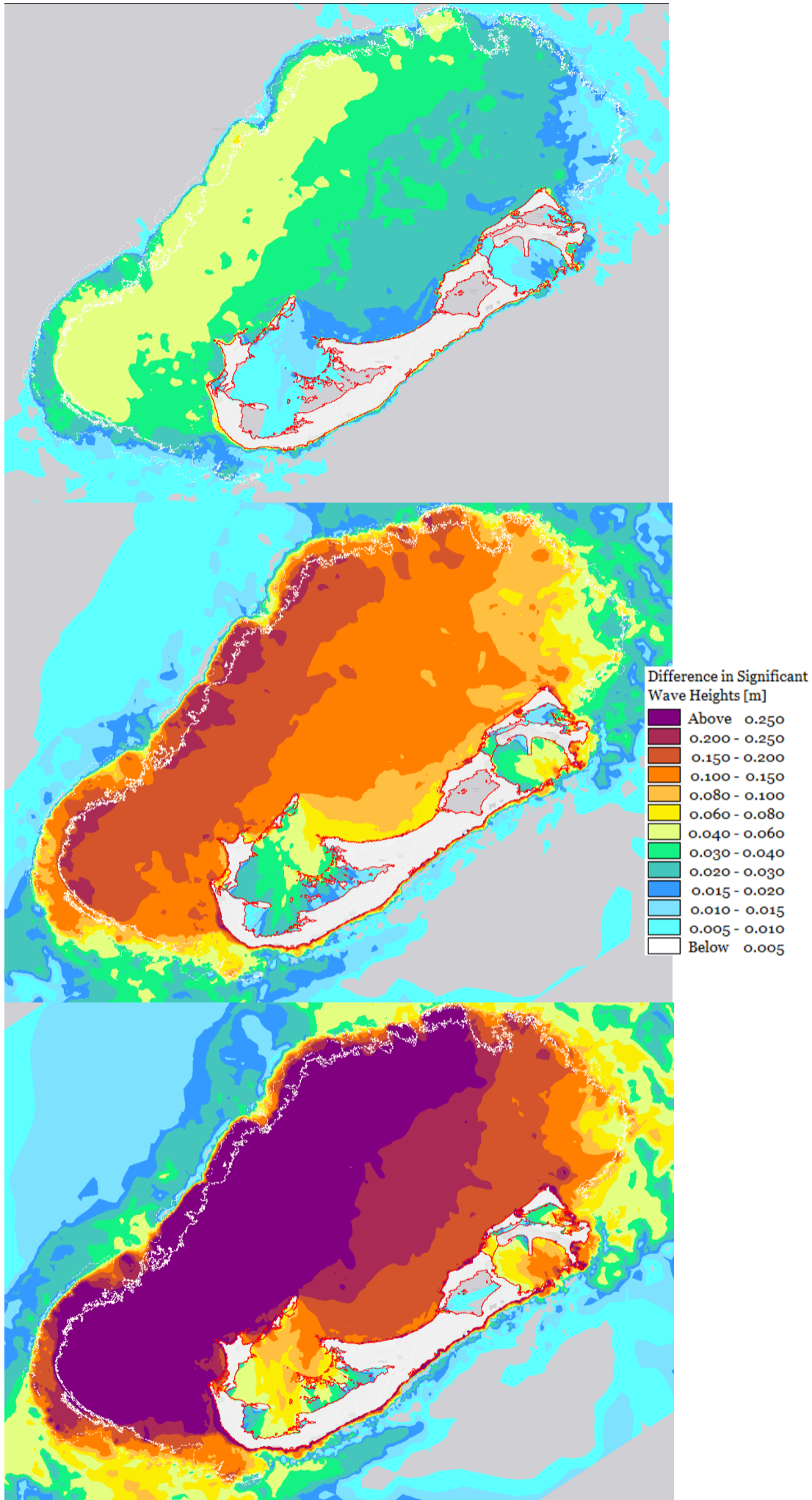


Figure 3.35 Predicted changes in the 99th percentile under the RCP 8.5 for 20-year (top), 50-year (middle) and 100-year (bottom) horizons

3.5.4 Swell Events

The computed annual wave climate revealed that swell waves – characterized by high energy, long period waves – impact Bermuda’s shorelines on rare occasions. Nevertheless, these swell waves were evaluated in detail because they have the potential to erode the coastlines and transport large amounts of sediment. Swell waves can damage shorelines with their inherent energy from a combination of high wave heights and long periods. To assess the vulnerability of this shoreline the time series of wave conditions representative of two winter swell events was extracted from the deep-water ERA5 database.

The two swell events were selected to represent the effect of swells originating from the north versus the south of Bermuda. The selection of these swell events from the 43-year database of wave data considered the following criteria:

- The significant wave heights should exceed the mean plus two standard deviations of data record;
- The wave period should be more than 10s;
- These conditions should not be as the result of a cyclone within 300km of Bermuda; and
- The conditions should be sustained for more than 5 days.

From this assessment, over 600 events were found with most coming from the north-northeast, attributable to winter storms in the north Atlantic Ocean. For events with dominant waves coming from the south, they were attributable to cyclones tracking south of Bermuda.

Swell Event 1: March 2018

The MIKE 21 model was used to investigate the shoreline response to the winter swell event (Figure 3.36). Time-varying wave heights, periods and directions characterising the swell events were input along the deep-water boundary of the numerical model. Figure 3.37 to Figure 3.38 shows the wave and current conditions at the peak of the swell event. A few critical observations include:

- When a swell event approaches from the north, the reef still reduces the wave heights by more than 150%. The offshore waves approach the reef at 2.5m in height and are effectively reduced to just under 1m along the north shore.
- A storm current is generated from the passage of a swell in this area. The wave energy creates a drift from the west to the east. Current speeds are greater than 0.8m/s along the south and the northern reef.
- This drift will create potential for significant sand movement.

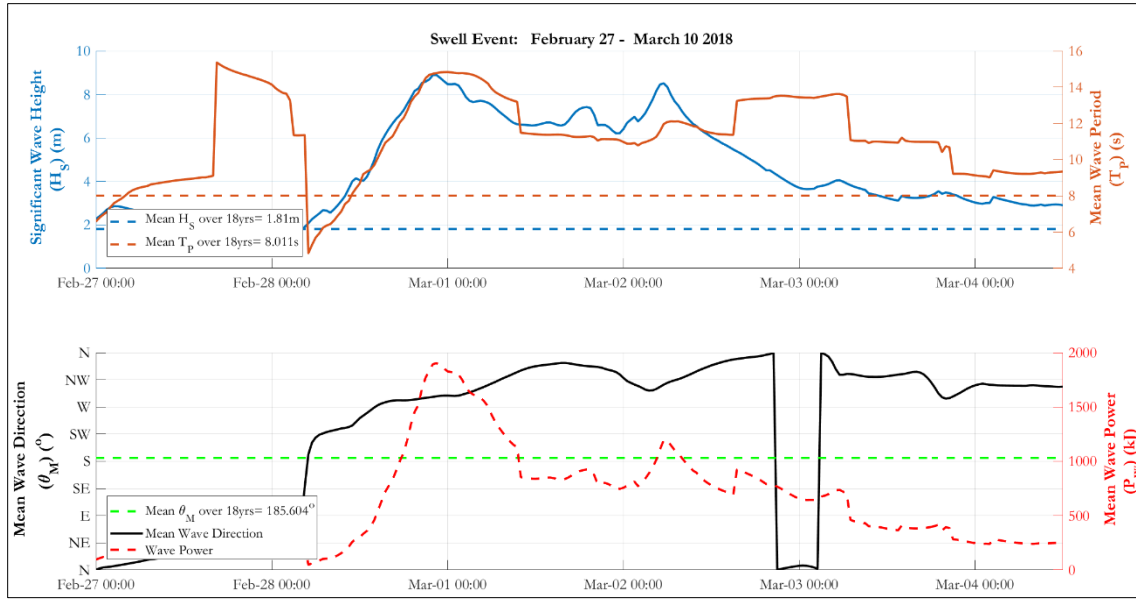


Figure 3.36 Offshore conditions March 2018 event

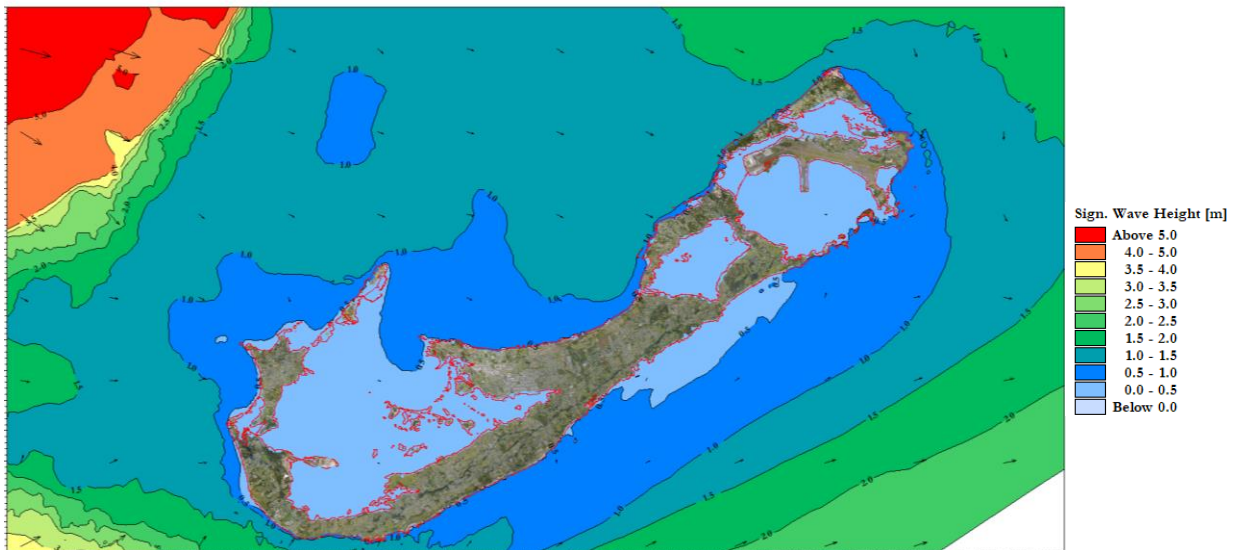


Figure 3.37 Significant wave heights at the peak of the swell March 2018 event

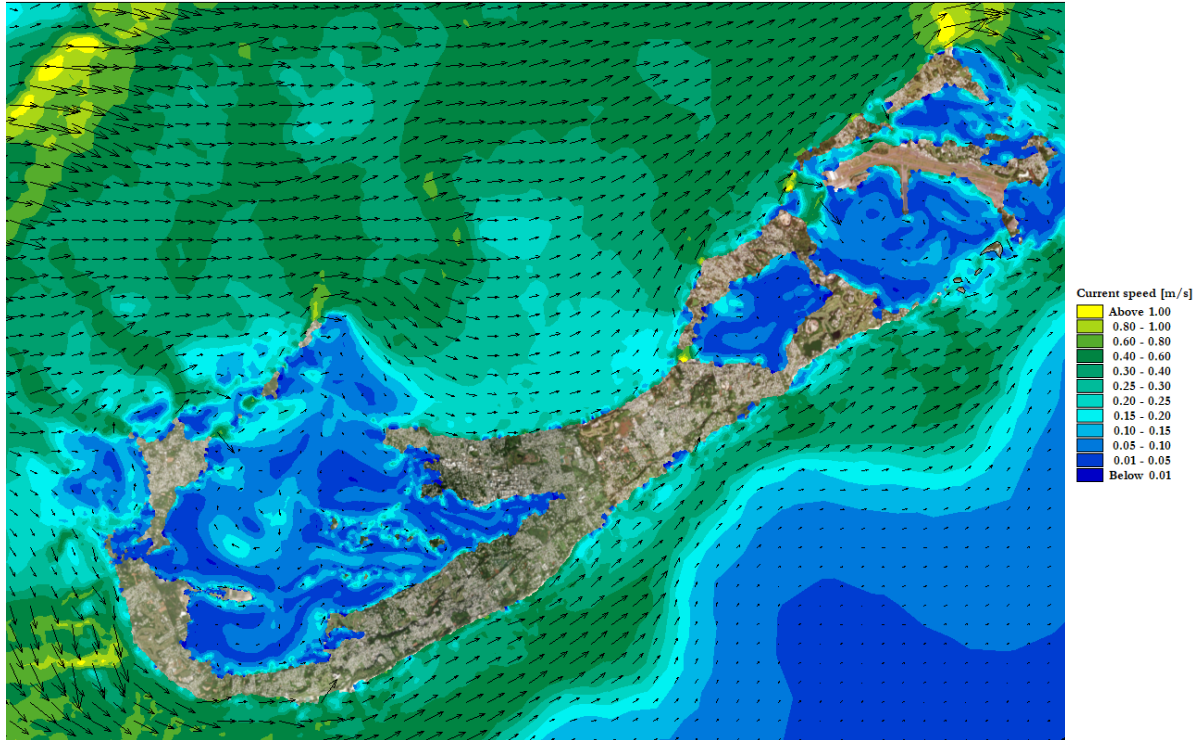


Figure 3.38 Current speeds at the peak of the swell March 2018 event

Swell Event 2: August 1995

The time-varying wave heights, periods and directions characterising a second swell was included to give an understanding of what happens as a result of southerly swell events. During this event, the wave heights were 5.5-6m along the south coast during the event (Figure 3.39 to Figure 3.41). The bimodal nature of Bermuda’s wave regime is evidenced by the generation of a north-easterly drift during the south swell event, which is the opposite of the event assessed above.

The implications garnered from this assessment suggests that:

- The south coast is more exposed to high wave energy events.
- There is potential for sediments to move both east and west along the south coast. However, a changing climate could cause an imbalance in this flow. As stated earlier, the southerly approaching swells resulted from hurricanes tracking south of the island. With predictions for stronger storms in the north Atlantic Ocean, this could mean swell events creating stronger currents towards the east and beaches may not be able to recover.

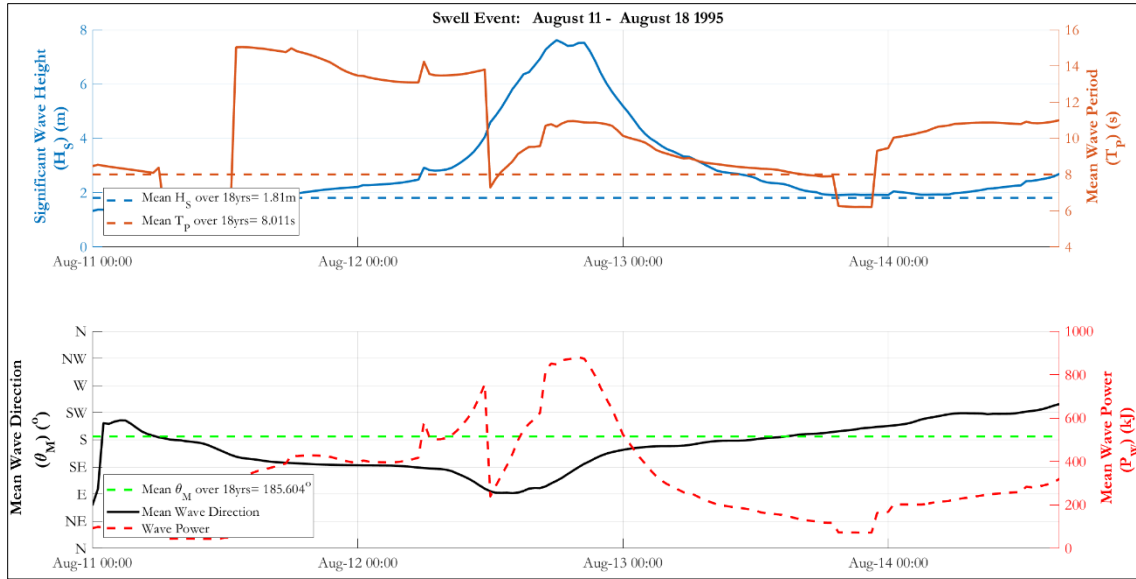


Figure 3.39 Offshore Conditions – August 1995 event

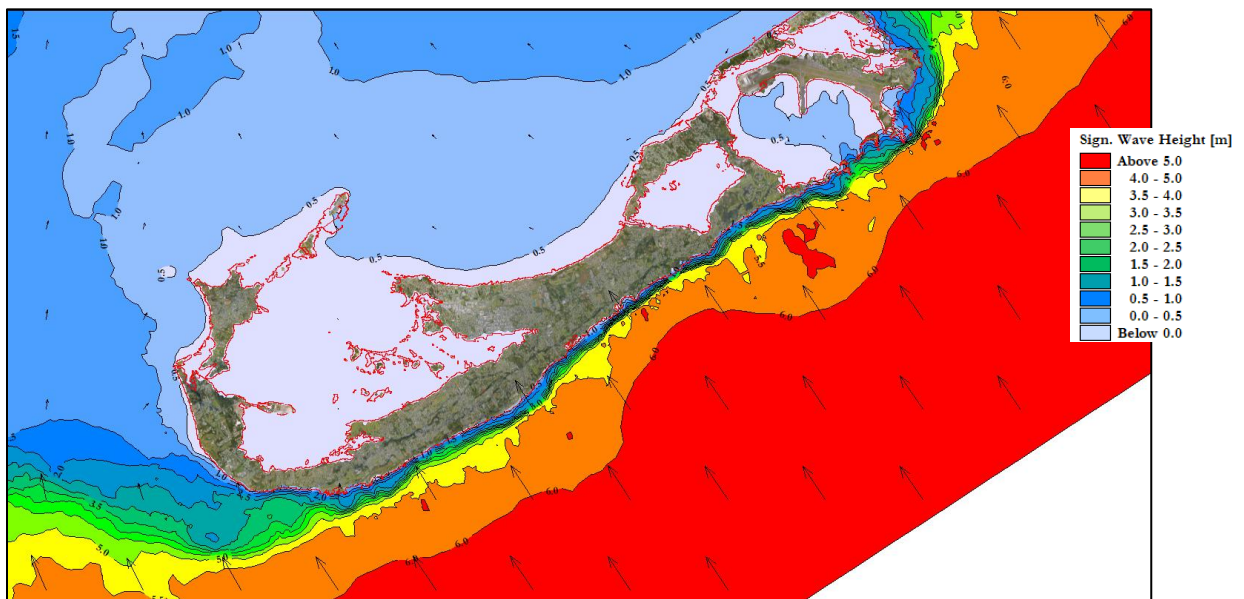


Figure 3.40 Significant wave heights at the peak of the swell – August 1995 event

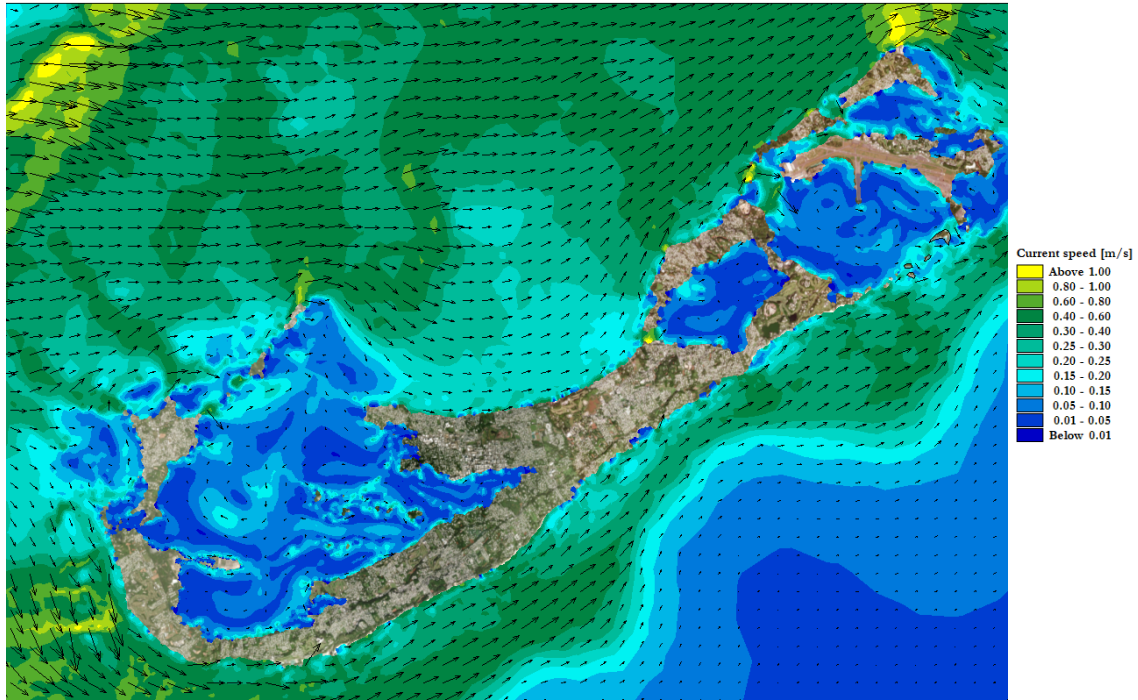


Figure 3.41 Current speeds at the peak of the swell – August 1995 event

4 Hurricane Risk Assessment

Tropical storms and hurricanes form frequently in the Atlantic Ocean each year from June to November. The storms generate high-energy waves, impacting shorelines in dramatic and abrupt ways.

Bermuda lies directly in ‘Hurricane Alley’, an area of water in the Atlantic Ocean within which hurricanes typically form because of the warmer sea surface temperatures there. Figure 4.1 shows the typical path of hurricanes in the north Atlantic basin, which tend to form between latitudes 5°N and 25°N off the west coast of Africa and then track across the Atlantic Ocean. Those formed at the lower latitudes are usually pushed on a westerly track by the north-east Trade Winds, whereas those of the higher latitudes track more to the north and north-west.

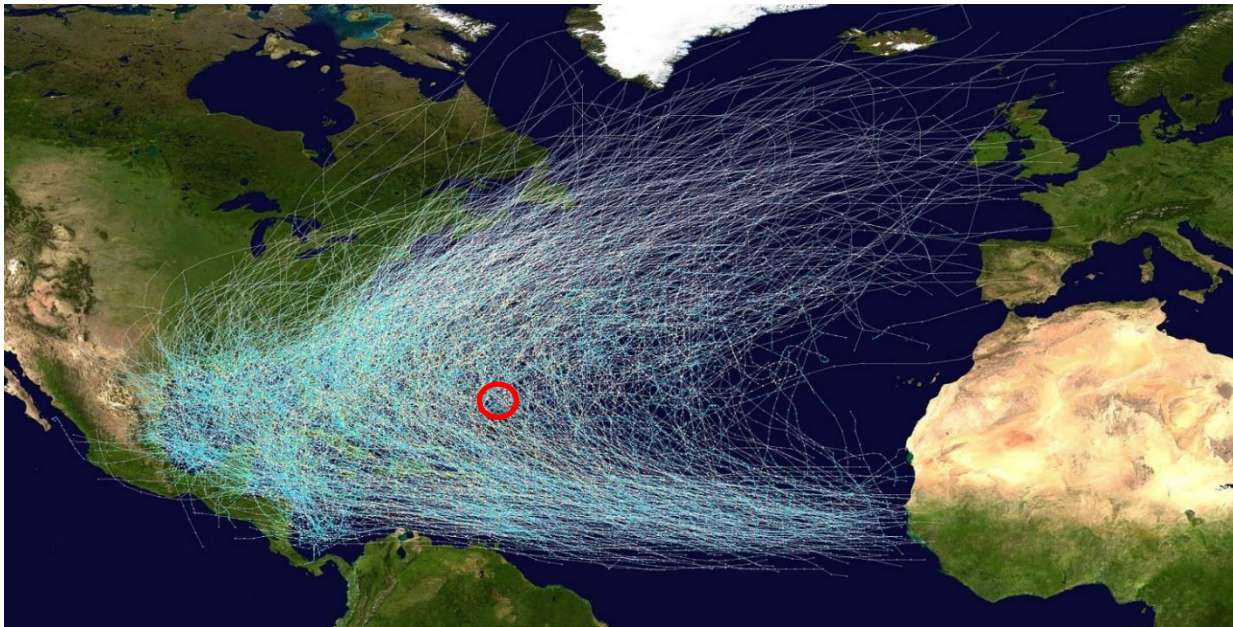


Figure 4.1 Atlantic hurricane tracks since 1851; approximate location of Bermuda is highlighted (red circle)

With respect to coastal risk and vulnerability in Bermuda, hurricanes have two immediate coastal hazards: (1) stronger waves and (2) higher water levels. These extreme conditions can be calculated using the MIKE 21 Spectral Wave (SW)/Hydrodynamic (HD) models. The models are forced with the highest deep-water wave and water level conditions to simulate the transformation of waves from deep-water to shallow water locations. For climate change analysis, it is important that the most realistic wave and water level conditions are applied in the simulation of these shallow water conditions. For these wave conditions, the values are selected through the process of hindcasting where conditions are calculated for a past event at a given time and location. Water levels are obtained by assessing the possible extreme tides and sea level rise conditions under hurricane conditions. The process is described briefly in the following paragraphs.

4.1 Historical Hurricane Activity

For the Atlantic Ocean, detailed information on tropical cyclones, including all hurricanes, has been collected by the US National Oceanic and Atmospheric Administration (NOAA), specifically at the National Hurricane Centre (NHC). This database historical hurricane information, dating from 1851 to 2019, contains storm tracks, wind speeds and several other parameters to accurately describe and simulate individual storms.

All hurricanes passing within a 300 km radius of Bermuda were extracted from the database and analysed using HurWave (SWI’s in-house computer program). The results show that since 1851 (over the past 171 years), 149 hurricanes and tropical storms passed within this distance. The total number of storms can be broken down according to the categories described by the Saffir Simpson scale. Figure 4.2 shows that Bermuda was more frequently hit by tropical storms (76), than major hurricanes (Category 3 and higher) (23).

Figure 4.3 shows the temporal distribution of storms. The graph shows that on occasion, several years pass without tropical storm or hurricane impact, but also on many occasions more than one storm can impact the area in any given year. Table 4-1 and Table 4-2 provide more detail about specific storms.

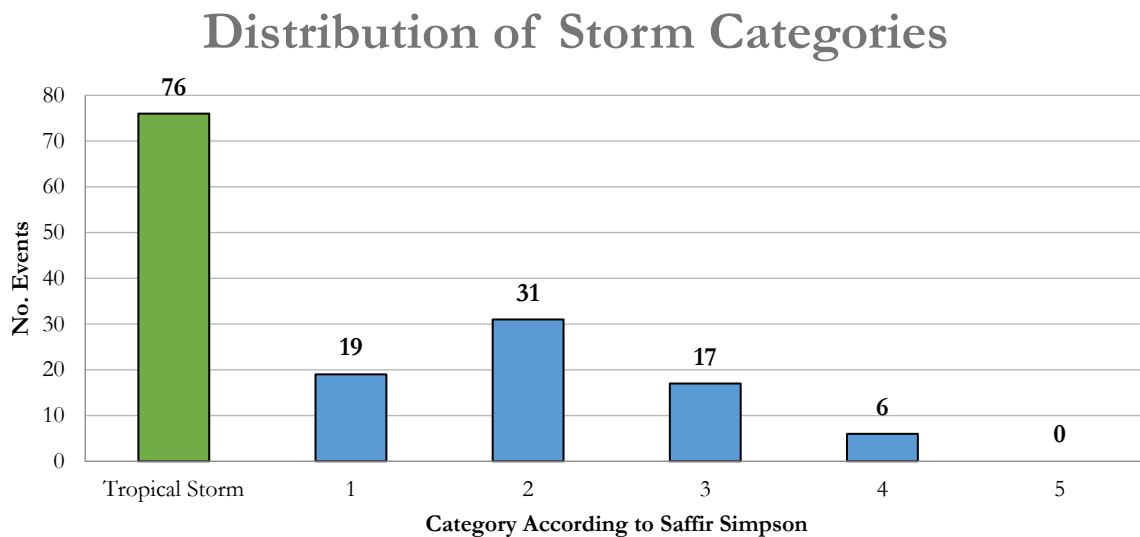


Figure 4.2 Distribution of storm events according to the Saffir Simpson Scale over the past 169 years

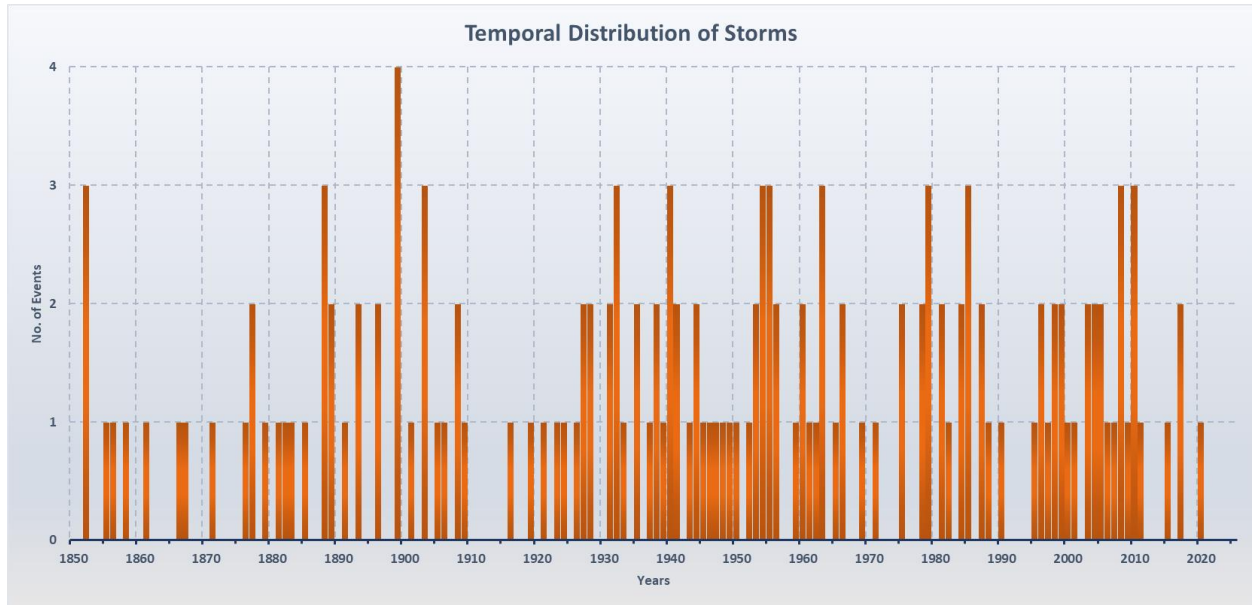


Figure 4.3 Temporal distribution of storms passing near the project site (300 km radius) from 1851

Table 4-1 Data for the five most recent Hurricanes category 3 and above

<i>Storm Name</i>	<i>Date Range</i>	<i>Max Wind Speed</i>	<i>Max Category</i>
Humberto 2019	Sep 12, 2019 to Sep 20, 2019	110	3
Nicole 2016	Oct 04, 2016 to Oct 19, 2016	120	4
Joaquin 2015	Sep 26, 2015 to Oct 15, 2015	135	4
Gonzalo 2014	Oct 11, 2014 to Oct 20, 2014	125	4
Ophelia 2011	Sep 20, 2011 to Oct 04, 2011	120	4

Table 4-2 Data for all category four hurricanes close by Bermuda

<i>Storm Name</i>	<i>Date Range</i>	<i>Max Wind Speed</i>	<i>Max Category</i>
Nicole 2016	Oct 04, 2016 To Oct 19, 2016	120	4
Gonzalo 2014	Oct 11, 2014 To Oct 20, 2014	125	4
Ophelia 2011	Sep 20, 2011 To Oct 04, 2011	120	4
Frances 1961	Sep 30, 1961 To Oct 10, 1961	115	4
Unnamed 1948	Sep 04, 1948 To Sep 17, 1948	115	4
Unnamed 1943	Aug 19, 1943 To Aug 27, 1943	120	4
Unnamed 1939	Oct 11, 1939 To Oct 18, 1939	120	4
Unnamed 1933	Aug 13, 1933 To Aug 28, 1933	120	4
Unnamed 1880	Sep 27, 1880 To Oct 04, 1880	120	4

4.2 Storm Tracks of Recent Hurricanes

Two hurricanes [Fiona (2022) and Nicole (2016)], representative of the more recent storms impacting Bermuda, were chosen for further modeling and analysis. Specifics from the hurricane tracks were extracted from the NOAA and Wunderground database for model input:

- Time (hour);
- Latitude (deg);
- Longitude (deg);
- Maximum wind speed (m/s);
- Radius to maximum wind speed (km);
- Central pressure (KPa); and
- Ambient pressure (KPa).

The numerical model that computes storm surge requires that hurricane track information be converted into time-varying wind speed and atmospheric pressure maps. There are several different tools to make this conversion, most of which assume the hurricane can be represented as a moving vortex. For this work, the method of Young and Sobey (1980) was used to define the spatial and time-varying wind speeds. This method is based on an exponential decrease in the wind speed away from the point of maximum wind. To create the maps, a relatively short time step of 1 hour was used to diminish the errors associated with interpolating a concentric radial phenomenon onto a rectangular and triangular grid.

Wave and water level conditions were computed using MIKE 21 at hourly intervals along the overall hurricane tracks. The result of this analysis indicates:

- At the centre of hurricanes like Hurricane Nicole and Fiona, offshore wave heights exceed 12m. Stronger cyclones like Nicole show that wave heights greater than 12m span a wider area.
- At the centre of the hurricanes, water levels are greater than 0.35m for Hurricane Fiona and 0.9m for of Hurricane Nicole. A water level increase is observed more than 200km from the centre.
- A passing hurricane/cyclone affects an area as large as 300km radius. For stronger hurricanes like Nicole (2016), the severe conditions can be greater than 300km away from its centre.
- Due to Bermuda's small size, using a static modeling approach for hurricane simulations is practical. This involves assigning a single value to the boundaries of the mesh mentioned earlier as opposed to running individual hurricanes. The underlying assumption is that conditions in Bermuda's offshore waters are consistent during a given hurricane. For example, the water level and wave height caused by hurricanes is anticipated to be uniform offshore Bermuda (across deeper waters). However, it's important to note that the subsequent nearshore modeling (to transform the offshore conditions to the nearshore) incorporates intricate dynamics related to energy propagation in shallower waters, such as wave refraction, wave growth and wind setup. Consequently, wave and surge conditions along Bermuda's various shorelines will be replicated accurately.

Figure 4.4 and Figure 4.5 show significant wave heights during Hurricanes Fiona and Nicole.

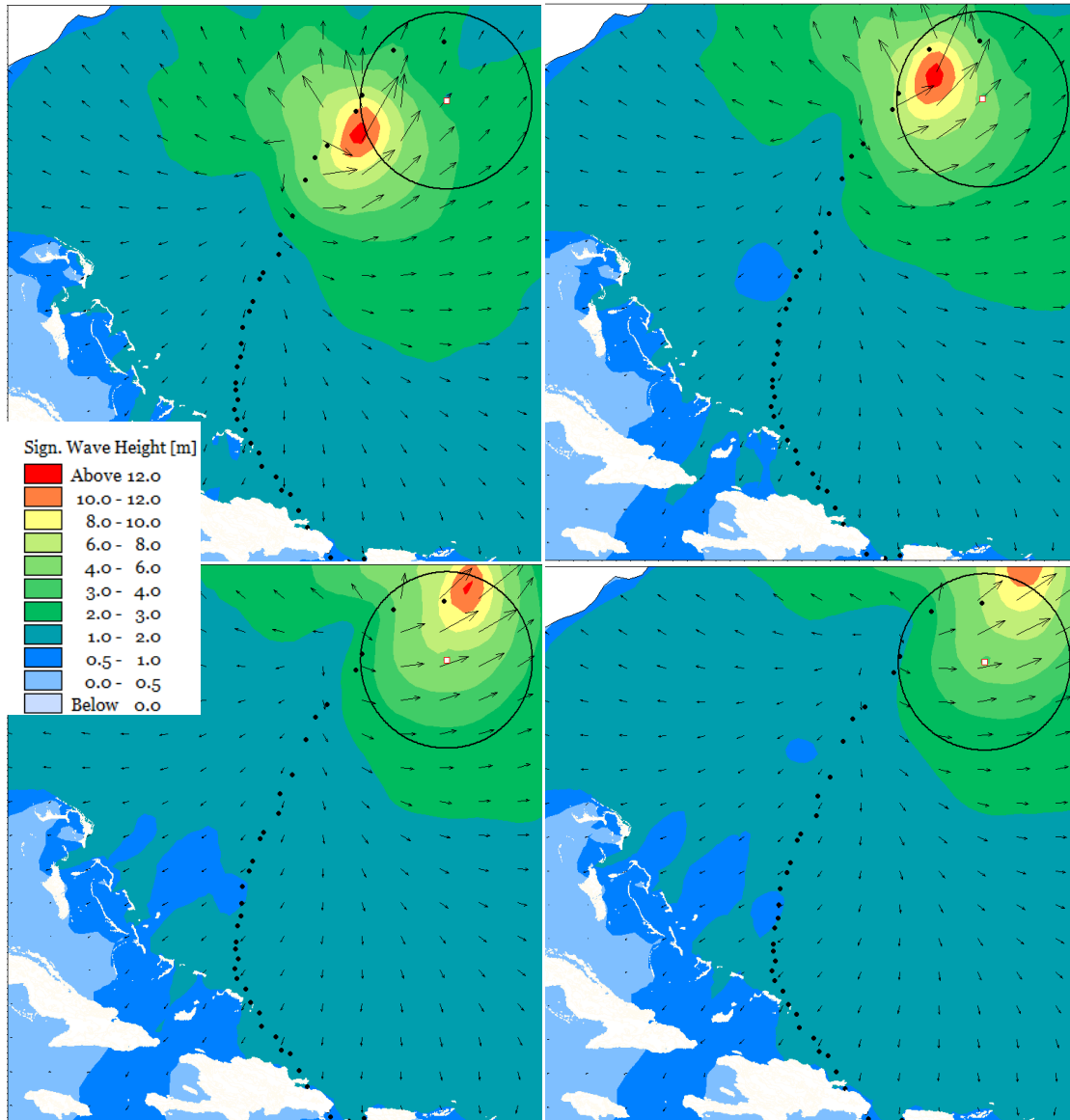


Figure 4.4 Significant wave height during Hurricane Fiona 2022 (from Sept 23 3AM to 5PM)

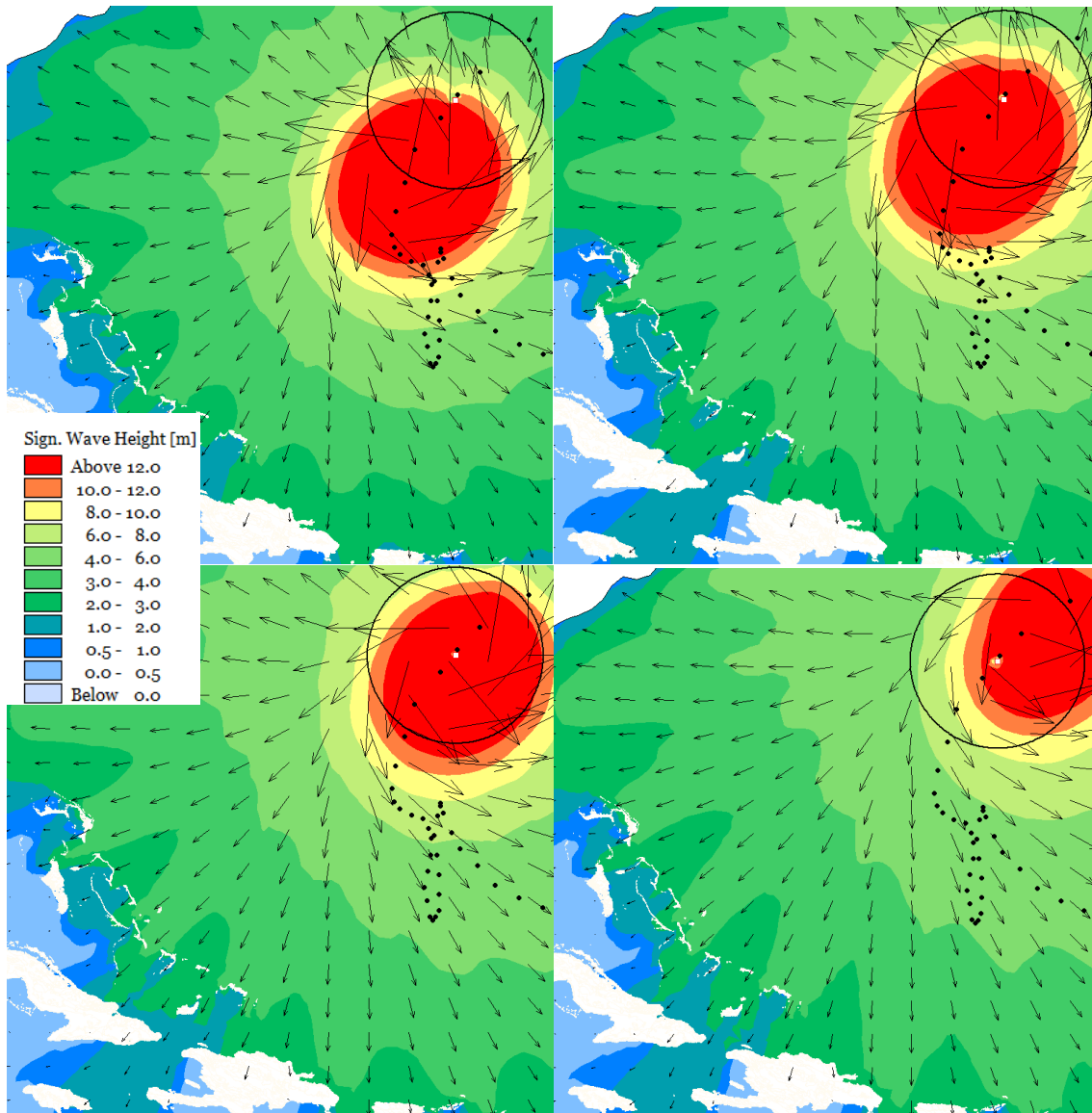


Figure 4.5 Significant wave height during Hurricane Nicole 2016 (from Oct 13 3AM to 9PM)

4.3 Deep Water Waves

Deep water wave parameters were calculated for each selected tropical cyclone using parametric hurricane models (Cooper, 1988; Young and Burchell, 1996). The resulting wave conditions were divided into directional sectors and each set was fit to a statistical function describing their exceedance probability. The wave parameter values for 25, 50, 100 and 150-year return periods were determined from the best-fit statistical distribution. The deep-water wave parameters corresponding to the 25, 50, 100 and 150-year return periods were computed for five directional sectors of incidence.

Table 4-2 shows the resulting wave heights, wind speeds, and periods for the directional sectors investigated. These wave parameters are subsequently applied in MIKE 21 SW with the inclusion of the static storm surge levels to obtain design wave heights in the nearshore of the selected areas for the different return periods.

Table 4-2 Deep water hurricane wave parameters (significant wave height (Hs), peak period (Tp) and wind speed (Vm) resulting from the 25, 50, 100 and 150-year return periods

<i>Directional Sector</i>	<i>Parameters</i>	<i>Return Period</i>			
		25	50	100	150
<i>North</i>	Hs (m)	5.67	6.55	7.36	7.81
	Tp (s)	9.84	10.78	11.61	12.05
	Vm (m/s)	14.93	17.13	19.15	20.26
<i>North-east</i>	Hs (m)	6.05	7	7.87	8.35
	Tp (s)	10.25	11.24	12.11	12.57
	Vm (m/s)	18.63	20.92	23.01	24.17
<i>East</i>	Hs (m)	8.44	9.36	10.22	10.68
	Tp (s)	12.65	13.51	14.27	14.68
	Vm (m/s)	21.86	24.4	26.73	28.02
<i>South-east</i>	Hs (m)	9.73	10.86	11.89	12.46
	Tp (s)	13.83	14.82	15.7	16.17
	Vm (m/s)	24.5	27.65	30.55	32.14
<i>South</i>	Hs (m)	10.16	11.34	12.43	13.03
	Tp (s)	14.21	15.24	16.15	16.63
	Vm (m/s)	23.85	26.64	29.21	30.62
<i>South-west</i>	Hs (m)	10.22	11.44	12.56	13.18
	Tp (s)	14.27	15.32	16.25	16.75
	Vm (m/s)	23.54	26.27	28.78	30.16
<i>West</i>	Hs (m)	9.21	10.25	11.21	11.74
	Tp (s)	13.36	14.3	15.13	15.58
	Vm (m/s)	22.45	25.06	27.44	28.76
<i>North-west</i>	Hs (m)	7.35	8.33	9.22	9.72
	Tp (s)	11.6	12.54	13.38	13.83
	Vm (m/s)	16.85	19.27	21.5	22.73

4.4 Storm Surge Components

4.4.1 Definition of Storm Surge Components

The elevated water level that accompanies hurricanes and creates flooding and causes damage to coastal infrastructure is known as storm surge. Put another way, storm surge is simply the increase in water level at the shoreline resulting from the passage of a storm.

Storm surge encompasses static and dynamic elements. The static aspects consist of inverse barometric pressure rise and wind set-up, while the dynamic components arise from wave set-up and

wave action on the shore. Unlike the relatively constant water levels associated with static surge elements, water levels in areas affected by wave action, termed the wave run-up zone, fluctuate as waves interact with the beach profile and move onto the land. Refer to Figure 4.6 for an illustration of storm surge components.

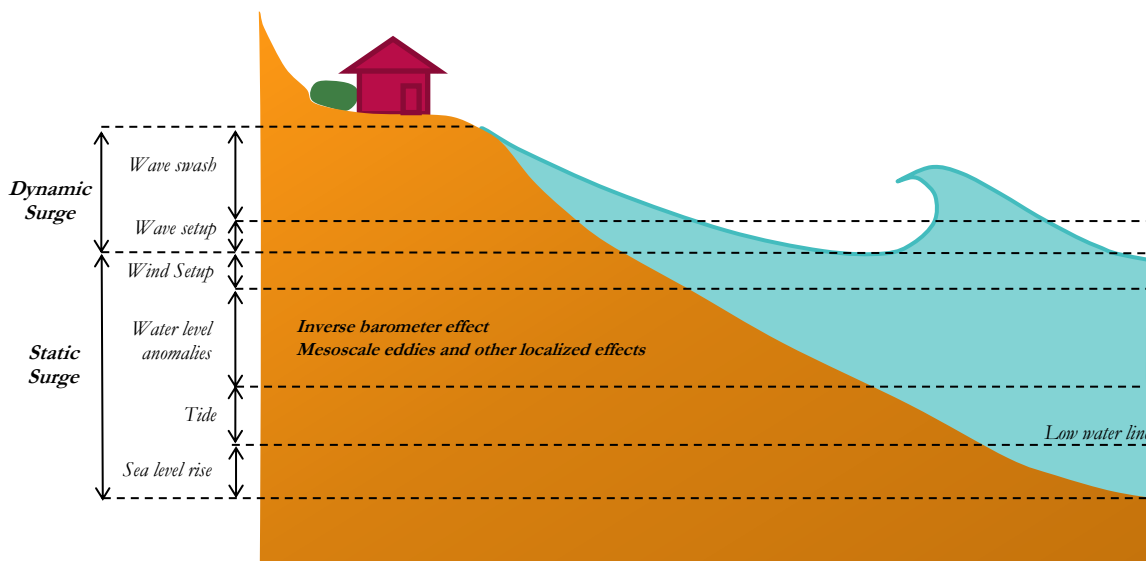


Figure 4.6 Components of storm surge

4.4.2 Tidal Input (HAT)

The initial water level estimated by hurricane wave climate modeling was determined from historical data obtained from tidal prediction software. For conservative reasons, SWI assumed the highest astronomical tide (HAT) for the surge modeling. The HAT was obtained from the ADMIRALTY Total Tide (ATT) program and is 0.85m above MSL.

4.4.3 Inverse Barometer Effect

The atmosphere constantly exerts pressure on the Earth and ocean. When low pressure systems move over a region, the sea level rises by a relative amount, while high pressure systems push down on the ocean, creating a drop in sea level. This is called the inverse barometer effect, as the higher the pressure, the lower the sea level, and vice versa.

Extremely low central pressures are normally associated with smaller and more intense hurricanes, which can have high sustained wind speeds. This is usually highest when the eye of the hurricane is closest to the site. This component was estimated from HurWave, which derived the values statistically using historical storm data.

4.4.4 Mesoscale Eddies

Mesoscale eddies are common features of the world's oceans, with a typical scale of about 100km and a lifespan between tens and hundreds of days (Shcherbina, 2010). These eddies can rotate anti-clockwise or clockwise and the gradients associated with their density fields drive ocean currents in much the same way that high- and low-pressure systems in the atmosphere force the wind field. Bermuda is affected by mesoscale eddies that result in both increased and lowered water levels. As shown in Figure 4.7 these eddies result in water level conditions that can cause worse flooding than

some tropical storms. Conversely, these eddies can also cause unusually low tides, as occurred in Bermuda over several months in 2010.

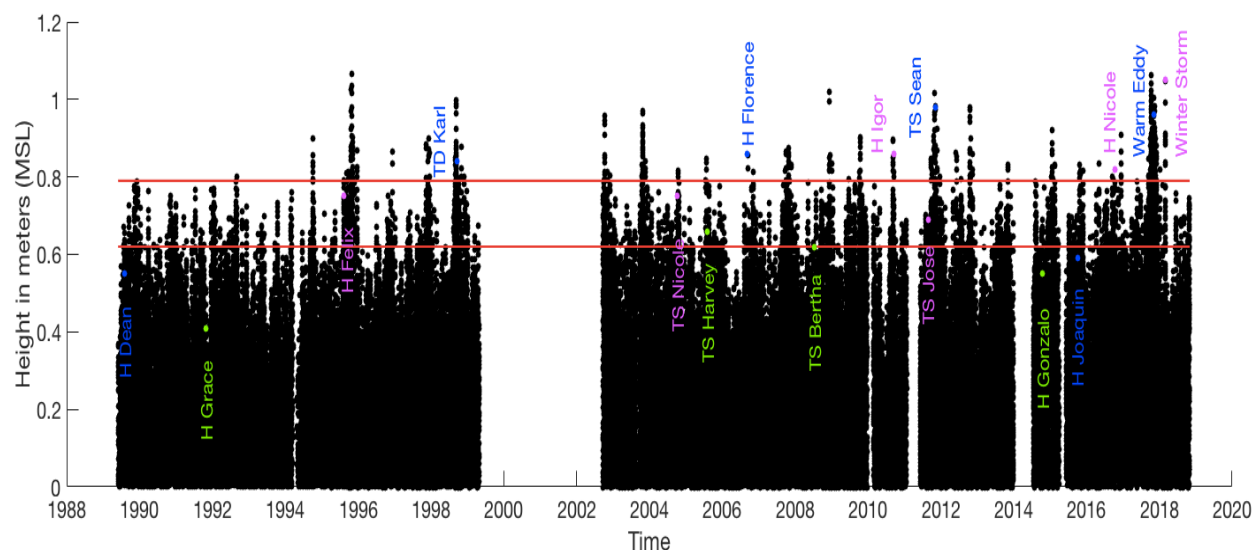


Figure 4.7 Extreme water level recorded at the St George's Station – Source: BWS

Tides are created by the gravitational forces from celestial bodies like the moon and sun acting on the waters of Earth. Those gravitational forces change as the relative positions of the Earth, sun, and moon change. Each of these changes is cyclical, repeating over time; and each change also has a measurable effect on the tides experienced at a shoreline. The effect of the myriad of motions of the earth and other celestial bodies have been studied and it was found there are approximately 37 constituents that affect the tides in an area. In general, the tides at a location are very predictable and several tidal models have been developed to predict the tides of an area.

Nonetheless, the water levels recorded at a local level can sometimes be different. In the case of Bermuda there were times when the calculated water level was very different from the measured water level. This is due to local influences. These local effects include the effect of wave and wind setup, frictional effects, as well as the mesoscale eddies.

Tide data obtained from NOAA³ for the St George's Station (ID: 2695540) from 1989 to 2018 were analysed. Every instance where the water level measured at St. George's Station **exceeded** the tidal level determined by tidal harmonics was extracted. These instances, for the purpose of this analysis, were referred to as positive surges. The difference between measured and calculated tides accounts for increases in water level that are not directly attributed to the tidal action. The filtering resulted in over 3800 events. Some of these events represent times when the maximum surge level was not more than 0.1m. To further filter out the positive significant surge events the following criteria had to be met:

³ https://tidesandcurrents.noaa.gov/sltrends/sltrends_station.shtml?id=2695540

1. During the time of the positive surge, no hurricanes should be within 300km of the island.
2. When wave energy in an area increases it causes wave set-up and wave run-up as described in Figure 4.6. This increases the ambient water levels and would be erroneous in the water level record and measurements. The analysis accounts for this by removing instances where the wave height is greater than the definition of a storm condition. That is, the wave height should be less than mean plus two standard deviations of the wave record from 1979. To do this, SWI looked at the ERA5 data record from 1979 for a point offshore Bermuda. This means that the significant wave heights should be less than is 3.7m.
3. For this analysis, only storm events where the maximum surge level was greater than 0.1m was considered.
4. The water surface elevation anomaly should last longer than 5 days.

Figure 4.9 shows the distribution of sustained positive surge events where the surge is greater than 0.1m, as well as where the event was longer than 5 days. These filtering routines shows 636 events with sustained positive surges. Table 4-3 to Table 4-4 show the ten longest events and the ten events with the largest surge. The data shows that these events can be more than 60 days long with a maximum surge greater than 0.4m.

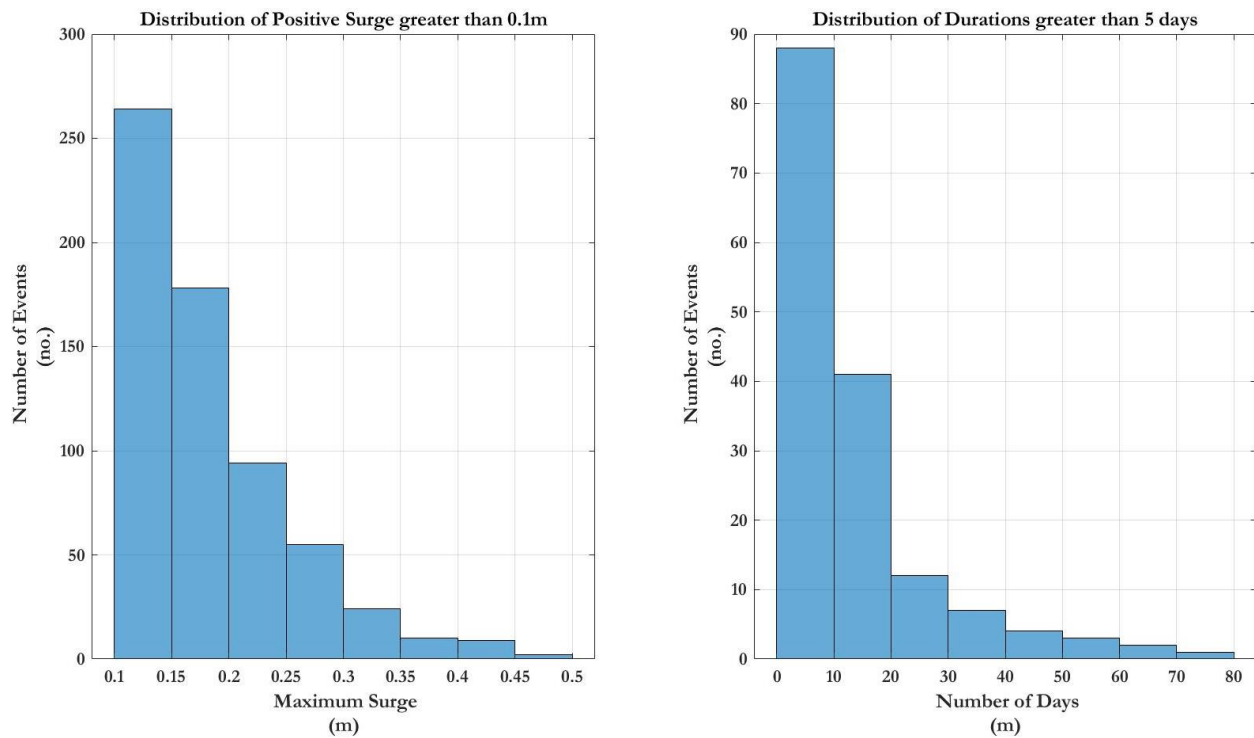


Figure 4.8 Distribution of positive surge events

Table 4-3 Positive surge events – ranked by duration

Start Date	End Date	Duration (days)	Maximum Surge (m)	Mean Surge(m)
"2017 09 29 09:00"	"2017 12 13 14:00"	75.20	0.482	0.267
"2009 06 18 05:00"	"2009 08 21 21:00"	64.66	0.279	0.092
"1995 09 20 09:00"	"1995 11 21 04:00"	61.79	0.435	0.177
"2016 06 07 08:00"	"2016 08 01 09:00"	55.04	0.252	0.119
"2007 09 10 12:00"	"2007 11 03 10:00"	53.91	0.344	0.127
"2005 07 10 16:00"	"2005 09 01 09:00"	52.70	0.237	0.091
"2017 08 11 02:00"	"2017 09 29 07:00"	49.20	0.292	0.134
"2016 08 22 12:00"	"2016 10 10 13:00"	49.04	0.413	0.113
"2012 05 14 11:00"	"2012 07 02 03:00"	48.66	0.289	0.096
"1997 05 07 04:00"	"1997 06 17 22:00"	41.75	0.215	0.078

Table 4-4 Positive surge events – ranked by maximum surge

Start Date	End Date	Duration (days)	Maximum Surge (m)	Mean Surge(m)
"2017 09 29 09:00"	"2017 12 13 14:00"	75.208	0.482	0.267
"2011 11 11 12:00"	"2011 11 27 09:00"	15.875	0.472	0.190
"2015 01 15 16:00"	"2015 01 27 16:00"	12	0.450	0.307
"2012 09 27 11:00"	"2012 10 28 17:00"	31.250	0.449	0.137
"2003 10 01 05:00"	"2003 11 10 01:00"	39.833	0.445	0.183
"2015 02 07 04:00"	"2015 02 11 23:00"	4.7916	0.439	0.195
"1998 09 02 18:00"	"1998 10 10 00:00"	37.250	0.438	0.191
"1995 09 20 09:00"	"1995 11 21 04:00"	61.791	0.435	0.177
"2009 01 18 22:00"	"2009 01 21 05:00"	2.2916	0.427	0.197
"2017 04 29 20:00"	"2017 05 31 15:00"	31.791	0.417	0.109

Figure 4.9 shows the predicted tide level, the verified water level, and the total positive surge for an October 2017 event. The positive surge in this event approaches a maximum of **0.482m**.

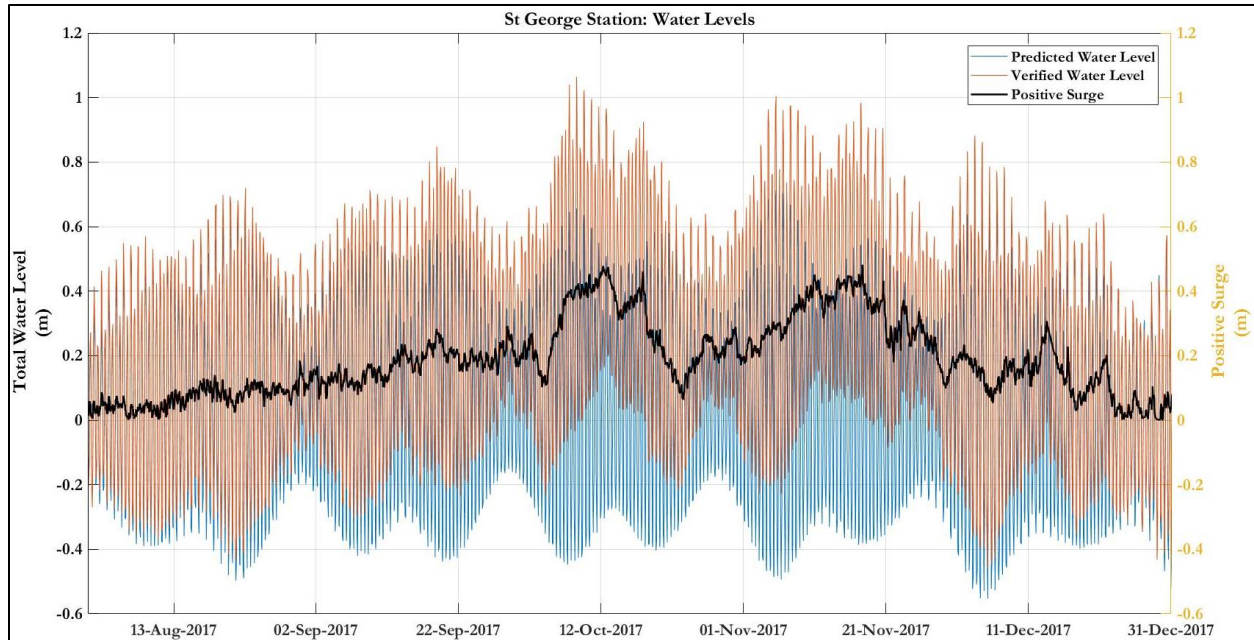


Figure 4.9 Positive surge event October 2017

4.4.5 Sea Level Rise

Within climate change modeling, RCPs (Representative Concentration Pathways) try to predict human behaviour and its associated impact on the climate. In assessing these future trends, experts make predictions of how concentrations of greenhouse gases in the atmosphere will change in the future because of human activities and estimates sea level rise based on those changes. Table 4-5 shows the rates of sea level rise we used in the numerical modeling (refer to Section 2.3.1).

Table 4-5 AR6 Report IPCC (2022) guidelines showing SLR used for numerical modeling

Horizon	RCP 4.5		RCP 8.5	
	Rate (mm/yr)	SLR (m)	Rate (mm/yr)	SLR (m)
20yr	5.7	0.114	6.6	0.132
50yr	7.7	0.385	10.5	0.525
100yr	7.7	0.770	10.5	1.05

4.4.6 Dynamic Surge

Wind Setup

As the wind blows over the water surface, it pushes water that piles up against the shoreline. The stronger the wind, the more energy is available to transfer, and the longer the wind blows the more time that is available for energy transfer. Wind set-up is minimal over shorter fetches; however, the

Bermudian coast is open to very long fetches. The wind speed and duration are critical factors affecting the storm surge value. This wind set-up component is shown in Figure 4.10.

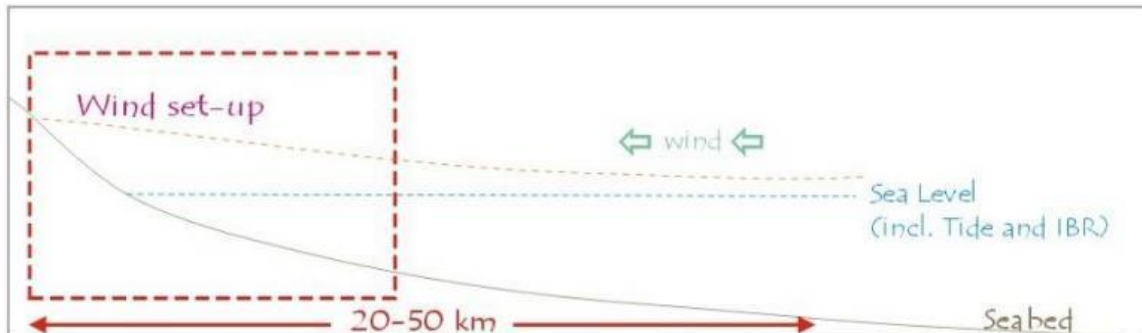


Figure 4.10 Sketch of the wind set-up component of storm surge

Wave Set-up and Wave Run-up

As waves approach the shoreline, they break and surge up a sloping surface, a phenomenon known as wave run-up, temporarily elevating water levels, particularly on inclining terrain. While vertical barriers like seawalls may deter run-up, they can also result in wave overtopping. This process occurs over a span of seconds and is typically calculated following the estimation of static storm surge values, as discussed in subsequent sections. It is important to note that numerical models often fail to fully account for wave run-up, potentially underestimating the total surge presented. The discrepancy between anecdotal reports of inundation levels and scientifically measured water levels during a storm can often be attributed to this difference between dynamic and static surge. People tend to report the highest water level reached, which may be consistently higher than the static water levels observed over longer periods. Therefore, vertical setback limits should consider dynamic surge factors.

The wind's force during a storm generates waves, with wave height in deep water being a crucial factor in predicting storm surge magnitude. Wave height not only influences wave breaking (wave set-up) but also determines the amount of wave energy available for surging onto land (wave run-up). Graphic illustrations of these components are depicted in Figures 4 11 and 4 12 below.

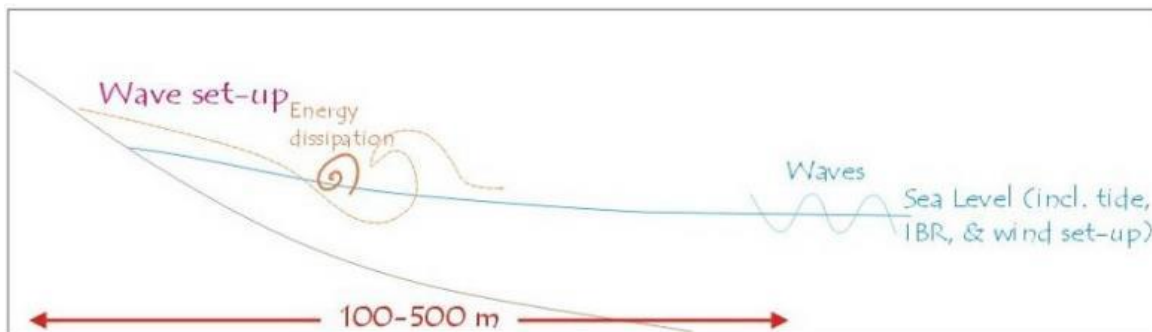


Figure 4.11 Sketch of the wave set-up component of storm surge

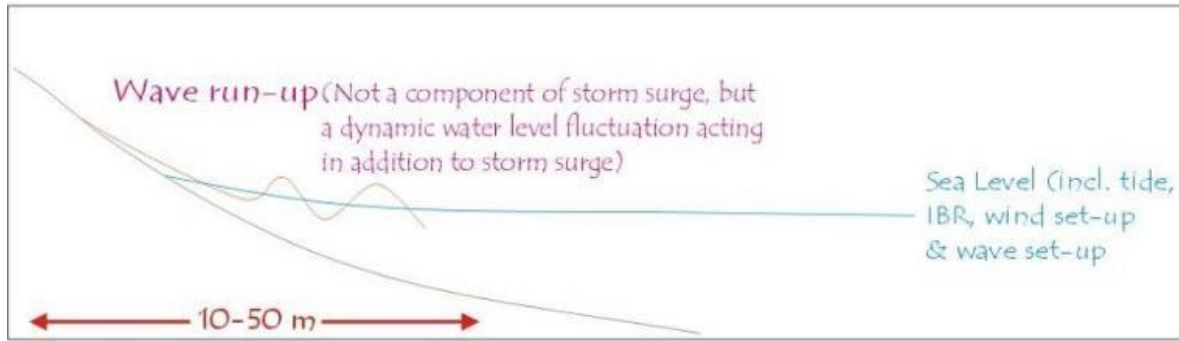


Figure 4.12 Sketch of the wave run-up component of storm surge

Table 4-6 and Table 4-7 provide calculated water levels for hurricane events of varying recurrence intervals under RCP 4.5 and RCP 8.5 scenarios, respectively.

Table 4-6 Calculation of water levels for 25, 50, 100 and 150-year hurricane returns periods for RCP 4.5

	Parameter	Return Period (years)				Notes	
		25	50	100	150		
Static Surge Components	IBR (m)	0.35	0.42	0.49	0.53	Determined through statistical hind-casting analysis	
	Highest Astronomical Tide (m)	0.84				Determined through historical analysis	
	Mean Rate of Sea Level Rise (mm/year)	5.7				RCP 4.5 Scenario value from IPCC AR6 research – see Table 4-5.	
	By year 2042 (20-yr horizon)	0.114					
	Mean Rate of Sea Level Rise (mm/year)	7.7					
	By year 2072 (50-year horizon)	0.385					
	Mean Rate of Sea Level Rise (mm/year)	7.7					
	By year 2122 (100-year horizon)	0.77					
	Total deep water surface level (m)		1.30	1.37	1.44	1.48	Sum of IBR, Highest Astronomical Tide, and Sea Level for 25-, 50-, 100- and 150-year return period event.
			1.57	1.64	1.71	1.75	
		1.96	2.03	2.10	2.14		
Mesoscale Eddies	0.48				Sum of IBR, Highest Astronomical Tide, Microscale Eddies, and Sea Level for 25-, 50-, 100- and 150-year return period event.		
Total deep water surface level (m)		1.78	1.85	1.92		1.96	
		2.05	2.12	2.19		2.23	
		2.44	2.51	2.58	2.62		
Dynamic Surge Components	Wind and Wave Setup	Based on wind speed and wave height, typically greater than 0.3m			To be computed using MIKE 21 HD and SW modules.		
	Wave Run-up	Wave run-up was not computed for this assessment					

Table 4-7 Calculation of water levels for 25, 50, 100 and 150-year hurricane returns periods for RCP 8.5

	Parameter	Return Period (years)				Notes	
		25	50	100	150		
Static Surge Components	IBR (m)	.35	0.42	0.49	0.53	Determined through statistical hind-casting analysis	
	Highest Astronomical Tide (m)	0.84					
	Mean Rate of Sea Level Rise (mm/year)	6.6					
	By year 2042 (20-yr horizon)	0.114					
	Mean Rate of Sea Level Rise (mm/year)	10.5					
	By year 2072 (50-year horizon)	0.385					
	Mean Rate of Sea Level Rise (mm/year)	10.5					
	By year 2122 (100-year horizon)	1.05					
	Total deep water surface level (m)	1.32	1.39	1.46	1.50		Sum of IBR, Highest Astronomical Tide, and Sea Level for 25-, 50-, 100- and 150-year return period event.
		1.72	1.79	1.86	1.90		
2.24		2.31	2.38	2.42			
Mesoscale Eddies	0.48				Sum of IBR, Highest Astronomical Tide, Microscale Eddies, and Sea Level for 25-, 50-, 100- and 150-year return period event.		
Total deep water surface level (m)	1.80	1.87	1.94	1.98			
	2.20	2.27	2.34	2.38			
		2.72	2.79	2.86	2.90		
Dynamic Surge Components	Wave Setup	Based on wind speed and wave height, typically greater than 0.3m			To be computed using MIKE 21 HD and SW modules.		
	Wave Run-up	Wave run-up was not computed for this assessment					

5 Nearshore Hurricane Waves and Water Levels

The MIKE 21 software, using both its SW (Surface Wave) and HD (Hydrodynamic) modules, conducted simulations of nearshore hurricane wave and water level conditions along Bermuda's coast through a coupled mode, allowing for the simulation of the interplay between waves and currents. This coupling between hydrodynamics and wave action is crucial for accurate storm surge predictions, especially in areas where wave setup significantly contributes to the overall storm surge. As substantial waves break in shallow waters or against a reef, they elevate the water level and generate localized currents. These currents, along with the altered water levels, enable waves to reach further inland.

For the analysis of Bermuda's coastline, eight directional sector scenarios were examined: east, northeast, north, northwest, west, southeast, south, and southwest. These scenarios were integrated with conditions derived from deep-water wave models for return periods of 25, 50, 100, and 150 years. The outcomes from the wave transformation modeling under various hurricane conditions are detailed in the following sections.

5.1 Present Day Conditions

In the present-day conditions, the influence of sea level rise was not considered. The results are shown in Figure 5.1 and Figure 5.2 following. Without the effects of climate change, the following was observed:

- The reef effectively protected the north shore from hurricane waves. The rim reef at the north reduced wave heights from 10m to approximately 2m at the north shore.
- Despite this reduction, significant wave heights between 1-2m affect the shoreline on the north coast under the 25-year return period event. Under the 150-year event, the wave heights on the north shore are 2-3m. These wave conditions will have significant wave run-up potential.
- Unlike the north shore, the south shore does not have protection from the reefs. As a result, the wave heights immediately offshore are 8-10m in height during a hurricane.
- The storm surge levels are less than 1.2m on the north shore, while along the south shore, the surge levels are greater than 1.6m.

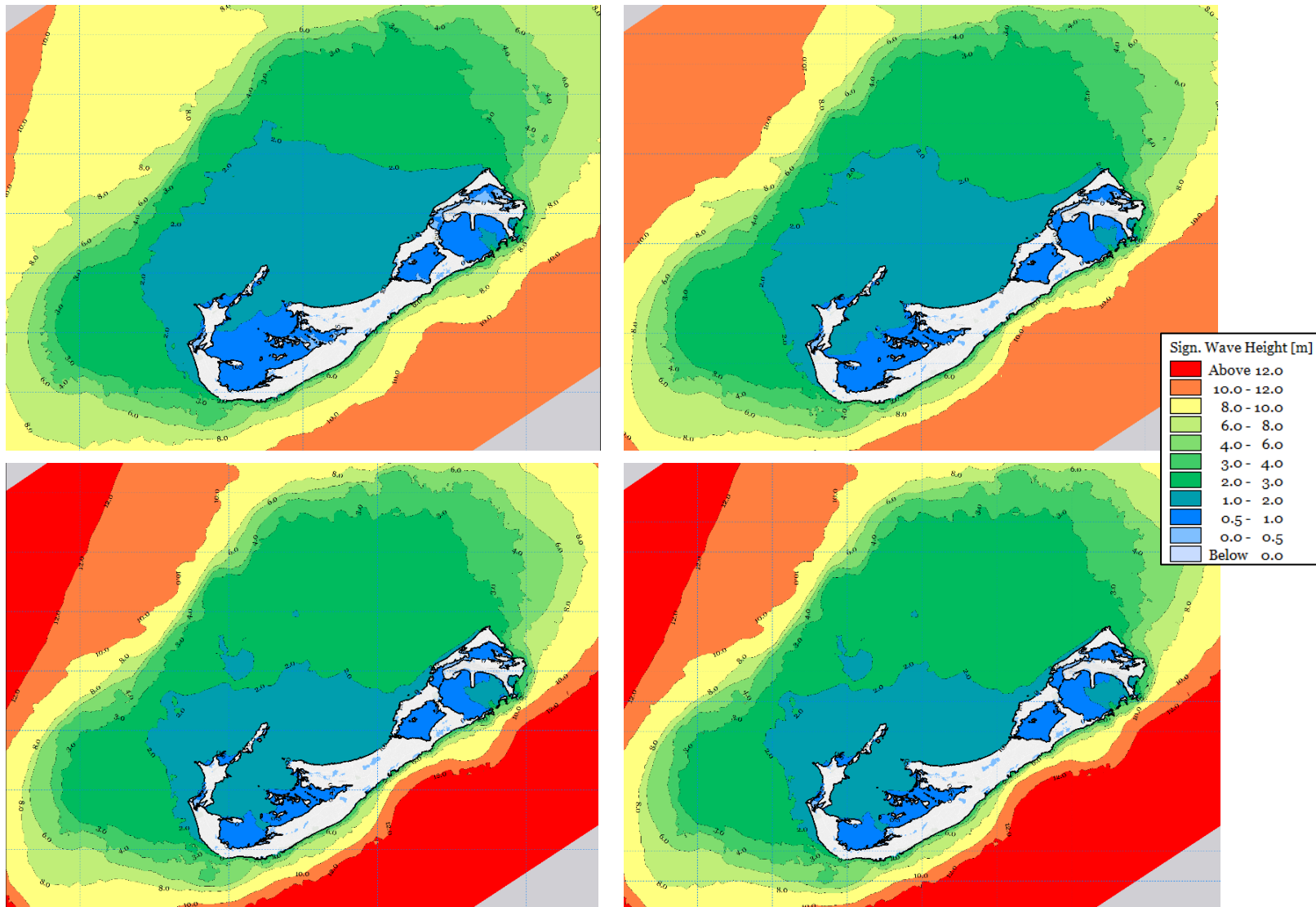


Figure 5.1 Hurricane wave heights computed for the 25-yr, 50-yr, 100-yr and 150-yr return period without the effect of SLR

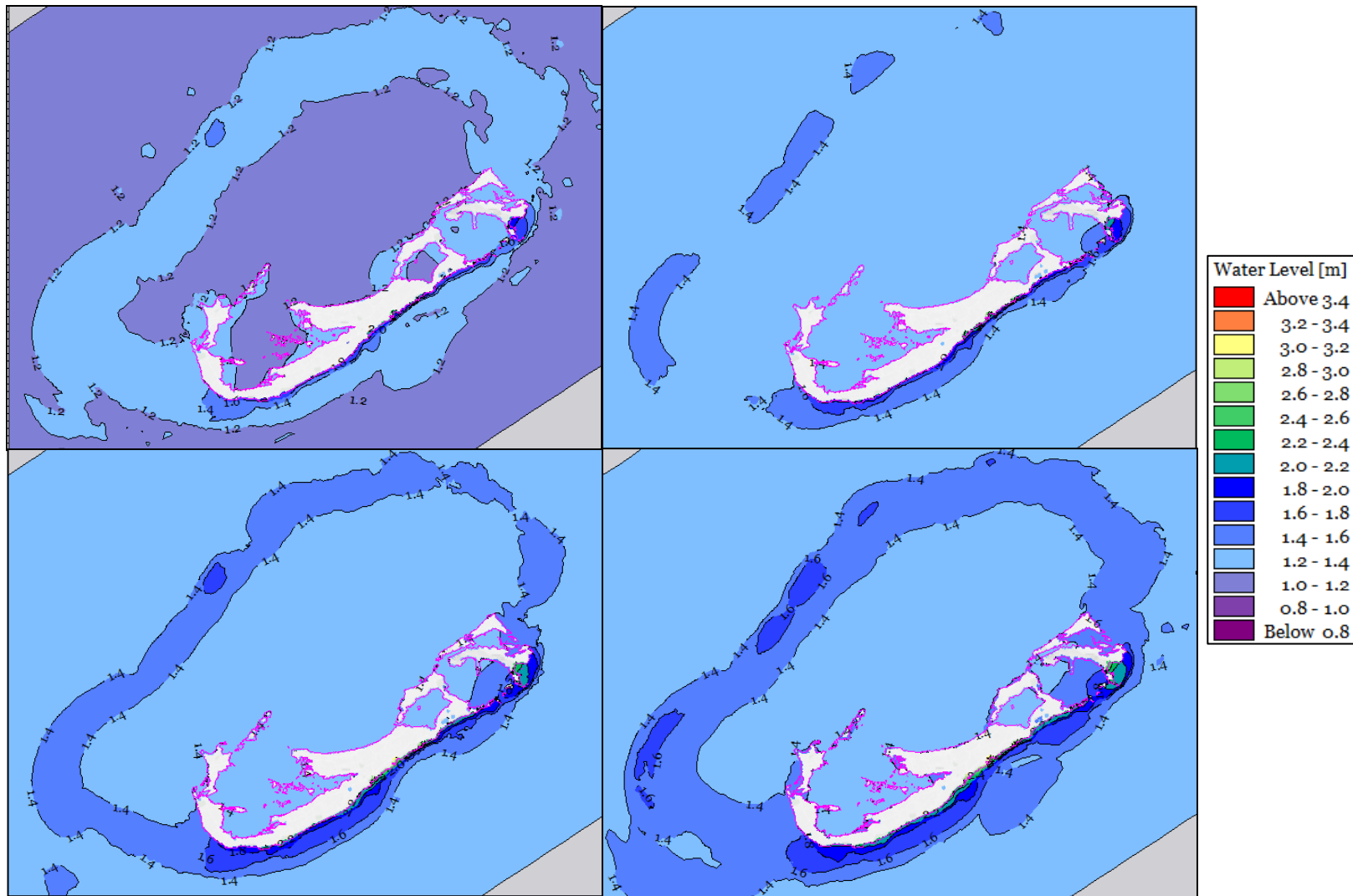


Figure 5.2 Storm surge computed for the 25-yr, 50-yr, 100-yr and 150-yr return period without the effect of SLR

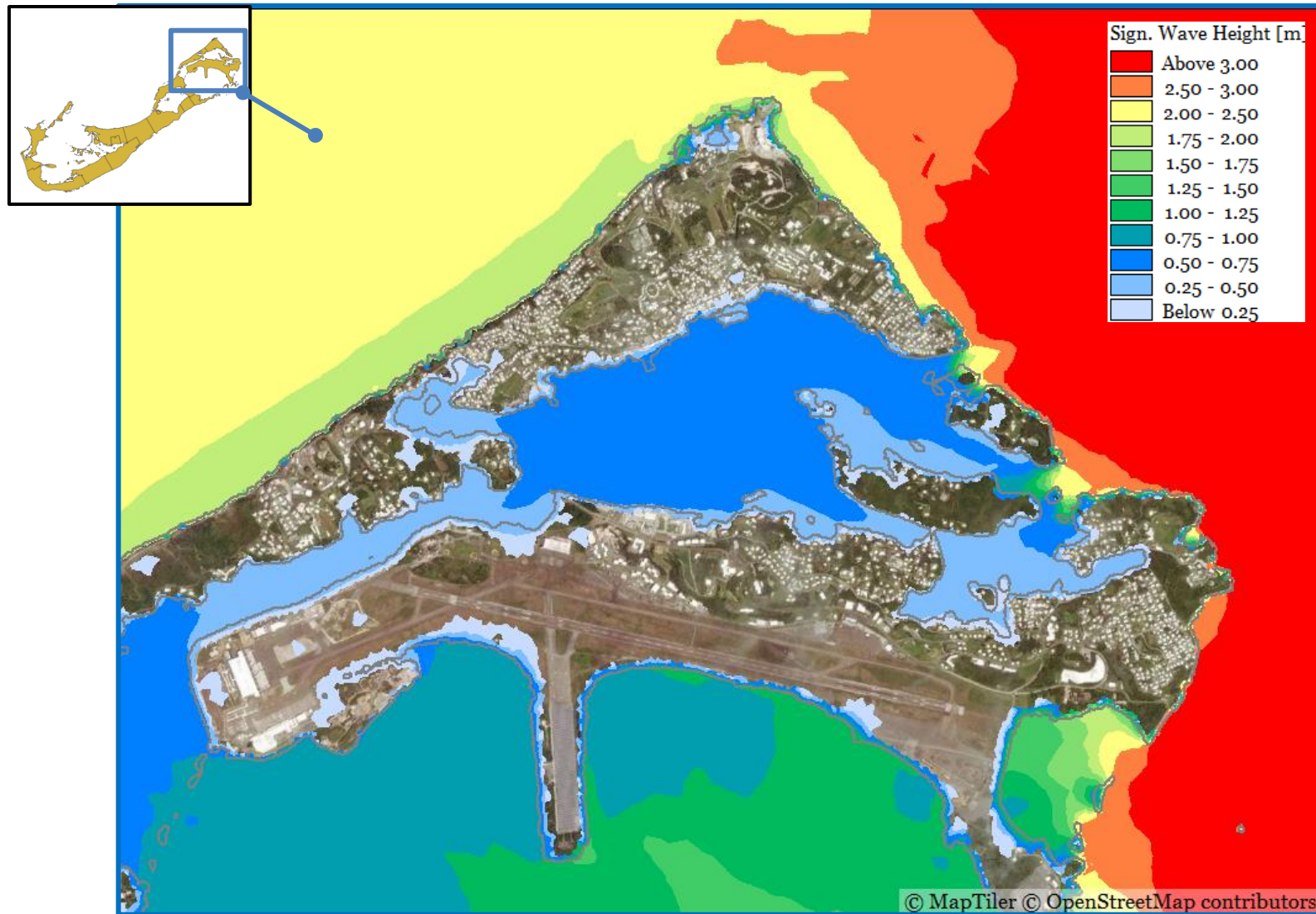


Figure 5.3 Computed hurricane wave height for Castle Harbour and the Town of St George's for the 150-Year Return Period

5.2 Hurricane Conditions under the RCP 4.5 and RCP 8.5 Scenarios

Based on the historical storm analysis, hurricane conditions (combination of a significant wave height, wave period, wind speed, and the inverse barometer rise) were computed for return periods (RP) of 1 in 25, 50, 100, and 150 years. The effects of sea level rise due to climate change on these conditions were examined using the mild (RCP 4.5) and extreme (RCP 8.5) scenarios in three-time horizons: 20 years (~2042), 50 years (~2072) and 100 years (~2122). This resulted in a total of 24 scenarios summarized in Table 5-1.

Figure 5.4 to Figure 5.7 present the 100-year time horizon conditions for the RCP 4.5 and 8.5 scenarios for the return periods 25-year, 50-year, 100-year and 150-year. Appendix E contains the other simulation results.

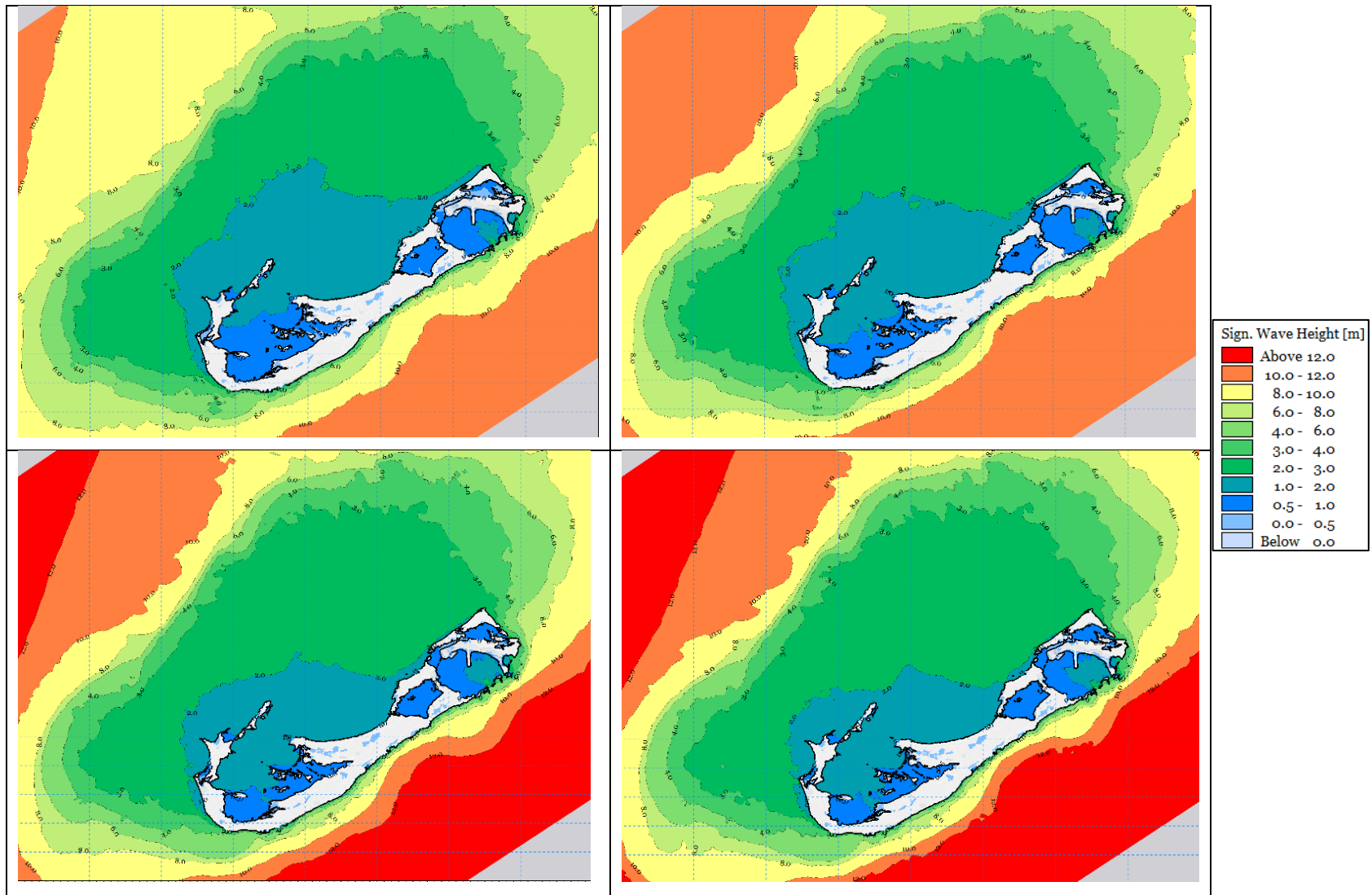


Figure 5.4 RCP 4.5 100-year horizon hurricane wave heights computed for the 25-yr, 50-yr, 100-yr and 150-yr return period with the effect of SLR

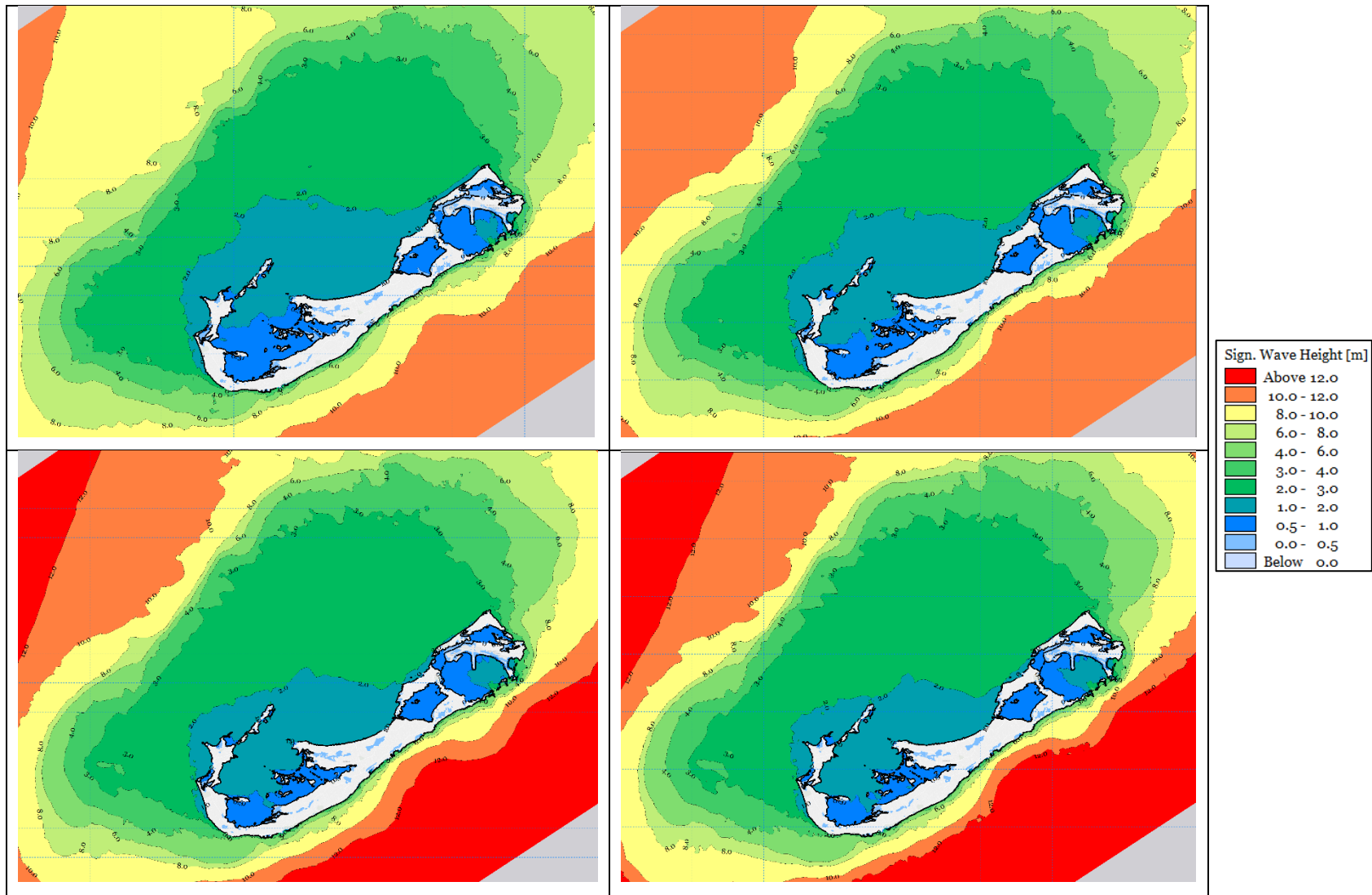


Figure 5.5 RCP 8.5 100-year horizon hurricane wave heights computed for the 25-yr, 50-yr, 100-yr and 150-yr return period with the effect of SLR

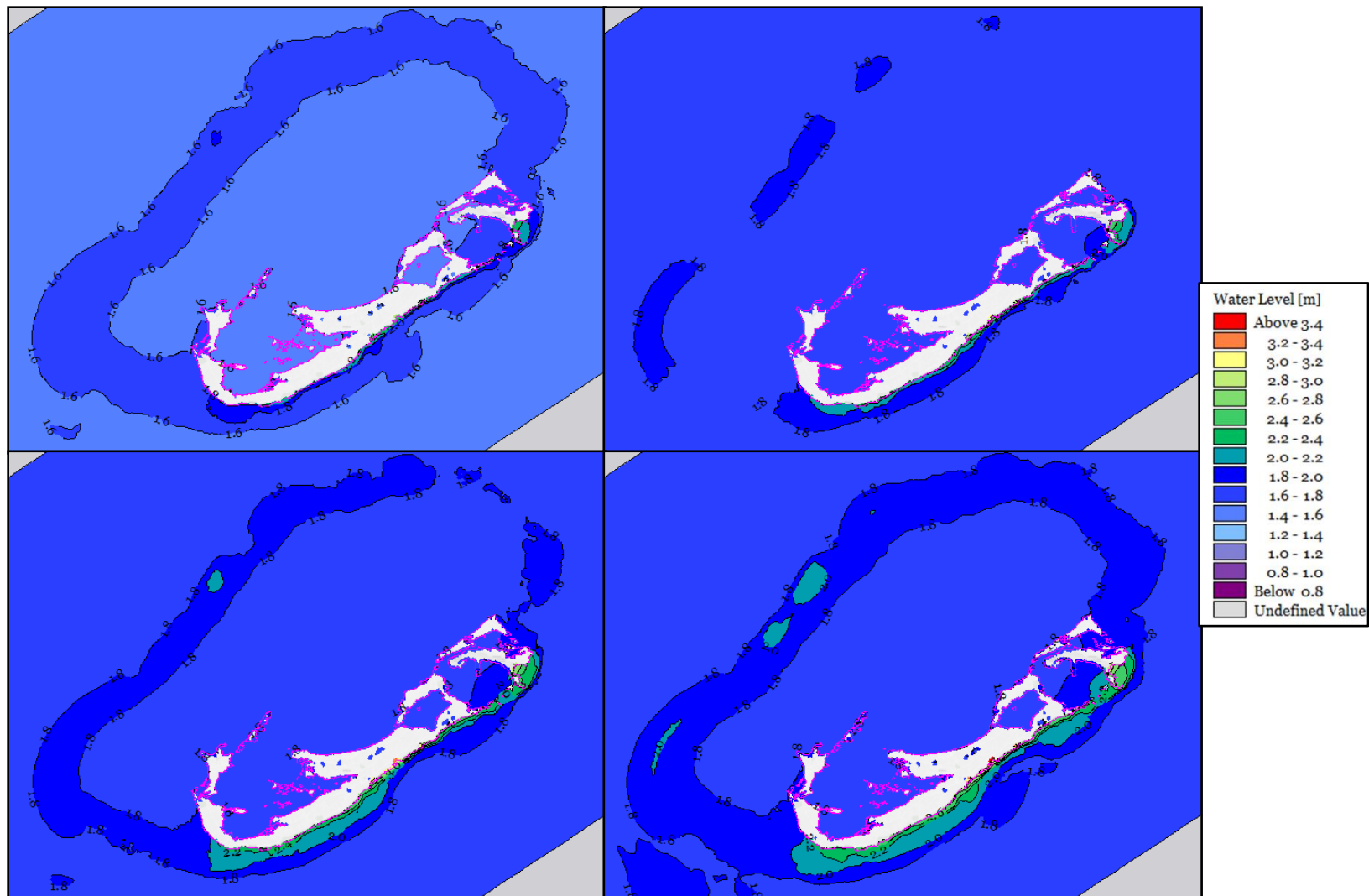


Figure 5.6 RCP 4.5 100-year horizon storm surge computed for the 25-yr, 50-yr, 100-yr and 150-yr return period with the effect of SLR

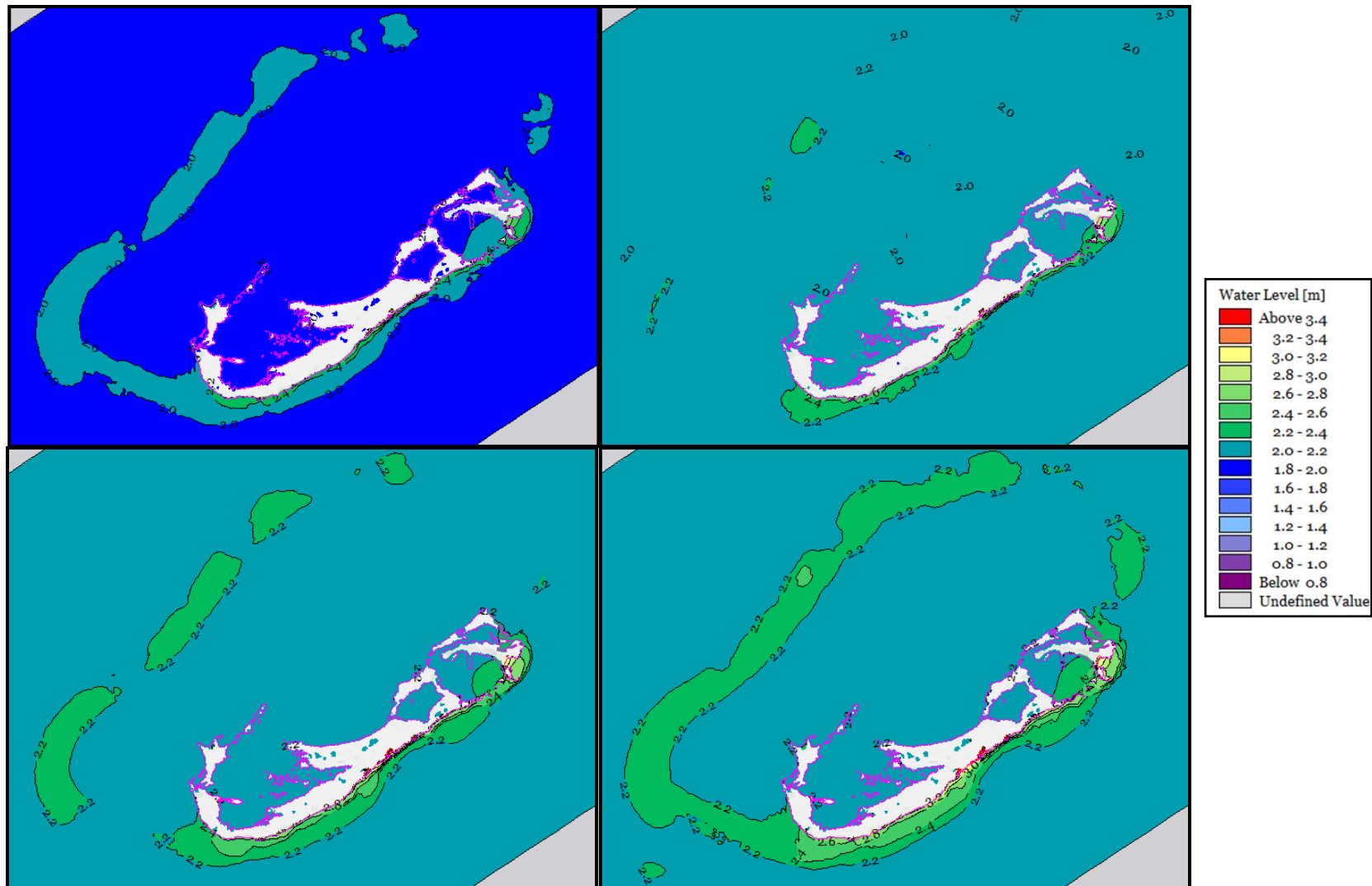


Figure 5.7 RCP 8.5 100-year horizon storm surge computed for the 25-yr, 50-yr, 100-yr and 150-yr return period with the effect of SLR

The differences between storm scenarios and the effects these various scenarios have on the wave and surge conditions is best described through tabulation of five comparison points around Bermuda (Figure 5.8).

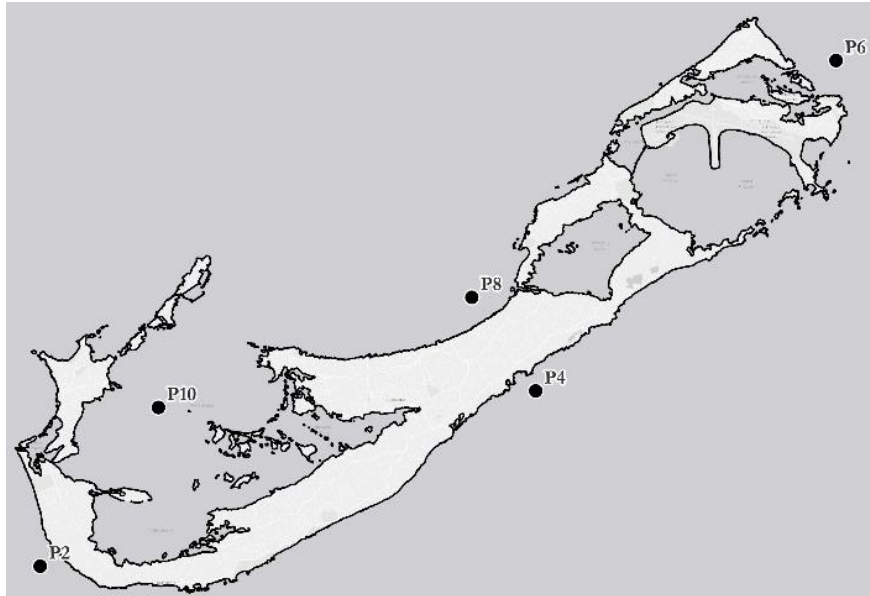


Figure 5.8 Comparison points for hurricane scenarios

Table 5-1 shows the “present day” wave heights for various return period storm events, along with the percentage increase in wave heights for the 25-, 50-, 100-, and 150-year return period storms for the locations shown in Figure 5.8.

The results show that the north shore is comparatively more vulnerable to sea level rise as the reef becomes less effective with greater water depths. This causes storm waves to get to the north shore and by extension the Great Sound area. For example, under the 100-year return period in an RCP 8.5 scenario, areas previously protected by the reef (P2, P8 and P10) will see increases in wave heights of 5.3% to 14.1%.

Table 5-1 Comparison of points along the Bermudian shoreline (significant wave heights)

South West P2	South P4	North East P6	North P8	Great Sound P10	Scenario	
2.86	7.96	4.94	1.40	0.96	Present	25yr Return Period
1.5%	0.3%	0.6%	1.0%	0.5%	4.5 20yr	
1.8%	0.4%	0.7%	1.2%	0.6%	8.5 20yr	
5.4%	1.1%	2.2%	3.6%	1.9%	4.5 50yr	
7.3%	1.5%	3.0%	5.0%	2.6%	8.5 50yr	
10.6%	2.2%	4.4%	7.4%	3.8%	4.5 100yr	
14.5%	2.9%	5.9%	10.4%	5.2%	8.5 100yr	
2.95	8.50	5.15	1.50	1.07	Present	50yr Return Period
1.5%	0.4%	0.7%	0.9%	0.5%	4.5 20yr	
1.8%	0.4%	0.8%	1.0%	0.6%	8.5 20yr	
5.3%	1.3%	2.3%	3.2%	1.9%	4.5 50yr	
7.2%	1.7%	3.1%	4.3%	2.6%	8.5 50yr	
10.5%	2.4%	4.5%	6.5%	3.8%	4.5 100yr	
14.4%	3.3%	6.2%	9.1%	5.2%	8.5 100yr	
3.04	8.94	5.32	1.59	1.17	Present	100yr Return Period
1.5%	0.4%	0.7%	0.8%	0.5%	4.5 20yr	
1.8%	0.5%	0.8%	0.9%	0.6%	8.5 20yr	
5.3%	1.3%	2.4%	2.8%	1.9%	4.5 50yr	
7.1%	1.8%	3.2%	3.9%	2.6%	8.5 50yr	
10.4%	2.6%	4.7%	5.8%	3.8%	4.5 100yr	
14.2%	3.5%	6.3%	8.1%	5.3%	8.5 100yr	
3.09	9.17	5.40	1.65	1.22	Present	150yr Return Period
1.5%	0.4%	0.7%	0.7%	0.5%	4.5 20yr	
1.7%	0.5%	0.8%	0.8%	0.6%	8.5 20yr	
5.2%	1.4%	2.4%	2.6%	1.9%	4.5 50yr	
7.1%	1.9%	3.2%	3.6%	2.6%	8.5 50yr	
10.3%	2.7%	4.7%	5.4%	3.8%	4.5 100yr	
14.1%	3.6%	6.4%	7.6%	5.3%	8.5 100yr	

5.3 Hurricane Conditions under the RCP 4.5 and RCP 8.5 (Consideration for Mesoscale Eddies)

The third wave/surge modeling assessment included the effect of a cyclone affecting Bermuda while there are mesoscale eddies concurrently affecting the local area (presented in Section 4). The maximum mesoscale eddy obtained from the earlier analysis resulted in the addition of 0.48m to the input water level. This would cause significantly more flooding when combined with hurricanes.

The results of this assessment are shown below (Figure 5.9 to Figure 5.13) for the RCP 4.5 and 8.5 in the next 100 years. The key vulnerable areas previously identified are more evident, namely:

- The town of St George’s;
- The airport;
- Dockyards;
- Castle Harbour; and
- The islands of the Great Sound

As expected, more areas are flooded, and the highest flood levels increased to 3.0-3.6m for the 100-year horizon. These values are seen along the south shore.

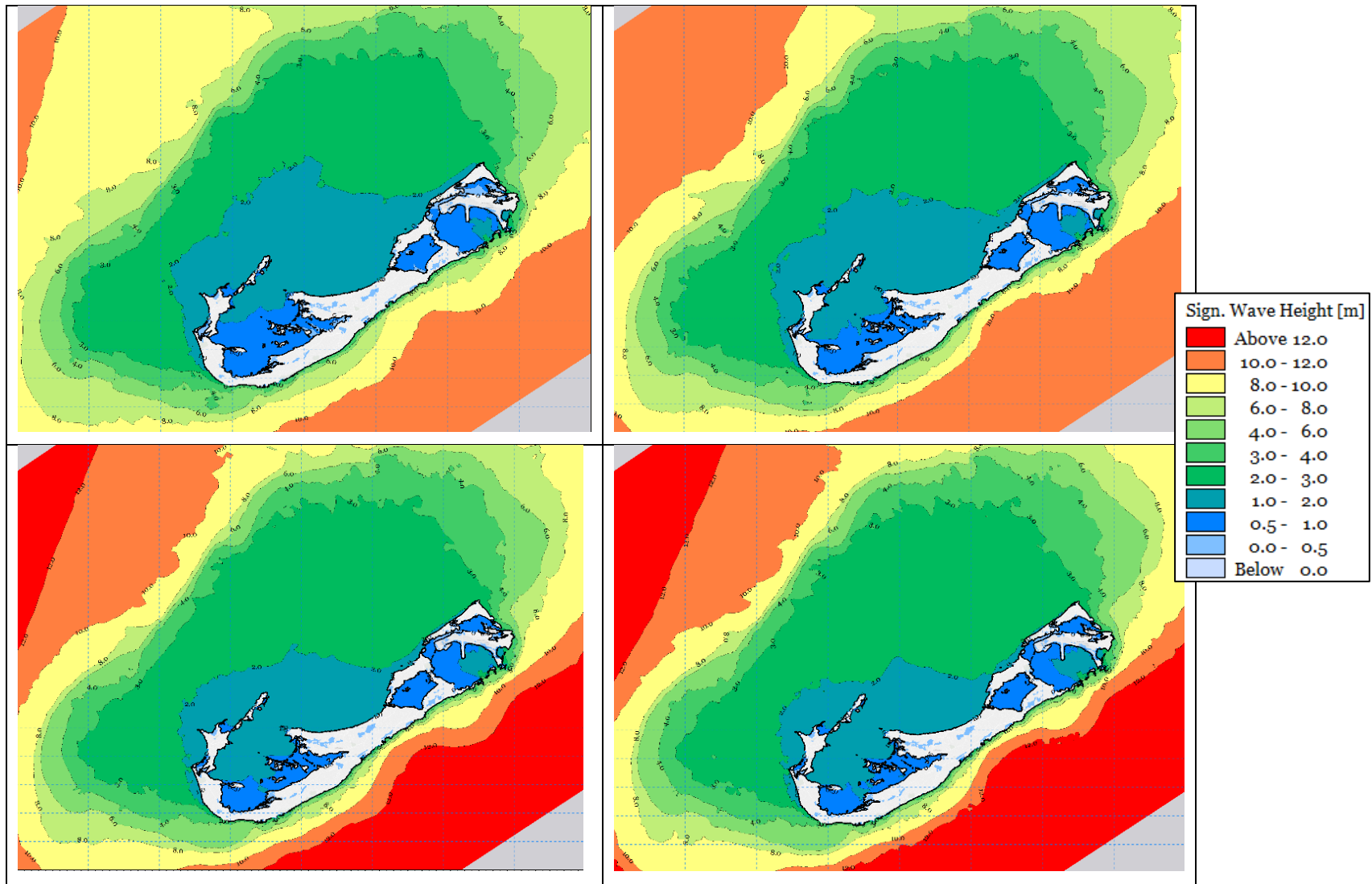


Figure 5.9 RCP 4.5 100-year horizon hurricane wave heights computed for the 25-yr, 50-yr, 100-yr and 150-yr return period with the effect of SLR and positive local effects like mesoscale eddies

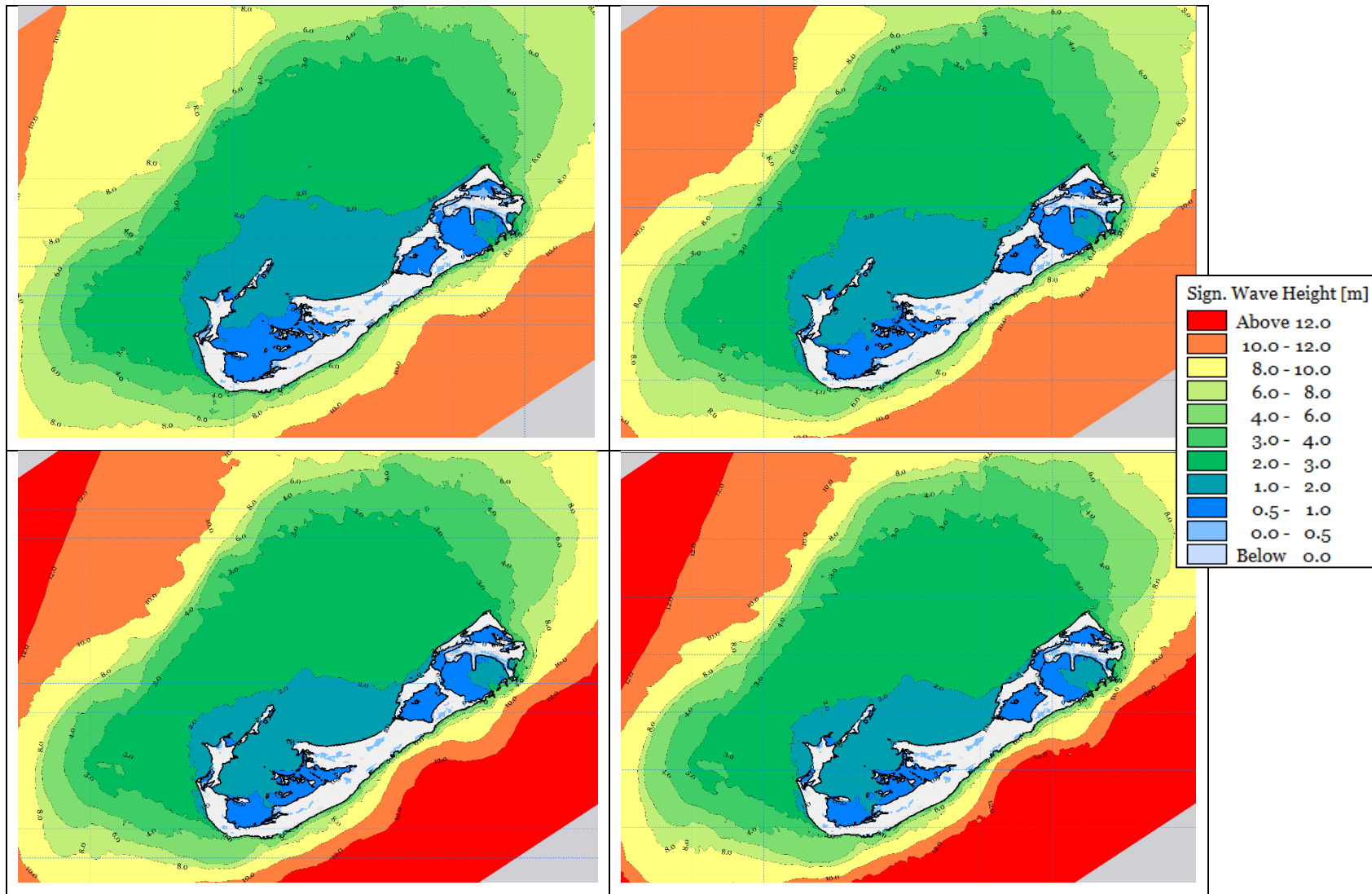


Figure 5.10 RCP 8.5 100-year horizon hurricane wave heights computed for the 25-yr, 50-yr, 100-yr and 150-yr return period with the effect of SLR and positive local effects like mesoscale eddies

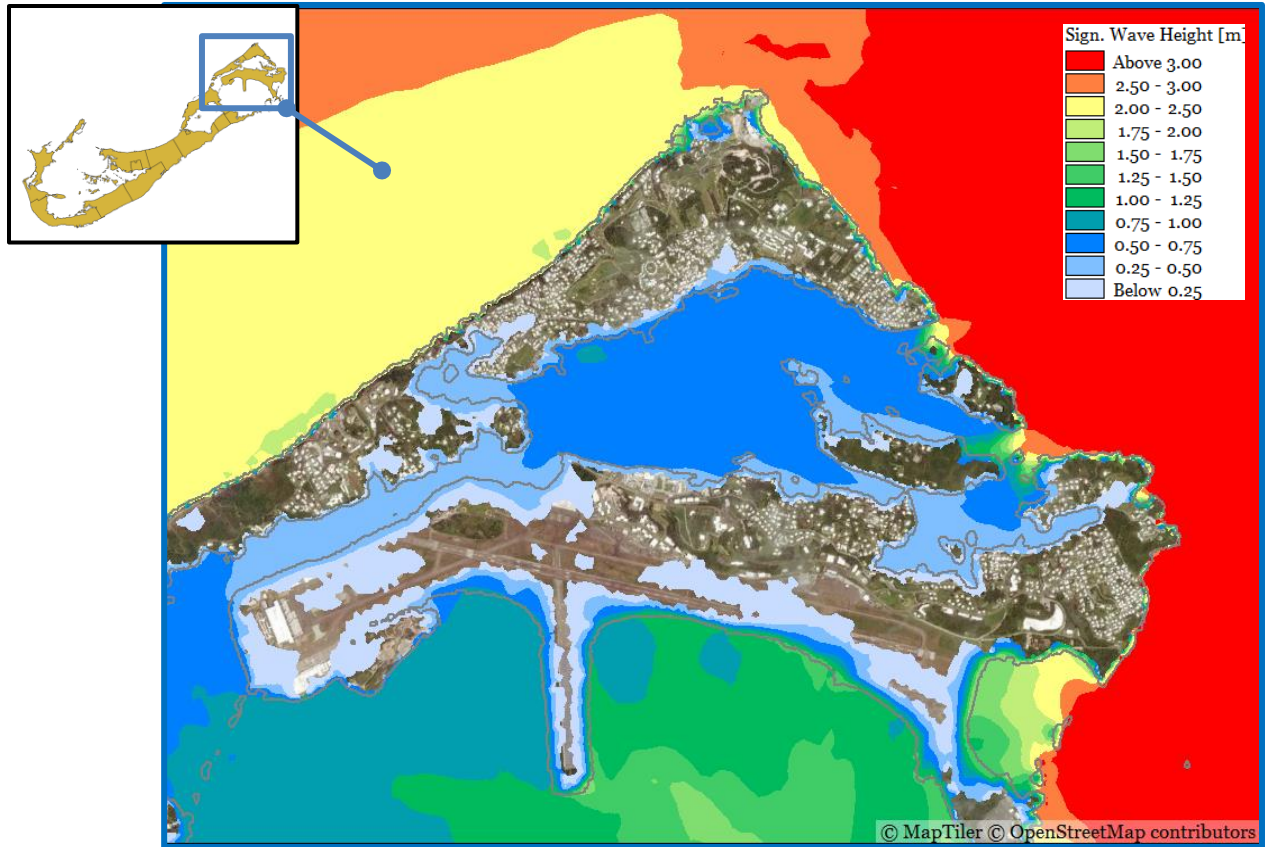


Figure 5.11 Computed hurricane wave heights for Castle Harbour and the Town of St George's for the 150-year return period considering the RCP 8.5 100yr horizon.

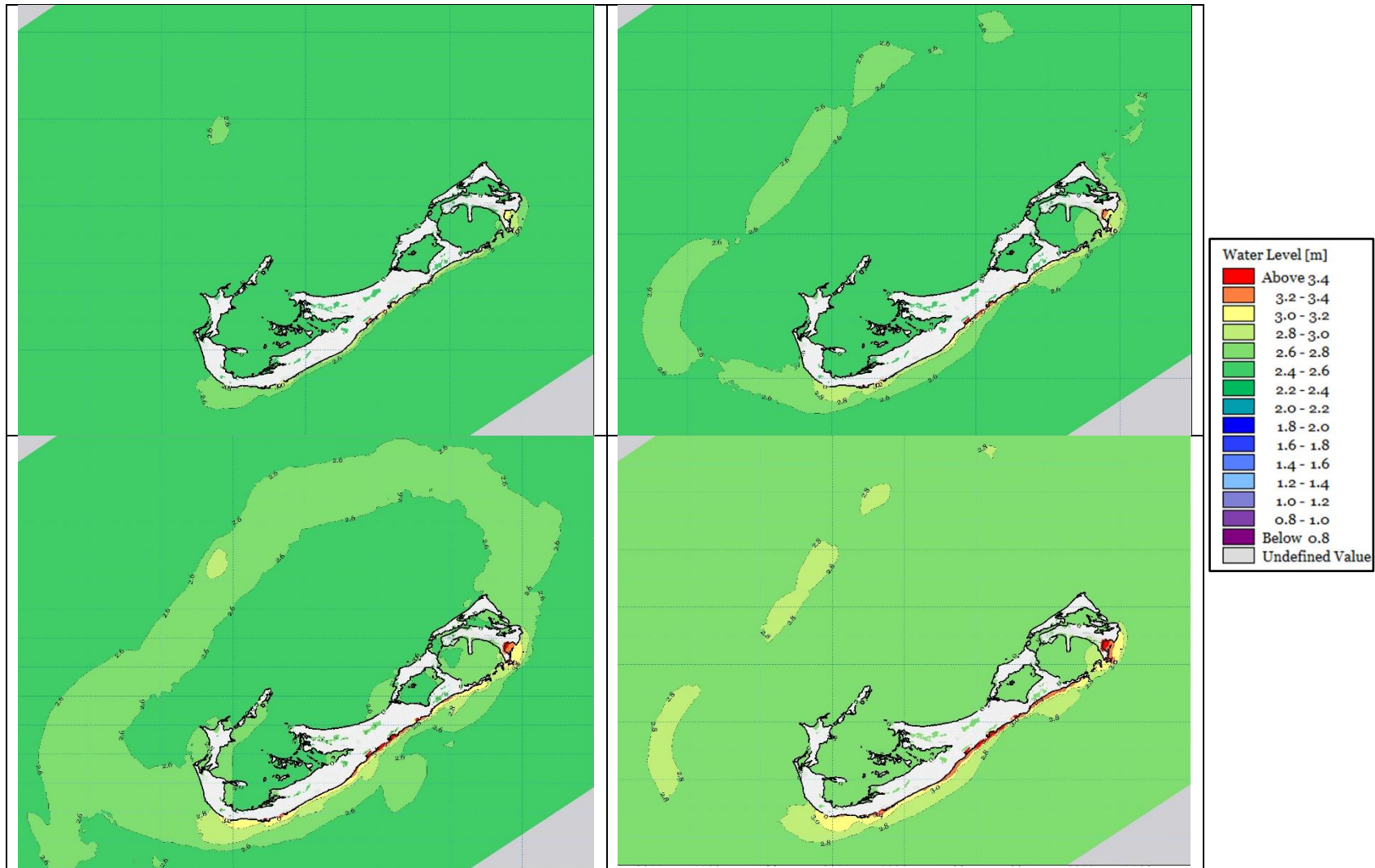


Figure 5.12 RCP 4.5 100-year horizon water levels computed for the 25-yr, 50-yr, 100-yr and 150-yr return period with the effect of SLR and positive local effects like mesoscale eddies

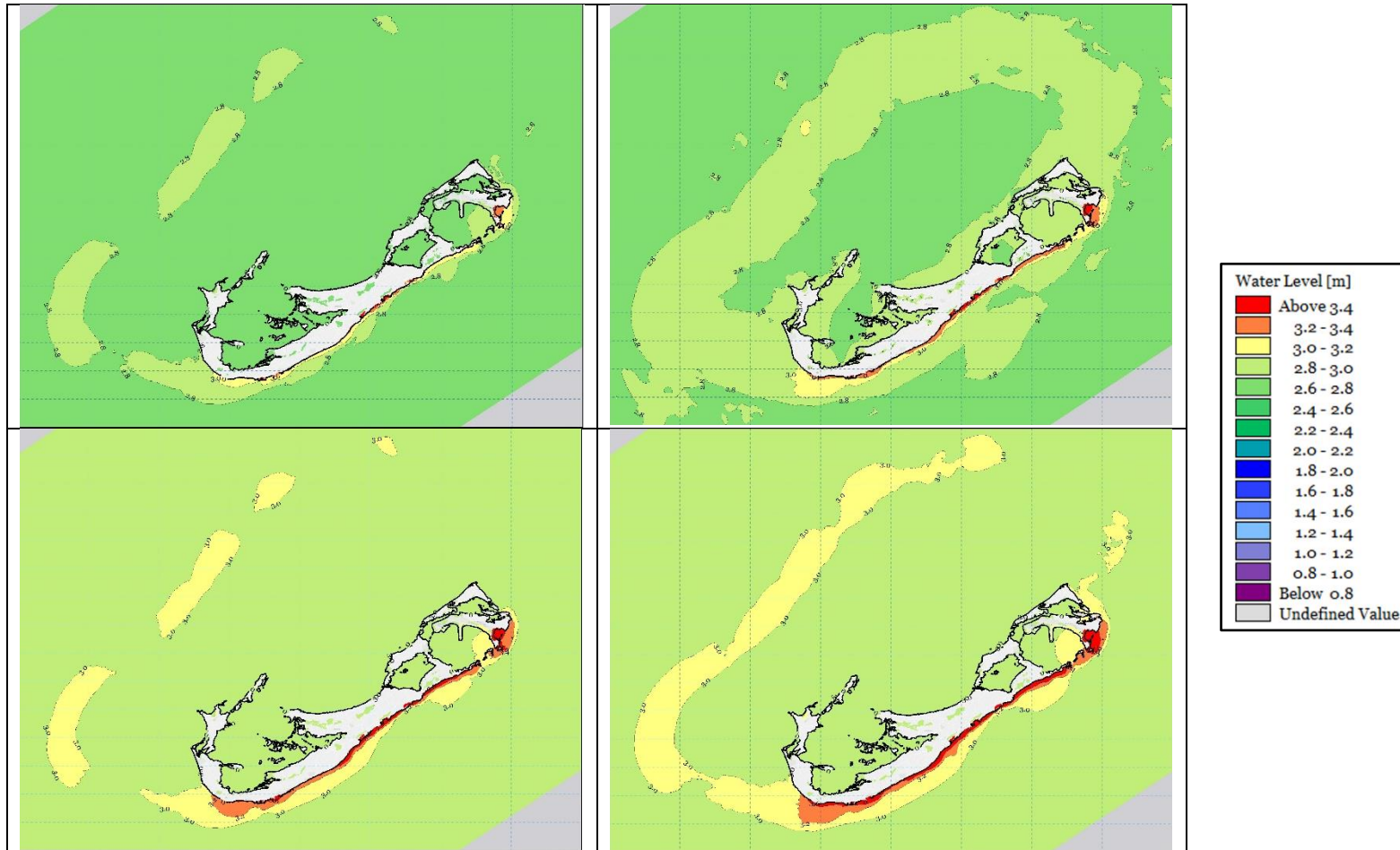


Figure 5.13 RCP 8.5 100-year horizon water levels computed for the 25-yr, 50-yr, 100-yr and 150-yr return period with the effect of SLR and positive local effects like mesoscale eddies

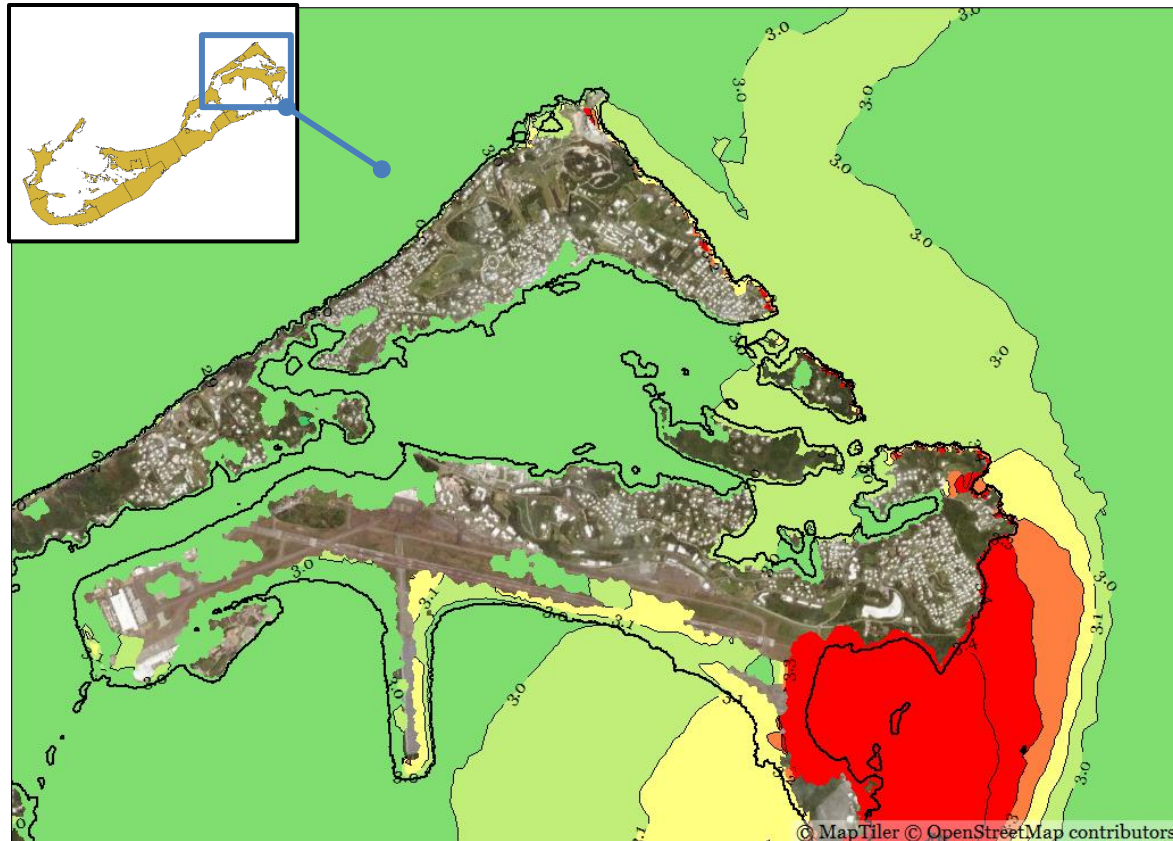


Figure 5.14 Computed storm surge for Castle Harbour and the Town of St Georges for the 150-year return period considering the RCP 8.5 100yr horizon

5.4 Change in Wind Speeds and Storm Intensity

From the available body of literature, the following changes related to future intensity and frequency of hurricane occurrences are noted:

- The number of hurricanes experienced in a given season is likely to decrease or remain unchanged in the future. Zhang, et al. (2019) for instance found an inversely proportional historical relationship between tropical cyclone frequencies and sea surface temperature (SST). That is, tropical cyclone activity decreased with an increase in the warmth of pools in which they form. This is with high confidence (tests of 90-99.9% for the respective pools). Storms in moderate pools (65th-90th percentile) decreased by 0.79 storms/decade and in the warm pools (>90th percentile) by 1.08 storms/decade. The suggestion is that with increases in future temperatures there may be reduced overall hurricane frequency in the future. These results are echoed in other reports such as the CSGM 2017 report (2017), the IPCC 2012 Special Report on Extremes (IPCC 2012) and Knutson et al. (2013).
- The effects of climate change from external forcing (e.g. greenhouse gases, aerosols, and volcanic eruptions) on tropical storm activity (over 1980 to 2018) is more evident in changes in spatial occurrence, rather than overall frequency of occurrence [Murakami et al (2020)].

Through observations and statistical analysis, the authors have determined that an increase in frequency in the North Atlantic, central Pacific and Arabian Sea is somewhat balanced by a corresponding decrease in the southern Indian Ocean, tropical western North Pacific, and South Pacific such that there is little net change in global frequency. The climate models employed do indicate a decreasing trend in the number of tropical storms in the North Atlantic resulting from increases in CO₂ concentrations (assuming no volcanic eruptions).

- As noted earlier, the Atlantic Multidecadal Oscillation (AMO), which is evidenced by periodic warming of the waters of the North Atlantic, appears to affect tropical storm events, in that positive phases of the AMO produces more tropical storms than the negative phase (Landsea, Vecchi, Bengtsson, & Knutson, 2010). A positive phase of the AMO commenced circa 2000.
- Hallam et al (2021) correlated an increase in tropical storm activity and intensity in Bermuda waters (between 1955 to 2019) to an increase in the sea surface and average ocean temperatures. The tropical storms analysed showed a more easterly genesis of tracks for 2000-2019 (positive AMO) as compared to 1980-1999 (negative AMO) and suggest this is related to increase in measured sea temperatures. These hurricanes that are spawned further east in the North Atlantic eventually hit Bermuda with marked ferocity. The authors compute that the maximum wind speeds for hurricanes in Bermuda have increased 30 knots from 1955 to 2019, and measure an average increase of 7.7 knots/decade from 1980 to 2009.
- The number of higher category hurricanes are likely to increase in the future. Studies (Bhatia et al., 2018, Bender et al., 2018 and Knutson et al., 2013) have shown an increasing trend in major Atlantic hurricanes. Bhatia et al. (2018) projected a 72.9 and 135.5 % increase in category 4 and 5 hurricanes respectively by end of the century under RCP 4.5. Bender et al. (2010) and Knutson et al. (2013) presented combined category 4 and 5 percentage increases of 100% and 40% respectively.
- Maximum wind speeds associated with hurricanes are likely to increase in the future as temperature increases (Trepanier 2020). For Bermuda, this rate is from 1 to 1.5 ms⁻¹ per °C. This implies an increase from current wind speeds by as much as 1.1ms⁻¹, 2.3ms⁻¹ and 3.5ms⁻¹ in the near-, medium- and long-term future respectively under RCP 8.5.

The aim of this assessment is to provide some context on how the values for waves heights under different return periods could change. For this assessment, we took the following steps.

- *Step 1* - All hurricanes passing within 300km of the site were extracted and the track information edited. All the tracks in the database were increased in magnitude based on the projected increase from the literature, that is 1.1ms⁻¹, 2.3ms⁻¹ and 3.5ms⁻¹ for the 20-year, 50-year and 100-year horizons.
- *Step 2* - All hurricanes passing with 300km were reassessed. The *Climate Profile and Projections for the Island of Bermuda* (Appendix A) proposes that the number of the number of storms Category 0 – 3 will decrease by 0.79 storms per decade while the stronger will increase by 1.08 storms per decade. Using this information, the hurricane track dataset was edited at random, to remove and include storms to select storms to create a new hurricane database (Figure 5.15).
- Once two datasets were created, the statistical analysis was performed to obtain the parameters for the return periods as shown in Table 5-2 below.

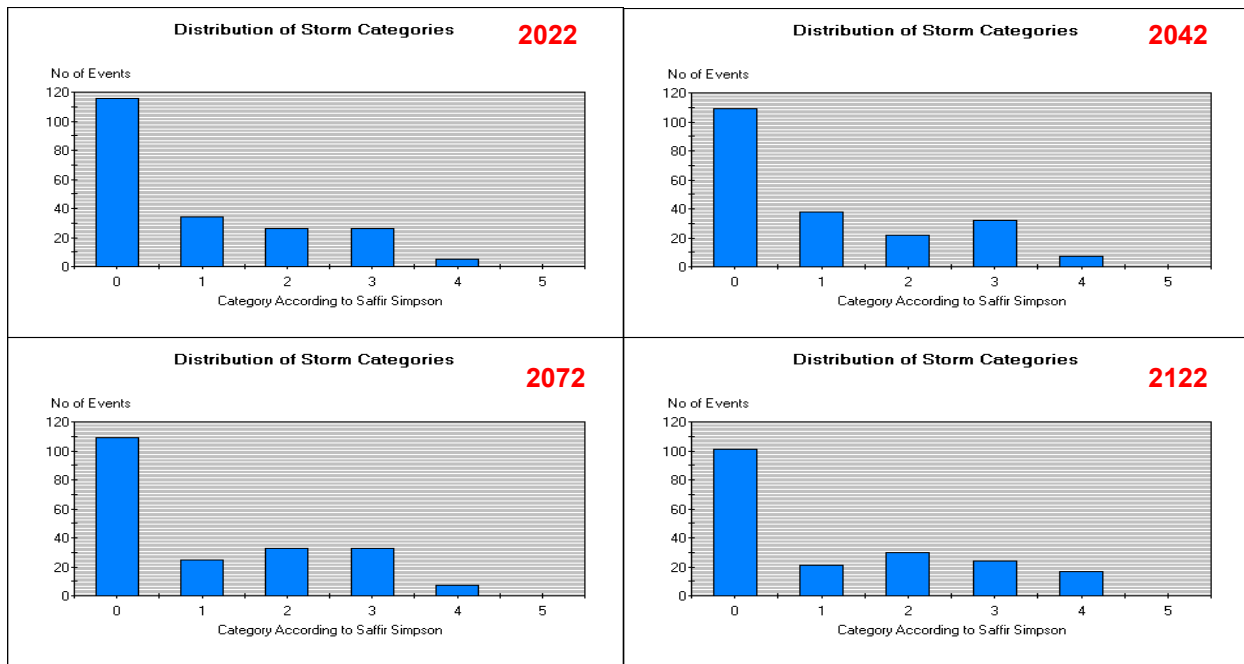


Figure 5.15 Distribution of storm categories

Table 5-2 Change in significant wave heights and wind speeds

		Wave and Windspeeds Due to the Expected Increase in Wind Speeds from to Climate Change						Wave and Windspeeds due to the expected increase in Wind Speeds and Change in Storm Intensity						
		PRESENT DAY		2042		2072		2122		2042		2072		2122
Return Period	Vs (m/s)	Hs (m)	Vs (m/s)	Hs (m)	Vs (m/s)	Hs (m)	Vs (m/s)	Hs (m)	Vs (m/s)	Hs (m)	Vs (m/s)	Hs (m)	Vs (m/s)	Hs (m)
5	22.62	8.9	1.33	1.12	2.92	2.25	4.55	3.37	1.95	1.42	4.33	3.37	4.24	5.62
10	27.74	10.5	1.15	1.90	2.60	2.86	4.15	4.76	1.66	1.54	3.79	3.81	4.22	6.67
25	33.62	12.4	1.01	1.61	2.35	3.23	3.81	4.03	1.46	1.31	3.33	3.23	4.10	6.45
50	37.59	13.7	0.96	1.46	2.23	2.92	3.67	4.38	1.38	1.26	3.14	2.92	4.07	6.57
100	41.27	14.9	0.90	1.34	2.13	2.68	3.56	4.03	1.31	1.14	2.98	2.68	4.00	6.04
150	43.31	15.6	0.88	1.28	2.08	2.56	3.49	3.85	1.27	1.18	2.91	2.56	3.95	5.77
200	44.71	16	0.85	1.25	2.06	2.50	3.44	3.75	1.25	1.02	2.86	2.50	3.91	6.25

With stronger storms, the offshore wave heights for shorter return periods have increased. Therefore, in the future, it can be expected that the 1 in 25-year and 50-year events will be stronger. This has implications for the design of coastal protection measures. In the Caribbean, for example, developers

typically choose the 1 in 50-year event to protect their assets. Under these changing conditions, within the next 20 years, the 1 in 50-year design wave height could be increased by up to 1.46%. The design values would have to be increased accordingly. Additionally, this may have implications for the design guidance set by Bermuda's Department of Planning.

The impact of an increase in wave conditions at the boundaries of the mesh, will mean more higher waves at the shorelines. That is to say, the 1.26-1.46% increase in the wave heights offshore will result in an approximately 5% increase in wave heights at the shoreline. This is an argument for recommending design parameters for more intense events, for example the 1 in 150-year storm.

6 Compound Flooding Analysis – Combined Surge and Rainfall effects in Mill Creek/Pembroke Marsh

In the context of coastal flooding, compound flooding analysis focuses on the interacting effects of multiple flood drivers, particularly storm surge and rainfall. This analysis is crucial because the combined impact of these factors can be significantly greater than the sum of their individual effects. By understanding how storm surge and rainfall interact, we can improve flood risk assessment, planning, and mitigation strategies, leading to increased preparedness and resilience.

This section outlines the approach to assess compound flooding risks in the Mill Creek/Pembroke Marsh vicinity, through application of the storm surge results obtained from the MIKE21 model (previously discussed) with integration of rainfall data within a separate modeling platform.

The Mill Creek and Pembroke Marsh catchment is recognized as one of the most vulnerable areas in Bermuda to rainfall-induced flooding due to several key factors:

- **Low-lying terrain:** The catchment area sits at a low elevation, making it susceptible to inundation during heavy rainfall events.
- **Seaward drainage:** Runoff from the marsh area naturally flows towards the sea, eventually discharging into the open ocean.
- **Storm surge amplification:** Previous storm surge modeling (MIKE21 results) have already demonstrated the amplifying effect of surge events traveling upstream along Mill Creek. Combining this data with rainfall predictions will likely extend the projected flood inundation zones.
- **Critical infrastructure at risk:** The catchment is unfortunately home to critical industries located along the stream, further highlighting the potential consequences of severe flooding events.

For these compelling reasons, the Mill Creek catchment will serve as a case study to demonstrate the potential impacts of compound flooding (combined storm surge and rainfall) in Bermuda. By analyzing this specific location, valuable insights can be gained and applied to broader flood risk management strategies across the island.

A comprehensive flood risk assessment methodology that considers the combined effects of rainfall and storm surge is recommended for other major watercourses in Bermuda. This methodology should involve further analysis of historical rainfall data for trends, application of the HEC-RAS flood simulation model with specific data such as topography and channel geometry, and major outflows, and finally presenting the results including flood inundation maps and flood depth and velocity data for various scenarios.

6.1 Description of Model

HEC-RAS (Hydrologic Engineering Center's River Analysis System) is a powerful software tool developed by the U.S. Army Corps of Engineers for hydraulic modeling of river and stream systems. It offers a wide range of functions to support floodplain management, river engineering, and hydraulic design projects. HEC-RAS allows users to simulate steady and unsteady flow conditions. In general, the inputs listed in the table below were included.

Table 6-1 Model inputs

<i>Input</i>	<i>Source</i>
<ul style="list-style-type: none"> • Geometric data, including cross-sectional profiles of the river channel. 	LIDAR Data from 2019
<ul style="list-style-type: none"> • Elevation data for the riverbed and floodplain. 	LIDAR Data from 2019 Streams Catchment Areas
<ul style="list-style-type: none"> • Hydraulic properties of materials involved, such as Manning's roughness coefficients. 	Soil Maps – Bermuda Geological Maps Land Use Maps – EOMAP Literature Review
<ul style="list-style-type: none"> • Boundary conditions, such as upstream flow rates or downstream water levels. 	Downstream water levels from MIKE21
<ul style="list-style-type: none"> • Hydrological data, including flow rates, rainfall patterns, and infiltration rates. 	Bermuda Weather Service Soil Data Literature Review
<ul style="list-style-type: none"> • Geospatial data, such as aerial imagery, topographic maps, and GIS data layers, to enhance accuracy and detail. 	Buildings layers, Road Layers, Soil Maps, etc.

6.2 Rainfall Data

In Bermuda, localized flooding events are a recurrent challenge, primarily triggered by heavy rainfall exceeding a threshold of 39.3mm in a 24-hour period (Johnston et al., 2018). These events have been particularly prevalent in low-lying areas of Pembroke Parish, including parts of Hamilton, where vulnerabilities to flooding are heightened due to the area's proximity to sea level. Despite efforts to address these issues, flooding remains a significant concern, often resulting in disruptions to traffic flow, property damage, and infrastructure disturbances. Concerns from the public and decision-makers have escalated in recent years, necessitating a deeper understanding of rainfall dynamics and their impact on flooding.

Historical rainfall data spanning from 1949 to 2016 reveal an increasing trend in rainfall accumulations and rain days, although with notable variability and no statistical significance. The recurrence interval analysis suggests that heavy rain days, meeting or exceeding the defined threshold, occur approximately once every 2.09 months (based on observations) or 1.70 months (using a fitted model). Despite these insights, predicting specific flood events remains challenging due to the stochastic nature of rainfall in Bermuda and the limitations associated with anecdotal flood reports.

6.2.1 Historical Data

The assessment included a thorough analysis of daily rainfall accumulation data spanning from 1949 to 2020 from the Bermuda Weather Service (BWS). This extensive dataset provided valuable insights into precipitation patterns over more than seven decades in the study area. Upon examining the data, it was found that the maximum daily rainfall accumulation recorded during this period was 197mm. This peak value serves as a significant reference point, illustrating the potential intensity of precipitation events experienced within the region.

The study also identified a notable rainfall event associated with Hurricane Nicole, during which the highest recorded rainfall accumulation reached 171mm for the day. This observation underscores the substantial impact that tropical cyclones can have on local weather conditions, including intense rainfall and subsequent flooding. Figure 6.1 shows the maximum rainfall per year across the 72 years of data. Consistent with the findings of the *Climate Profile and Projections for the Island of Bermuda* (Appendix A), no definitive trend of increase or decrease in annual rainfall is observed.

It is important to clarify that the rainfall measurements discussed here pertain to daily accumulations, encompassing rainfall occurring throughout the entire day. This means that even brief instances of rainfall, lasting only an hour, are recorded as 24-hour accumulations. For the purposes of rainfall modeling, understanding the intensity of these rainfall events is crucial. To gauge the intensity of rainfall affecting Bermuda, historical data provided by the Bermuda Weather Service was examined. The data sources encompassed two reports authored by W. A. Macky from the Bermuda Meteorological Office: Technical Note No. 1⁴, covering the period from 1891 to 1932, and Technical Note No. 8⁵, covering the period from 1933 to 1942.

⁴http://www.weather.bm/climateArchiveDocuments/1943_to_1958_Macky_Reports/1943_01_01_No1_The_Rainfall_And_Water_Supply_Of_Bermuda.pdf

⁵ http://www.weather.bm/climateArchiveDocuments/1943_to_1958_Macky_Reports/1957_10_01_No8_The_Rainfall_Of_Bermuda.pdf

Technical Note No. 1 (1891-1932):

- Maximum intensity within one hour: 3.51 inches (89.15 mm)
- Maximum intensity within three hours: 4.25 inches (107.95 mm)
- Based on 41 years of data, the average intensity is estimated to be 98.55mm over 2 hours.

Technical Note No. 8 (1933-1942)

- Maximum intensity over one hour: 2.09 inches (53.09 mm)
- Maximum intensity over three hours: 2.43 inches (61.72 mm)
- Based on 9 years of data, the average intensity is estimated to be 57.41mm over 2 hours.

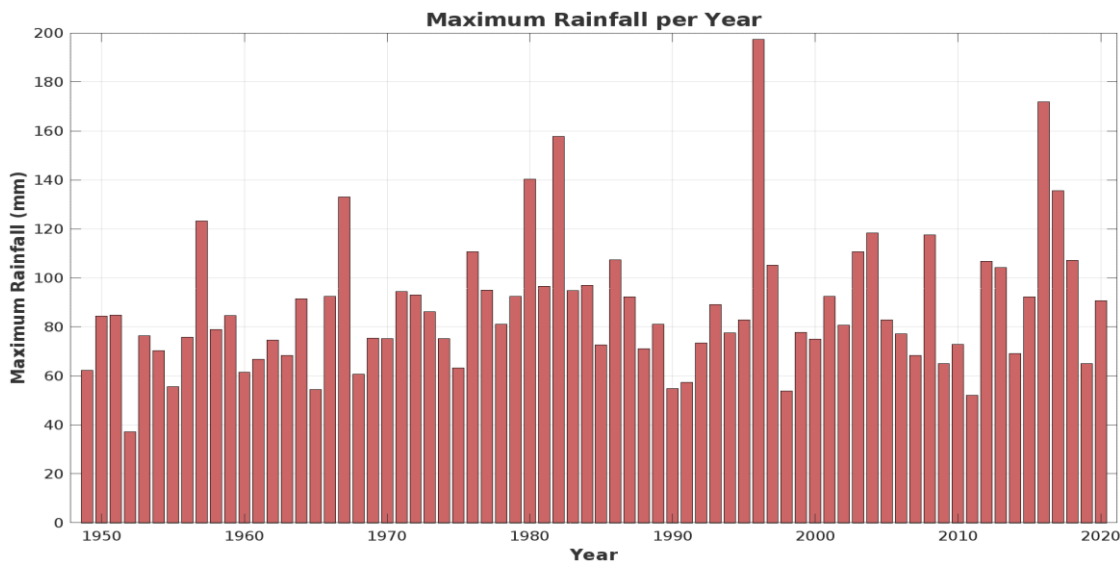


Figure 6.1 Maximum daily rainfall per year

6.2.2 Selection of Return Period and the Impact of Climate Change

The daily rainfall data was statistically analysed to derive the extreme return periods. The data was fit to a Weibull plot, a widely employed method in hydrological assessments for analysing the probability distribution of extreme events (Figure 6.2). The results of this analysis yielded return periods for various precipitation thresholds (Table 6-2).

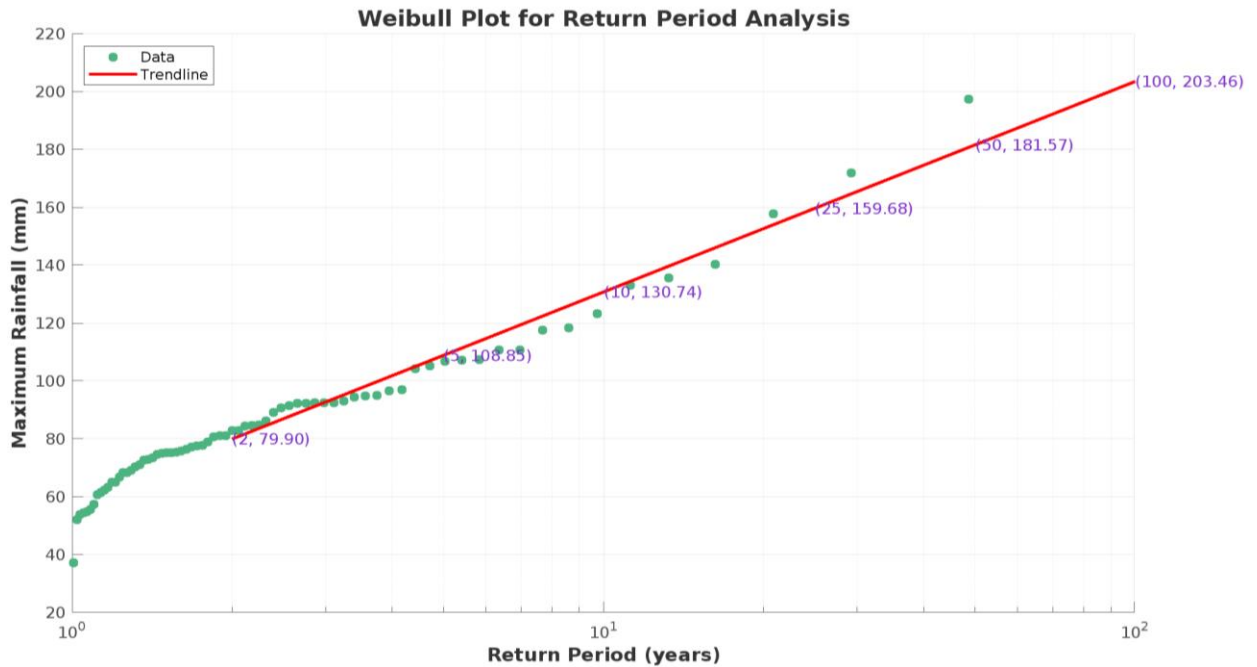


Figure 6.2 Probability of Exceedance for 24-hour rainfall

Table 6-2 Extracted return periods for 24hr rainfall amounts (using 1949 – 2021)

Return Period	Probability of Exceedance (%)	Normal Rainfall (mm)	Increased Rainfall due to Climate Change (mm)
1 in 2yr	50%	79.9	103.9
1 in 5yr	20%	108.8	141.5
1 in 10yr	10%	130.7	170.0
1 in 25yr	4%	159.7	207.6
1 in 50yr	2%	181.6	236.0
1 in 100yr	1%	203.5	264.5

Climate change modeling projections indicate varying trends in mean annual rainfall changes over the medium and long term. Specifically, the RCPs suggest a range of mean annual projected changes, with potential increases of 3% to 48% by the end of the century. Additionally, projections indicate an increase in the intensity of hurricanes, leading to higher winds and greater rainfall (between 20% and 33%). To account for these changes, **the current rainfall data was adjusted by 30%** to simulate the potential increase in rainfall under extreme climate scenarios.

The modeling approach for the combined surge/rainfall forcing adopted the Florida Department of Transportation (FDOT) 2024 guidelines⁶ for coastal areas, which pertain to creeks and small rivers flowing into tidal water bodies. The FDOT's recommendation is to apply the peak flow from a 10-year storm with surge-driven tailwater.

In analysing the precipitation data and its implications for hydrological modeling, the adjustment of the 1 in 10-year historical normal rainfall from 131mm to 170mm to account for climate change effects is insightful. This revision is particularly cogent when juxtaposed with the 171mm rainfall observed during Hurricane Nicole, supporting the updated modeling parameters. The FDOT's guidance on employing a 10-year storm flowrate in tandem with storm surge considerations is aptly applied here. Moreover, the maximum BWS rainfall record from 1949 to 2020 at 197mm further substantiates the decision to adjust rainfall values in the context of increased precipitation trends associated with climate change. These analyses underscore the necessity of integrating historical data with contemporary climate projections to enhance the resilience and accuracy of hydrological models.

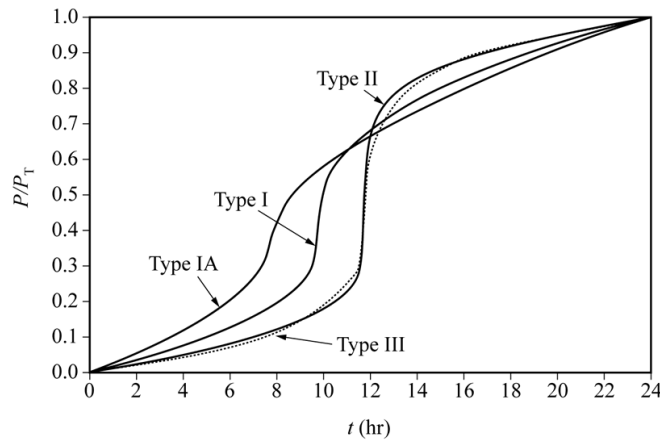


Figure 6.3 SCS (NRCS) Rainfall types (Source Nicklow et al., 2006)

6.2.3 Runoff Hydrographs

In the absence of intensity data, hourly rainfall information was estimated using the NRCS (Natural Resources Conservation Service) curves. For Bermuda, the Type 3 curve was assumed, which provides a framework for estimating rainfall depths for various durations. The Type 3 curve accounts for the temporal distribution of rainfall and is widely used in hydrological analyses. The NRCS Type 3 curve incorporates the antecedent moisture condition (AMC) of the soil, which refers to the soil's wetness level before a rainfall event. This is crucial because drier soil can absorb more water before runoff occurs compared to saturated soil. Types 1, 1A, and 2 are simpler and do not consider AMC, potentially leading to inaccurate runoff estimates, especially during wet periods when the soil is already saturated and generates more runoff.

The NRCS Type 3 curve has three distinct segments representing different runoff rates based on the rainfall intensity:

Initial segment: Low runoff rate for low rainfall intensity, reflecting initial infiltration and surface storage.

⁶ FDOT Drainage Manual, Topic No. 625-040-002, Effective: January 2024 Drainage Manual

Middle segment: Increased runoff rate with increasing rainfall intensity as infiltration capacity is exceeded.

Final segment: Constant high runoff rate for very high rainfall intensity, indicating saturated soil conditions and limited infiltration.

Based on the 1-in-10-year event calculated earlier, a daily rainfall of 130.74mm was replicated using the NRCS Type 3 Curve, illustrated in the figure below. The curve begins with minimal rainfall and peaks in intensity for approximately 2 hours around the 12-hour mark. Under normal rainfall conditions, the maximum intensity is 32.69mm per hour, resulting in a cumulative intensity of around 65.38 mm over 2 hours. This closely aligns with recorded intensities from 1933-1942, suggesting that the NRCS Type 3 Curve adequately represents extreme rainfall in Bermuda. However, to accommodate climate change effects, this value was increased by 30%, resulting in an average intensity of 42.49mm per hour over 1 hour. The resulting stage hydrograph was then inputted into the HECRAS model to generate flows across the Pembroke catchment.

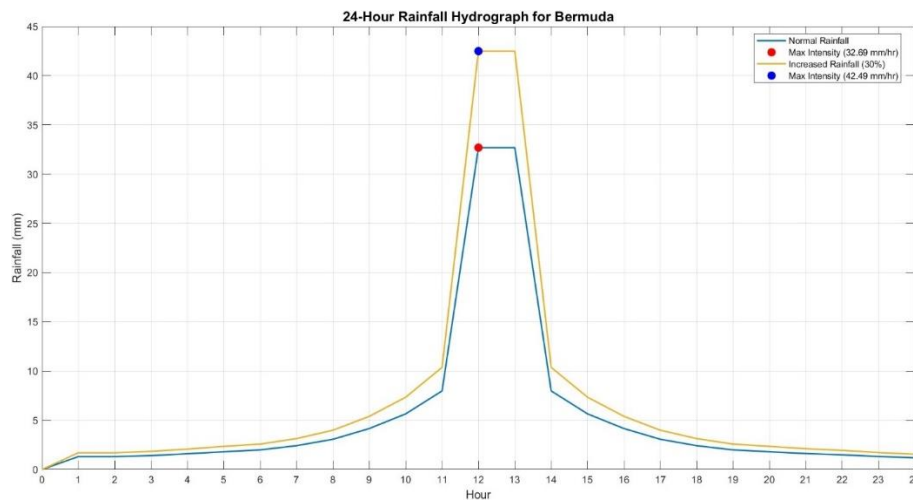


Figure 6.4 Recreated hydrograph for rainfall modeling

6.3 Surge Conditions at Mill Creek

Downstream conditions were configured based on the MIKE21 results outlined earlier. At Mill Creek, wave conditions are relatively subdued compared to Bermuda's ambient shoreline due to its location within the creek. While significant wave run-up is not anticipated, the static surge at the creek's mouth is expected to propagate inland significantly. Specifically, the influence of the static surge will extend along the Pembroke Canal up to Woodlands Road. The table below provides static surge values at the mouth of the Pembroke Canal that were used to drive the HEC RAS model.

Table 6-3 Surge levels in Mill Creek

<i>Return Period</i>	<i>Horizon</i>	<i>RCP 4.5</i>	<i>RCP 8.5</i>
25 year	20 year	1.39	1.54
	50 year	1.63	1.98
	100 year	2.11	2.46
50 year	20 year	1.48	1.63
	50 year	1.72	2.07
	100 year	2.20	2.55
100 year	20 year	1.56	1.67
	50 year	1.80	2.15
	100 year	2.28	2.63
150 year	20 year	1.61	1.74
	50 year	1.85	2.20
	100 year	2.33	2.67

6.4 Results

Figure 6.5 shows the rainfall modeling outcomes under the RCP 8.5 scenario for a 100-year projection into the future, focusing on a 1 in 50-year event. The top image illustrates the surge's impact on the Pembroke Canal, while the second image illustrates the repercussions of a 1 in 10-year rainfall event. Lastly, the third image demonstrates the effects of a 30% increase in rainfall intensity during the 1 in 10-year event. The findings reveal two primary types of flooding: overflow from the banks and pocket flooding in low-lying areas.

The analysis indicates water depths ranging from approximately 1.3 to 1.7m along the channel, extending from the shoreline of Mill Creek to the Pembroke Marsh. The water flows from the catchment via the streamlines (Figure 6.6) and eventually reaches the main channel. Notable areas of concern include:

- Properties along St. Johns Road, Mill Creek Road, and Pitts Bays Road, which filter to Baker Lane. In this area, the channel overflows, flooding the area with 0.5-1.5m of water, exacerbated by a combination of rainfall, surge, and channel overflow.
- Western Stars Sports Club (Dandy Town) along the bank of the channel.
- Bermuda Athletic Association (Goose Gosling Field), which acts as a detention area but is still lower than ambient areas.
- At the point where the channel changes direction at Laffan Street/Saltus Grammar School, significant overflow causes flooding ranging from 0.4-1.2m.
- Dellwood Middle School also experiences flooding due to bank overtopping and lower terrain.
- Pembroke Marsh Playground and North Street are notable flood plains, with flooding reaching up to 1.5-1.7m under this event.

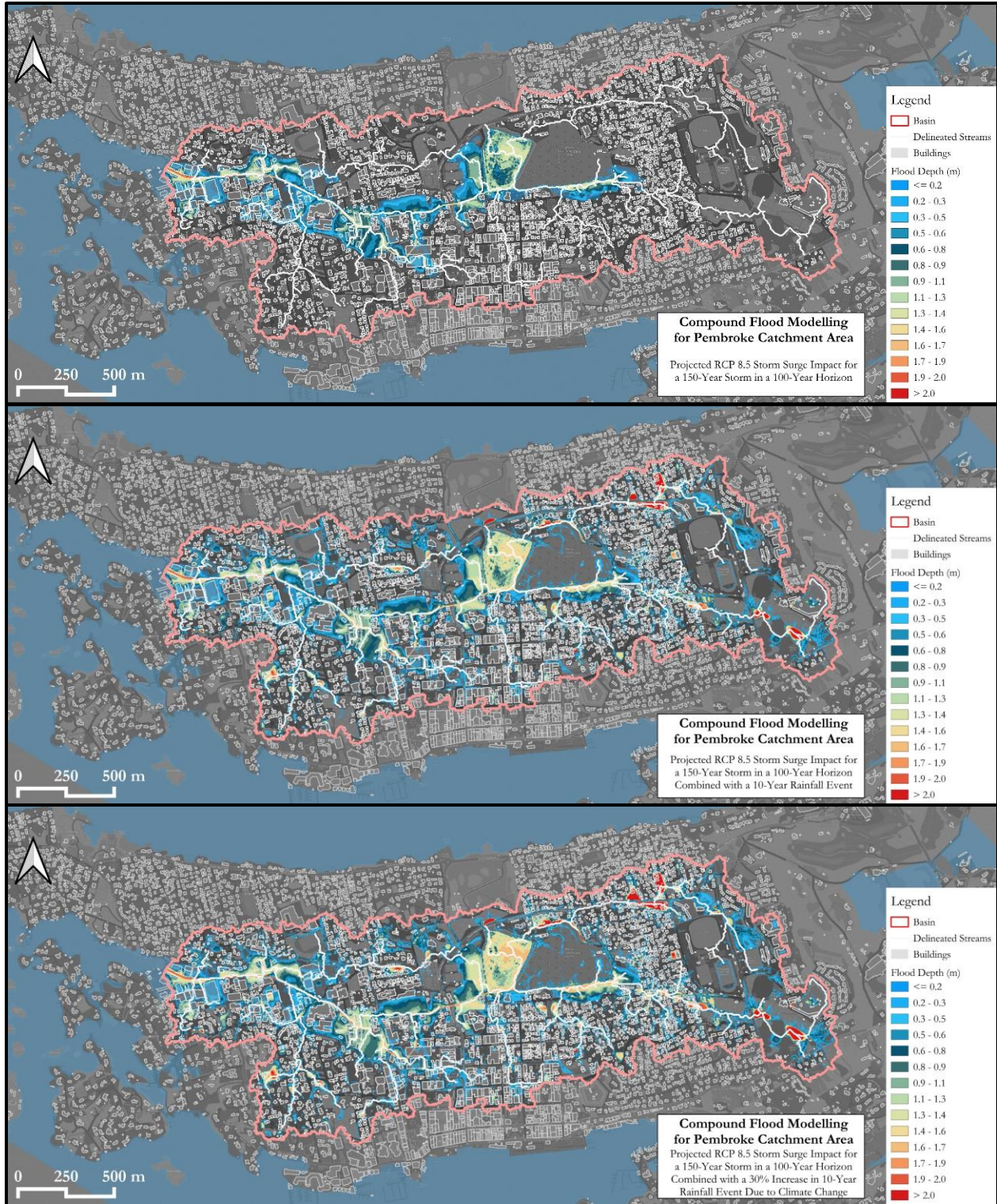


Figure 6.5 Flood depth induced by storm surge (top), rainfall and storm surge combined (middle), rainfall and storm surge considering climate change impact (bottom)

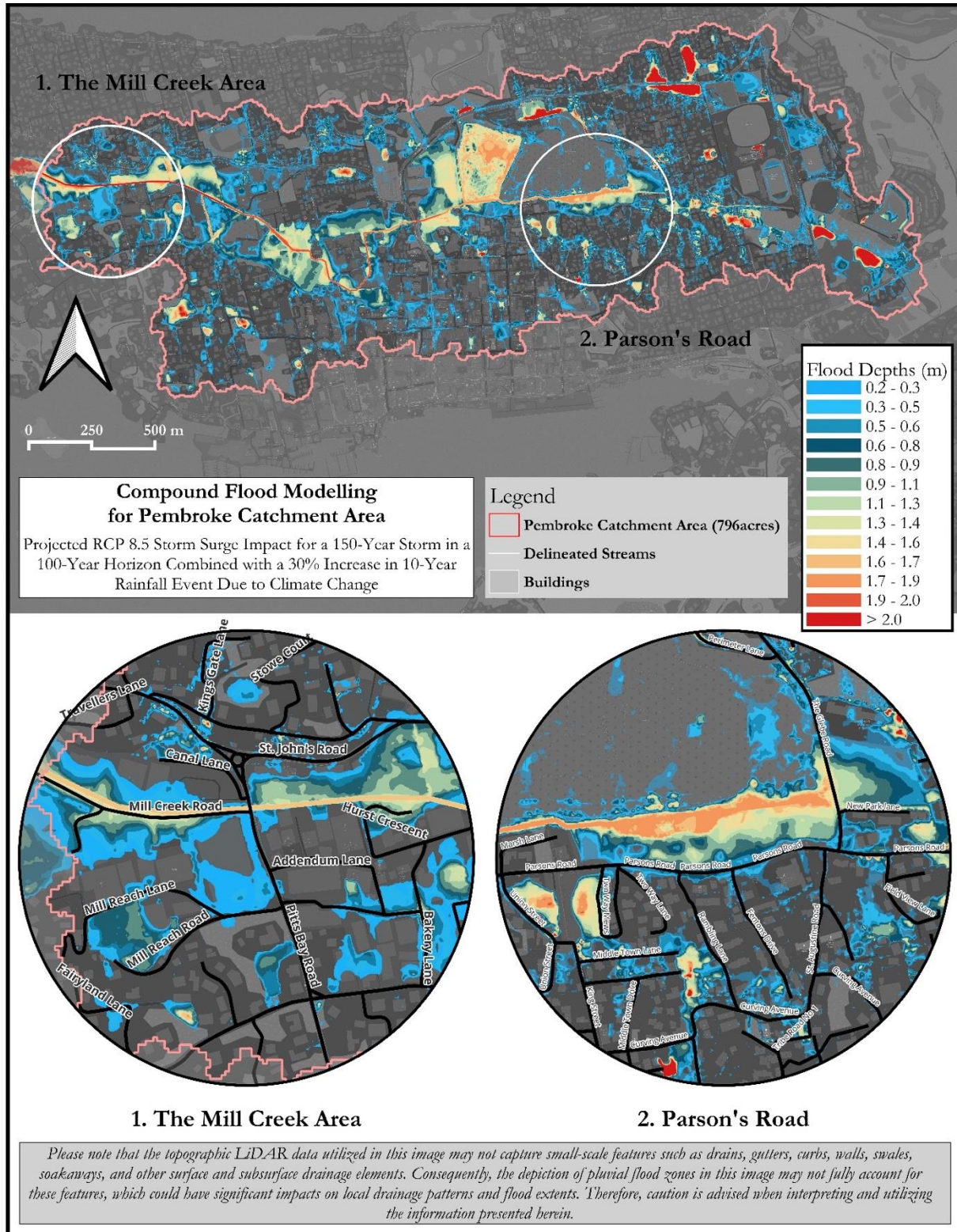


Figure 6.6 Flood induced by rainfall and storm surge combined under the RCP 8.5 climate change scenario

The results confirm previous studies highlighting pocket flooding across the 756-acre catchment area. Notable areas with pocket flooding include:

- To the northeast of the catchment along Palmetto/Roberts Avenue, where flooding reaches up to 3m, affecting several residences both north and south of the roadway. The model's limitations exclude manmade interventions, focusing on terrain and natural stream flows.
- Bermuda Arboretum is a natural detention pond area, relieving surrounding areas without impacting critical assets.
- Land adjacent to Kings, Curving Avenue, and Curving Court.
- Old Rectory Lane.
- Cedar Avenue.
- Along Palmetto Road, water depths measure 2.6-2.8m, with flooding exceeding 2.6m due to depressions in the terrain.

Despite the model's limitations in identifying existing drainage features, these findings provide a conservative estimate of potential flood scenarios. Channel overtopping (from 0.1 to 1.3m) is observed at the Bermuda Athletic Association, Ghost Gosling Field, and Woodlands Road, surpassing the United Nations Office of Disaster Risk Reduction's (UNDRR) threshold for flood risk mapping.

These observations were compared to newspaper reports and offer valuable insights into the model's accuracy, particularly when compared to natural stream flow within the catchment. Although some discrepancies are noted, the data reflects maximum flood levels within the catchment area.

6.5 Current Model Limitations

The model results offer valuable insights into potential flood-prone areas, providing a foundational understanding of the impact of rainfall during major hurricane surge events. Using a detailed LiDAR elevation file with a 0.5m grid spacing, the model accurately predicts natural stream locations and the topographical layout of the area. This precision enhances the model's ability to identify areas where land slopes towards the sea, aiding in the assessment of flood risks.

However, several limitations within the model must be acknowledged. One significant constraint is the inability to consider all drainage features present in the area. While the model effectively captures natural stream flow patterns, it fails to account for man-made interventions such as roadways, which can obstruct natural drainage paths. The absence of a drainage path file impedes the model's ability to accurately simulate water flow dynamics, particularly in areas where human modifications alter natural terrain. Moreover, the model lacks critical data from land use and soil maps, limiting its comprehensive understanding of the terrain. The terrain file, although meticulously generated from LiDAR data, required editing to remove elevations that may not correspond to actual land features. These limitations, particularly stemming from the terrain file, impose constraints on the model's accuracy and reliability in predicting flood scenarios.

While the model results offer valuable insights, they should be interpreted with caution, recognizing the inherent limitations. The model serves as a useful tool for preliminary flood risk assessment but may not provide exhaustive or precise predictions due to its constraints. Future iterations of the model would benefit from addressing these limitations to enhance its effectiveness in assessing flood hazards accurately.

7 Beach Erosion Modeling

The previous sections identified the wave climate responsible for erosion and the areas susceptible to erosion. The objective of this section is to quantify the extent and rate of erosion due to sea level rise. The erosion risk mapping can then be used to establish setback limits and planning for future development needs. The mapping of the shoreline retreat and the subsequent erosion risk mapping take into consideration the latest computed sea level rise values calculated using the Bruun rule.

7.1 Historical Erosion Trends

The shoreline shape is impacted, and largely formed, by the nearshore wave climate it is exposed to. For example, a sandy beach may accrete when the sediment volumes being transported to the beach are larger than those leaving the beach. Conversely, an erodible shoreline may also erode when sediment volumes being transported to the beach are less than those leaving the beach.

The historical movement of a shoreline is a valuable tool in obtaining an initial understanding of the long-term changes of the shoreline. Shoreline morphology can be extracted from historical maps, surveys, aerial photos and satellite imagery. The methodology used in this assessment included:

1. Procure available Google Earth satellite images of the shoreline,
2. Georeferenced satellite images using ArcGIS,
3. Trace the shoreline in each of the images,
4. Compare the traced shorelines using fixed reference points.

There are limitations to this method and uncertainties that mostly centre on the nature of the shoreline position at the time a satellite image is captured. Possible errors that could limit the accuracy of the analysis are summarized in the Table 7-1 below.

Table 7-1 Possible errors to limit accuracy of shoreline trend analysis

Error	Description
Seasonal error	Many beaches have seasonal cycles of erosion and accretion. Because high resolution satellite images are limited for small islands, images cannot be selected on seasonal time frames;
Tidal fluctuation error	The satellite images were obtained without regard to tidal cycles, which can result in inaccuracies on the digitized shoreline (though it should be noted the tide range in Bermuda is quite small);
Digitizing error	The error associated with digitizing the shoreline;
Pixel error	The pixel size in orthorectified images is 0.5m, which means anything within 0.5m cannot be resolved;
Rectification error	Satellite images are corrected, or rectified, to reduce displacements caused by lens distortions, Earth curvature, refraction, camera tilt, and terrain relief using remote sensing software.

The results indicate that for the period analyzed (2003 – 2018), along the south-western coast the shoreline has the potential to have variations in width between 29 and 42m. Along the south-eastern coast the shoreline change is between 16-18m. The sandy beaches at the north see less change with only 9-12m of beach width movement.

There is no clear trend of erosion or accretion when looking at the beaches on a large scale. As Figure 7.1 shows, there is erosion and accretion at any given beach, both on the south and north shores.

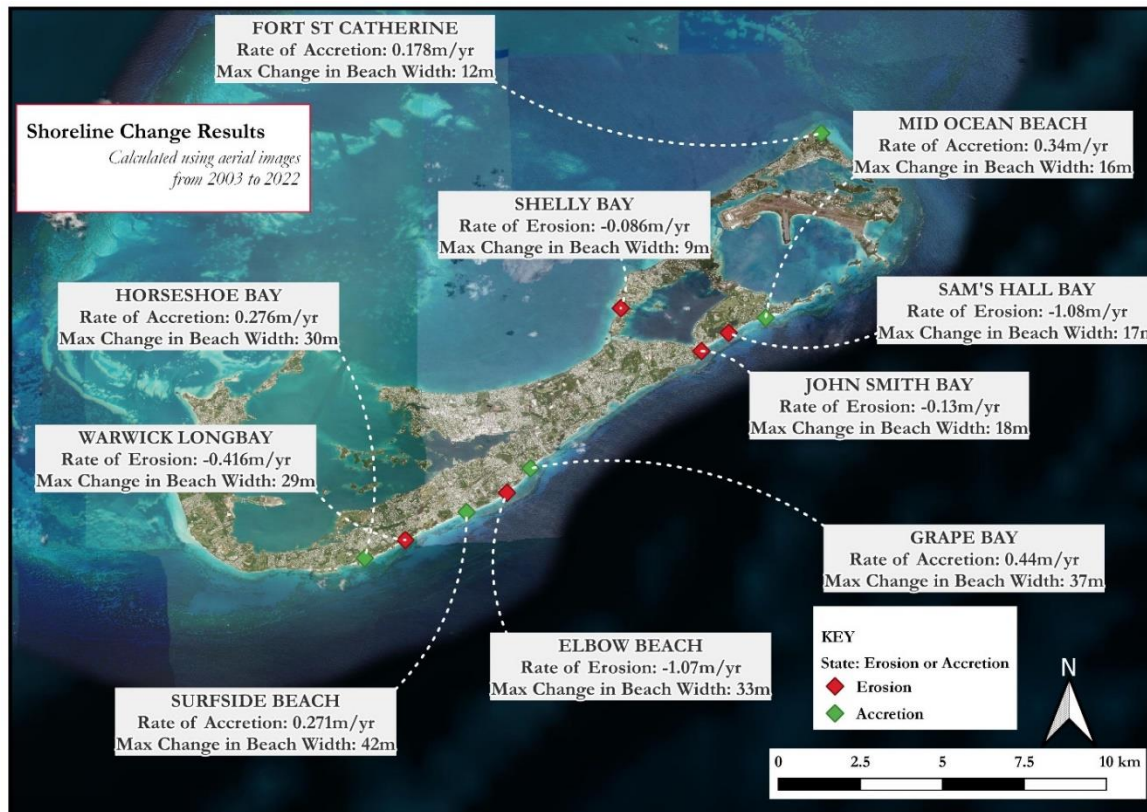


Figure 7.1 Summary for shoreline change assessment

7.2 Shoreline Retreat Calculations

7.2.1 Uniform Shoreline Retreat

The IPCC report states that a 1cm rise in sea level erodes beaches about 1m horizontally. This becomes a large issue for developed beaches that with infrastructure less than 5m from the ocean (IPCC, 1998). By this definition, the expected shoreline retreat would be uniform across the areas. Table 7-2 below shows the result of this uniform calculation. The table shows that in the next 100 years, the shoreline can retreat by 77-105m from the existing shoreline. This level of erosion/shoreline retreat would compromise several beaches and other critical infrastructure along the shores of Bermuda. There are clear limitations with this approach. This approach does not consider:

1. Site conditions like slope of the nearshore areas

2. Wave conditions that affect the movement of sediments along the shoreline.

A more applicable assessment tool, the Bruun Rule, is presented below and considers a few more environmental parameters that affect the shoreline retreat.

Table 7-2 Expected retreat based on the simple retreat rule.

Scenario	Expected Shoreline Retreat		
	20 years	50 years	100 years
RCP 4.5	10.8m	38.5m	77.0m
RCP 8.5	15.4m	52.5m	105.0m

7.2.2 Results of Bruun Rule Calculations

The first and best-known model relating shoreline retreat to an increase in local sea level was that proposed by Per Bruun (1962). The Bruun Rule states that a typical concave-upward beach profile erodes sand from the beach face and deposits it offshore to maintain constant water depth. The rule can be applied to correlate sea-level rise with eroding beaches, as it estimates the response of the shoreline profile to sea-level rise.

This simple model states that the beach profile is a parabolic function whose parameters are entirely determined by the mean water level and the sand grain size. Figure 7.2 below gives a representation of the Bruun Rule. The analysis by Bruun assumes that with a rise in sea level, the equilibrium profile of the beach and shallow offshore area moves upward and landward. The Bruun Rule was used to form the basis for the estimation of surface of land loss due to erosion.

The Bruun rule is applied to correlate SLR with beach erosion, as it estimates the response of the shoreline profile to SLR using the mean annual wave climate (IPPC 1998) including both daily and swell waves. The methodology used to map erosion risk is described in the following sections.

Unfortunately, the Bruun Rule also has severe limitations, especially in complex systems such as Bermuda. Some of these limitations are noted in the assumptions inherent in its formulation, such as:

- straight and parallel nearshore bottom contours,
- consistency in a sandy erodible beach throughout,
- no longshore transport,
- no cliff or hardened shoreline.

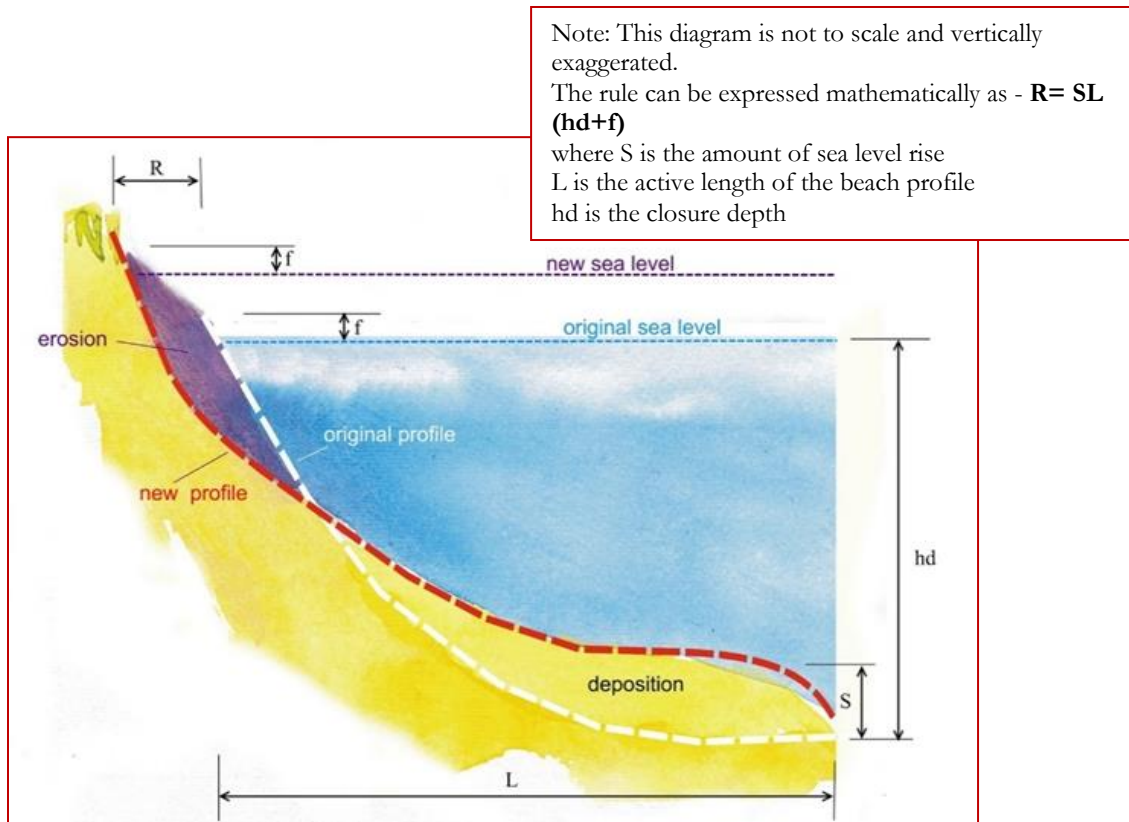


Figure 7.2 Definition sketch of the Bruun Rule applied to determine coastal retreat on sandy shoreline

As such, the erosion profiles calculated below should be considered with caution.

The Bruun Rule needs the active slope of sand transport as one of the parameters. The active slope starts from the depth of closure to the shoreline. The depth of closure requires a long-term record of data to calculate where there is no movement of sediment offshore. In lieu of this, the depth of closure can be estimated by calculating where the waves can no longer affect the movement of sand.

7.2.3 Depth of Closure

The Depth of Closure, or zone of active sediment movement, can be calculated from Hallermeier (1981) based on the 99th percentile wave heights. The formula was subsequently simplified by Houston (1995) to express the depth of closure as a function of the mean annual wave height according to the following equation:

$$H_{in} = 8.9 H_s$$

Where H_{in} is the “inner” (closer to shore) closure depth at the seaward limit of the littoral zone, and H_s the mean annual significant wave height.

Figure 7.3 shows the resulting zone of active sediment transport from the shoreline out to the depth of closure calculated using the 99th percentile wave conditions.

Results indicate that:

- the zone of active sediment movement includes the rim reef.
- within the lagoon there is little potential for sediment movement.
- along the south coast shows a band of 100 – 120m of active sediment transport.
- along the north shore it shows that a narrower band of less than 60m.

The formulation of the Brunn Rule shows that gentler slopes result in more shoreline retreat under SLR. Therefore, the coastal shoreline which have a wider zone of active transport will have higher shoreline retreat values.

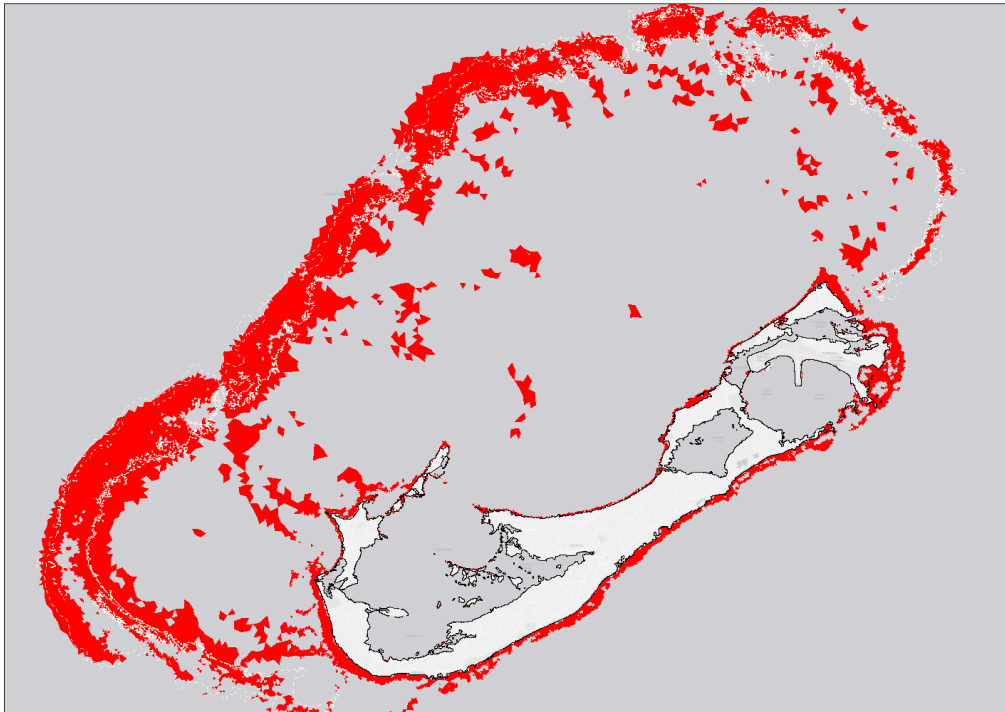


Figure 7.3 Zone of active sediment movement

Sandy shorelines longer than 50m were assessed. Figure 7.4 shows that under the RCP 4.5 and 8.5 SLR scenarios, in the year 2100 the southern beaches will recede between 30m and 65m using the Brunn Rule. The results further show that:

- The rates of shoreline retreat for RCP 4.5 and 8.5 in 2050 are comparable;
- In 2050, the shoreline along the south coast is expected to retreat 10-25m;
- In 2100, the differences in shoreline retreats are more pronounced between the two RCP scenarios;
- Along the south shore, at beaches like Horseshoe Bay, the shoreline retreat can be up to 60m in 2100. Warwick Long Bay could also retreat by up to 40m in 2100; and

- The maximum retreat calculated is 75-85m. This was close to the Dockyards, in an area with a wider zone of active transport as is visible on the active zone of transport plot above.

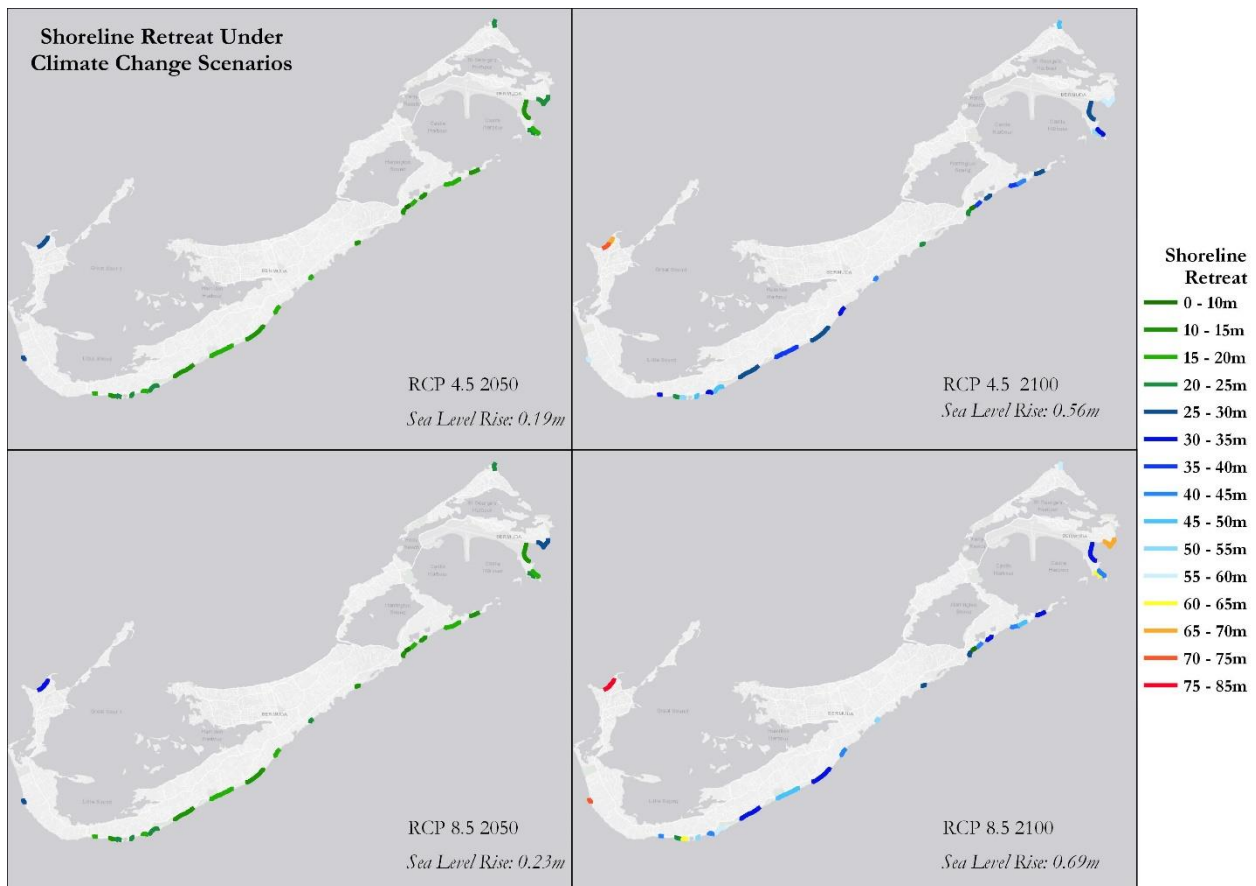


Figure 7.4 Horizontal shoreline retreat considering the average SLR rise projections (RCP 4.5) and the worst case SLR rise projections (RCP 8.5) for the 20- and 50-year horizons

The Brunn Rule has some limitations so caution must be taken when interpreting the results. Each sandy location would have site specific conditions that affect the shoreline retreat. For example, the nearshore wave conditions could be affected by the presence of reefs and rock formations. The retreat would also be limited by hard substrates such as a cliff face. Erosion of a cliff face would in turn act as a supply of sediment to the beach. Anthropogenic influences could limit the shoreline retreat in the future via coastal protection.

7.3 Erosion Under Swell Events

Another way of assessing the retreat of the shoreline is to look at how the shoreline would be affected by events that cause erosion. For example, long period swell events (as described in Section 3.5.4) will likely cause notable erosion. In the future, it is probable these events will be more common. As noted

previously, Bermuda can also expect stronger hurricanes, which can also severely alter beach conditions.

For this assessment, sediment movement under the effect of two swell events was assessed using the MIKE ST module. The morphological model (ST) takes results from the SW and HD modules and computes the sediment transport at each point in the computational mesh. Pre-calculated sediment transport tables are used to improve the model's efficiency. These transport tables are calculated using the Stokes 1st order wave theory, which was found to be the best method to accurately reproduce the wave-induced near-bed velocities, both in the shoaling and the surf zones. In the shoaling region, wave asymmetry results in onshore-directed net sediment transport, which is typically small. In the surf zone, wave breaking, and the associated undertow are the dominant mechanisms, which in most cases results in offshore-directed cross-shore sediment transport.

A mean grain size diameter of 0.42mm and a grading coefficient of 1.1 were taken as constants for the sediment properties. These are average conditions of the sand samples collected and results are shown in Figure 7.5 and Table 7-3. The layer thicknesses in the nearshore locations assumed to contribute to the sediment transport were assigned a constant value of 2m (Figure 7.6).

The results show:

- When a swell event originates north of Bermuda the reef provides protection for the north of island. As described previously, wave heights will increase with rising sea levels that reduce the efficiency of the reef to attenuate wave energy.
- When a swell event originates south of Bermuda, the southern shoreline is directly affected by erosion.
- On the north shore, the sandy areas within the lagoon are protected from erosion. Despite relatively large waves affecting offshore areas, there was no notable erosion predicted along the north shore for swell events.
- Most of the sediment movement occurs on the rim reef. Sediment in the vicinity of the rim reef shows erosion of up to 0.95m.
- On the south shore, the sandy areas are generally eroded by up to 0.5m, with a notable 0.8m of erosion closer to Horseshoe Bay.
- The zone of erosion along the south shore is wider than that along the north shore. This implies that sediment movement occurs over a wider area. This observation leads to questions of whether sediment could be lost to the deeper areas offshore the south coast.

The level of erosion on the south coast will be affected by more frequent, high intensity hurricanes. The ability for the beaches to recover after these events will affect the stability of the beaches in the future. A total of 14 swell events were found on average per year in the 43-year wave record from ERA5. As discussed in Section 3.5.4, a swell event is considered when the significant wave heights exceed the mean H_s plus two standard deviations of data record. The events can originate from the north (more likely) and from the south. These swell events cause current flow and sediment flow in opposing directions. That is, when the swell event is from the north, the current flows toward the east; when the swell event is from the south the current flows to the west. If there is no equilibrium, there

could be net erosion of the beaches in the south. This is a phenomenon that should be assessed in further detail.

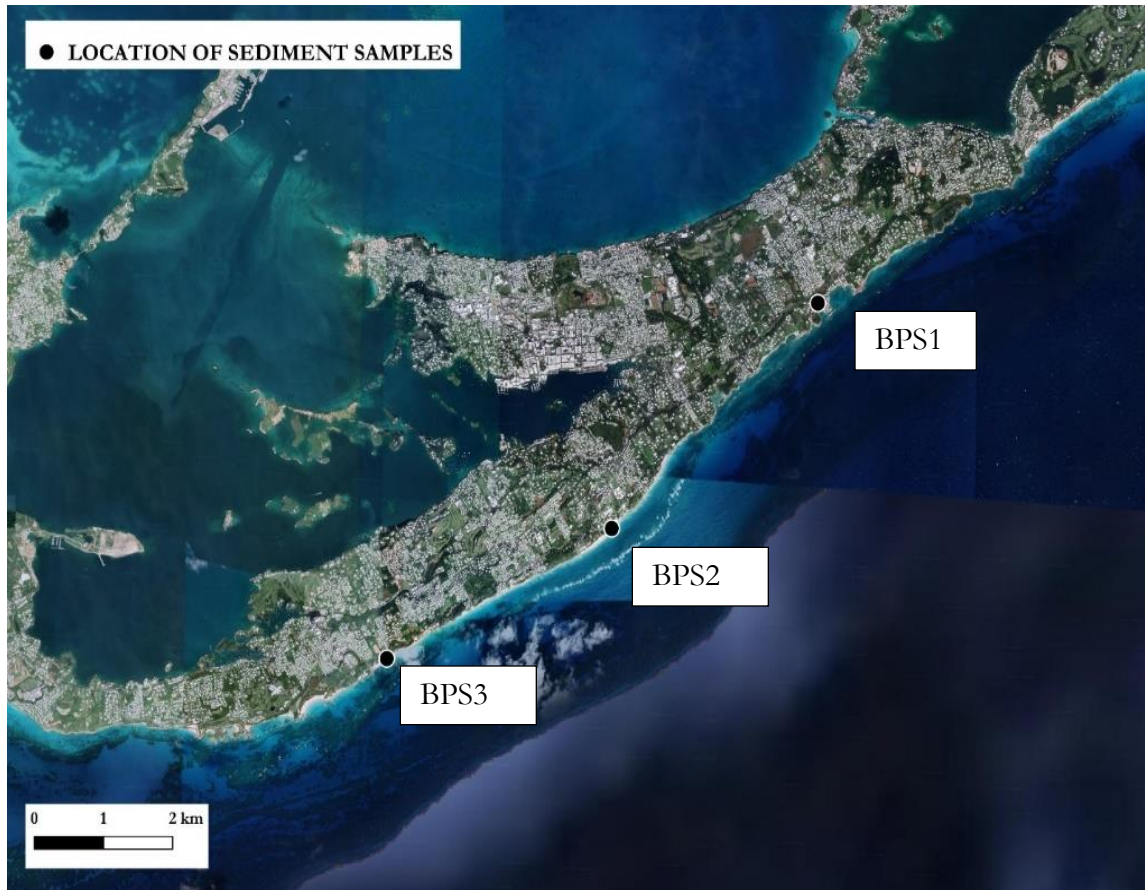


Figure 7.5 Locations of sediment sampling

Table 7-3 Results of sand sample analysis

Sample	Grain Size Diameters (mm)					
	D10	D16	D30	D50	D60	D90
BPS 1	0.260	0.280	0.316	0.368	0.399	0.593
BPS 2	0.514	0.618	0.848	1.239	1.449	2.610
BPS 3	0.296	0.321	0.376	0.483	0.561	0.887
	%Gravel	%Sand	%Silt/Clay	Cc	Cu	
BPS 1	0.0	99.8	0.0	0.963	1.535	
BPS 2	13.9	86.0	0.0	0.966	2.819	
BPS 3	0.3	99.6	0.0	0.851	1.895	

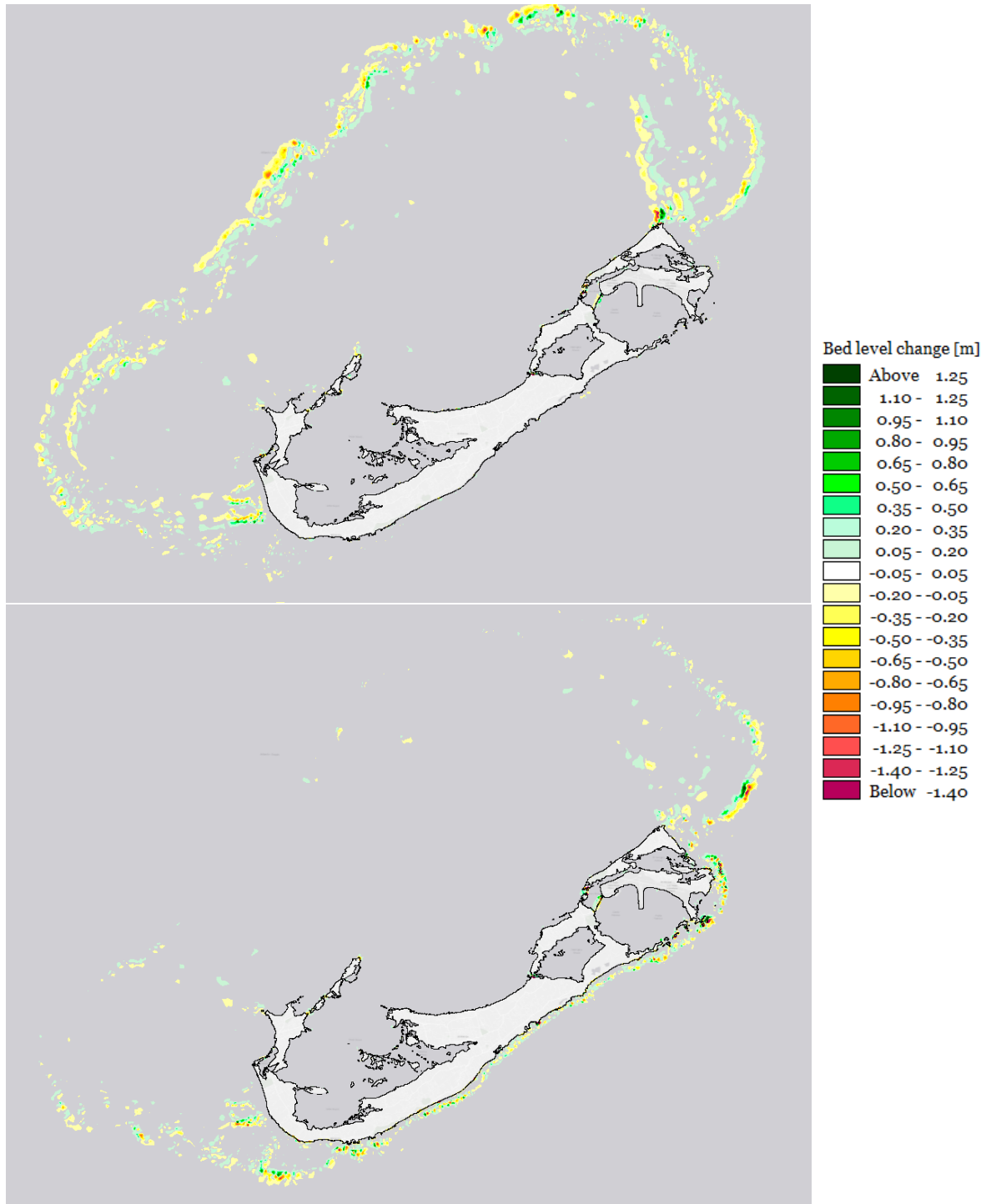


Figure 7.6 Bed level change at the end of swell events - March 2018 (top) and August 1995 (bottom)

8 Cliff Erosion Assessment

8.1 Cliff Setting

Bermuda’s coastal cliffs outcrop at many locations and are composed primarily of Pleistocene dune calcarenites (aeolianites) and associated beach calcarenites (Vacher, et al., 1997). Minor outcrops of marine deposited limestones and fossil soils (paleosols) also exist (Rowe, 2021). The aeolianite deposits include five main formations with the older and harder rocks lower in the rock column (Vacher et al. 1997). Taller cliffs are primarily located on the eastern and south-eastern areas of the island. The present cliffs formed as the Pleistocene rocks were cut back during the Holocene transgression and subsequent sea level still stand. The cliffs are fronted by a shore platform and sometimes calcareous beaches composed of sand, gravel, and coral fragments. In some areas beaches are absent and the cliffs are in continuous contact with the ocean. The cliffs exhibit karstic weathering and complex morphology (Bird, 2010) including caves, notches (Neumann, 1966; Moses, 2013), and arches. In some locations, seawalls, revetements, notch fills, and other engineering measures have been installed to prevent erosion and improve slope stability.

Coastal cliffs in Bermuda can be broadly categorized into two general types. The first type are coastal cliffs that plunge directly into the ocean and are in continuous contact with the ocean waves (Figure 8.1).



Figure 8.1 Example of coastal cliffs in Bermuda without beaches: Spittal Pond area (left), north of Building Bay Beach (center), and Great Head (right)

The second main type of coastal cliffs are those fronted by sand and gravel beaches, and waves are not in continuous contact with the cliffs (Figure 8.2).



Figure 8.2 Example of coastal cliffs in Bermuda with fronting beaches: Surf Side Beach (left), Pink Beach West (center), and Marley Beach (right)

8.2 Cliff Erosion Processes

The coastal cliffs of Bermuda are exposed to a range of physical, chemical, and biological weathering processes, which can weaken the cliff material to varying degrees and lead to cliff erosion. In Bermuda, some weathering factors that are visually apparent and/or have been documented in the literature include: (1) root wedging, particularly from Casuarina trees, (2) bioerosion from marine life (i.e. boring sponges, mollusks, etc.; Neumann 1966), and (3) dissolution of limestone rock, in some locations forming caves (karst; Mylroie et al. 1995).

Coastal cliff erosion can be broadly attributed to marine and subaerial (including subsurface) erosion mechanisms (Trenhaile, 1987; Sunamura, 1992). Marine erosional processes (e.g. wave-driven impact pressures and abrasion) act directly at the cliff base, but only when tides and other water level fluctuations allow waves to reach the cliff (Young et al., 2016). Impacts to coastal cliffs from waves may increase as sea levels rise; this is an important concern for Bermuda and the focus of the current report. However, impacts to coastal cliff erosion from sea level rise will vary around the island based on several factors.

One factor that influences wave-driven cliff erosion is basic exposure to wave energy. A protective shelf and shallow reefs help limit wave exposure on the northern coast cliffs of Bermuda, while the southern coastal cliffs are exposed to relatively higher wave energy. The Smith Warner International (SWI) 2004 *Coastal Erosion Vulnerability Assessment* found that wave action during storm events was the primary driver of erosion, compared to day-to-day wave action. SWI (2004) documented numerous coastal cliff failures related to 2003 Hurricane Fabian and noted observations of several wave-driven processes related to these failures including cliff overstepping from basal erosion, surface stripping that exposed softer and more erodible cliff material, and high-pressure water jets extending to high cliff elevations helping to trigger upper cliff failures. SWI (2004) also found that offshore bathymetry (which influences wave conditions at the coastline), rock dip (which can affect the type of failure), and the degree of rock fracturing also influence erosion rates in Bermuda.

The evolution of coastal cliffs can be generally conceptualized as a three-stage cycle. In Stage 1, waves erode the cliff base, causing notch development or cliff steepening, and reducing cliff stability. Eventually, in Stage 2, a slope or block failure occurs, depositing talus material at the cliff base. The talus temporarily protects the cliff from direct wave action until the talus is removed during Stage 3, restoring direct wave attack, and completing the cycle (Young et al., 2009). The time span of the cycle and persistence of the talus material is variable.

This general erosion cycle is observed in Bermuda. Large blocks of limestone (cemented paleo dunes) occur on beaches in many locations around the island of Bermuda, reflecting that seacliff failures in Bermuda can occur in large blocks, resulting in many meters of inland retreat at once. However, the blocks of material do not immediately erode, and can temporarily act to protect cliffs from additional wave attack. As the blocks erode, sand-size material in the rock can be retained on the beach, while finer grained material is more swiftly carried offshore.

Beaches are another important factor to consider for wave-driven cliff erosion. Cliff fronting beaches can also provide natural erosion protection to the seacliffs by preventing waves from impacting the cliff when the combined wave and tide conditions do not generate wave runup levels that exceed the beach conditions.

For cliffs with fronting beaches, the rate of cliff retreat, and resulting hazards associated with cliff retreat, in response to ocean-driven erosion related to sea level rise will depend upon several factors, including future wave conditions, the frequency and length of time that runup exceeds the beach level and waves can impact cliffs, and the physical cliff properties such as hardness of the cliff material. For cliffs without fronting beaches that are already in continuous contact with the ocean, change to cliff erosion rates will mostly depend on possible changes in nearshore wave conditions. An additional factor to consider for all cliffs is the presence of weak layers in the cliffs that may experience new or increased wave attack as sea level rises.

8.3 Historical Cliff Erosion Rates

Detailed quantitative assessments of cliff retreat rates in Bermuda are not available. However, several significant cliff failure events have been documented. For example, in 2003 the eye of Hurricane Fabian passed about 80 km to west of Bermuda and generated sustained wind speeds of 190 km/h over the land. The hurricane caused extensive damage including seawall failures, structural damage, and coastal erosion including cliff failures (SWI, 2004). Jones (2012) also reported two major cliff collapses just east of the Grand Atlantic development (now the Bermudian Resort) and at Southlands Beach prior to the arrival of Tropical Storm Leslie in 2012.

Airborne LiDAR surveys conducted in 2004 and 2019 potentially provide an opportunity to quantitatively analyze coastal change, including cliff retreat, over the time period between the surveys. The 2004 LiDAR dataset is sparse, with a density of about 0.058 points/m² (1 point per 17m²) and spans about 24 km along the southern side of Bermuda and about 2.7 km in the cross-shore direction. The dataset includes the offshore bathymetry to depths of about 60m. The 2019 dataset is also relatively sparse, with a similar point density of about 0.053 points/m² (1 point per ~19m²) but includes full coverage of Bermuda and the surrounding areas to depths of about 60m. Both LiDAR datasets were converted to digital elevation models with 4m resolution (16 m² grid cells) and used for preliminary topographic change analysis. Initial inspection revealed significant noise levels at many coastal cliff locations and other similar features with rapid elevation changes. The noise was generated by the low data resolution, data gaps in cliff areas, edge effects, vegetation, and interpolation. Unfortunately, the topographic cliff changes are typically relatively small compared to the available data resolution (1 point per 17-19m²), preventing confidence in quantitative change analysis of the coastal cliffs.

Quantifying historical coastal cliff retreat rates might be possible in Bermuda if historical high resolution topographic surveys or orthorectified aerial images could be obtained for this purpose. Current and future cliff retreat rates could be quantified with new, subsequent high-resolution LiDAR surveys.

Although the existing LiDAR datasets could not be used to conduct extensive quantitative cliff retreat analysis, the two LiDAR datasets were compared for the area east of Bermudian Resort where a large failure occurred in 2012 (Jones, 2012). The LiDAR comparison suggests about 30m alongshore of the cliff top retreated about 5m in some areas, corresponding to a retreat rate of 33cm/yr between the 2004 and 2019 LiDAR datasets. Note, this case represents an episodic event and probably represents the high range of historic cliff retreat rates. Long term historical average retreat rates are likely lower.

8.4 Impacts of sea level rise

In many cliff settings around the world, the rate of cliff retreat is expected to increase as sea levels rise. Most models that estimate future cliff retreat rates considering sea level rise require known historical cliff retreat rates as a model input and calibration, which are generally not available for Bermuda. The vulnerability of Bermuda's coastal cliffs was therefore qualitatively assessed for 20-, 50-, and 100-year time horizons for sea level rise scenarios RCP 4.5 and 8.5. Future cliff vulnerability was evaluated using available data sources including present and future wave conditions, geologic conditions and lithology, and site settings. The assessment included an on-site visit to visually evaluate present conditions and to collect data including rock hardness (obtained with a Schmidt hammer) and photos of representative erosional processes. The 20-, 50-, and 100-year time horizons were compared to baseline conditions to evaluate future changes. Overall, qualitative vulnerability was assessed primarily between sites using relative wave exposure, rock hardness, site conditions, and modeled beach retreat. Parameters that were qualitatively evaluated fall into three categories: (1) beach, (2) geologic, and (3) wave conditions.

8.4.1 Beach conditions

When cliffs become sufficiently undercut or weakened from wave action or other weathering processes, cliff failures occur. Beaches can provide a natural buffer to wave exposure of the cliffs. If combined conditions of wave action and sea level exceeds the beach conditions, waves can directly attack the cliffs. Wider and higher elevation beaches provide relatively more protection compared to narrow, low elevation beaches.

For the cliffs currently continuously in contact with the waves, such as rocky headlands and cliffs without fronting beaches, future vulnerability can be primarily related to changes in nearshore wave height (assuming no geologic changes of the cliff face in contact with the ocean as sea levels rise). In areas with deep water presently at the cliff base, there may be relatively little change in cliff base wave conditions as sea levels rise.

Sites were assessed using beach condition factors including beach presence, beach elevation, beach slope, historical beach width, and modeled Bruun rule shoreline retreat estimates. Beach elevation and slope were estimated from the 2004 and 2019 lidar data. Historical beach widths were estimated from historical shoreline analysis (Section 7.1) and Bruun rule beach retreat estimates (Section 7.2). Note, the basic Bruun rule model does not consider the presence of coastal cliffs behind the beach. Beaches without backing cliffs will likely retreat faster in response to sea level rise compared to beaches backed by cliffs, which will provide more resistance to wave erosion. Beaches backed by cliffs will also likely have a lagged response to sea level rise. Note that beaches are inherently dynamic and change with time, so these estimates of observed beach conditions are interpreted as representative snapshots in time and should not be considered absolute.

8.4.2 Geologic conditions

Geologic conditions were evaluated using *in situ* measurements and observations. *In situ* cliff rock strength measurements were obtained with a Proceq Schmidt hammer at the cliff base using the ASTM method (mean value of ten measurements with outliers removed; ASTM, 2013). Schmidt hammer rebound values are strongly correlated ($r^2 = 0.96$) with uniaxial compressive strength (Katz et al., 2000). At many of the beaches visited for this project, a paleosol layer was observed in the cliffs just above the back beach elevation. The Schmidt Hammer typically could not measure rock hardness in the paleosol layers, because the material was too weak and the hammer action did not register. Indeed,

the material in these layers could easily be scraped away by hand. In contrast, the limestone material surrounding paleosol layers was much harder, although it varied in hardness and in the degree of weathering/pitting of the material, which would result in variability in overall rock resistance to erosion.

The site visit observations suggest that beaches often form in Bermuda at locations where a paleosol layer is located near the cliff at an elevation potentially exposed to wave action. In some locations, such as below the Bermudian Resort development, seawalls were observed that appear to have been placed to protect a paleosol layer near the base of the cliff, just above the back beach.

8.5 Evaluated Sites

Twenty representative sites were selected for evaluation based on available data sources (Figure 8.3, Table 8-1).

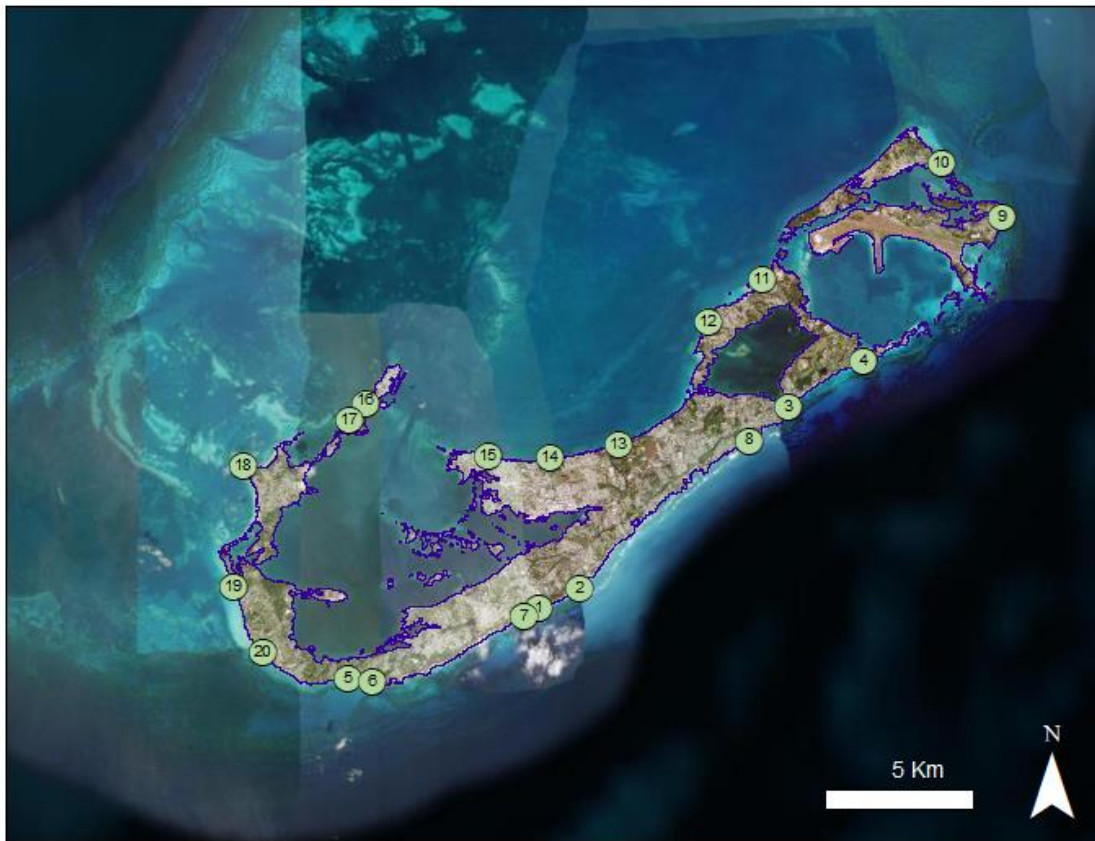


Figure 8.3 Locations of the twenty representative coastal cliff sites

Table 8-1 General site settings and parameters of beach and geologic conditions, and existing wave climate

Site Name	Site Number	Beach Present	Cliff	Back Beach Elevation (m)	Beach slope (°)	Historical Beach Width (m)	Cliff Hardness (Schmidt Hammer)	Cliff Elevation (m)	Lower Cliff Paleosol Observed	Foreshore Setting	Waves Hs (m)* mean	Waves Hs (m)* 99th
Surf Side Beach	1	Yes	Yes	1-3	3.6, 4.6	0-40	19.5, 21, 0, 16.5	22	Yes	Sediment Dominated	0.5	1.0
Elbow Beach	2	Yes	Partial	2-4	3.1, 3.9	10-100	0, 10, 0, 11, 45, 14.5	10-20	Yes	Sediment Dominated	0.5	1.1
John Smith	3	Yes	Partial	3-4	3.8, 4.1	30-70	19.5, 33	5-10	Yes	Sediment Dominated	0.4	1.1
Rosewood Club	4	Yes	Partial	3-5	2.7, 3.5	40-80	42.5, 41, 45	20-25	No	Sediment Dominated	0.5	1.3
Church Bay	5	Yes	Yes	2-4	7.3	—	27, 12.5	15-20	Yes	Sediment Dominated	0.5	0.9
The Reefs Resort	6	Yes	Yes	2-4	6.2, 5.1	—	25	20-25	Yes	Sediment Dominated	0.5	1.0
Marley Beach	7	Yes	Yes	2-3	2.5, 2.6	—	15, 9.5, 11.5, 12, 11.5, 32, 13.5,	20	Yes	Rock / Sediment	0.3	0.7
Spittal Pond	8	No	Yes	—	—	—	34.5, 21.5, 19.5	3-20	No	Rock Dominated	0.5	1.4
Great Head	9	No	Yes	—	—	—	41	20-30	No	Rock Dominated	0.7	1.8
Barry Road	10	No	Yes	—	—	—	29.5	3-5	No	Rock Dominated	0.6	1.2
Railway Trail near Callen Glen Dr.	11	No	Yes	—	—	—	44, 20, 12.5	5-10	No	Rock Dominated	0.4	0.8
Railway Trail near Lynwood Dr.	12	No	Yes	—	—	—	29, 24.5, 15.5	3-5	No	Rock Dominated	0.4	0.8
Robinson Bay Park	13	No	Yes	—	—	—	10.5	5-8	No	Coral Dominated	0.2	0.3
Ducking Stool Park	14	No	Yes	—	—	—	27.5	5-10	No	Rock Dominated	0.4	0.7
Clarence Cove	15	No	Yes	—	—	—	13.5	10-20	No	Rock Dominated	0.4	0.7
Dockyard - Pulpit Rock	16	No	Yes	—	—	—	15.5, 13, 26.5	5	Yes	Rock Dominated	0.4	0.7
Theo's Cove	17	Partial	Partial	—	—	—	15	3	No	Sediment Dominated	0.2	0.3
Daniels Head	18	Partial	Partial	—	—	—	29.5	5-10	No	Sediment Dominated	0.3	0.4
Hog Bay Park	19	No	Yes	—	—	—	36, 22.5	2-5	No	Sediment Dominated	0.2	0.3
West Whale Bay Park	20	Partial	Yes	—	—	—	24.5, 17	5-15	No	Sediment Dominated	0.4	0.5

* Median of study site

Sites 1-8 were primarily located on the southern side of Bermuda and had a beach fronting the cliffs except site 8 (Spittal Pond) where there is no protective beach. Site 2 (Elbow Beach), 3 (John Smith), and 4 (Rosewood Club) are only partially backed by coastal cliffs. Sites 3 (John Smith), site 4 (Rosewood), and 6 (Reefs Resort) are pocket beaches. Sites 9 (Great Head) and 10 (along Barry Road) are located on the northeast portion of Bermuda and do not have any protective beaches. Site 9 (Great Head) is characterized by high cliffs that plunge into relatively deep water. Sites 11-15 are located on the northern facing part of Bermuda, sheltered from wave energy by an extensive shelf, and generally lack protective beaches. Sites 16-20 are on the western side of Bermuda and include variable amounts of beach and cliff extent.

8.5.1 Beach Conditions

Back beach elevation conditions at sites 1-7 generally ranged from about 1-5 m (Table 8-1). The lowest elevation beaches were at sites 1 (Surf Side) and 7 (Marley Beach), while site 4 (Rosewood) was the most elevated. Generalized historical beach widths (available for sites 1-4) ranged from about 0-100 m, with site 1 (Surf Side) the narrowest. Site 2 (Elbow Beach) exhibited the largest range (combined temporal and alongshore) of 10-100 m in width. Sites 2-4 all had maximum historical beach widths of at least 70 m.

Future Bruun rule beach retreat estimates for a 100-year horizon ranged 15-36m for RCP 4.5, and 19-44m for RCP 8.5. The lowest beach retreat for RCP 8.5, 100-year horizon was at site 6 (Reefs Resort, 19m), while sites 1 (Surf Side), 4 (Rosewood), and 7 (Marley Beach) had estimated retreats of 42-44 m. 50-year horizon beach retreat ranged up to 13m and 15m, for RCP 4.5 and 8.5, respectively.

8.5.2 Geologic Conditions

Weak paleosol layers near the cliff base were observed near the cliff base at sites 1-7 and 16, and generally correspond to sites with extensive beaches. The exception was at site 8 (Rosewood Beach) where a paleosol layer was not observed, but possibly concealed by shore protection and vegetation. Rock hardness observations ranged from 0-45 around the island. Relatively weak cliff layers (rebound values <15) were observed at sites 1, 2, 5, 7, 11, 13, and 15-17, while relatively hard cliff layers (rebound values >35) were observed at sites 2, 4, 9, and 11. A relatively large range of rock hardness was observed at site 2 (Elbow Beach, 0-45) and site 11 (Railway Trail, 12.5-44).

8.5.3 Wave Conditions

Future wave conditions at each site were evaluated for both the standard day to day wave climate (Figure 8.4) as well as changes related to hurricanes (Figure 8.5). Day to day wave exposure generally increased with rising sea levels with 99th percentile wave heights increasing up to 25% and 59% by 2100, over present conditions for RCP 4.5 and 8.5, respectively. Relative wave height increases were largest at sites 17, 19, and 20, all located on the west side of Bermuda. The smallest change in relative wave heights was site 9 (Great Head) where the cliff plunges into relatively deep water.

Of the sites evaluated for this work, site 8 (Spittal Pond) and site 9 (Great Head) are most exposed to present and future hurricane waves. Modeled hurricane wave height estimates ranged up to an increase of 0.5m for a 100 year event under RCP 8.5 and a 50 year forecast horizon (Figure 8.5). However, many of the expected changes in hurricane wave heights remain <0.3m across all sites and future climate scenarios. The largest and smallest increases are expected at sites 1-8 (maximum modeled increase 0.4-0.5m), and sites 11-19 (modeled increase of <=0.3m), respectively.

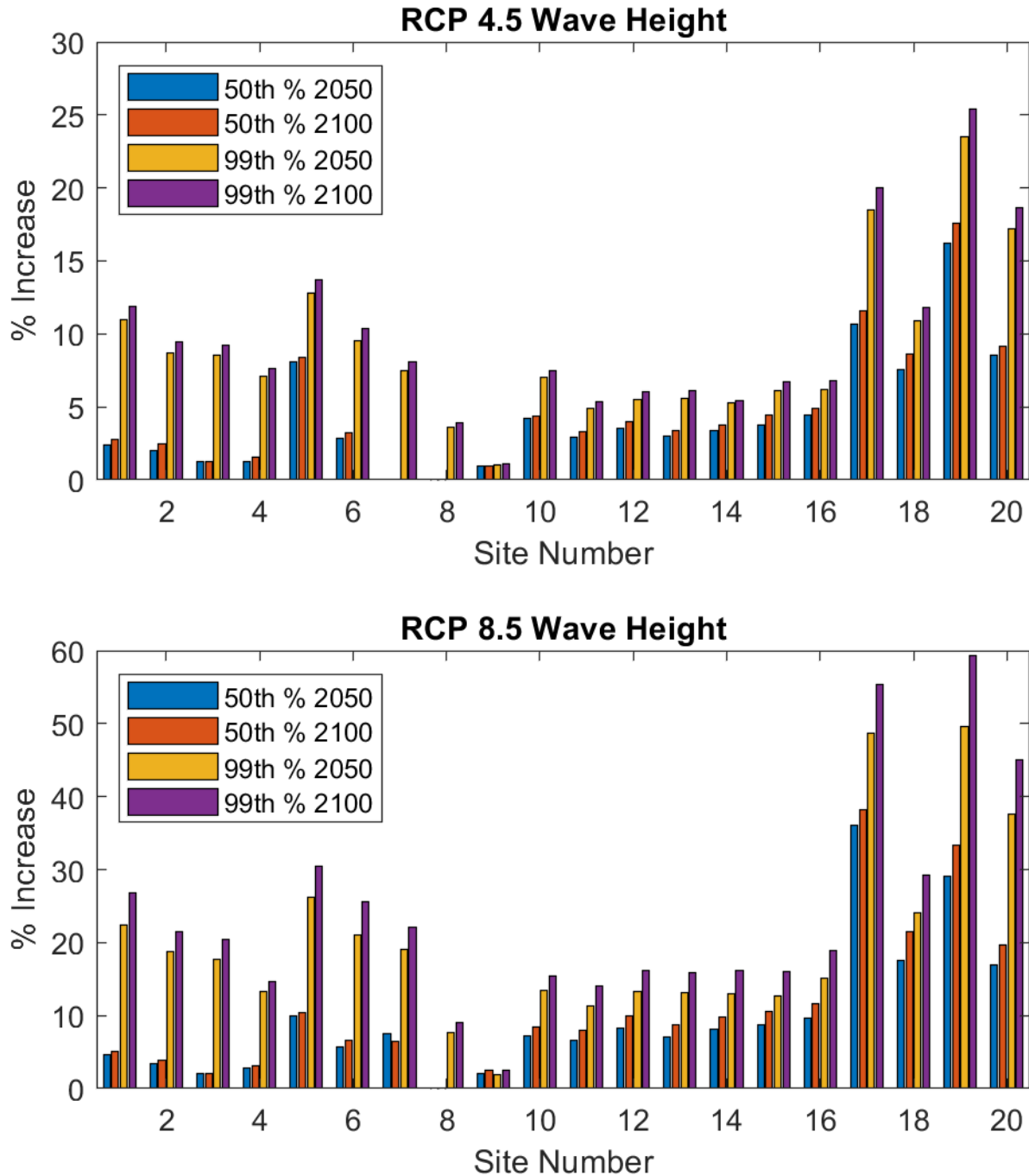


Figure 8.4 Modeled changes in standard wave condition at each site for the 50th and 99th percentile of wave heights expected in both 2050 and 2100; RCP 4.5 (top) and RCP 8.5 (bottom) future climate model scenarios

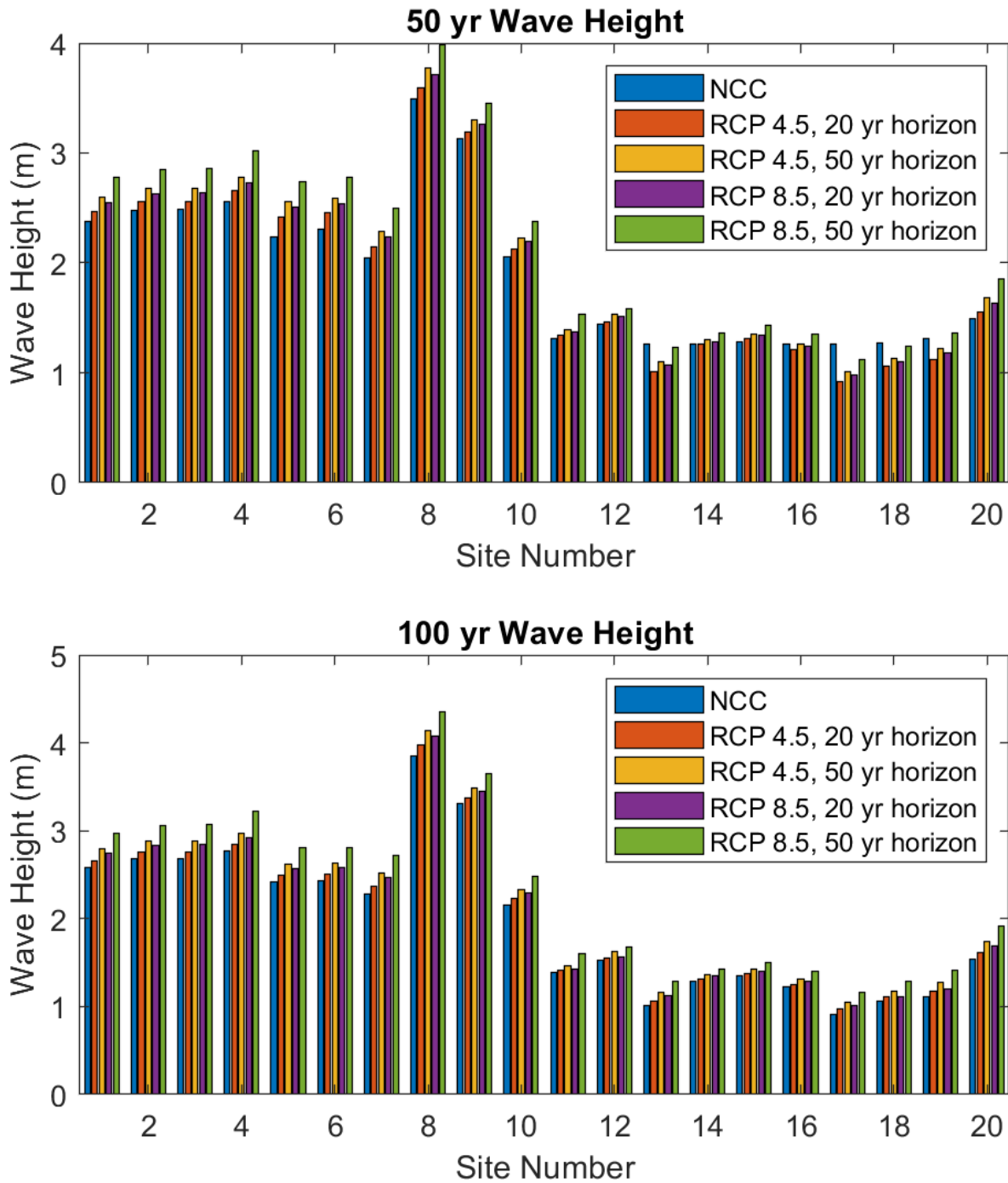


Figure 8.5 Modeled future hurricane wave conditions for climate scenario RCP 4.5 and 8.5 compared to no climate change (NCC) for 20- and 50-year forecast time horizons; 50-year return period wave height (top) and 100-year return period wave height (bottom)

8.6 Qualitative Comparison

A qualitative summary of present and future beach, geologic, and wave conditions show variable factors to consider for different parts of Bermuda (Table 8-2). Paleosol layers and beaches exist at many south shore sites evaluated. The south shore has relatively large present-day waves compared to the west and north shores. Standard day to day wave conditions on the south shore are expected to increase moderately, while the largest increase is forecast to occur on the west shore. Standard day to day wave condition changes on the north and east shore are expected to be relatively small. Expected changes in hurricane wave conditions are highest and lowest, on the south and west shore, respectively.

The combined factors of weak cliff materials, small volume beaches, forecasted beach retreat, and increasing day to day and hurricane wave conditions at many south shore sites, suggest that these sites will be relatively more susceptible to increased erosion as sea levels rise compared to other areas. In particular, site 1 (Surf Side) and 7 (Marley Beach) are likely to experience increased cliff erosion. The west shore is relatively vulnerable to increased standard day to day wave conditions, while the north and east shore appear relatively sheltered to future wave changes compared to other areas. Future conditions and changes at sites 8 (Spittal Pond) and 9 (Great Head) are primarily related to potential increases in hurricane wave conditions.

Table 8-2 Color coded qualitative relative comparison between sites for various beach, geologic, and wave conditions and forecasts

Site Name	Site Number	Beach Present	~ Back Beach Elevation (m)	Historical Beach Width Minimum (m)	Cliff Hardness Minimum (Schmidt Hammer)	Lower Cliff Paleosol Observed	Waves Hs (m) *		Waves Standard Conditions, % Change *								Waves Hurricane Conditions (m) *						Brunn Rule Shoreline Change (m)								
							Present		RCP 4.5				RCP 8.5				NCC		RCP 4.5		RCP 8.5		RCP 4.5		RCP 8.5						
							mean	99th %	50th %	99th %	50%	99th %	50%	99th %	50 Yr	100 Yr	20 year horizon	50 yr horizon	20 year horizon	50 yr horizon	50 yr horizon	100 yr horizon	50 year horizon	100 year horizon	100 year horizon						
									2050	2100	2050	2100	2050	2100	2050	2100	50 Yr	100 Yr	50 Yr	100 Yr	50 Yr	100 Yr	50 Yr	100 Yr	50 year horizon	100 year horizon	100 year horizon				
Surf Side Beach	1	Yes	2	0	0	Yes	0.5	1.0	2	3	11	12	5	5	22	27	2.4	2.6	2.5	2.7	2.6	2.8	2.6	2.7	2.8	3.0	13	34	14	42	
Elbow Beach	2	Yes	3	10	0	Yes	0.5	1.1	2	2	9	9	3	4	19	22	2.5	2.7	2.6	2.8	2.7	2.9	2.6	2.8	2.9	3.1	9	24	10	29	
John Smith	3	Yes	3.5	30	19.5	Yes	0.4	1.1	1	1	9	9	2	2	18	20	2.5	2.7	2.6	2.8	2.7	2.9	2.6	2.8	2.9	3.1	7	20	8	24	
Rosewood Club	4	Yes	4	40	41	No?	0.5	1.3	1	2	7	8	3	3	13	15	2.6	2.8	2.7	2.8	2.8	3.0	2.7	2.9	3.0	3.2	13	36	15	44	
Church Bay	5	Yes	3	—	12.5	Yes	0.5	0.9	8	8	13	14	10	10	26	31	2.2	2.4	2.4	2.5	2.6	2.6	2.5	2.6	2.7	2.8	11	29	12	36	
The Reefs Resort	6	Yes	3	—	25	Yes	0.5	1.0	3	3	10	10	6	7	21	26	2.3	2.4	2.5	2.5	2.6	2.6	2.5	2.6	2.8	2.8	6	15	6	19	
Marley Beach	7	Yes	2.5	—	9.5	Yes	0.3	0.7	0	0	7	8	8	6	19	22	2.0	2.3	2.1	2.4	2.3	2.5	2.2	2.5	2.5	2.7	13	34	14	42	
Spittal Pond	8	No	—	—	19.5	No	0.5	1.4	0	0	4	4	-1	-1	8	9	3.5	3.9	3.6	4.0	3.8	4.1	3.7	4.1	4.0	4.4	—	—	—	—	
Great Head	9	No	—	—	41	No	0.7	1.8	1	1	1	1	2	2	2	3	3.1	3.3	3.2	3.4	3.3	3.5	3.3	3.4	3.5	3.6	—	—	—	—	
Barry Road	10	No	—	—	30	No	0.6	1.2	4	4	7	8	7	8	13	15	2.1	2.2	2.1	2.2	2.2	2.3	2.2	2.3	2.4	2.5	—	—	—	—	
Railway Trail near Callen Glen Dr.	11	No	—	—	12.5	No	0.4	0.8	3	3	5	5	7	8	11	14	1.3	1.4	1.3	1.4	1.4	1.5	1.4	1.4	1.5	1.6	—	—	—	—	
Railway Trail near Lynwood Dr.	12	No	—	—	15.5	No	0.4	0.8	4	4	6	6	8	10	13	16	1.4	1.5	1.5	1.6	1.5	1.6	1.5	1.6	1.6	1.7	—	—	—	—	
Robinson Bay Park	13	No	—	—	10.5	No	0.2	0.3	3	3	6	6	7	9	13	16	1.3	1.0	1.0	1.1	1.1	1.2	1.1	1.1	1.1	1.2	1.3	—	—	—	—
Ducking Stool Park	14	No	—	—	27.5	No	0.4	0.7	3	4	5	5	8	10	13	16	1.3	1.3	1.3	1.3	1.3	1.4	1.3	1.3	1.4	1.4	—	—	—	—	
Clarence Cove	15	No	—	—	13.5	No	0.4	0.7	4	4	6	7	9	11	13	16	1.3	1.3	1.3	1.4	1.4	1.4	1.3	1.4	1.4	1.5	—	—	—	—	
Dockyard - Pulpit Rock	16	No	—	—	13	Yes	0.4	0.7	4	5	6	7	10	12	15	19	1.3	1.2	1.2	1.3	1.3	1.3	1.2	1.3	1.4	1.4	—	—	—	—	
Theo's Cove	17	Partial	—	—	15	No	0.2	0.3	11	12	19	20	36	38	49	55	1.3	0.9	0.9	1.0	1.0	1.1	1.0	1.0	1.1	1.1	1.2	—	—	—	—
Daniels Head	18	Partial	—	—	29.5	No	0.3	0.4	8	9	11	12	18	21	24	29	1.3	1.1	1.1	1.1	1.1	1.2	1.1	1.1	1.1	1.2	1.3	—	—	—	—
Hog Bay Park	19	No	—	—	22.50	No	0.2	0.3	16	18	24	25	29	33	50	59	1.3	1.1	1.1	1.2	1.2	1.3	1.2	1.2	1.4	1.4	—	—	—	—	
West Whale Bay Park	20	Partial	—	—	17	No	0.4	0.5	9	9	17	19	17	20	38	45	1.5	1.5	1.6	1.6	1.7	1.7	1.6	1.7	1.9	1.9	—	—	—	—	

* Median of study site

Colors are relative within each factor, with darker blues representing increasing factors that are expected to result in increased cliff erosion rates.



8.7 Modified Scape Model

In addition to the qualitative assessment above, a simple model was used to estimate future conditions based on the rate of historical sea level rise (3.84 ± 0.4 mm/year; Climate Studies Group Mona, 2022), estimated future rates of sea level rise (5.4 - 9.6 mm/yr for RCP 4.5, and 7.1-14.8 mm/yr for RCP 8.5; Climate Studies Group Mona, 2022), and a range of estimated historical cliff retreat rates spanning 5-33 cm/yr. The upper range represents the observed rate of about 33 cm/yr estimated from the lidar data east of the Bermudian Resort.

Future retreat was estimated using the modified SCAPE model (Walkden and Dickson, 2008; Ashton et al., 2011; Table 8-3), which assumes cliff erosion is primarily driven by wave action. The modified SCAPE model assumes future cliff retreat depends on historical cliff retreat, and historical and future sea level rise. The modified SCAPE model is expressed as a relatively simple relationship but was derived from detailed process-based modeling of soft cliff coasts using the full SCAPE model version (*Soft Cliff and Platform Erosion*, Walkden and Dickson, 2008). Therefore, the modified SCAPE model is considered more physics-based compared to the other simplified coastal erosion models.

Table 8-3 Modeled future cliff retreat rates for RCP 4.5 and 8.5 based on the Modified SCAPE model for a range of potential historical retreat rates

Future Retreat Rate (cm/yr)						
	RCP 4.5			RCP 8.5		
	SLR 5.7 mm/yr	SLR 7.7 mm/yr	SLR 7.7 mm/yr	SLR 6.6 mm/yr	SLR 10.5 mm/yr	SLR 10.5 mm/yr
Historical Retreat Rate (cm/yr)	20 Year Horizon	50 Year Horizon	100 Year Horizon	20 Year Horizon	50 Year Horizon	100 Year Horizon
5	6	7	7	7	8	8
10	12	14	14	13	17	17
20	24	28	28	26	33	33
33	41	47	47	44	55	55

8.8 Summary

A qualitative comparison of 20 coastal cliff sites spread throughout Bermuda was conducted. The coastal cliffs can be divided into two main categories: those with and without a fronting beach. Cliffs with fronting beaches mostly occur on the south shore. Beaches of sufficient volume can provide

protection to wave-driven cliff erosion. However, the cliffs fronted by beaches were often observed to have a weak rock layer (paleosol) near the cliff base that is relatively susceptible to erosion. As sea levels rise, forecasted increasing wave heights and modeled beach retreat make these cliffs particularly vulnerable to climate change and increased erosion rates. Alternatively, relatively low or moderate increases in future erosion rates are expected at sites with relatively small forecast changes in wave conditions, such as on the north coast, and where cliffs plunge directly into deep water (e.g., headlands). The modeled increase in day-to-day wave conditions was highest on the west coast, suggesting a potential moderate acceleration of future cliff retreat rates at those sites.

If sea level rise causes waves to interact with a paleosol layer (or other weak layer) that is not currently actively eroded by waves, erosion rates would likely accelerate. The elevation and locations of the paleosol layers varied along the coastline and are not currently mapped in sufficient detail to allow geographic analysis of this factor. This could be useful as an area of focus for future studies. Additional observations such as high resolution lidar and/or imagery are also needed to develop a detailed inventory of quantitative coastal cliff changes in Bermuda, required to calibrate and develop robust models of coastal cliff evolution under future climate scenarios.

9 Hydrogeologic Assessment

Impacts of rising sea level on the hydraulic balance between aquifers and the ocean will likely threaten freshwater resources and aquatic ecosystems along many coastline areas around the world, and in many cases, for some distance inland in small oceanic islands. It is vital to understand the vulnerability of groundwater systems to these rising sea levels and saltwater intrusion and to assess and understand the factors that determine the magnitude of system response. Sea water (or salt water) intrusion is defined as the lateral landward migration of the sea water-fresh water interface in the subsurface. Vulnerability in this context is defined by the rate and magnitude of salinization (or salinification) of coastal aquifers and changes in groundwater flow to the sea. This understanding is critical to developing effective management and adaptation plans in coastal zones. Salinization can occur from lateral saltwater intrusion at depth and infiltration from surface due to coastline transgression and storm surge inundation. Changes in groundwater flux to the ocean can affect groundwater discharge and circulation of saltwater through the offshore subsurface. This can alter both ocean aquatic ecosystems and ocean chemical composition.

Bermuda's fresh-water lenses float on the underlying saline groundwater due to the density differences between fresh and salt water. Sea water rise is translated throughout the subsurface of Bermuda through the highly permeable Walsingham Formation rocks with the result that a rise in sea levels is translated into a comparable rise of the freshwater lenses. The interface zone of mixing of fresh and saline water at the base of the lenses and the water table will rise at the same rate on average.

The rise and fall of the sea level at the coast of Bermuda is translated inland and causes the freshwater lenses to rise and fall as well. Since the topography of Bermuda rises relatively steeply from the shoreline, the rise of the freshwater lenses are not likely to intercept the ground surface except for a limited area near the coast in the foreseeable future. Therefore, the shape of the groundwater lenses in cross-section are predicted to stay the same assuming extraction and recharge remain constant. This is a recharge limited system as rather than a topography limited system and the horizontal hydraulic gradient (and thus the groundwater flow to the sea) will remain the same in the future assuming the hydraulic conductivity of the aquifer is more or less the same above the existing water table as it is below the existing water table and the recharge remains the same.

In the coastal areas the sea level rise combined with the maximum tidal effect plus half the steric anomaly plus meso scale effects is currently (2022) calculated to have resulted in saline water some 1.49m above OD⁷ intruding into the subsurface or 1.23m above existing calculated sea level. Glasspool (2008) estimated sea level rise without including meso scale anomalies. In this study half the steric anomaly is used plus the meso scale effect since the rise in sea level will deposit salt within the pores of the rock or soil which will stay in situ for a period even after the sea levels decline in the annual cycle. This saline water will slowly drain by gravity or be slowly displaced by recharging infiltration but at a much slower rate than the daily and seasonal effects controlling sea level rise and intrusion into the rock and soil matrix.

The effects of tidal damping diminish the range of oscillations of the water table moving inland from the coasts. Vacher (1974) shows that on the north shore of Bermuda and moving inland, the tidal

⁷ Ordnance datum was set at a mean sea level (msl) of 0.000m in 1963 from tide gauge records at the Bermuda Biological Station. (Johnson, 1984 cited in Ellison, 1993). Glasspool 2008, gave msl as 0.21 m AOD. Plotting these values on a graph gives a 2022 msl of 0.26m AOD.

oscillation in the Central Lens is reduced to 10cm at 100-120m from the north shore and reduced to 2cm within 200 m from the north shore. The maximum tidal range at the coasts during spring tides is 1.2m. This Central Lens north of the line of east-west trending inland ponds is underlain by the Langton Aquifer with its relatively low permeability rocks. The higher permeability Brighton Aquifer to the south has the 10cm contour of tidal oscillation at approximately 500-600m from the south shore, and the 2cm contour at approximately 800m from the south shore. Therefore, the effects of rising sea levels will be greater inland from the south shore in the Brighton Aquifer than on the north shore in the Langton Aquifer inland from the ocean.

Barometric effects on sea level occur every few days. For a drop in air pressure of 1 mb (0.1 Kpa) sea level rises 1cm. Since barometric pressure varies every few days it would be prudent to include a component of sea level rise due to varying atmospheric pressure and a value of 25cm has therefore been used.

Capillary effects of migrating salt into the vadose zone have not been included in the estimates of salinization. Further studies are required in different environments and soil types to determine the scope and extent of capillary effects.

With the projected sea level rise from the calculated 2022 sea level in relation to Bermuda Ordnance Datum, future projected sea level rises under RCP 4.5 are given with reference to this datum are given in Table 9-1.

Table 9-1 Projected sea level rise and elevation above Bermuda Ordnance Datum, RCP 4.5

Year	Years from Present	Projected Sea Level Rise (m) extrapolated from Mona data	Projected sea level above present level (m) above OD
2022	0		0.26
2042	20	0.18	0.44
2072	50	0.36	0.62
2122	100	0.66	0.92

The sea level rise for 2122 for both RCP 4.5 and 8.5 was calculated from graphing the Mona data plus OD and extrapolating to 2122. There is no allowance for the acceleration of sea level rise that may occur. Table 9-2 shows projected sea level rise under RCP 8.5 in relation to the Bermuda Ordnance Datum.

Table 9-2 Projected sea level rise and elevation above Bermuda Ordnance Datum, RCP 8.5

Year	Years from present	Projected Sea Level Rise (m)	Projected Sea Level above Present Level m above OD
2022	0		0.26
2042	20	0.18	0.44
2072	50	0.45	0.71
2122	100	0.85	1.1

Table 9-3 shows the expected sea level rise around Bermuda which includes tidal effects, the local steric anomaly and meso scale effects for RCP 4.5 and 8.5. This will also be the projected maximum rise of the groundwater lenses including the water table at the coasts. The tidal effect on groundwater lens rise will diminish fairly rapidly and progressively inland from the coasts.

Table 9-3 Projected sea level rise around Bermuda plus tidal, steric and meso Scale Effects, RCP 4.5 and 8.5 equals total groundwater lens rise at the coasts

Years From Present (2022)	RCP	Sea Level Rise Above OD m	Maximum Tidal Height m	Local Steric Anomaly m	Meso Scale Effects m	Barometric Pressure Effects m	Bermuda subsidence below 2022 level (m)	Total projected groundwater rise above OD (m)
0	4.5	0.26	0.6	0.125	0.25	0.25	0	1.49
20	4.5	0.44	0.6	0.125	0.25	0.25	0.018	1.68
50	4.5	0.62	0.6	0.125	0.25	0.25	0.045	1.89
100	4.5	0.92	0.6	0.125	0.25	0.25	0.09	2.24
0	8.5	0.26	0.6	0.125	0.25	0.25	0	1.49
20	8.5	0.44	0.6	0.125	0.25	0.25	0.018	1.68
50	8.5	0.71	0.6	0.125	0.25	0.25	0.045	1.98
100	8.5	1.10	0.6	0.125	0.25	0.25	0.09	2.42

The cumulative maximum sea level rise (therefore groundwater rise at the coasts) at any given time as a result of these effects will occur relatively infrequently. Spring tides occur twice each lunar month at new or full moons. Neap tides occur twice a month and occur when the sun and moon are 90 degrees from each other, at 1st and 3rd quarter. Barometric pressure effects vary daily or every few days and can be dramatic during relatively rare hurricanes which hit Bermuda. The local steric anomaly peaks in October each year at its maximum level of 12.5cm and six months later it is at -12.5cm. Meso scale effects can occur at any time around Bermuda and they emerge from instabilities of the strongly horizontally sheared motions of the Gulf Stream. These eddies often take the form of well-defined rings extending to great depth and can last for weeks to over a year. (NOAA <https://oceanservice.noaa.gov/facts/eddy.html>).

In addition, the entire landmass of Bermuda is sinking at a rate of 0.9 mm/yr. which will add to apparent sea level rise of 9.9cm after 100 years. Satellite GPS vertical motion velocity data published by the Jet Propulsion Laboratory in the US indicates that the island has been subsiding at the rate of 0.9 mm/year since 1993. These data have been derived from the vertical motion sensor positioned at the Bermuda Institute of Ocean Sciences. This subsidence will add to apparent sea level rise of 9.9 cm after 100 years. (Glasspool, 2008, JPL website <https://www.sonel.org/-JPL14-.html>)

This subsidence has been added to the total sea level rise in Table 9-3.

Table 9-4 gives the total projected maximum groundwater lens rise at the inland ponds in the Central Lens area. Maximum tidal effects in these areas are diminished because of damping and the maximum

rise due to tidal effects is approximately 2cm. The exception to this is the area around and east of the Pembroke Canal where the maximum tidal effect will be 10cm (Vacher, 1974).

Table 9-4 Maximum central lens rise at inland ponds

Years From Present (2022)	RCP	Sea Level Rise Above OD m	Maximum Tidal Height m	Local Steric Anomaly m	Meso Scale Effects m	Barometric Pressure Effects m	Bermuda Subsidence Below 2022 Level m	Total Projected Maximum Central Lens Rise in and Around Inland Ponds, Above OD m
0	4.5	0.26	0.02	0.125	0.25	0.25	0	0.91
20	4.5	0.44	0.02	0.125	0.25	0.25	0.018	1.10
50	4.5	0.62	0.02	0.125	0.25	0.25	0.045	1.31
100	4.5	0.92	0.02	0.125	0.25	0.25	0.09	1.66
0	8.5	0.26	0.02	0.125	0.25	0.25	0	0.91
20	8.5	0.44	0.02	0.125	0.25	0.25	0.018	1.10
50	8.5	0.71	0.02	0.125	0.25	0.25	0.045	1.40
100	8.5	1.10	0.02	0.125	0.25	0.25	0.09	1.84

It is questionable whether the inland ponds (with the possible exception of Pembroke Marsh West) will become more saline as sea level rises. From the literature, it appears that the Central Lens underlies the NE-SW line of ponds and the lens will rise with rising sea levels. With the two interpretations of the degree of hydraulic connection between the ponds and the Central Lens groundwater, it is likely that the ponds will rise over the years and least as much as average sea level around Bermuda rises. If the hydraulic connection is stronger, then some oceanic oscillations will be transmitted inland resulting in a higher water level in the ponds at various times than from sea level rise alone. The conclusion of this analysis is that the ponds in the Central Lens and the immediate surrounding area will not suffer from an increase in salinity in the foreseeable future. Monitoring of the ponds' water levels would be useful to ascertain the degree of hydraulic connection between the ponds and the Central Lens.

The saltwater ponds generally lie close to the south coasts. These are generally brackish as they lie in more permeable bedrock formations. Tidal effects are transmitted inland with less damping than along the north shore in the less permeable rocks.

The area at the west end of Pembroke Marsh West and towards the west coast from the marsh area to the Pembroke Canal will likely see an increase in salinization. Tidal effects of groundwater level rise

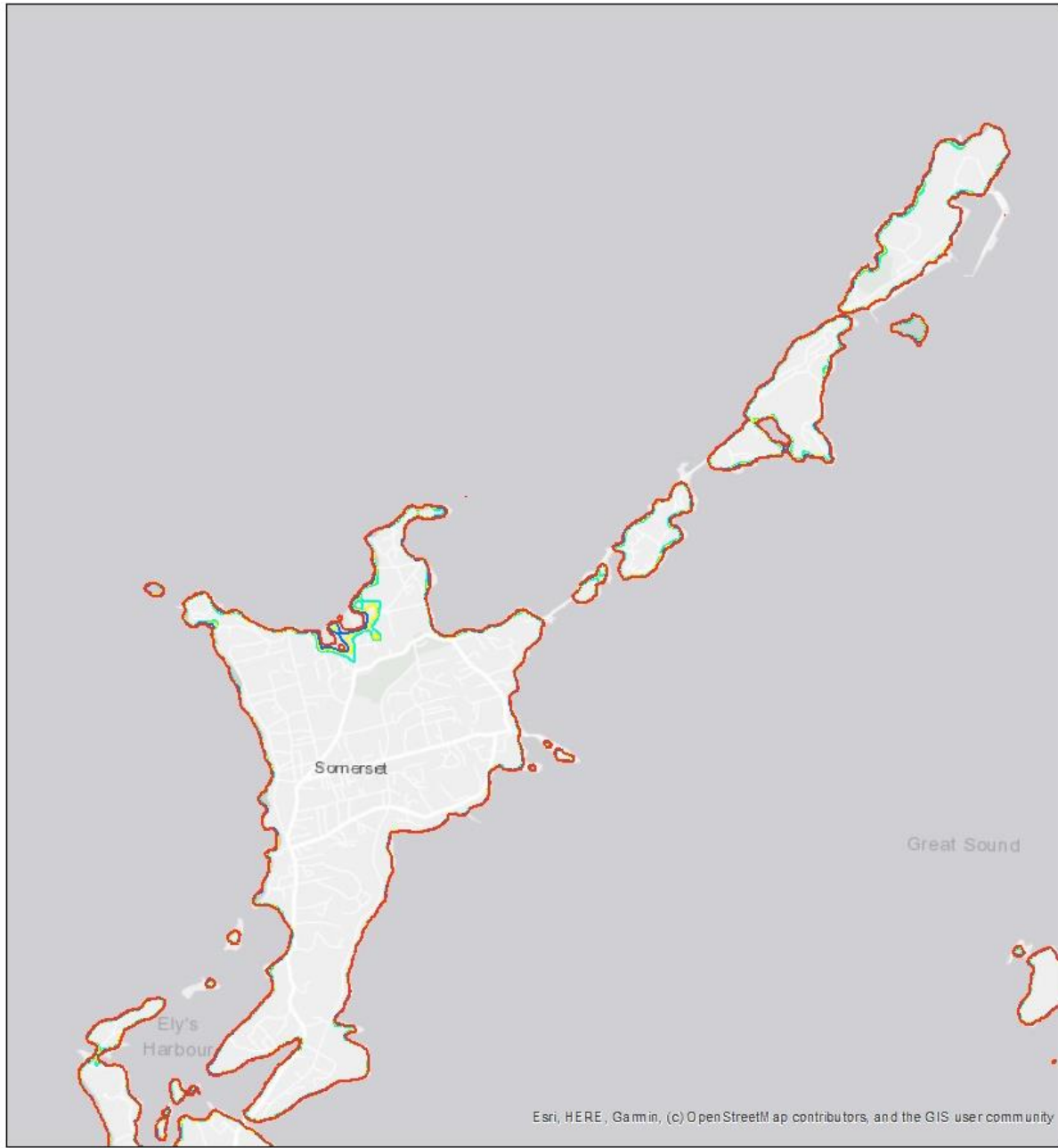
will be strongest in the canal and rapidly diminish inland to about 2cm in the Pembroke Marsh West. The other components of sea level rise will affect salinity levels in the groundwater around the Pembroke Canal and east possibly to the marsh.

As explained above saline groundwater rising with oscillations of the ocean in areas just at the coast of Bermuda and for some distance inland will introduce saline conditions in rocks containing freshwater aquifers progressively higher in elevation as sea levels rise. Saline water will displace fresh or brackish water in the pores of the rocks of the Langton Aquifer and the pores and fractures and solution channels of the Brighton Aquifer with the greatest impact being at and near the coast. Even with the relatively infrequent occurrence of a spring tide with the passage of a low-pressure area, with the October high steric anomaly and under the influence of a meso scale eddy, saline water will fill soil and rock pores to an elevation indicated on Table 9-3. With a decline in ocean levels (low tide, negative steric anomaly, high atmospheric pressure) some of this water will drain by gravity and the influence of recharging precipitation but the process is much slower than the water level rise. Chemical changes will occur relatively slowly and will involve cation exchange involving sodium, calcium and magnesium. This process is complicated by the migration of the interface zone inland as sea levels rise and by the presence of the vadose zone above the oscillating water table where saline water could migrate as a result of chemical diffusion and dispersion processes. In addition, evapotranspiration could act as a pump to induce upward flow of saline or brackish water. Soil in agricultural areas near the coast may see a decline of production over the years depending on their elevation in relation to sea level.

The Government of Bermuda Digital Terrain Model (DTM) was used as the basis to produce maps showing land areas in Bermuda below the future maximum projected sea level (plus transient effects) elevation changes for two scenarios and three future points in time. The DTM works from the ordnance datum of 0m elevation. Current mean sea level without oscillations detailed above was calculated in this study as 0.26m above OD (2022).

Figure 9.1 to Figure 9.12 show maximum projected groundwater rises (sea level plus transient effect rises) for present day, 20, 50 and 100 years under RCP 4.5 and 8.5.

The complete hydrogeologic report is attached as Appendix F



BERMUDA - CLIMATE CHANGE STUDY

DOCKYARD RCP 4.5

LEGEND

- Present Groundwater Elevation 1.49 m Above OD
- Projected Groundwater Rise 1.68 m Above OD
- Projected Groundwater Rise 1.89 m Above OD
- Projected Groundwater Rise 2.24 m Above OD

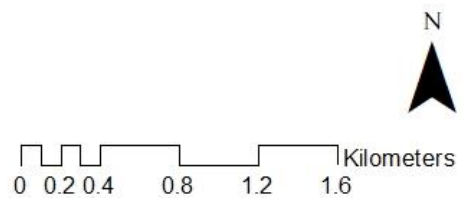
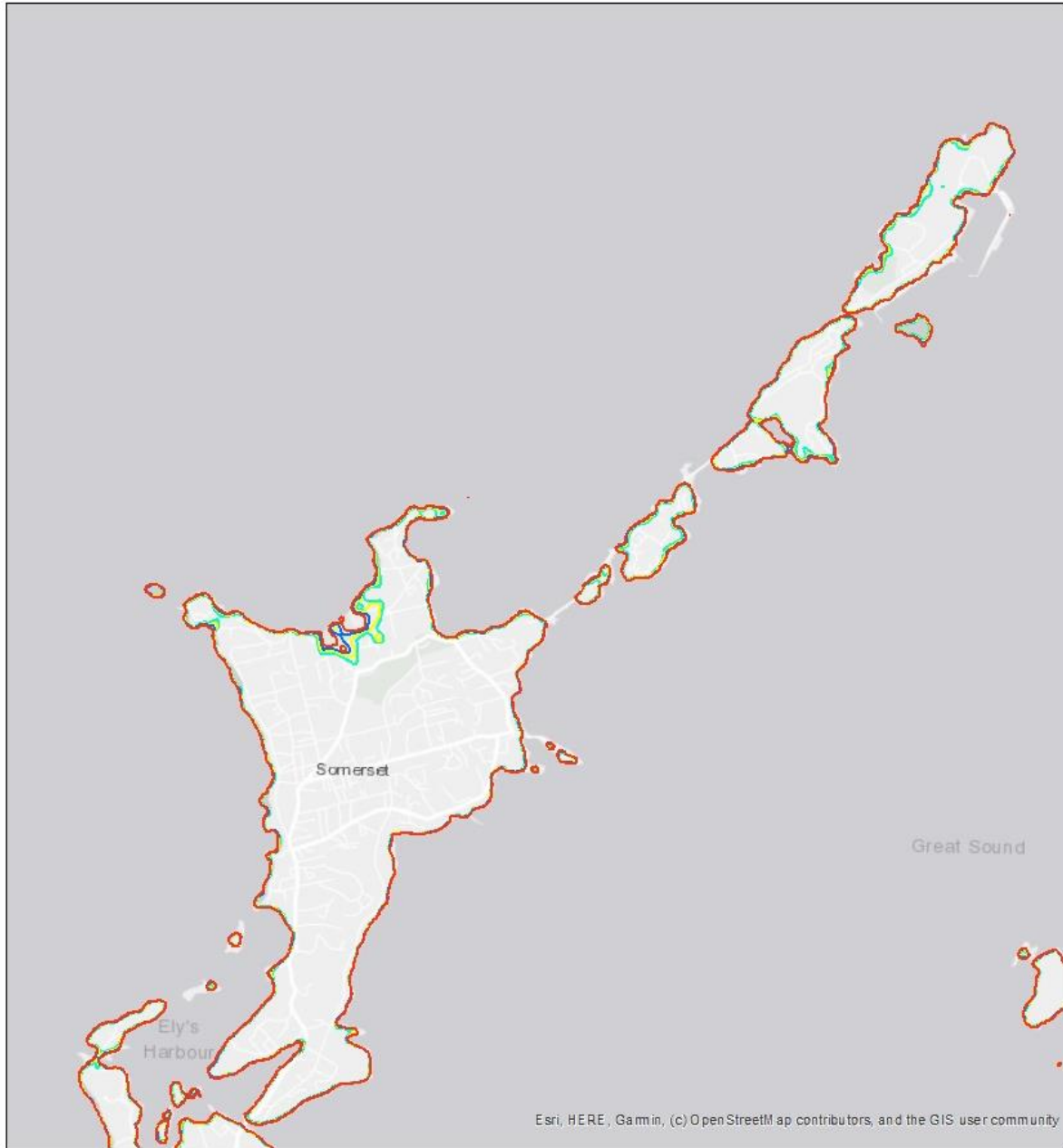


Figure 9.1 Predicted groundwater rise for the Dockyard area for RCP 4.5



BERMUDA - CLIMATE CHANGE STUDY

LEGEND

- Present Groundwater Elevation 1.49 m Above OD
- Projected Groundwater Rise 1.68 m Above OD
- Projected Groundwater Rise 1.98 m Above OD
- Projected Groundwater Rise 2.42 m Above OD

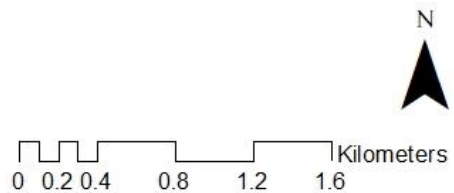
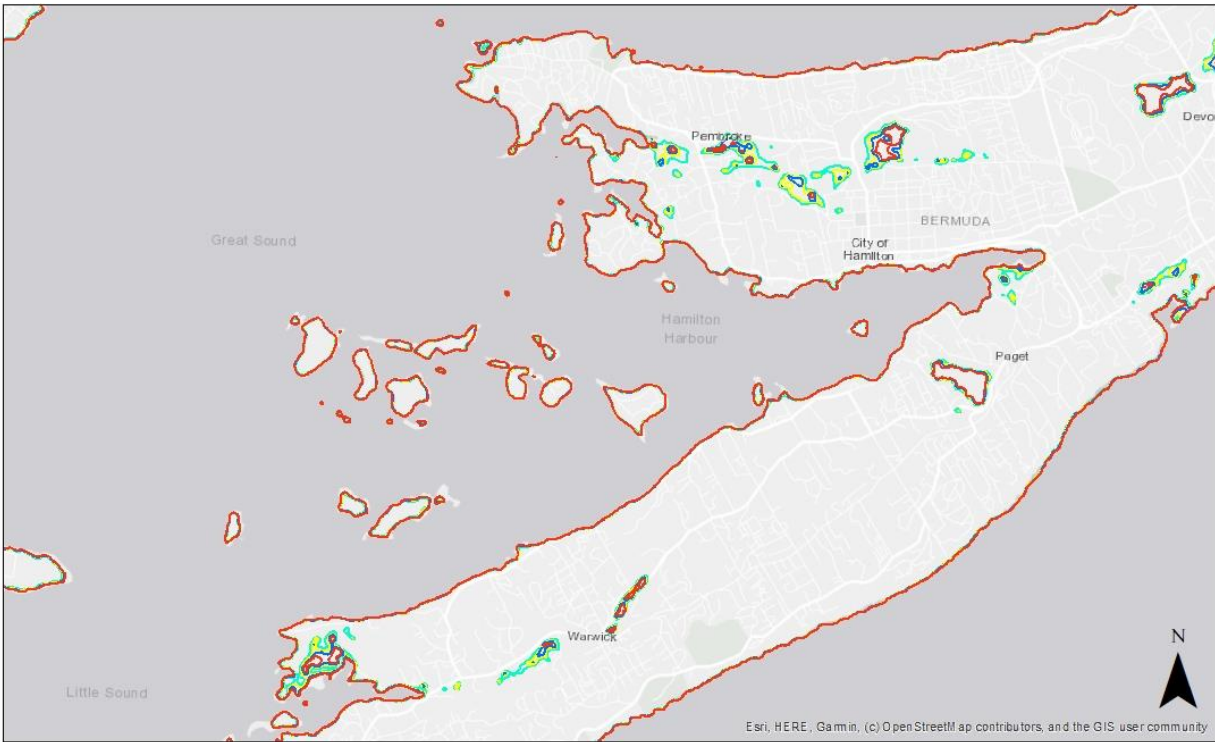


Figure 9.2 Predicted groundwater rise for the Dockyard area for RCP 8.5



BERMUDA - CLIMATE CHANGE STUDY
GREAT SOUND RCP 4.5

LEGEND

- Present Groundwater Elevation 1.49 m Above OD
- Projected Groundwater Rise 1.89 m Above OD
- Projected Groundwater Rise 1.68 m Above OD
- Projected Groundwater Rise 2.24 m Above OD

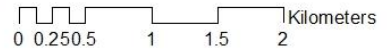
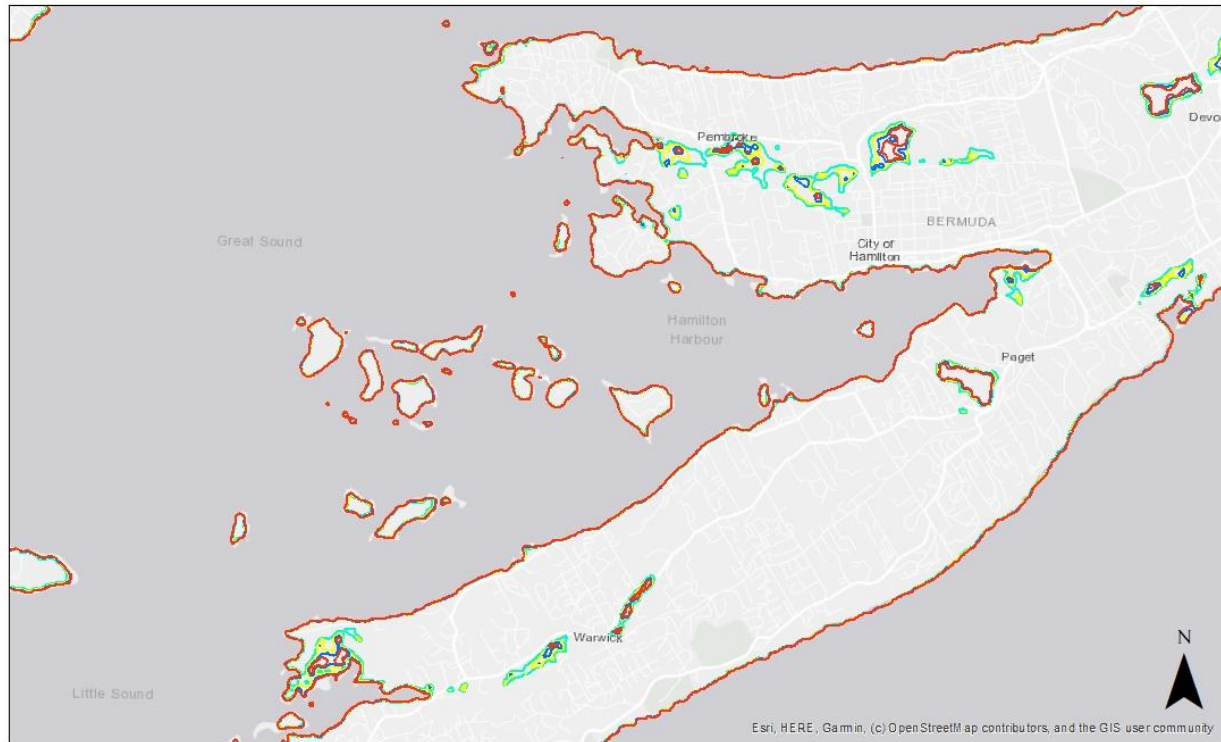


Figure 9.3 Predicted groundwater rise for the Great Sound area for RCP 4.5

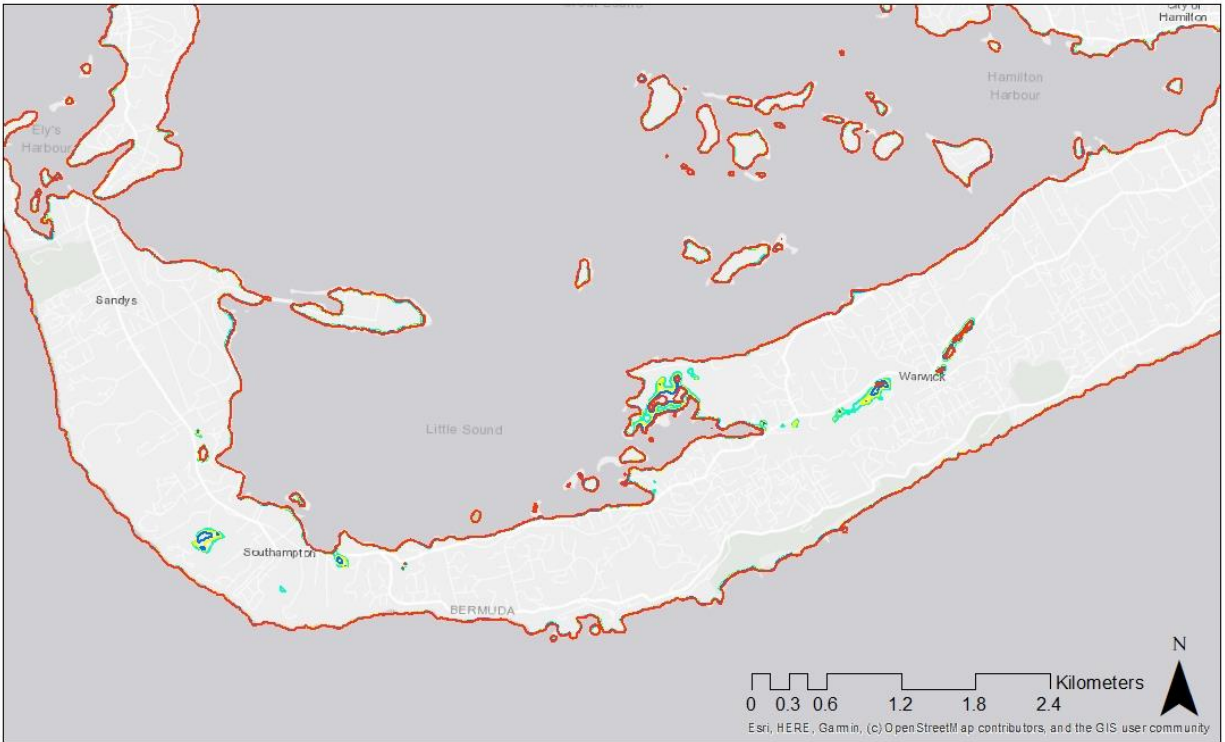


BERMUDA - CLIMATE CHANGE STUDY
GREAT SOUND RCP 8.5

LEGEND

- Present Groundwater Elevation 1.49 m Above OD
 - Projected Groundwater Rise 1.98 m Above OD
 - Projected Groundwater Rise 1.68 m Above OD
 - Projected Groundwater Rise 2.42 m Above OD
- 0 0.25 0.5 1 1.5 2 Kilometers

Figure 9.4 Predicted groundwater rise for the Great Sound area for RCP 8.5

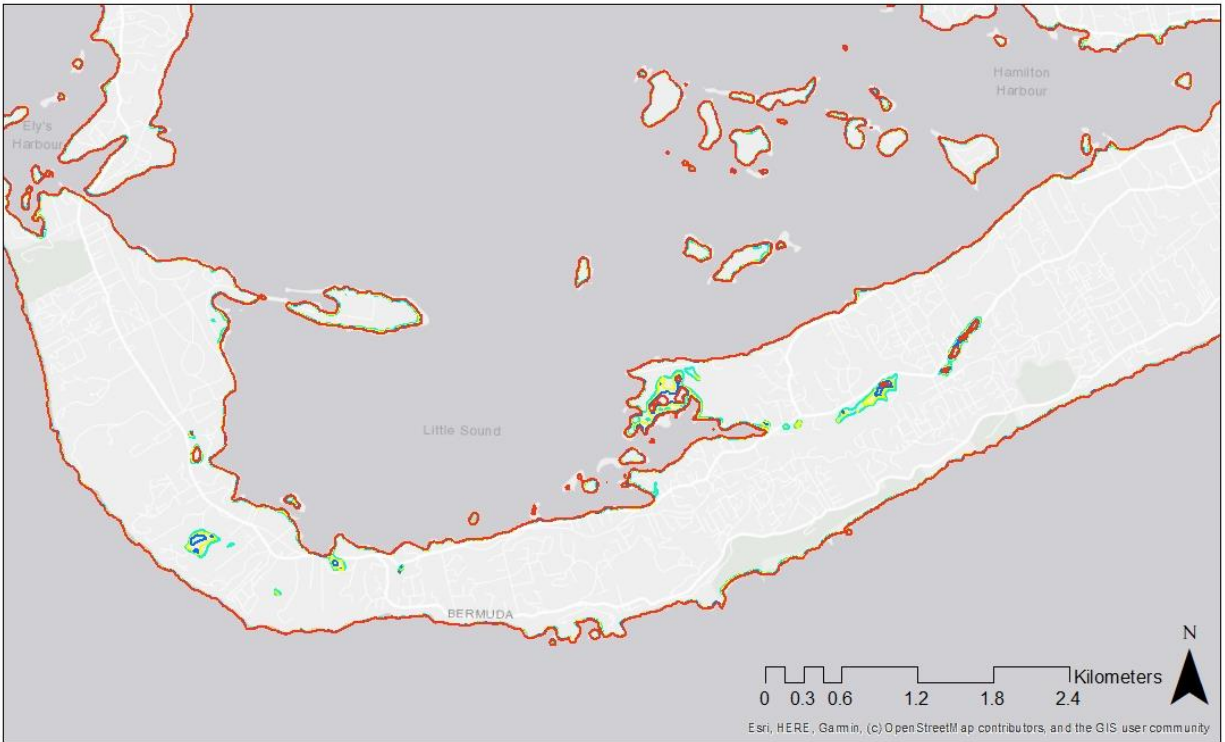


BERMUDA - CLIMATE CHANGE STUDY
SOUTH COAST BEACHES RCP 4.5

LEGEND

- Present Groundwater Elevation 1.49 m Above OD
- Projected Groundwater Rise 1.89 m Above OD
- Projected Groundwater Rise 1.68 m Above OD
- Projected Groundwater Rise 2.24 m Above OD

Figure 9.5 Predicted groundwater rise for south coast beaches for RCP 4.5

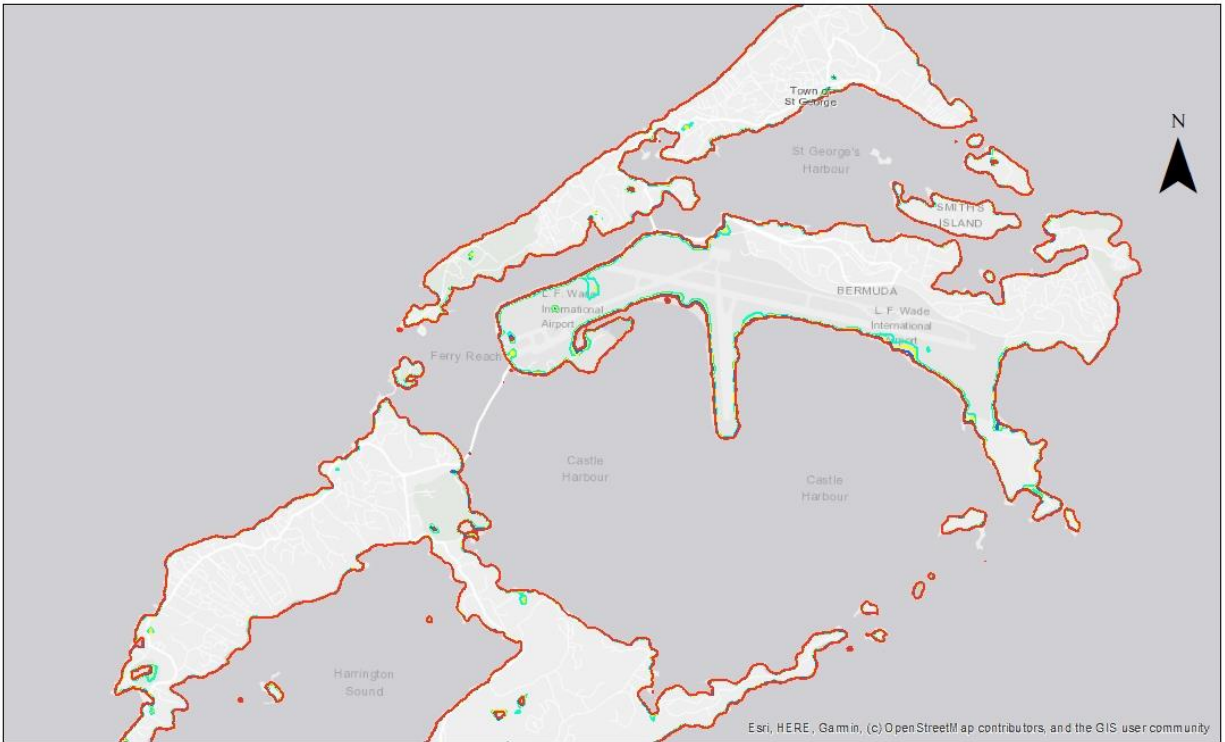


BERMUDA - CLIMATE CHANGE STUDY
SOUTH COAST BEACHES RCP 8.5

LEGEND

- Present Groundwater Elevation 1.49 m Above OD
- Projected Groundwater Rise 1.98 m Above OD
- Projected Groundwater Rise 1.68 m Above OD
- Projected Groundwater Rise 2.42 m Above OD

Figure 9.6 Predicted groundwater rise for south coast beaches for RCP 8.5



BERMUDA - CLIMATE CHANGE STUDY
ST. GEORGE'S AND CASTLE HARBOURS RCP 4.5

LEGEND

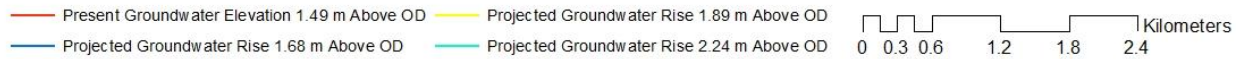
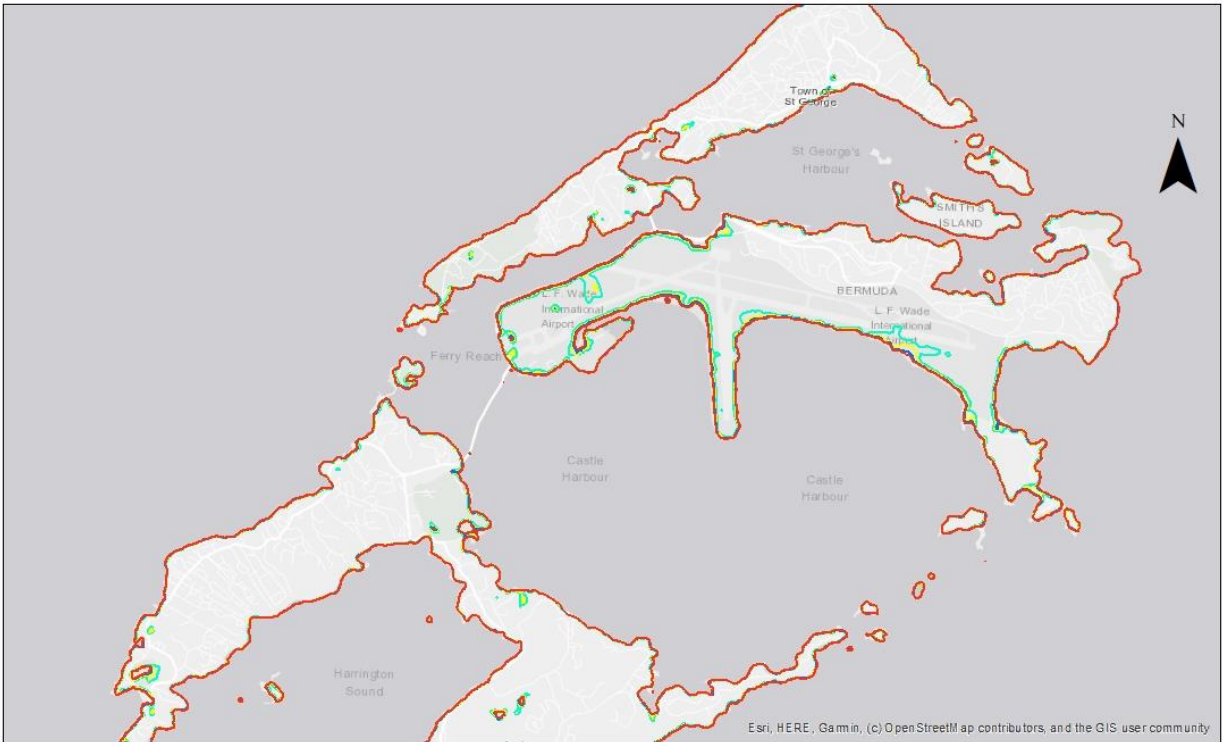


Figure 9.7 Predicted groundwater rise for St George's and Castle Harbour for RCP 4.5

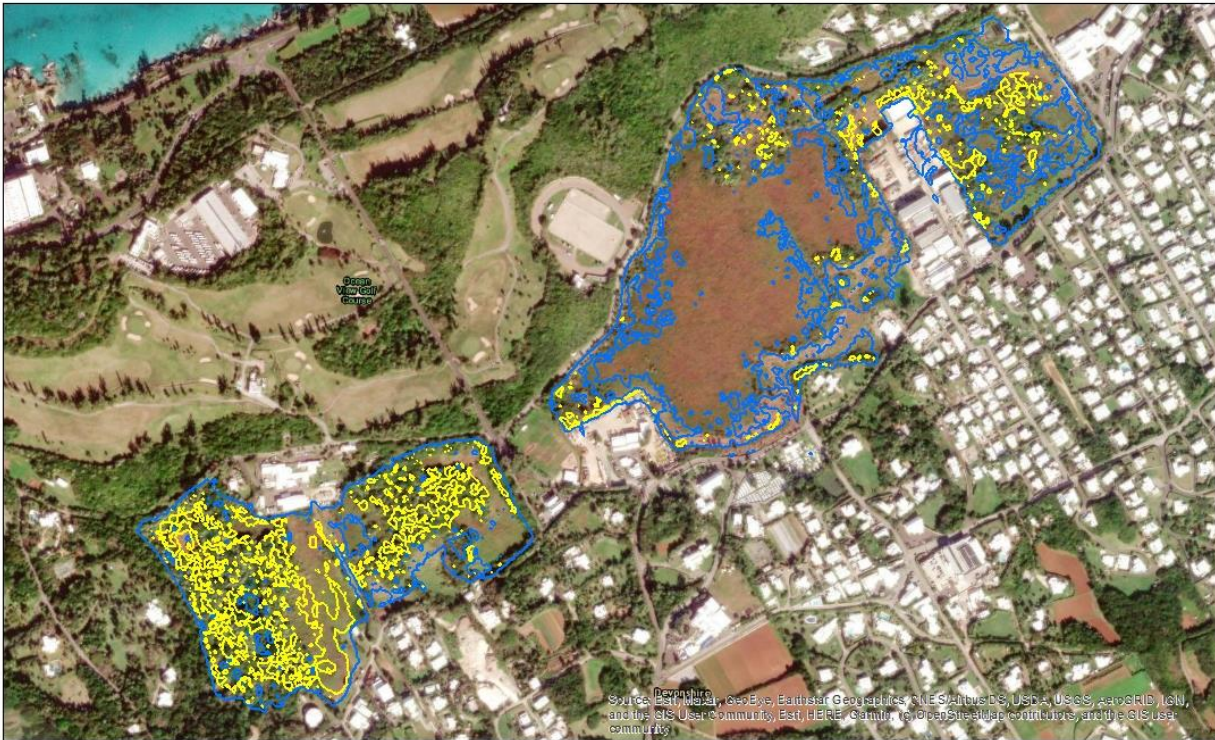


BERMUDA - CLIMATE CHANGE STUDY
ST. GEORGE'S AND CASTLE HARBOURS RCP 8.5

LEGEND

- Present Groundwater Elevation 1.49 m Above OD
 - Projected Groundwater Rise 1.68 m Above OD
 - Projected Groundwater Rise 1.98 m Above OD
 - Projected Groundwater Rise 2.42 m Above OD
- 0 0.3 0.6 1.2 1.8 2.4 Kilometers

Figure 9.8 Predicted groundwater rise for St George's and Castle Harbour for RCP 8.5



BERMUDA - CLIMATE CHANGE STUDY
DEVONSHIRE MARSH RCP 4.5

LEGEND

- Projected Maximum Central Lens Rise 1.31m
- Projected Maximum Central Lens Rise 1.66m

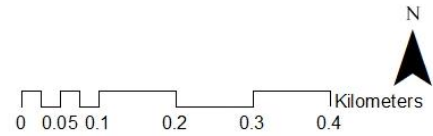
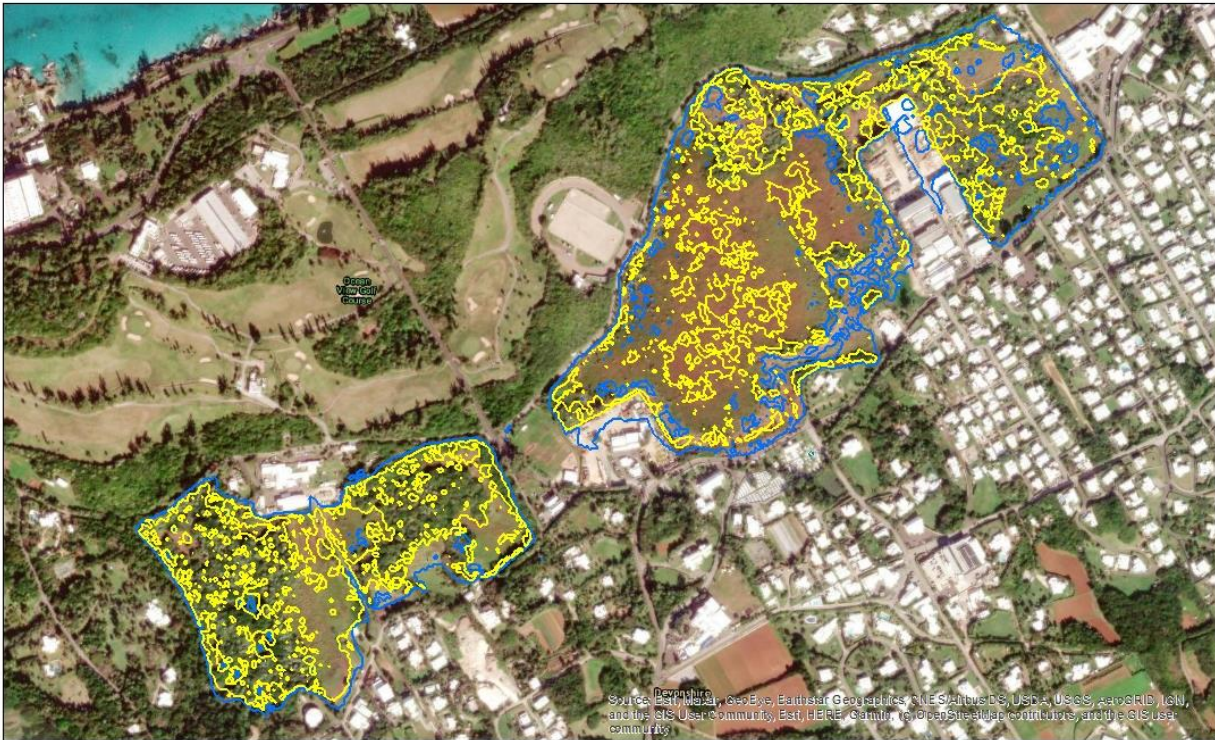


Figure 9.9 Predicted groundwater rise for Devonshire Marsh for RCP 4.5



BERMUDA - CLIMATE CHANGE STUDY
DEVONSHIRE MARSH RCP 8.5

LEGEND

- Projected Maximum Central Lens Rise 1.40m
- Projected Maximum Central Lens Rise 1.84m

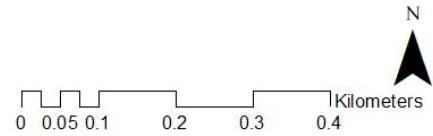


Figure 9.10 Predicted groundwater rise for Devonshire Marsh for RCP 8.5



BERMUDA - CLIMATE CHANGE STUDY
PEMBROKE MARSH RCP 4.5

LEGEND

- Projected Maximum Central Lens Rise 1.10m
- Projected Maximum Central Lens Rise 1.31m
- Projected Maximum Central Lens Rise 1.66m

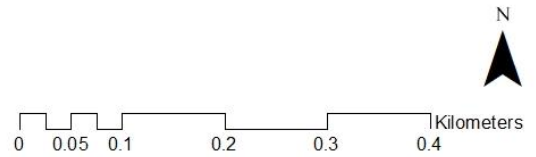


Figure 9.11 Predicted groundwater rise for Pembroke Marsh for RCP 4.5



BERMUDA - CLIMATE CHANGE STUDY
PEMBROKE MARSH RCP 8.5

LEGEND

- Projected Maximum Central Lens Rise 1.10m
- Projected Maximum Central Lens Rise 1.40m
- Projected Maximum Central Lens Rise 1.84m

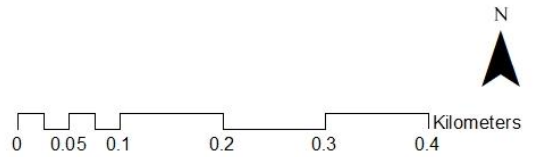


Figure 9.12 Predicted groundwater rise for Pembroke Marsh for RCP 8.5

10 Next Steps

The understanding presented in the coastal processes analysis, together with the results from the extreme sea level analysis, will be used to perform a coastal vulnerability assessment. This will include a review of the potential for flooding and erosion of coastal areas, and the potential for extreme events that would disrupt other coastal and marine activities.

To analyse potential solutions that may be appropriate to mitigate the effects of coastal erosion, SWI will employ the concept of “geomorphic units”. The coastline will be divided into geomorphic units or “sediment cells” that define relatively self-contained units within which sediment circulates. The net balance between sediment inputs and losses from within each geomorphic unit determines, to a large extent, whether a coastline is retreating or advancing.

11 Works Cited

- Attorney General's Chambers, TCI. (2018, March 13). *2017 Ordinance*. Retrieved from The Government of Turks and Caicos Islands: <https://www.gov.tc/agc/laws/annual-laws/2017-laws/2017-ordinances>
- M.M. Ball, R. M. (1985). Seismic structure and stratigraphy of northern edge of Bahaman-Cuban collision zone. *American Association of Petroleum Geologists Bulletin*, 1275-1294.
- Barnett, R. S. (1975). Gulf Coast Association of Geological Societies Transactions. *Basement Structure of Florida and its Tectonic Implications*, 122-142.
- Bates, N. (2007, September 19). Interannual variation of the oceanic CO₂ sink in the subtropical gyre of the North Atlantic Ocean over the last 2 decades. *Journal of Geophysical Research: Oceans*. doi: <https://doi.org/10.1029/2006JC003759>
- Bender, MA., Knutson, TR., Tuleya RE., Sirutis JJ., Vecchi, GA., Garner, ST., and Held, IM., (2010). Modeled Impact of Anthropogenic Warming on the Frequency of Intense Atlantic Hurricanes. *Science*. 22 Jan 2010 Vol 327, Issue 5964
- Bermuda Zoological Society. (2001). Bermuda Biodiversity Project (unpublished data).
- Bhatia, K.T., Vecchi, G.A., Knutson, T.R. et al. (2019). Recent increases in tropical cyclone intensification rates. *Nat Commun* 10, 635. <https://doi.org/10.1038/s41467-019-08471-z>
- Bird, E. (. (2010). *Encyclopedia of the world's coastal landforms*. Springer.
- Bounds, J. H., & Ferguson, J. A. (2018, February 2). *Turks and Caicos Islands*. Retrieved from Encyclopedia Britannica: <https://www.britannica.com/place/Turks-and-Caicos-Islands>
- Coates, K. F. (2013). Introduction to Bermuda: Geology,. *Coral Reefs of the World*. doi:DOI 10.1007/978-94-007-5965-7_10
- Fourqurean, J. W. (2019). Decadal Monitoring in Bermuda Shows a Widespread Loss of Seagrasses Attributable to Overgrazing by the Green Sea Turtle *Chelonia mydas*. *Estuaries and Coasts*, 1524-1540.
- Global Strategy Tentative List - Turks and Caicos*. (2018, March 13). Retrieved from UNESCO : <http://whc.unesco.org/en/tentativelists/5682/>
- Hallam, Samantha; Guishard, Mark; Josey, Simon A; Hyder, Pat; Hirschi, Joel (2021). Increasing tropical cyclone intensity and potential intensity in the subtropical Atlantic around Bermuda from an ocean heat content perspective 1955–2019, *Environmental Research Letters*, <https://dx.doi.org/10.1088/1748-9326/abe493>, 10.1088/1748-9326/abe493, 2021/03/02, IOP Publishing, 034052, 3, 16, 1748-9326
- Henry, H. (1964). Effects of dispersion on salt encroachment in coastal aquifers:. *US Geological Survey Water-Supply Paper*, C71-C84.
- Hurrell, J. W. (2003). The North Atlantic Oscillation: Climatic Significance and Environmental Impact. *American Geophysical Union*.
- Hurrell JW, Kushnir Y, Ottersen G, Visbeck M (2003) An overview of the North Atlantic Oscillation. *Geophys Monogr Geophys Union* 134:1–36. <https://doi.org/10.1029/134GM01>

- Hutching, C. D. (1977). *The story of the Turks and Caicos Islands*. Wisconsin: University of Wisconsin - Madison.
- Jones, R. &. (2010). Sewage contamination of a densely populated coral 'atoll' (Bermuda). . *Environmental Monitoring and Assessment*, 179. 309-24.
- Jones, S. (2012, September 18). Major rock fall occurs near Grand Atl. *Bermuda Sun*. Bermuda. Retrieved from <http://bermudasun.bm/MobileContent/NEWS/News/Article/Major-rock-fall-occurs-near-Grand-Atlantic-site/24/270/60639>
- Kerr, R. M. (1987). Beach and shoreface ooid deposition on shallow interior banks, Turks and Caicos islands, British West Indies. *Journal of Sedimentary Research*, 976-982.
- Kersell, J. E. (1988). Government administration in a very small microstate: Developing the Turks and Caicos Islands. *Public Administration and Development*, 169-181.
- Kline, S. W. (2014). The unsteady nature of sea cliff retreat due to mechanical abrasion, failure and comminution feedbacks. *Geomorphology*, 53-67.
- Knutson, T. R., F. Zeng, and A. T. Wittenberg, 2013: Multimodel assessment of regional surface temperature trends: CMIP3 and CMIP5 twentieth century simulations. *J. Climate*, 26, 8709–8743,
- Knutson, T. R., F. Zeng, and A. T. Wittenberg, 2014: Seasonal and annual mean precipitation extremes occurring during 2013: A U.S. focused analysis [in “Explaining Extremes of 2013 from a Climate Perspective”]. *Bull. Amer. Meteor. Soc.*, 95(9), S19–S23
- Kogure, T. A. (2006). Effect of the development of notches and tension cracks on instability of limestone coastal cliffs in the Ryukus, Japan. *Geomorphology*, 236-244.
- Landsea, C. W., Vecchi, G. A., Bengtsson, L., & Knutson, T. R. (2010). Impact of Duration Thresholds on Atlantic Tropical Cyclone Counts. *Journal of Climate*, 2508-2519.
- Lavis, D. S. (2022, March 23). Director, Bermuda Department of the Environment and Natural Resources. (D. Ruttan, Interviewer)
- Moses, C. (2013). Tropical rock coasts: Cliff, notch and platform erosion dynamics. *Progress in Physical Geography: Earth and Environment*, 37(2), 206-226. doi:<https://doi.org/10.1177/0309133312460073>
- Murakami, Hiroyuki, Delworth, Thomas Cooke, William Zhao, Ming Xiang, Baoqiang Hsu, Pang-Chi F.L. (2020). Detected climatic change in global distribution of tropical cyclones, 2020/05/19, doi: 10.1073/pnas.1922500117, 10.1073/pnas.1922500117, *Proceedings of the National Academy of Sciences*, 10706, 10714, 117, 20.
- Murdoch TJT, H. M. (2008). *A multi-scale assessment of the benthic communities of Bermuda's shallow water platform focusing on existing MPA's & control sites to enhance local management practices. Bermuda reef ecosystem assessment and mapping (BREAM) report.*
- Neumann, A. (1966). Observations on Coastal Erosion in Bermuda and Measurements of the Boring Rate of the Sponge. *Limnology and oceanography*, 11(1), 92-108. doi:<https://doi.org/10.4319/lo.1966.11.1.0092>
- Orth, R. J. (2006). A Global Crisis for Seagrass Ecosystems. *BioScience*, 987-996.

- Pereira, Jorge & Paiva, Vitor & Ceia, Filipe & Ramos, Jaime. (2020). Facing extremes: Cory's shearwaters adjust their foraging behaviour differently in response to contrasting phases of North Atlantic Oscillation. *Regional Environmental Change*. 22. 10.1007/s10113-020-01662-1.
- Plummer, L. V. (1976). Hydrogeochemistry of Bermuda: A Case History of Ground-Water Diagenesis of Biocalcarenes. *GSA Bulletin*, 1301-1316. doi:[https://doi.org/10.1130/0016-7606\(1976\)87<1301:HOBACH>2.0.CO;2](https://doi.org/10.1130/0016-7606(1976)87<1301:HOBACH>2.0.CO;2)
- Rance, A. (2022, March 23). Managing Director, Bermuda Water Works. (D. Ruttan, Interviewer)
- Rowe, M. (1981). The Central Lens of Bermuda: A Ghyben-Herzberg Lens in disequilibrium, M.Sc. Project. London: University College of London.
- Rowe, M. (1984). The freshwater "Central Lens" of Bermuda. *Journal of Hydrology*, 165-176. doi:[https://doi.org/10.1016/0022-1694\(84\)90038-6](https://doi.org/10.1016/0022-1694(84)90038-6)
- Rowe, M. (1991). Bermuda. In A. (. Falkland, *Hydrology and Water Resources of Small Islands, a Practical Guide* (pp. 333-338). Paris: UNESCO.
- Sarkis, S. V. (2013). Total economic value of Bermuda's coral reefs: a summary. *Coral Reefs of the World*.
- Shcherbina, A. G. (2010). Three-dimensional structure and temporal evolution of submesoscale thermohaline intrusions in the North Pacific subtropical frontal zone. *Journal of Physical Oceanography*, 1669–1689.
- Smith Warner International Limited. (2004). *Bermuda Coastal Erosion Vulnerability Assessment Final Report*. Kingston, Jamaica.
- Steinhoff, N. (n.d.). <https://oceanographicmagazine.com/features/bermuda-seagrass/>.
- Sunamura, T. (1982). A wave tank experiment on the erosional mechanism at a cliff base. *Earth Surface Processes and Landforms*, 333-343. doi:<https://doi.org/10.1002/esp.3290070405>
- Sunamura, T. (1992). *Geomorphology of rock coasts*. Chichester: Wiley. doi:<https://doi.org/10.1177/030913339401800416>
- Thomson, J. (1989). Modeling groundwater management options for small limestone islands: the Bermuda example. *Groundwater*, 147-154. doi:<https://doi.org/10.1111/j.1745-6584.1989.tb00434.x>
- from chloride concentration of the freshwater lenses. *Journal of Hydrology*, 20-37.
- Trenhaile, A. (1987). *The geomorphology of rock coasts*. Oxford: Clarendon Press. doi:<https://doi.org/10.1177/030913338801200215>
- Trepanier JC. North Atlantic Hurricane Winds in Warmer than Normal Seas. *Atmosphere*. 2020; 11(3):293. <https://doi.org/10.3390/atmos11030293>
- Vacher, H. (1974). *Groundwater hydrology of Bermuda*. Hamilton, Bermuda: Government of Bermuda Public Works Dept.
- Vacher, H. a. (1980). Hydrology of small oceanic islands - utility of an estimate of recharge inferred
- Vacher, H. H. (1995). Nomenclature, concepts and status of multiple systems of classifications. In H. a. Curran, *Terrestrial and Shallow Marine Geology of the Bahamas and Bermuda* (pp. 271-294).

- Wingate, D. B. (2003). Implications of global warming and sea-level rise for coastal nesting birds in Bermuda. *A Sense of Direction: a conference on conservation in UK Overseas Territories and other small island communities*, (pp. 214-256).
- Young, A. P. (2008). Instability investigation of cantilevered seacliffs. *Earth Surface Processes and Landforms*, 1661-1677.
- Young, A. P. (2009). Rain, waves, and short-term evolution of composite seacliffs in southern California. *Marine Geology*, 1-7. doi:<https://doi.org/10.1016/j.margeo.2009.08.008>
- Young, A. P. (2016). Observations of coastal cliff base waves, sand levels, and cliff top shaking: Cliff base waves and cliff top shaking. *Earth Surface Processes and Landforms*, 1564-1573.
- Zhang, B. et al 2019 Changes of tropical cyclone activity in a warming world are sensitive to sea surface temperature environment. *Environ. Res. Lett.* 14 124052

Appendix A - Climate Profile and Projections for the Island of Bermuda



CLIMATE PROFILE AND PROJECTIONS FOR THE ISLAND OF BERMUDA

Prepared By:



THE UNIVERSITY OF THE WEST INDIES
MONA CAMPUS, KINGSTON 7, JAMAICA, WEST INDIES

Contributing Authors:

LEONARDO CLARKE, MICHAEL TAYLOR & DERON MAITLAND

Submitted To:

SMITH WARNER INTERNATIONAL LIMITED
Unit 13, Seymour Park, 2 Seymour Avenue
Kingston 10, Jamaica, West Indies

May 31, 2022

BLANK PAGE

Table of Contents

About This Document.....	4
List of Figures.....	5
List of Tables.....	8
List of Acronyms and Abbreviations.....	10
Executive Summary.....	11
1.0 Introduction.....	12
2.0 Data & Methodology.....	13
2.1 Data Sources - Historical.....	13
2.2 Data Sources - Projections.....	14
2.2.1 Representative Concentration Pathways:.....	14
2.2.2 General Circulation Models:.....	15
2.2.3 Regional Climate Models:.....	15
2.3 Methodology.....	17
3.0 Results and Discussion.....	18
3.1 Surface Air Temperature.....	18
3.1.1 Temperature Climatology.....	18
3.1.3 Temperature Extremes.....	22
3.1.4 Sea Surface Temperature.....	27
3.2 Rainfall.....	29
3.2.1 Rainfall Climatology.....	29
3.2.3 Rainfall Extremes.....	32
3.4 Sea Level Rise.....	36
3.4.1 Historical Sea Level Rise.....	39
3.4.2 Projected Sea Level Rise.....	43
.....	47
3.5 Hurricanes.....	48
3.5.1 Historical Hurricanes.....	48
3.5.2 Hurricane Projections.....	52
4.0 Summary and Conclusions.....	54
References.....	55

About This Document

This document presents the characterization of the historical and future projected climate for the island of Bermuda from four data products: (i) station data, (ii) gridded data, (iii) reanalysis data and (iv) simulated outputs from three global climate models namely GFDL-ESM2M, MPI-ESM-MR and HadGEM2-ES.

Future projections are based on outputs from a General Circulation Model (GCM) downscaled using a Regional Climate Model (RCM) running representative concentration pathway (RCP) experiments. Section 2 has a brief overview of models and RCPs. Parameters for which downscaled projection data are unavailable are presented based on findings from a review of the available literature.

This document forms part of the larger Climate Vulnerability Assessment (CVA) being undertaken by Smith Warner International Limited. It is sectioned as follows:

- **Section 1 – Introduction:** This section provides a brief introduction, specifically detailing the domain for the analysis.
- **Section 2 – Data and Methodology:** This section gives a brief description of the datasets used for analysis and their sources. It also details the methodologies used in analyzing the data and provides a brief overview of global climate models (GCMs), regional climate models (RCMs) and the representative concentration pathways (RCPs) utilized by the Intergovernmental Panel on Climate Change (IPCC).
- **Section 3 – Results and Discussion:** This section presents the results and analyses. It is sectionalized according to climate variable, including air temperature, precipitation, sea level rise, hurricanes, etc. Results are presented for climatology, annual trends, and extreme events.
- **Section 4 – Summary and Conclusions:** This section summarizes the results presented in the previous sections and is followed by a list of references.

List of Figures

Figure 1 – Geographical Location of Bermuda.	12
Figure 2 – Visualization of GCM and RCM Scales (Hannah, 2015).	16
Figure 3– Historical Air Temperature Climatology. Climatology is presented for Mean (green lines), Maximum (orange lines) and Minimum (blue line) Air Temperature. Data shown for station data (LFWade) and reanalysis (ERA5). Base period: 2006 - 2021.	18
Figure 4 – Time scale decomposition for the historical temperature anomaly time series for the Bermuda region. Generated using IRI Map Room Tool. Data Source: CRU.	19
Figure 5 – Reanalysis and modelled historical climatological mean air temperature, baseline period (1980-2005). Data shown for reanalysis (ERA5) and modelled (GFDL, Had and MPI) data.	20
Figure 6 – Annual mean air temperature for the period 1980 to 2100. Data over the historical period are from ERA5 (1980 – 2021) and LFWade (2006 – 2021), while projections (2006 to 2100) are from GFDL, Had and MPI under RCP 2.6 and RCP 8.5. The modelled historical baseline values are also plotted. Units: °C.	21
Figure 7 – Annual Percentage of Hot Days (TX90p). Days when Maximum Temperature exceeds the 90th Percentile. Data over the historical period up to 2021 are from ERA5 and LFWade. Projections (2006 to 2100) are from GFDL, Had and MPI under RCP 2.6 and RCP 8.5. The models historical baseline values are also plotted. Units: %	23
Figure 8 – Annual Percentage of Hot Nights (TN90p). Days when Minimum Temperature exceeds the 90th Percentile. Data over the historical period up to 2021 are from ERA5 and LFWade. Projections (2006 to 2100) are from GFDL, Had and MPI under RCP 2.6 and RCP 8.5. The models historical baseline values are also plotted. Units: %	24
Figure 9 – Annual heatwave duration. That is the longest duration of a heatwave in days. Data over the historical period up to up to 2021 are from ERA5 and LFWade. Projections (2006 to 2100) are from GFDL, Had and MPI under RCP 2.6 and RCP 8.5. Units: Days.	25
Figure 10 – Annual Sum of Cooling Degree Days. Cooling Degree Days are calculated using a base temperature of 18 degrees. Data over the historical period up to up to 2021 are from ERA5 and LFWade. Projections (2006 to 2100) are from GFDL, Had and MPI under RCP 2.6 and RCP 8.5. Units: Cooling degree days.	26
Figure 11 –Historical and projected climatological mean sea surface temperature (SST) for the medium (2040 to 2060) and long (2070 to 2090) term for RCP 2.6 and 8.5. Data shown for NOAA and modelled	

(Had) data. Medium and long term are denoted by M and L respectively. The climatology over the historical baseline period (1982-2005) shown for comparison..... 27

Figure 12 – Annual average sea surface temperature, NOAA and Had. Data over the historical period up to 2020 (2005) are from NOAA (Had). Projections (2006 to 2100) are from Had under RCP 2.6 and RCP 8.5. The modelled (Had) historical baseline values are also plotted. Units: °C..... 28

Figure 13 – Historical Rainfall Climatology. Data shown for station data (LFWade), reanalysis (ERA5) and modelled (downscaled GFDL, Had and MPI). 30

Figure 14 – Annual Rainfall Trend. Data shown for Station data (LFWade), reanalysis (ERA5) and modelled (downscaled GFDL, Had and MPI). Measure data was unavailable. Units: mm/day. 31

Figure 15 – Annual Number of Heavy Rainfall (R20mm) Days. Number of days when precipitation \geq 20 mm. Data over the historical period up to up to 2021 are from ERA5 and LFWade. Projections (2006 to 2100) are from GFDL, Had and MPI under RCP 2.6 and RCP 8.5. Units: days. 32

Figure 16 – Annual Number of Consecutive Dry Days (CCD) Days. Maximum number of consecutive dry days (when precipitation is $<$ 1.0 mm). Data over the historical period up to up to 2021 are from ERA5 and LFWade. Projections (2006 to 2100) are from GFDL, Had and MPI under RCP 2.6 and RCP 8.5. Units: days. 33

Figure 17 – Annual Number of Consecutive Wet Days (CWD) Days. Maximum number of consecutive wet days (when precipitation is \geq 1.0 mm). Data over the historical period up to up to 2021 are from ERA5 and LFWade. Projections (2006 to 2100) are from GFDL, Had and MPI under RCP 2.6 and RCP 8.5. Units: days. 34

Figure 18 – Annual Total Rainfall (prctot) for days when rainfall is \geq 1mm. Data over the historical period up to up to 2021 are from ERA5 and LFWade. Projections (2006 to 2100) are from GFDL, Had and MPI under RCP 2.6 and RCP 8.5. Units: mm..... 35

Figure 19 – Mean sea level daily evolution. Data since January 1993 (in cm) and from the satellite altimeter observations estimated in the global ocean, derived from the average of the gridded sea level maps weighted by the cosine of the latitude. During 1993-1998, the dashed line shows an estimate of the global mean sea level corrected for the TOPEX-A instrumental drift, based on comparisons between altimeter and tide gauges measurements. Source: Copernicus Marine Service (CMEMS). <https://marine.copernicus.eu/> 40

Figure 20 – Climatology of Sea level change in Bermuda from tide gauge data. 41

Figure 21 – Time series of monthly sea level change in Bermuda 2004-2008..... 41

Figure 22 – Mean annual sea level rise for Bermuda from satellite altimetry. Data shown for nearest grid box to coordinates Lat: 32.373N and Lon: 64.703W. Solid line shows linear trend. Source: The Copernicus Climate Change Service (C3S): <https://cds.climate.copernicus.eu/>..... 42

Figure 23 – Local sea-level projections at St. Georges, Bermuda RCPs 2.6 (blue), 4.5 (orange) and 8.5 (red). The solid lines represent multi-model medians, the shaded areas capture the 66% uncertainty range. Dashed lines show median sea-level projections including expert judgement revised Antarctic ice-sheet contributions from Bamber et al. (2019). Climate Analytics Local SLR Tool (CMIP5). 45

Figure 24 – Sea-level change for SSP scenarios for Bermuda resulting from processes in whose projection there is medium confidence and 83rd percentile range. Projections are relative to a 1995-2014 baseline. The plot below shows the projection and uncertainties for 'Total Sea Level Change'. NASA Sea Level Projection Tool..... 46

Figure 25 – Showing local sea-level rise projections at 2100 for Bermuda Showing the current coast(A), SSP2-4.5: approximately 0.5m(B) and SSP5-8.5: Approximately 1m(C). Source: IDB (2018)..... 47

Figure 26 – Zones of likely origin and track density of storms by month during the hurricane season from August-October. Source: NOAA. 49

Figure 27 – Frequency and Category of Hurricanes Passing within 50km of Bermuda, Presented by Decades (1981 to 2020). Data from the NOAA HURDAT2 Dataset. 49

Figure 28 – Tracks of Hurricanes Passing within 50km of Bermuda (1981 to 2021). Data from the NOAA HURDAT2 and IBTrACS Datasets. 51

Figure 30 – Percentage Difference of Major Hurricane Days between 1986-2005 and 2081-2100 by the HiFLOR model. White crosses represent not statistically significant grid boxes (Bhatia,et. al, 2018, p.8298). 53

Figure 31 – (a) Strength of the Local Relationship between the Observed per Event Maximum Wind Intensity and the average (“normal”) August–October SST in °C. (b) Significance of the Relationship.(Trepanier 2020). 53

List of Tables

Table 1 – List of Datasets for Historical Analysis.....	13
Table 2 – List of Datasets for Future Analysis.	14
Table 3 – Description of the four Representative Concentration Pathway Scenarios (2014). The shaded rows indicate the RCPs used for this report.....	15
Table 4 – Summary of Climate Extremes.....	17
Table 5 – Projected monthly change in mean air temperatures for the medium (2040 to 2060) and long (2070 to 2090) term for RCP 2.6 and 8.5 with respect to the model baseline (1980 to 2005). Units °C.	20
Table 6 – Slopes of linear trend for Figure 6. Units: °C per decade	22
Table 7 – Historical and projected average annual percentage of hot days and hot nights.	24
Table 8 – Projected Average Annual Heatwave Duration.....	25
Table 9 – Projected Average Annual Cooling Degree Days. Percentage changes are given in brackets.	26
Table 10 – Historical climatologies and projected change in mean sea surface temperature climatology. Historical baseline period (1982-2005). Change is with respect to the model baseline.	28
Table 11 – Slope values of linear trends for observed and modelled annual average sea surface temperatures.....	28
Table 12 – Historical precipitation climatologies and projected change.....	30
Table 13 – Slopes of linear trends for Figure 14. Units (mm/day)/decade.....	31
Table 14 – Historical and Future Climate Change Data Sources.	37
Table 15 – Average Rate of Global Mean Sea Level Rise.	40
Table 16 – Mean rate of sea level rise averaged over the Caribbean basin.	40
Table 17 – Projected mean global SLR. Relative to 1986-2005. Source: SROCC (IPCC 2019).....	44
Table 18 – Projected mean global SLR. Source: AR6 (IPCC 2022).....	44
Table 19 – Local sea-level projections at St. Georges, Bermuda for RCP2.6 (blue), RCP4.5 (orange) and RCP8.5 (red). The second column shows the multi-model median, column three shows the 66% uncertainty range, and column four shows the 90% uncertainty range. Shown in brackets are sea-level projections including expert judgement revised Antarctic ice-sheet contributions from Bamber et al. (2019). Climate Analytics Local SLR Tool (CMIP5).	44
Table 20 – Sea level projections for 5 SSP scenarios, relative to a baseline of 1995-2014, in meters at St. Georges/ Esso Pier (Bermuda). Individual contributions are shown for the year 2100. Median values (likely ranges) are shown. Average rates for total sea-level change are shown in mm yr-1. The SSP5-8.5	

low confidence column incorporates a representation of the potential effect of low-likelihood, high-impact ice sheet processes that cannot be ruled out. This column shows the 17th-83rd percentile range factoring into account information from structured expert judgement and from a model incorporating Marine Ice Cliff Instability. NASA Sea Level Projection Tool. 46

Table 21 – Summary of Hurricanes Passing within 50km of Bermuda (1981 to 2020). Data from the NOAA HURDAT2 Dataset. 50

Table 22– Summary of Trends and Projections at a Glance..... 54

List of Acronyms and Abbreviations

AR5	Fifth Assessment Report
C3S	Copernicus Climate Change Service
CRU	Climatic Research Unit
CMEMS	Copernicus Marine Environment Monitoring Service
CSGM	Climate Studies Group Mona
ECMWF	European Centre for Medium-Range Weather Forecasts
GCM	General Circulation Model or Global Climate Model
GFDL-ESM2M	Geophysical Fluid Dynamics Laboratory - Earth System Model
GHG	Greenhouse Gas
HadGEM2-ES	Hadley Centre Global Environment Model version 2 – Earth System
IPCC	Intergovernmental Panel on Climate Change
KNMI	Royal Netherlands Meteorological Institute ()
LFWade	LF Wade International Airport
MPI-ESM-MR	Max Planck Institute - Earth System Model - Mixed Resolution
NOAA	National Oceanic and Atmospheric Administration
RCM	Regional Climate Model
RCP	Representative Concentration Pathways
RegCM	ICTP Regional Climate Model

Executive Summary

Summary of Trends and Projections at a Glance.

Historical Trend	Projection
<p>Temperature</p> <p>Air temperature varies throughout the year with the highest temperatures from July to September and lowest in January to March. Mean temperature has been increasing between 0.22°C and 0.6°C per decade.</p> <p>Hot days and nights have also been increasing at a rate of 4% and 3% per decade, respectively.</p>	<p>Temperature is expected to continuously increase with global warming. In the medium term (2040-2060) the projected annual increase is between 0.6 and 1.7 for the RCPs. In the long term (2070-2090) the projected annual increase is between 0.6 and 3.2 °C for the RCPs.</p> <p>Hot days and nights are increasing and will account for nearly 100% of days by end of century under RCP 8.5.</p> <p>Heatwave durations are increasing and will reach near 60 days by the end of century under RCP 8.5.</p>
<p>Rainfall</p> <p>The island’s climatology exhibits a bimodal rainfall pattern with peaks in January and September, with the September peak receiving more rainfall.</p> <p>Interannual variability dominates the rainfall record with no real linear trend.</p>	<p>The RCPs suggest no real trend toward the end of the century. In the medium term (2040-2060), mean annual projected change is 4 to 11% over the two RCPs examined. In the long term (2070-2090), mean annual projected change is 3 to 48%.</p> <p>Extreme events will be characterised by significant interannual variability. However, rainfall indices reflect no real overall trends with projected change in consecutive dry days (CDD) (between 0.1 and 0.2 days/decade) and changes in consecutive wet days (CWD) (0 and 0.2 days/decade).</p>
<p>Sea Surface Temperature</p> <p>SST are highest during August to September and coolest during December to April. SSTs are increasing at a rate of 0.26 °C per decade.</p>	<p>SSTs are projected to increase at a rate of 0.07 °C (0.43 °C) per decade under RCP 2.6 (8.5). In the medium term (2040-2060) monthly projected increase ranges from 0.6 to 1.7 °C (1.0 – 2.3 °C) for RCP 2.6 (8.5). In the long term (2070-2090) monthly projected increase ranges from 0.8 to 1.7 °C (2.5 – 4.0 °C) for RCP 2.6 (8.5).¹</p>
<p>Sea Level Rise</p> <p>Bermuda lies in an area of the Caribbean Basin that has experienced sea level rise of more than 3.84 mm/year.</p>	<p>By 2100, mean SLR is projected to be approximately 0.47 m for SSP1—2.6 and between 0.69 and 0.82m for SSP5-8.5.</p> <p>If expert judgement including revised Antarctic ice-sheet contributions are considered then by 2100, mean SLR for Bermuda is projected to be approximately 1.46m for SSP5-8.5.</p>
<p>Hurricanes</p> <p>Over the last 4 decades there were 21 storms passing within 50km of Bermuda. Between 5 and 8 storms passed per decade except for 1991 to 2000 when no storms were recorded passing within 50km.</p>	<p>The future will likely be characterized by more intense hurricanes with high winds and greater rainfall. A likely increase in rainfall rate of between 20% and 33% is projected particularly near the hurricane core by the end of the century.</p>

¹ For SLR, instead of RCPs, changes are presented for four future Shared Socio-economic Pathways (SSPs), namely, SSP1-2.6, SSP2-4.5, SSP3-7.0, SSP5-8.5. SSPs are a new method of assessing future scenarios which seeks to combine the knowledge of the physical sciences of climate change with the societal impacts brought on by the vulnerability caused by climate change. The SSPs and RCPs are not directly comparable however SSP1-2.6 is related to RCP2.6 as it corresponds to significant and immediate emissions cuts, leading to net zero and eventually negative annual emissions in the second half of the century while SSP5-8.5 represents the high end of the range of future pathways (corresponding to RCP8.5) and is the worst-case scenario pathway.

1.0 Introduction

This document details the historical and projected climatology, extremes, and trends for the island of Bermuda for a range of climate parameters, based on station, gridded, reanalysis and simulated climate data. Historical and future climatologies, annual trends, and extremes are presented. Also included is information on sea level rise and hurricanes based on a review of literature.

The analysis characterising the historical and future projected climate for the island of Bermuda are based on four data products: (i) station data, (ii) gridded data, (iii) reanalysis data and (iv) simulated outputs from three global climate models (GFDL-ESM2M, MPI-ESM-MR and HadGEM2-ES). The specific datasets utilised are presented in section 2. It is to be noted that station data was limited in scope for this analysis.

Bermuda is a British island territory located in the North Atlantic Ocean. It is an archipelago of 7 main islands and about 170 additional islets and rocks. It is situated about 1,050 km east of Cape Hatteras, North Carolina, USA. The archipelago is about 40 km long and averages less than 1.6 km in width. The largest island is Main Island, 22.5 km long. Bermuda is geographically located at latitude 32.3051°N and longitude 64.7529°W. See Figure 1.

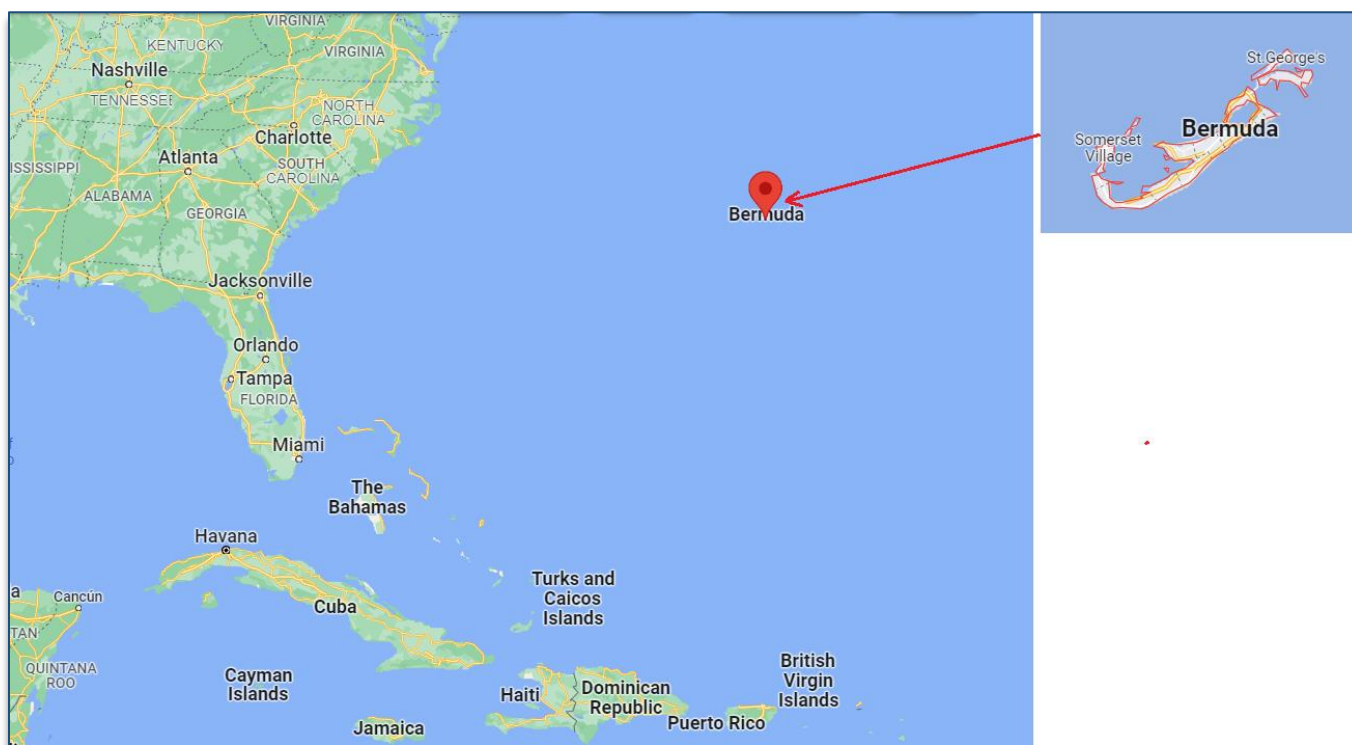


Figure 1 – Geographical Location of Bermuda.

2.0 Data & Methodology

This section details the datasets utilised in the production of this document and how they were processed and analysed. Specifically, it details the data sources, resolution, type, and the methodology utilised in the processing and analysis of the data. Also provided is an overview of climate models and a discussion on the process by which future projections are generated and the uncertainties associated with this type of data.

The temperature and rainfall results are based on the analysis of four types of data: (i) station data, (ii) gridded data, (iii) reanalysis data and (iv) simulated outputs from three global climate models namely GFDL-ESM2M, MPI-ESM-MR and HadGEM2-ES, herein referred to as GFDL, MPI and Had respectively. Tables 1 and 2 give summaries of the datasets utilised, their type, source, and resolution.

2.1 Data Sources - Historical

The gridded dataset utilised is from the Climatic Research Unit (CRU) from the University of East Anglia (temperature and rainfall). CRU TS (Climatic Research Unit gridded Time Series) is a widely used climate dataset on a 0.5° latitude by 0.5° longitude grid over all land domains of the world except Antarctica. It is derived by the interpolation of monthly climate anomalies from extensive networks of weather station observations. Reanalysis data is from ERA 5, which is the latest climate reanalysis product produced by the Copernicus Climate Change Service (C3S) at the European Centre for Medium-Range Weather Forecasts (ECMWF). ERA5 provides hourly estimates of a large number of atmospheric, land and oceanic climate variables. The data cover the Earth on a 30km grid and resolve the atmosphere using 137 levels from the surface up to a height of 80km. ERA5 combines vast amounts of historical observations into global estimates using advanced modelling and data assimilation systems. Both datasets were accessed from the Climate Explorer database (see Table 1).

Table 1 – List of Datasets for Historical Analysis.

Variables	Analysis	Source	Dataset	Resolution		Units
				Temporal	Spatial	
Air Temperature Mean, Max & Min	Climatology, Trends & Extremes	Royal Netherlands Meteorological Institute (KNMI) Climate Explorer https://climexp.knmi.nl/	ERA5 & CRU	Daily	0.5°	°C
Precipitation						mm/day
Sea Surface Temperature	Climatology & Trends		NOAA Reynolds OI	Monthly	1.0°	°C
Hurricane	Trends	NOAA https://coast.noaa.gov/hurricanes/	HURDAT2 & IBTrACS	--	--	--
Sea Level Rise		Literature	--	--	--	--
		Copernicus Marine Environment Monitoring Service (CMEMS) https://marine.copernicus.eu/	CMEMS	--	0.25°	--

Sea surface temperatures are from the Reynolds OI SST dataset, hurricane data from the NOAA National Hurricane Center HURDAT2 and NOAA National Centers for Environmental Information IBTrACS data sets, and sea level rise from the Copernicus Marine Environment Monitoring Service (CMEMS).

2.2 Data Sources - Projections

Precipitation and air temperature data for future projections are extracted from the outputs of RegCM, a regional climate model (RCM) from the International Centre for Theoretical Physics (ICTP). These outputs are downscaled values of outputs from the GFDL, MPI and Had General Circulation Models (GCMs), configured to run utilising the representative concentration pathways (RCPs) described by the RCP 2.6 and RCP 8.5 scenarios. The downscaling was done by the Climate Studies group, Mona (CSGM). A brief overview of GCMs, RCMs and RCPs are provided below as a context for users when interpreting the results from simulated data.

Future projections for sea surface temperatures are from the HadGEM2-ES model while information on future hurricanes and sea level rise data are extracted from the literature.

Table 2 – List of Datasets for Future Analysis.

Variables	Analysis	Source	Dataset	Resolution		Units
				Temporal	Spatial	
Air Temperature Mean, Max & Min	Climatology, Trends & Extremes	CSGM	RegCM Downscaled GFDL-ESM2M, MPI-ESM- MR and HadGEM2-ES (RCP 2.6 and RCP8.5)	Daily	0.25°	°C
Precipitation						mm/day
Sea Surface Temperature	Climatology & Trends	KNMI Climate Explorer	HadGEM2-ES (RCP 2.6 and RCP8.5)	Monthly	1.25°	°C
Hurricane	Trends	As reported in the literature.				
Sea Level Rise		As reported in the literature.				

2.2.1 Representative Concentration Pathways:

Climate projections are simulated based on future expectations (scenarios) of the earth's environment. In this regard, future simulations of the Earth's climate employ one of several standard scenarios used by the Intergovernmental Panel on Climate Change (IPCC). In this report the scenarios employed are representative concentration pathways (RCPs). RCPs are factor amalgamated greenhouse gas emission (GHG) scenarios used by the IPCC, which categorize possible future climates of the world. Factors weighed into the scenarios include energy use, economic activity, and land use. See the IPCC climate change report (2014) for more details. There are four (4) defined scenarios, namely RCP 2.6, 4.5, 6 and 8.5, each representing a future subjected to a specific radiative forcing value because of the predicted cumulative GHG emission quantities. Table 3 summarizes the 4 RCP scenarios and their GHG emission ranges in parts per million (ppm). Downscaled data for RCP 4.5 and RCP 8.5 were available for use.

Table 3 – Description of the four Representative Concentration Pathway Scenarios (2014). The shaded rows indicate the RCPs used for this report.

RCP Scenario/ Radiative Forcing	Description	Likely End of Century Global Mean Surface Temperature Increases
2.6	Low GHG Emissions or neutered impact through social and economic behavioural changes directed towards major mitigation. Denoted by a GHG range ≥ 430 ppm and ≤ 530 ppm.	0.3°C to 1.7 °C
4.5	Intermediate mitigation. Denoted by a GHG range ≥ 530 ppm and ≤ 720 ppm.	1.1°C to 2.6°C
6.0	Low intermediate mitigation which falls closer to a business-as-usual behaviour. Denoted by a GHG range ≥ 720 and ≤ 1000 ppm.	1.4°C to 3.1°C
8.5	High GHG Emissions through a business-as-usual behaviour or low behavioural change towards GHG mitigation. Denoted by a GHG range > 1000 ppm.	2.6°C to 4.8°C

2.2.2 General Circulation Models:

Future climates are simulated by global climate models (GCMs). These models are configured utilising GHG emissions from a specified RCP along with other parameters. GCMs utilise mathematical equations governing the conservation laws and physical processes to mimic the behaviour of atmospheric motion and their land and ocean interactions. There are numerous GCMs available and are run by various organizations around the world. The skill of individual GCMs varies in performance, with some better suited for specific regions of the globe. The performance of each is normally determined through statistical validation against observed datasets, see for instance Liu, Xu, & Li (2017), Ahmed, Sachindra, Shahid, Demire, & Chung (2019) and Shi, Wang, Qi, & Chen, (2018).

2.2.3 Regional Climate Models:

Data outputted from GCMs are of a coarse resolution, usually greater than 125 km. At coarser/lower resolutions, small island states or even local country scales are generally not represented well or identified at all. See for example Cantet, Déqué, Palany, & Maridet (2014) and Gao, et al. (2008). To have a more accurate representation of smaller regions the output of a GCM can be used as boundary conditions for a regional climate model (RCM), which downscales the GCM to a higher resolution (see Figure 2). The higher resolution allows for the study of the influence on dynamics posed by highly variable physical factors; for example, topography, land use and land–sea differences, see for instance Filippo (2019) and Wang, et al. (2004). The RCM model used in this report is the ICTP RegCM. The RCM domain chosen was centred over the Caribbean Sea, with the domain adopting a horizontal resolution of 0.22 degrees (approximately 25km) with 63 vertical atmosphere levels.

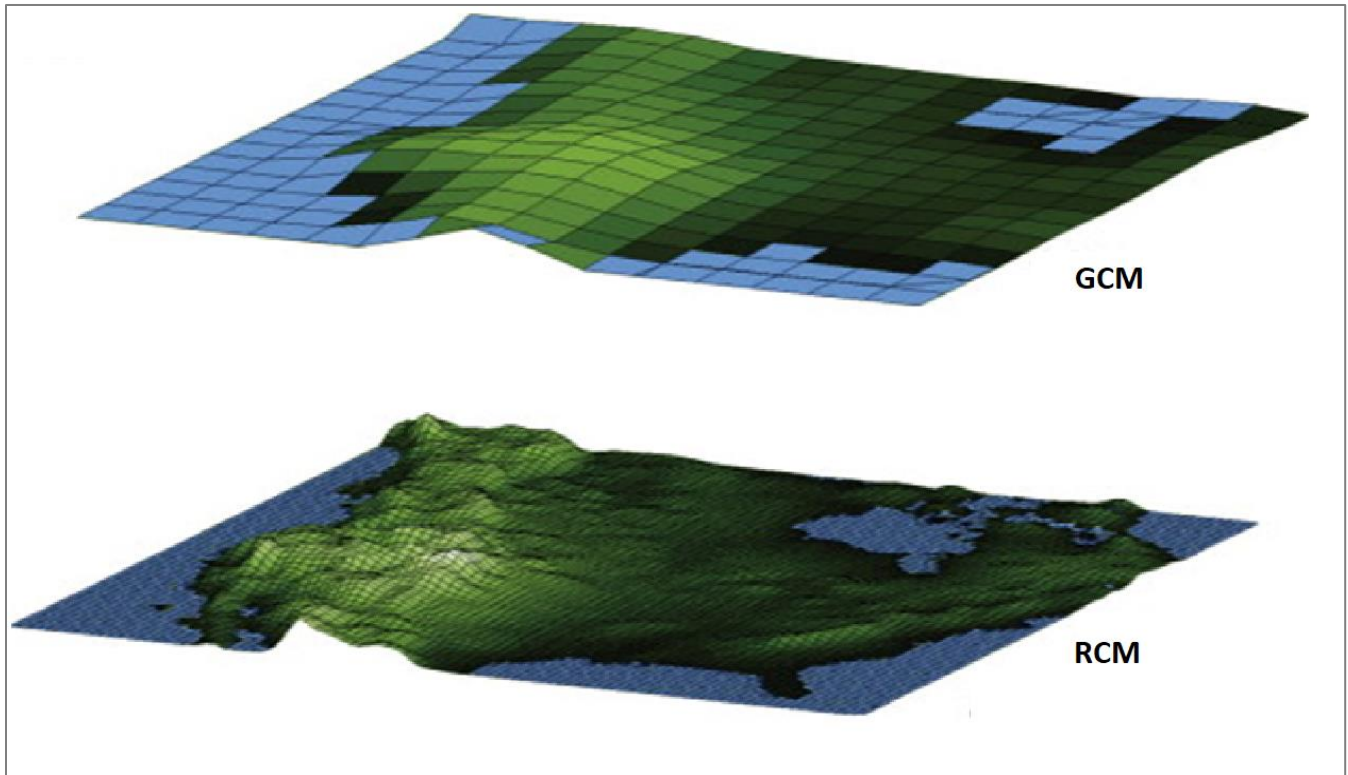


Figure 2 – Visualization of GCM and RCM Scales (Hannah, 2015).

2.3 Methodology

Data in the report are presented in tables, graphs and figures representing climatology, trends, and extremes. Climatologies are calculated as averages over a prolonged period (normally 30 years). Where not specified, the period utilised in this document is 1980 to 2005. This period was chosen to align with the data from all the available sources. For temperature and rainfall, the extremes examined are summarised in Table 4.

Indices utilized are those recommended by the World Meteorological Organization's Expert Team on Sector-Specific Climate Indices (ET-SCI) and are generated utilising the Clim pact open-source package, see www.climpact-sci.org for more information.

A decomposition of the annual rainfall and temperature data is also performed to identify the percentage of variance contributed by linear trend, decadal trend and interannual variability. This decomposition is done with the aid of the Map Room tool from the International Research Institute for Climate and Society (IRI). Decomposition is done on the Climatic Research Unit (CRU) dataset.

Where gridded and reanalysis data are utilised the grid boundaries used for extraction encompass 32.24N to 32.40N degrees latitude and 64.90W to 64.63W degrees longitude unless otherwise specified.

Table 4 – Summary of Climate Extremes

Extreme Name	Calculation	Units
Number of Heavy Rain Days (R20mm)	Number of days when precipitation \geq 20 mm	# of days
Total Precipitation (PRCPTOT)	Annual total wet-day precipitation	Millimetres
Consecutive Dry Days (CDD)	Maximum number of consecutive dry days (when precipitation is $<$ 1.0 mm)	# of days
Consecutive Wet Days (CWD)	Maximum number of consecutive wet days (when precipitation is \geq 1.0 mm)	# of days
Percentage of Hot Days (TX90p)	Percentage of days when maximum temperature $>$ 90 th percentile	%
Percentage of Warm Nights (TN90p)	Percentage of days when minimum temperature $>$ 90 th percentile	%
Heatwave Duration (HWD)	The length of the longest heatwave identified by heatwave number (HWN) when maximum temperature $>$ 90 th percentile	Days
Cooling Degree Days (CDDcoldn)	The annual sum of mean temperature minus 18°	Degree Days

3.0 Results and Discussion

This section presents the results and analysis of the climate data for the island of Bermuda. The variables analysed are temperature and rainfall and their extremes, as well as hurricanes, and sea level rise.

3.1 Surface Air Temperature

3.1.1 Temperature Climatology

Figure 3 presents the historical monthly climatologies of average maximum, mean and minimum air temperature for the island of Bermuda. The climatologies are calculated over the period 2006 to 2021.

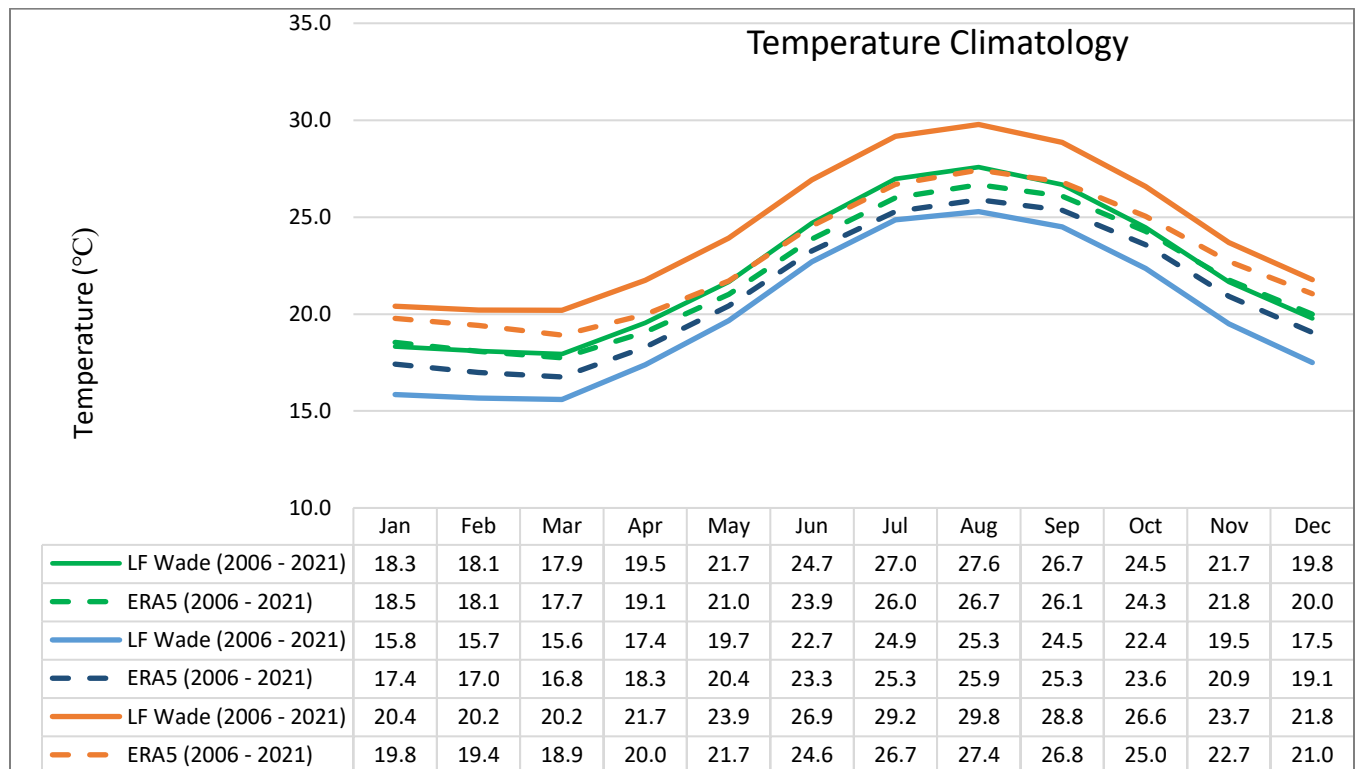


Figure 3– Historical Air Temperature Climatology. Climatology is presented for Mean (green lines), Maximum (orange lines) and Minimum (blue line) Air Temperature. Data shown for station data (LFWade) and reanalysis (ERA5). Base period: 2006 - 2021.

The following are noted:

- Annual recorded mean air temperature ranges between 17.9 to 27.6 °C (range 9.6 degrees) for LFWade and 18 and 26.7 °C (8.6 degrees) for ERA 5, with an approximately monthly range between 4.2 to 4.6°C for LFWade and 1.3 to 2.5°C for ERA5. A similar pattern is observed for the monthly averages of maximum and minimum temperatures.
- Peak temperature values occur between July and September, while the coolest temperatures are experienced from January to March.
- Maximum temperature values may reach as high as 30 °C (28°C) in August for LFWade (ERA5), while minimum temperature values may drop to 20°C (19°C) in March.

Figure 4 presents the historical temperature anomaly time scales decomposition for the Bermuda region. These graphs were generated using the IRI Map Room tool utilising the CRU dataset. Decomposition of the data shows that the linear trend accounts for approximately 25% of the changes seen in the temperature record, with interannual variability accounting for 44% and decadal variability accounting for approximately 24% of the change seen.

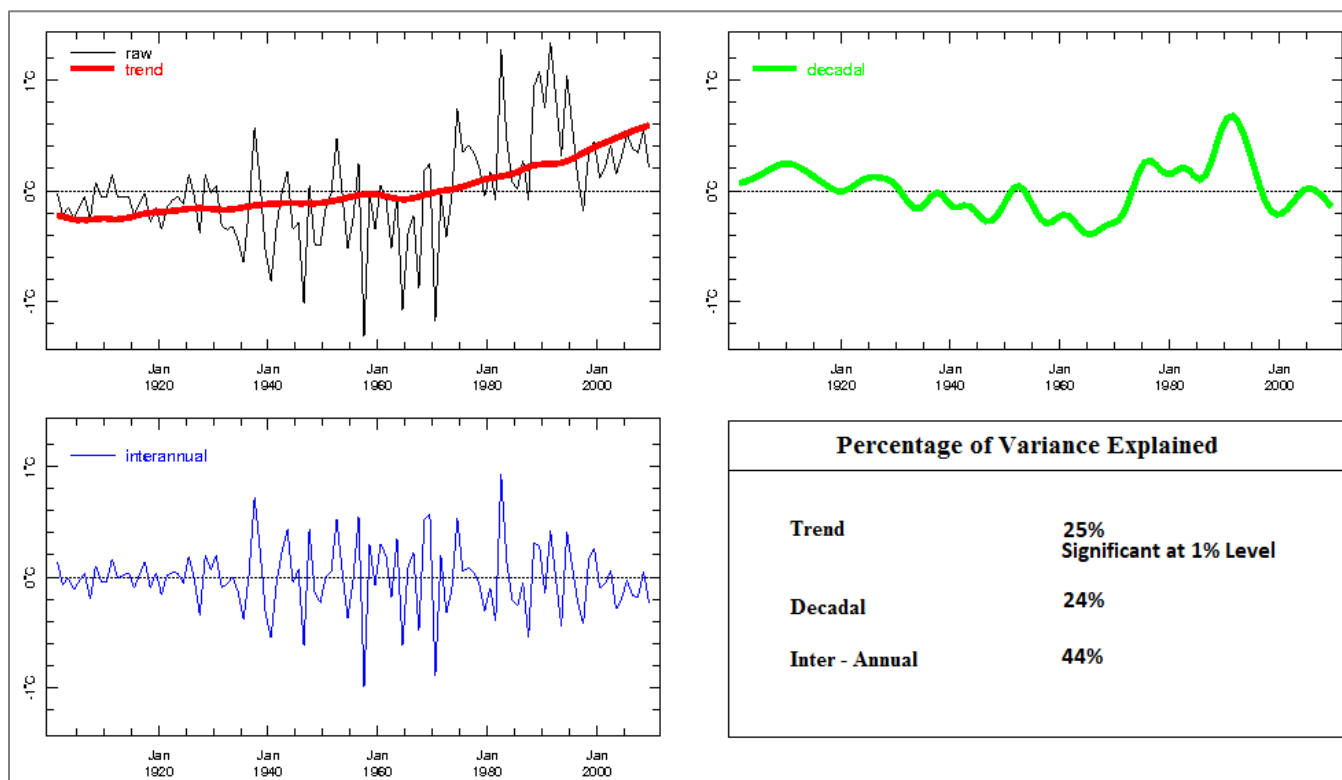


Figure 4 – Time scale decomposition for the historical temperature anomaly time series for the Bermuda region. Generated using IRI Map Room Tool. Data Source: CRU.

Figure 5 presents the historical monthly climatologies of average mean air temperature for ERA5, GFDL, Had and MPI² and Table 5, the projected future changes with respect to the baseline (1980 to 2005).

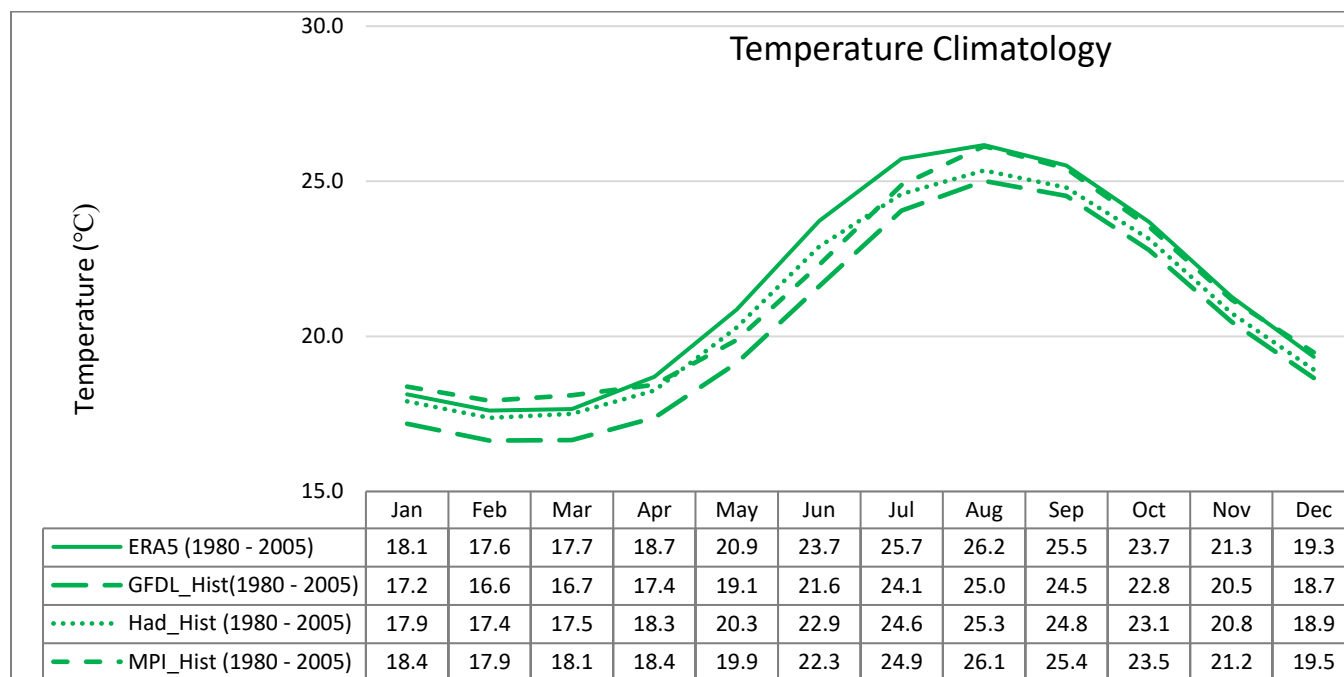


Figure 5 – Reanalysis and modelled historical climatological mean air temperature, baseline period (1980-2005). Data shown for reanalysis (ERA5) and modelled (GFDL, Had and MPI) data.

Table 5 – Projected monthly change in mean air temperatures for the medium (2040 to 2060) and long (2070 to 2090) term for RCP 2.6 and 8.5 with respect to the model baseline (1980 to 2005). Units °C.

RCP	Period	Model	Jan	Feb	Mar	Apr	May	Jun	Jul	Aug	Sep	Oct	Nov	Dec
2.6	Medium	GFDL	0.8	0.8	0.5	0.8	0.8	0.9	1.0	1.0	0.9	0.8	0.8	0.6
		Had	1.2	1.0	1.1	1.3	1.2	0.9	1.1	1.1	1.2	1.4	1.5	1.3
		MPI	0.5	0.4	0.3	0.5	0.6	0.8	0.7	0.9	0.9	0.8	0.7	0.6
	Long	GFDL	0.6	0.5	0.3	0.6	0.7	1.0	0.8	0.9	0.8	0.7	0.7	0.4
		Had	0.8	0.7	0.7	1.0	1.2	1.1	1.1	1.1	1.2	1.3	1.3	1.2
		MPI	0.6	0.6	0.5	0.7	0.9	0.8	0.8	0.8	0.9	0.9	1.0	0.9
8.5	Medium	GFDL	1.2	1.0	0.9	0.9	1.3	1.5	1.4	1.7	1.5	1.4	1.4	1.1
		Had	1.5	1.4	1.5	1.6	1.7	1.7	1.8	1.8	1.9	2.0	2.1	1.9
		MPI	0.8	0.7	0.6	0.9	1.0	1.4	1.5	1.8	1.8	1.4	1.4	0.9
	Long	GFDL	2.0	1.7	1.8	1.9	2.0	2.6	2.6	2.7	2.4	2.3	2.3	2.0
		Had	2.9	2.5	2.5	2.7	3.1	3.2	3.4	3.4	3.4	3.8	3.9	3.6
		MPI	1.9	1.5	1.5	1.9	2.1	2.9	2.9	3.1	3.2	2.7	2.7	2.2

² GFDL, Had and MPI² respectively refer to the GFDL-ESM2M, MPI-ESM-MR and HadGEM2-ES General Circulation Models mentioned in Section 2.2.

The following are noted:

- The models' historical climatologies captures well the pattern and reasonably well the reanalysis values with a slight underestimation in most months.
- The historical climatological pattern, not shown, is also maintained in the future, with the highest temperatures occurring from July and September and the coolest from January to March.
- Temperature is expected to increase under both RCP 2.6 and 8.5 scenarios with higher temperature increases under RCP 8.5.
- The average annual and seasonal increases over the two RCPs for the medium term (2040-2060) are: 0.6-1.7 °C annual; 0.5-1.6 °C for December through February; 0.5-1.6 °C for March through May; 0.8-1.7 °C for June through August; and 0.7-2.0 °C for September through November.
- The average annual and seasonal increases over the two RCPs for the long term (2070-2090) are: 0.6-3.2 °C annual; 0.5-3.0 °C for December through February; 0.5-2.8 °C for March through May; 0.8-3.3 °C for June through August; and 0.6-3.8 °C for September through November.

Figure 6 presents the annual average air temperature for both the historical (reanalysis and modelled) and future projections under RCP 2.6 and 8.5 scenarios. Table 6 presents the slopes of the linear trend.

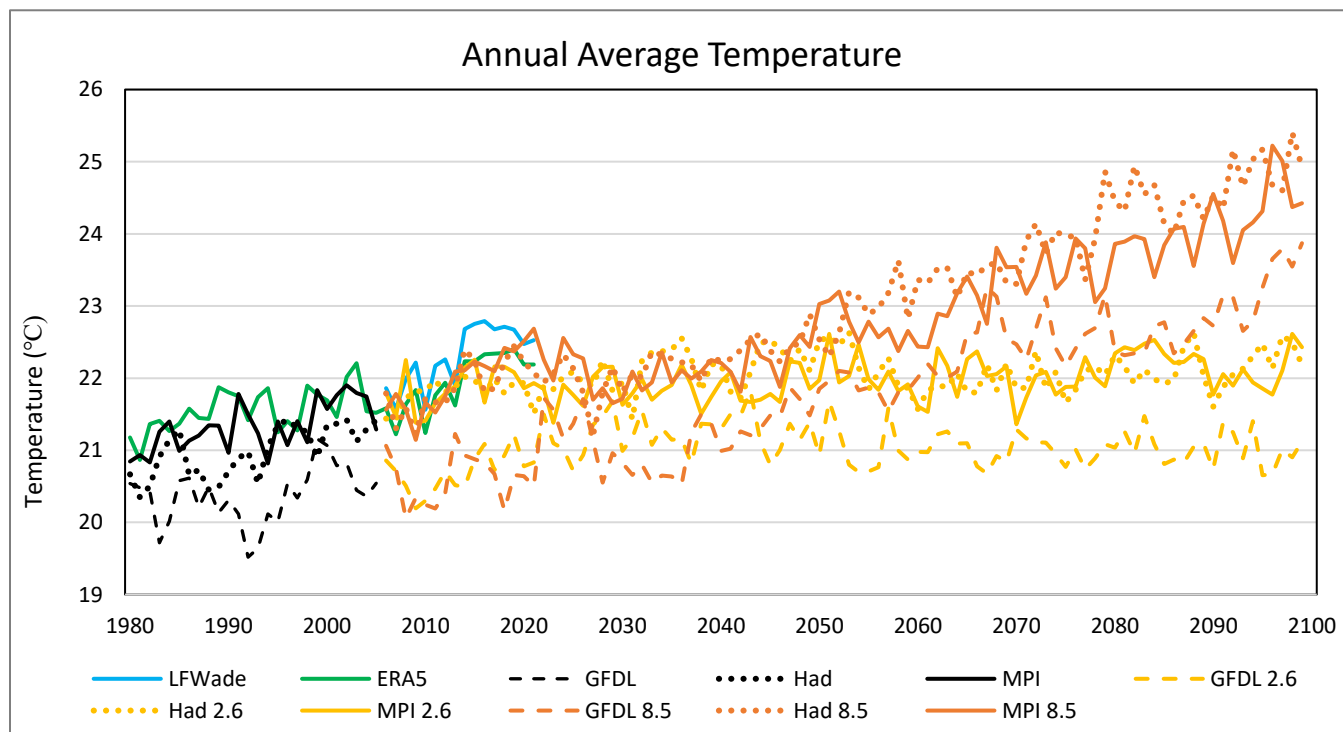


Figure 6 – Annual mean air temperature for the period 1980 to 2100. Data over the historical period are from ERA5 (1980 – 2021) and LFWade (2006 – 2021), while projections (2006 to 2100) are from GFDL, Had and MPI under RCP 2.6 and RCP 8.5. The modelled historical baseline values are also plotted. Units: °C.

The following are noted:

- Annual average temperature shows a linear increasing trend of between 0.17-0.6°C/decade for the historical period. The models' baseline data underestimates the ERA5 reanalysis data, however, the increasing trend is evident across all datasets.
- Under both future scenarios, air temperature increases with a larger trend for RCP 8.5 than for RCP 2.6 (Table 6).

Table 6 – Slopes of linear trend for Figure 6. Units: °C per decade

Historical					RCP 2.6			RCP 8.5		
LFWade	ERA 5	GFDL	Had	MPI	GFDL	Had	MPI	GFDL	Had	MPI 8.5
0.6	0.22	0.17	0.32	0.28	0.01	0.03	0.04	0.32	0.38	0.3

3.1.3 Temperature Extremes

Figure 7 presents the historical and future trends in the annual percentage of days when maximum temperatures are above the 90th percentile (hot days). The base period is 2006 to 2021. The following are noted:

- The RCP 8.5 scenario shows a continuous increase in the number of hot days through the end of the century. Under RCP 8.5, the percentage of days when maximum temperatures exceed the 90th percentile of the baseline period increases to near 100% by the end of the century, i.e., most days (>90%) are expected to be considered very hot by current standard of definition.
- Under RCP 2.6 the percentage of days when maximum temperatures exceed the 90th percentile of the baseline period, levels off at current levels and remain through to the end of century.
- See Table 7 for the projected increases for the medium and long term.

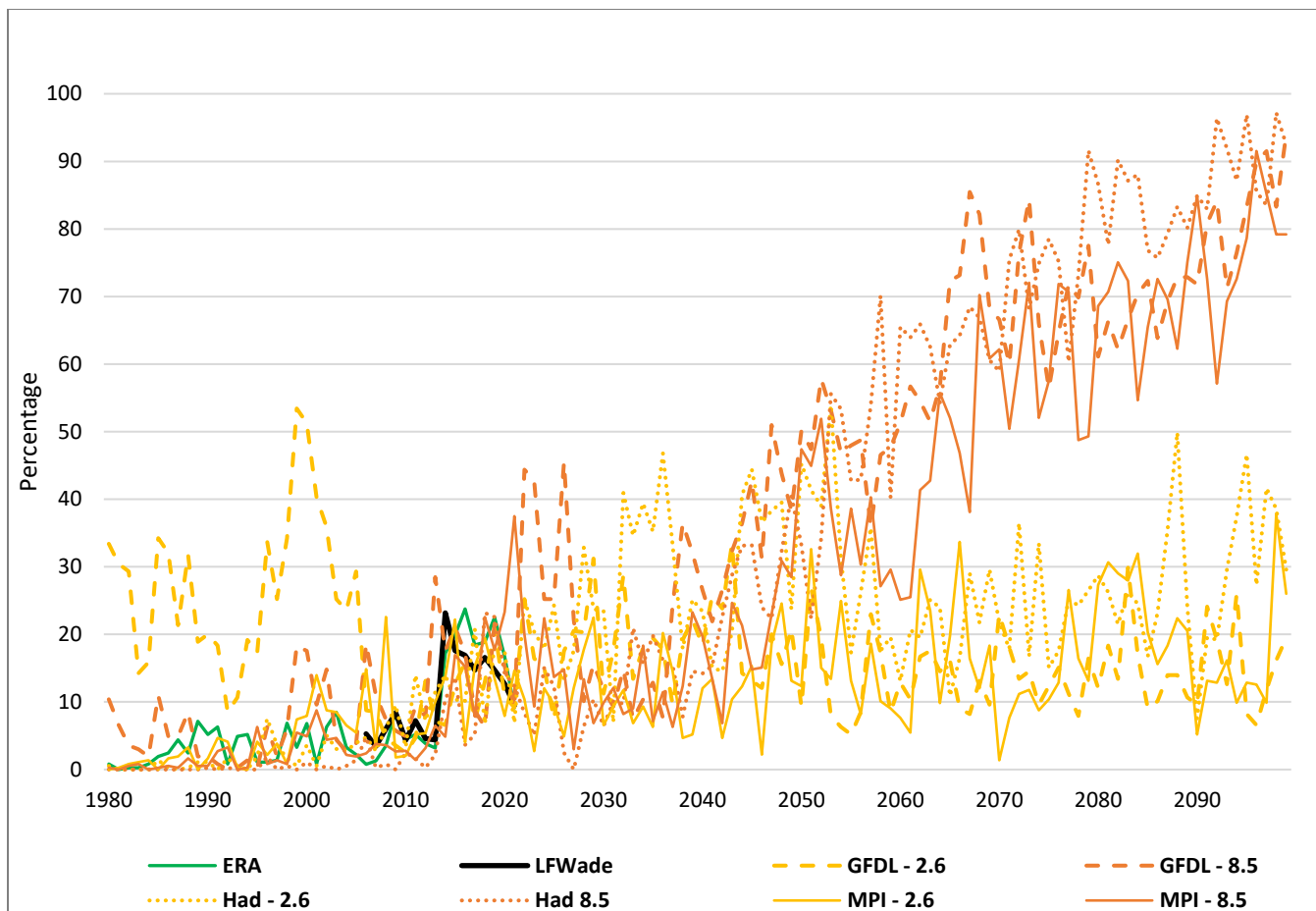


Figure 7 – Annual Percentage of Hot Days (TX90p). Days when Maximum Temperature exceeds the 90th Percentile. Data over the historical period up to 2021 are from ERA5 and LFWade. Projections (2006 to 2100) are from GFDL, Had and MPI under RCP 2.6 and RCP 8.5. The models historical baseline values are also plotted. Units: %

Figure 8 presents the historical and future trends in the annual percentage of days when minimum temperatures are above the 90th percentile (hot nights). The base period 2006 to 2021. The following are noted:

- The RCP 8.5 scenario show a continuous increase in the number of hot nights through the end of the century. Under RCP 8.5 the percentage of days when minimum temperatures exceed the 90th percentile of the baseline period, reaches 100% by the end of century, i.e., by this time most nights (>90%) will be considered a warm night.
- Under RCP 2.6 the percentage of days when minimum temperatures exceed the 90th percentile of the baseline period, levels off at current levels and remain through to the end of century.
- See Table 7 for the projected increases for the medium and long term.

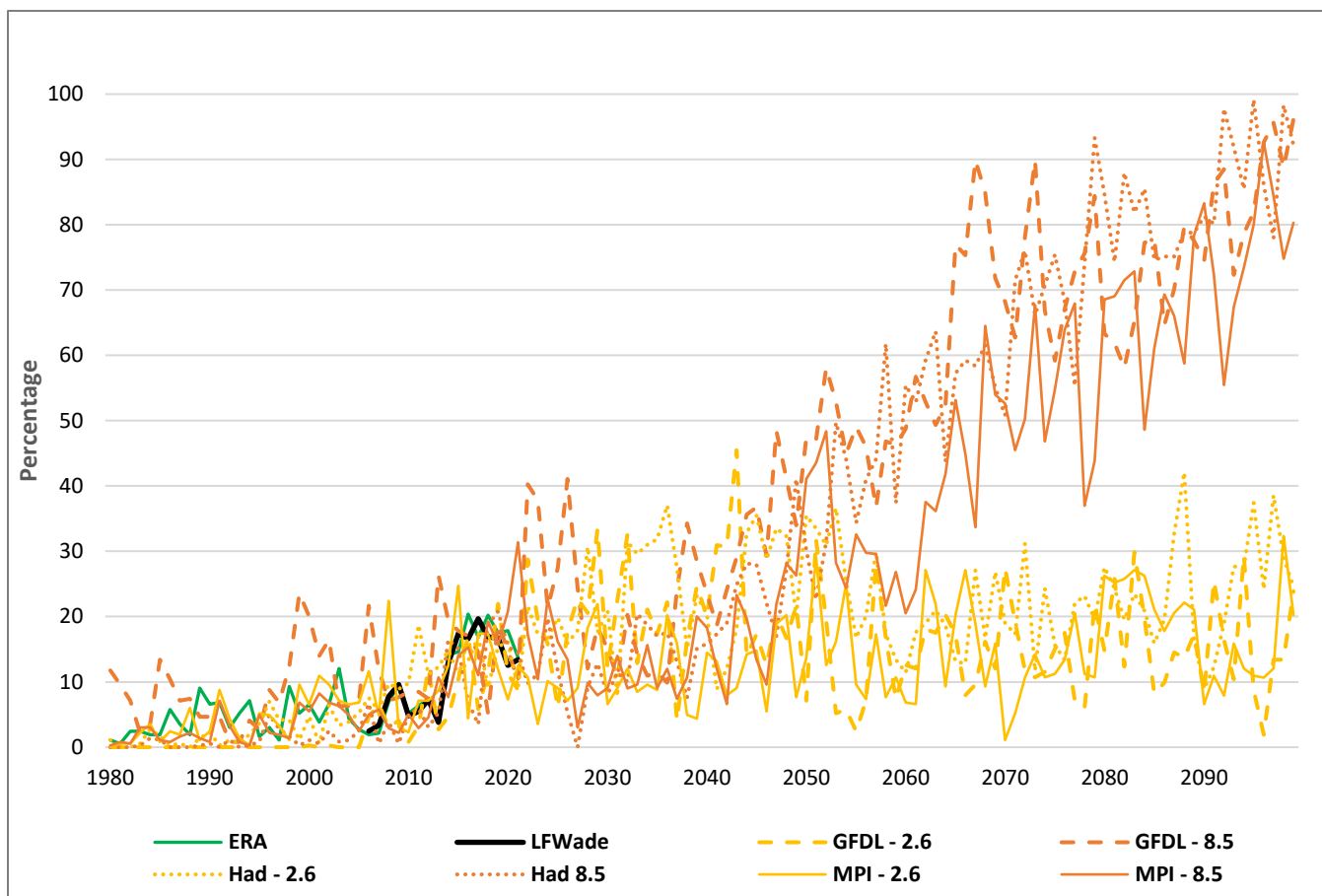


Figure 8 – Annual Percentage of Hot Nights (TN90p). Days when Minimum Temperature exceeds the 90th Percentile. Data over the historical period up to 2021 are from ERA5 and LFWade. Projections (2006 to 2100) are from GFDL, Had and MPI under RCP 2.6 and RCP 8.5. The models historical baseline values are also plotted. Units: %

Table 7 – Historical and projected average annual percentage of hot days and hot nights.

Parameter	Historical (2006 to 2021)					2040 to 2060						2070 to 2090					
	LFWade	ERA5	GFDL	Had	MPI	2.6			8.5			2.6			8.5		
						GFDL	Had	MPI	GFDL	Had	MPI	GFDL	Had	MPI	GFDL	Had	MPI
TX90P (%)	11	11	11	9	10	16	30	14	42	37	29	14	25	18	69	78	65
TN90P (%)	11	11	11	10	10	18	24	13	40	33	25	15	21	17	71	75	61

Figure 9 and Table 8 present the historical and future trends for the annual duration of heat waves for Bermuda. It is to be noted that there is a significant increase in heatwave duration under RCP 8.5, moving from an average of approximately 4 days historically to between 12 and 28 by the end of the century. That is, by the end of the century the longest duration of a heatwave, as defined by current standards, will last up to a month. See Table 8 for the projected durations for the medium and long term. There is no major change in heat wave duration under RCP 2.6.

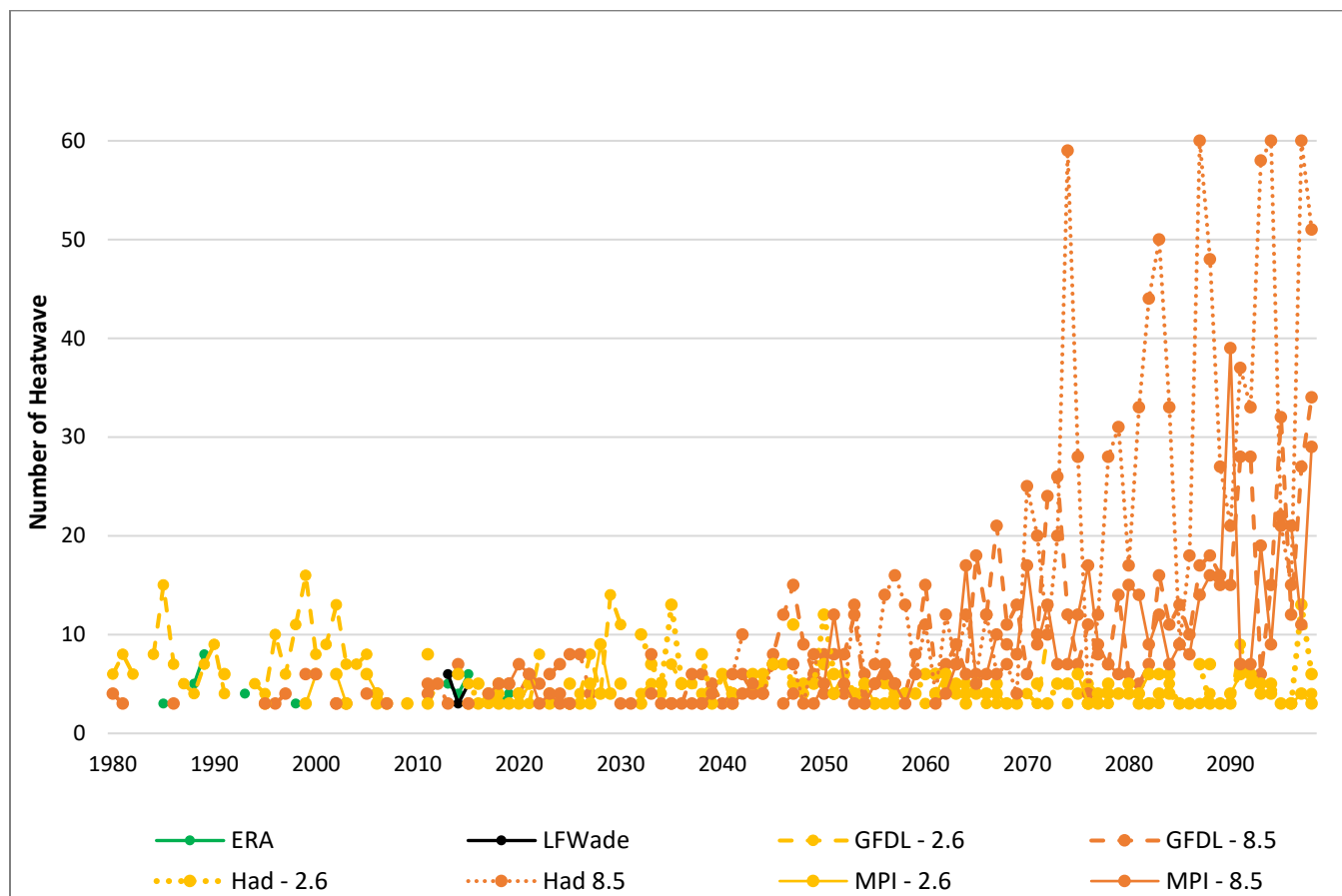


Figure 9 – Annual heatwave duration. That is the longest duration of a heatwave in days. Data over the historical period up to up to 2021 are from ERA5 and LFWade. Projections (2006 to 2100) are from GFDL, Had and MPI under RCP 2.6 and RCP 8.5. Units: Days

Table 8 – Projected Average Annual Heatwave Duration.

Parameter	Historical (2006 to 2021)					2040 to 2060						2070 to 2090					
	LFWade	ERA5	GFDL	Had	MPI	2.6			8.5			2.6			8.5		
						GFDL	Had	MPI	GFDL	Had	MPI	GFDL	Had	MPI	GFDL	Had	MPI
HWD	4	4	4	5	4.5	4	5	5	7	8	5	4	4	5	12	28	12

Figure 10 presents historical and projected cooling degrees days trends for Bermuda. The following are noted:

- The historical period suggests a linear trend, increasing at a rate of 173 (LFWade) and 69 (ERA) cooling degree days per decade. There were approximately 1591 (1298) cooling degree days annually in 2006 (1982) which increases to approximately 1713 (1602) cooling degree days in 2021 for LFWade and ERA respectively.
- Future projections show linear trends of increases of approximately 19 to 35 cooling degree days per decade under RCP 2.6 and 87 to 124 cooling degree days per decade under RCP 8.5 annually. Table 9 gives the historical and projected annual average for the medium and long term. Percentage changes are given in brackets.

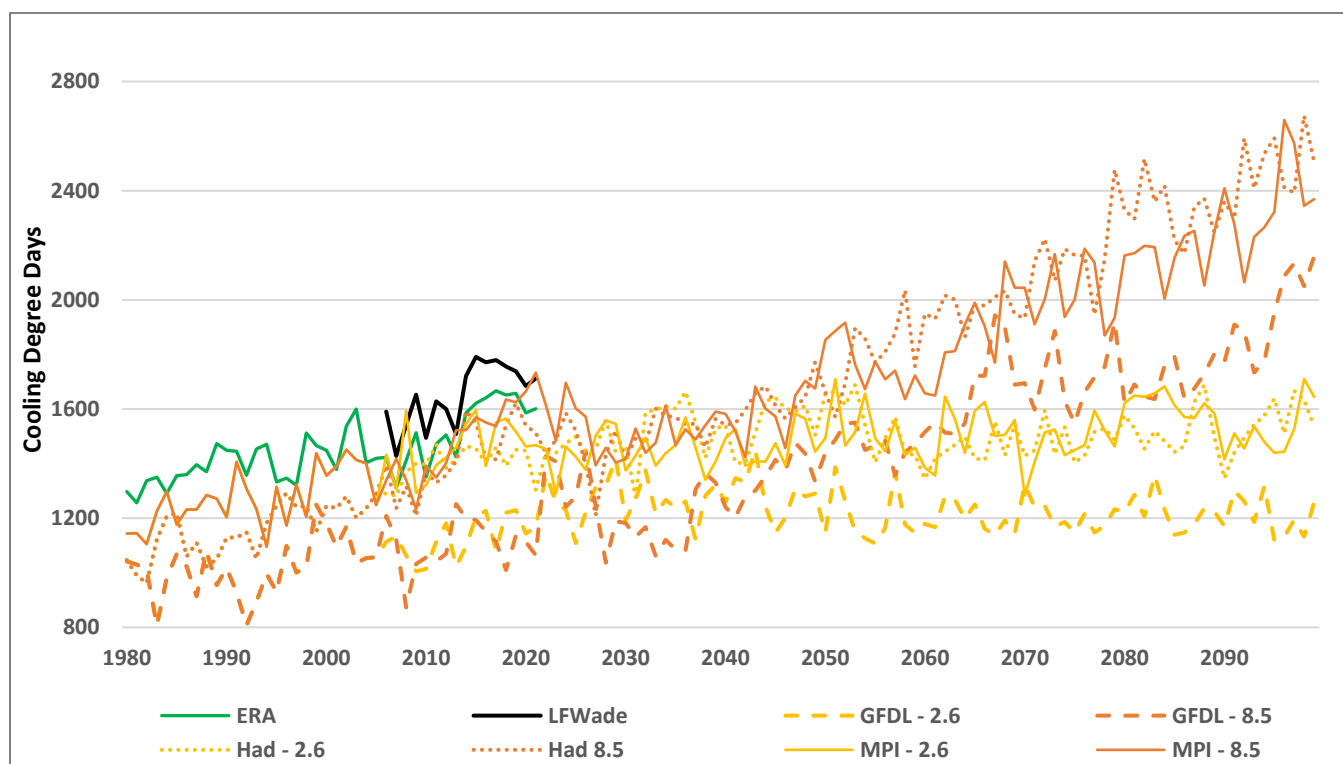


Figure 10 – Annual Sum of Cooling Degree Days. Cooling Degree Days are calculated using a base temperature of 18 degrees. Data over the historical period up to up to 2021 are from ERA5 and LFWade. Projections (2006 to 2100) are from GFDL, Had and MPI under RCP 2.6 and RCP 8.5. Units: Cooling degree days

Table 9 – Projected Average Annual Cooling Degree Days. Percentage changes are given in brackets.

Parameter	Historical (2006 to 2021)					2040 to 2060						2070 to 2090					
	LFWade	ERA5	GFDL	Had	MPI	2.6			8.5			2.6			8.5		
						GFDL	Had	MPI	GFDL	Had	MPI	GFDL	Had	MPI	GFDL	Had	MPI
CDDCold	1650	1526	1114	1412	1465	1242 (10)	1537 (10)	1490 (2)	1411 (28)	1719 (21)	1676 (14)	1213 (8)	1497 (7)	1537 (5)	1710 (55)	2242 (57)	2108 (43)

3.1.4 Sea Surface Temperature

Figure 11 and Table 10 present the historical and projected sea surface temperature (SST) for the Bermuda region. The following are noted:

- SST varies throughout the year with the highest temperatures occurring during August to September and coolest during January to April. This pattern holds true for both historical and projected SSTs.
- The modelled data follows reasonably well the reanalysis data. There is however a slight cold bias from October to April in the model compared to the reanalysis.
- SST is project to increase under both RCPs with higher values expected under RCP 8.5. Table 10 gives the projected changes with respect to the modelled historical (1982 to 2005).

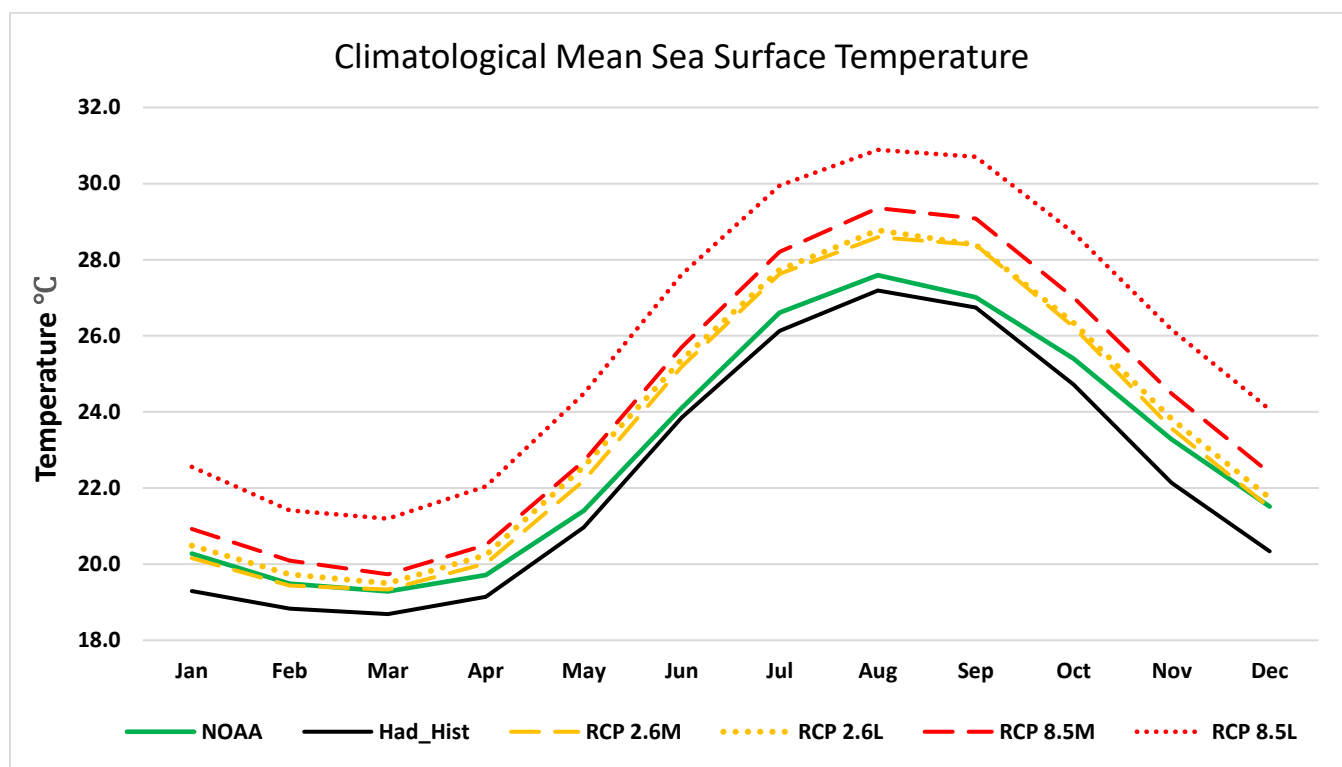


Figure 11 –Historical and projected climatological mean sea surface temperature (SST) for the medium (2040 to 2060) and long (2070 to 2090) term for RCP 2.6 and 8.5. Data shown for NOAA and modelled (Had) data. Medium and long term are denoted by M and L respectively. The climatology over the historical baseline period (1982-2005) shown for comparison.

Figure 12 presents the average annual SST for the period 1861 to 2100 of the Bermuda region. The following are noted:

- NOAA data indicate that over the historical period analysed, SSTs have been increasing at a rate of approximately 0.26°C per decade.

- SSTs are projected to continue increasing through the end of this current century. Under RCP 2.6 the rate of increase is projected to be 0.07°C per decade. The rate is 0.43°C per decade under RCP 8.5. See Table 11.

Table 10 – Historical climatologies and projected change in mean sea surface temperature climatology. Historical baseline period (1982-2005). Change is with respect to the model baseline.

Dataset	Jan	Feb	Mar	Apr	May	Jun	Jul	Aug	Sep	Oct	Nov	Dec
NOAA	20.3	19.5	19.3	19.7	21.4	24.1	26.6	27.6	27.0	25.4	23.3	21.5
Had_Hist	19.3	18.8	18.7	19.1	21.0	23.9	26.1	27.2	26.7	24.7	22.1	20.3
4.5M	0.9	0.6	0.6	0.9	1.2	1.3	1.5	1.4	1.7	1.5	1.4	1.2
4.5L	1.2	0.9	0.8	1.1	1.6	1.5	1.6	1.6	1.7	1.6	1.7	1.4
8.5M	1.6	1.3	1.0	1.4	1.7	1.8	2.1	2.2	2.3	2.3	2.3	2.1
8.5L	3.3	2.6	2.5	2.9	3.5	3.8	3.8	3.7	4.0	4.0	4.0	3.7

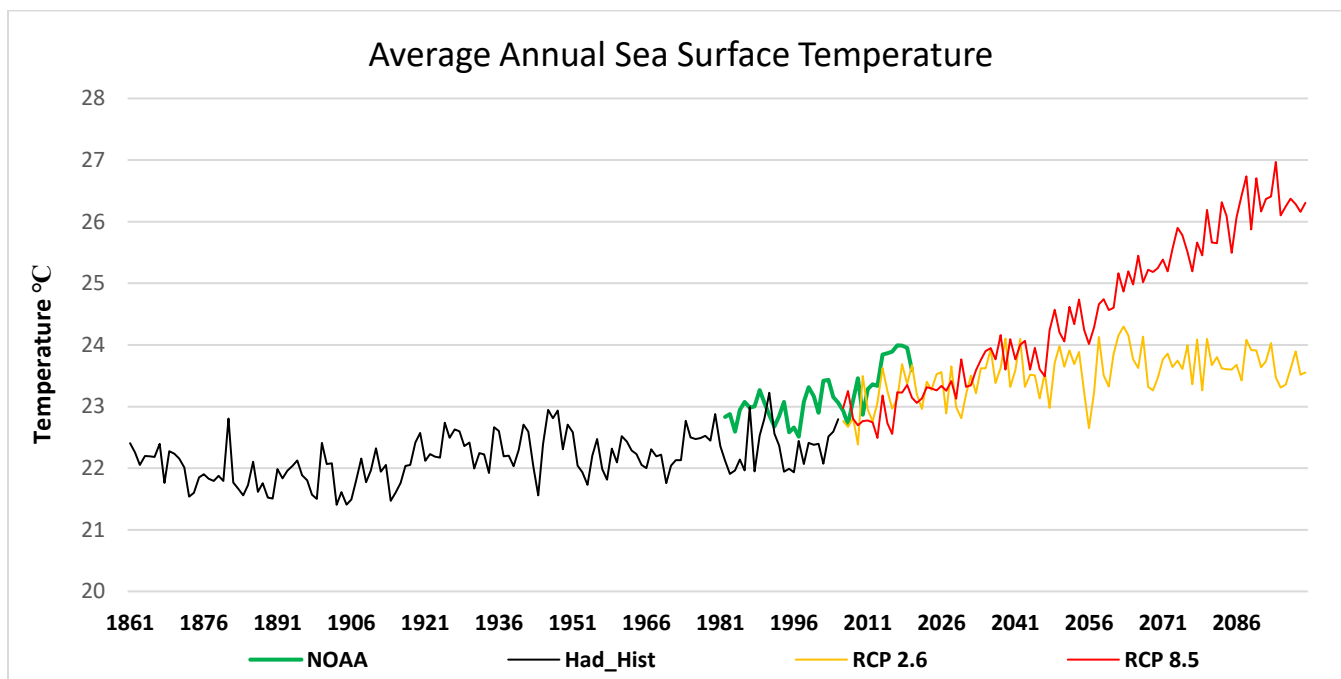


Figure 12 – Annual average sea surface temperature, NOAA and Had. Data over the historical period up to 2020 (2005) are from NOAA (Had). Projections (2006 to 2100) are from Had under RCP 2.6 and RCP 8.5. The modelled (Had) historical baseline values are also plotted. Units: °C.

Table 11 – Slope values of linear trends for observed and modelled annual average sea surface temperatures.

NOAA	Had_Hist	RCP 2.6	RCP 8.5
0.26 °C per decade	0.04 °C per decade	0.07 °C per decade	0.43 °C per decade

3.2 Rainfall

Historical and projected analyses for climatology, trends and extremes in rainfall are presented in figures 13 to 18 and tables 12 and 13.

3.2.1 Rainfall Climatology

Figure 13 presents the historical monthly climatologies of average precipitation for the island of Bermuda. The historical is for two periods 2006 to 2021 (LFWade and ERA5) and 1980 to 2005 ERA5. The historical climatologies for the models are also shown (1980 to 2005). Again, the simulated values are RegCM downscaled values of GFDL, Had and MPI (RCP 2.6 and 8.5). The two periods are chosen to allow for comparison of the datasets, 2006 to 2021 to compare the observed LFWade to the reanalysis ERA5 and 1980 to 2005 to compare ERA5 to the historical model datasets. The following are noted:

- The ERA5 datasets do a good job of capturing the climatological pattern and values of the observed dataset (LFWade). The differences, mostly observed in July and August, could be attributed to LFWade being point data while ERA5, gridded data for the island as a whole.
- A bimodal rainfall pattern is exhibited with peaks in January and September. The September peak receives approximately 25% more rainfall than the January peak.
- The models' historical climatologies underestimate the observed data more so in the cooler months, November to April.

Table 12 gives the historical precipitation climatologies for the observed, reanalysis and model datasets. Also given are the projected changes in precipitation for the medium and long term compared to the modelled base line (1980 to 2005). The following are noted.

- Projected changes are varied based on the specific model in both the medium and long term.
- The average annual and seasonal changes over the two RCPs for the medium term (2040-2060) are: -4 to 11% annual; 0 to 15% for December through February; 5 to 33% for March through May; -15 to 18% for June through August; and 1 to 27% for September through November.
- The average annual and seasonal changes over the two RCPs for the long term (2070-2090) are: 3 to 48% annual; 0 to 13 % for December through February; 2 to 49% for March through May; -9 to 47 % for June through August; and -4 to 34% for September through November

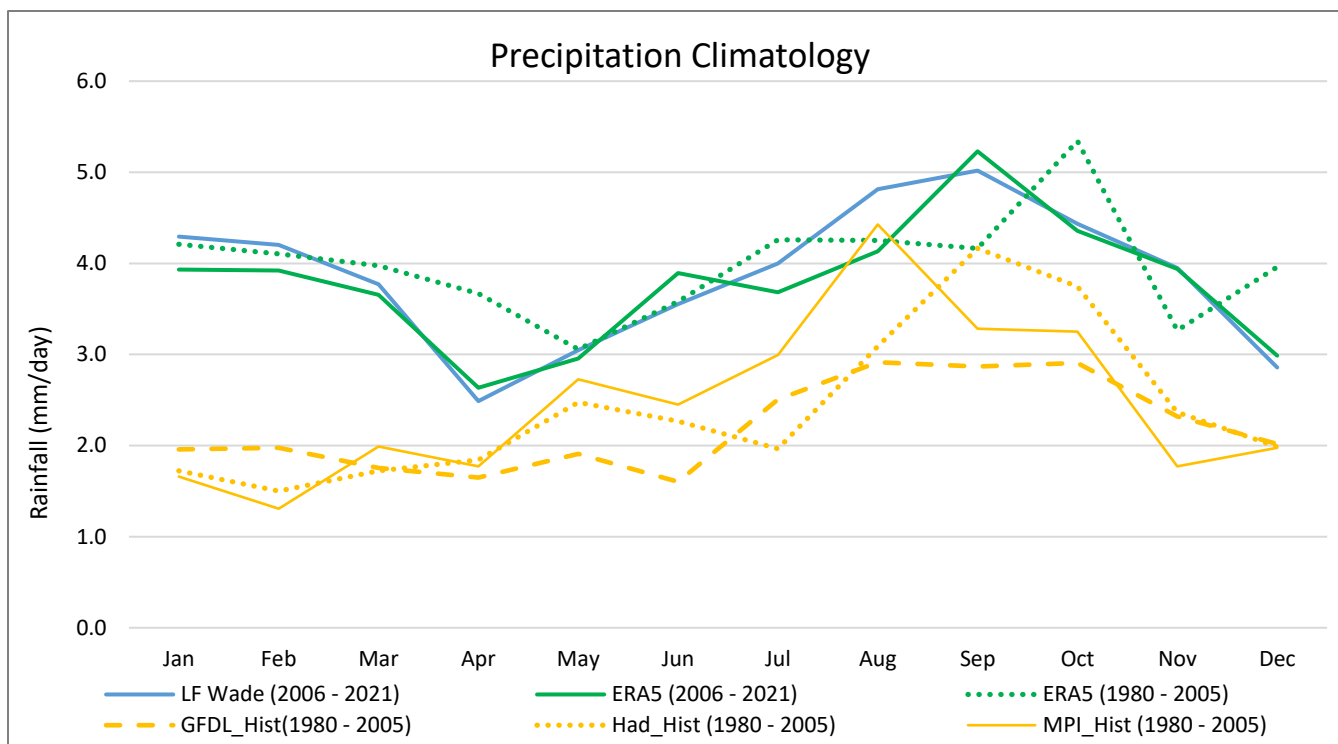


Figure 13 – Historical Rainfall Climatology. Data shown for station data (LFWade), reanalysis (ERA5) and modelled (downscaled GFDL, Had and MPI).

Table 12 – Historical precipitation climatologies and projected change.

Dataset	Jan	Feb	Mar	Apr	May	Jun	Jul	Aug	Sep	Oct	Nov	Dec	Unit
LF Wade (2006 - 2021)	4.3	4.2	3.8	2.5	3.0	3.6	4.0	4.8	5.0	4.4	3.9	2.9	mm/day
ERA5 (1980 - 2005)	4.2	4.1	4.0	3.7	3.1	3.6	4.3	4.3	4.2	5.3	3.3	4.0	
GFDL_Hist(1980 - 2005)	2.0	2.0	1.8	1.6	1.9	1.6	2.5	2.9	2.9	2.9	2.3	2.0	
Had_Hist (1980 - 2005)	1.7	1.5	1.7	1.8	2.5	2.3	2.0	3.1	4.2	3.7	2.4	2.0	
MPI_Hist (1980 - 2005)	1.7	1.3	2.0	1.8	2.7	2.5	3.0	4.4	3.3	3.3	1.8	2.0	
GFDL_2.6 (2040 - 2060)	4%	2%	-2%	32%	40%	28%	9%	18%	-3%	18%	-11%	-1%	Percent
Had_2.6 (2040 - 2060)	51%	20%	23%	46%	30%	-20%	8%	-11%	-4%	-4%	13%	-29%	
MPI_2.6 (2040 - 2060)	10%	27%	-14%	42%	-6%	-29%	-17%	0%	29%	-6%	6%	4%	
GFDL_2.6(2070 - 2090)	11%	9%	-1%	56%	10%	24%	-32%	-16%	1%	-30%	17%	19%	
Had_2.6 (2070 - 2090)	30%	21%	0%	19%	-12%	-28%	6%	-4%	-7%	-3%	9%	9%	
MPI_2.6 (2070 - 2090)	20%	32%	14%	43%	-8%	-8%	5%	-6%	11%	-16%	20%	4%	
GFDL_8.5 (2040 - 2060)	10%	-1%	26%	39%	21%	-6%	-12%	28%	7%	5%	-2%	-1%	
Had_8.5 (2040 - 2060)	12%	25%	26%	6%	14%	-9%	36%	-28%	-7%	-6%	41%	5%	
MPI_8.5 (2040 - 2060)	0%	40%	3%	12%	-2%	-27%	-9%	-1%	30%	-17%	68%	10%	
GFDL_8.5 (2070 - 2090)	5%	8%	28%	59%	-10%	65%	21%	-12%	-9%	6%	5%	-1%	
Had_8.5 (2070 - 2090)	83%	65%	58%	65%	23%	21%	112%	8%	-18%	43%	47%	74%	
MPI_8.5 (2070 - 2090)	12%	33%	6%	49%	-11%	8%	27%	20%	33%	-3%	71%	18%	

Figure 14 presents the historical and projected changes in annual average precipitation. The following are noted:

- Over the period of analysis there seem to be no real linear trend for both the historical and projected data. The data, however, exhibits significant interannual variability throughout the period.
- See Table 13 for the slope values.

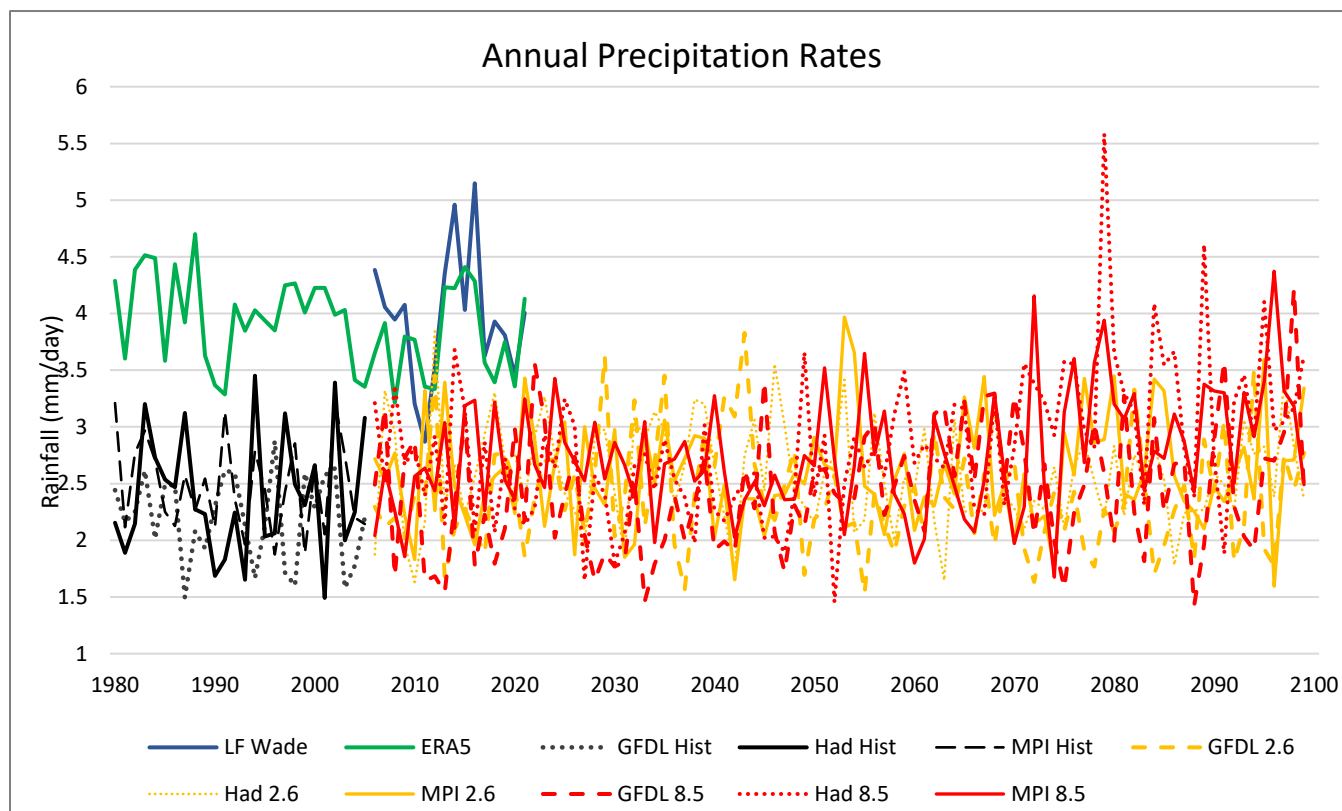


Figure 14 – Annual Rainfall Trend. Data shown for Station data (LFWade), reanalysis (ERA5) and modelled (downscaled GFDL, Had and MPI). Measure data was unavailable. Units: mm/day.

Table 13 – Slopes of linear trends for Figure 14. Units (mm/day)/decade.

Historical					2.6			8.5		
LFWade	ERA5	GFDL	Had	MPI	GFDL	Had	MPI	GFDL	Had	MPI
0.00	-0.10	-0.07	0.06	-0.01	-0.01	-0.02	0.02	0.05	0.10	0.06

3.2.3 Rainfall Extremes

Figure 15 presents the annual number of heavy rainfall days (R20mm). This is shown for station, reanalysis, and the modelled data. The following are noted:

- The station and reanalysis datasets exhibit significant interannual variability and show slight linear trends with slopes of 0.7 days/decade and -0.9 days/decade respectively.
- The modelled data also exhibit considerable interannual variability with no real linear trends. This is true for both RCP 2.6 (moving from 10/12 days to 11 days and 8/12 days in the medium and long term respectively) and RCP 8.5 (moving from 8/12 days to 11 days and 10/17 days in the medium and long term respectively).

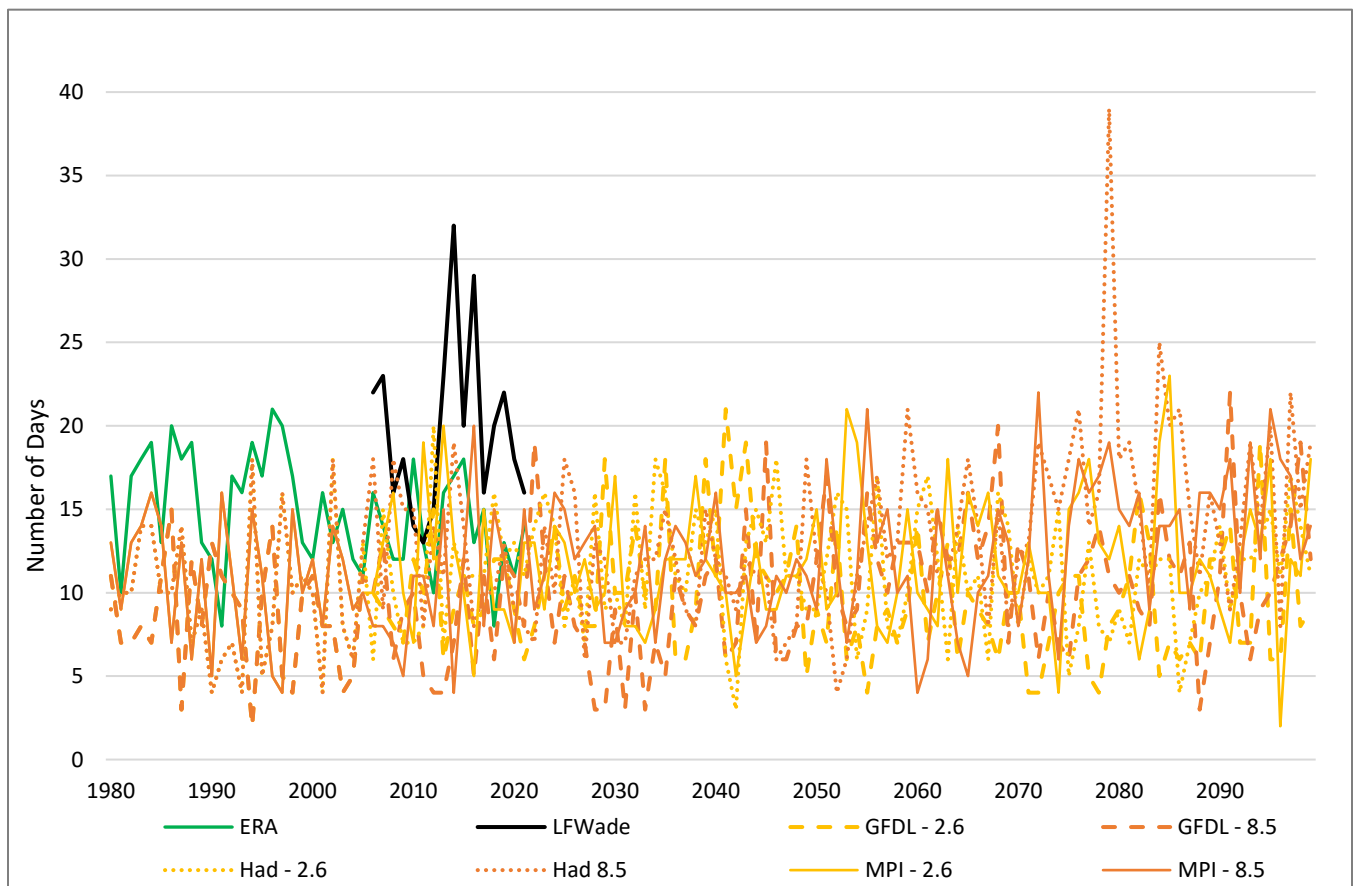


Figure 15 – Annual Number of Heavy Rainfall (R20mm) Days. Number of days when precipitation ≥ 20 mm. Data over the historical period up to up to 2021 are from ERA5 and LFWade. Projections (2006 to 2100) are from GFDL, Had and MPI under RCP 2.6 and RCP 8.5. Units: days.

Figure 16 presents the annual number of consecutive dry days (CCD). This is shown for station, reanalysis, and the modelled data. The following are noted:

- The station and reanalysis datasets exhibit significant interannual variability and show slight linear trends with slopes of 1.2 days/decade and 1.3 days/decade respectively.
- The modelled data also exhibit considerable interannual variability with no real linear trends. This is true for both RCP 2.6 (moving from 21/24 days to 23/25 days and 19/23 days in the medium and long term respectively) and RCP 8.5 (moving from 20/23 days to 21/23 days and 20/21 days in the medium and long term respectively).

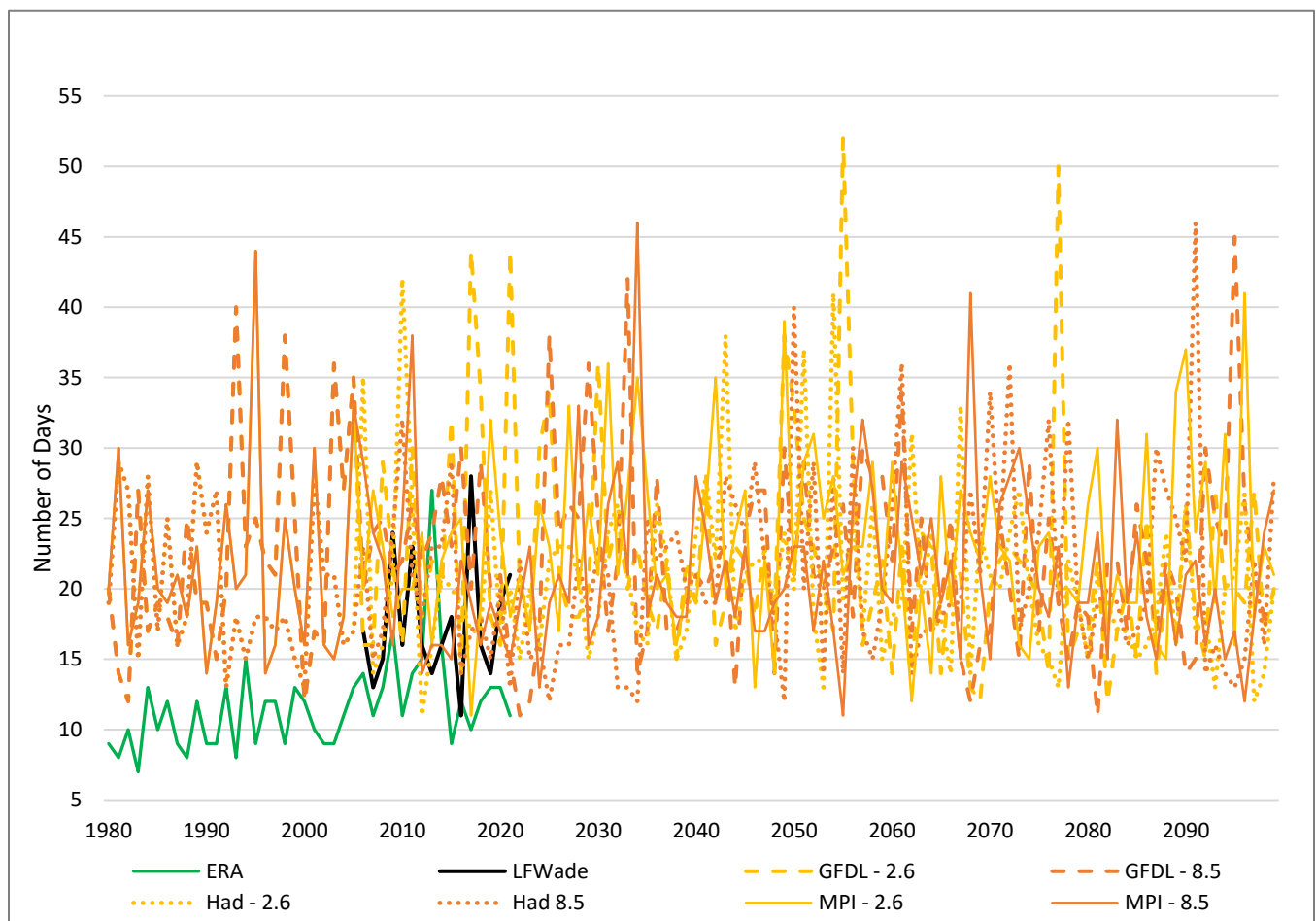


Figure 16 – Annual Number of Consecutive Dry Days (CCD) Days. Maximum number of consecutive dry days (when precipitation is < 1.0 mm). Data over the historical period up to up to 2021 are from ERA5 and LFWade. Projections (2006 to 2100) are from GFDL, Had and MPI under RCP 2.6 and RCP 8.5. Units: days.

Figure 17 presents the annual number of consecutive wet days (CWD). This is shown for station, reanalysis, and the modelled data. The following are noted:

- The station and reanalysis datasets exhibit significant interannual variability and show no real linear trends with slopes of 0.1 days/decade and 0.2 days/decade respectively.
- The modelled data also exhibit considerable interannual variability with no real linear trends. This is true for both RCP 2.6 (moving from 6/7 days to 5/6 days and 6 days in the medium and long term respectively) and RCP 8.5 (moving from 6/7 days to 6/7 days and 5/7 days in the medium and long term respectively).

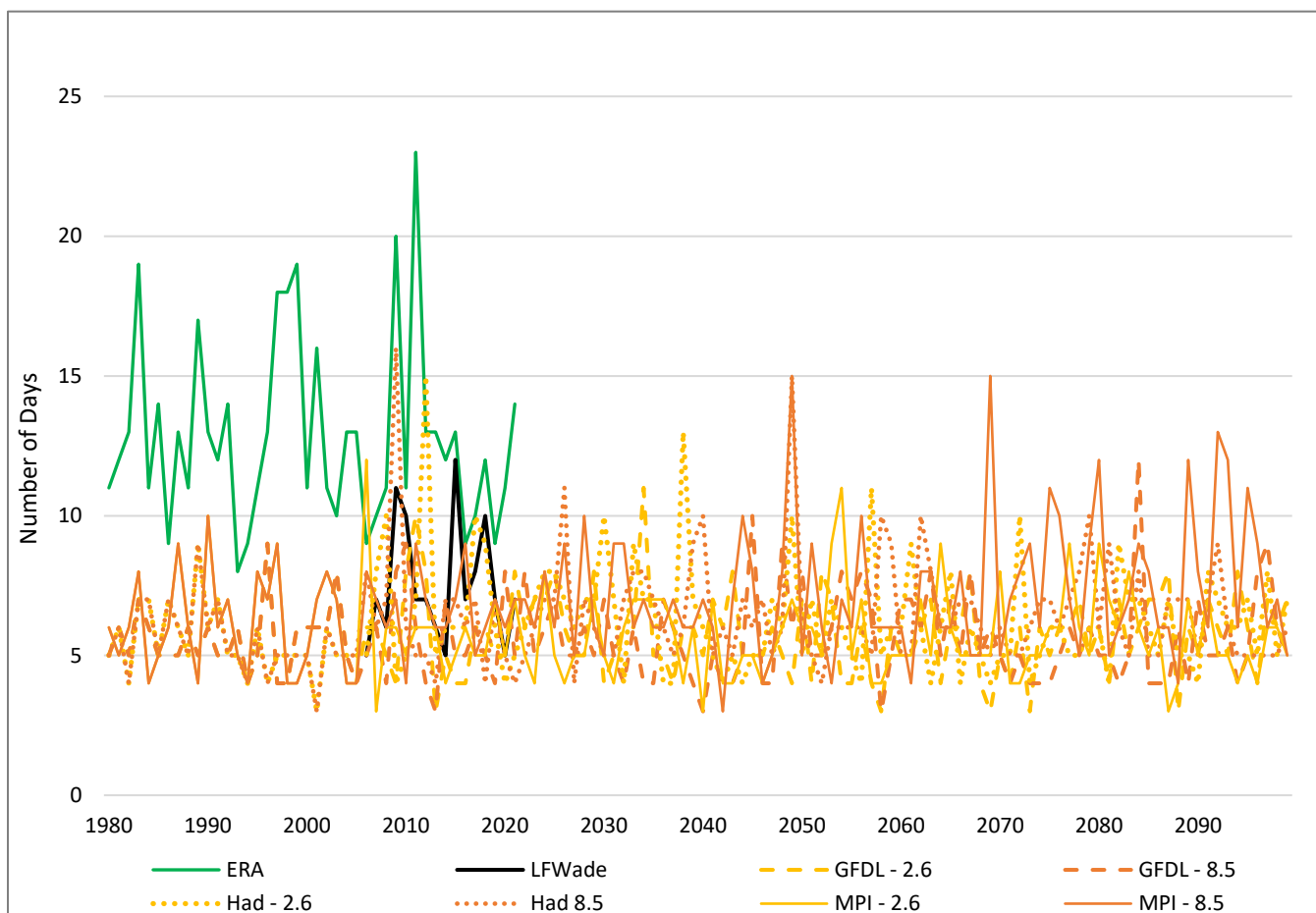


Figure 17 – Annual Number of Consecutive Wet Days (CWD) Days. Maximum number of consecutive wet days (when precipitation is ≥ 1.0 mm). Data over the historical period up to up to 2021 are from ERA5 and LFWade. Projections (2006 to 2100) are from GFDL, Had and MPI under RCP 2.6 and RCP 8.5. Units: days.

Figure 18 presents the annual total rainfall on wet days (prctot) for Bermuda. This is shown for station, reanalysis, and the modelled data. The following are noted:

- The station and reanalysis datasets exhibit significant interannual variability and show linear trends with slopes of -35 mm/decade and 7 mm/decade respectively.
- The modelled data also exhibit considerable interannual variability with no real (slight) linear trends for RCP 2.6 (8.5). With RCP 2.6 (moving from 816/915 mm/year to 865/900 mm/year and 796/931 mm/year in the medium and long term respectively) and RCP 8.5 (moving from 804/944 mm/year to 855/926 mm/year and 865/1187 days in the medium and long term respectively).

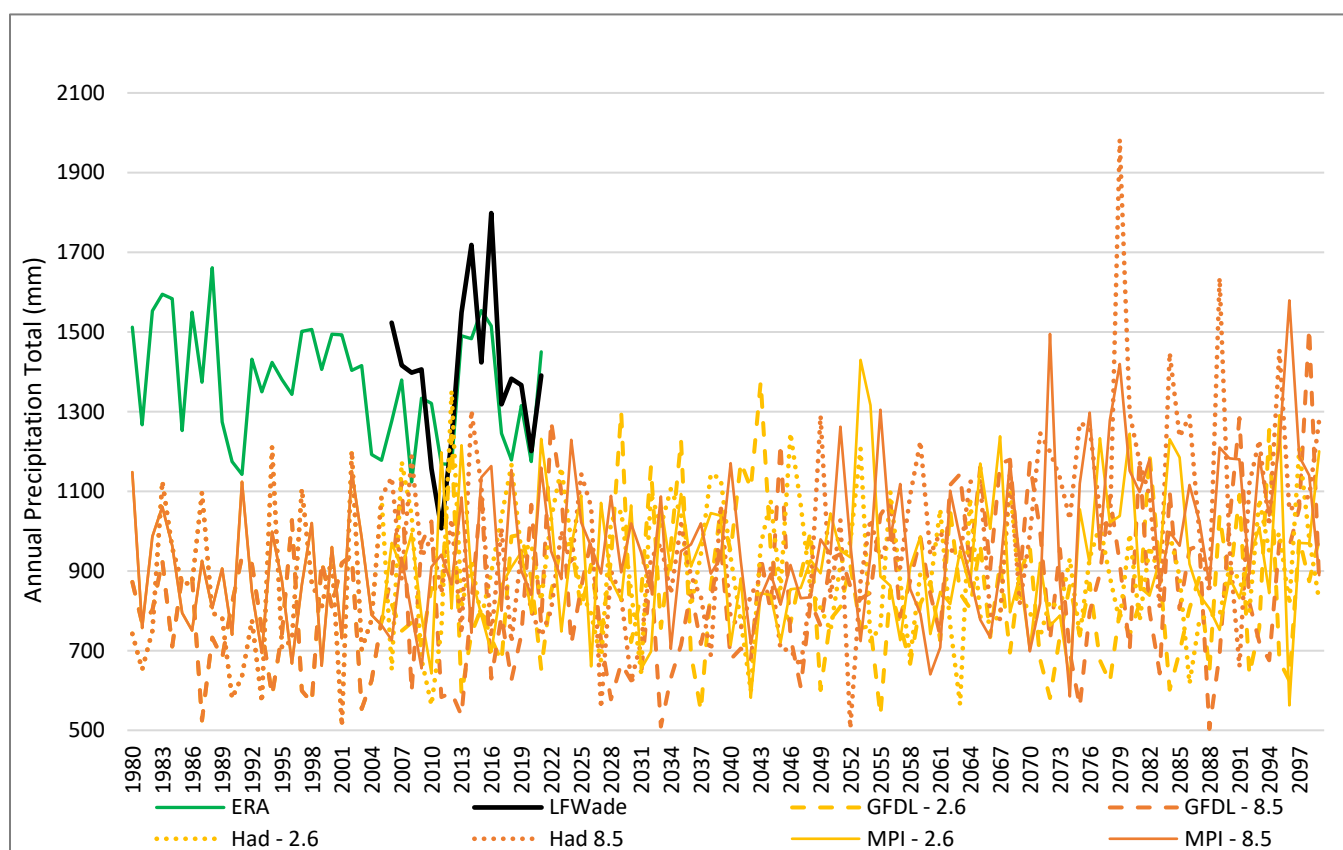


Figure 18 – Annual Total Rainfall (prctot) for days when rainfall is ≥ 1 mm. Data over the historical period up to up to 2021 are from ERA5 and LFWade. Projections (2006 to 2100) are from GFDL, Had and MPI under RCP 2.6 and RCP 8.5. Units: mm.

3.4 Sea Level Rise

This section provides the trends in historical and projected mean sea level. Also presented are trends for the Globe and Caribbean as context for interpreting the data for the island. The general approach taken in presenting the results is outlined below.

- **Historical and Future Change:** The report is divided into two sections. Section 3.4.1 examines historical changes in sea level. Section 3.4.2 examines projections of sea level rise up to 2100. Table 13 provides a summary of datasets utilised.
- **The Global Context:** In presenting each section, results for the globe, and where applicable and available, the region are presented first. The wider global context is useful for interpreting regional and sub regional results, especially for a particular Caribbean territory.
- **Multiple Data Sources:** This report relies on multiple authoritative data sources. The use of multiple sources is to ensure that as complete as possible a picture is provided as well as for consistency and consensus purposes. For historical and future trends and projection at the global scale, the report relies on the IPCC's Special Report on Oceans and Cryosphere in a Changing Climate (SROCC) (IPCC 2019) and the recently released IPCC's Sixth Assessment Report (AR6) (IPCC 2022). For historical trends Bermuda, published literature, tide gauge data and satellite altimetry data are used. For projection trends for Bermuda, results from two climate data sites/tools are used. Detailed explanations about the data sources are given at the beginning of each section.
- **Future Scenarios:** Instead of RCPs, changes are presented for four future Shared Socio-economic Pathways (SSPs), namely, SSP1-2.6, SSP2-4.5, SSP3-7.0, SSP5-8.5 (Pörtner et al., 2022). SSPs are a new method of assessing future scenarios which seeks to combine the knowledge of the physical sciences of climate change with the societal impacts brought on by the vulnerability caused by climate change. SSPs incorporate adaptation and mitigation research to create more holistic approach to future projections by combining them with future emission and concentration scenarios with socio-economic development pathways. SSP1-2.6 is described as the 'sustainability' development pathway, SSP2-4.5 referred to as the 'middle of the road' development pathway, SSP3-7.0 referred to as 'regional rivalry' development pathway, SSP4-6.0 referred to as 'inequality' development pathway and SSP5-8.5 described as a 'fossil fuel intensive' development pathway. (See Riahi et al., 2017 for more details on SSPs). The SSPs and RCPs are not directly comparable however SSP1-2.6 is related to the previous RCP2.6 from the fifth assessment report as it corresponds to significant and immediate emissions cuts, leading to net zero and eventually negative annual emissions in the second half of the century. Under SSP-2.6 global warming stays just below 2°C at the end of the century when compared to pre-industrial (pre-1900) levels. SSP2-4.5 corresponds to emissions reductions which are roughly in line with the upper bounds of the latest Nationally Determined Contributions and global warming of around 2.7°C at the end of the 21st century. SSP3-7.0 corresponds with a medium-high development pathway. Under this SSP no additional climate change policy is put in place and there are high non-CO₂ related emissions which leads to a pathway which would be roughly in the middle of the previous RCP6.0 and RCP8.5 SSP5-8.5 corresponds to very high emissions, no additional climate policy and intensive fossil fuel dependent development which is the worst-case scenario pathway.

Table 14 – Historical and Future Climate Change Data Sources.

Region	Source	Note	Reference
Historical			
Globe	Intergovernmental Panel on Climate Change Fifth Assessment Report (AR5)	Synthesis reports of latest global studies at the time of publication. Long term and more recent trend estimates.	IPCC (2013)
	Special Report on Oceans and Cryosphere in a Changing Climate (SROCC)	Synthesis reports of latest global studies at the time of publication. Long term and more recent trend estimates.	IPCC (2019)
	Copernicus Marine Service Ocean State Report, Issue 4 (2020) (OSR4)	Synthesis reports of satellite altimetry estimates. Data since 1993 to present.	https://doi.org/10.1080/1755876X.2020.1785097
Caribbean	Peer reviewed Literature	Various studies providing information on sea level rise for the Caribbean from tide gauge measurements and merged tide gauge and satellite altimetry data.	Torres and Tsimplis (2013) Palanisamy <i>et al.</i> , (2012)
Bermuda	The Copernicus Climate Change Service (C3S)	Satellite Altimetry Data 1993-present. Data resolution: 0.25° x 0.25°.	https://cds.climate.copernicus.eu/
	The National Aeronautics and Space Administration (NASA)	Sea Level Evaluation and Assessment Tool (SEA Tool)	https://sealevel.nasa.gov/sea-level-evaluation-tool
	University of Hawaii Sea Level Centre.	Tide Gauge Data	Retrieved from: http://uhslc.soest.hawaii.edu/data/
Future			
Globe	Special Report on Oceans and Cryosphere in a Changing Climate (SROCC)	Synthesis reports of latest global modelling studies at the time of publication. This report provides estimates based on literature largely published after the Fifth Assessment Report of the IPCC (AR5).	IPCC (2019)
	Intergovernmental Panel on Climate Change Sixth Assessment Report (AR6): Climate Change 2022 Impacts, Adaptation and Vulnerability	Synthesis reports of latest global studies climate change at the time of publication. Long term and more recent trend estimates of sea level change. The NASA Sea Level Projection Tool was developed by NASA and the IPCC to visual sea level rise projections from the recent IPCC (AR6)	IPCC (2022) https://sealevel.nasa.gov/ipcc-ar6-sea-level-projection-tool
Bermuda	Intergovernmental Panel on Climate Change Sixth Assessment Report (AR6): Climate Change 2022 Impacts, Adaptation and Vulnerability	Synthesis reports of latest global studies climate change at the time of publication. Long term and more recent trend estimates of sea level change. The NASA Sea Level Projection Tool was developed by NASA and the IPCC	IPCC (2022) https://sealevel.nasa.gov/ipcc-ar6-sea-level-projection-tool

		to visual sea level rise projections from the recent IPCC (AR6)	
	Sea-Level Rise Threats in the Caribbean: Data, tools, and analysis for a more resilient future.	See above	IDB (2018) *See Footnote ³
	Climate Analytics Local SLR Tool	The Tool provides projected sea levels around the globe for different RCPs at different levels of warming. The projections are available at the local level. Data retrieved for Grid box centered on latitude 10N, longitude 60W. Projections as relative to 2006.	http://localslr.climateanalytics.org/ *See Footnote

The following things should be noted about the Climate Analytics Tool:

- The projections are based on two different sea level models that build on top of the IPCC reports.
- The first set of models are those used in Kopp et al. (2014) extended by data based on Rasmussen et al. (2018).
- The second set of models are for Kopp et al. (2014) extended by data based on Rasmussen et al. (2018) and include revised Antarctic ice-sheet contribution based on expert judgement presented in Bamber et al. (2019).
- The Bermuda projections are for a grid box which does not incorporate any tide gauge data from a station in St. George, Bermuda.

3.4.1 Historical Sea Level Rise

Figures 19 to 22 and Table 15 present information related to historical mean sea level rise for the Globe and Bermuda. The following are noted:

Globe:

- There is an acceleration in global mean sea level rise (GMSL) which is projected to continue with increased global warming. Global mean sea level from tide gauges and altimetry increased from 1.4 mm/year over the period 1901–1990 to 2.1 mm/year over the period 1970–2015 to 3.2 mm/year over the period 1993–2015 to 3.6 mm/year over the period 2006–2015. See Figure 20 and Table 14.
- New calculations presented in the Fourth CMS Ocean State Report 2020 (OSR) premised on satellite altimetry corroborates that global mean sea level rise is accelerating, with this rate increasing by 0.12 ± 0.073 mm/year each year. See Table 15.

Bermuda:

- Bermuda is one of the few small islands with a long and reliable tide gauge record from which sea level analysis can be done. St. Georges record captures sea level data from 1985-2019 with small gaps. Figure 20 presents the climatology of the uninterrupted years of data spanning 2004 to 2008. The highest and lowest values are observed in October and April respectively.
- Figure 21 gives the monthly sea level change in Bermuda for 2004-2008. A trend of increasing sea level is observed throughout this 5-year period.
- Figure 22 gives the annual mean sea level plot for the nearest relevant grid box to Bermuda Station (Latitude 32.373N and Longitude 64.703W) from the C3S data for the period of 1993-2020. The observed linear trend of sea level rise is approximately 3.84 ± 0.4 mm/year. This is not significantly different from trend of 3.47mm/year which obtained from the Sea Level Evaluation and Assessment Tool (Latitude 32.25N and Longitude 64.75W). These values are close to the global mean sea level rise 3.7 ± 0.4 mm/year (Pörtner et al., 2022).

Table 15 – Average Rate of Global Mean Sea Level Rise.

Source	Period	Rate (mm/year)	Description
GLOBAL			
IPCC (2019)	1901-1990	1.4 ± 0.6	Tide gauge
	2006-2015	3.6 ± 0.4	Tide gauge + Satellite Altimetry
IPCC (2022)	1901-2018	2.3 ± 0.6	Tide gauge + Satellite Altimetry
	2006-2018	3.7 ± 0.4	Tide gauge + Satellite Altimetry
OSR4	1993-2018	3.3 ± 0.4	Satellite Altimetry
	1993 - 2010	2.5 ± 1.3	Satellite Altimetry after correction for Global Isostatic Adjustment (GIA)

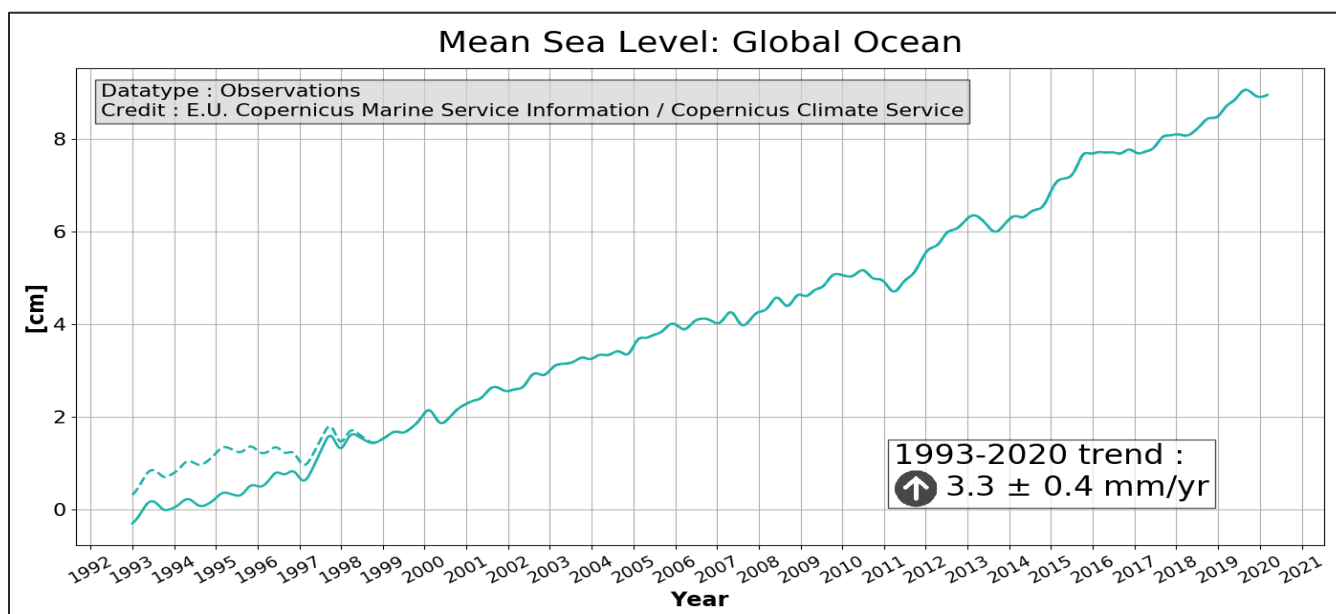


Figure 19 – Mean sea level daily evolution. Data since January 1993 (in cm) and from the satellite altimeter observations estimated in the global ocean, derived from the average of the gridded sea level maps weighted by the cosine of the latitude. During 1993-1998, the dashed line shows an estimate of the global mean sea level corrected for the TOPEX-A instrumental drift, based on comparisons between altimeter and tide gauges measurements. Source: Copernicus Marine Service (CMEMS). <https://marine.copernicus.eu/>

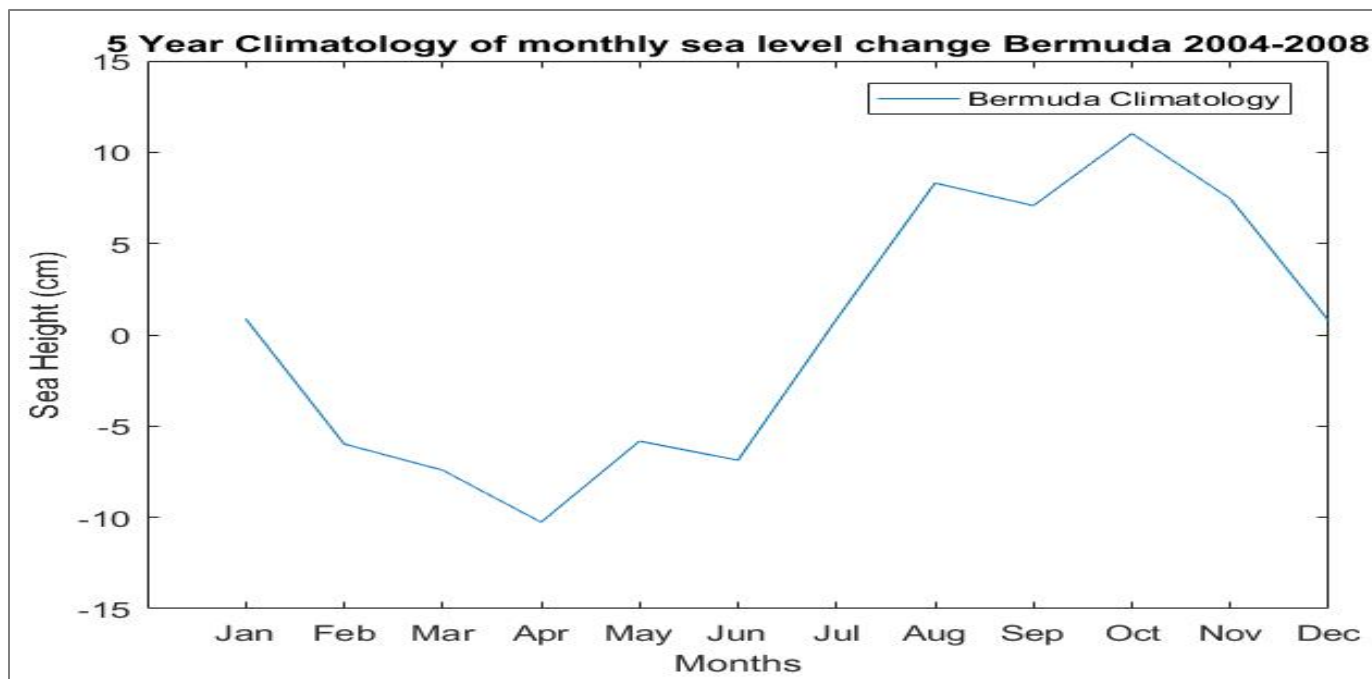


Figure 20 – Climatology of Sea level change in Bermuda from tide gauge data.

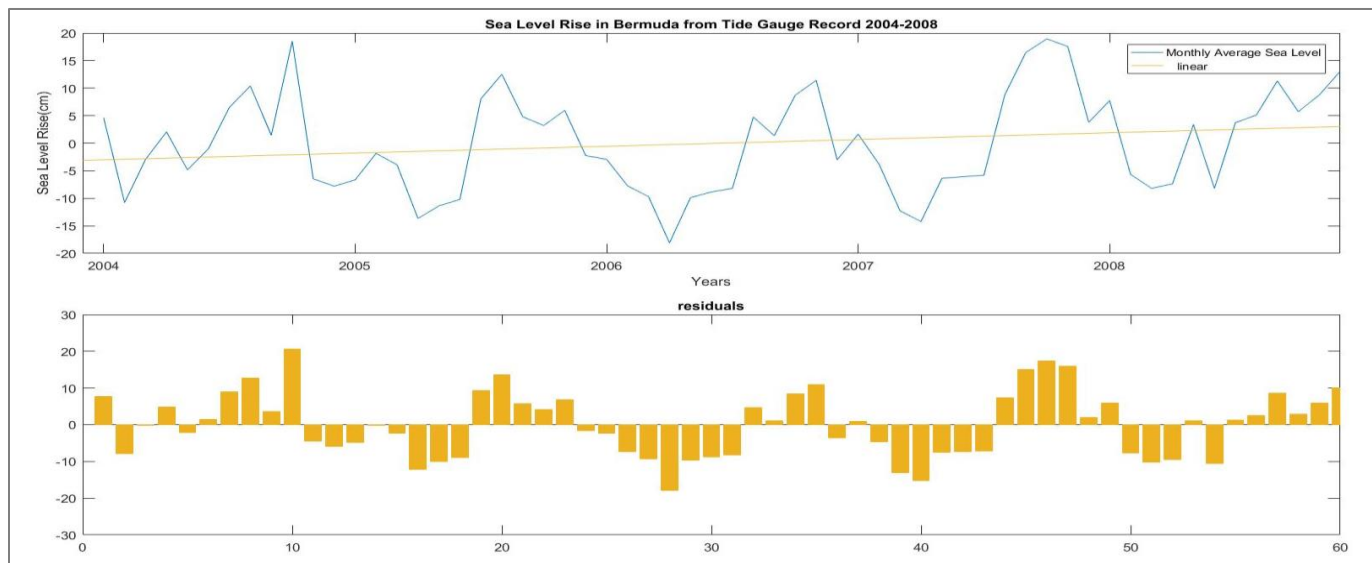


Figure 21 – Time series of monthly sea level change in Bermuda 2004-2008

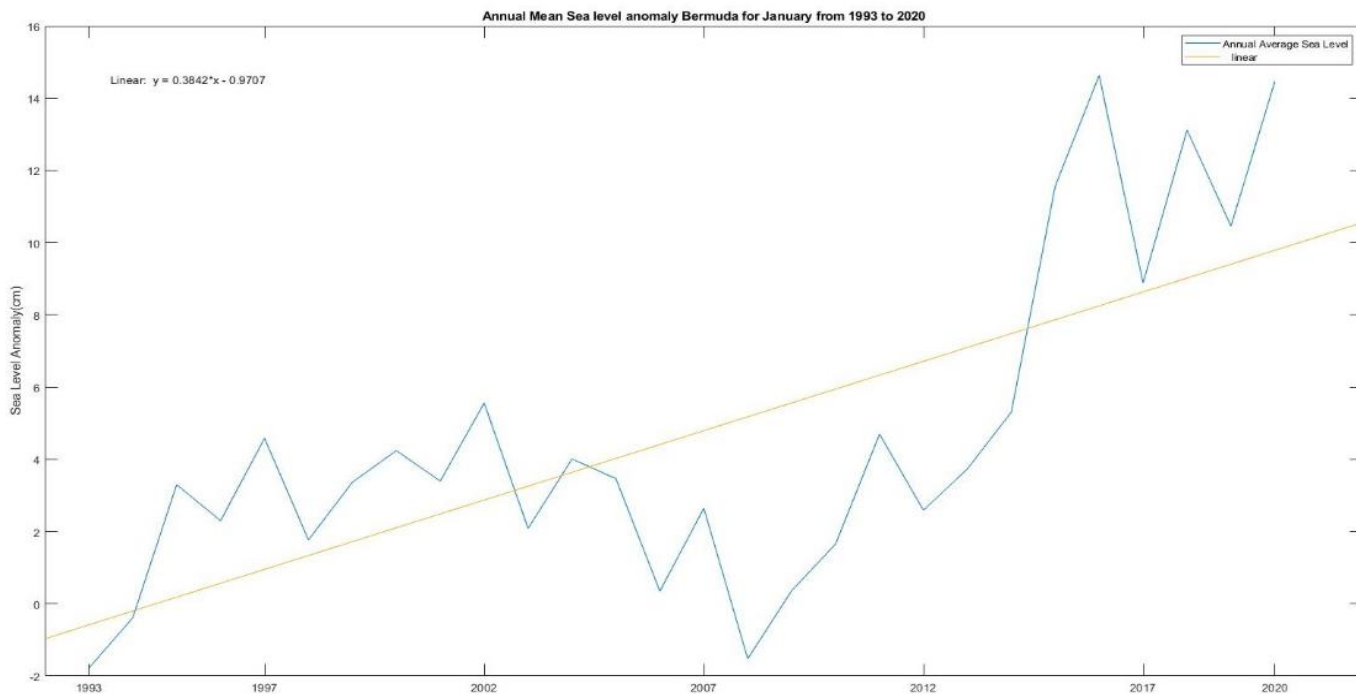


Figure 22 – Mean annual sea level rise for Bermuda from satellite altimetry. Data shown for nearest grid box to coordinates Lat: 32.373N and Lon: 64.703W. Solid line shows linear trend. Source: The Copernicus Climate Change Service (C3S): <https://cds.climate.copernicus.eu/>

3.4.2 Projected Sea Level Rise

The following are noted about the projected future sea level rise:

- For global mean SLR, generally, variations across RCPs are small up to 2050 but diverge in the second half of the century (IPCC 2019). IPCC (2019) notes: “*Future rise in GMSL caused by thermal expansion, melting of glaciers and ice sheets and land water storage changes, is strongly dependent on which RCP emission scenario is followed. SLR at the end of the century is projected to be faster under all scenarios, including those compatible with achieving the long-term temperature goal set out in the Paris Agreement.*” The SROCC (IPCC 2019) also notes that “Under RCP 8.5, estimates for 2100 are higher and the uncertainty range larger than in AR5.” “Mean sea level rise projections are higher by 0.1 m compared to AR5 under RCP 8.5 in 2100, and the likely range extends beyond 1 m in 2100 due to a larger projected ice loss from the Antarctic Ice Sheet (medium confidence). The uncertainty at the end of the century is mainly determined by the ice sheets, especially in Antarctica.”
- The AR6 (IPCC 2022) projects that the sea rate of sea level rise will continue to accelerate and thus sea levels will continue to rise throughout the 21st century with virtual certainty. Table 18 shows the estimates for projections of mid-century SLR and end-of-century of the best-case scenario (SSP1-1.9) and the worst-case development pathway scenario (SSP5-8.5). These estimates are not significantly different from the estimates of the SROCC (IPCC 2019) report.
- For Bermuda, there is good consensus across the two mapping tools examined about sea level rise. Though RCPs and SSPs are not directly comparable, by 2050, mean SLR is projected to 0.23m for RCP4.5 and 0.21m SSP2-4.5; while by 2100, mean SLR is projected to be 0.53m for RCP4.5 and 0.56 for SSP5-8.5. AR6 (IPCC 2022) suggests that if expert judgement on high impact ice-sheet processes and inputs from a model incorporating Marine Ice Cliff Instability are considered then by 2100, SLR may reach up to 1.46m for Bermuda according to SSP5-8.5. These projections are less than estimates of global mean sea level rise by 2100 which are 0.56m for SSP2-4.5 and 0.77m SSP5-8.5.
- Projections show significant land loss across the entire mainland Bermuda, with the Sandy’s and St. Georges seeing significant inundation. See Figure 25.

Table 17 – Projected mean global SLR. Relative to 1986-2005. Source: SROCC (IPCC 2019)

RCP		SLR	Rate (mm/year)
RCP 2.6	2050	0.24 m (0.17–0.32 m, likely range)	
	2100	0.43 m (0.29 – 0.59 m likely range)	~ 4 mm year-1 (2–6 mm/yr, likely range)
RCP 8.5	2050	0.32 m (0.23–0.40 m, likely range)	
	2100	0.84 m (0.61–1.10 m, likely range)	~ 15 mm/year (10–20 mm/year, likely range)

Table 18 – Projected mean global SLR. Source: AR6 (IPCC 2022)

RCP		SLR
SSP1-1.9	2050	0.18 m (0.15–0.23 m, likely range)
	2100	0.38 m (0.28– 0.55 m, likely range)
SSP5-8.5	2050	0.23 m (0.20–0.30 m, likely range)
	2100	0.77 m (0.63–1.02 m, likely range)

Table 19 – Local sea-level projections at St. Georges, Bermuda for RCP2.6 (blue), RCP4.5 (orange) and RCP8.5 (red). The second column shows the multi-model median, column three shows the 66% uncertainty range, and column four shows the 90% uncertainty range. Shown in brackets are sea-level projections including expert judgement revised Antarctic ice-sheet contributions from Bamber et al. (2019). Climate Analytics Local SLR Tool (CMIP5).

Year	Local Sea Level Rise (m)			
	RCP	Median	Uncertainty Ranges	
			66%	90%
2030	2.6	13 [13]	7-19 [8-18]	2-24 [5-22]
	4.5	12	6-19	1-24
	8.5	12 [14]	5-20 [6-22]	0-26 [1-28]
2050	2.6	23 [26]	15-33 [17-37]	9-41 [10-49]
	4.5	23	14-34	7-43
	8.5	25 [32]	14-37 [20-46]	7-47 [11-61]
2100	2.6	48 [64]	27-73 [42-92]	14-100 [27-124]
	4.5	53	28-82	12-110
	8.5	65 [102]	34-102 [61-160]	14-136 [37-243]

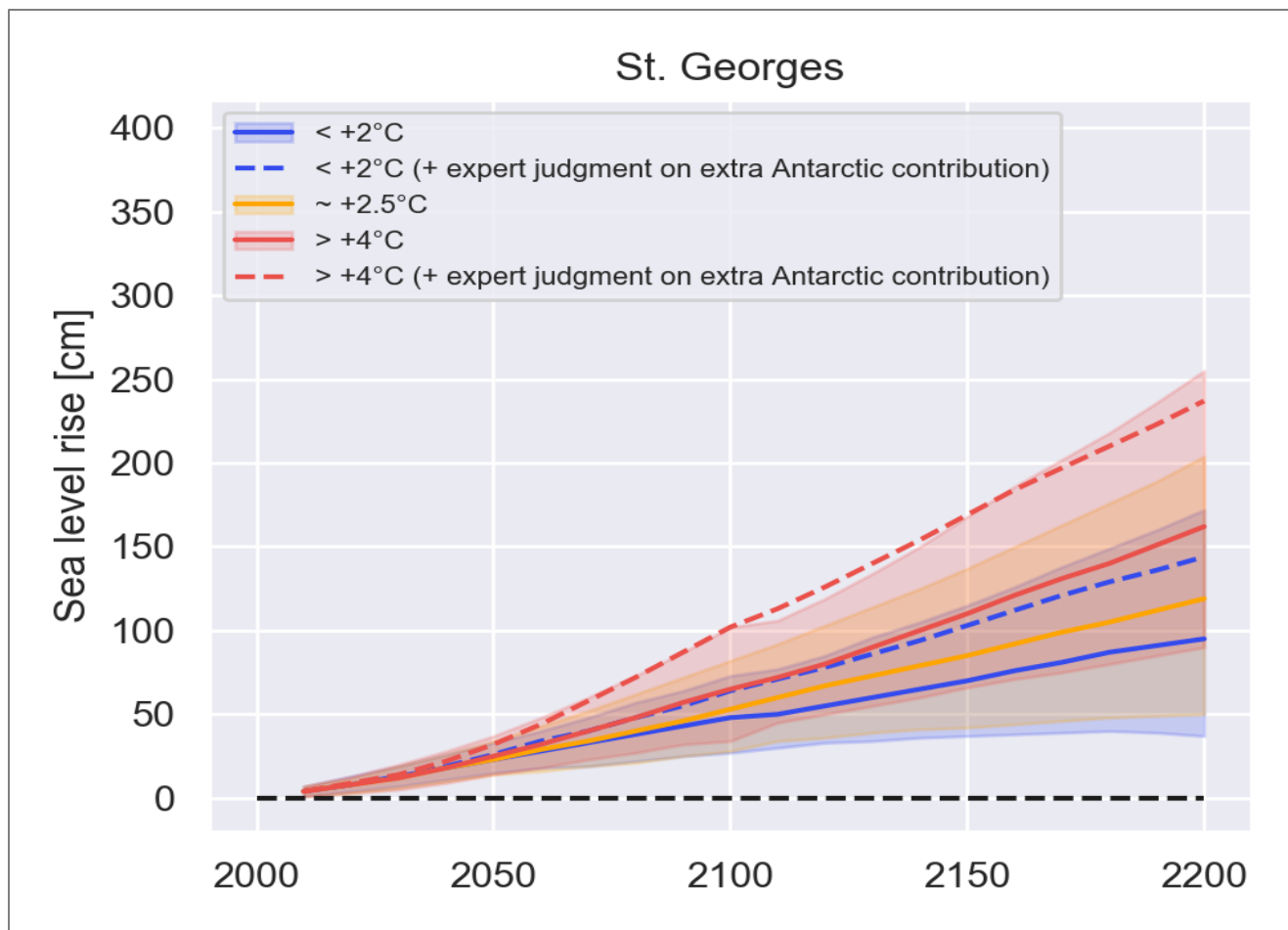


Figure 23 – Local sea-level projections at St. Georges, Bermuda RCPs 2.6 (blue), 4.5 (orange) and 8.5 (red). The solid lines represent multi-model medians, the shaded areas capture the 66% uncertainty range. Dashed lines show median sea-level projections including expert judgement revised Antarctic ice-sheet contributions from Bamber et al. (2019). Climate Analytics Local SLR Tool (CMIP5).

Table 20 – Sea level projections for 5 SSP scenarios, relative to a baseline of 1995-2014, in meters at St. Georges/ Esso Pier (Bermuda). Individual contributions are shown for the year 2100. Median values (likely ranges) are shown. Average rates for total sea-level change are shown in mm yr⁻¹. The SSP5-8.5 low confidence column incorporates a representation of the potential effect of low-likelihood, high-impact ice sheet processes that cannot be ruled out. This column shows the 17th-83rd percentile range factoring into account information from structured expert judgement and from a model incorporating Marine Ice Cliff Instability. NASA Sea Level Projection Tool.

SLR (m)	SSP1-1.9	SSP1-2.6	SSP2-4.5	SSP3-7.0	SSP5-8.5	SSP5-8.5 Low Confidence
Total (2050)	0.18 (0.10, 0.28)	0.19 (0.14, 0.27)	0.21 (0.13, 0.30)	0.22 (0.14, 0.31)	0.23 (0.15, 0.33)	0.24 (0.15, 0.40)
Total (2100)	0.43 (0.30, 0.63)	0.47 (0.30, 0.69)	0.56 (0.37, 0.83)	0.65 (0.44, 0.93)	0.69 (0.47, 1.03)	0.82 (0.47, 1.46)
Rates (mmyr ⁻¹)	SSP1-1.9	SSP1-2.6	SSP2-4.5	SSP3-7.0	SSP5-8.5	SSP5-8.5 Low Confidence
Rate (2040-2060)	4.6 (3.2, 6.9)	4.6 (2.6, 7.5)	5.4 (3.8, 8.1)	5.7 (4.1, 8.1)	6.6 (4.6, 9.4)	7.1 (4.6, 14.9)
Rate (2080-2100)	4.4 (2.2, 7.4)	5.6 (3.0, 9.2)	7.7 (3.5, 13.0)	9.6 (5.2, 15.2)	10.5 (5.2, 17.7)	14.8 (5.2, 31.4)

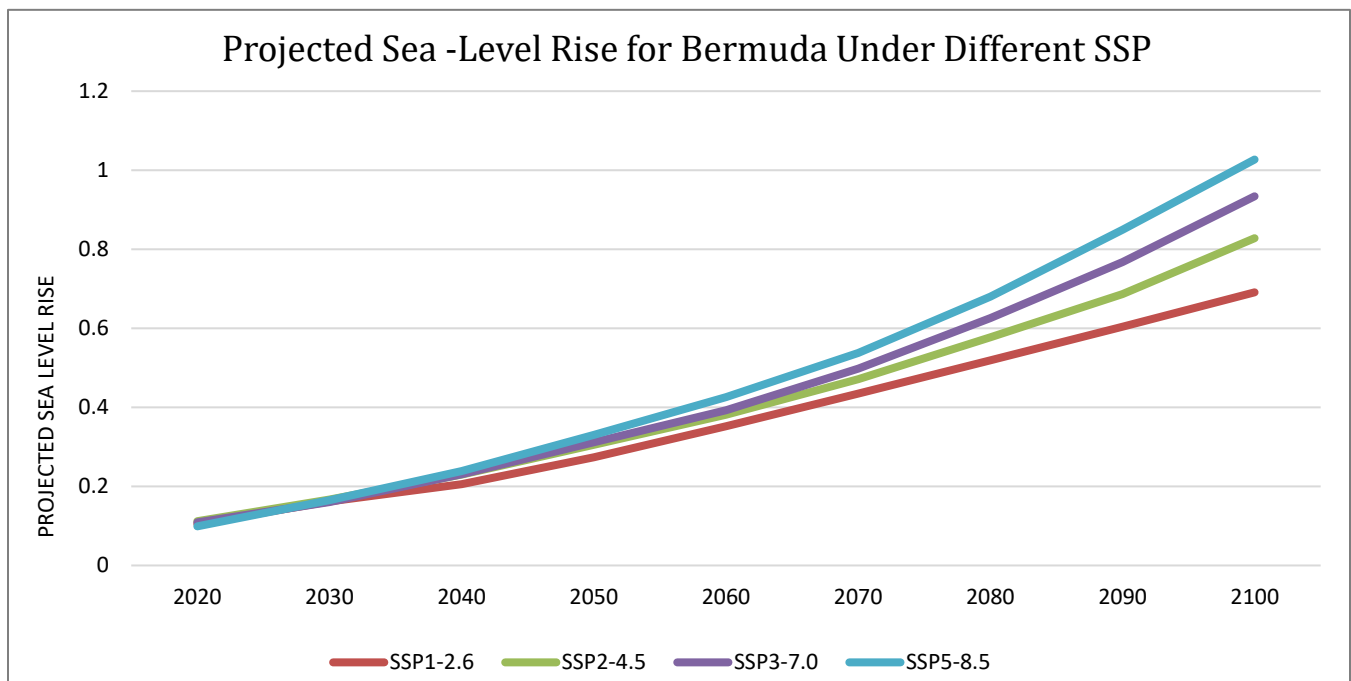


Figure 24 – Sea-level change for SSP scenarios for Bermuda resulting from processes in whose projection there is medium confidence and 83rd percentile range. Projections are relative to a 1995-2014 baseline. The plot below shows the projection and uncertainties for 'Total Sea Level Change'. NASA Sea Level Projection Tool.



Figure 25 – Showing local sea-level rise projections at 2100 for Bermuda Showing the current coast(A), SSP2-4.5: approximately 0.5m(B) and SSP5-8.5: Approximately 1m(C). Source: IDB (2018).

3.5 Hurricanes

3.5.1 Historical Hurricanes

The following points (adapted from the State of the Caribbean Climate (CSGM 2020)) are noted about historical trends:

- The hurricane season in the North Atlantic spans June to November. This coincides with the period when the Gulf of Mexico, the Caribbean Sea, and the north Tropical Atlantic are most conducive to convective activity. During this time of the year, the region is characterised by weak easterly trade winds, decreased vertical wind shear, and SSTs in excess of 26°C. In tandem, these create ideal conditions for tropical cyclone (TC) activity.
- This does not preclude storm or hurricane activity in May or December. The peak of the North Atlantic season is from mid-August to late October, with a primary peak around September 10th. A secondary peak occurs around the middle of October, which is mainly for the Caribbean Sea and the Gulf of Mexico region, after which the number of storms drops off quickly through the end of the season.
- The mean areas of origin and prevailing tracks shift during the hurricane season. From June through August, the areas of origin shift from the western Caribbean Sea and Gulf of Mexico (June) into the Atlantic Ocean (August-September). This coincides with the eastward expansion of the Atlantic warm pool which results in water temperatures becoming warmer in the north tropical Atlantic thereby allowing easterly waves coming off the African coast to develop into storms and hurricanes. By October, the water temperatures in the north Tropical Atlantic east of the Caribbean basin start to cool and wind shear increases, and storm genesis and activity generally shifts back into the Caribbean Sea and Gulf of Mexico, where the water temperatures are still very warm. See Figure 26.
- Most measures of Atlantic hurricane activity show a marked increase since the early 1980s when high-quality satellite data became available (Bell et al. 2012; Bender et al. 2010; Emanuel 2007; Landsea and Franklin 2013). These include measures of intensity, frequency, and duration as well as the number of strongest (category 4 and 5) storms.
- The El Niño-Southern Oscillation phenomenon plays a significant role in modifying hurricane activity in the North Atlantic from year to year. El Niño contributes to fewer Atlantic hurricanes while La Niña contributes to more Atlantic hurricanes.

For each of the last 4 decades, Bermuda has had between 5 and 8 storms passing within 50 km of the island except for 1991 to 2000 which saw no storms passing within 50km. Several of the storms can be considered as direct hits to the island. See Table 21 and figures 27 and 28.

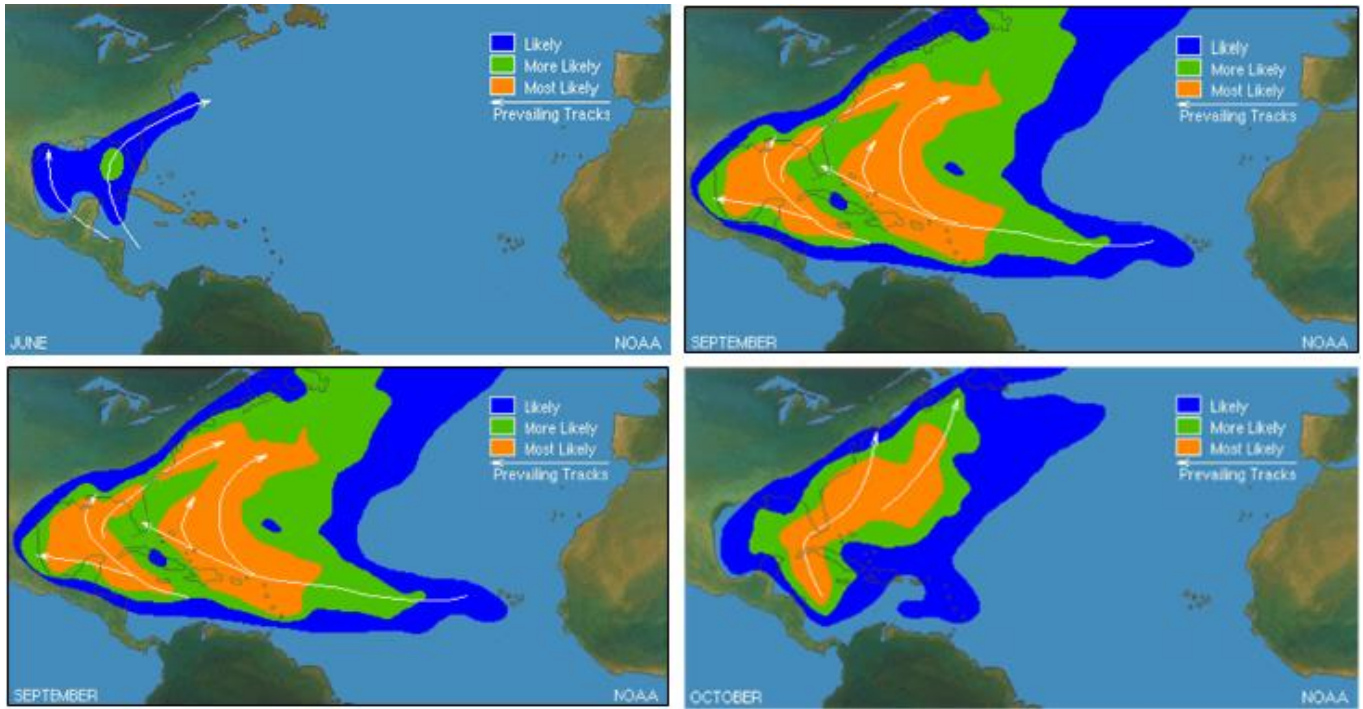


Figure 26 – Zones of likely origin and track density of storms by month during the hurricane season from August-October. Source: NOAA.

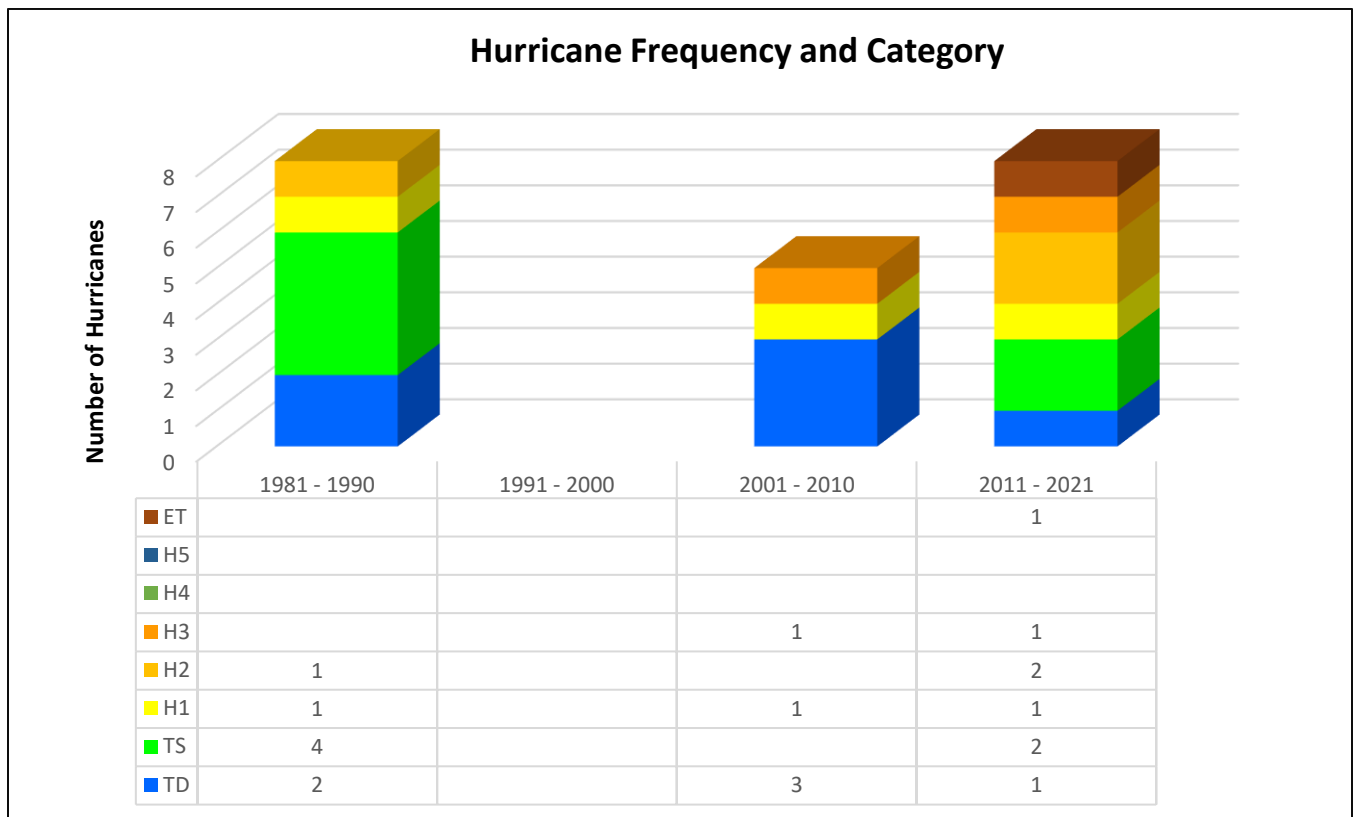


Figure 27 – Frequency and Category of Hurricanes Passing within 50km of Bermuda, Presented by Decades (1981 to 2020). Data from the NOAA HURDAT2 Dataset.

Table 21 – Summary of Hurricanes Passing within 50km of Bermuda (1981 to 2020). Data from the NOAA HURDAT2 Dataset.

Year	Name	Area		Life			Range
		Category	Min Pressure (mb)	Category	Max Wind Speed (kt)	Min Pressure (mb)	
1981	Emily	TS	990	H1	80	966	25
1981	Floyd	TS	1003	H3	100	975	25
1984	Gustav	TD	1009	TD	45	1006	25
1984	Hortense	TS	1006	H1	65	993	25
1986	Unnamed	TD	NA	TD	30	NA	25
1987	Arlene	TS	998	H1	65	987	50
1987	Emily	H1	974	H3	110	958	25
1989	Dean	H2	971	H2	90	968	25
2001	Karen	TS	991	H1	70	982	25
2003	Fabian	H3	950	H4	125	939	25
2005	Harvey	TS	995	TS	55	994	50
2008	Bertha	TS	995	H3	110	952	50
2010	Igor	H1	953	H4	135	924	50
2012	Chris	TS	1004	H1	75	974	50
2013	Gabrielle	TS	1004	TS	55	1003	25
2014	Fay	H1	984	H1	70	983	25
2014	Gonzalo	H2	952	H4	125	940	25
2016	Nicole	H3	959	H4	120	950	25
2019	Jerry	TD	1001	H2	90	976	25
2020	Arthur	ET	989	ET	55	989	50
2020	Paulette	H2	971	H2	90	965	25

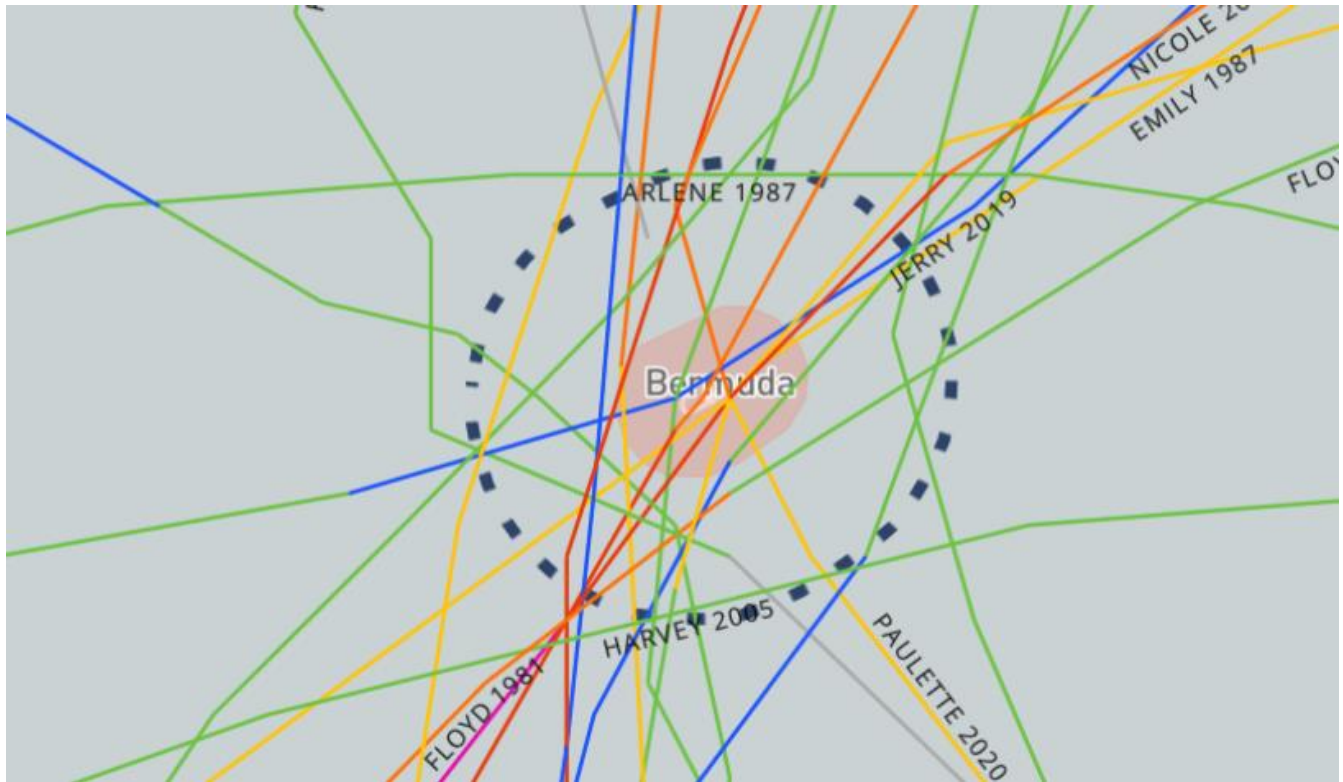


Figure 28 – Tracks of Hurricanes Passing within 50km of Bermuda (1981 to 2021). Data from the NOAA HURDAT2 and IBTrACS Datasets.

3.5.2 Hurricane Projections

From the available body of literature examined the following changes related to future intensity and frequency of hurricane occurrences are to be noted:

- The number of hurricanes experienced in a given season is likely to decrease or remain unchanged in the future. Zhang, et al. (2019) for instance found an inversely proportional historical relationship between tropical cyclone frequencies and sea surface temperature (SST). That is, tropical cyclone activity decreased with an increase in the warmth of pools in which they form. This is with high confidence (tests of 90-99.9% for the respective pools). Storms in moderate pools (65th-90th percentile) decreased by 0.79 storms/decade and in the warm pools (>90th percentile) by 1.08 storms/decade. The suggestion is that with increase in future temperatures there may be reduced overall hurricane frequency in the future. These results are echoed in other reports such as the CSGM 2017 report (2017), the IPCC 2012 Special Report on Extremes (IPCC 2012) and Knutson et al. (2013).
- The number of higher category hurricanes are likely to increase in the future. Studies (Bhatia et al., 2018, Bender et al., 2018 and Knutson et al., 2013) have shown an increasing trend in major Atlantic hurricanes. (Bhatia et al. 2018) projected a 72.9 and 135.5 % increase in category 4 and 5 hurricanes respectively by end of century under RCP 4.5. Bender et al. (2010) and Knutson et al. (2013) presented combined category 4 and 5 percentage increases of 100% and 40% respectively. Figure 29 shows projected hurricane frequency increase as a percentage with respect to 1986 to 2005.
- Rainfall rates associated with hurricanes are likely to increase in the future. Warmer temperatures are associated with greater convection and more moisture in the atmosphere. Knutson et al. (2013) indicated a likely increase in rainfall rate of between 20% and 33% particularly near the hurricane core for the late twenty-first century from an ensemble of models run under the SRES A1B scenario and RCP 4.5.
- Maximum wind speeds associated hurricanes are likely to increase in the future as temperature increases (Trepanier 2020). Figure 30 from Trepanier (2020) shows the expected rate at which wind speed changes with temperature. For Bermuda, this rate is between 1 to 1.5 ms⁻¹ per °C. This implies an increase from current wind speed by as much as 1.1ms⁻¹, 2.3ms⁻¹ and 3.5ms⁻¹ in the near-, medium- and long-term future respectively under RCP 8.5.

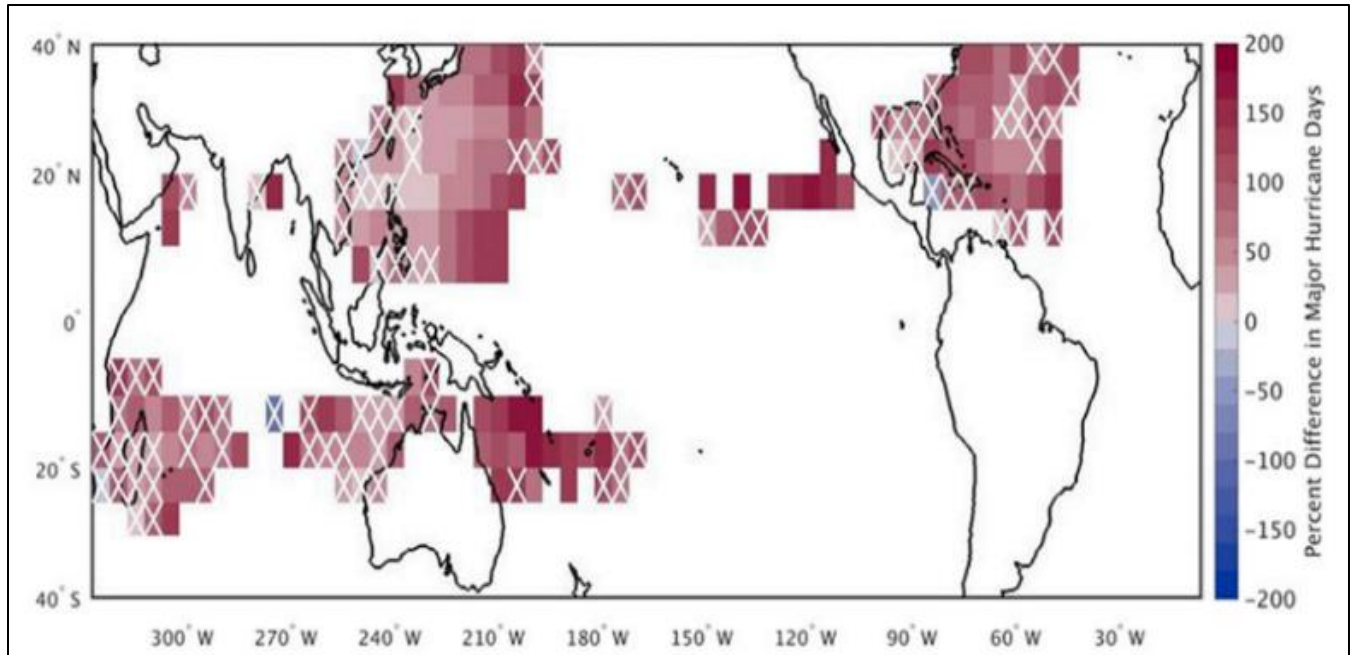


Figure 29 – Percentage Difference of Major Hurricane Days between 1986-2005 and 2081-2100 by the HiFLOR model. White crosses represent not statistically significant grid boxes (Bhatia, et. al, 2018, p.8298).

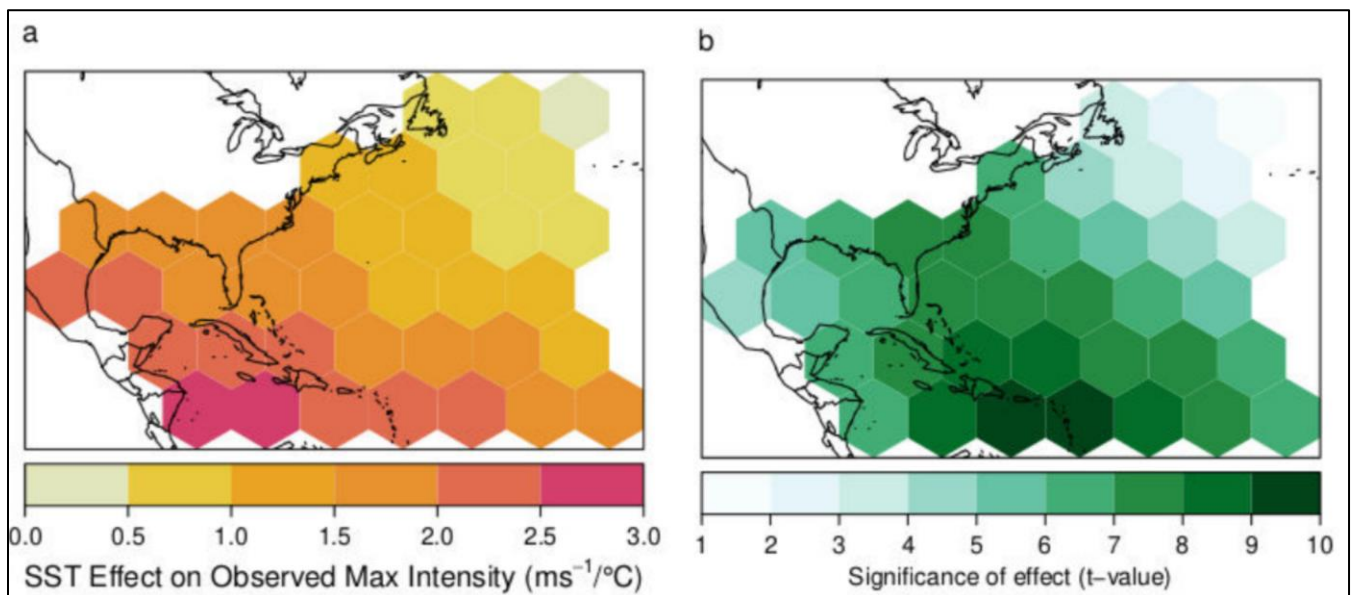


Figure 30 – (a) Strength of the Local Relationship between the Observed per Event Maximum Wind Intensity and the average (“normal”) August–October SST in °C. (b) Significance of the Relationship. (Trepanier 2020).

4.0 Summary and Conclusions

Table 22– Summary of Trends and Projections at a Glance.

Historical Trend	Projection
<p>Temperature</p> <p>Air temperature varies throughout the year with the highest temperatures from July to September and lowest in January to March. Mean temperature has been increasing between 0.22°C and 0.6°C per decade.</p> <p>Hot days and nights have also been increasing at a rate of 4% and 3% per decade respectively.</p>	<p>Temperature is expected to continuously increase with global warming. In the medium term (2040-2060) the projected annual increase is between 0.6 and 1.7 for the RCPs. In the long term (2070-2090) the projected annual increase is between 0.6 and 3.2 °C for the RCPs.</p> <p>Hot days and nights are increasing and will account for nearly 100% of days by end of century under RCP 8.5.</p> <p>Heatwave durations are increasing and will reach near 60 days by the end of century under RCP 8.5.</p>
<p>Rainfall</p> <p>The island’s climatology exhibits a bimodal rainfall pattern with peaks in January and September, with the September peak receiving more rainfall.</p> <p>Interannual variability dominates the rainfall record with no real linear trend.</p>	<p>The RCPs suggest no real trend toward the end of the century. In the medium term (2040-2060) mean annual projected change is 4 to 11% over the two RCPs examined. In the long term (2070-2090) mean annual projected change is 3 to 48%.</p> <p>Extreme events will be characterised by significant interannual variability. However, rainfall indices reflect no real overall trends with projected change in consecutive dry days (CDD) (between 0.1 and 0.2 days/decade) and changes in consecutive wet days (CWD) (0 and 0.2 days/decade).</p>
<p>Sea Surface Temperature</p> <p>SST are highest during August to September and coolest during December to April. SSTs are increasing at a rate of 0.26 °C per decade.</p>	<p>SSTs are projected to increase at a rate of 0.07 °C (0.4.3 °C) per decade under RCP 2.6 (8.5). In the medium term (2040-2060) monthly projected increase ranges from 0.6 to 1.7 °C (1.0 – 2.3 °C) for RCP 2.6 (8.5). In the long term (2070-2090) monthly projected increase ranges from 0.8 to 1.7 °C (2.5 – 4.0 °C) for RCP 2.6 (8.5).</p>
<p>Sea Level Rise</p> <p>Bermuda lies in an area of the Caribbean Basin that has experienced sea level rise of more than 3.84 mm/year.</p>	<p>By 2100, mean SLR is projected to be approximately 0.47 m for SSP1—2.6 and between 0.69 and 0.82m for SSP5-8.5.</p> <p>If expert judgement including revised Antarctic ice-sheet contributions are considered then by 2100, mean SLR for Bermuda is projected to be approximately 1.46m for SSP5-8.5.</p>
<p>Hurricanes</p> <p>Over the last 4 decades there were 21 storms passing within 50km of Bermuda. Between 5 and 8 storms passed per decade except for 1991 to 2000 when no storms were recorded passing within 50km.</p>	<p>The future will likely be characterized by more intense hurricanes with high winds and greater rainfall. A likely increase in rainfall rate of between 20% and 33% is projected particularly near the hurricane core by the end of the century.</p>

References

- Ahmed, K., Sachindra, D. A., Shahid, S., Demire, M. C., & Chung, E.-S. (2019). Selection of multi-model ensemble of general circulation models for the simulation of precipitation and maximum and minimum temperature based on spatial assessment metrics. *Hydrology and Earth System Sciences*, 23, 4803–4824. doi:<https://doi.org/10.5194/hess-23-4803-2019>
- Bamber, J. L., Oppenheimer, M., Kopp, R. E., Aspinall, W. P., & Cooke, R. M. (2019). Ice sheet contributions to future sea-level rise from structured expert judgment. *Proceedings of the National Academy of Sciences of the United States of America*, 166(23), 11195–11200.
- Bender, M. A., Knutson, T. R., Tuley, R. E., Sirutis, J. J., Vecchi, G. A., Garner, S. T., & Held, I. M. (2010). Modeled impact of anthropogenic warming of the frequency of intense Atlantic hurricanes. *Science*, 327. doi:DOI: 10.1126/science.1180568
- Bhatia, K., Vecchi, G., Murakami, H., Underwood, S., & Kossin, J. (2018). Projected Response of Tropical Cyclone Intensity and Intensification in a Global Climate Model. *Journal of Climate*, 31, 8281–8303. Retrieved from http://www.bamboodream.sakura.ne.jp/hiroblog/wp-content/papercite-data/pdf_paper/Bhatia_etal_2018_JCLI.pdf
- Cantet, P., Déqué, M., Palany, P., & Maridet, J.-L. (2014). The importance of using a high-resolution model to study the climate change on small islands: the Lesser Antilles case. *Tellus A: Dynamic Meteorology and Oceanography*, 66(1). doi:<https://doi.org/10.3402/tellusa.v66.24065>
- Charlton, C. S., Stephenson, T. S., Taylor, M. A., & Douglas, C. A. (2021). Characterizing Bushfire Occurrences over Jamaica Using the MODIS C6 Fire Archive 2001–2019. *Atmosphere*, 12(3), 390.
- Church, J. A., Clark, P. U., Cazenave, A., Gregory, J. M., Jevrejeva, S., Levermann, A., . . . Unnikrishnan, A. S. (2013). Sea Level Change. *Climate Change 2013: The Physical Science Basis. Contribution of Working Group I to the Fifth Assessment Report of the Intergovernmental Panel on Climate Change* [Stocker, T.F., Qin, D., Plattner, G.-K., Tignor, M., Allen, S.K., Boschung, J.]. Cambridge, United Kingdom and New York, NY, USA: Cambridge University Press.
- Clarke, L. A., Taylor, M. A., Centella-Artola, A., Williams, M. S. M., Campbell, J. D., Bezanilla-Morlot, A., & Stephenson, T. S. (2021). The Caribbean and 1.5° C: Is SRM an Option?. *Atmosphere*, 12(3), 367.
- Climate Studies Group, Mona (CSGM). (2017). *State of the Jamaican Climate 2015: Information for Resilience Building (Full Report)*. Kingston, Jamaica: Produced for the Planning Institute of Jamaica (PIOJ).
- Climate Studies Group Mona (Eds) 2020: *State of the Caribbean Climate*. Produced for the Caribbean Development Bank.
- Elguindi, N., Bi, X., Giorgi, F., Nagarajan, B. P., Solmon, F., Rauscher, S., . . . Giuliani, G. (2011, May). *Regional Climatic Model RegCM User Manual Version 4.1*. Trieste, Italy.

- Emanuel, Kerry. "Environmental factors affecting tropical cyclone power dissipation." *Journal of Climate* 20, no. 22 (2007): 5497-5509
- Filippo, G. (2019). Thirty Years of Regional Climate Modeling: Where Are We and Where Are We Going next? *Journal of Geophysical Research: Atmospheres*. Retrieved from <https://agupubs.onlinelibrary.wiley.com/doi/10.1029/2018JD030094>
- Funk, C. C., Peterson, P. J., Landsfeld, M. F., Pedreros, D. H., Verdin, J. P., Rowland, J. D., ... & Verdin, A. P. (2014). A quasi-global precipitation time series for drought monitoring. *US Geological Survey data series*, 832(4), 1-12.
- Gouirand, I., Moron, V., & Sing, B. (2020). Seasonal atmospheric transitions in the Caribbean basin and Central America. *Climate Dynamics*, 55(7), 1809-1828
- Hannah, L. (2015). Chapter 2 - The Climate System and Climate Change. In *Climate Change Biology* (2nd ed., pp. 13-53). Santa Barbara: Elsevier. Retrieved from <https://www.sciencedirect.com/topics/earth-and-planetary-sciences/general-circulation-model>
- Liu, P., Xu, Z., & Li, X. (2017). Projection of Climate Change Scenarios in Different Temperature Zones in the Eastern Monsoon Region, China. *Water*, 9(5). doi:<https://doi.org/10.3390/w9050305>
- Holland, G., & Bruyère, C. L. (2014). Recent intense hurricane response to global climate change. *Climate Dynamics*, 42(3-4), 617-627. <https://doi.org/10.1007/s00382-013-1713-0>
- IPCC. (2012). *Climate change: new dimensions in disaster risk, exposure, vulnerability, and Managing the Risks of Extreme Events and Disasters to Advance Climate Change Adaptation*. Cambridge, UK and New York, NY, USA: Cambridge University Press.
- IPCC. 2013. "Climate Change 2013: The Physical Science Basis. Contribution of Working Group I to the Fifth Assessment Report of the Intergovernmental Panel on Climate Change" [Stocker, T.F., D. Qin, G.-K. Plattner, M. Tignor, S.K. Allen, J. Boschung, A. Nauels, Y. Xia, V. Bex and P.M. Midgley (eds.)]. Cambridge University Press, Cambridge, United Kingdom and New York, NY, USA, 1535 pp, doi:10.1017/CBO9781107415324
- IPCC, 2019: IPCC Special Report on the Ocean and Cryosphere in a Changing Climate [H.-O. Pörtner, D.C. Roberts, V. Masson-Delmotte, P. Zhai, M. Tignor, E. Poloczanska, K. Mintenbeck, A. Alegría, M. Nicolai, A. Okem, J. Petzold, B. Rama, N.M. Weyer (eds.)].
- Keetch, J. J., & Byram, G. M. (1968). *A drought index for forest fire control* (Vol. 38). US Department of Agriculture, Forest Service, Southeastern Forest Experiment Station.
- Knutson, T. R., Sirutis, J. J., Vecchi, G. A., Garner, S., Zhao, M., Kim, H.-S., . . . Villarini, G. (2013). Dynamical Downscaling Projections of Twenty-First-Century Atlantic Hurricane Activity: CMIP3 and CMIP5 Model-Based Scenarios. *Journal of Climate*, 33. Retrieved from <https://journals.ametsoc.org/doi/full/10.1175/JCLI-D-12-00539.1>

- Knutson, T., Camargo, S. J., Chan, J. C. L., Emanuel, K., Ho, C. H., Kossin, J., ... Wu, L. (2019). Tropical cyclones and climate change assessment. *Bulletin of the American Meteorological Society*, 100(10), 1987–2007. <https://doi.org/10.1175/BAMS-D-18-0189.1>
- Kopp RE, DeConto RM, Bader DA, Hay CC, Horton RM, Kulp S, Oppenheimer M, Pollard D, Strauss BH (2017) Evolving Understanding of Antarctic Ice-Sheet Physics and Ambiguity in Probabilistic Sea-Level Projections. *Earth's Future*.
- Landsea, Christopher W., and James L. Franklin. "Atlantic hurricane database uncertainty and presentation of a new database format." *Monthly Weather Review* 141, no. 10 (2013): 3576-3592.
- Mapes, B. E., Buening, N., Kang, I. S., Kiladis, G. N., Schultz, D. M., & Weickmann, K. M. (2007). Strides, steps and stumbles in the march of the seasons. *Bull. Amer. Met. Society*.
- Palanisamy, H., M. Becker, B. Meyssignac, O. Henry, and A. Cazenave. 2012. "Regional sea level change and variability in the Caribbean Sea since 1950." *Journal of Geodetic Science* 2(2): 125-133.
- Riahi, K., Rao, S., Krey, V., Cho, C., Chirkov, V., Fischer, G., . . . Rafaj, P. (2011). RCP 8.5—A scenario of comparatively high greenhouse gas emissions. *Climatic Change*.
- Ryu, J. H., & Hayhoe, K. (2014). Understanding the sources of Caribbean precipitation biases in CMIP3 and CMIP5 simulations. *Climate dynamics*, 42(11-12), 3233-3252.
- Shi, F., Wang, Z., Qi, L., & Chen, R. (2018). An Assessment of GCM Performance at a Regional Scale. *Hindawi Advances in Meteorology*, 2018. doi:<https://doi.org/10.1155/2018/7641019>
- Stephenson, Tannecia S., Lucie A. Vincent, Theodore Allen, Cedric J. Van Meerbeek, Natalie McLean, Thomas C. Peterson, Michael A. Taylor et al. "Changes in extreme temperature and precipitation in the Caribbean region, 1961–2010." *International Journal of Climatology* 34, no. 9 (2014): 2957-2971.
- Taylor, M. A., Clarke, L. A., Centella, A., Bezanilla, A., Stephenson, T. S., Jones, J. J., ... & Charlery, J. (2018). Future Caribbean climates in a world of rising temperatures: The 1.5 vs 2.0 dilemma. *Journal of Climate*, 31(7), 2907-2926.
- Taufik, M., Setiawan, B. I., & van Lanen, H. A. (2015). Modification of a fire drought index for tropical wetland ecosystems by including water table depth. *Agricultural and Forest Meteorology*, 203, 1-10.
- Thomson, A., Calvin, K., Smith, S., Kyle, G., Volke, A., Patel, P., . . . Edmonds, J. (2011). RCP4.5: a pathway for stabilization of radiative forcing by 2100. *Climatic Change*.
- Torres, R.R., and M.N. Tsimplis. 2014. "Sea level extremes in the Caribbean Sea." *Journal of Geophysical Research: Oceans* 119 (8): 4714-4731.
- Trepanier, J. C. (2020). North Atlantic Hurricane Winds in Warmer than Normal Seas. *Atmosphere*, 11. doi:10.3390/atmos11030293
- Vichot-Llano, A., Martinez-Castro, D., Giorgi, F., Bezanilla-Morlot, A., & Centella-Artola, A. (2021). Comparison of GCM and RCM simulated precipitation and temperature over Central America and the Caribbean. *Theoretical and Applied Climatology*, 143(1), 389-402.

Walters, D., Baran, A. J., Boutle, I., Brooks, M., Earnshaw, P., Edwards, J., ... & Zerroukat, M. (2019). The Met Office Unified Model global atmosphere 7.0/7.1 and JULES global land 7.0 configurations. *Geoscientific Model Development*, 12(5), 1909-1963.

Wang, Y., Leung, L. R., McGREGOR, J. L., Lee, D. K., Wang, W. C., Ding, Y., & Kimura, F. (2004). Regional climate modeling: progress, challenges, and prospects. *Journal of the Meteorological Society of Japan. Ser. II*, 82(6), 1599-1628.

Zhang, B., Zhang, R., Pinker, R., Feng, Y., Nie, C., & Guan, Y. (2019). Changes of tropical cyclone activity in a warming world are sensitive to sea surface temperature environment. *Environmental Research Letters*.

Appendix B – Description of the Numerical Models



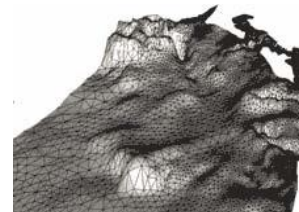
MIKE 21 is a professional engineering software package for the simulation of flows, waves, sediments and ecology in rivers, lakes, estuaries, bays, coastal areas and seas. The modeling system is designed in an integrated modular framework with a variety of add-on modules. This, in combination with the range of dedicated and easy to use tools and editors, allow you to customise your personal software package to suit your own specific needs, whether for simple or more complex 2D flow modeling needs.

MIKE 21 provides

- A complete and effective design environment
- An advanced GUI combined with a series of highly efficient computational engines
- GUI facilities for easy applications
- GIS integration
- Free tools, eg for processing of model data in MATLAB
- Integration with urban and water resource models for flood modeling
- Modules for virtually any kind of 2D water modeling needs
- Open, flexible and easy ecology and water quality modeling
- Sophisticated tools for data handling, analysis and visualization
- Multiple computational grid options ensuring optimal model application
- Well-proven technology with 30+ years of track record
- Widely used by thousands of engineers and scientists worldwide

Flow Model Versions

MIKE 21 FM is based on an unstructured mesh and uses a cell-centred finite volume solution technique. The mesh is based on linear triangular elements. The FM version is particularly well suited for modeling large complex areas that, at the same time, require a detailed resolution of specific features.



Hydrodynamics



The hydrodynamic modules provide the basis for computations performed in many other modules but can also be used alone. They simulate the water level variations and flows in response to a variety of forcing functions on flood plains, in lakes, estuaries and coastal areas.

In MIKE 21 the HD modules solve the vertically integrated equations for the conservation of continuity and momentum, i.e., the Saint Venant equations on rectangular, flexible or curvilinear grids covering the area of interest, when provided with the bathymetry, bed resistance coefficients, wind field, hydrographic boundary conditions, etc.

The effect of waves on the currents can be included in various ways, e.g., by apparent bed roughness. Including wave-induced flow in the model is done by specifying wave radiation stresses, which then will enter the momentum equations. These can also be imported directly from the wave models MIKE 21 SW/NSW or PMS.

The effects of sources and sinks like precipitation and evaporation, river discharge, intakes and outlets from power stations, etc are included in the hydrodynamic equations. The impact of hydraulic structures (bridge piers or piles, weirs, etc) on the flow conditions can also be included. A valuable facility in MIKE 21 is its capability to compute the flow in an area that sometimes dries out and sometimes is flooded, e.g., tidal flats and flood plains.

MIKE 21 C, the flow model for the curvilinear version, includes helical three-dimensional flow that occurs in curved flows, especially in river bends. Helical flow is a principal secondary flow phenomenon in rivers that has a significant influence on the sediment transport direction and hence the morphological changes in the river channel.

The US Federal Emergency Management Agency (FEMA) has officially approved MIKE 21 HD and NHD for use in national flood insurance program studies (NFIS) for applications in both coastal and riverine environments.

SW Spectral Wave Module



MIKE 21 SW is a new 3rd generation spectral wind-wave model that simulates the growth, decay and transformation of wind-generated waves and swell in offshore and coastal areas. MIKE 21 SW solves the spectral wave action balance equation formulated in either Cartesian or spherical coordinates. At each element, the wave field is represented by a discrete two-dimensional wave action density spectrum.

The model includes the following physical phenomena; wave growth by action of wind, non-linear wave-wave interaction, dissipation by white-capping, dissipation by wave breaking, dissipation due to bottom friction, refraction due to depth variations, and wave-current interaction.

The discretisation of the governing equations in geographical and spectral space is performed using the cell-centred finite volume method. In the geographical domain an unstructured mesh is used. The time integration is performed using a fractional step approach where a multi-sequence explicit method is applied for the propagation of wave action. **MIKE 21 SW** includes two different formulations:

- fully spectral formulation

- directional decoupled parametric formulation

MIKE 21 SW is used for the assessment of wave climates in offshore and coastal areas - in hindcast and forecast mode. A major application area is the design of offshore, coastal and port structures for which accurate assessment of wave loads is of utmost importance to the safe and economic design of these structures.

MIKE 21 SW is particularly applicable for simultaneous wave prediction and analysis on regional scale and local scale. Coarse spatial and temporal resolution is used for the regional part of the mesh and a high-resolution boundary and depth-adaptive mesh is describing the shallow water environment at the coastline.

MIKE 21 SW is also used for the calculation of the sediment transport, which, to a great extent, is determined by wave conditions and associated wave-induced currents. The wave-induced current is generated by the gradients in radiation stresses that occur in the surf zone. **MIKE 21 SW** can be used to calculate the wave conditions and associated radiation stresses. The long-shore currents and sediment transport are then calculated using the flow and sediment transport models available in the **MIKE 21** package.

Coupled Model FM



MIKE 21/3 Coupled Model FM is a truly dynamic modeling system for application within coastal and estuarine environments. It is composed of following modules:

- Hydrodynamic Module
- Spectral Wave Module
- Transport Module
- ECO Lab Module
- Mud Transport Module
- Sand Transport Module (only 2D simulations)

The Hydrodynamic Module and the Spectral Wave Module are the basic computational components of the **MIKE 21/3 Flow Model FM**. Using **MIKE 21/3 Coupled Model FM** it is possible to simulate the mutual interaction between waves and currents using a dynamic coupling between the Hydrodynamic Module and the Spectral Wave Module. The **MIKE 21/3 Coupled Model FM** also includes a dynamic coupling between the Mud Transport and the Sand Transport models and the Hydrodynamic Module and the Spectral Wave Module. Hence, a full feedback of the bed level changes on the waves and flow calculations can be included.

Application Areas

The application areas are generally problems where flow and transport phenomena are important, with an emphasis on coastal and marine applications, where the flexibility inherited in the unstructured meshes can be utilized.

MIKE 21/3 Coupled Model FM can be used for investigating the morphological evolution of the nearshore bathymetry due to the impact of engineering works (coastal structures, dredging works etc.).

The engineering works may include breakwaters (surface-piercing and submerged), groins, shoreface nourishment, harbours etc. MIKE 21/3 Coupled Model FM can also be used to study the morphological evolution of tidal inlets.

It is most suitable for medium-term morphological investigations (several weeks to months) over a limited coastal area. The typical dimensions are about 10km in the alongshore direction and 2km in the offshore direction. The computational effort can become quite large for long-term simulations, or for larger areas.

The main features of the MIKE 21 Coupled Model FM are as follows

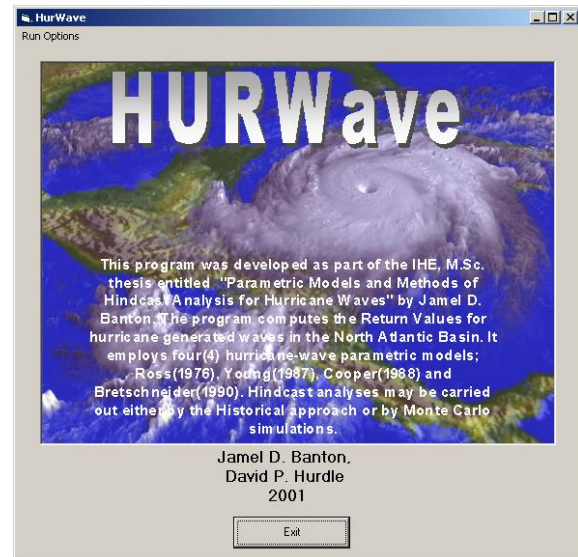
- Dynamic coupling of flow and wave calculations
- Fully feedback of bed level changes on flow and wave calculations
- Easy switch between 2D and 3D calculations (hydrodynamic module and process modules)
- Optimal degree of flexibility in describing bathymetry and ambient flow and wave conditions using depth-adaptive and boundary-fitted unstructured mesh.

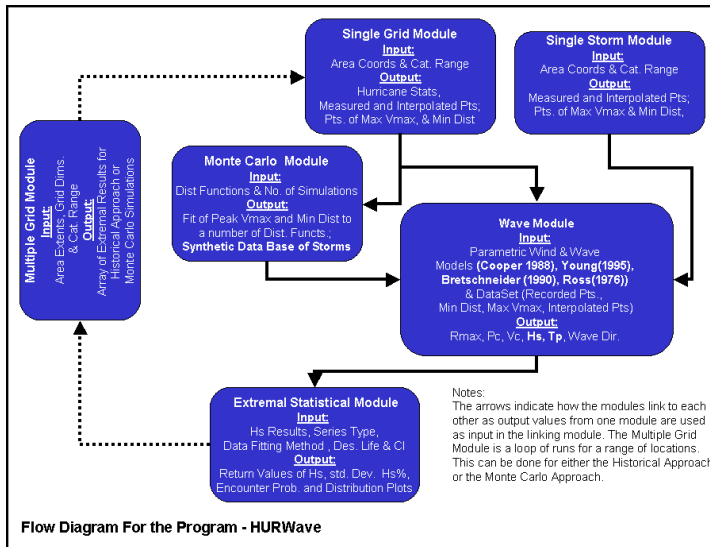
HurWave

A package of Hurricane Parametric Wave Models and Extremal Statistical Analyses by Jamel D. Banton.

HURWave combines the database of the National Oceanic and Atmospheric Administration (NOAA), of hurricane tracks, with wind and wave distribution algorithms to statistically determine deep-water design wave conditions at any location within the Caribbean and the Gulf of Mexico.

The program consists of 6 main modules, namely: The Single Grid Module; The Single Storm Module; The Wave Module; The Extremal Statistical Module; The Monte Carlo Module; and The Multiple Grid Module. These are shown in the flow chart following.



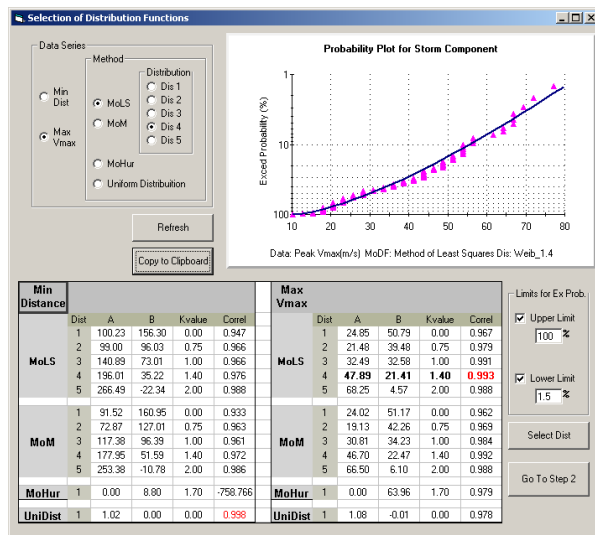


Program Capabilities:

The NOAA database consists of Atlantic hurricane track positions along with wind and pressure conditions at 6-hour intervals, since the late 19th century. For any specified location within the North Atlantic Basin, HURWave searches this database for Tropical storms and hurricanes that have passed within a specified distance from the point of interest. The program produces a number of statistical descriptions for this result.

The Monte Carlo Approach

An alternative method to using just the NOAA database of storms is to generate a much larger synthetic database of storms from the statistical properties of those that actually occurred. This Monte Carlo approach is capable of generating hundreds of probable storms for a particular location, thereby simulating tracks that may occur in the future. This approach was developed from research observations of multi-decadal trends in hurricane frequency and intensity. The research and method are presented in the paper “Long term variability of hurricane trends and a Monte Carlo approach to design” by Smith, Warner and Banton, presented at The International Conference for Coastal Engineering (ICCE 2002).



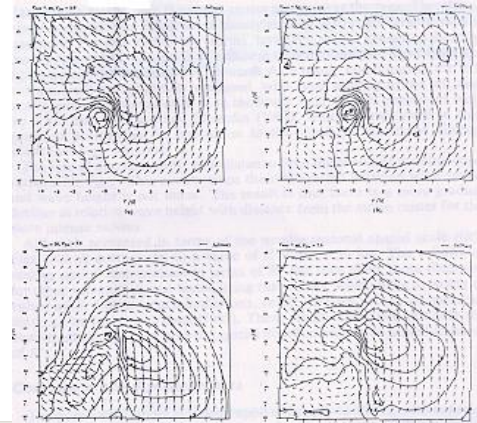
Parametric Wave Modeling

A number of widely used wind and wave models are applied to produce a hindcast dataset of hurricane wave conditions at the point in question. These models include Cooper (1988) and Young (1995).

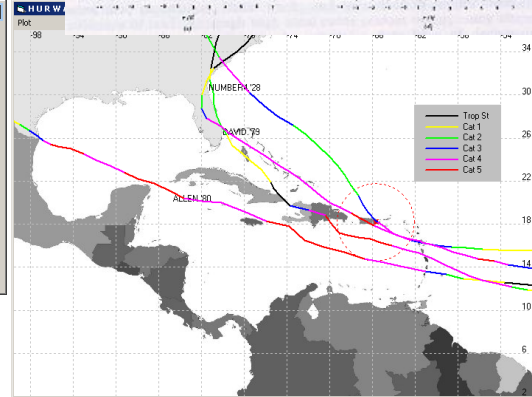
The Cooper model was developed by statistically analyzing the output from numerical wind and wave models for 6 Gulf of Mexico hurricanes. The storms used covered a wide cross-section of hurricane conditions.

In the case of Young, he first developed an extensive synthetic database by running a numerical wave prediction model for a wide range of hurricane parameters. The data from these numerical experiments were then used to clarify the wave generation process within hurricanes and further to develop the parametric model suitable for wave prediction in deep water. This model was further calibrated with over 100 measurements made by the GEOSAT satellite.

With the results of these models, a range of extremal statistical analyses may be carried out in HURWave. The extremal methods applied are based on work published by Yoshima Goda in 1988 for statistically analyzing extreme events such as hurricane waves. Distribution functions such as Weibull and Fischer Tippet (Type I) are fitted to the model results and the best fit chosen. The results include the values for wind, wave and water level conditions for various return periods.



Return Wave Heights and Variations																				
Return Values For The Peak Value Series																				
Rp	FT - I				Weibull															
	Hs	σ	Hs%	EP	k = 0.75			k = 1.00			k = 1.40			k = 2.00						
	Hs	σ	Hs%	EP	Hs	σ	Hs%	EP	Hs	σ	Hs%	EP	Hs	σ	Hs%	EP				
2	4.15	0.2	4.4	100.0	3.54	0.2	3.8	100.0	3.81	0.2	4.1	100.0	4.09	0.2	4.4	100.0	4.32	0.2	4.6	100.0
5	5.92	0.3	6.2	100.0	5.52	0.4	5.8	100.0	5.82	0.4	6.1	100.0	6.02	0.4	6.3	100.0	6.11	0.3	6.4	100.0
10	7.14	0.4	7.4	99.5	7.25	0.5	7.5	99.5	7.34	0.6	7.6	99.5	7.29	0.4	7.6	99.5	7.18	0.3	7.5	99.5
20	8.33	0.5	8.6	92.3	9.16	0.7	9.5	92.3	8.87	0.8	9.2	92.3	8.47	0.5	8.8	92.3	8.11	0.4	8.4	92.3
25	8.70	0.5	9.0	87.0	9.80	0.8	10.1	87.0	9.36	0.8	9.6	87.0	8.84	0.6	9.1	87.0	8.39	0.4	8.7	87.0
50	9.87	0.6	10.2	63.6	11.89	1.0	12.2	63.6	10.88	1.0	11.2	63.6	9.93	0.6	10.2	63.6	9.20	0.5	9.5	63.6
100	11.03	0.7	11.3	39.5	14.09	1.2	14.4	39.5	12.40	1.2	12.7	39.5	10.97	0.7	11.3	39.5	9.95	0.5	10.2	39.5
CI = 95 %																				
Cor= 0.996 Cor= 0.996 Cor= 0.991 Cor= 0.991 Cor= 0.998																				



Appendix C – Numerical Model Set Up & Validation

An important step in implementing a sustainable coastal defence scheme is to determine the prevailing conditions that dictate coastal change at the site of interest. This section describes the numerical model validation that was used to describe the existing coastal processes at the project site, including the prevailing operational wave climate, the extreme (hurricane) wave climate and the resulting sediment transport and beach morphology.

The operational wave climate refers to the day-to-day distribution of wave heights, periods and directions. These wave conditions contribute to sediment movement within the beach system and are responsible for long-term morphological changes. For coastal engineering design, operational wave conditions are typically used to determine the most appropriate design solution in terms of types and layout of the structures.

The extreme wave climate refers to waves associated with tropical storms and hurricanes, to which the Atlantic Ocean is vulnerable each year from June to November. Dramatic and abrupt changes to the coastline can occur as a result of these storms. In general, coastal protection structures are designed to withstand wave attack from these extreme storm events. For example, in the selection of an armour stone size that would be required for a coastal structure, or in determination of design wave forces that may occur, extreme waves are used. These conditions occur only very infrequently, and decades or centuries of data must be explored to adequately describe the statistics.

Numerical models were therefore used to develop a working representation of the wave and current environment throughout the project site, and to understand how shoreline stabilization measures will affect the coastal environment on a day-to-day basis.

The MIKE suite of computer models, created by the Danish Hydraulic Institute was used for the analysis. MIKE 21 is a professional engineering software package for the simulation of flows, waves, sediments and ecology in rivers, lakes, estuaries, bays, coastal areas and seas.

The MIKE 21 model uses various modules to simulate hydrodynamic variances in surface elevation and currents (HD) as well as spectral waves (SW). Coupling of the two modes means that the mutual interaction between waves and currents is simulated and results from one module are passed back and forth to the other module in order to improve the efficiency and accuracy of the simulations.

The spectral wave (SW) module computes the transformation of wind waves as they grow, propagate and break in the nearshore zone. The hydrodynamic (HD) module computes the currents and water level patterns. Linked together (HD+SW) the modules can compute wave-induced currents and can also be used for storm surge calculations. Ultimately both modules can be used for sediment transport computations using the sediment transport (ST).

Wave Model Validation

Two steps were taken for the wave model validation. (1) to evaluate the MIKE Spectral Wave model's suitability as a credible tool for precisely computing nearshore wave processes, and (2) to analyze the dependability of the long-term wave database, which is needed to validate the long-term hydrodynamics (wave-induced currents) at the project site. The procedures are explained below.

Accuracy of Long Term Wave Data Base

The model was forced with the time series of the ERA 5 deep water wave conditions.

For both methods the validation was as follow

1. Extract the time series of the resulting significant wave heights, peak wave period and mean wave directions at the physical location of each of the four instruments and coinciding with the same time period of the measurements.
2. Compare the model results to the measured wave data.
3. Calculate the error between the measured and modeling values.
4. Calculate the various parameters listed below to assess whether the model falls within acceptable range of numerical model performance/ standards.
5. If not develop a correlation factor between the model results and instrument measurements and apply where necessary to the long-term offshore wave climate.

Error Parameters

The effectiveness of the model was assessed by computing statistical error parameters such as:

- Mean Error (ME) (Measure of general offset between measurements and simulations).
- Mean Absolute Error (MAE) (overall measure of comparison similar to RMSE but puts less emphasis on the largest errors as compared to RMSE where errors are squared).
- Root Mean Square Error (RMSE) (gives a relatively high weightage to large errors).
- Coefficient of Determination (R^2) (statistical measure of how close the data are to the fitted regression line).
- Coefficient of Efficiency (used to assess the predictive power of hydrological models).
- Index of Agreement (used to assess dispersion between model predictions and field recordings. Values closer 1 indicate a stronger the agreement between the two data sets). While it's difficult to find guidelines for what values might represent a good agreement, values meaningfully larger than 0.5 are considered to represent good model performance based on Willmott, et al (1985).

The Root Mean Square Error (RMSE) and Normalized RMSE (NRMSE) calculations can be used to quantitatively assess model calibration. RMSE is a useful indicator as it sums the difference between the computed and measured values. The values that can be assessed include wave heights, tide height, current speed and direction (or Easting and Northing current components). Because these differences may be positive or negative, the value is squared before being averaged so that the absolute error is preserved, according to the following formula:

$$RMSE = \sqrt{\frac{\sum_{i=1}^n (X_{obs,i} - X_{model,i})^2}{n}}$$

where X_{obs} is observed values and X_{model} is modeling values at time/place i .

The RMSE has the same units as the input parameters, in this case wave height (m). When comparing model performance at different locations it can be helpful to use the normalized RMSE, as this

provides an indication of the amount of error relative to the range of observed wave heights. NRMSE is calculated as follows:

$$NRMSE = \frac{RMSE}{X_{obs,max} - X_{obs,min}}$$

The Coefficient of Efficiency NSE (Nash and Sutcliffe, 1970) indicates how well the plot of observed versus simulated fits the 1:1 line in the scatter plot. NSE ranges between $-\infty$ and 1.0 (1 inclusive), with NSE = 1 being the optimal value. Values between 0.0 and 1.0 are generally viewed as acceptable levels of performance, whereas values below zero are considered less acceptable

For the Index of Agreement values closer 1 indicate a stronger agreement between the two data sets. While it's difficult to find guidelines for what values might represent a good agreement, values meaningfully larger than 0.5 are considered to represent good model performance based on Willmott, et al (1985).

Wave Height Comparisons

The time series comparison are presented in the following figures for each instruments forcing with offshore ERA5 wave model parameters.

The error calculations are presented in the following tables also with both methods.

For instrument I1 West:

- The coefficient of determination was 0.79 which indicates that the model explains 79% of all the variability of the response data around its mean.
- The Coefficient of Efficiency NSE (Nash and Sutcliffe, 1970) was 0.65 which is considered a good level for model performance.
- The Index of Agreement is 0.88. While it's difficult to find guidelines for what values might represent a good agreement, values meaningfully larger than 0.5 are considered to represent good model performance based on Willmott, et al (1985). Values between 0 and 0.5 are considered to represent acceptable level of model performance.
- The RMS error is 0.19m which corresponds to an absolute error of 16%.
- The average measured wave heights was 0.87m while the modeling was 0.76m creating an average difference of 0.11m.

This provided reasonably accurate comparisons of the instrument-measured values (blue) and model-predicted wave heights (red), with depiction of wave height variations between peaks and lows. The comparisons showed that the simulated variations in wave height between daytime (peak) and nighttime (lows) are being shown with a respectable level of accuracy.

All the indices utilized for model validations are regarded as having adequate model performance. This statistical technique verified the model, allowing for the quantification of any effects across a long-term database of daily wave conditions on the project site's nearshore.

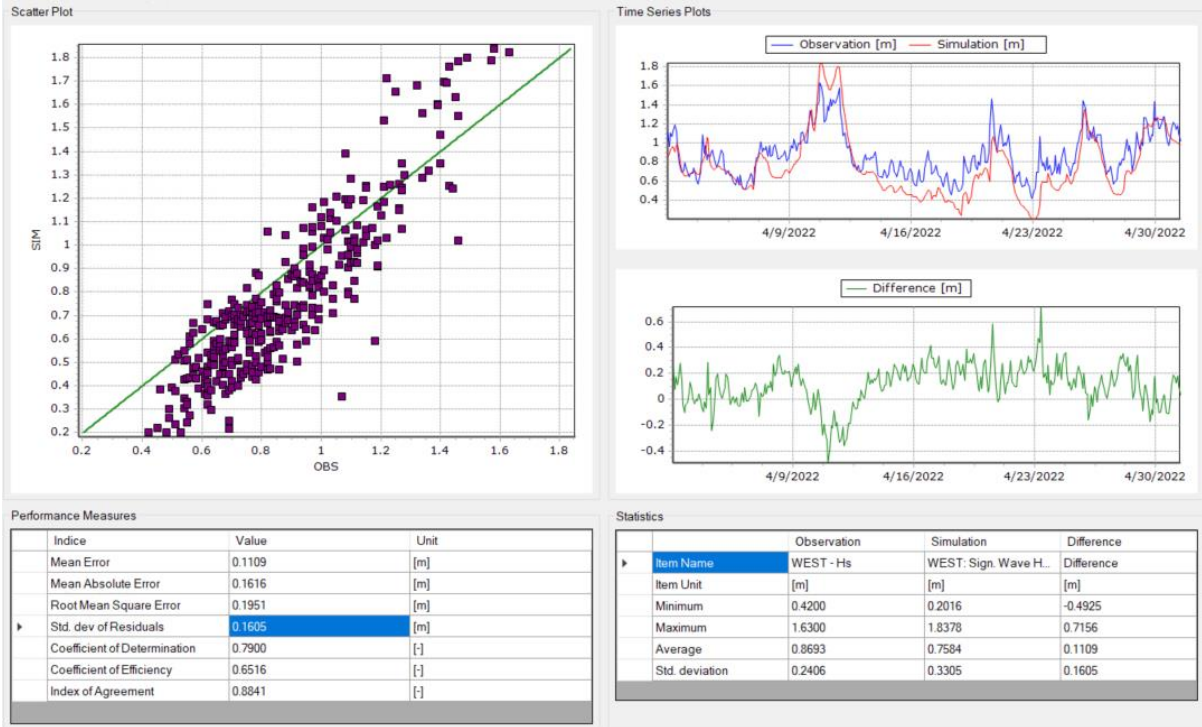
For instrument I2 East:

- The coefficient of determination was 0.74 which indicates that the model explains 74% of all the variability of the response data around its mean.
- The Coefficient of Efficiency NSE (Nash and Sutcliffe, 1970) was 0.69 which is considered a good level for model performance.
- The Index of Agreement is 0.92. While it's difficult to find guidelines for what values might represent a good agreement, values meaningfully larger than 0.5 are considered to represent good model performance based on Willmott, et al (1985). Values between 0 and 0.5 are considered to represent acceptable level of model performance.
- The RMS error is 0.13m which corresponds to an absolute error of 11%.
- The average measured wave heights was 0.6m while the modeling was 0.58m creating an average difference of 0.02m.

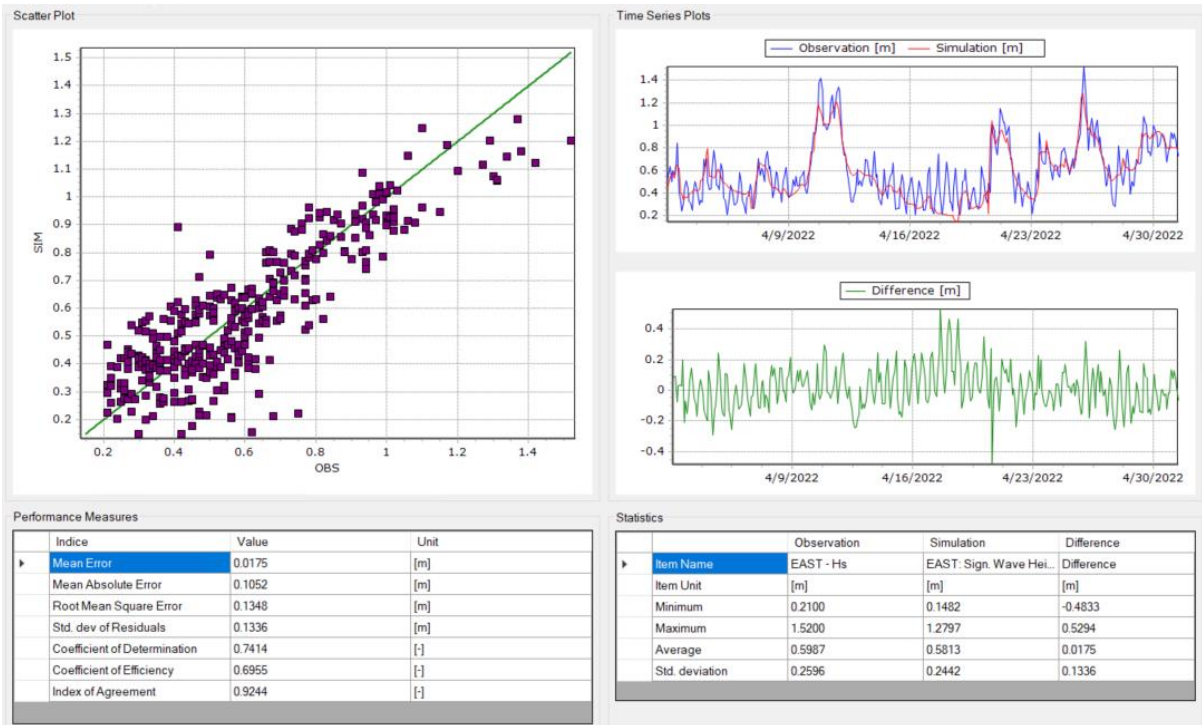
Error Parameters

<i>I1 West ADCP</i>	Index of Agreement	Guidelines	Score	NSE	Guidelines	Score	RMSE (%)	Guidelines ±%	Score
	0.88	>0.5	Pass	0.65	−∞ - 1	Pass	19.5	10	Marginal
<i>I2 East ADCP</i>	Index of Agreement	Guidelines	Score	NSE	Guidelines	Score	RMSE (%)	Guidelines ±%	Score
	0.92	>0.5	Pass	0.69	−∞ - 1	Pass	13.4	10	Marginal

Williams, J. J., & Esteves, L. S. (2017). Guidance on Setup, Calibration, and Validation of Hydrodynamic, Wave, and Sediment Models for Shelf Seas and Estuaries. In *Advances in Civil Engineering* (Vol. 2017, pp. 1–25). Hindawi Limited.



Instrument I1 West - ADCP instrument measured wave heights vs modeling predicted wave heights comparison



Instrument I2 East - ADCP instrument measured wave heights vs modeling predicted wave heights comparison

Directions

For instrument I1 West:

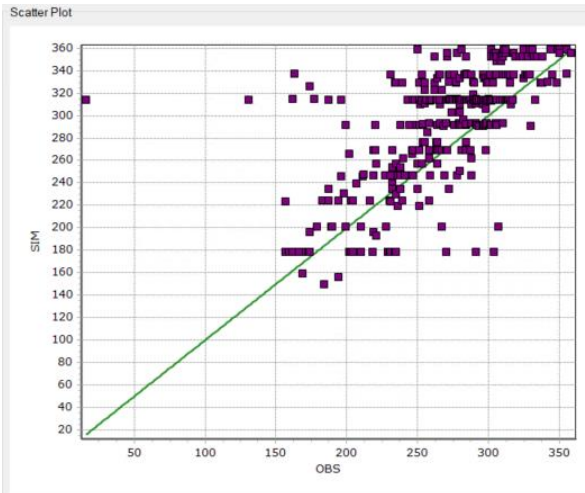
- The measured waves had a lesser variance in direction, ranging from 130° to 358° while the modeling directions ranged from 150° to 359°. The average measured mean wave direction was 268.8° while the modeling was 292.3°, creating an average difference of 23.4°.
- The RMS error is 46.5° corresponding to a relative error of 20%.

For instrument I2 East:

- The measured waves had a lesser variance in direction, ranging from 0° to 360° while the modeling directions ranged from 1.5° to 359°. The average measured mean wave direction was 191.4° while the modeling was 270.8°, creating an average difference of 79.4°.
- The RMS error is 152.2° corresponding to a relative error of 42%.

<i>West ADCP</i>	RMSE	Obs Mean	Guidelines ± (%) obs mean	Score
Peak Wave Period			20	Marginal
Mean Wave Direction	46.56	268.79°	30	Pass
<i>East ADCP</i>	RMSE	Obs Mean	Guidelines ± (%) obs mean	Score
Peak Wave Period			20	Marginal
Mean Wave Direction	152.2	191.4°	30	Fail

Calculated errors from Peak Period and Wave Direction between model-predicted and instrument measured



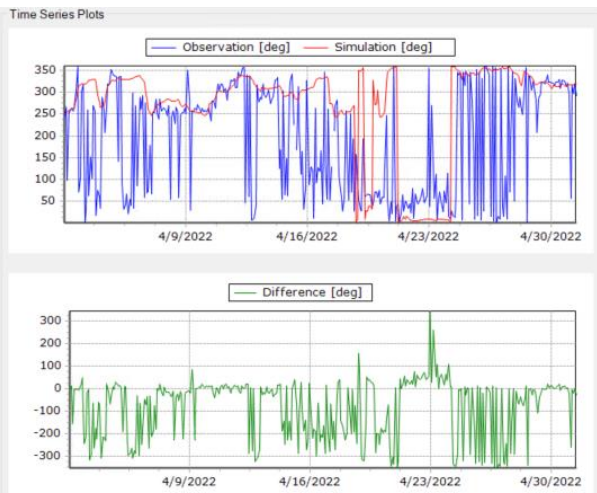
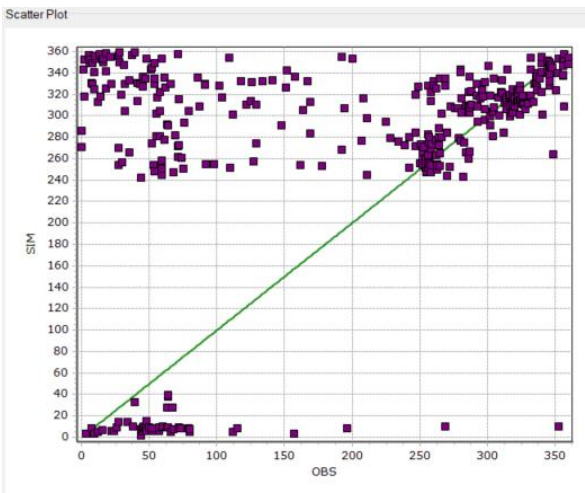
Performance Measures

Index	Value	Unit
Mean Error	-23.5532	[deg]
Mean Absolute Error	34.0035	[deg]
Root Mean Square Error	46.5467	[deg]
Std. dev of Residuals	40.1478	[deg]
Coefficient of Determination	0.4304	[-]
Coefficient of Efficiency	0.1602	[-]
Index of Agreement	0.7646	[-]

Statistics

	Observation	Simulation	Difference
Item Name	WEST - Wave Direction	WEST: Peak Wave Di...	Difference
Item Unit	[deg]	[deg]	[deg]
Minimum	16.0000	150.0752	-297.9366
Maximum	358.0000	358.9366	125.0633
Average	268.7938	292.3470	-23.5532
Std. deviation	45.2564	50.7935	40.1478

Instrument West D1 – ADCP instrument measured wave directions vs modeling predicted wave directions



Performance Measures

Index	Value	Unit
Mean Error	-79.3751	[deg]
Mean Absolute Error	99.9118	[deg]
Root Mean Square Error	152.1954	[deg]
Std. dev of Residuals	129.8578	[deg]
Coefficient of Determination	0.1293	[-]
Coefficient of Efficiency	-1.1460	[-]
Index of Agreement	0.6319	[-]

Statistics

	Observation	Simulation	Difference
Item Name	EAST - Wave Direction	EAST: Mean Wave Dir...	Difference
Item Unit	[deg]	[deg]	[deg]
Minimum	0.0000	1.5423	-352.0298
Maximum	360.0000	358.9722	343.1108
Average	191.4153	270.7903	-79.3751
Std. deviation	123.7579	103.8920	129.8578

Instrument East D1 – ADCP instrument measured wave directions vs modeling predicted wave directions



Hydrodynamic Model Validation

To comprehend how tidal currents or wave-induced currents will affect the coastal environment on a daily basis, it is crucial to establish a complete understanding of the operational hydrodynamic climate, similar to how nearshore wave dynamics must be understood. Therefore, numerical models were employed to comprehend the site's hydrodynamic climate.

The global tide model from DTU (Denmark Technical University) was used to calculate water level inputs to the model borders in addition to the water depths, which are specified over the whole model domain using the flexible mesh. The model has received widespread approval as being sufficiently accurate for studies of this scale after being tested at various Caribbean locations. The validation process is explained here:

- The water level forcing from the DTU model results were extracted at the boundary locations of the hydrodynamic models.
- Other forcing to the model included wind and wave radiation stress from the ERA 5 global wave model, seabed roughness and eddy viscosity.
- The hydrodynamic model computes nearshore currents forced by water level variations, from the DTU model. The operational hydrodynamics were developed and transformed to the nearshore using the hydrodynamic module to produce real-time hydrodynamic variances in current velocities, and surface elevation (HD) coinciding with the time of the measurement period.
- Wave and currents were determined at each simulation time step over the computational mesh.
- The validation involved comparing the various measurements and model-predicted values.
- The last step was calculating the error between instrument-measured and model-predicted and adjusting various model parameters to minimize model versus measured errors according to the *Foundation of Water Research Guidelines* for assessing hydrodynamic model performance.

The Foundation for Water Research published *A Framework for Marine and Estuarine Model Specifications in the UK* in 1993, which is one of the only documents providing standards for assessing hydrodynamic model performance. These guidelines suggest accuracy levels as follows:

- Water levels to within $\pm 15\%$ during spring tidal ranges and $\pm 20\%$ during neap tidal ranges.
- Current speeds to within $\pm 200\text{mm/s}$ or $\pm 10\text{-}20\%$ of the observed speed; and
- Current directions to within ± 20 degrees

To quantify the capabilities of the numerical model, the modeling water levels and u and v velocities were compared to the measured water levels and measured u and v velocities. The comparison was evaluated using the root mean square error (RMSE) and the normalized root mean squared error (NRMSE) for the water level.

RMSE is a useful indicator of model calibration as it sums the difference between the computed and measured values. The values that can be assessed include tide height and current speed and direction (or Easting and Northing current components). Because these differences may be positive or negative,

the value is squared before being averaged so that the absolute error is preserved, according to the following formula:

$$RMSE = \sqrt{\frac{\sum_{i=1}^n (X_{obs,i} - X_{model,i})^2}{n}}$$

where X_{obs} is observed values and X_{model} is modeling values at time/place i .

The NRMSE has the same units as the input parameters, in the case of tide height (m). When comparing model performance at different locations it can be helpful to use the normalized RMSE, as this provides an indication of the amount of error relative to the range of observed tide heights. NRMSE is calculated as follows:

$$NRMSE = \frac{RMSE}{X_{obs,max} - X_{obs,min}}$$

The table below indicates the RMSE and NRMSE computed between model-predicted and instrument-measured at the four instrument locations. Overall results indicate that the predicted tides match the measured levels relatively well in terms of both height and phase, with the calculated error levels well within $\pm 20\%$ range indicated in the *Guidelines from the Foundation for Water Research*.

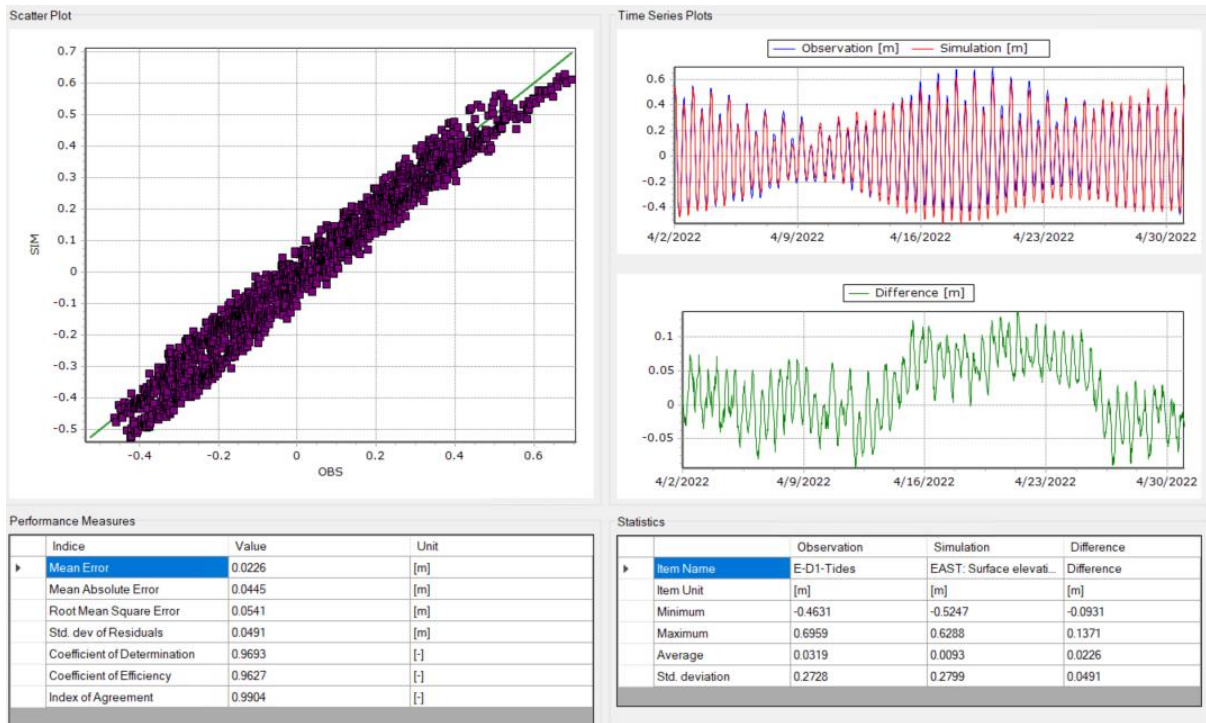
Calculated errors between model predicted and instrument measured tide heights

Location	Tide Height Comparison					
	RMSE (mm)	Guidelines	Score	NRMSE (%)	Guidelines	Score
West – D1	54.1	±150-200mm	Pass	4.67%	±15-20%	Pass
East – D1	67.8		Pass	5.62%		Pass

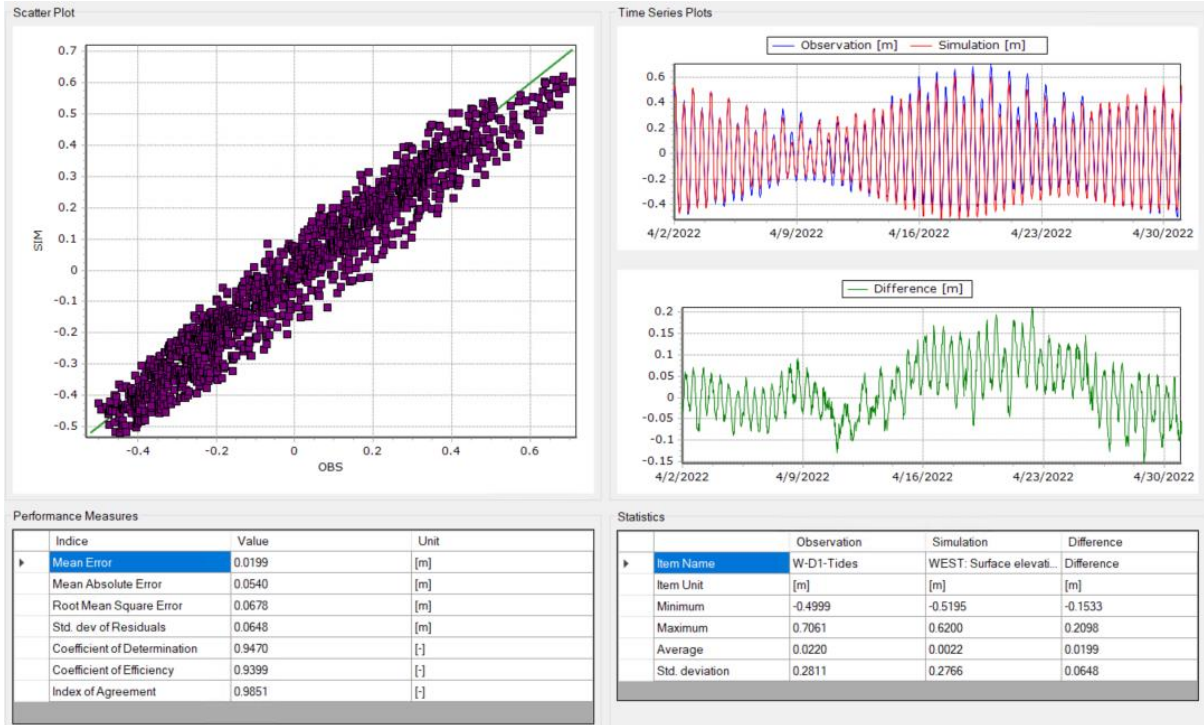
The results of the RMSE and the NRMSE computed between model predicted (depth averaged) and instrument measured easting and northing velocities are listed in the following tables. Results indicate that the calculated errors are within range of model calibration guidance (within $\pm 0.2\text{m/s}$ or $\pm 10-20\%$). A typical scatter and progressive vector plot of the measured versus modeling is presented below for all instruments and indicate the model reproduces the recorded in both intensity and direction.

Calculated errors from northing and easting velocities between model-predicted and instrument measured at Caye Caulker

I1 (West) ADCP	<i>Easting and Northing Comparison (ADCP West)</i>					
	RMSE (m/s)	Guidelines	Score	NRMSE (%)	Guidelines	Score
Easting (U Vel)	0.07	±0.2 m/s	Pass	38	±10-20%	Fail
Northing (V Vel)	0.12		Pass	36		Fail
I2 (East) ADCP	<i>Easting and Northing Comparison (ADCP East)</i>					
	RMSE (m/s)	Guidelines	Score	NRMSE (%)	Guidelines	Score
Easting (U Vel)	0.08	±0.2 m/s	Pass	41	±10-20%	Fail
Northing (V Vel)	0.04		Pass	24		Pass

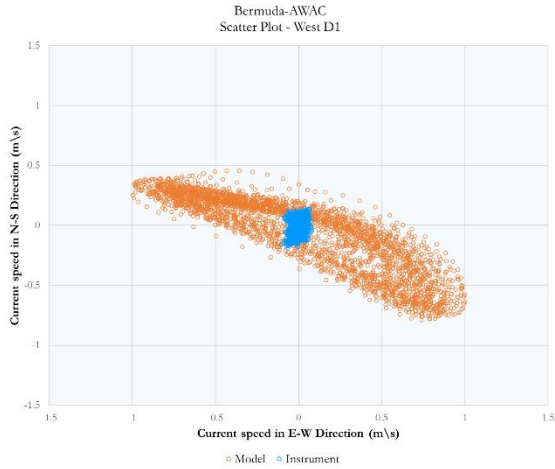


ADCP instrument measured tides vs modeling predicted tides comparison at location West D1



ADCP instrument measured tides vs modeling predicted tides comparison at location East D1

ADCP – Depth Average Currents



Deployment Details:

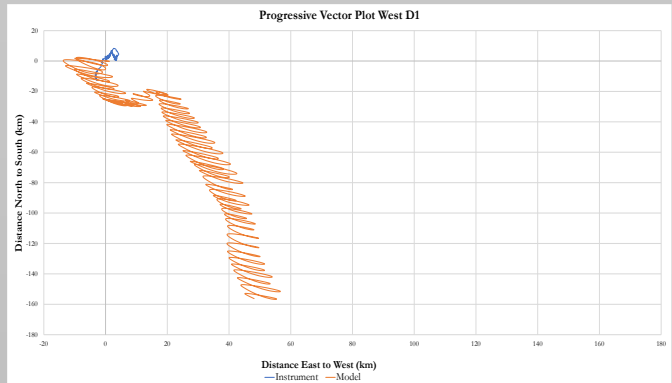
Currents measured using ADCP April 1 to May 1, 2022

Recordings at 30-minute intervals

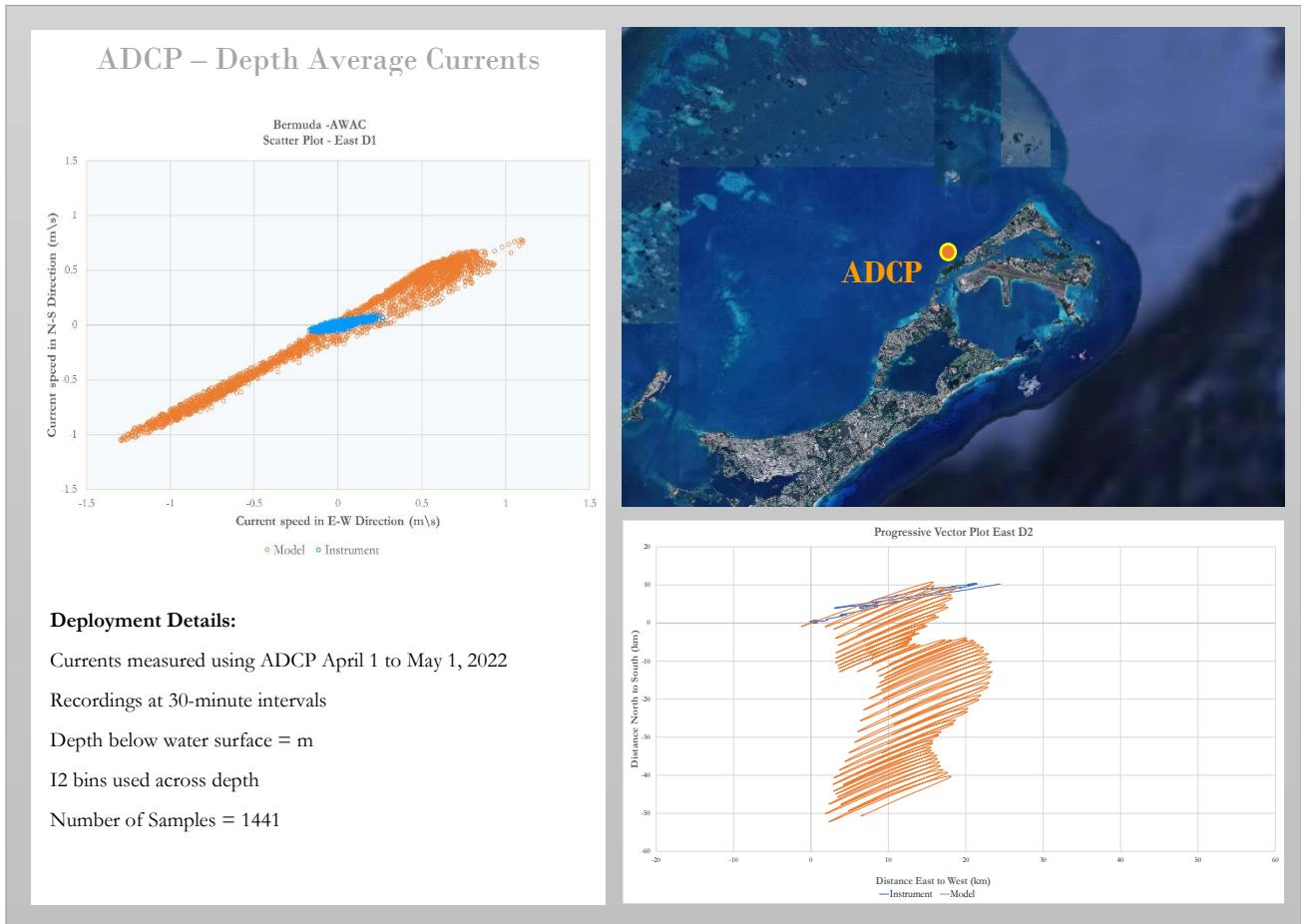
Depth below water surface = m

12 bins used across depth

Number of Samples = 1441



ADCP West D1 measured scatter vs modeling scatter u (east-west) and v (north-south) components of the velocities and corresponding progressive vector plot.



ADCP East D1 measured scatter vs modeling scatter u (east-west) and v (north-south) components of the velocities and corresponding progressive vector plot.

The hydrodynamic model was determined to fulfill the minimum requirements for model performance based on the guidelines provided in the section above. Overall, it was determined that the validation findings were adequate and that the model could calculate hydrodynamic parameters with a respectable degree of accuracy.

Summary of Validated Model

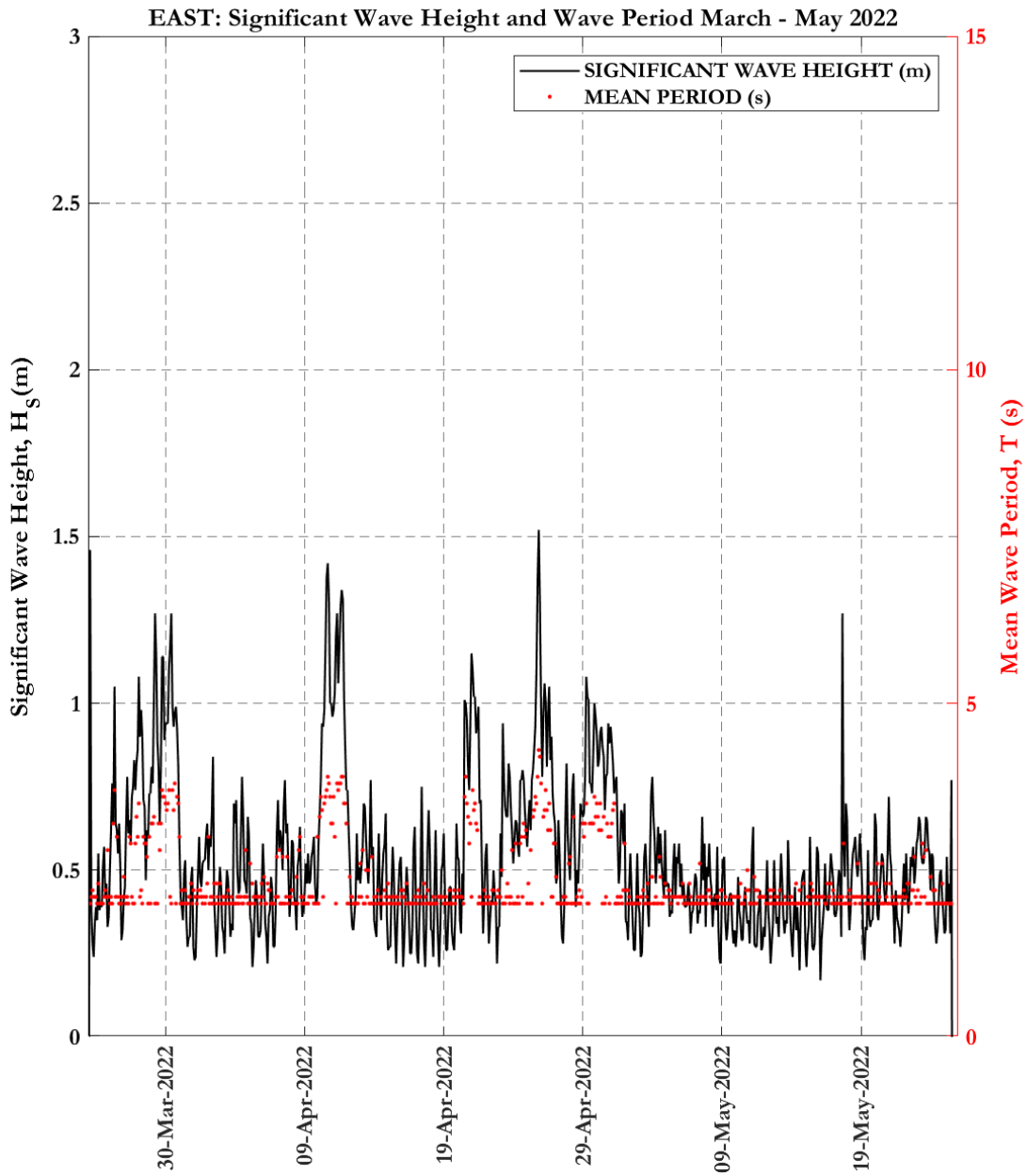
The numerical model was calibrated for correlation with waves and tides at several points offshore Bermuda.

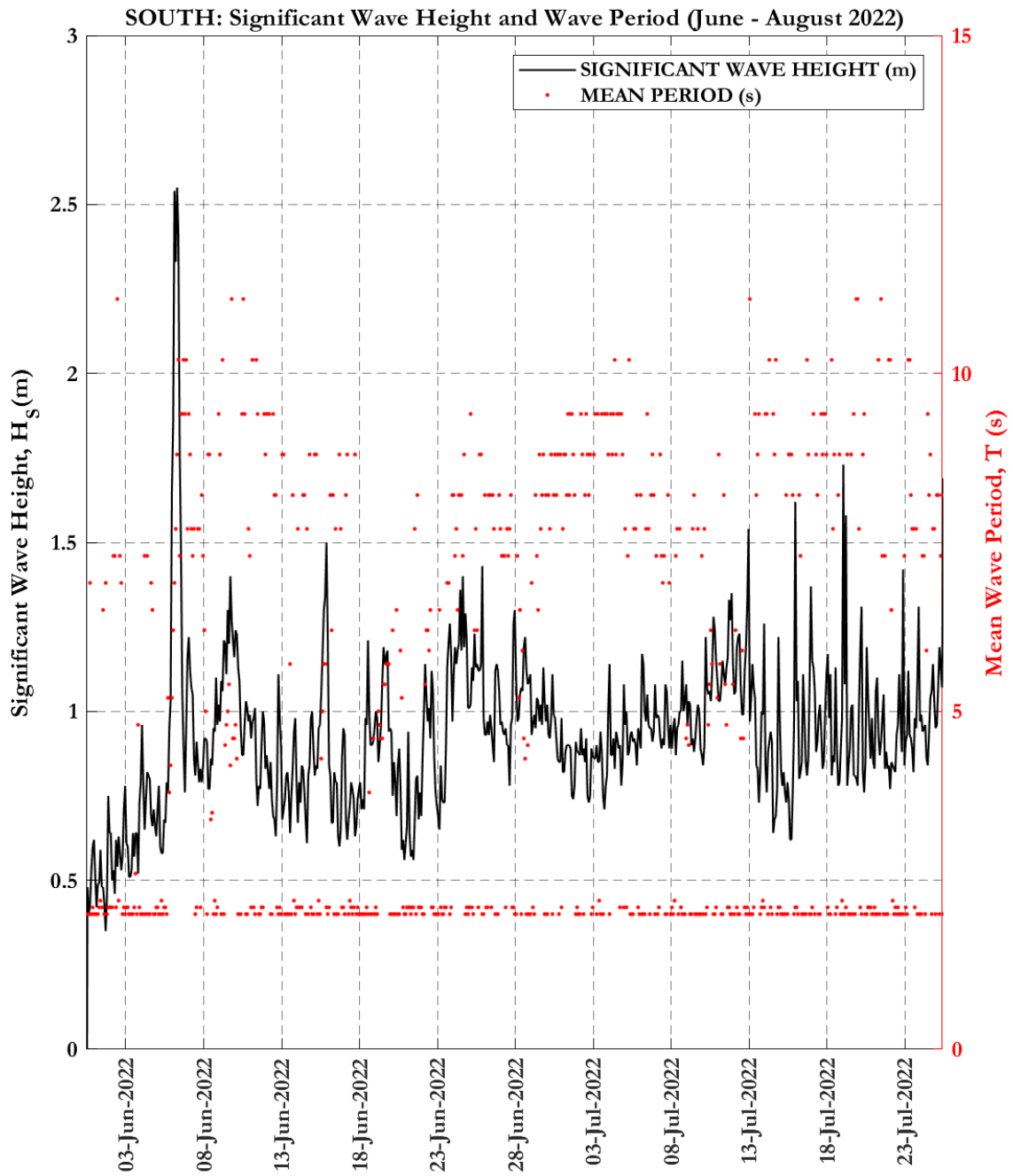
The calibration exercises undertaken can be summarized as follows:

- The wave model performed well:
 - The Index of Agreement between modeling wave heights and measured wave heights were acceptable for both instruments. Comparison of the actual values revealed an average difference of 0.11m and 0.02m respectively i.e. the model tended to overestimate the wave heights by roughly 0.06m.
 - The model predicted the peak wave periods well, comparison of the actual values revealed an average difference of 0.02s for West D1 and 4.3s for East D1 i.e. the model tended to underestimate the wave periods more to the south.
 - The dominant wave direction of the model approached from the NW for West D1 and East D1, which were relatively close to the same direction measured.
- The tide model also performed well, with all tides in sync with the measured tides and just minor underestimations of the measured highs and lows. The calculated RMSE percentages ranged from 4.67% to 5.62%. These errors were close to the acceptable maximum allowed by the guidelines of $\pm 15-20\%$.

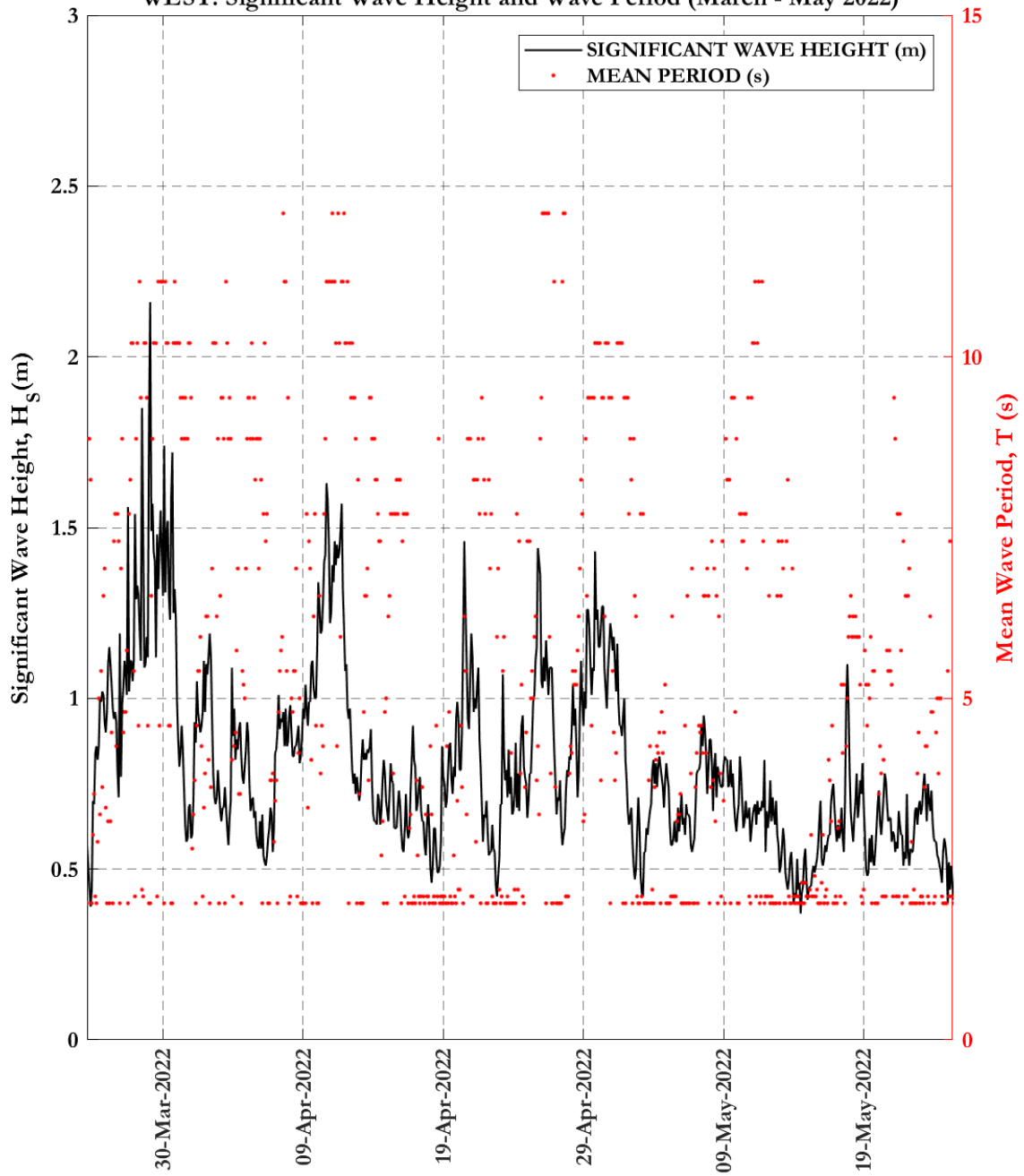
Overall, the MIKE 21 model performed within the guidelines for both spectral waves and tides. The model can therefore be expected to be capable of representing the average conditions that occur within the bay and should be able to both represent the existing coastal processes and, in the future, evaluate the impacts of any proposed design on ambient surroundings.

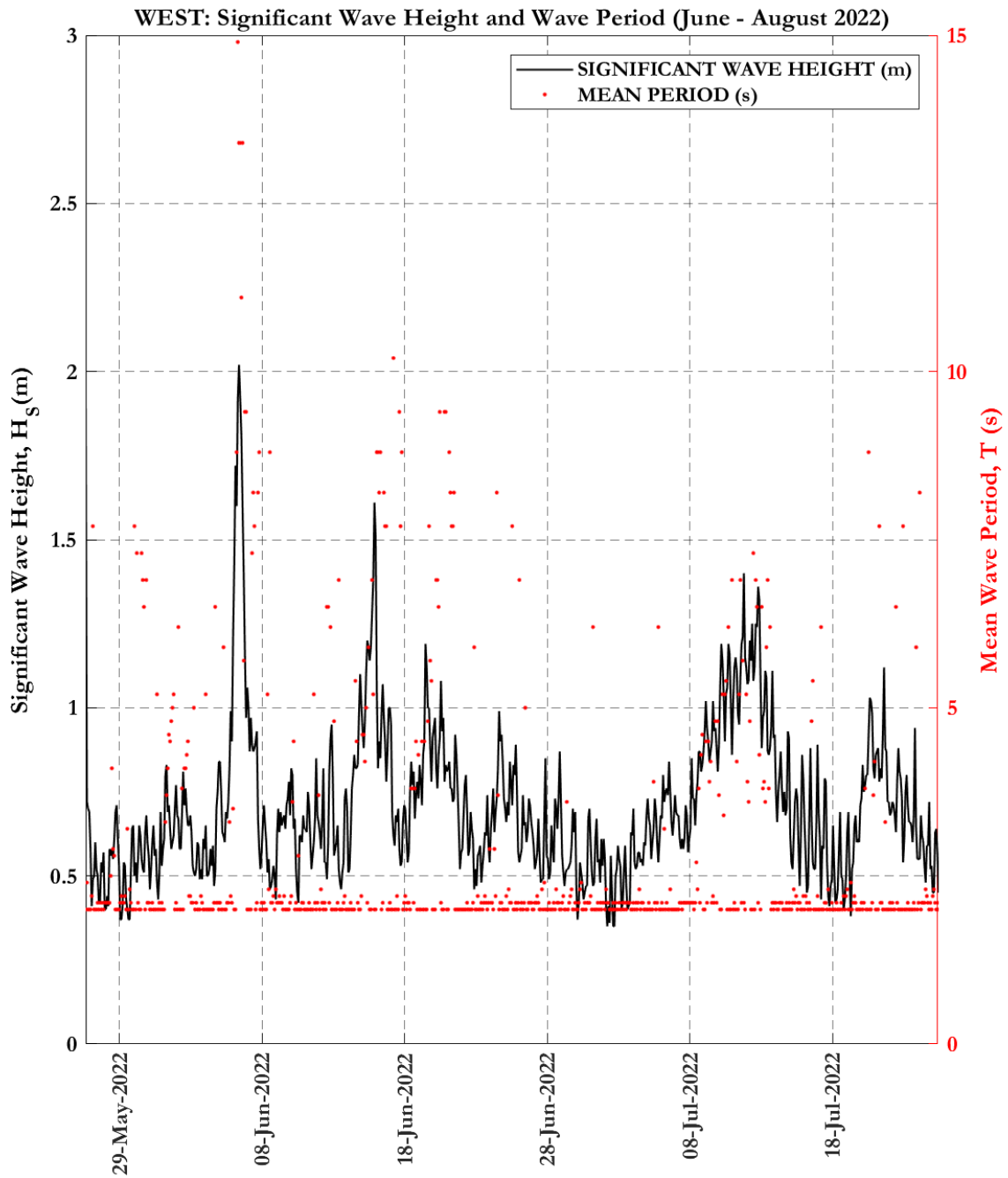
Appendix D – Measured Data

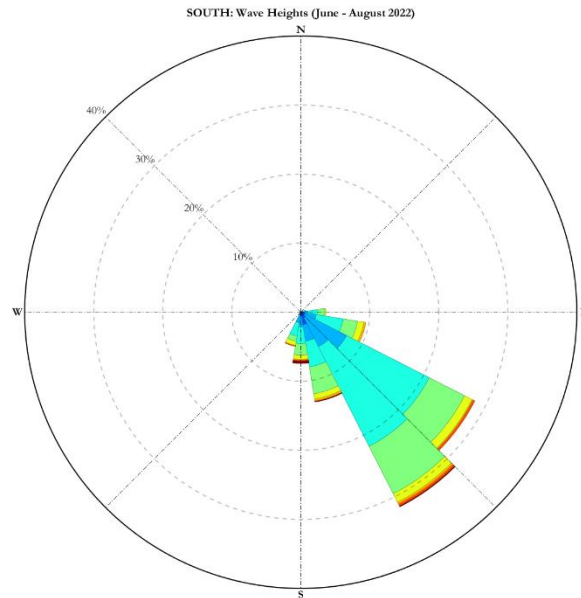
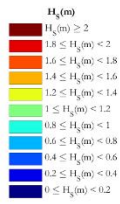
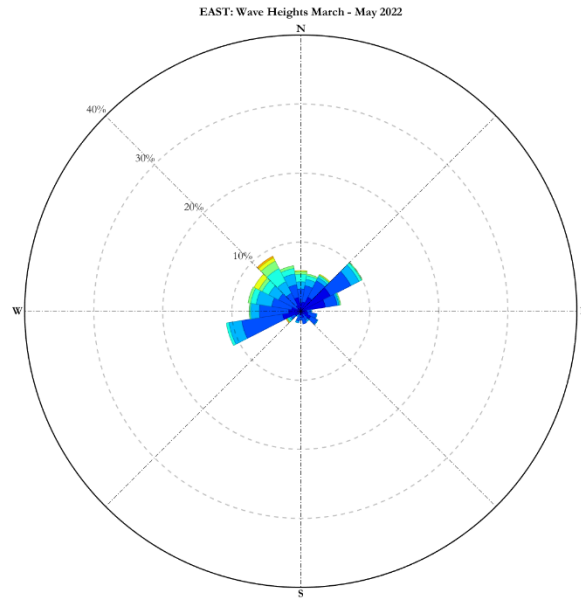
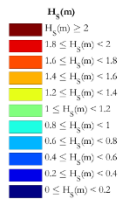


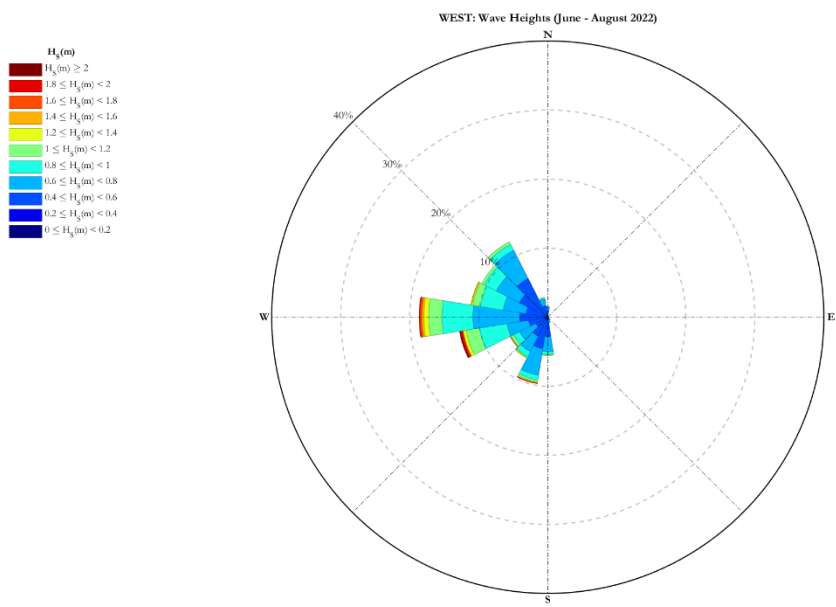
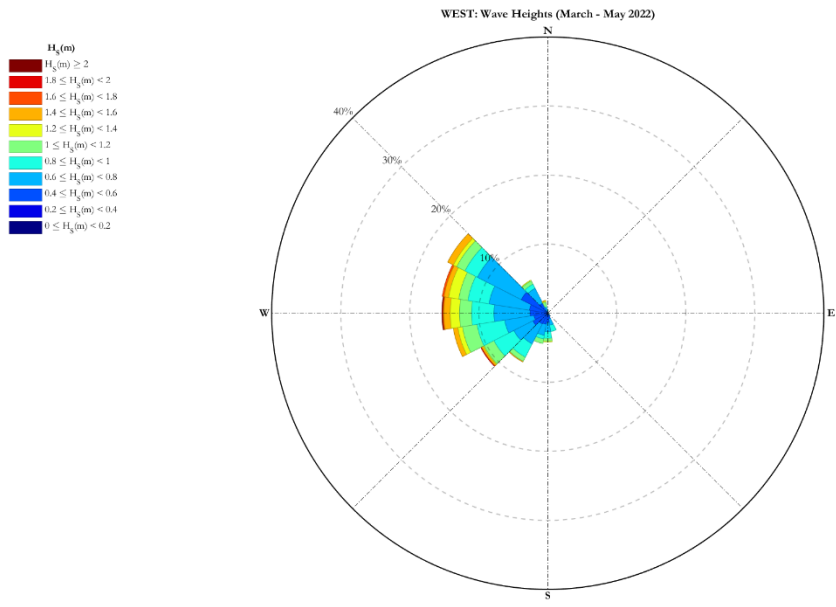


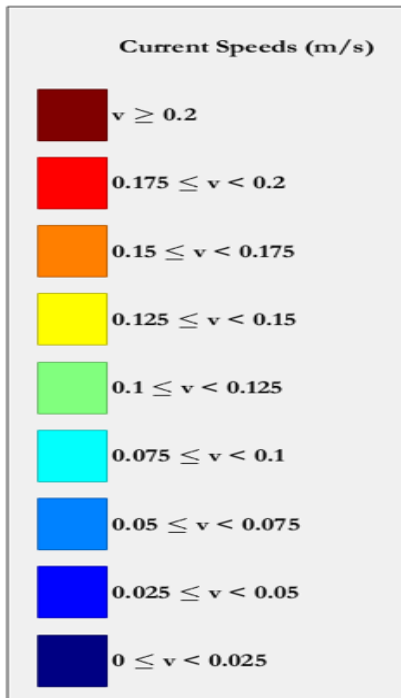
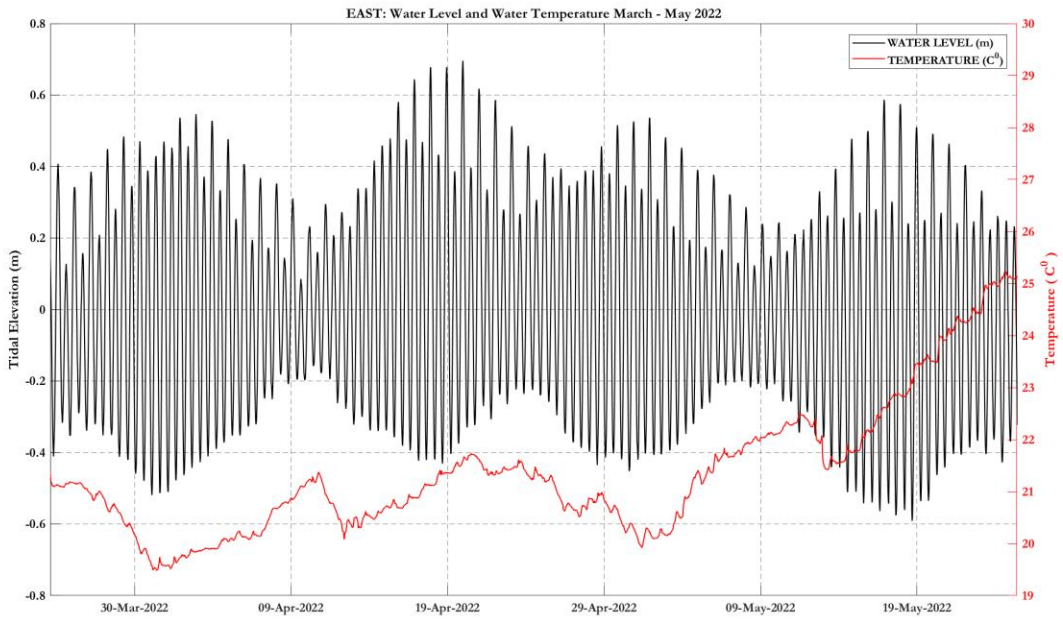
WEST: Significant Wave Height and Wave Period (March - May 2022)

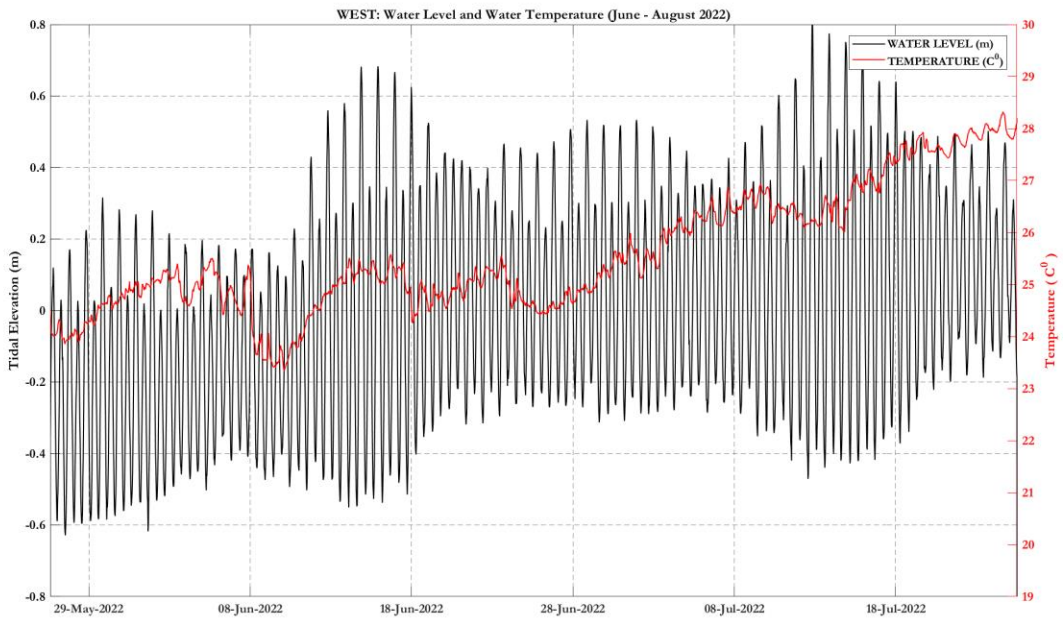
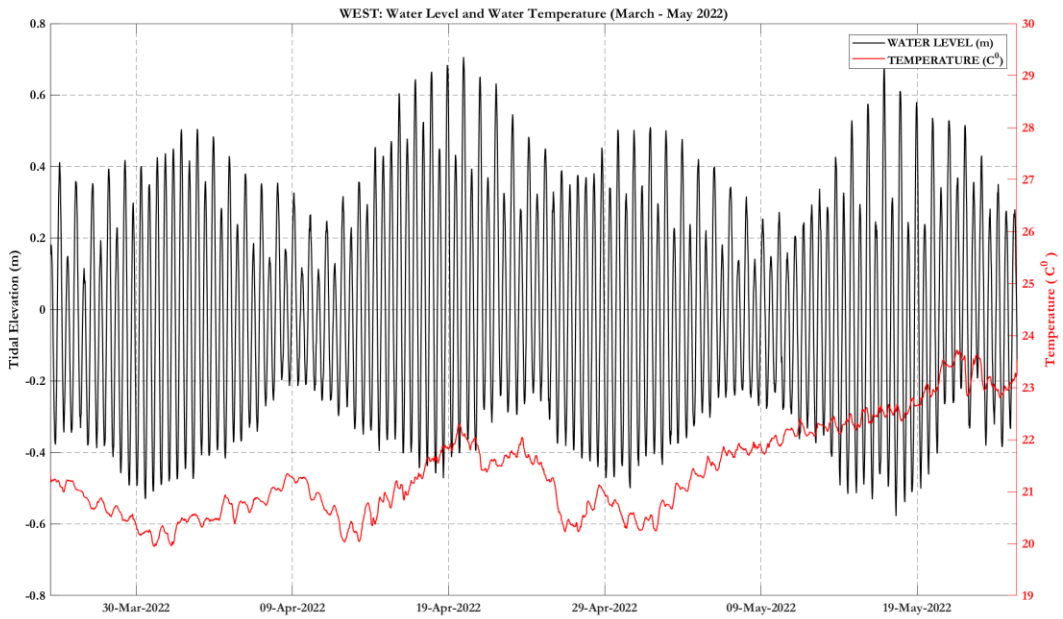


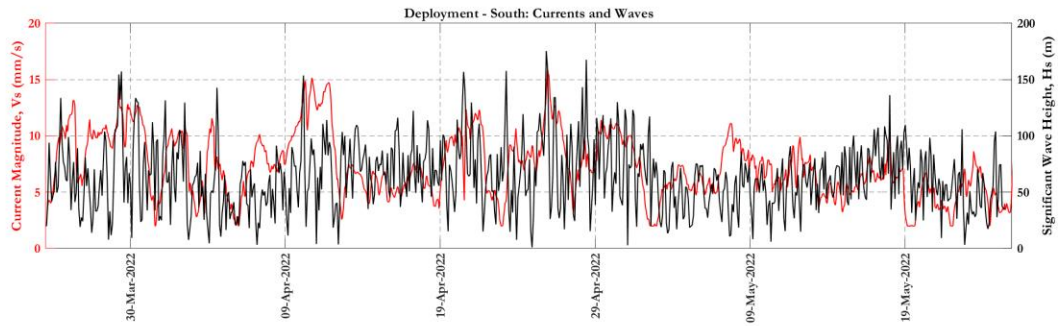
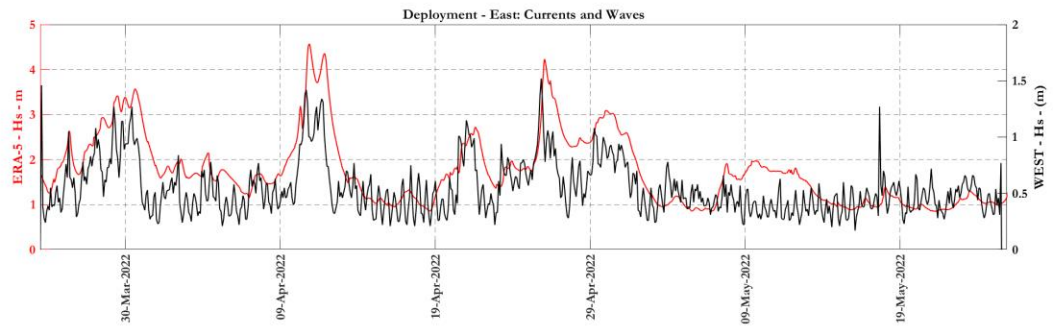
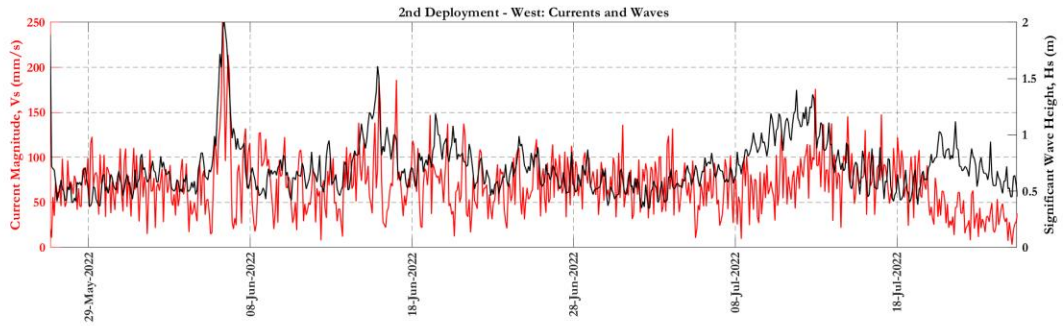
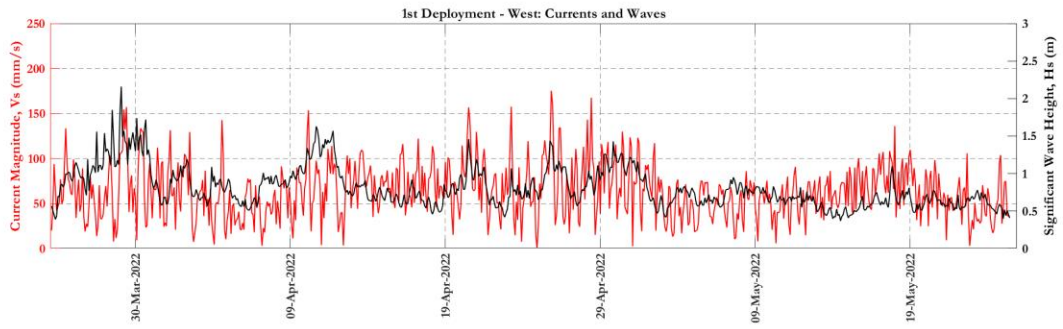


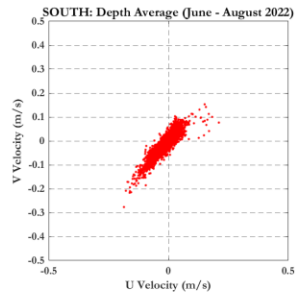
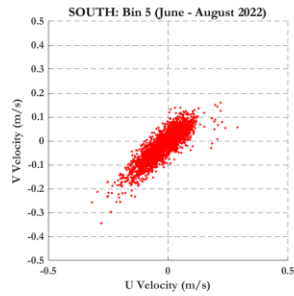
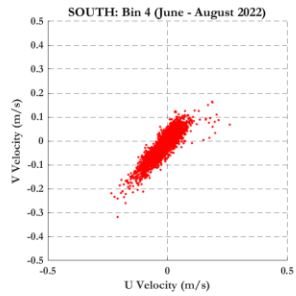
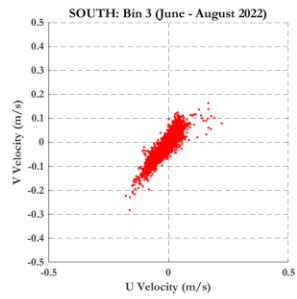
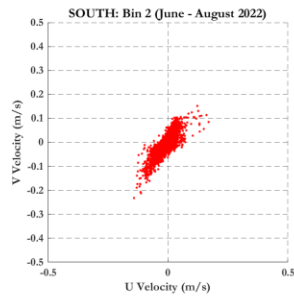
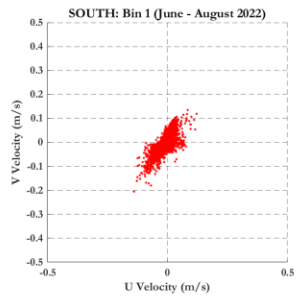
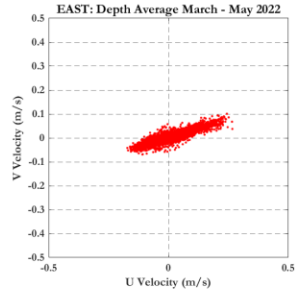
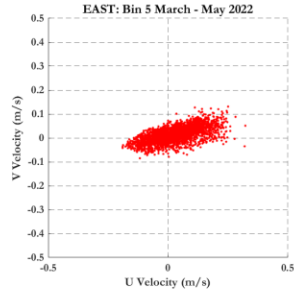
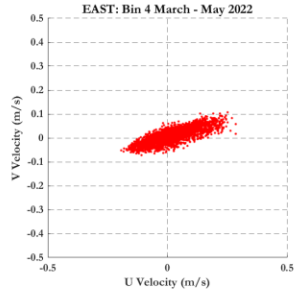
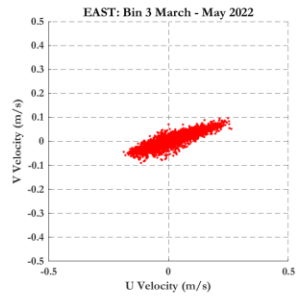
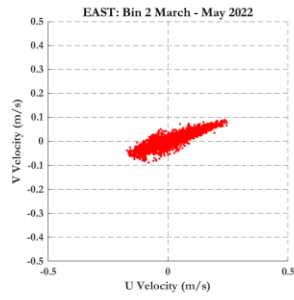
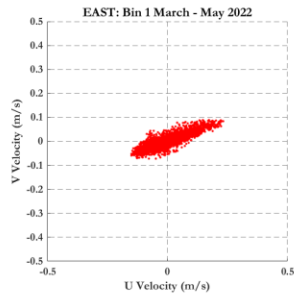


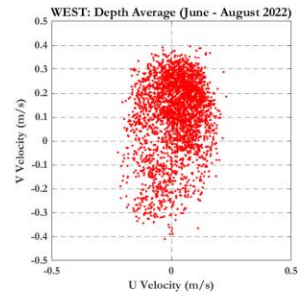
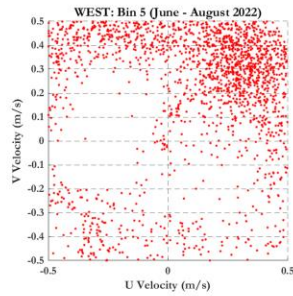
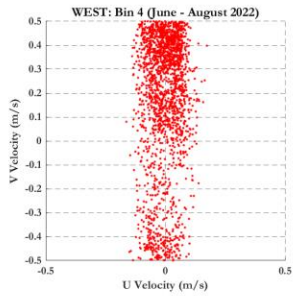
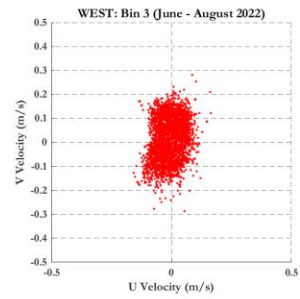
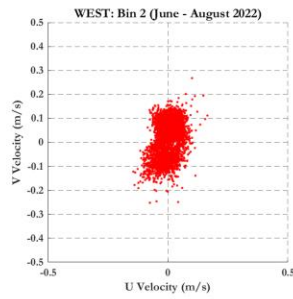
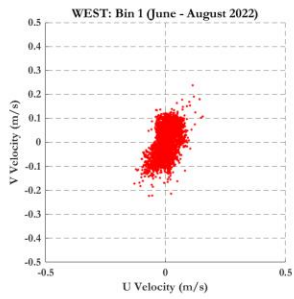
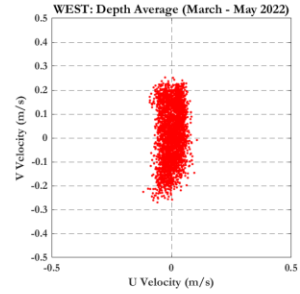
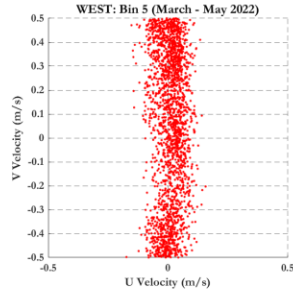
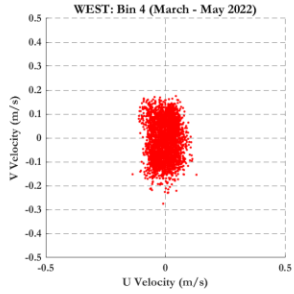
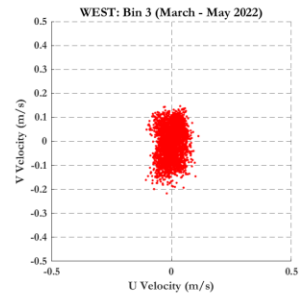
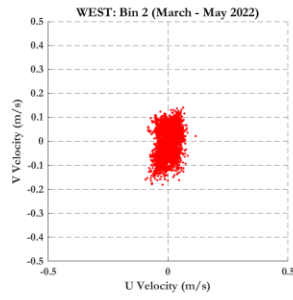
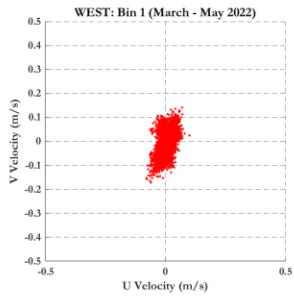


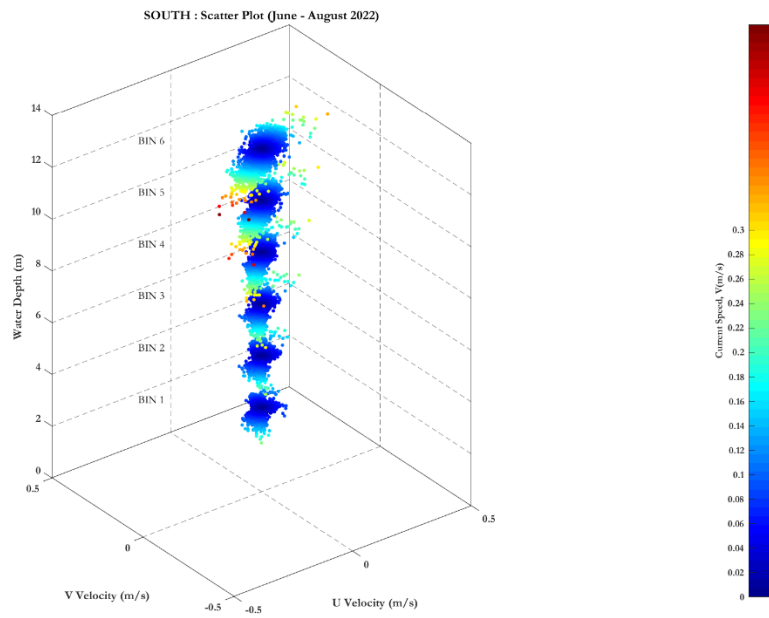
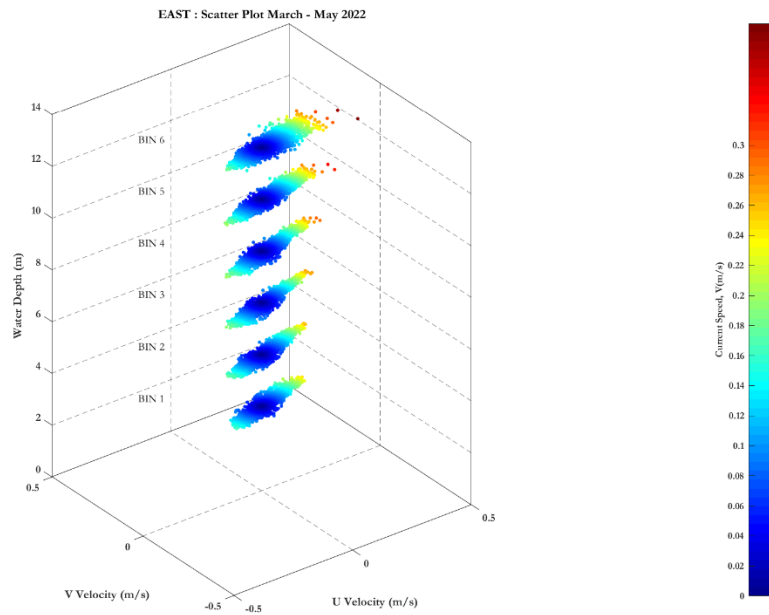


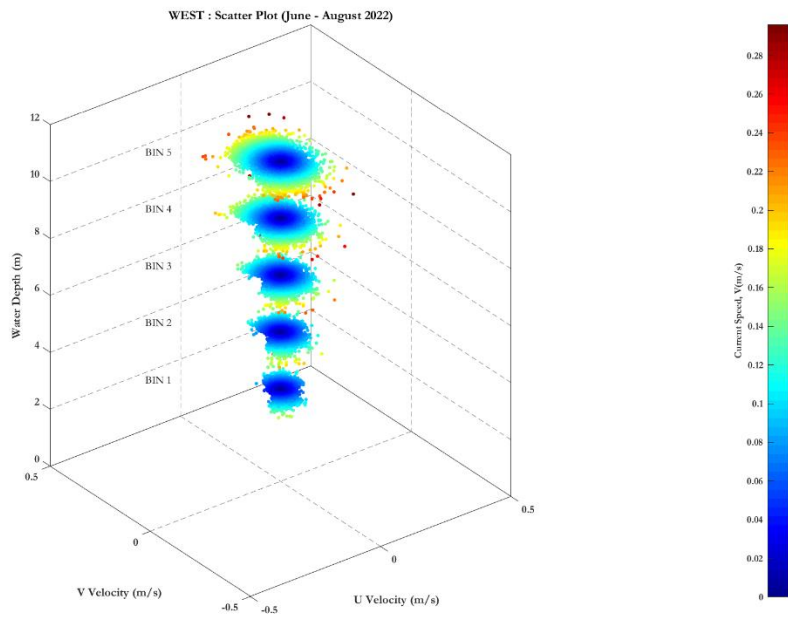
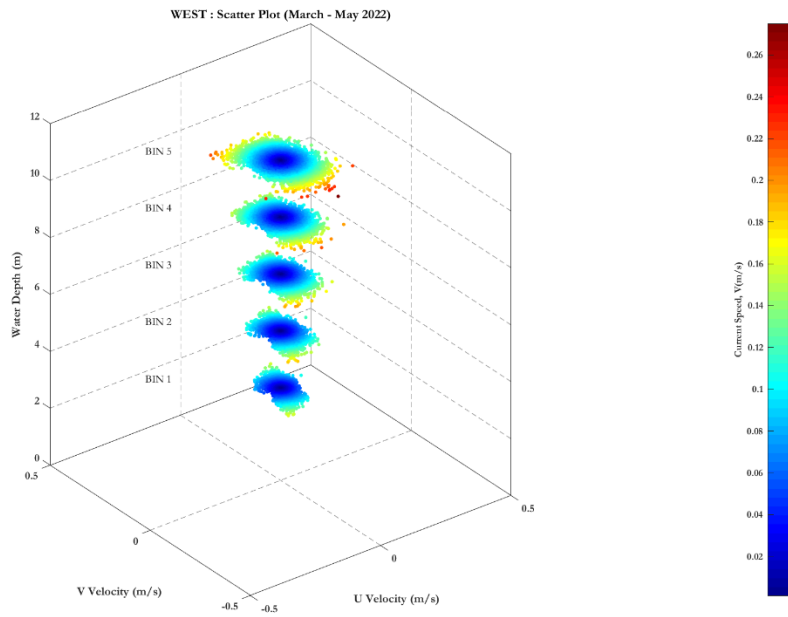


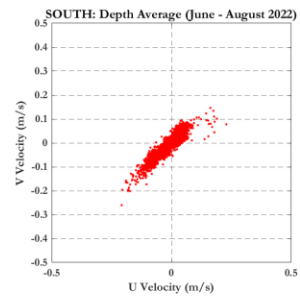
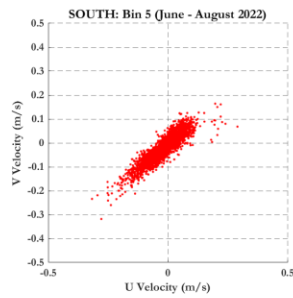
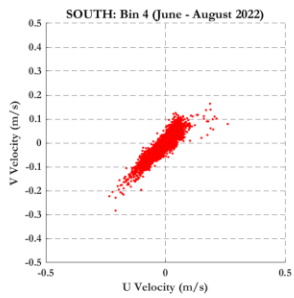
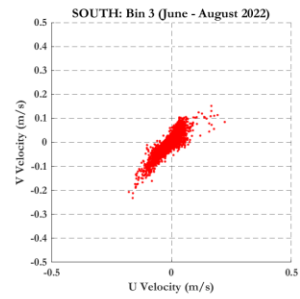
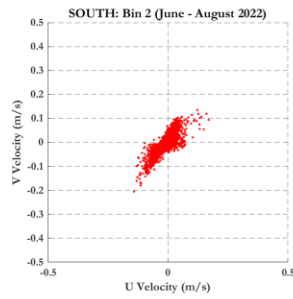
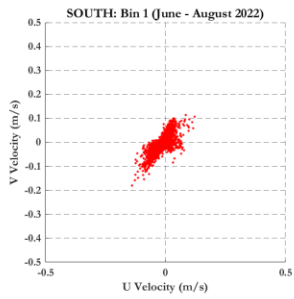
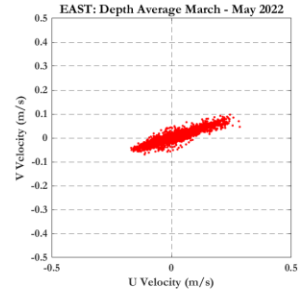
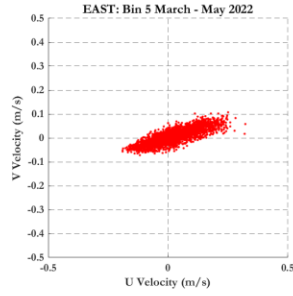
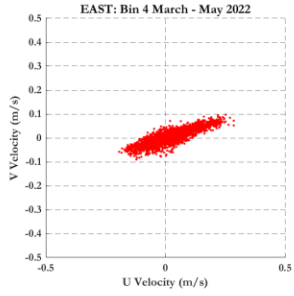
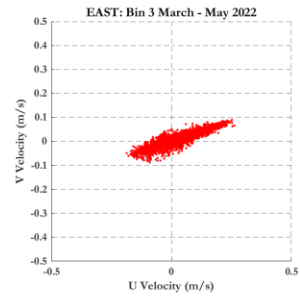
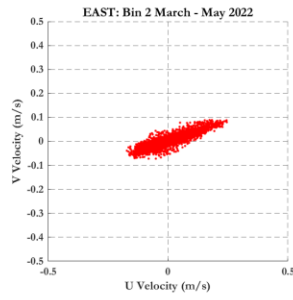
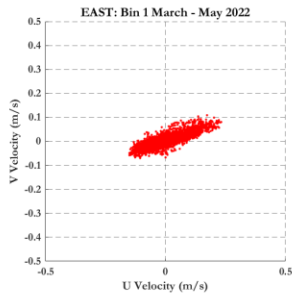


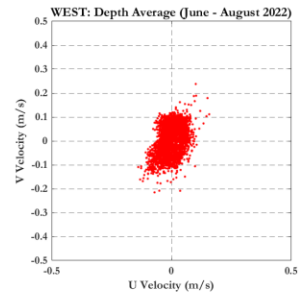
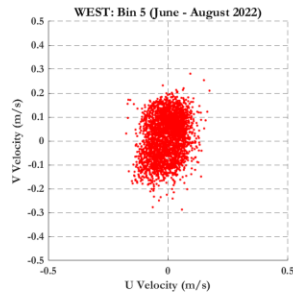
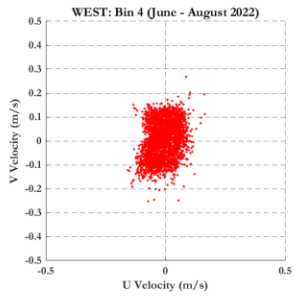
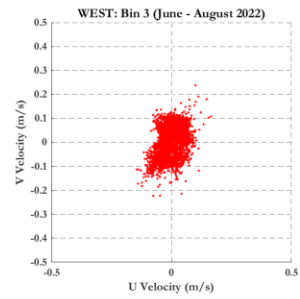
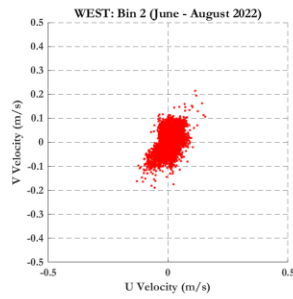
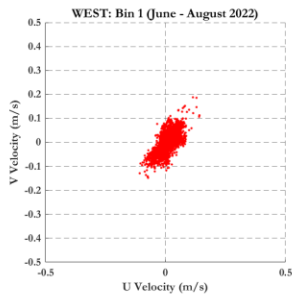
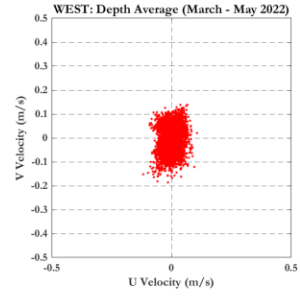
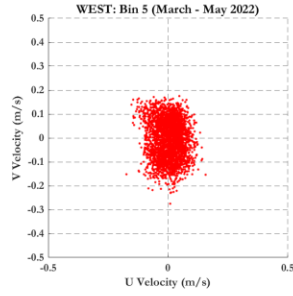
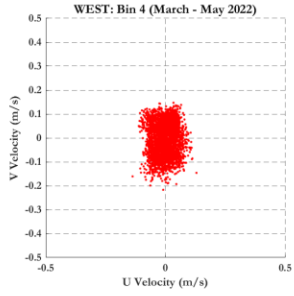
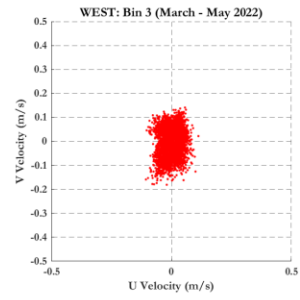
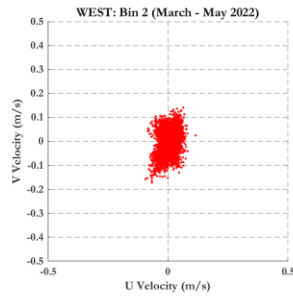
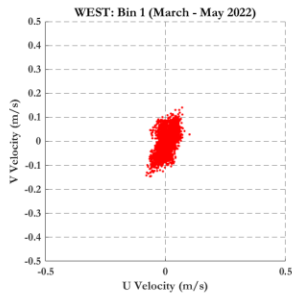


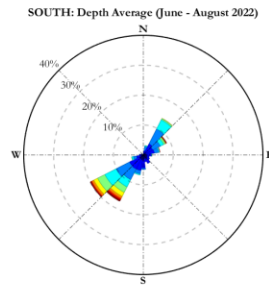
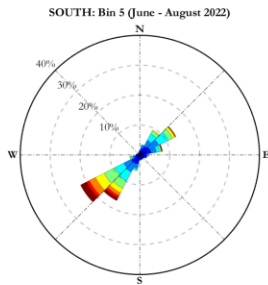
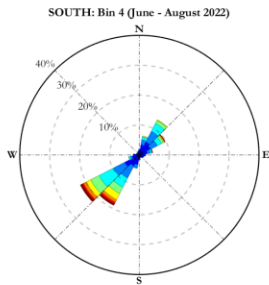
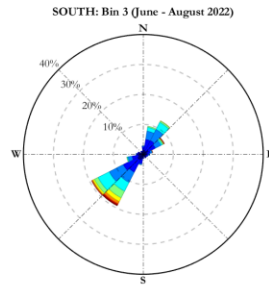
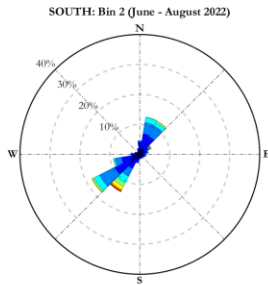
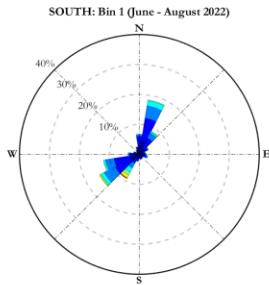
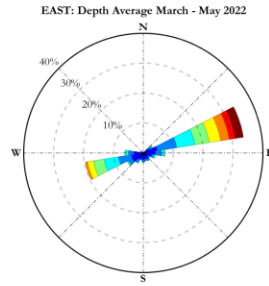
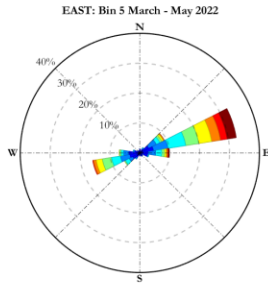
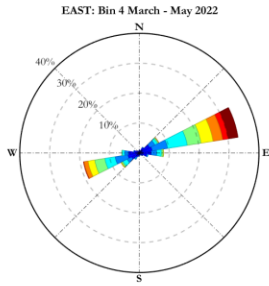
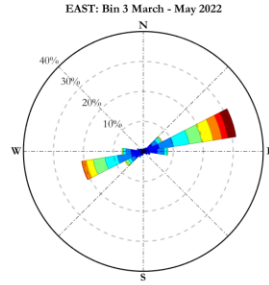
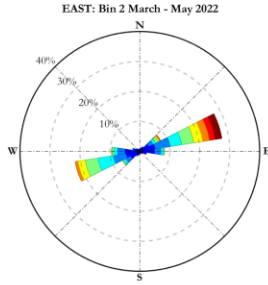
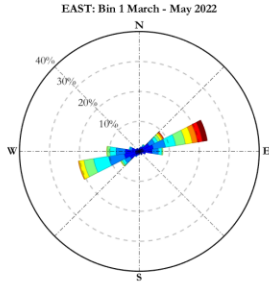


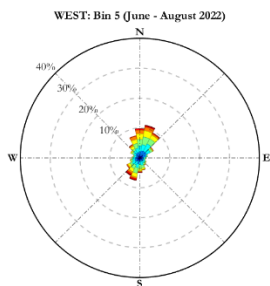
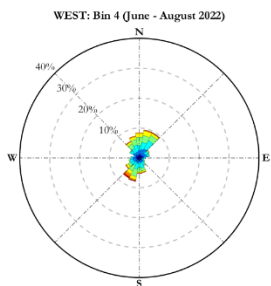
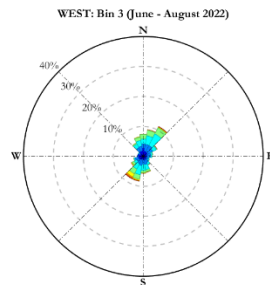
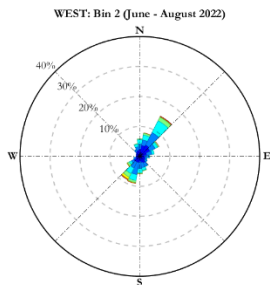
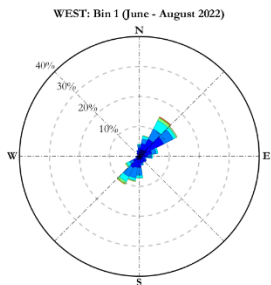
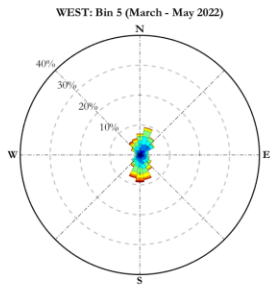
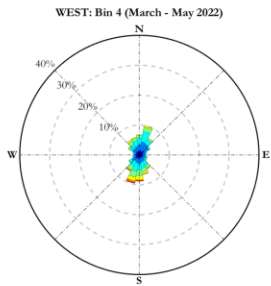
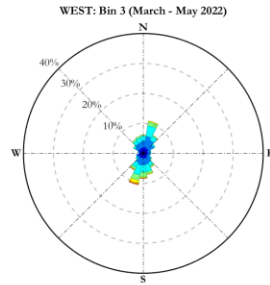
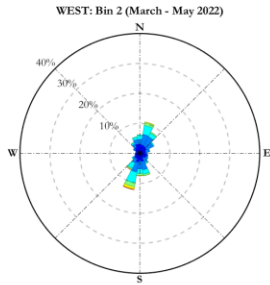
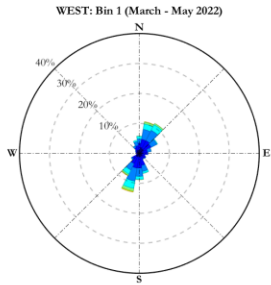


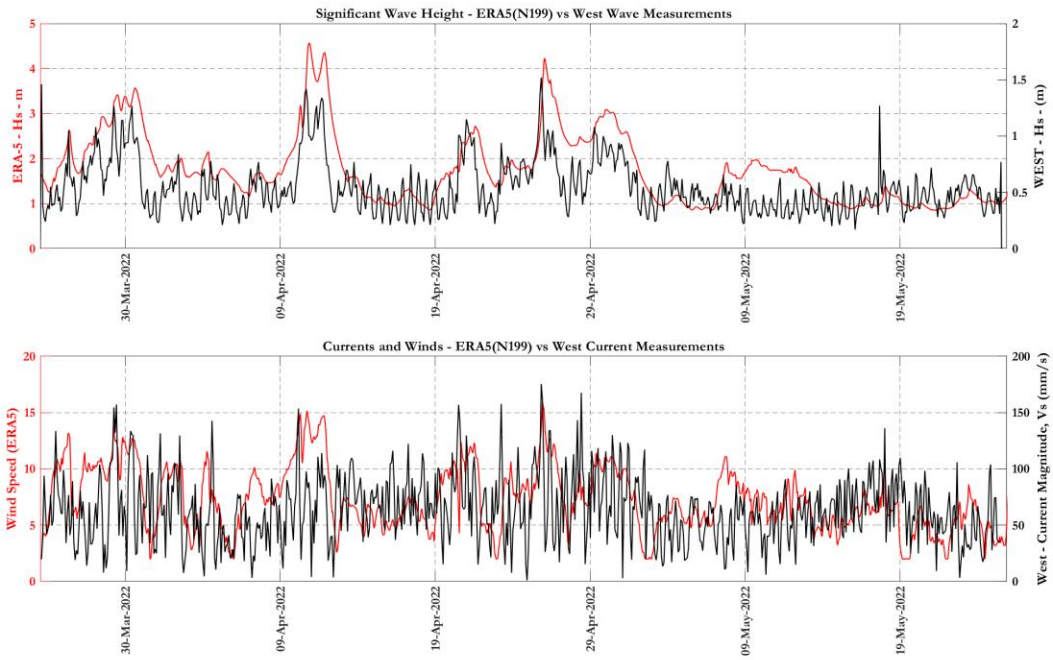




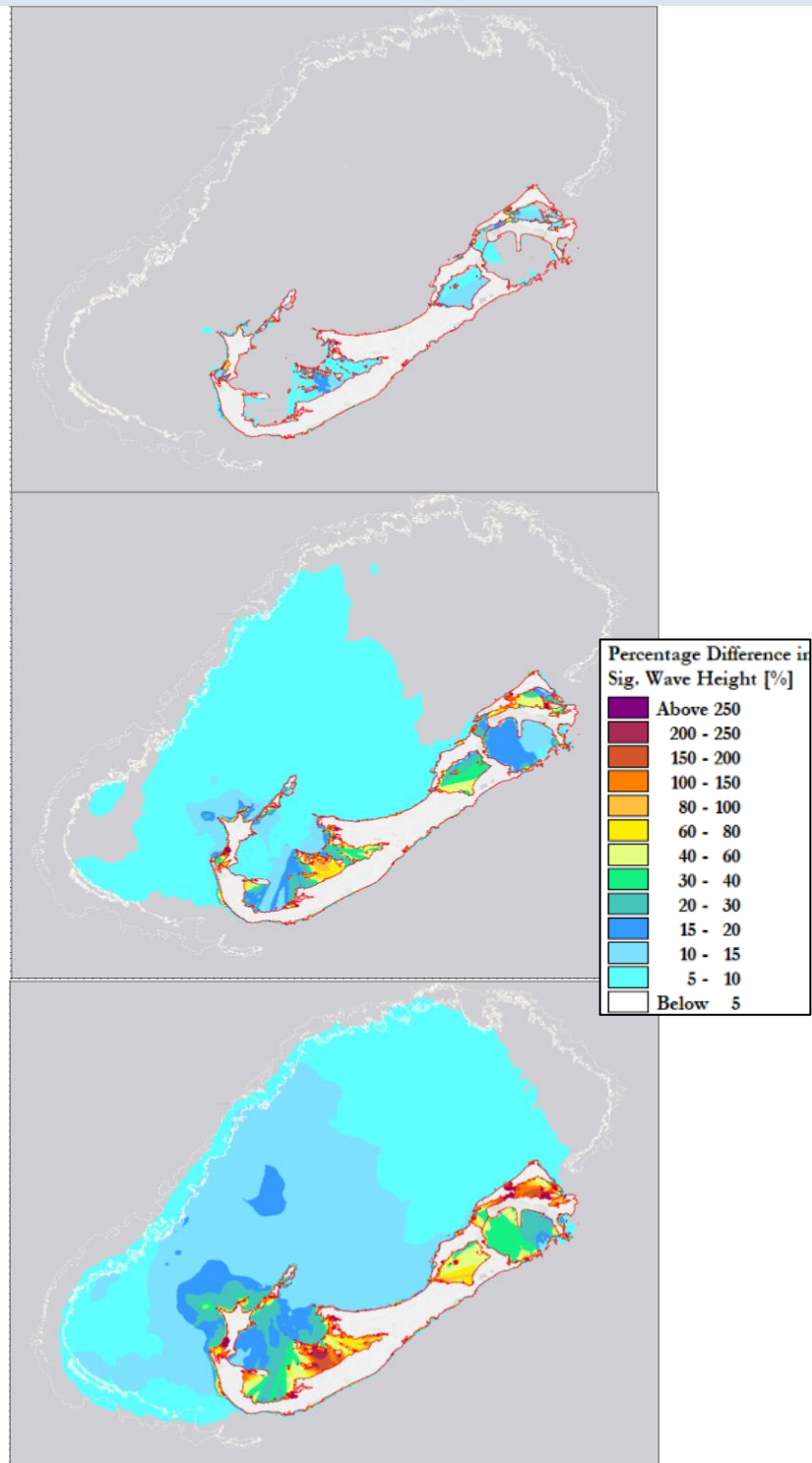




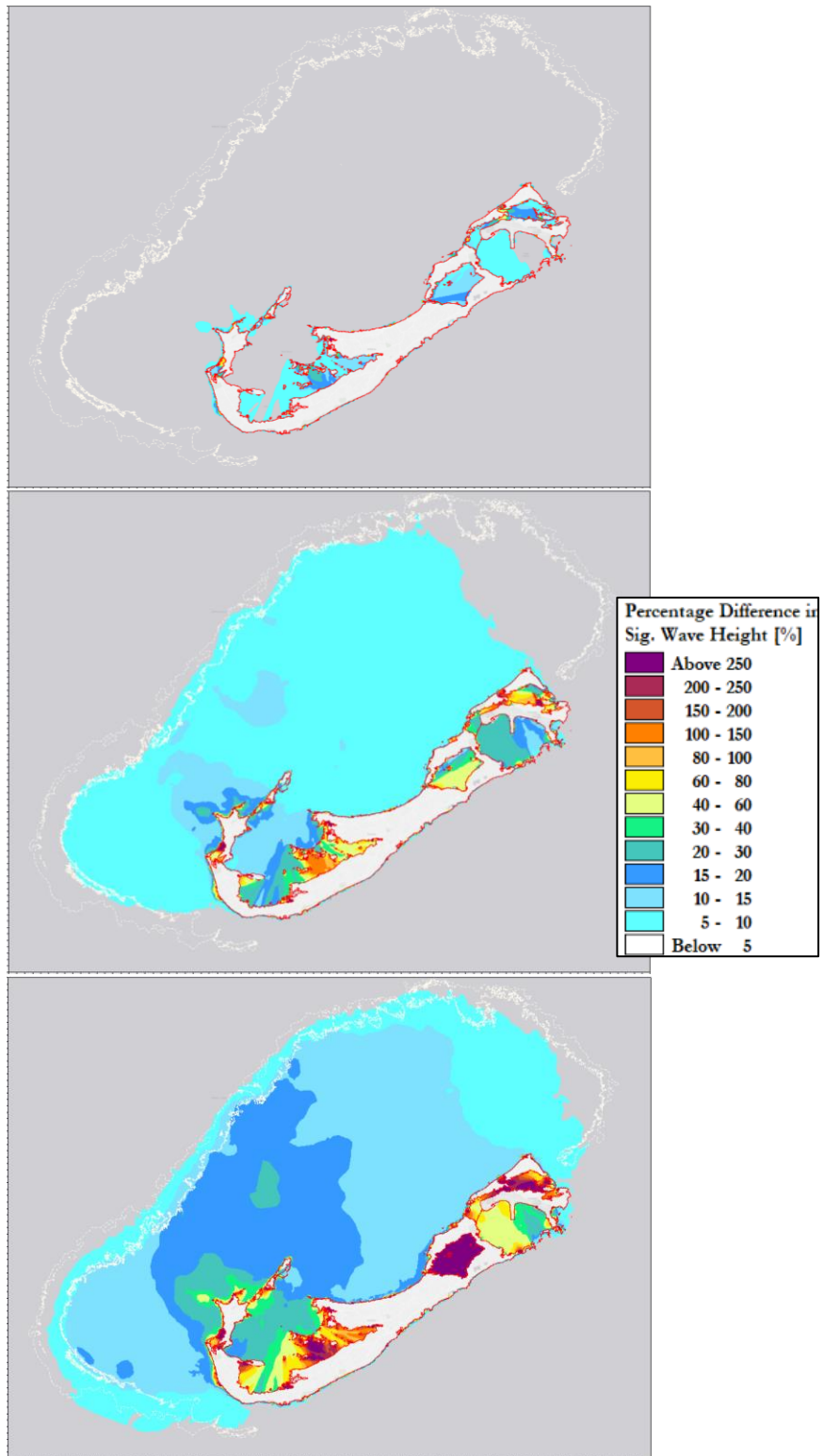




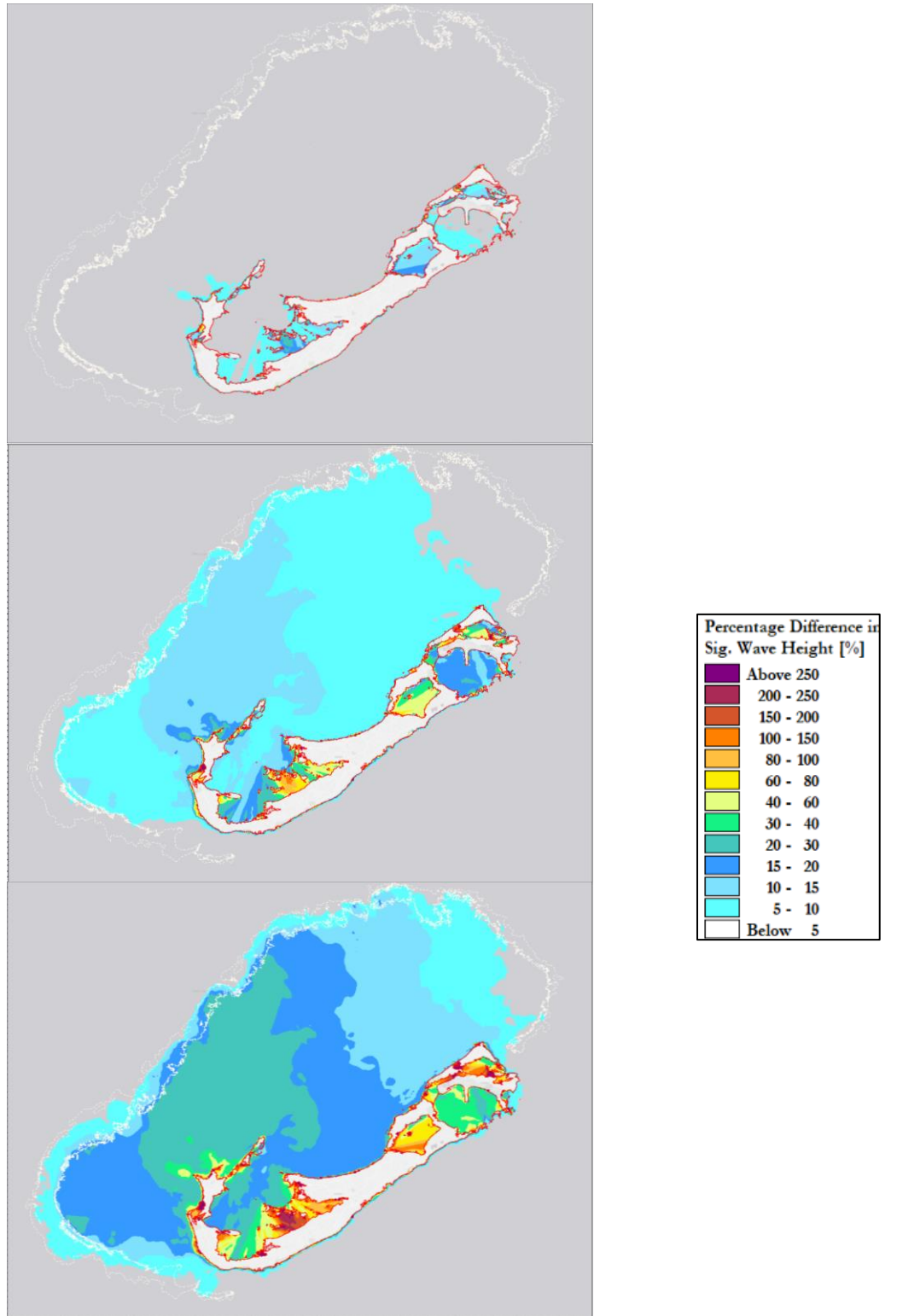
Appendix E – Additional Plots



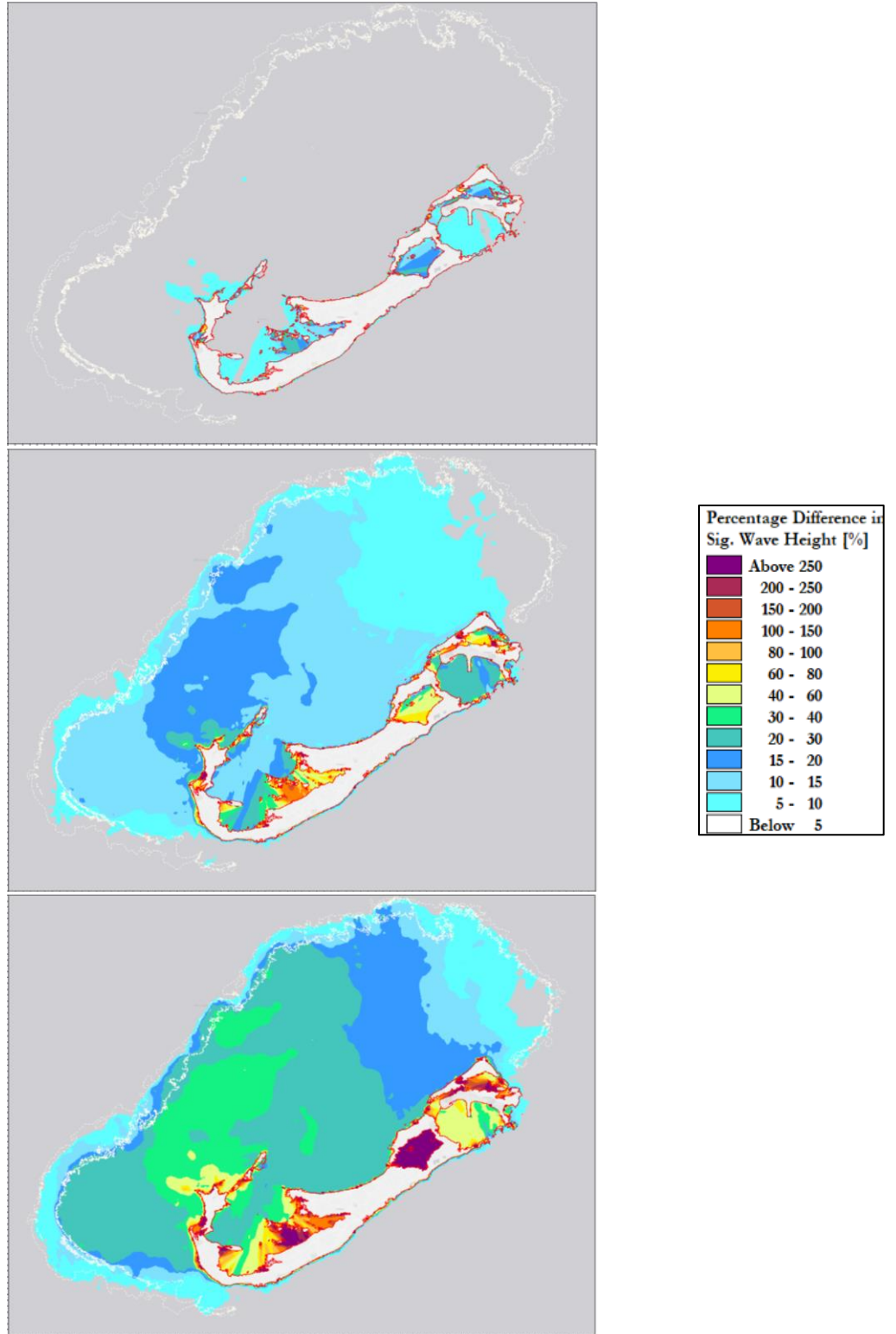
Changes in the Mean Wave Conditions under the RCP 4.5 for 20-year (top), 50-year (middle) and 100-year (bottom) horizons



Changes in the Mean Wave Conditions under the RCP 8.5 for (a) 20-year, (b) 50-year and (c) 100- year horizons

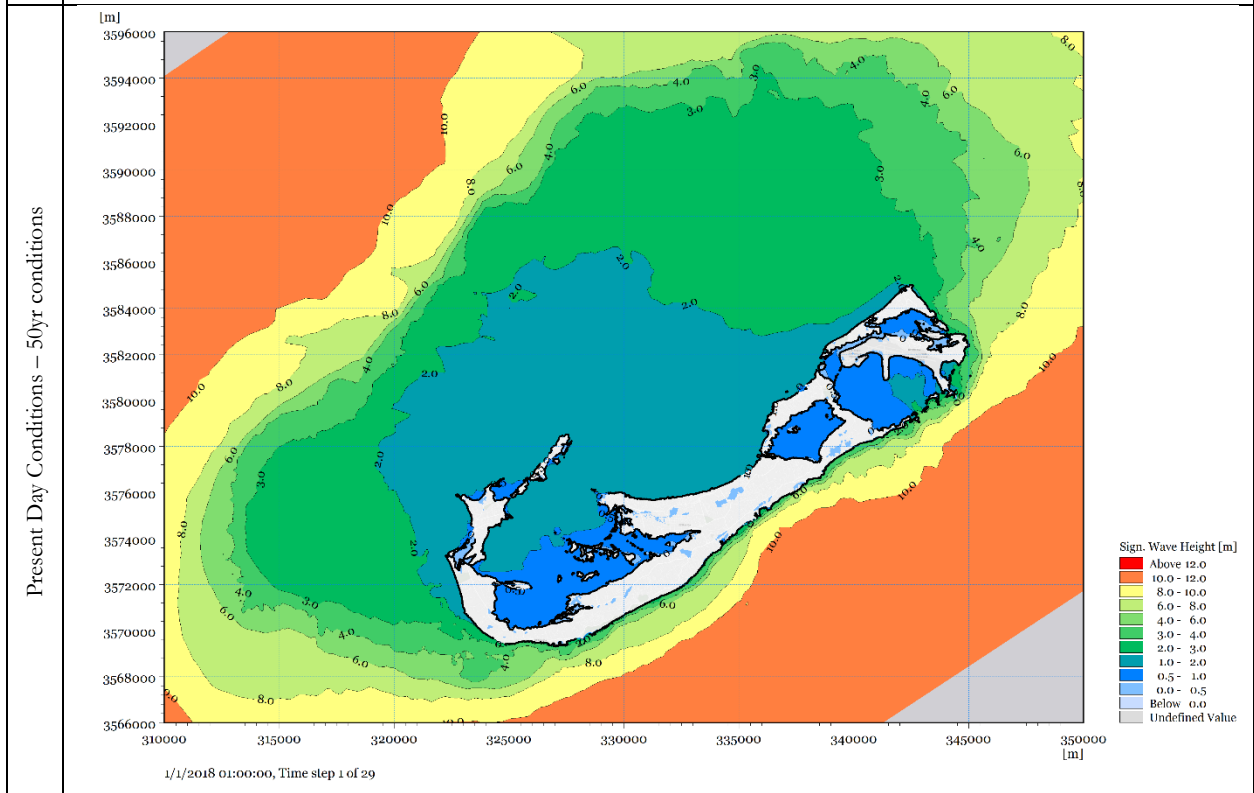
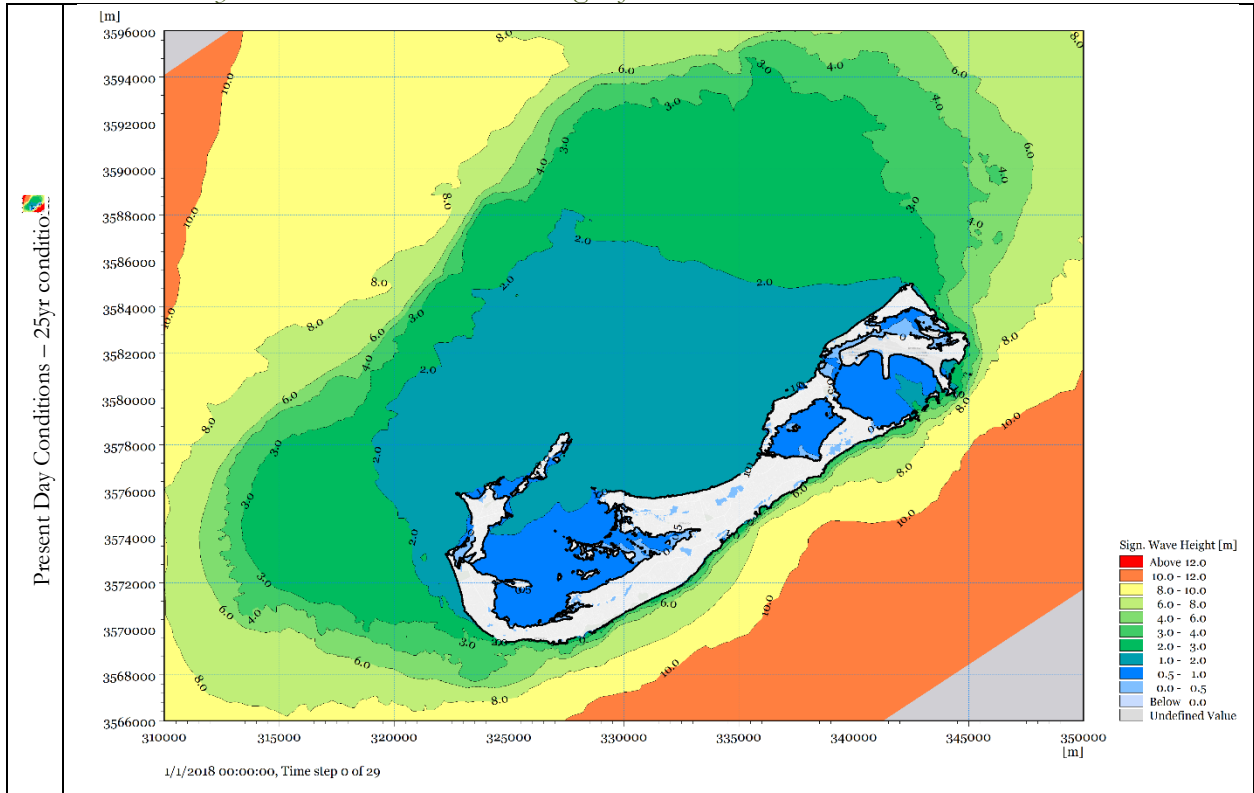


Changes in the 99th percentile under the RCP 4.5 for (a) 20-year, (b) 50-year and (c) 100- year horizons

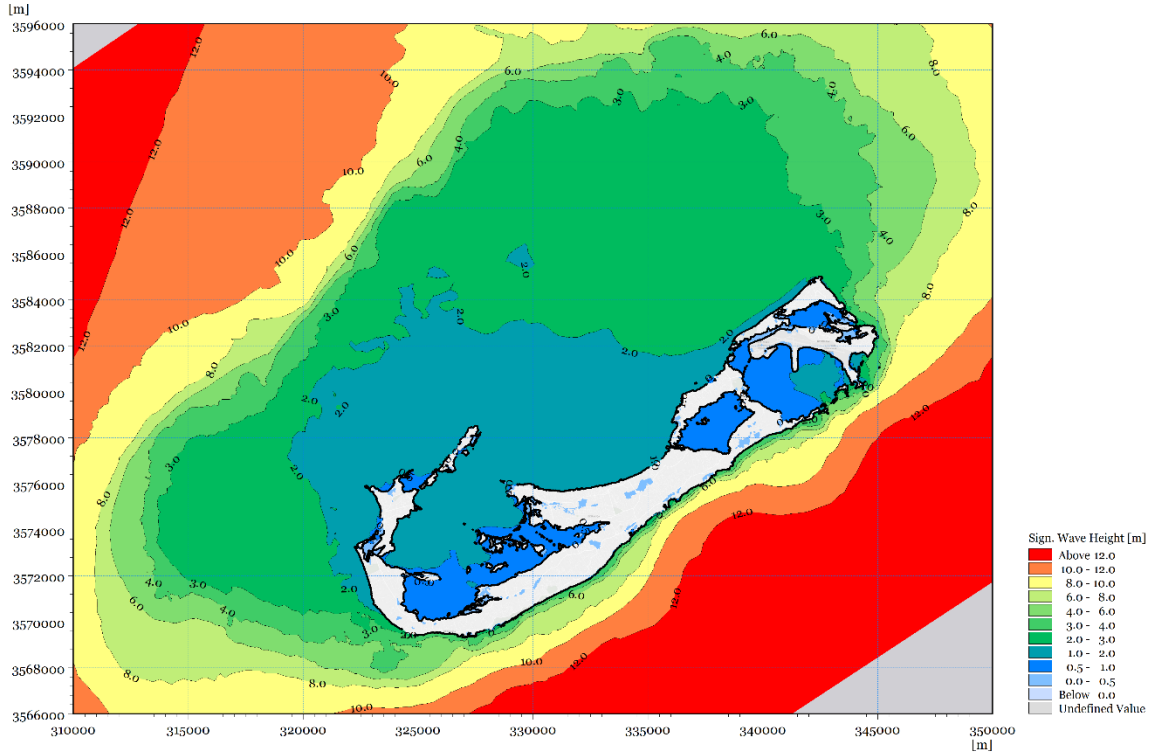


Changes in the 99th percentile under the RCP 8.5 for (a) 20-year, (b) 50-year and (c) 100- year Horizons

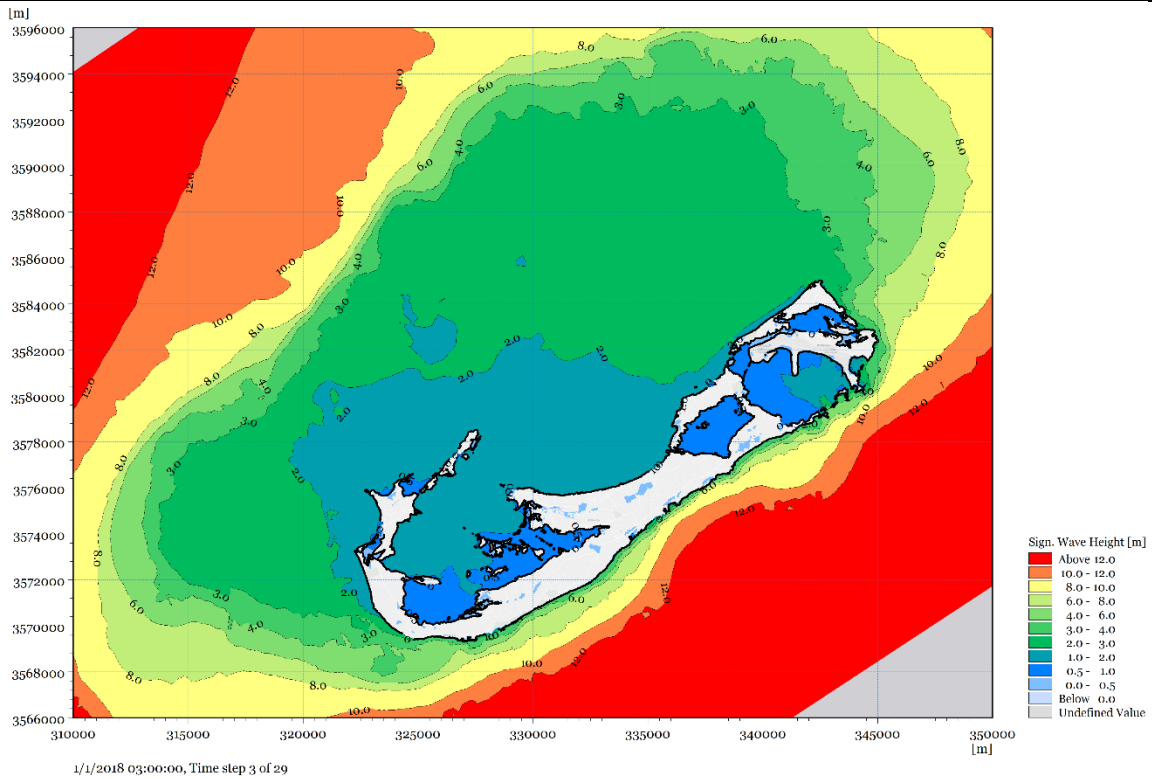
Present Day Conditions – Bermuda including reefs



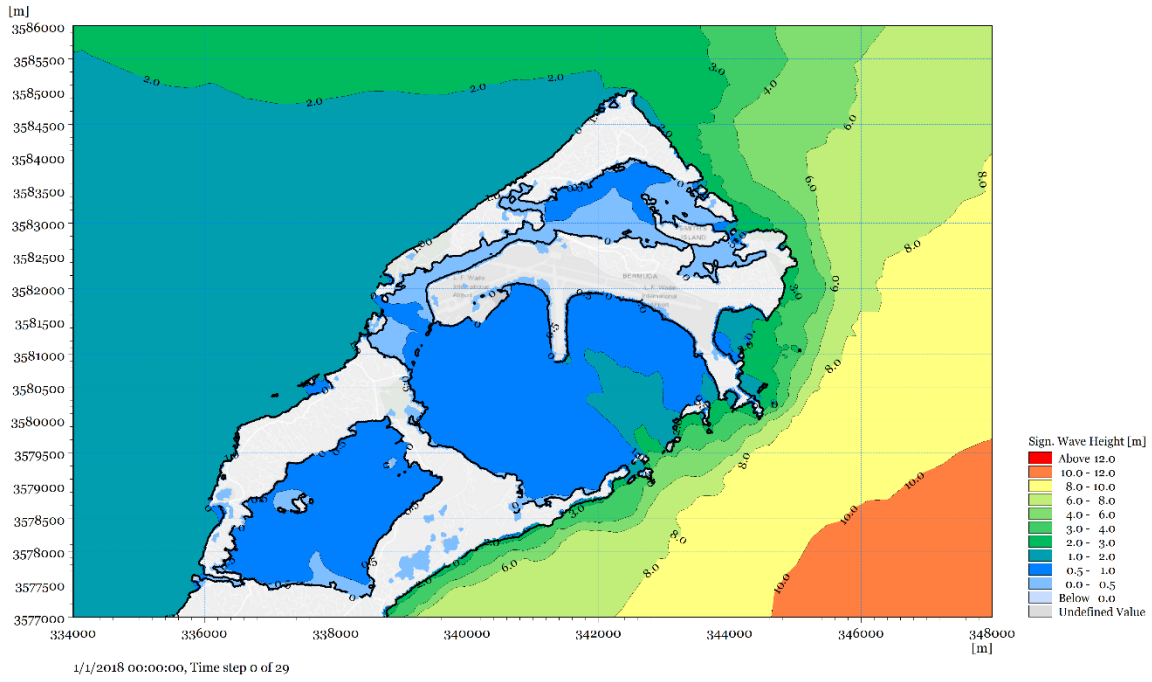
Present Day Conditions – 100yr conditions



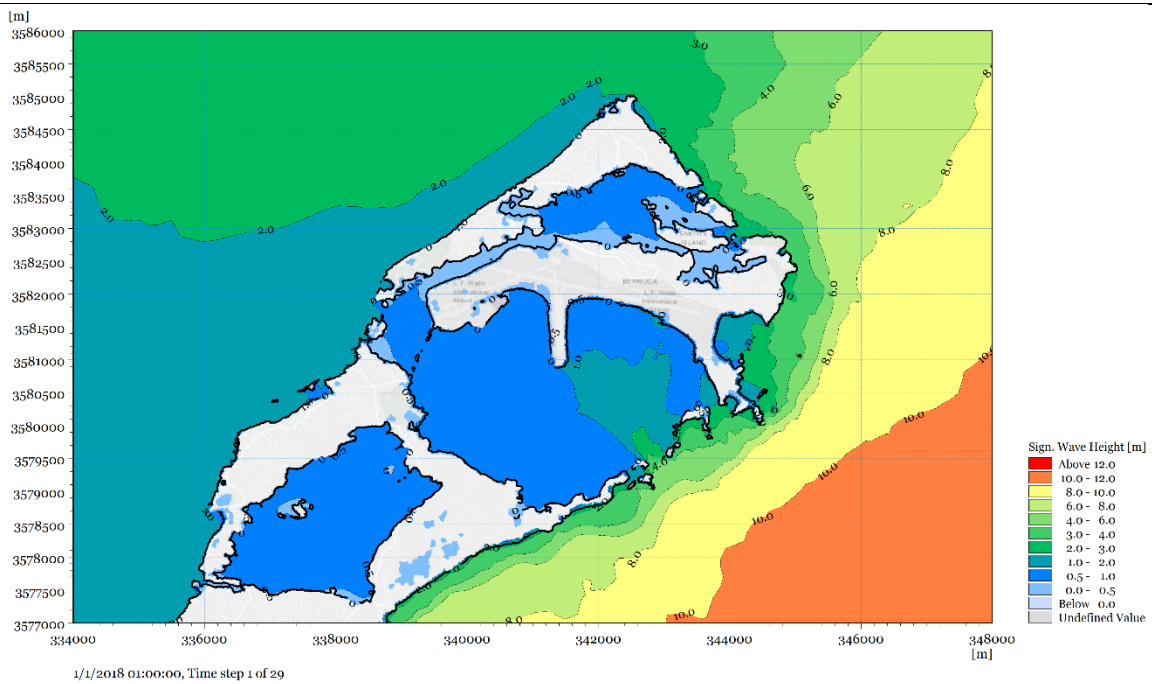
Present Day Conditions – 150yr conditions



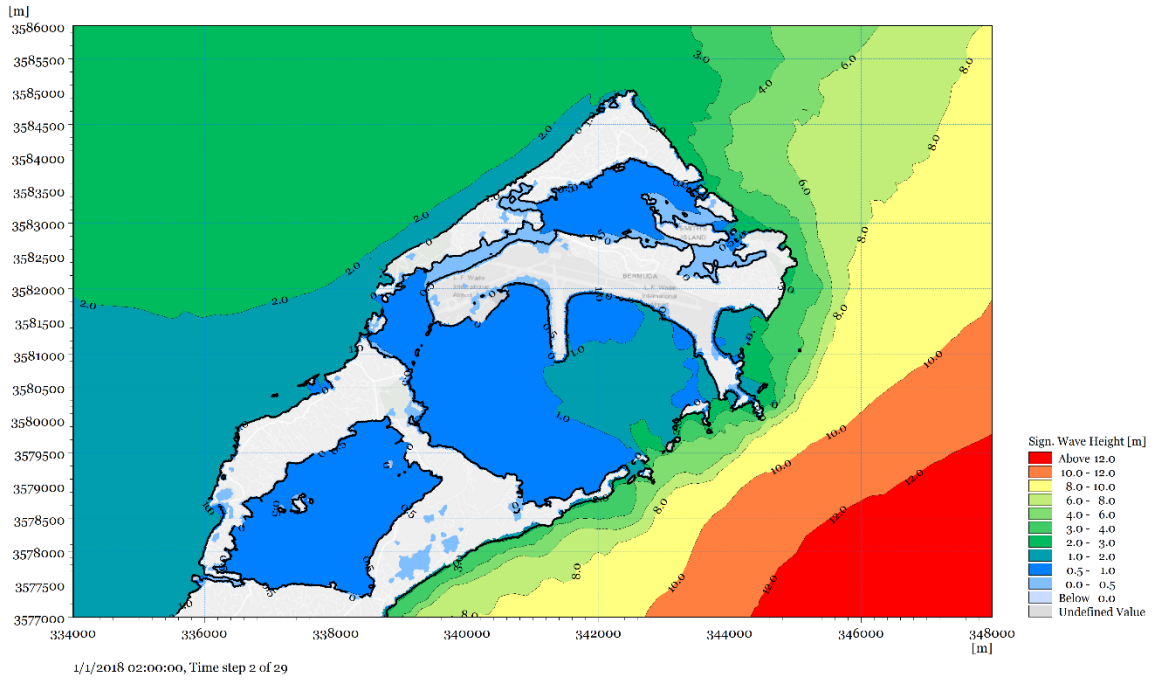
Present Day Conditions – 25yr conditions



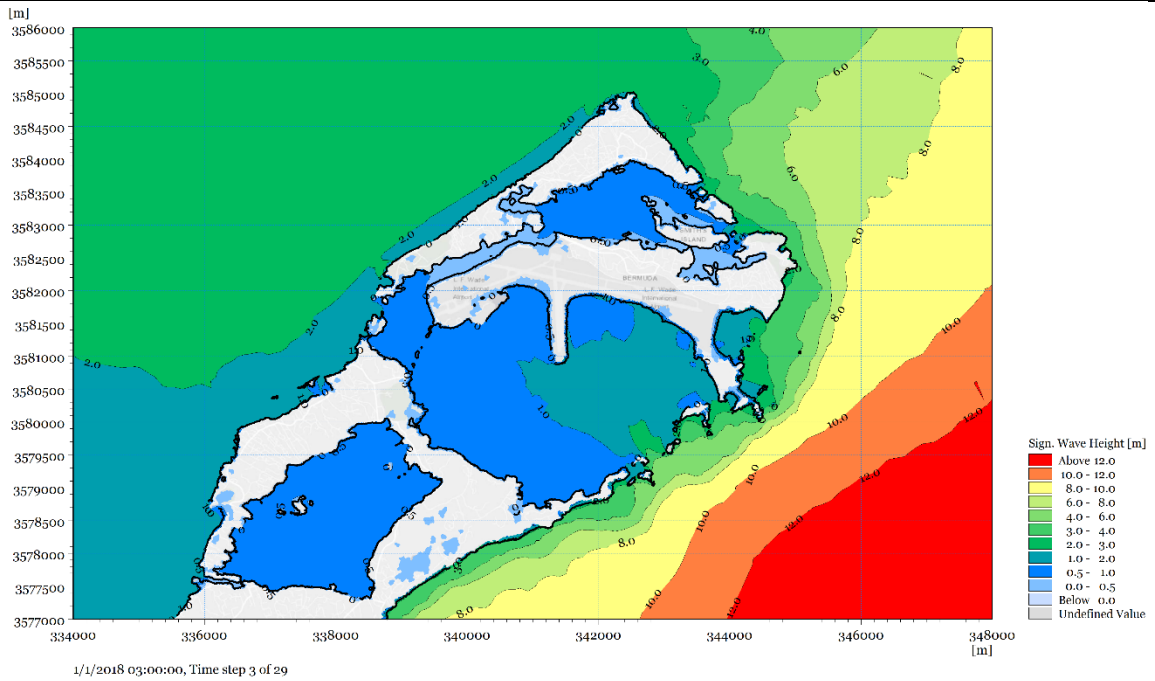
Present Day Conditions – 50yr conditions



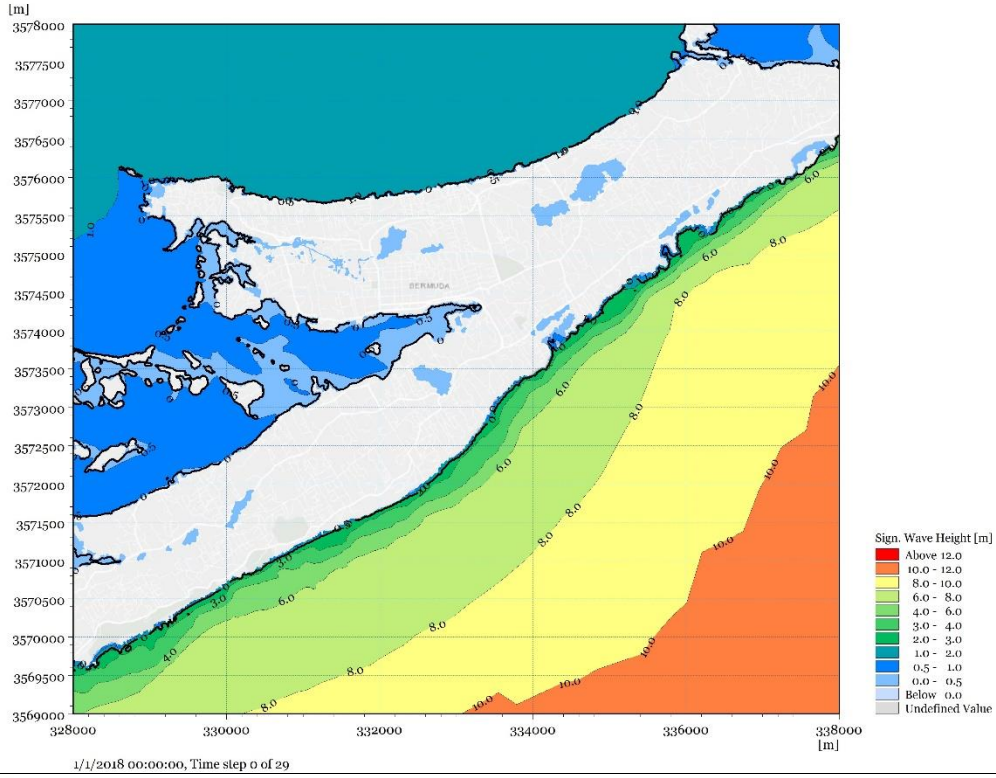
Present Day Conditions – 100yr conditions



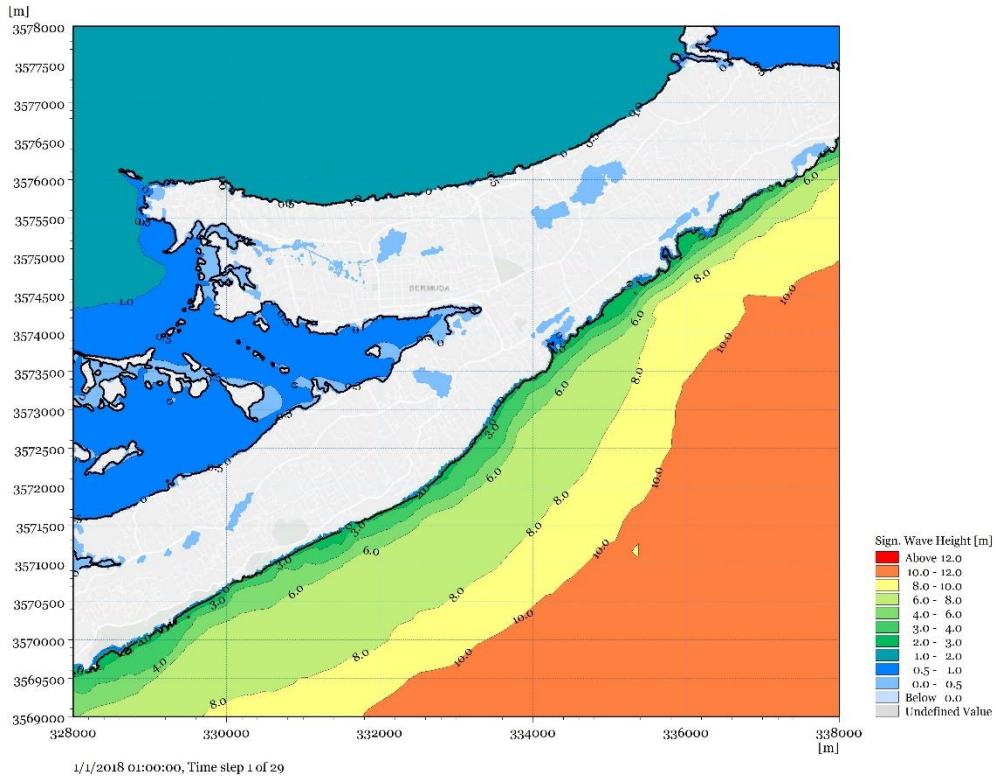
Present Day Conditions – 150yr conditions



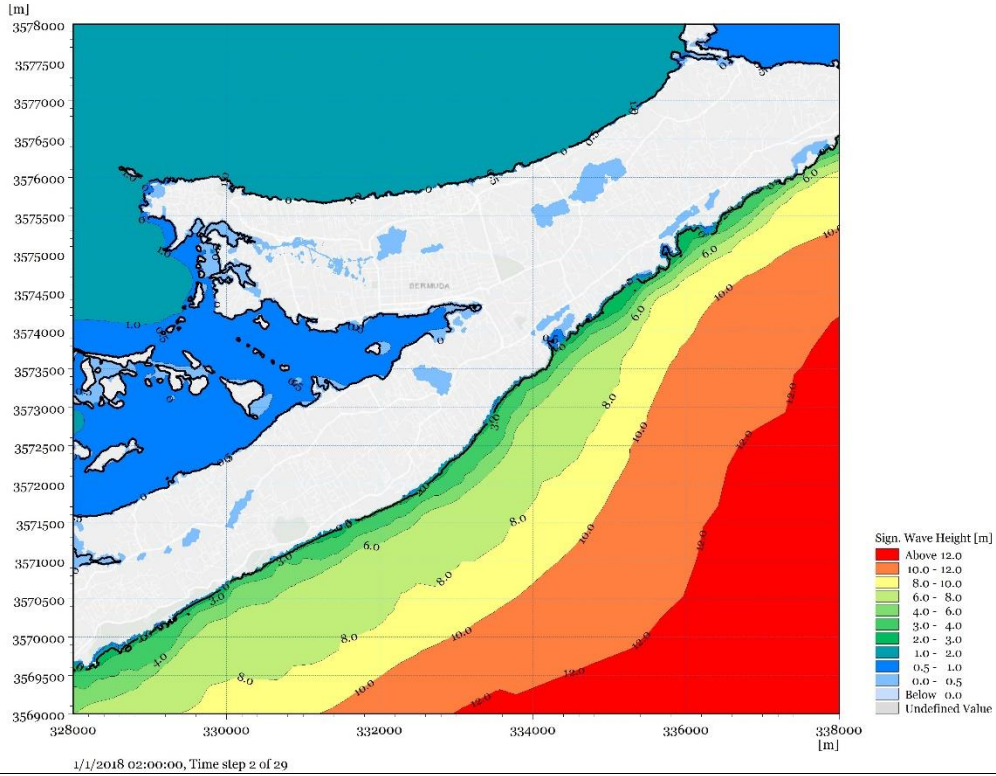
Present Day Conditions – 25yr conditions



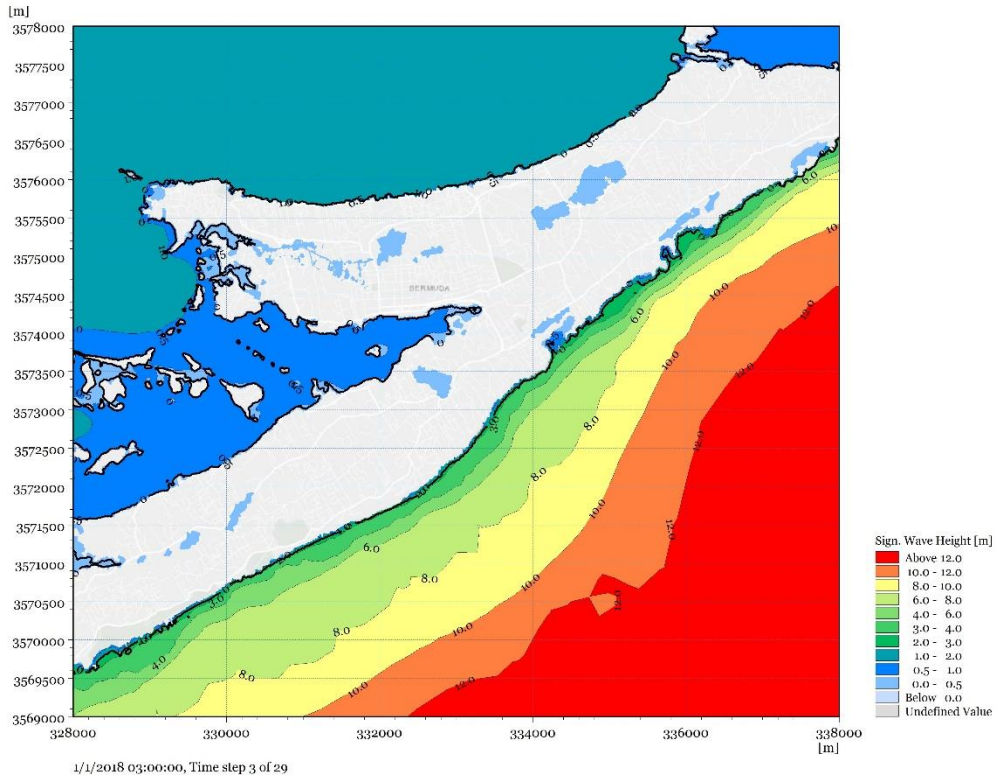
Present Day Conditions – 50yr conditions



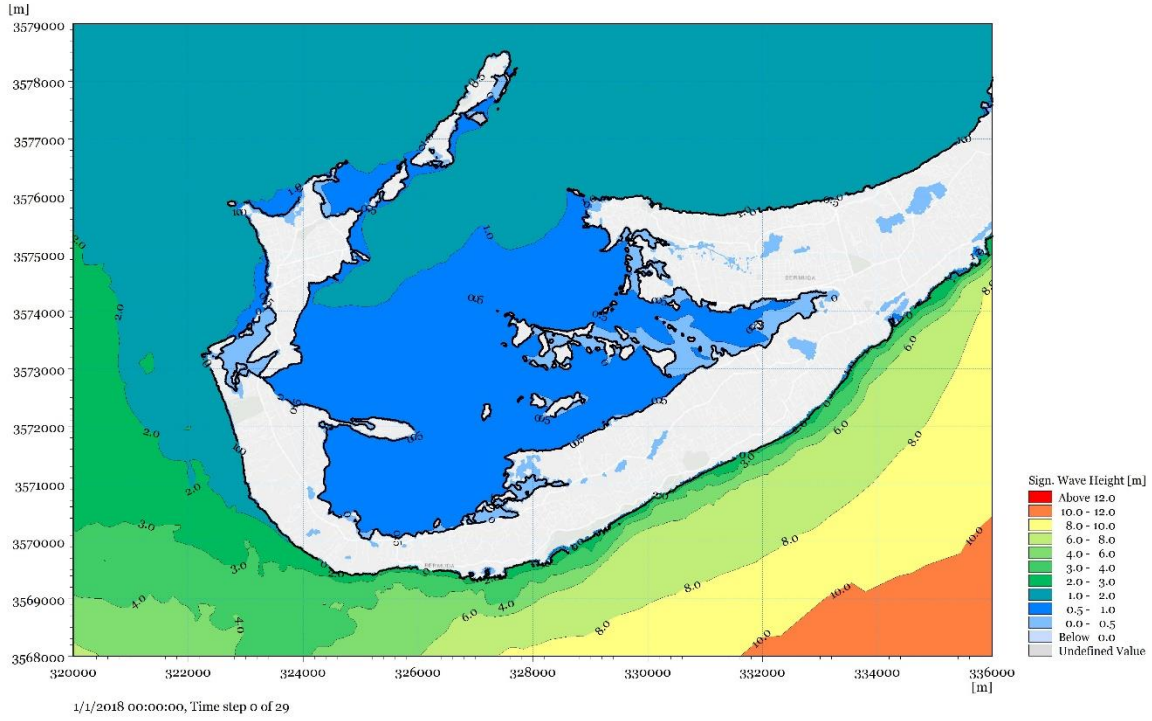
Present Day Conditions – 100yr conditions



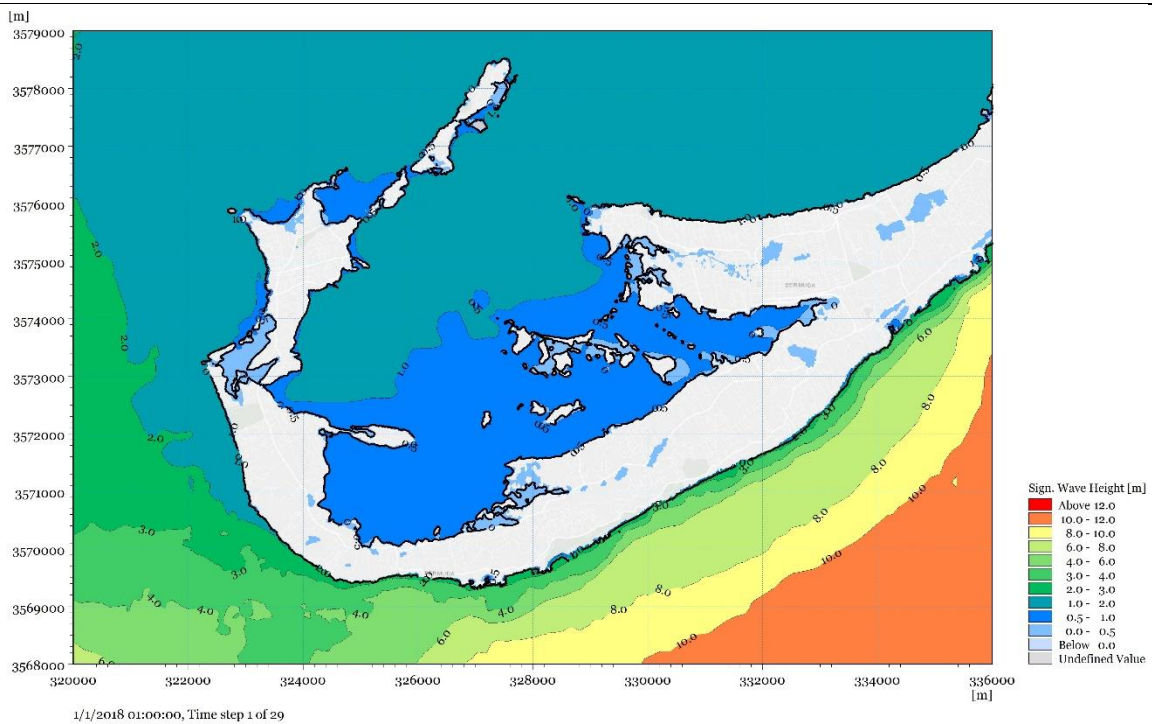
Present Day Conditions – 150yr conditions



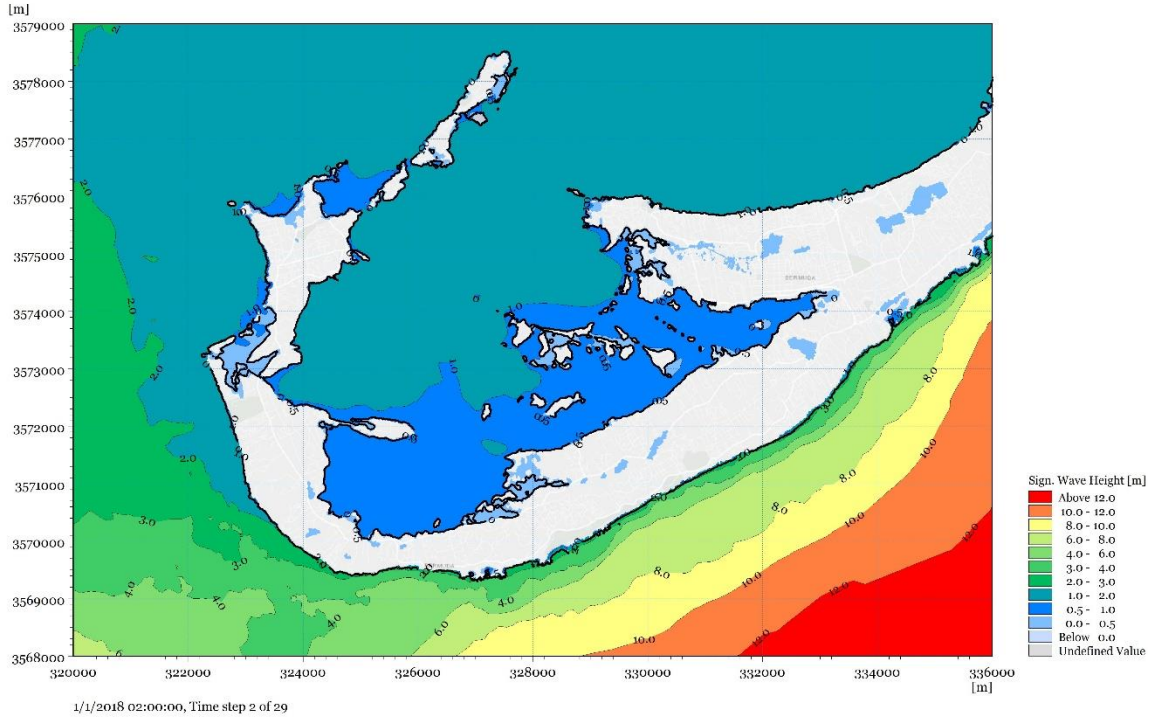
Present Day Conditions – 25yr conditions



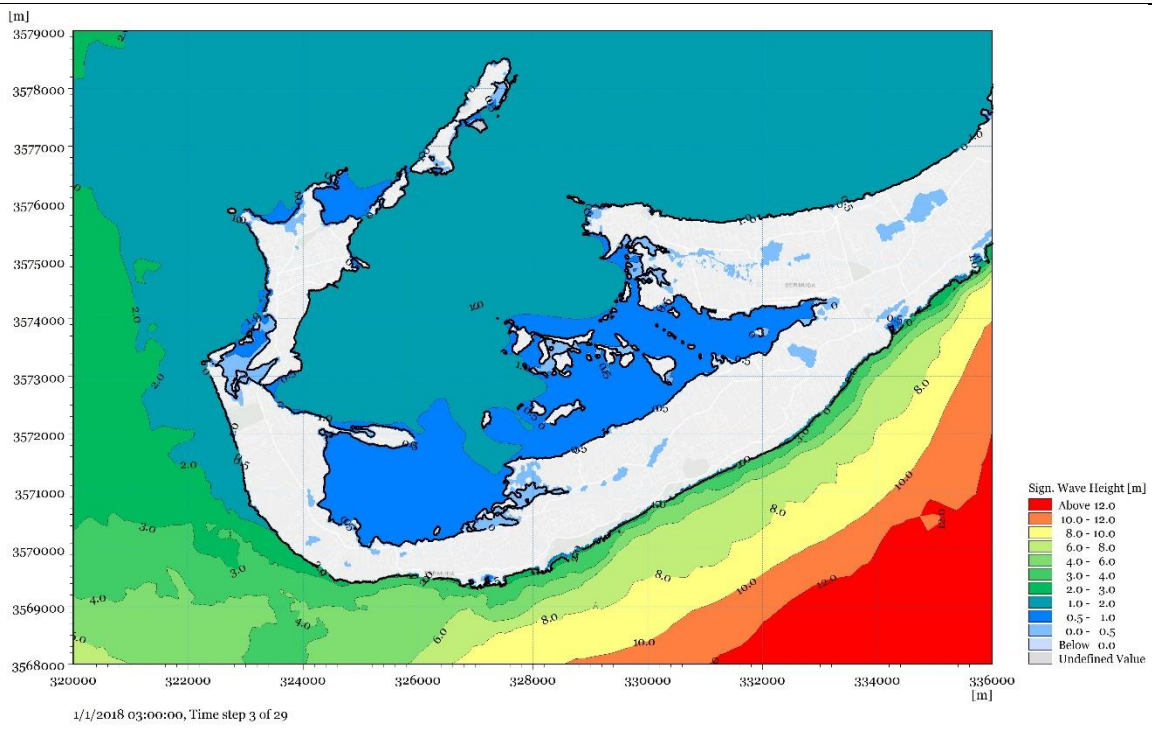
Present Day Conditions – 50yr conditions



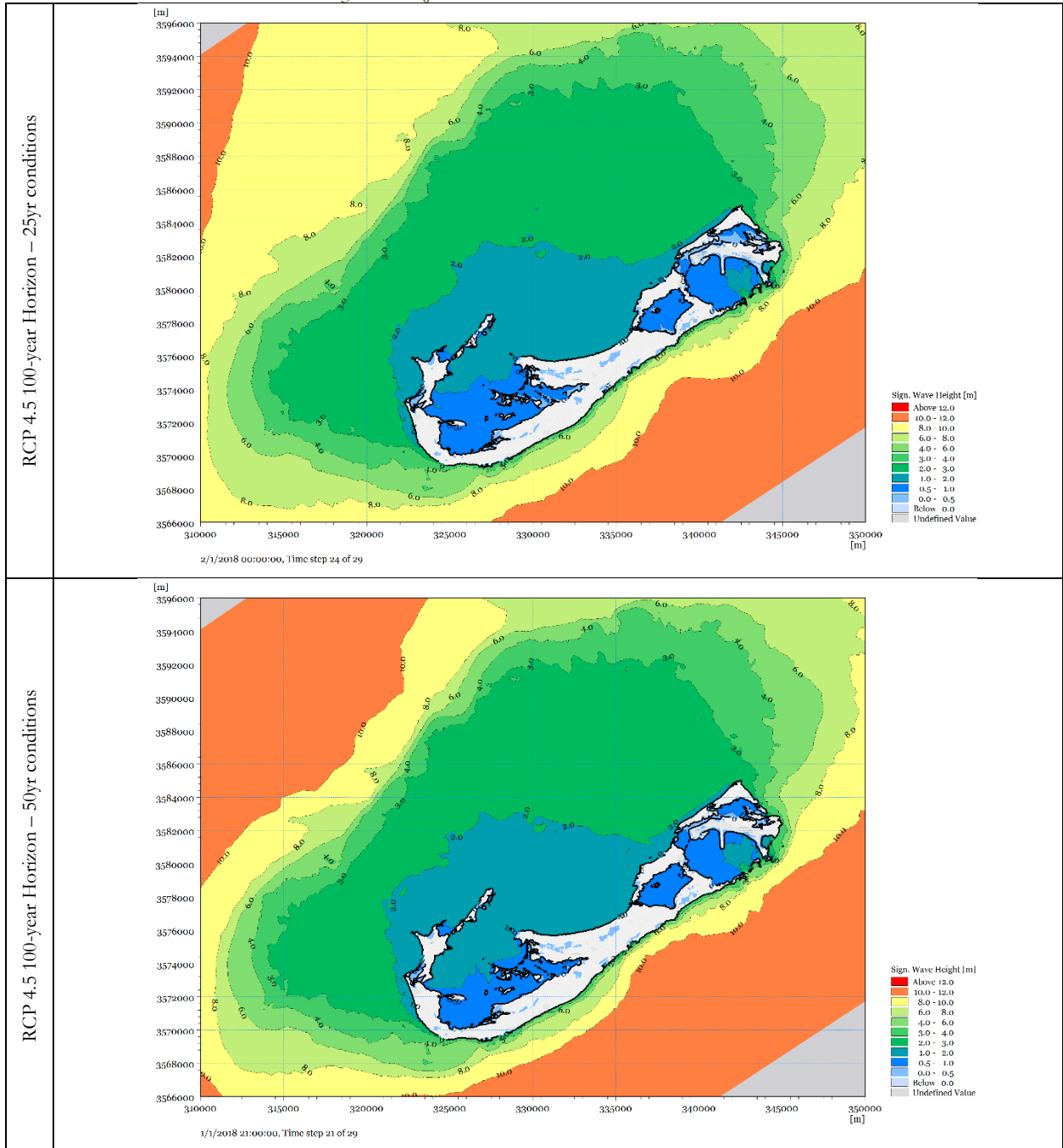
Present Day Conditions – 100yr conditions



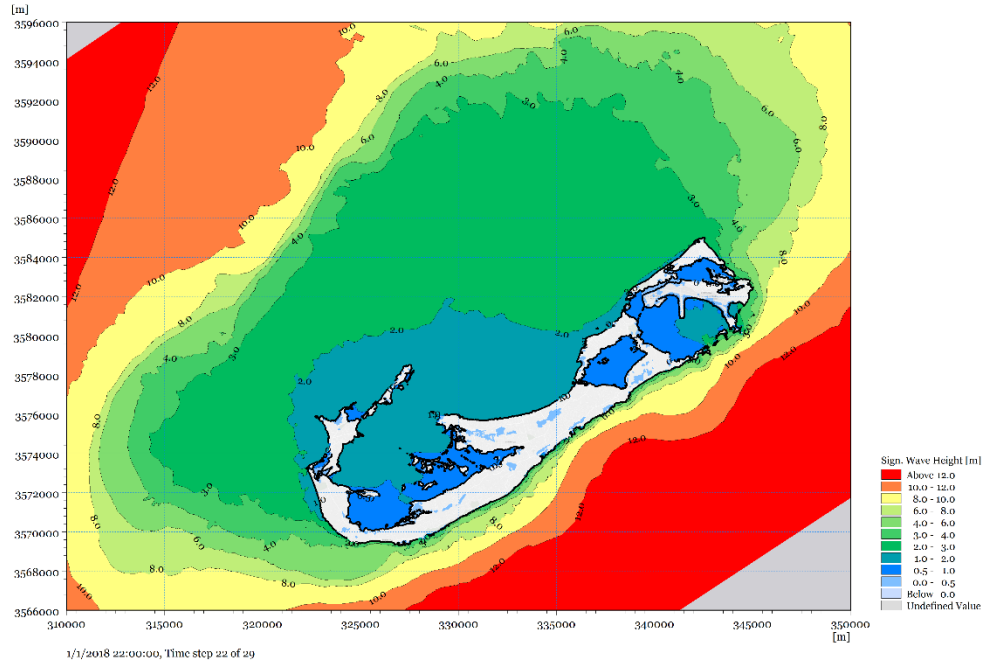
Present Day Conditions – 150yr conditions



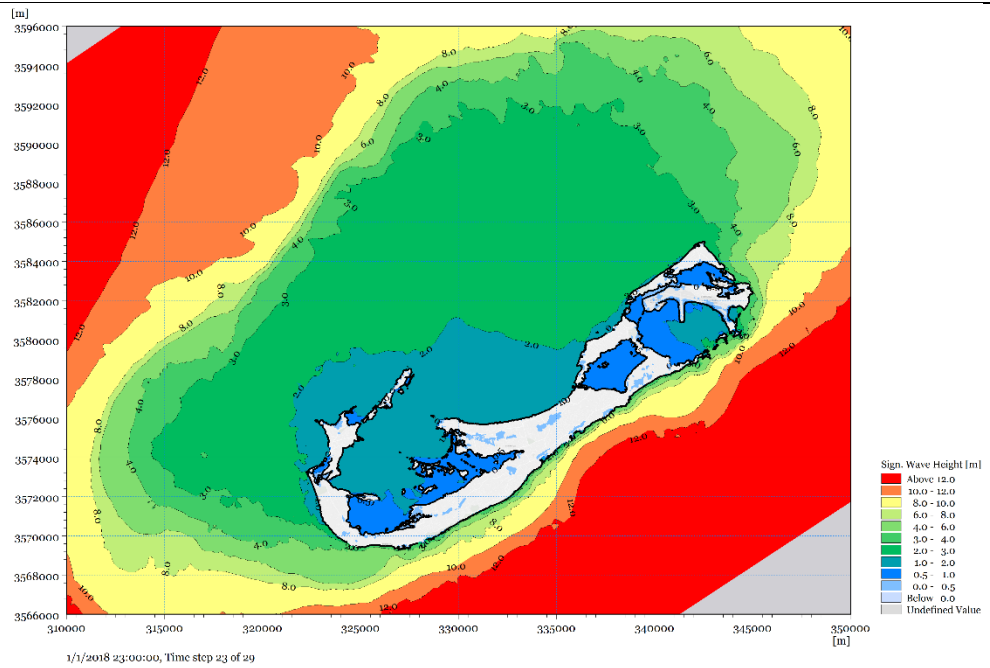
RCP 4.5 – Bermuda – 100yr Horizon



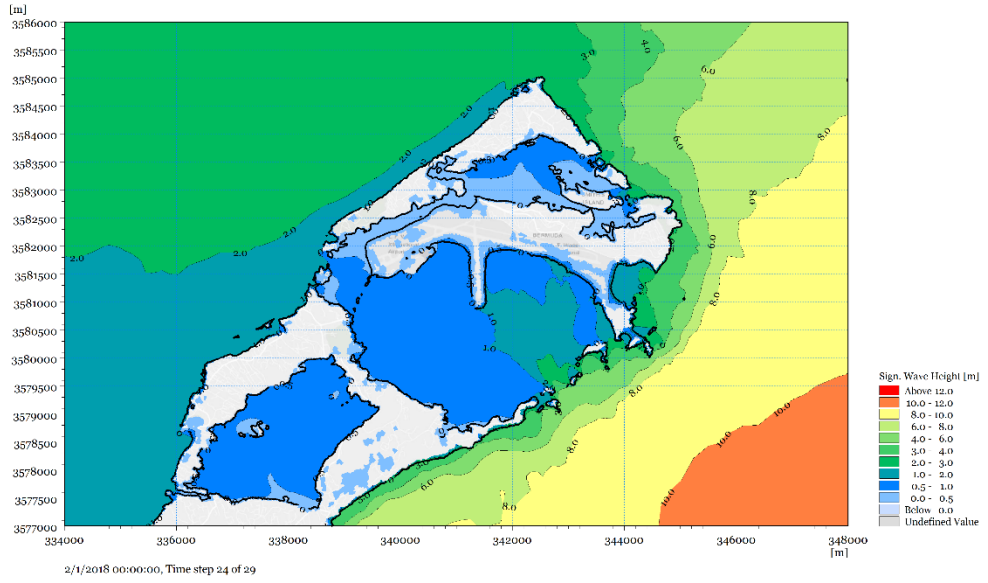
RCP 4.5 100 year Horizon – 100yr conditions



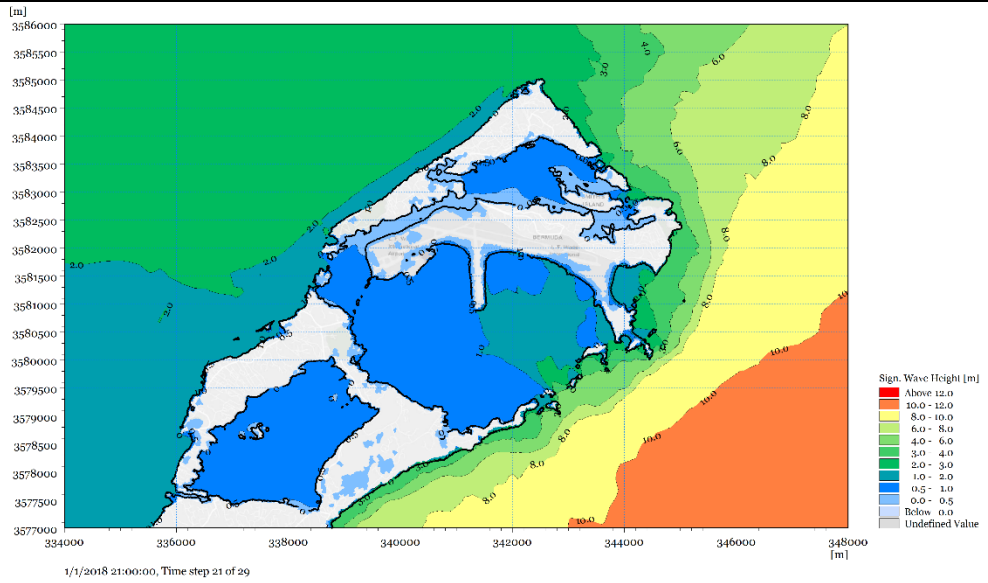
RCP 4.5 100 year Horizon – 150yr conditions



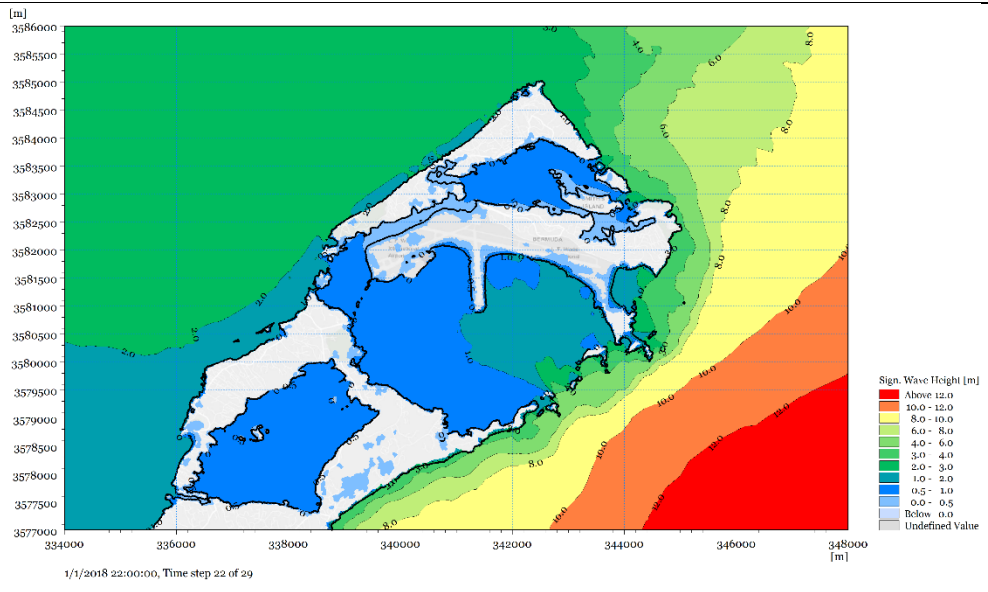
RCP 4.5 100-year Horizon – 25yr conditions



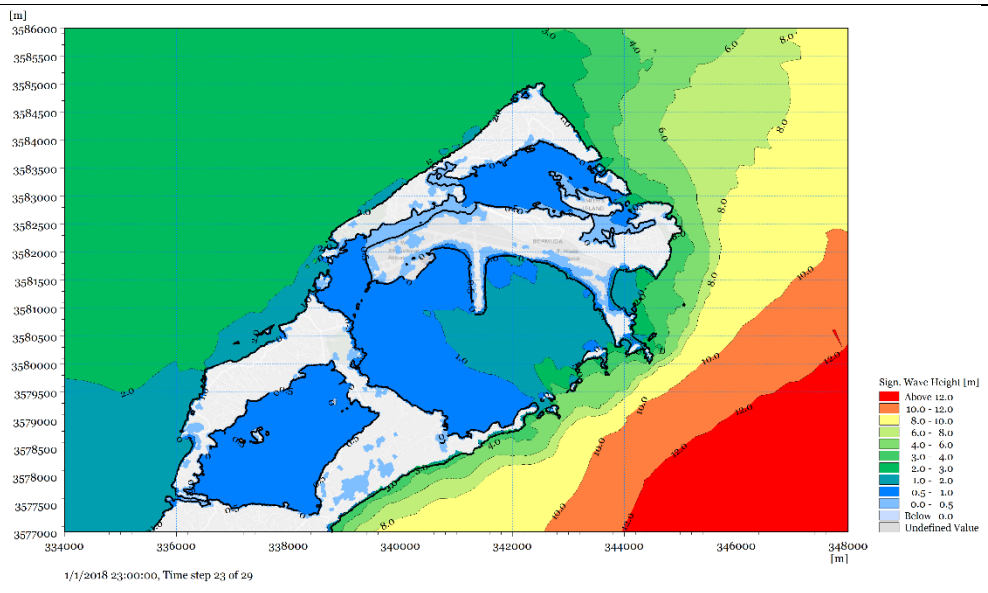
RCP 4.5 100-year Horizon – 50yr conditions



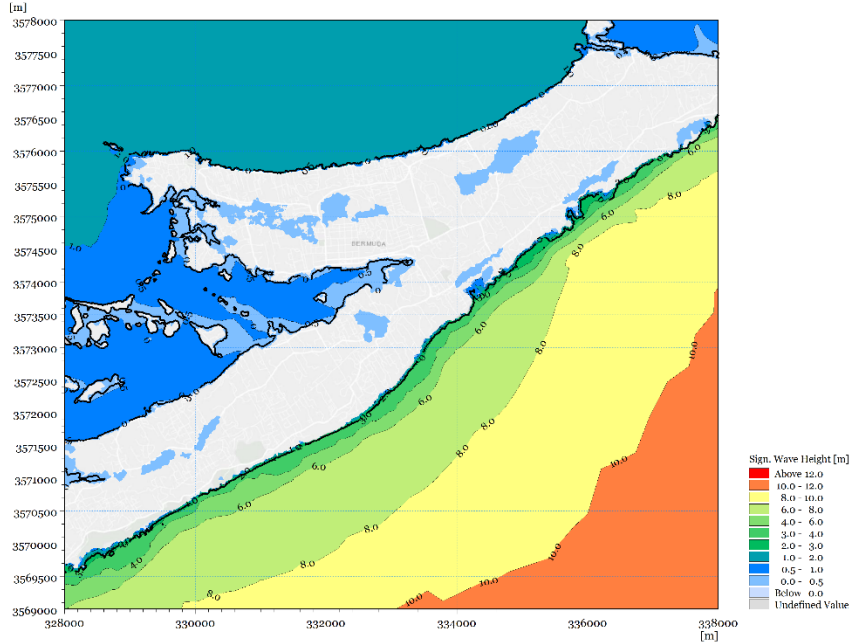
RCP 4.5 100 year Horizon – 100yr conditions



RCP 4.5 100 year Horizon – 150yr conditions

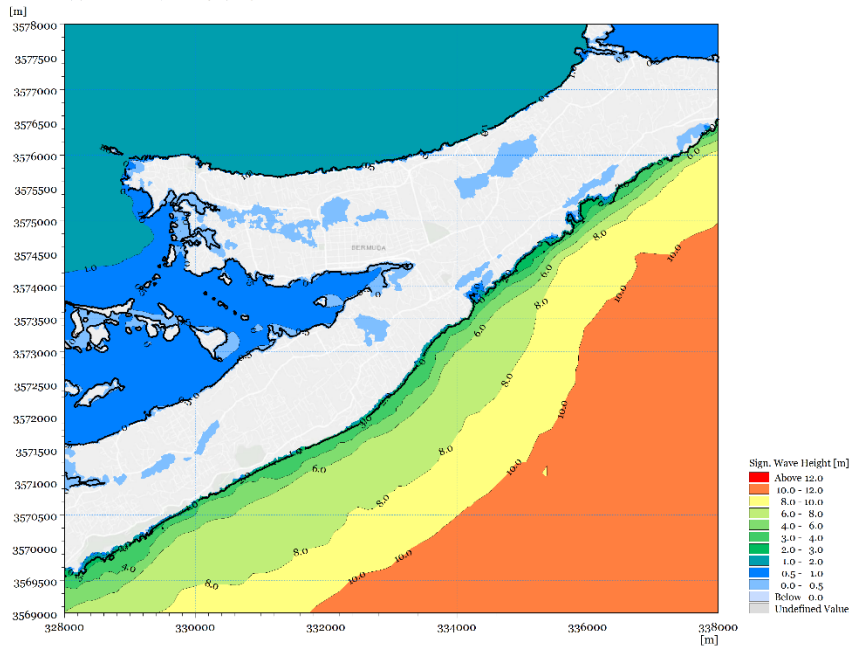


RCP 4.5 100-year Horizon – 25yr conditions

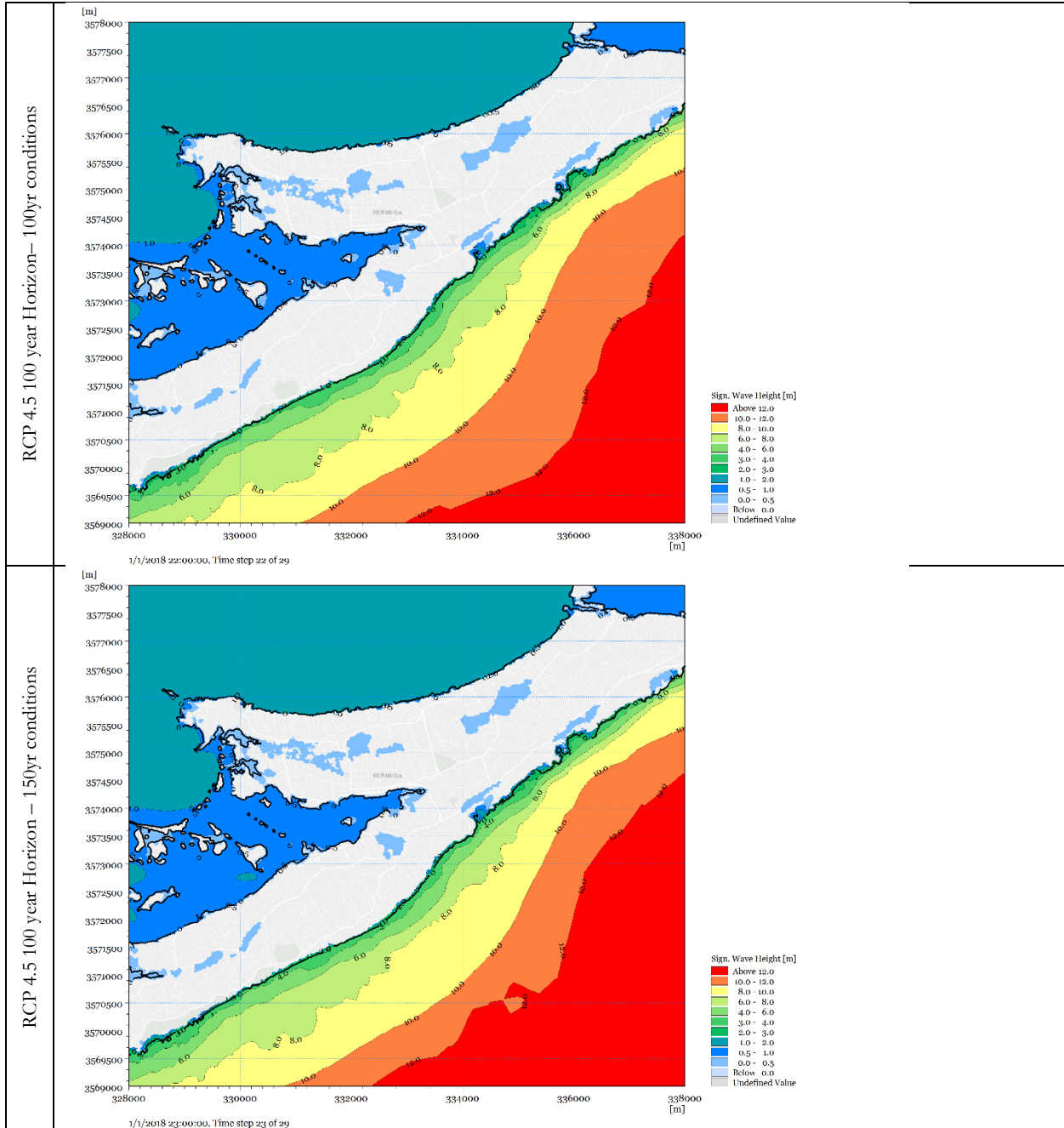


2/1/2018 00:00:00, Time step 24 of 29

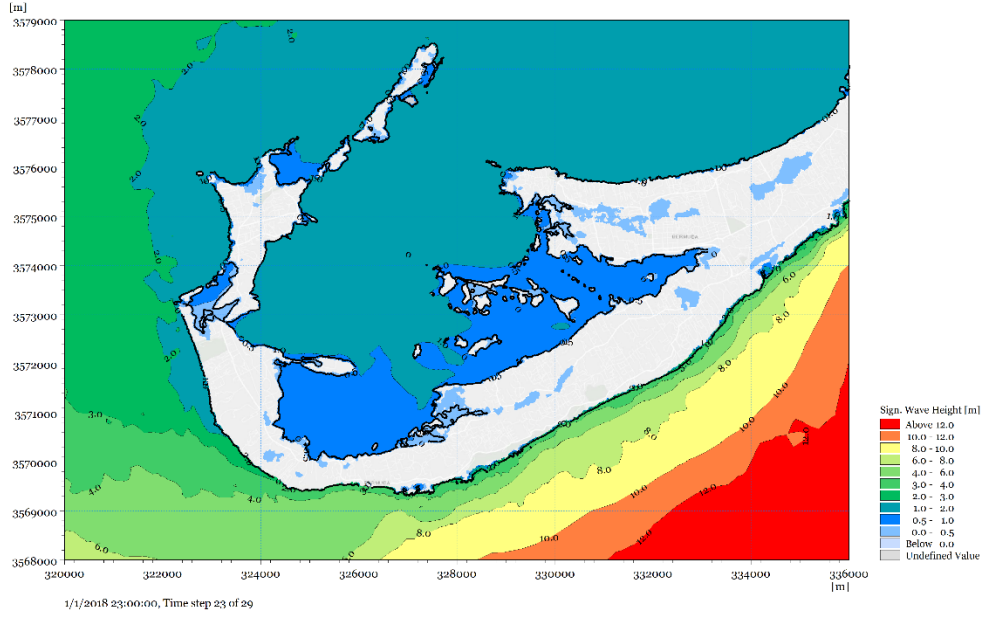
RCP 4.5 100-year Horizon – 50yr conditions



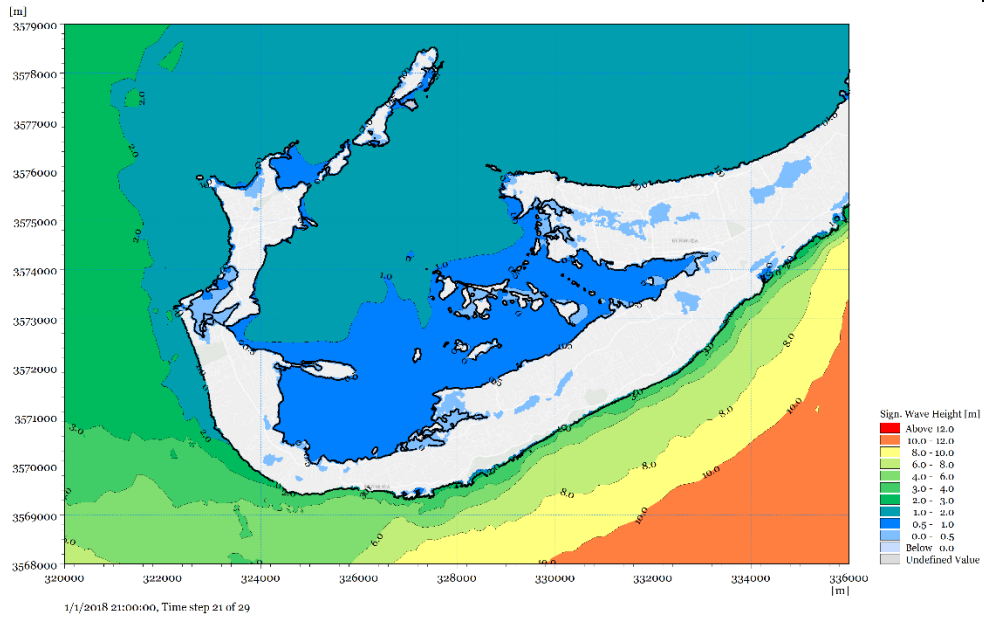
1/1/2018 21:00:00, Time step 21 of 29



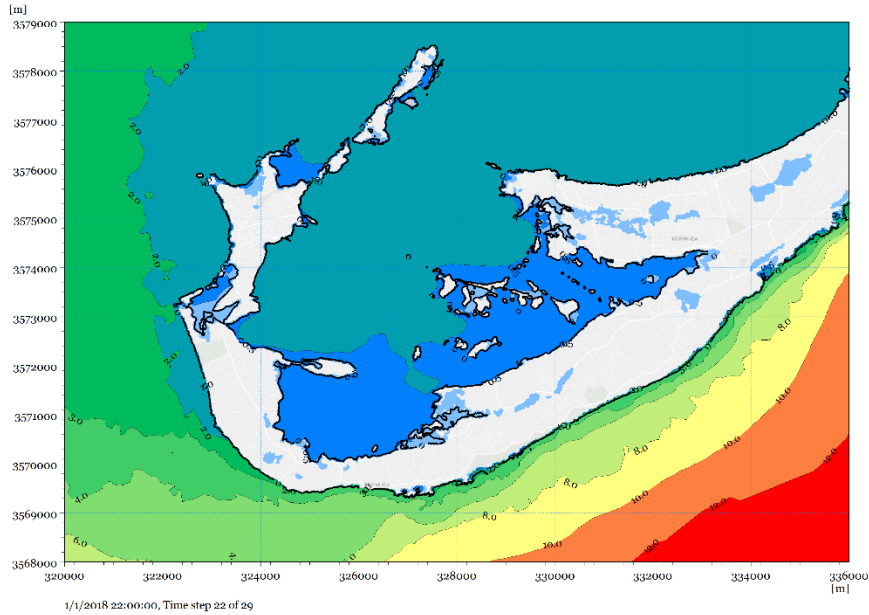
RCP 4.5 100-year Horizon – 25yr conditions



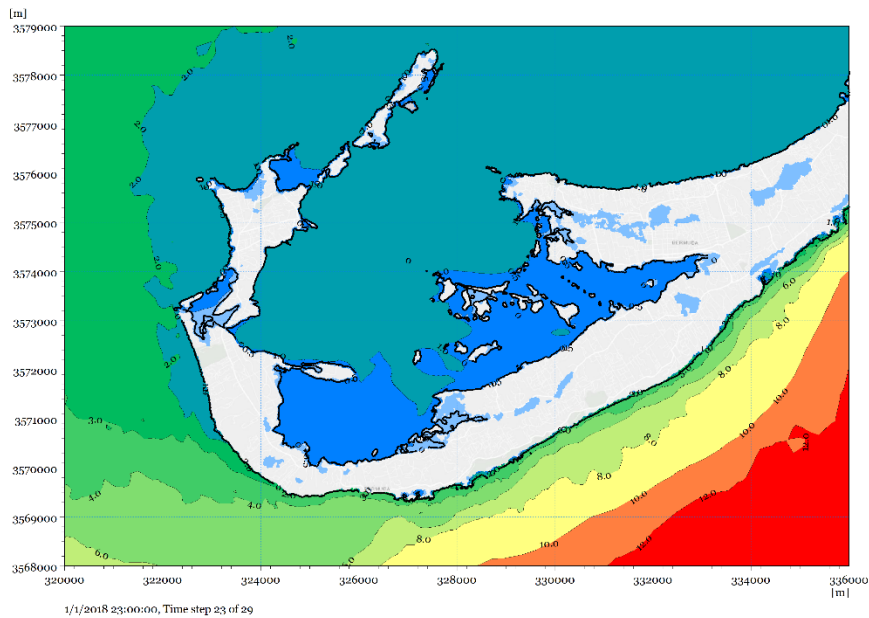
RCP 4.5 100-year Horizon – 50yr conditions



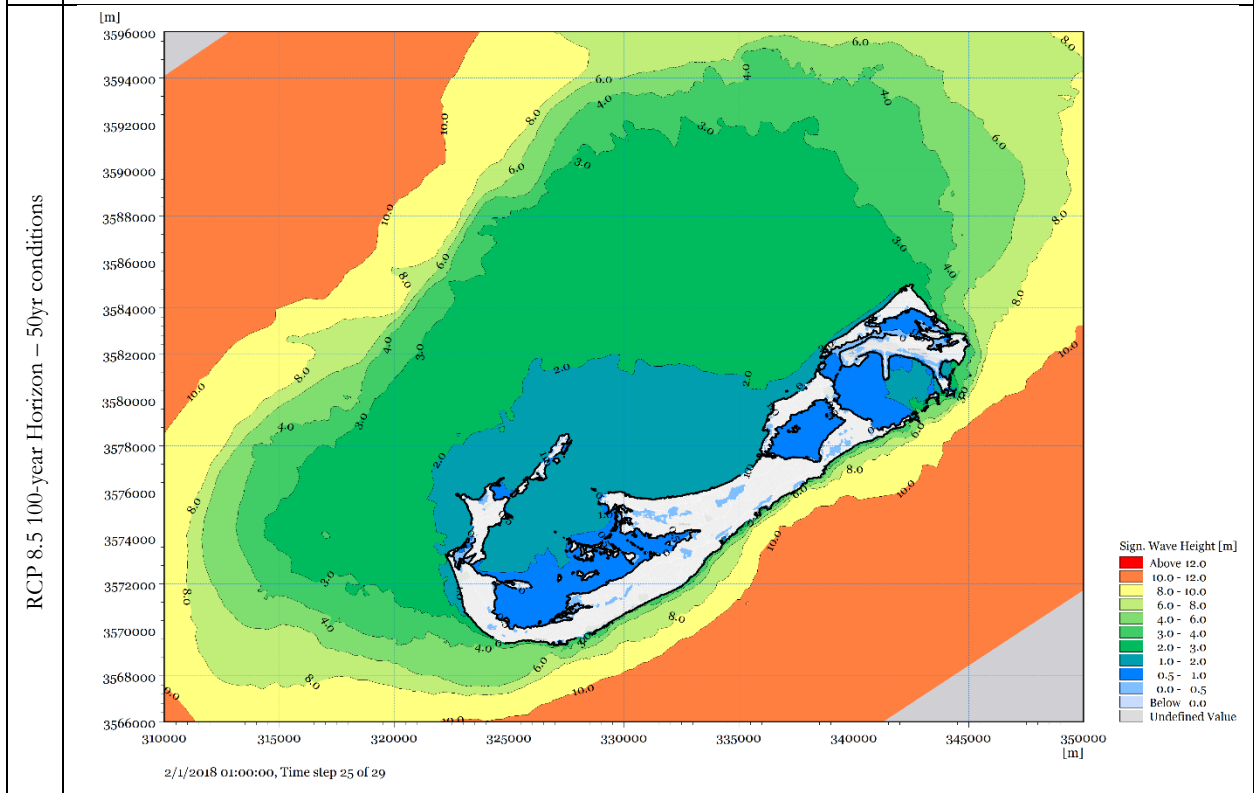
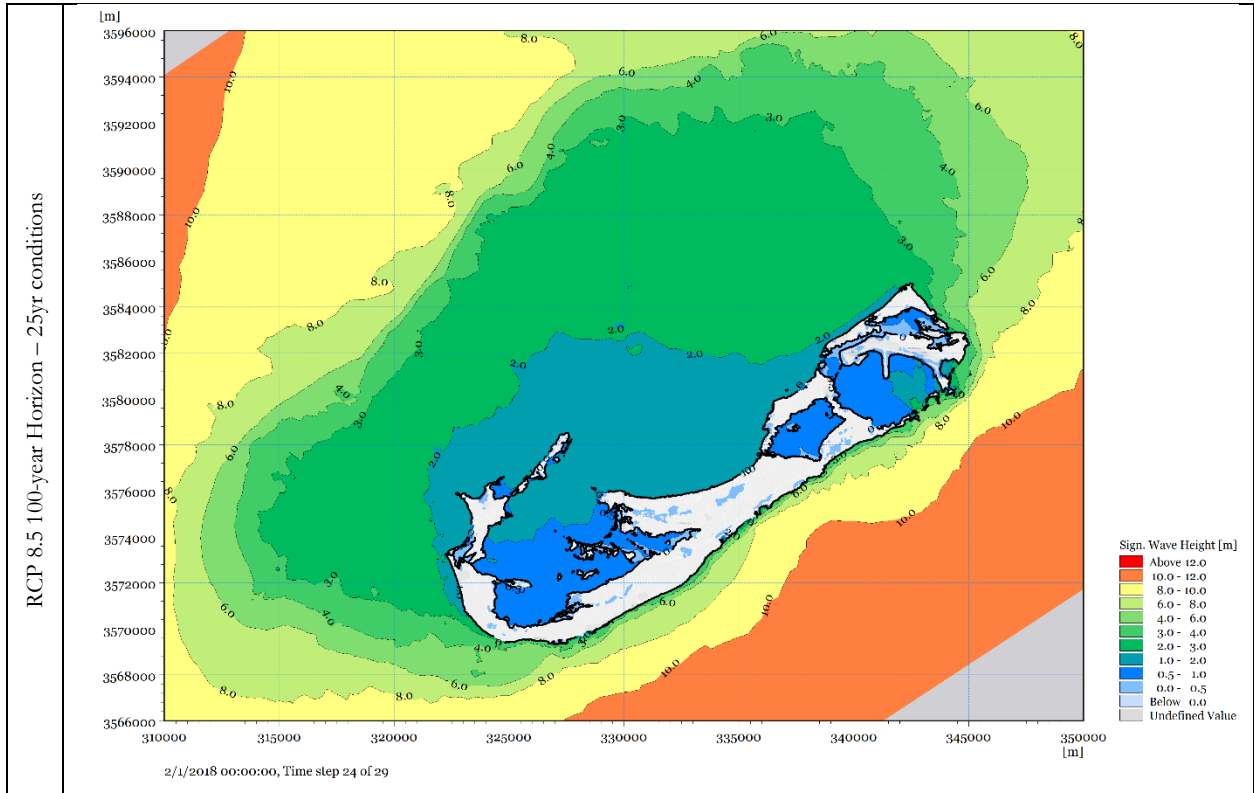
RCP 4.5 100 year Horizon – 100yr conditions



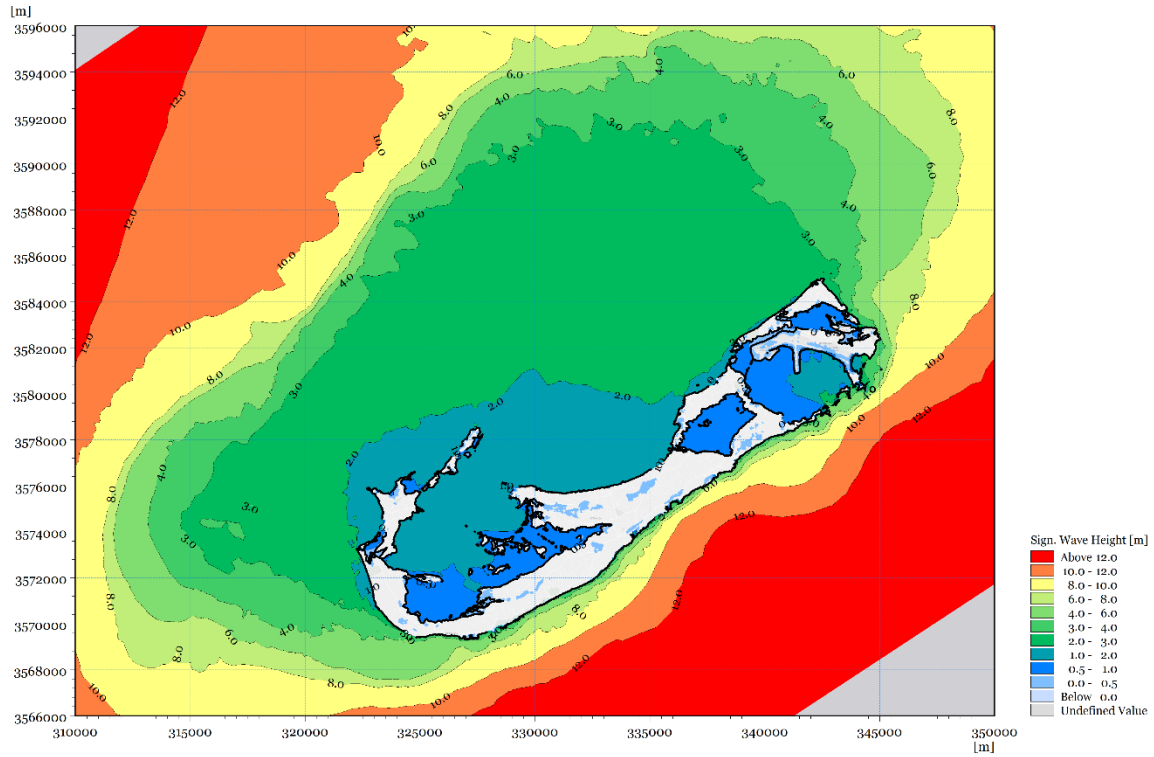
RCP 4.5 100 year Horizon – 150yr conditions



RCP 8.5 – Bermuda

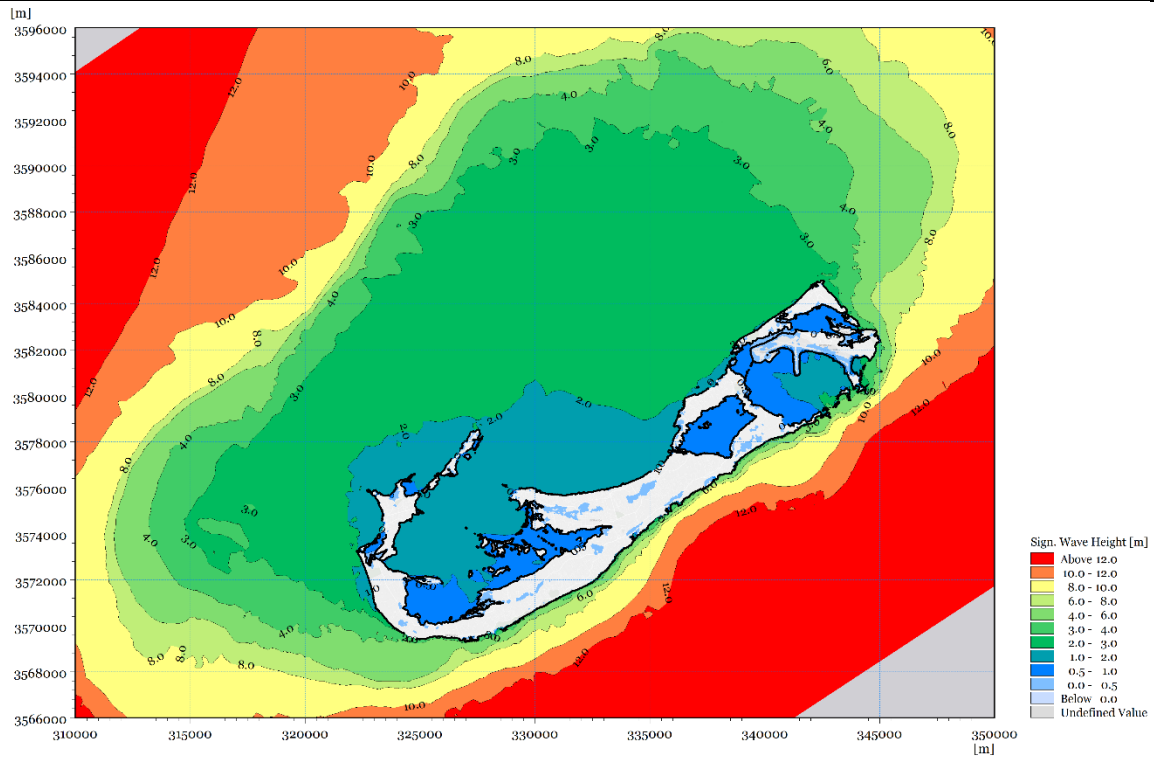


RCP 8.5 100 year Horizon – 100yr conditions



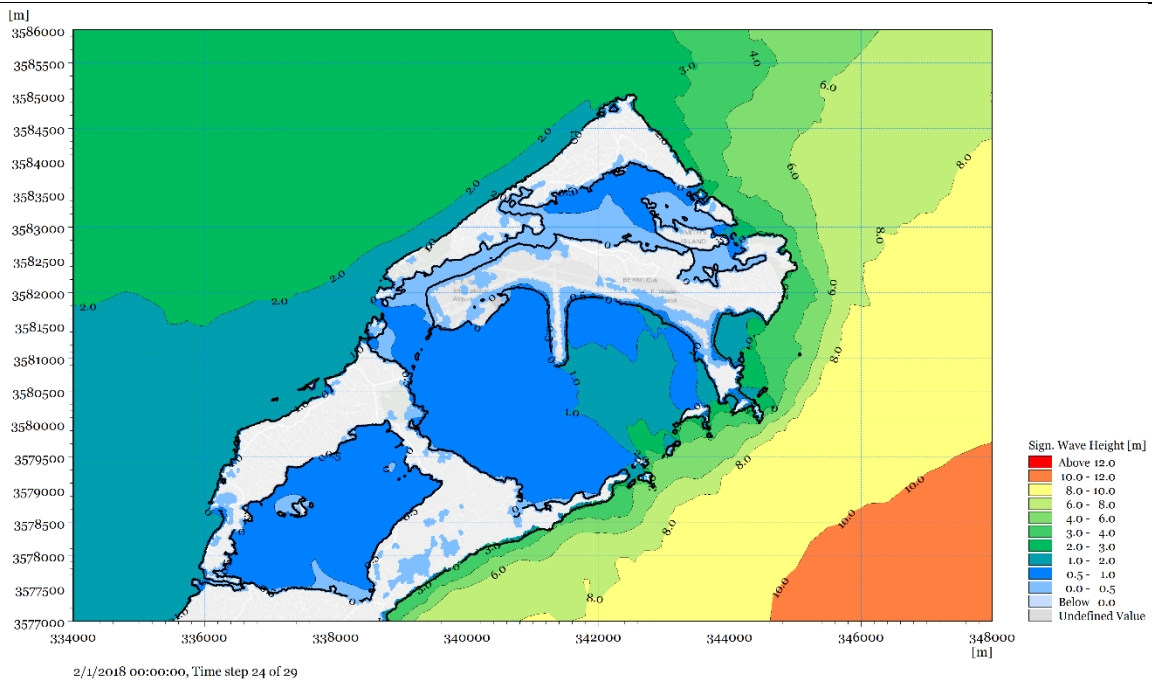
2/1/2018 02:00:00, Time step 26 of 29

RCP 8.5 100 year Horizon – 150yr conditions

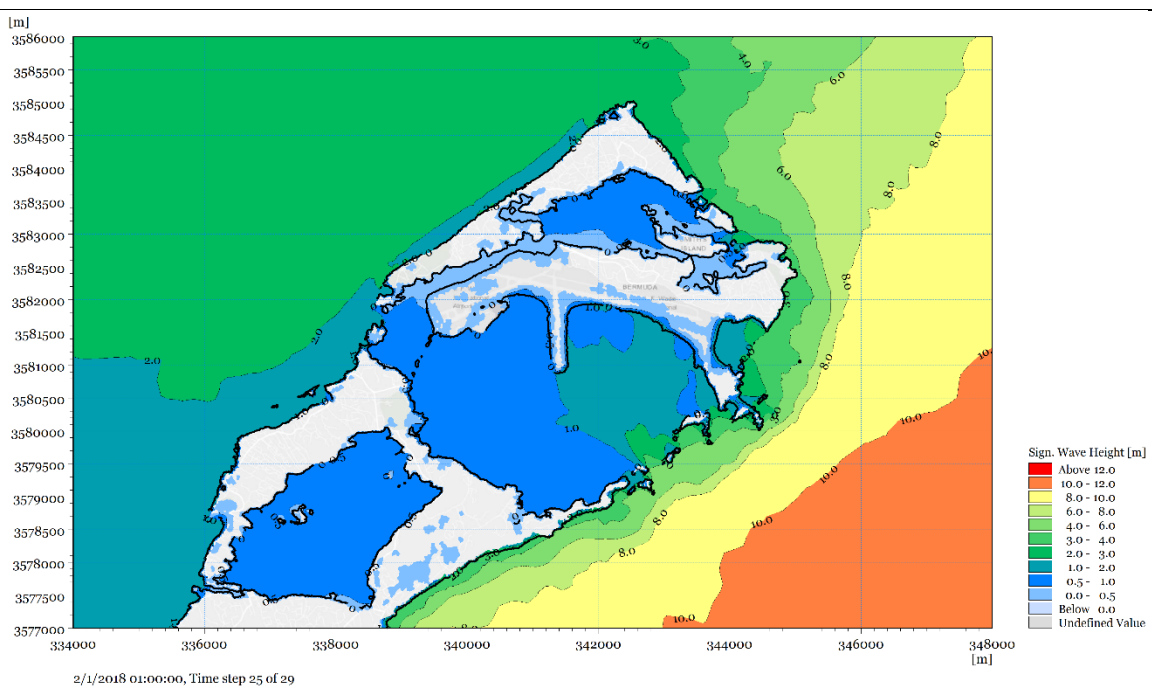


2/1/2018 03:00:00, Time step 27 of 29

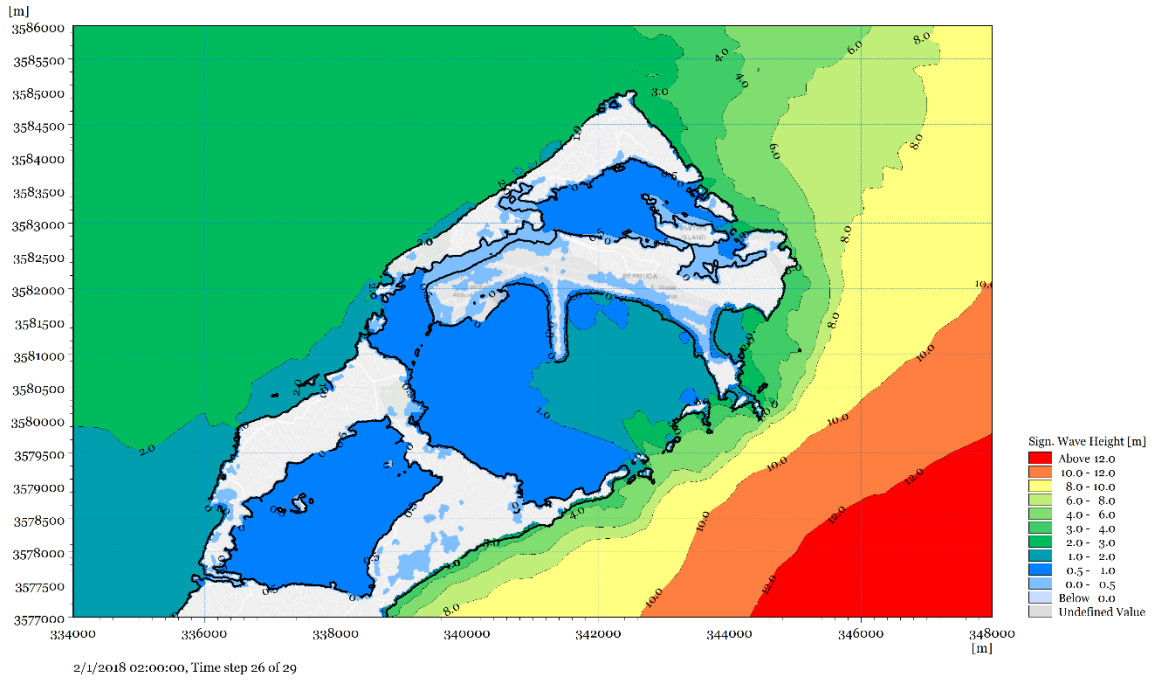
RCP 8.5 100-year Horizon – 25yr conditions



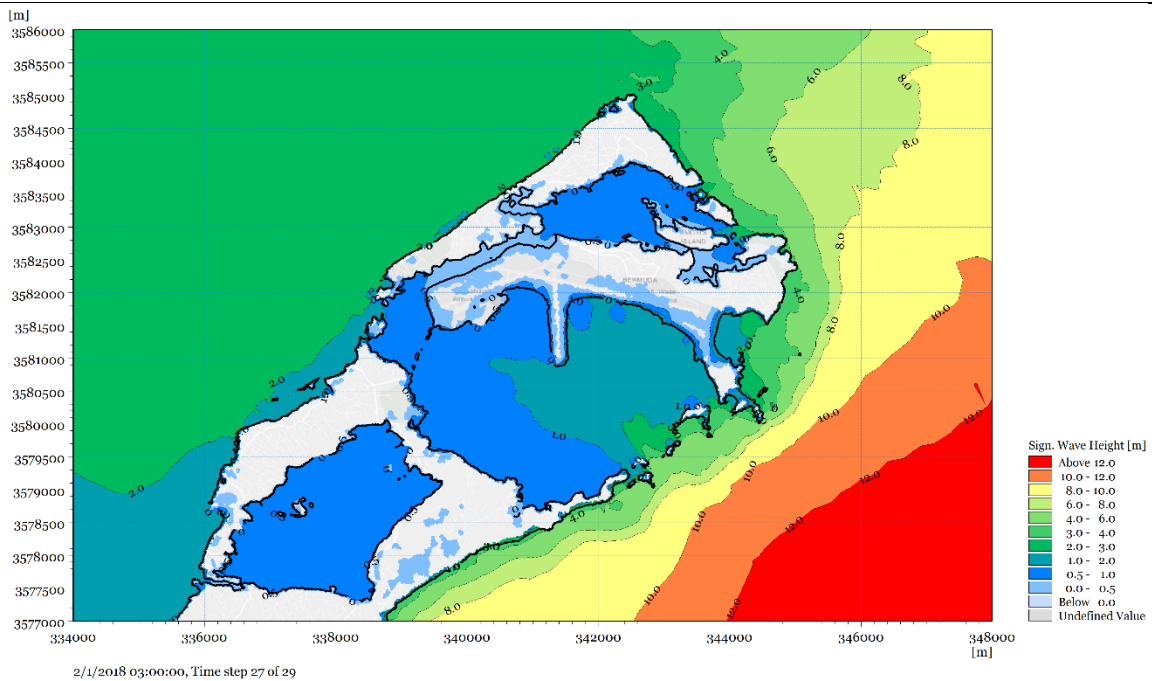
RCP 8.5 100-year Horizon – 50yr conditions



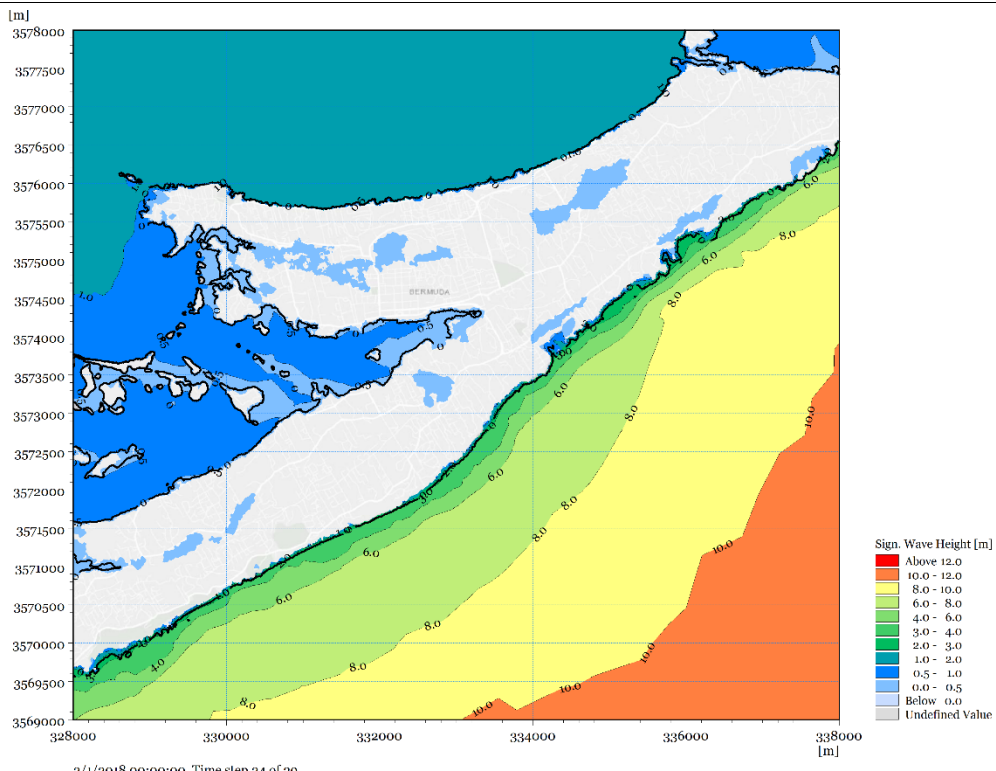
RCP 8.5 100 year Horizon – 100yr conditions



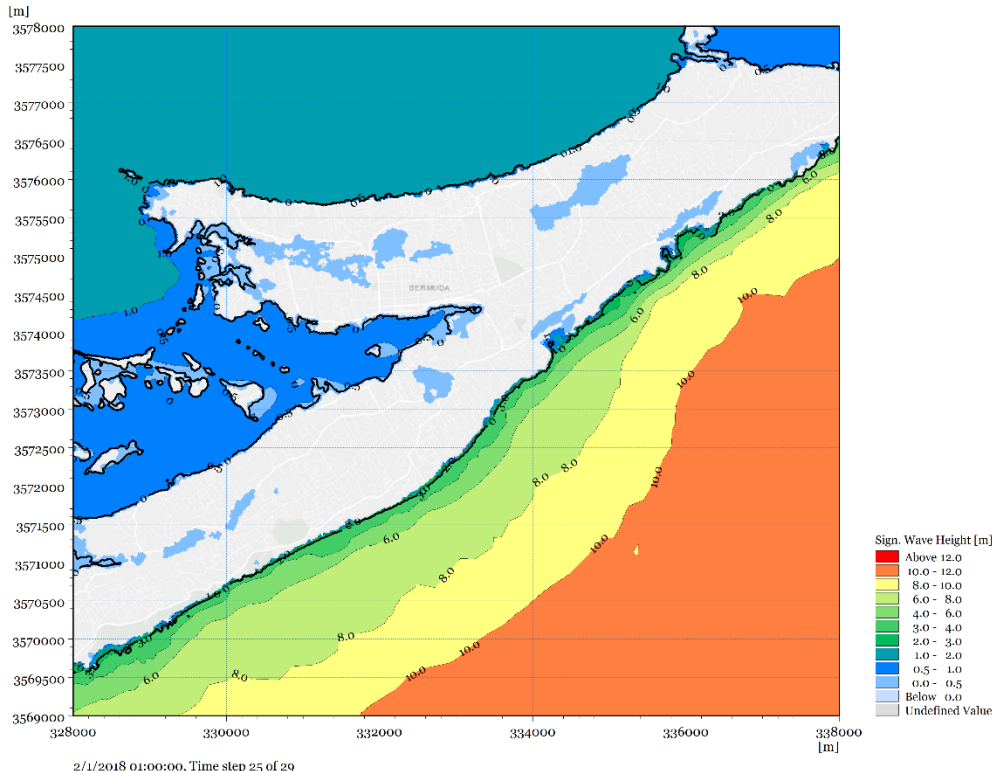
RCP 8.5 100 year Horizon – 150yr conditions



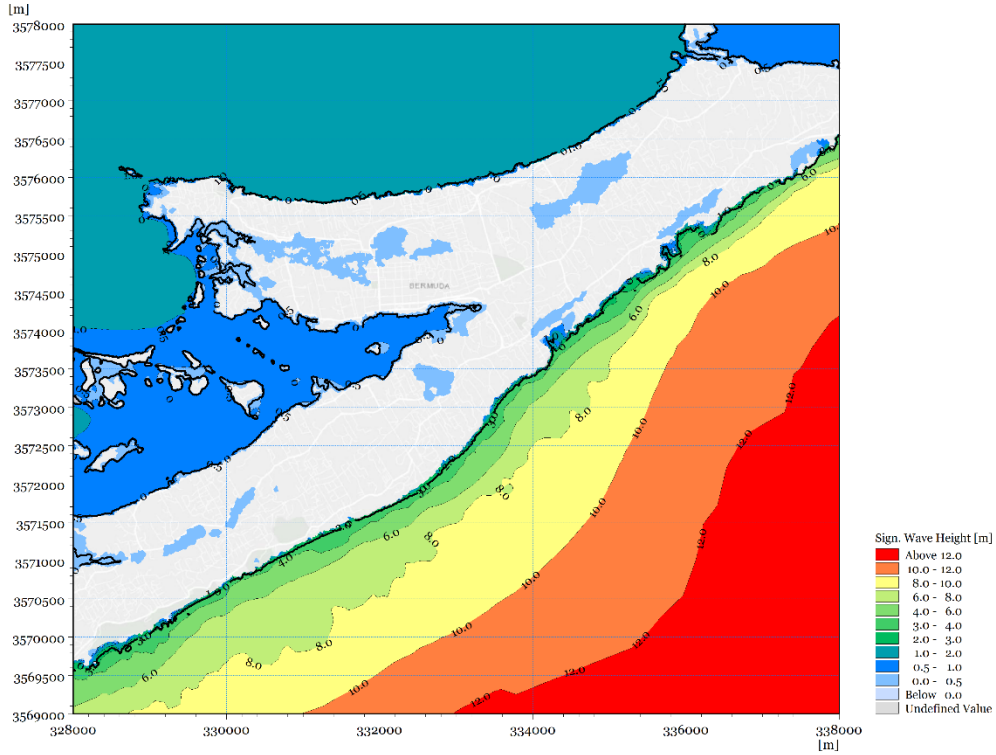
RCP 8.5 100-year Horizon - 25yr conditions



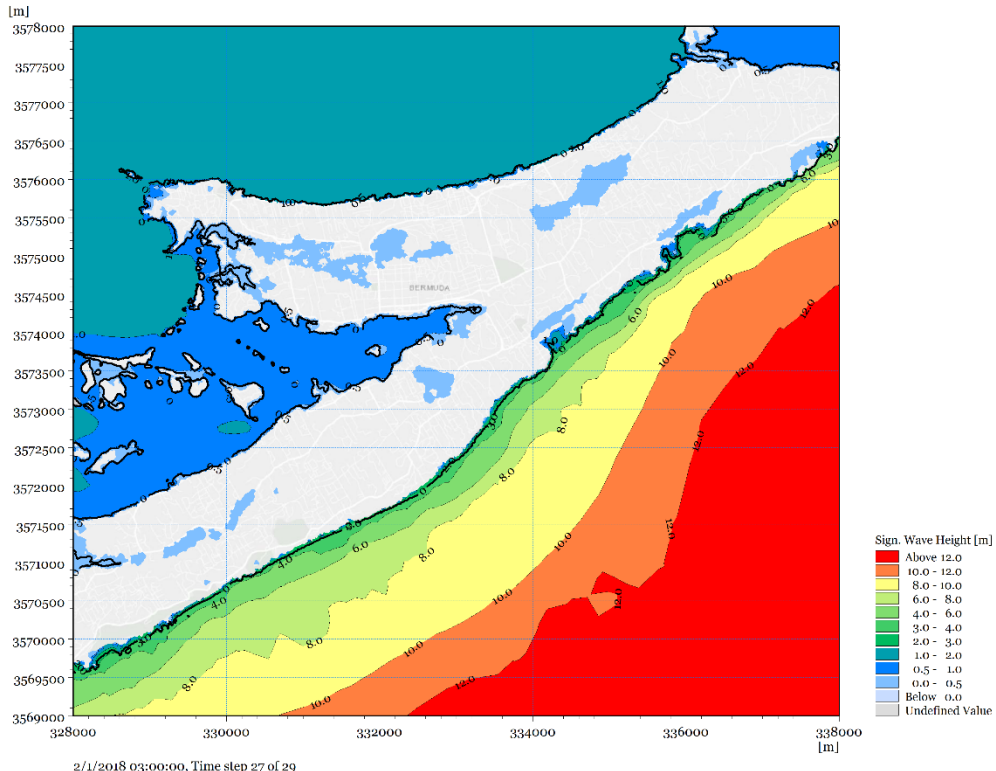
RCP 8.5 100-year Horizon - 50yr conditions



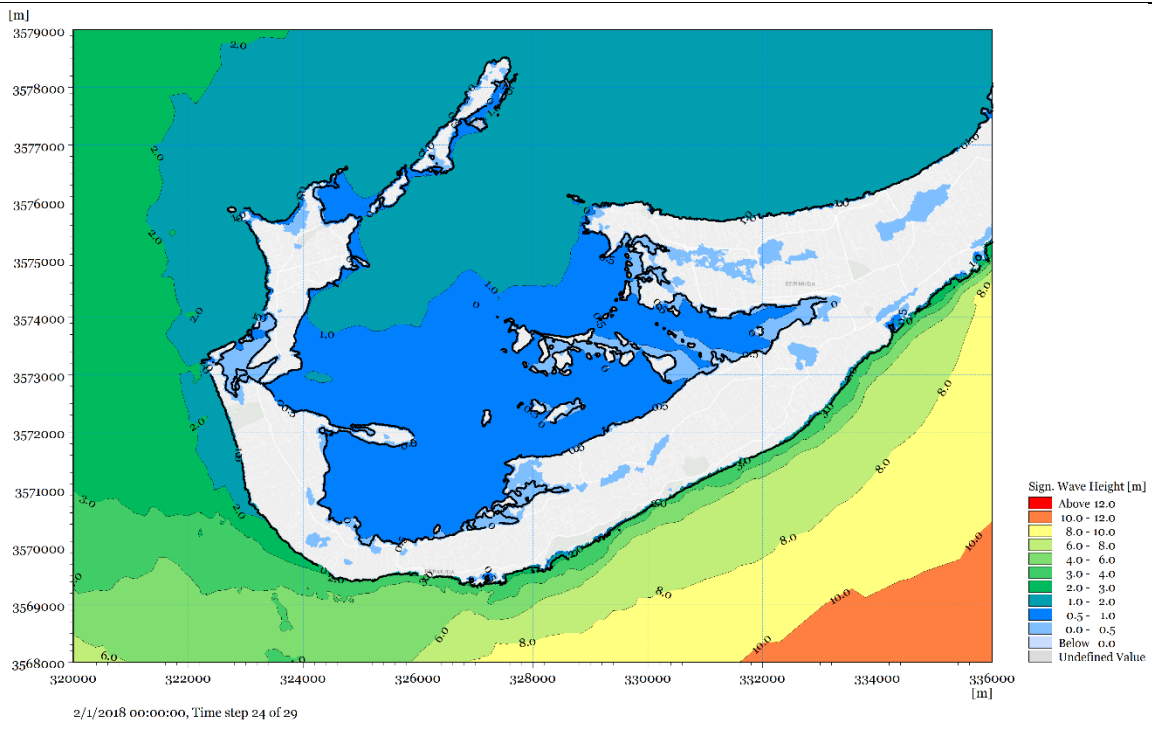
RCP 8.5 100 year Horizon – 100yr conditions



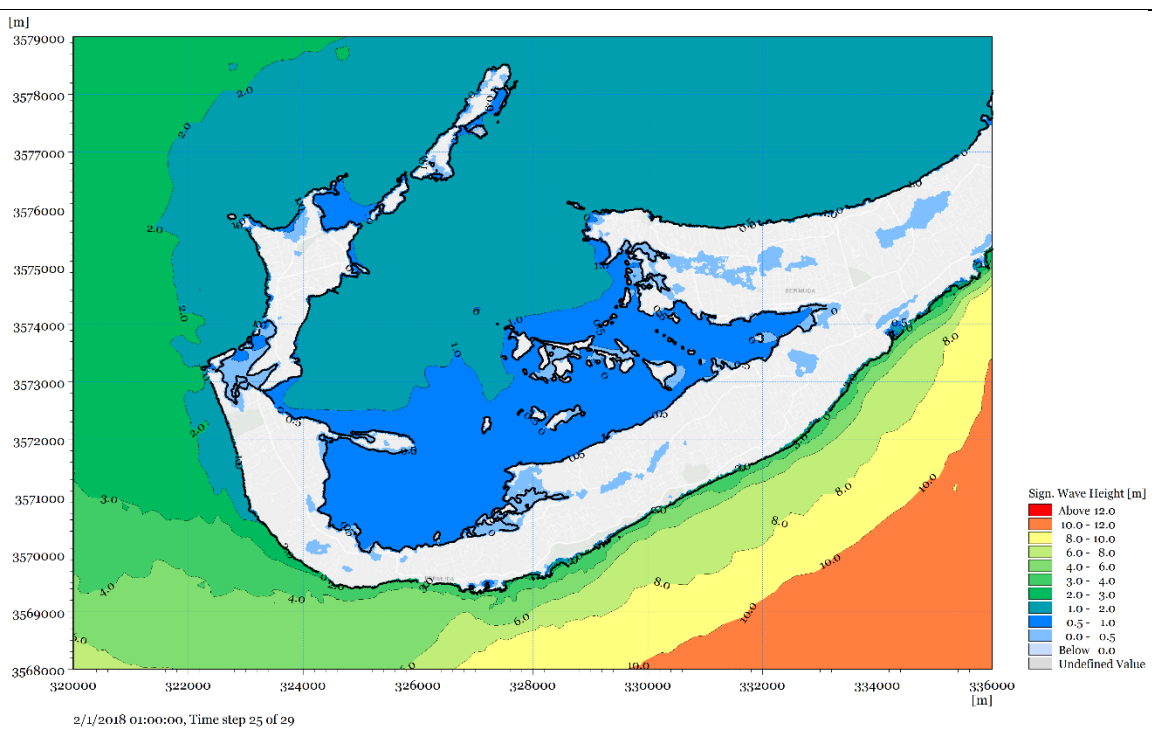
RCP 8.5 100 year Horizon – 150yr conditions



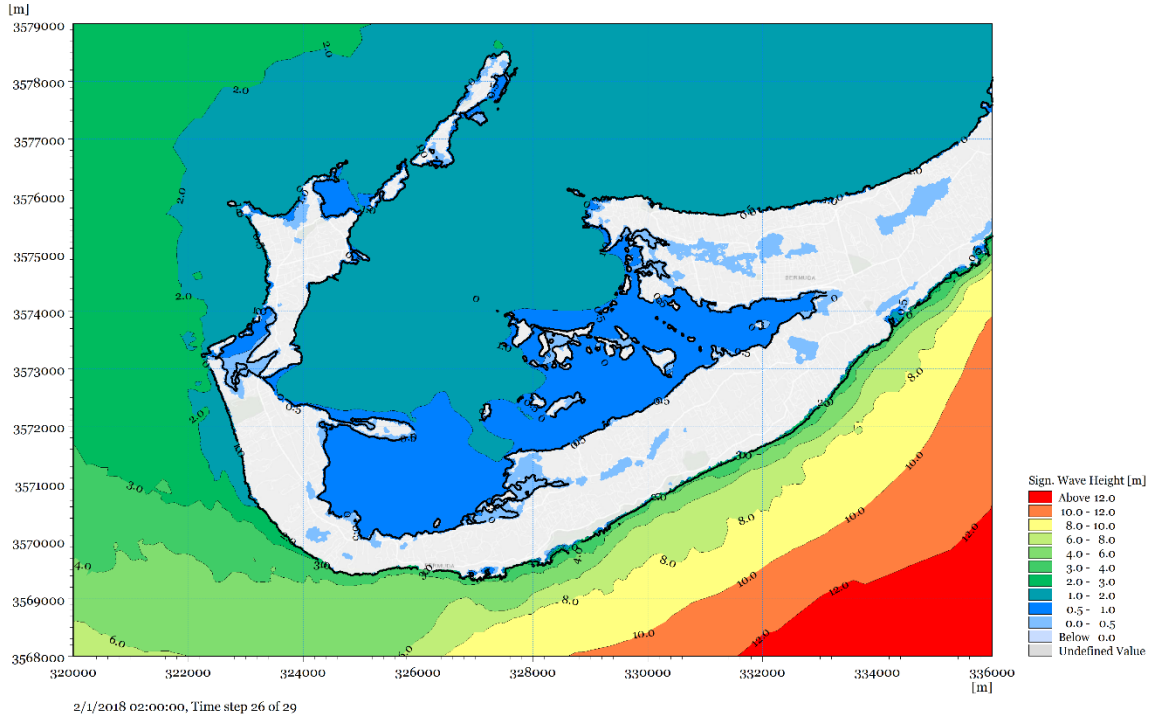
RCP 8.5 100-year Horizon - 25yr conditions



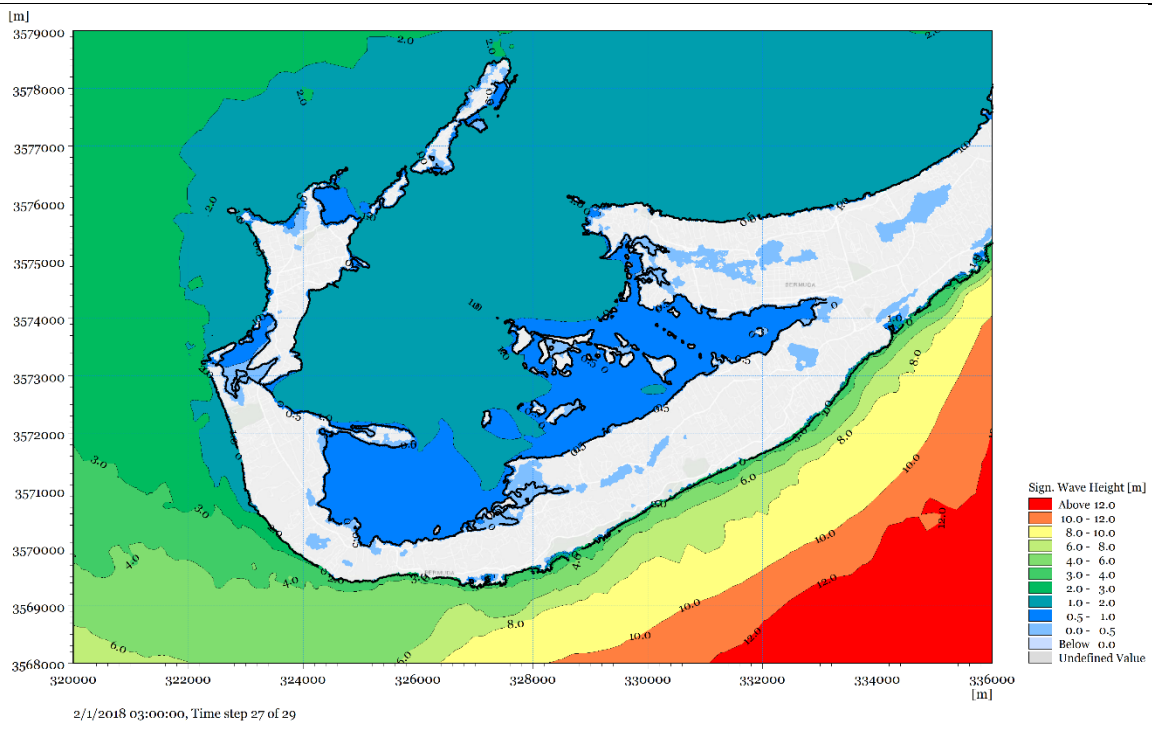
RCP 8.5 100-year Horizon - 50yr conditions



RCP 8.5 100 year Horizon – 100yr conditions



RCP 8.5 100 year Horizon – 150yr conditions



Appendix F – Hydrogeology Modeling Report



Bermuda Modelling Report - Hydrogeology

Nov 30, 2022

Introduction

Impacts of rising sea level on the hydraulic balance between aquifers and the ocean will likely threaten fresh water resources and aquatic ecosystems along many coastline areas around the world, and in many cases, for some distance inland in small oceanic islands. It is vital to understand the vulnerability of groundwater systems to these rising sea levels and salt water intrusion and to assess and understand the factors that determine the magnitude of system response. Sea water (or salt water) intrusion is defined as the lateral landward migration of the sea water-fresh water interface in the subsurface. Vulnerability in this context is defined by the rate and magnitude of salinization (or salinification) of coastal aquifers and changes in groundwater flow to the sea. This understanding is critical to developing effective management and adaptation plans in coastal zones. Salinization can occur from lateral saltwater intrusion at depth and infiltration from surface due to coastline transgression and storm surge inundation. Changes in groundwater flux to the ocean can affect groundwater discharge and circulation of saltwater through the offshore subsurface. This can alter both ocean aquatic ecosystems and ocean chemical composition.

Groundwater systems underlying land masses which are characterized by dry conditions (evapotranspiration exceeding rainfall) and/or low topography are vulnerable to changes caused by sea-level rise. Those oceanic islands and continental coastlines characterized by low topography are particularly vulnerable to salinization of fresh water aquifers. Studies (Werner and Simmons, 2009), (Michael et al, 2013),(Haitjema and Mitchell-Bruker, 2005) have determined that the response of recharge-limited systems (specified flux systems) to sea level rise is largely minimal, whereas topography-limited systems (specified heads systems) are vulnerable to sea level rise for various combinations of permeability, vertical anisotropy in permeability, and recharge. A recharge-limited system

is a system where the main controlling factor is the amount of infiltration from precipitation and induced recharge from rainfall harvesting. A topography-limited system is characterized by low relief with a substantial percentage of the topography slightly above sea level. Bermuda is predominantly a recharge-limited system as explained below. These studies also found that hydrogeologic properties (differences in permeability, distance to a hydraulic divide, and recharge) and the characteristics of the settings are more important factors to consider than uncertainties in projections of sea level rise and inland to coast hydrologic shifts. (Werner and Simmons, 2009), (Michael et al, 2013),(Haitjema and Mitchell-Bruker, 2005) The results of these studies have implications for the management of coastal aquifers subject to sea-level rise. The resulting sea water intrusion may be somewhat mitigated if water resource managers are able to allow ground water levels to rise commensurate with sea-level rise.

In the Werner and Simmons study, two conceptual models were tested and were considered to provide realistic endmembers on the likely range of behavior that could be expected in the field: (1) flux-controlled systems, in which ground water discharge to the sea is maintained assuming similar hydraulic conductivities despite changes in sea level. Groundwater level rise is the same as sea-level rise and horizontal hydraulic gradients are maintained, and (2) head-controlled systems, whereby hydrogeologic controls such as ground surface, surface water bodies or pumping wells or infiltration galleries maintain the inland head in the aquifer despite sea-level changes. The sea water-fresh water interface migration due to sea-level rise is a function of hydrogeologic variables including aquifer thickness, recharge rate, hydraulic conductivity, and the rate of ground water discharge to the sea.

Werner and Simmons (2009) concluded that flux-controlled systems are associated with minimum sea water intrusion as a result of sea-level rise and that head-controlled systems are associated with maximum sea water intrusion as a result of sea-level rise. For constant flux conditions, the upper limit for sea water intrusion due to sea-level rise (up to 1.5 m) is no greater than 50 m for typical values of recharge, hydraulic conductivity, and aquifer depth.

For the constant head case, the magnitude of salt water toe migration is on the order of hundreds of meters to in excess of a kilometre for the same sea-level rise.

Physically, a specified flux boundary condition represents a system that has sufficient thickness of unsaturated zone (difference between ground elevation and water table elevation) to accommodate any water-table rise. The elevation of the water table is limited only by the flux of water to the system, or its recharge: a flux-controlled system [Werner and Simmons, 2009] or a recharge-limited system. The piezometric rise in recharge-limited systems caused by an increase in sea level has been called a “lifting” effect [Chang et al., 2011]. Recharge-limited systems are less vulnerable to sea-level rise because the horizontal hydraulic gradient between land and sea can be maintained and thus groundwater flux to the sea remains the same.

Conversely, in topography-limited systems (specified head systems) the water table is near to land surface such that an increase in sea level causing the freshwater lens to rise results in intersection of the water table with the land surface and increased overland discharge from newly created springs or seeps. Topography-limited systems are more vulnerable to sea-level rise because the hydraulic head on the freshwater, landward side cannot rise in response to a rise on the seaward side.

Bermuda, characterized by topography that generally rises relatively steeply from the coast, could be characterized as a recharge-limited system as opposed to a topography-limited system, and, its freshwater lenses are not as vulnerable as those lenses characterized as topographic-limited systems.

The fresh groundwater lenses do discharge to the sea in a dynamic system that is more or less in equilibrium. However, there are two areas in Bermuda where substantial drainage of the Central Lens may be occurring and the groundwater flux to the sea may increase because the horizontal hydraulic gradient will increase with sea level rise: one by drainage into a reentrant bay (Foot of the Lane) and the other into Mill Creek which drains into the human-made Pembroke Canal.

Groundwater flux is determined by the equation $Q=KiA$

Where: Q is flux m^3/day

K is hydraulic conductivity m/day

i is horizontal hydraulic gradient m/m

A is the cross-sectional area through which flow occurs

For a given hydraulic conductivity and cross-sectional area flux will depend on the magnitude of the horizontal hydraulic gradient. With sea level and accompanying freshwater lens rise, in most instances the horizontal hydraulic gradient will remain the same. In some areas with groundwater rise, a seepage face may develop in topography that rises slowly from sea level which will increase the horizontal hydraulic gradient and therefore groundwater flux. The areas noted may exhibit this phenomenon because groundwater flow lines converge strongly around these features. There may be other places where this occurs which are not as obvious; observers should monitor the gradual appearance of new springs and seeps along the coastlines.

Vacher (1974) indicates that there is a natural westerly component of flow in the Brighton Aquifer due to the reentrant shoreline at Foot of the Lane at Crow Lane Park. (approximate UTM coordinates E 547900 N 132800). The Town Hill Formation rocks are an effective drain in this area. In addition, he asserts that the Pembroke Canal drains the Central Lens into the eastern Hamilton Harbour. However, Thomson (1989) says that this latter outflow is unlikely to take place as the Canal runs over a reclaimed peat marsh and is not connected to the aquifer. Further work in this area is warranted to determine the degree of hydraulic connection between the Central Lens and the Mill Creek/Pembroke Canal. Lavis (2022) has carried out some preliminary work in the area of Mill Creek and the east-west line of marshes in the Central Lens area investigating whether the marshes and Mill Creek are hydraulically connected to the Central Lens. Preliminary work indicates the possibility of a perched groundwater body in the Mills

Creek Area possibly above the peat layer. There was no indication of a tidal signature and it is suspected that the peat acts as a leaky confining layer/aquitard.

Evidence supporting the existence of the drain to Mill Creek and the Pembroke Canal is the steep horizontal hydraulic gradient in the Central Lens between the Salisbury Yard well and the St. John's West well which does indicate a component of westward groundwater flow towards the area of the upper reaches of Mill Creek and the downstream Pembroke Canal.

If both of these locations do act as drains to the Central Lens, then, as sea levels rise and the Central Lens rises in concert with sea levels, the horizontal hydraulic gradients between the lens centres and the drainage locations discussed may increase resulting in more flow to these 'drains' and depletion of the freshwater resource in the lens. This should be confirmed by a field study.

Bermuda does have some anthropogenic features which place parts of the Central Lens into the category of a head-controlled system. In this case hydrogeologic controls such as pumping wells and infiltration galleries will maintain the inland hydraulic head in the aquifer despite sea-level changes. Maintaining pumping rates and levels in wells can be controlled but infiltration galleries, such as those employed by the Bermuda Water Works Limited (BWW) are at a fixed elevation. Sea level rise lifting the Central Lens will result in a decrease of the horizontal hydraulic gradient between the water level in the galleries and the sea level. This will alter the shape and extent of the cone of influence induced from pumping this water but it is difficult to ascertain whether pumping and sea level rise over the years has decreased the flow of fresh water to the ocean especially when the pumping rates are not constant. A decrease in flow of fresh water to the ocean implies inland movement of the salt water interface-sea water intrusion. An analysis of the changes in the water table in relation to sea level over the years and into the future is required.

Vacher (1974) does show the inferred water table depression around the BWW as a result of pumping 571,000 lgpd (2,596 m³/d) in 1974. The 0.1 ft. (0.03 m) drawdown contour does intercept the north coast. The total drawdown of the pumping at BWW is more than 0.3 ft (0.09 m). While this may not seem very significant, with the sea level rise between 1974 and 2022 of 0.26 m, and assuming drawdown is the same (ie assuming pumping is the same) this drawdown must have increased substantially on a percent difference basis. Because the cone of depression around a groundwater withdrawal system represents the surface expression of the area where groundwater flows toward the extraction facilities, salt water intrusion in the aquifer where the cone of depression intersects the north shore would likely have increased if this pumping rate was maintained.

However, BWW reduced its abstraction substantially after 1974. According to the data, in 1974 about 571,000 IGPD (2,596 m³/d) was abstracted by BWW and about 133,000 IGPD (605 m³/d) by the government's Prospect wells. BWW's abstraction rate decreased after 1978 to <300,000 IGPD (1,363 m³/d) by 1989, after which it stabilized at around 350,000 IGPD (1,591 m³/d). Given the reduction in pumping rate, the cone of depression has likely been reduced in extent since 1974 and may not intercept the coast to the north of the infiltration galleries and wells thus reducing the possibility of sea water intrusion caused by pumping in this area. Continued monitoring and analysis of the changes in the water table in relation to sea level over the years is required.

Current field work (Lavis, 2022) shows that there is a clear reduction of the thickness of the lens between the water table and the 3% salinity point in the vicinity of the cone of depression (i.e. around the Devonshire Marsh area) shown in Vacher (1974). It is likely that this thinning has been there since the mid 1970's. However, after reduction in the pumping rate after 1974, it is likely that a reduction in the extent of the cone of depression occurred and with a concurrent increase in the depth from the water table to the 3% salinity location predominantly on the outer reaches of the cone of depression. (S. Lavis, Aug. 16, 2022 personal communication) This increase in the thickness of the fresh water lens occurs because any rise in the elevation of the water table will increase the depth of the salt water interface by an average of 40 times, the Ghyben-Herzberg ratio.

Thomson (1989) discusses a groundwater steady-state model of the Central Lens which was run with and without existing wells in order to see the effect of rates of abstraction. The average abstraction (the 1980-84 average) was 4500 m³/d. Without it, the water table was predicted to be up to 10 cm higher, implying that abstraction has thinned the lens by up to 4 m, using the 40:1 ratio. This corresponds with field observations: in the early 1970's, before abstraction became widespread, the maximum lens thickness was 14 m, whereas it is now 10 m. (Thomson 1989)

Bermuda currently experiences on average more or less equal rainfall distributed throughout the year and a surplus of rainfall over evapotranspiration. (Clarke, L., Taylor, M., and Maitland, D., May 31, 2022). One of the possibilities of climate change is interruption of rainfall patterns with increasing drought periods and droughts of longer duration. This will result in changes to the recharge-evapotranspiration balance and possibly deplete the volumes of the fresh water lenses. Increases of the intensity of precipitation are likely to occur in Bermuda, thus increasing recharge and runoff and flooding of low-lying areas. Maximum recharge is equal to vertical hydraulic conductivity which depends on the characteristics of the subsurface so increased intensity of precipitation does not necessarily mean increased recharge.

Bermuda differs in hydrogeological conditions from other small islands in two ways: (1) internal marshes, major discharge areas elsewhere, may act as barriers to ground-water flow; and (2) development of a high density of housing (typical of only a few small oceanic islands) has significantly increased Bermuda's recharge, because of domestic waste water and road drainage contributions.

Geology

The approximately 139 islands of Bermuda sit atop a long-extinct, mid-ocean volcanic seamount about 1,000km east of the Carolinas in the North Atlantic Ocean. The oceanic crust is estimated to have formed about 124 million years ago from sea floor spreading at the Mid-Atlantic Ridge. The history of the Bermuda Rise and the Bermuda Pedestal is

known from seismic-reflection studies and deep drilling of the Bermuda Rise (Tucholke, Vogt et al., 1979; Tucholke and Mountain, 1986). The occurrence on the western Bermuda Rise of an abrupt change from deposition of turbidites from the continental margin to deposition of pelagic sediments dates the initial uplift of the rise as middle to late-middle Eocene (45-50 Ma). The occurrence of volcanoclastic turbidites 140 km southeast of Bermuda indicates that the Bermuda volcanoes built up to sea level and were being actively eroded during the late-middle Eocene to early Oligocene (43-35 Ma). The end of deposition of the volcanoclastics and, by inference, the end of subaerial erosion and the time that the Bermuda volcanic rocks subsided below sea level, was in the late Oligocene (25 Ma). (Vacher and Rowe, 1997)

Rising from the ocean bottom are four northeast-to-southwest trending volcanic peaks, including the Bermuda Pedestal (the only emergent peak), and the submerged Challenger, Argus, and Bowditch seamounts. Ocean waves eroded the exposed Bermuda Pedestal so that by 20-25 million years ago the former volcano was a relatively flat surface, the Bermuda Platform. The product of this erosion would have been beaches and seabed sediments made up of black volcanic sand. The platform, with its surrounding reefs, became a sheltered refuge in the middle of the Atlantic for shallow-water marine life including corals, molluscs, foraminifera, and algae. Over time, their skeletons broke down and accumulated, burying the whole platform in carbonate sand. (Vacher and Rowe, 1997)

During the Pleistocene Epoch (2.5 million years to 12,000 years BP) sea levels fluctuated by more than 100m during periods of glacial advance and retreat. These rising and falling sea levels were key in the generation and distribution of carbonate sediments on the Bermuda Platform. Over the last million years (approximately) the cycles increased in amplitude, and it's believed that the limestone islands of Bermuda formed during this period. Proof of seven of such cycles exists in five limestone formations and at least six well-developed fossil soils (paleosols) throughout the islands. These paleosols are thin (0.3-1.0 m thick), undulating layers of regosols interbedded with the limestones, separating the geological formations in some cases.

Waves and currents on the Platform moved the sand around and created shoals and eventually low-lying islands. Where wind-blown sand became trapped among vegetation above the high tide level, dunes formed and grew. Despite occasional storm damage, the islands continued to grow, assisted by the ongoing breakdown of the skeletons of shallow water marine creatures, which continued to create carbonate sand. During the Pleistocene, the Bermuda Islands repeatedly underwent partial inundation and re-emergence. The land areas were continuously attacked and reduced by rain and ground water but repeatedly renewed, during times of submergence, by deposition of marine limestone and by contemporaneous additions of shore-born and wind-transported carbonate sand, now eolianite. Paleosols formed under subaerial conditions and were buried beneath later deposits and constitute important stratigraphic markers. The igneous rock appears to have been exposed during some low marine stands, and the former shorelines seem to be recorded by submerged terraces. The major karst features are largely below sea level, and they date from times of continental glaciations. (Bretz, J. H., 1960. Vacher and Rowe, 1997)

The present-day Bermuda Platform consists of four geomorphological-ecological provinces: a reef-front terrace at 20m depth; a main reef composed of 4m deep coral algal reefs; a 16m deep lagoon in the north and the islands themselves forming a northeast trending chain along the southern edge of the platform.

The limestones of Bermuda consist mostly of cemented dunes, or eolianites. The five limestone formations in order of decreasing age are: the Walsingham, the Town Hill (lower and upper members), the Belmont, the Rocky Bay and the Southampton. They represent successive major episodes of dune building on Bermuda. Variations in the physical character, or lithology, of these formations are primarily age-related. There is a gradation of physical and chemical alteration, (diagenesis), increasing from the youngest to the oldest limestones. Figure 1 shows the geology of Bermuda.

The principal agent of diagenetic change that has acted on Bermuda's limestones is rainwater. As it penetrates, or percolates, through the surface-soil this water becomes

weakly acidic. Carbonate sand grains comprising the skeletal remains of marine organisms composed of unstable high-magnesium calcite and aragonite are altered or dissolved. The calcium carbonate is then re-deposited, or precipitated, in the pores of the limestone as stable low-magnesium calcite cement.

In Bermuda, the youngest and therefore least altered and least cemented limestones belong to the Southampton Formation. Older limestones of the Rocky Bay and Belmont Formations are better cemented but still retain a primary granular texture, like beach sand. Increasingly, in the Upper and Lower Members of the Town Hill Formation and the Walsingham Formation, the grains become corroded and more tightly cemented. (Vacher and Rowe, 1997). Figure 1 shows the geology of Bermuda.

Hydrogeology

In the Southampton and Rocky Bay Formation. rocks water can occur and is constrained to move only between the sand grains that comprise the rock. In Belmont Formation rocks, as the grains themselves are partly corroded in the process of conversion to more stable carbonate mineral species, and as the rock is partially dissolved, thus containing pencil size solution channels and small caves, water flows through a larger and more connected pore space. In the Walsingham Formation. rocks, the solutional openings are coalesced into room-sized caves and the intervening rock is tightly cemented, so that water flows largely through underground channels. The characteristics of the Town Hill Formation in terms of cementing and primary and secondary porosity lie between those of the Belmont and Walsingham Formations. The permeability (hydraulic conductivity) of Bermudian rocks ranges upward from that of well-sorted sand (youngest rocks) of the Southampton and Rocky Bay Formations to that of a rock with an anastomosed network of well-defined open channels (oldest carbonate rocks) of the Walsingham Formation.

There is a stratigraphic partitioning of the upper saturated zone. According to current nomenclature (Rowe, 1991; Vacher et al., 1995), the partitioning involves two hydrostratigraphic units: the Langton Aquifer and the Brighton Aquifer. The Langton

Aquifer consists of the Southampton, Rocky Bay and Belmont Formations. The Brighton Aquifer consists of the upper and lower members of the Town Hill Formation.

There is an extensive literature on the geology and hydrogeology of Bermuda (e.g., Vacher et al., 1974, 1978a,b; Plummer et al., 1976; Rowe, 1984; Thomson 1989; Morse and Mackenzie, 1990) that uses an earlier hydrostratigraphic nomenclature that may lead to confusion if used in conjunction with the more recent geologic map and the stratigraphic column (Vacher et al., 1989, 1995). Earlier, the stratigraphic control was described in terms of two units: the Paget Formation and the Belmont Formation. The Paget Formation of those papers corresponds to the Langton Aquifer of the current nomenclature, and the Belmont Formation of those papers parallels the Brighton Aquifer now. Confusing the synonymy is the fact that "Belmont" during the early stages of the geologic mapping (1970s) was used for the vast body of rocks between the Walsingham Formation and what is now known as the Rocky Bay Formation. Now, the Belmont is restricted to the definition of Land et al. (1967), and nearly all of the volume of rock between Walsingham and Rocky Bay is identified as Town Hill Formation. It is this volume that, in the saturated zone, constitutes the Brighton Aquifer.

The underlying Walsingham Formation is characterized, in terms of groundwater, as a salt water aquifer. The Langton Aquifer comprises the youngest limestone and is where the important fresh water lenses are centred. The Brighton Aquifer does contain significant fresh water but not as extensively as the Langton.

The hydraulic conductivity of the Langton Aquifer is some 30-120 m/day. The hydraulic conductivity of the Brighton Aquifer is on the order of 1,000 m/day, which clearly reflects increased secondary porosity (fractures and solutional channels). In addition to these two aquifers, there is a hydrostratigraphic unit corresponding to the Walsingham Formation. This formation does not usually figure largely in discussions of Bermuda hydrogeology because it is highly cavernous and generally occupied by salty where it is below sea level.

The freshwater lenses are localized in the Langton Aquifer. Groundwater in the Brighton Aquifer is generally brackish at the water table. Where fresh groundwater does occur in the Brighton Aquifer, it is usually an extension of a lens centered in the Langton Aquifer such as in the Central Lens. The distribution of rock types affect the flow of groundwater. Several marshes occur in an approximately east-west direction along the contact of the Rocky Bay Formation rocks and the Belmont Formation rocks. North of the marshes the Central Lens is in the Southampton and Rocky Bay Formation rocks, and south of the marshes the lens is in the Belmont rocks.

The value of Bermuda limestone as a ground water aquifer is dependent on the intergranular porosity (porosity between the grains) and permeability (referred to as hydraulic conductivity where groundwater flow is considered). To be capable of storing rain water, porosity must be high and the permeability must be low, as in the youngest formations. Due to diagenesis, the pore spaces of older limestones become cemented and secondary channels are opened up by ground water flow, a process called karstification which causes a large increase in permeability, and ultimately creates caves. The oldest limestones, with their high permeability, are therefore susceptible to sea water intrusion and are for the most part occupied by saline ground water. It is the youngest formations, particularly the volumetrically dominant Rocky Bay Formation, within which the nuclei of significant "fresh" ground water bodies, known as "lenses", have formed. The four main lenses which have accumulated in this way and have been exploited for public water supply are the Somerset Lens (most of Somerset Island west of Beacon Hill Road, area 1.2 km²), the Port Royal Lens (previously called the Southampton Lens, West of Middle Road, in the vicinity of Port Royal Golf Course, in western Southampton and southern Sandys Parishes, area 1.1 km²), the Central Lens of Pembroke and Devonshire (previously called the Warwick and Devonshire Lenses, an elongate body just north of South Road in eastern Southampton Parish, around Horseshoe Bay, and in Devonshire, Western Smith's and northern Pembroke Parishes, area 7.2 km²) and the St. George's Lens (area 0.38 km²) in the St. George area. At its peak, sustainable abstraction of low salinity ground water for public water supply exceeded 4.55×10^6 L/day. (Vacher 1974).

The groundwater lenses are shown on Figure 2 and 3. Figure 2 shows the location of the lenses underlying different areas of the island and the salinity gradations between fresh and salt groundwater and Figure 3 shows the names and configurations of the lenses.

Information provided for this report was predominately about the Central Lens which spans the Langton and Brighton Aquifers in an elongated shape in the central area of the island.

The ideal Ghyben-Herzberg fresh groundwater lens (named after the hydrogeologists who first explained the dynamics) is the basic model for a fresh water lens. Its upper surface is the water table that separates the aerated zone from the underlying saturated zone. Its lower surface is the interface separating fresh groundwater from underlying sea water.

In the simplest case, the lens is in hydrostatic equilibrium, so that the elevation of the water table above sea level, and the depth of the interface below sea level are mutually related. The relationship is the Ghyben-Herzberg Principle (G-H) and involves the depth of the interface below sea level, the elevation of the water table, the densities of sea water and fresh water. The densities of fresh water and sea water are such that the Ghyben-Herzberg balance equals approximately 40 (since density depends on the temperature of the water, the GH balance can vary somewhat from this quantity). This means that at any point the interface below sea level is 40 times the difference between the elevation of the water table at that location and sea level and the thickness of the lens at that point is 41 times the elevation of the water table at that location. The portion that is below sea level is 40/41 times the difference between the elevation of the water table at that location and sea level. The volume of fresh water that is below sea level is 40/41 (97.6%) of the volume of the lens.

As an example suppose the top of the ideal lens is 1 m above sea level (asl). The bottom of the salt water/fresh water interface is therefore 40 m below sea level (bsl). The volume of fresh water below sea level is 40/41 of the volume of the lens. Saline ocean water can

permeate through the limestones relatively easily, especially the oldest Walsingham Formation. Fresh water from precipitation infiltrates from the surface and forms lenses 'floating' on the saline water. The interface between the fresh and saline water is not sharp and tends to migrate up and down depending on precipitation, storm events, tides etc. The location of the midpoint of the interface can be calculated by the G- H equation for steady-state conditions.

The G-H relationship does not describe the elevation of the water table, only the position of the interface relative to the position of the water table. The position of the water table depends on the amount of fresh groundwater circulation through the lens and the time for water to migrate to the shoreline where it is discharged to the ocean.

The G-H relationship is based on the supposition that fresh and salty water are not miscible and are separated by a surface of zero thickness. In real world situations, the water table and the interface are continually fluctuating, so that in the neighbourhood of the interface the two bodies alternately and repeatedly invade each other, and the waters do mix. Thus, a transition zone of mixed, brackish water is present between the overlying unmixed fresh groundwater and the underlying undiluted salty groundwater. In the transition zone, the chemical composition of the groundwater changes progressively with depth, from the composition of the overlying fresh water to that of the underlying salty groundwater which is essentially equivalent in chemical composition to sea water.

The midpoint of the transition zone (50% relative salinity) is the interface of the idealized no-mixing lens. The real-world lenses have three volumes of groundwater that are distinct: 1) the interface-bounded lens with the water table as the upper surface and the lower surface is the position of the 1:1 mixture of fresh and salt water. 2) The transition zone with gradational upper and lower boundaries which are placed (conveniently and arbitrarily) at the position of the 1% (99 parts fresh groundwater and 1 part seawater) and 99% blends respectively. 3) The fresh water nucleus of which the upper surface is the water table and the lower surface is arbitrarily placed at the 1% blend.

The first two volumes of groundwater described above can be considered fundamental and independent bodies in that their size and geometry depend on different fundamental hydrologic phenomena which include the circulation through the island of rain-derived fresh water, and the efficiency of the blending caused by the up and down motion of the interface. The geometry of the third volume is dependent on the other two above it i.e. the fresh water nucleus is the interface bounded lens minus the upper half of the transition zone.

Relative salinity is indicative of the amount of mixing in the transition zone and is expressed as the percentage of one of the end members in the mixing blend, either fresh water or seawater. This can be measured using electrical conductivity probes which are linearly dependent on the total concentration of dissolved solids. Thus the RO plant operated by Bermuda Water Works can operate with a salinity of 5000ppm but the preferred salinity is 3000 ppm. (Allan Rance, Managing Director, Bermuda Water Works, March 23, 2022 pers. comm.)

The groundwater monitoring program carried out by the government hydrogeologists included over a hundred drilled boreholes in 1991. Most of the boreholes penetrate into the seawater beneath the freshwater lenses and underlying transition zone. Salinity profiles have been measured with an electrical conductivity probe.

Relative salinity ranges from zero in the fresh water nucleus to 100% in undiluted seawater. The salinity profiles give information on the structure of the transition zone and the quantity of recharge-derived water in the lens. The salinity data generally produce straight lines when relative salinity is plotted on a probability scale vs. depth on an arithmetic scale. These probability-paper plots indicate a simple error-function variation of relative salinity vs. depth, which is consistent with one-dimensional dispersion models. The error-function variation also means that the depth of particular percentiles of relative salinity can be read easily from the graphs. One of these, where the relative salinity is 50%, is taken as the position of the "interface", that is, where the base of the freshwater lens would be if there were no mixing. The thickness between the water table and this

50% datum provides a measure of the "meteoric water inventory"; the (smaller) thickness of freshwater from a water-resources standpoint, of course, is given by the break in slope of the relative salinity curve at the top of the transition zone.

Across the island, the depth of the interface (50% relative salinity), the thickness of the transition zone (1% to 99%), and the thickness of the freshwater lens (depth to 1% relative salinity) all vary with the hydrostratigraphy and illustrate the geologic control on the distribution of fresh and brackish groundwater. Compared to the Brighton Aquifer, the lower-permeability Langton Aquifer impedes the escape of recharge-derived fresh groundwater. Also, tides and other sea-level variations are less effective in mixing the freshwater and saltwater in the Langton Aquifer than in the Brighton Aquifer. The transition zone decreases in thickness inland in both units but more rapidly per unit distance in the Langton Aquifer than in the Brighton Aquifer.

Recharge (infiltration from precipitation) has been evaluated in a variety of ways and, over the years, has been repeatedly revised upwards. In the early study, Vacher (1974; Plummer et al., 1976) used a water-budget accounting method to estimate recharge and actual evapotranspiration from monthly averages of rainfall and potential evapotranspiration and ignored the unnatural contributions; the result was about 18 cm/yr (12% of the annual rainfall of 150 cm/yr). Rowe (1981) applied a conceptually similar scheme but coupled it to a land zonation based on percentage coverage by housing, roads and marshlands; by including such processes as road runoff and recharge through cesspits, the recharge result increased to about 30 cm/yr. Vacher and Ayers (1980) obtained values of 35-45 cm/yr from three independent methods: evaluation of outflows and change in storage (hence inflows, by difference) in an area of diversion around a major development area; fitting of the lens geometry by G-H equations with independently inferred values of hydraulic conductivity; and the ratio of the Cl⁻ concentration in rainfall to that in the freshest part of the lenses. In his summary paper on the Central Lens, Rowe (1984) indicated that the earlier values from the water-budget accounting for natural surfaces were too low, because they were derived from monthly rather than daily values.

Rowe (1984) suggested that the actual value for recharge including the unnatural contributions, may range up to 55-65 cm/yr in some places.

The most recent estimate of recharge is in connection with a steady-state model of the Central Lens (Thomson, 1989) developed as part of a U.N. study. In that model, the recharge is a distributed parameter which varies according to percentage of rooftop coverage. In Bermuda, most households capture water from their roofs and then dispose of it in soakaways after use. Thomson (1989) calculated cell-by-cell recharge as a weighted average of 90% of the rainfall that falls on impervious surfaces (roofs and roads) and the somewhat high figure of 25% of the annual rainfall that falls on natural surfaces. With these assumptions, combined with the percentage coverage by paved surfaces (5-40%), Thompson obtained recharge rates of 40-75 cm/yr. (Thomson, 1989). The same assumptions, of course, imply that in areas where the percentage coverage by pavement exceeds 22%, more than half of the recharge is obtained by recycling from these paved surfaces (with the total recharge being about 39% of the rainfall). This includes a significant fraction of the area of the Central Lens (Thomson, 1989).

Transient Behaviour

Effects of sea level: With the exception of dug wells in some of the marshes, all the dug wells and boreholes in Bermuda are tidal (that is their water level fluctuations are influenced by rising and ebbing tides), and most are strongly tidal. For a given distance inland of the shoreline, the tidal fluctuation is markedly larger in the Brighton Aquifer than in the Langton aquifer, indicating greater dampening in the latter unit. The water table fluctuation is not a simple scaled down version of ocean tides: The semidiurnal inequality is significantly enhanced in the water table fluctuation, indicating that the diurnal component passes through more easily than the semidiurnal component.

Hydrographs taken from the marshes show a non-tidal water level variation related to changes in freshwater storage. The marsh levels rise rapidly in response to rainfall, decay

exponentially after the rainfall, and fluctuate with a diurnal periodicity in response to evapotranspiration-driven withdrawal.

In contrast, recharge events due to rainfall are not at all evident in hydrographs from boreholes in the limestone. As already noted, the dominant water table fluctuations correlate with changes in sea level, not with volumetric changes in the lens. Attempts to subtract out the sea-level variation in order to look at volume-related residuals have been frustrated by the uniqueness of the sea-level influence at each borehole (Rowe, 1984).

Comparison of yearly averages do reveal variations due to recharge (Rowe, 1984). Maps of the annual average water table in the Central Lens are now available for several decades (although not available for this study). During wet years, the reduced water levels can be 50% higher than those of dry years. The interface (50% relative salinity), however, is not in G-H equilibrium with this interannual variation. In a single borehole, the ratio of water table elevation to the depth of the interface can vary from 1:25 in wet years to 1:58 in dry years. Thus the interface lags in its response to these water-table changes (Rowe, 1984). These results argue against the use of G-H models to simulate transient variation of the meteoric water inventory stored in the lens.

The long-term averages of eight years of data indicate that under steady-state conditions the Central Lens configuration supports the G-H theory. On a yearly average basis, however, the degree of disequilibrium is substantial. The water table is shown to be far more responsive to variations in recharge than is the interface and possible causes for this are discussed below. On less than a yearly average basis the water table levels are dominated by the influence of sea level (tides and barometric fluctuations). Demonstration of a relatively stable lens thickness, below sea level, allows a less cautious approach to management of pumping rates than previously taken. A maximum permissible thinning of the lens is considered as 45% in fresh areas and 60% in brackish areas. Under these conditions it is calculated from Henry's equation (Henry, 1964) that ~ 75% of recharge could be abstracted.

Consistent with the G-H principle, the Bermuda groundwater lenses float in the sea water almost entirely below sea level. Their maximum thicknesses range from 3m to 10m. The lenses have been developed for water supply purposes, through wellfields operated by the Bermuda Government and by private water companies using wells, horizontal tunnels and infiltration galleries. Following treatment by reverse osmosis, this ground water is delivered to the public via a limited network of “mains” pipelines and by “water truckers”.

All the groundwater lenses correlate with occurrences of the Southampton, Rocky Bay and Belmont Formation rocks. The interface bounded lens tends to swell in the Southampton and Rocky Bay Formation rocks and thin in the Belmont Formation rocks because of the hydraulic conductivity contrast. In the Central Lens, as it crosses the Rocky Bay/Belmont Formation contact, the midline of the transition zone rises abruptly and levels off at a lesser depth in the Belmont. The Southampton and Rocky Bay Formations act as a dam, and the Belmont Formation as a drain due to changes in hydraulic conductivity. The transition zone thins in the inland direction and does so at a greater rate per unit distance from the shoreline in the Southampton and Rocky Bay Formation rocks than in the Belmont Formation. The result is that at a given distance inland from the shoreline, the transition zone is considerably thicker in Belmont rocks than in Southampton and Rocky Bay rocks. In the Prospect section, the transition zone attains its least thickness in the Southampton and Rocky Bay Formation rocks. Southward, as the transition zone crosses the Rocky Bay/Belmont contact the relative salinity surfaces diverge abruptly. This thickening and thinning of the transition zone is related to the considerably greater damping of tidal and other oscillations of the water table in Southampton and Rocky Bay rocks as opposed to Belmont rocks. Thus the geographic distribution of fresh and brackish groundwater in Bermuda reflects the hydraulic characteristics of the rocks on the thickness of the interface-bounded lens and the thickness of the transition zone. These two effects, though mutually independent, are each dependent on hydraulic conductivity and oppose each other. As the lens crosses from relatively low hydraulic conductivity Southampton and Rocky Bay rocks that occur on the north side of the island into relatively high hydraulic conductivity Belmont rocks

that occur on the south side of the island, the interface-bounded lens thins abruptly and the transition zone thickens abruptly. As the thickness of the fresh water nucleus is the thickness of the interface-bounded lens minus the thickness of the upper half of the transition zone, the effect of the distribution of rock types of contrasting permeability on the thickness of fresh groundwater is pronounced. (Vacher, 1974)

The result of this pronounced geologic control is that the interface-bounded lenses and the fresh-water nuclei are not symmetric, as they would be if the island were composed of a single, homogeneous rock type. Instead, there is a pronounced asymmetry such that the axis of any particular lens or fresh water nucleus is displaced from the centreline of the island toward the shoreline composed of younger formations. This phenomenon could be important in the prediction of future climate changes on the groundwater regime.

Central Lens

In the area of the Central Lens, 866 ha. of the land surface are underlain by unmixed fresh water, and of that 340 ha. have 6 m or more thickness of fresh water, and 73 ha. have in excess of 10.7 m thickness of fresh water. The volume of rock that is saturated with fresh groundwater is $5.0 \times 10^7 \text{ m}^3$. Assuming a conservative porosity of 20%, the volume of fresh water in the Central Lens is estimated at $1.0 \times 10^7 \text{ m}^3$. In 72% of the area where a freshwater layer occurs, it is greater than 3 m thick, in 28% of the area of naturally occurring fresh groundwater, the nucleus is 3-6 m thick, in 56% of the area in which there is fresh groundwater the thickness is less than 6 m. More than 10.7 m of fresh groundwater occurs in the Prospect area over an area of 80 ha., or less than 10% of the area of naturally occurring fresh groundwater. (Vacher, 1974)

There is a zone of brackish water bounded by the surfaces of the 1% and 10% relative salinity. This zone represents the appropriate composition for desalination by some RO plants and electrodialysis plants that utilize brackish water. The volume of this brackish zone in the central lens is about $4.6 \times 10^6 \text{ m}^3$. (Vacher, 1974).

Summary of the occurrence of groundwater in Bermuda

The occurrence of fresh and brackish groundwater can be summarised as follows:

- a) Fresh groundwater is presently being extracted from five separate areas comprising approximately 1,012 ha. or 20% of the area of Bermuda
- b) The largest area is that underlain by the Central Lens.
 - i) It contains about 9.1×10^5 m³ of fresh water (Vacher, 1974).
 - ii) it attains its maximum thickness, about 15 m, in the Prospect area.
 - iii) it covers an area of some 870 ha. about 75% of which is presently yielding fresh water to household wells
- c) Slightly brackish groundwater laterally surrounds and lies beneath the fresh water nuclei. This slightly brackish water is a mixture of fresh groundwater and seawater, the percentage of the latter component ranging from 1% to 10% with a TDS range of 600-3300 ppm.
 - i) the aureole of slightly brackish water associated with the Central Lens contains about 4.6×10^6 m³ water.
 - ii) the area from which water of this quality is presently (1974) being produced by household wells in the Main Island is more than 1,200 ha.

The distribution of fresh and brackish groundwater is orderly both geographically and in three dimensions and it bears a systematic relation to the occurrence of geologic units. The two key variables that together determine the nature of the groundwater at a given locality are:

- i) The thickness of the interface-bounded lens i.e. the depth below the water table of the midline of the transition zone and

- ii) The thickness of the upper half of the transition zone i.e. the depth range between groundwater of 1% and 50% salinity

Where the thickness of the interface-bounded lens exceeds the thickness of the upper half of the transition zone, there is a layer of unmixed fresh groundwater, and its thickness is given by the difference of the two. Where the thickness of the interface-bounded lens is less than the thickness of the reconstructed upper half of the transition zone, the groundwater at the water table is brackish, and its composition can be determined approximately by the difference. Further, the increase in relative salinity with depth, that is, the composition of the groundwater at a particular position above the midline of the transition zone depends on the overall thickness of the zone. (Vacher 1974).

The geometry of the interface-bounded lens and the transition zone, and hence the geographic distribution of fresh and brackish water, reflects the fact that relatively low permeability limestone of the Southampton and Rocky Bay Formations occurs on the north side of the island and relatively high permeability limestone of the Town Hill and Belmont Formations occurs on the south side of the island.

- i) The interface-bounded lens swells in the Southampton and Rocky Bay Formation rocks and thins in the Town Hill and Belmont Formations.
- ii) The transition zone, which, in general, thins in the inland direction, does so at a greater rate in the Southampton and Rocky Bay rocks than in the Town Hill and Belmont rocks.
- iii) The net results is that the various freshwater nuclei are mostly or entirely in the Southampton and Rocky Bay Formation rocks.

The continuity equation for hydrologic elements is called the Hydrologic Equation and gives a water budget for the reservoir. The equation states that if the amount of water entering the component at a given instant in time exceeds the amount of water leaving that component (ie the groundwater regime), at that time, then the amount of water stored there is increasing.

The concept of safe yield used to mean that extraction at the rate of recharge would maintain the groundwater reservoir. Extraction greater than recharge begins depletion of the reservoir. However, in the case of fresh water lenses the upper and lower boundaries of the lenses are movable surfaces; their position in space is dictated by the volume of flow and its route within and through the lens.

The following analysis illustrates the water budget elements before and after human caused development:

Before development: total inflow (recharge) = total outflows + change in volume

Total outflow = shoreline discharge + total pumping

Therefore, before development recharge = shoreline discharge

In the final adjusted state:

Shoreline discharge = recharge - pumping

During the transitional state between the commencement of increased extraction and the final adjusted state, shoreline discharge steadily decreases to reach its final lower rate. At that time total outflows exceed recharge so the volume of the lens steadily decreases. The volume of the lens that is adjusted to the imposed extraction is less than the volume prior to the extraction. The result of the extraction (in this case assuming the use is consumptive and is not returned to the ground) is that the lens decreases to a lesser volume. Therefore planning for decreases of fresh groundwater in storage and how much decrease can be tolerated is essential. The framework for these kinds of considerations involves the relationship of the volume of the lens to the internal routing of water within it. Assessing this cycle is made more complicated with sea level rise and salt water intrusion.

This assessment requires a periodically updated quantitative hydrologic budget for each groundwater lens. The exercise must include an evaluation of the amount of rainfall and evapotranspiration as well as the assessment of the quantities of water that flow through the soil zone into the underlying rock and through the subsystem that includes household tanks and cesspits. The recharge to the groundwater table is a key variable affecting the distribution of fresh and salty groundwater, the chemistry of the fresh groundwater, the vertical fluctuations of the water table, and the drawdown of the water table in response to pumping.

The paths through which water passes from atmosphere to the groundwater in Bermuda are as follows:

- 1) Rainfall lands on vegetated soils. A portion of rainfall is absorbed by vegetation and transmitted back to the aquifer by evapotranspiration. Some runs off to natural depressions where it either evaporates from the soil, is transpired by plants or infiltrates into the underlying limestones entering the aerated or vadose zone. The water moves downward under the influence of gravity but is resisted by capillary forces within the pore spaces. The water that the pore spaces do not hold percolates downward through the vadose zone and enters the water table as groundwater recharge.
- 2) Rainfall lands on the marshes. The marshes likely represent outcroppings of the groundwater reservoir, due to the presence of thick peat deposits underlying the marshes, there is a muted hydraulic connection between the groundwater in the marshes and groundwater in the limestones. Water is continuously available to plants in the marsh. Some of the rain that falls on the marshes is directly transmitted back to the atmosphere by evaporation from the water surface and evapotranspiration from vegetation. During the period in which water levels in the marsh are higher than in the surrounding limestone, the remaining water (that is the amount of rainfall that exceeds evapotranspiration) flows from the marsh into the limestone reservoir. During

- periods when the rainfall cannot satisfy the needs of the plants in the marsh, the marsh acts as an evapotranspiration-driven pump. During these periods groundwater flows back into the marsh from the limestone reservoir and the water surface in the marsh is lower than the water table in the surrounding limestone. On an annual or longer term basis there is probably recharge of the groundwater reservoir from the marshes.
- 3) Pembroke Marsh East was Pembroke's waste disposal site and now serves as a composting site. According to Vacher (1974) calculations indicate some $2.55 \times 10^4 \text{ m}^3$ per year infiltrate the waste and enter the reservoir. This water then flows both north and south becoming progressively diluted by clean groundwater in the lens as it discharges into the ocean. Thomson (1989) disputes this recharge of the groundwater lenses from the waste disposal site. It is likely that the actual situation lies in between the scenarios of Vacher and Thomson. This is because the base of this marsh is a thick layer of peat deposits up to 15 m thick (Vacher, 1974) which is not likely to be impermeable. Although peat has a low hydraulic conductivity, this layer could constitute a leaky confining layer between shallow and deep groundwater allowing some leachate seepage into the Central Lens. Leachate flow through the peat would result in significant adsorption of organic pollutants which may be present in the leachate due to its high adsorptive capacity. Peat has significant quantities of labile organic carbon which is essential to the retardation process.
 - 4) Anthropogenic sources of water (rainfall that short-circuits the natural elements of the infiltration process) include buildings that have a constructed catchment area on the roof where the water is routed to individual storage tanks for domestic use. Nearly all households use cesspits for human waste disposal. In some areas (Hamilton and Prospect) the waste water is carried in a sewer system to be discharged in the ocean, in some cases after a septic system stage.

- 5) Constructed waterproof surfaces are drained (in some cases) by wells drilled to the water table. In other areas water runs off from roads and infiltrates into the soil, is then evapotranspired by plants or is evaporated from the road surface. In most cases the new routes water takes are short cuts in the hydrologic cycle. These short cuts represent significant alteration of both the quantity and quality of the infiltrating water. Under natural conditions in Bermuda nearly 90% of the water that infiltrates the soil is transmitted back to the atmosphere by evapotranspiration before reaching the water table. (Vacher, 1974) In contrast to this, it has been estimated that 80% of rainfall that lands on roof catchments goes through a cesspit and enters the groundwater reservoir. For water that falls on roof catchments and is discharged to a sewage system which discharges into the ocean, the rainwater bypasses all natural storage functions. It is estimated that 10% of rainfall is lost from storage in built-up areas with roof catchments where the sewage is discharged into the ocean. (Vacher, 1974)
- 6) Water that is extracted from the groundwater reservoir by wells, tunnels and infiltration galleries: The characteristics of the various routes and their effect on the overall water budget depend on the use and subsequent fate of the pumped water. Water that is extracted for gardening use or crop irrigation goes back into the soil and a significant portion of it is evapotranspired back to the atmosphere. This is net outflow from the reservoir. Water that is extracted for human use in sewered areas goes into the ocean and is consumptive use, an outflow from the reservoir. Some water is extracted from the reservoir and transported by pipeline or truck and represents an outflow from the reservoir.

As noted earlier, the first calculation of recharge over the 688 ha. Central Lens was approximately 16% of the rainfall that falls on the area (18 cm/year average) Vacher (1974). Vacher and Ayers (1980) obtained values of 35-45 cm/yr using three independent

methods. Rowe (1981) calculated 30 cm/yr but included road runoff and infiltration through cesspits. Rowe (1984) calculated 55-65 cm/yr recharge including unnatural contributions such as infiltration through cesspits. Thomson obtained recharge rates of 40-75 cm/yr using a steady-state model. (Thomson, 1989).

From the water budget calculations, it was estimated that the average water use by Bermudans is 136 L/day.

For the Central Lens: About one quarter of the water that passes through the saturated zone of the Central Lens has passed through a cesspit. This practice of capturing rooftop rain has increased the flow into the reservoir by 4.41×10^5 m³/yr. (Vacher, 1974) The use of sewers and discharge to the ocean reduces the water entering the reservoir. This flow has been estimated to be 10% of annual rainfall.

Approximately 2.55×10^4 m³/yr of recharge from precipitation flows through the Pembroke Dump waste and into the reservoir. No information on the extent of the leachate plume from the Pembroke dump appears to be available. It is not known what the concentrations of leachate related parameters are or whether there are any organic contaminants of consequence in the plume and whether the leachate is attenuated naturally by dilution, dispersion and diffusion and retardation or emerges on the shoreline to discharge into the ocean. Given that the base of the marsh upon which the landfill was built, it is possible that much of the leachate generated over the years has been attenuated by the highly adsorptive nature of the peat and that the facility may be characterized as a natural attenuation site.

The Central Lens appears to be shrinking according to Vacher (1974) because of the large amount of water exported from the area. This is, however, being offset by the significant volume of water that is directly recharged through the cesspits. Bermuda Water Works reduced its extraction from 2,596 m³/d to 1,591 m³/d between 1978 and 1989 (S. Lavis, personal communication) which would have likely reduced or reversed the shrinkage of the lens.

The Water Table

The water table is the air-water interface in the subsurface where the water pressure is equal to atmospheric pressure and is the top of the saturated zone of the aquifer. Below the water table surface the pores and fractures of the porous medium are saturated. Above the water table surface is the capillary fringe which includes both the tension-saturated and unsaturated portions of the vadose zone. The water table is variable in elevation geographically. The elevation of the water table at any location represents the hydraulic head at that location. Hydraulic head is the potential energy per unit mass of the flowing groundwater. Groundwater flows from areas of high hydraulic head (high elevation of the water table) to areas of lower hydraulic head, ultimately sea level (in Bermuda's case). The shape of the water table surface is not constant and varies with topography as well as with recharge from precipitation and atmospheric pressure changes, and, in the case of small oceanic islands such as Bermuda, oscillates up and down with oceanic tides, the local steric anomaly and meso scale effects. Long term sea level rise from climate change also affects the elevation of the water table at any point. The configuration of the water table, specifically the elevation of the water table at multiple points across the landscape as measured by wells and springs, indicates the hydraulic head and thus the nature of the groundwater flow system and the hydraulic properties of the porous medium through which the water flows. A contour map of the water table surface, measured in terms of elevation above sea level, shows lines of equal potential. The horizontal hydraulic gradient, indicated by the space between the contours, is the slope of the water table. The relation connecting groundwater flux in m³/day to hydraulic gradient (metres decline over distance in metres) is Darcy's Law:

$$q = -KA \frac{dh}{dl}$$

Where: q is the flux of groundwater m³/day

K is the hydraulic conductivity m/day

$\frac{dh}{dt}$ is the hydraulic gradient m/m

A is the cross sectional area perpendicular to the direction of flow m²

Typical units are shown but any consistent set of units can be used.

The natural, vertical fluctuations of the water table are of two fundamental kinds:

- 1) The fluctuations resulting from intermittent recharge (infiltration from precipitation). This affects the volume of fresh water stored in the interface bounded lens over time.
- 2) Fluctuations from changes in the level of the surrounding ocean which are not related to changes in volume of the interface-bounded lens. They reflect the vertical motion of the entire lens as seawater moves in and out of the island beneath the lens in response to the changing ocean levels.

Recharge Related Fluctuations

A recharge event will cause the water table to rise once the infiltrating precipitation reaches the water table. This would also increase the thickness of the fresh-water column thus disturbing the hydrostatic equilibrium and the interface between fresh and saline water underlying the lens lowers in elevation. After the recharge event ends, the water table subsides in an exponential decay curve declining to the elevation where hydrostatic balance is restored. The dynamics depend on the densities of fresh and saline water which vary with dissolved solids content and temperature. Since the temperature of both sea water and precipitation vary between summer and winter, the thickness of the fresh water lens and the location of the mixing zone between fresh and salt water will vary seasonally all other factors being equal.

Fluctuations Related to Changes in Sea Level.

Changes in ocean levels around Bermuda are easily translated into the island's interior because of the very permeable nature of the Walsingham Formation. As the sea level oscillates from tidal and barometric forcing, these oscillations are transmitted inland and affect the position of the water table. The entire fresh water lens moves up and down in concert with the water table. This rise and fall effect decreases in magnitude away from the shoreline. The controlling factors of the magnitude of the oscillations are the permeability of the rocks and the amplitude and period of the sea level oscillation. The response to ocean oscillations can be explained with a mathematical model where the amplitude of the fluctuation drops to zero following an exponential decay function with increasing distance from the shoreline; the lag time increases linearly inland from the shoreline, and the damping varies inversely with the period of fluctuation. (Vacher, 1974). Observing the response of the water table in terms of daily elevation and seasonal changes over the long term is important in assessing the performance of the fresh water lenses in response to the influences outlined above.

Data recorded for the 1974 Vacher study showed tidal oscillations at numerous well locations which reflect the passage of a train of inland moving, progressively dampened waves generated from the shoreline. Longer period fluctuations are a dominant feature of wells that penetrate the limestone reservoir and are related to the response of sea level changes to atmospheric pressure. These are similar waves to those produced by tidal oscillations. In the ocean the pressure related sea level fluctuations are obscured by the larger amplitude tidal oscillations. For the water table this pattern is reversed. The amplitude of fluctuations due to changes in atmospheric pressure is greater than that of the tidal oscillations. Longer period, pressure related fluctuations of sea level are less attenuated within the porous media than generated by tidal oscillations.

As the fresh water lens rises the groundwater flow from the centre of the lens toward the shoreline increases and subsequently decreases once the elevation of the water table decreases. There is a lag time between periods of high tide and the maximum rise of the water table depending on how far from the shoreline the maximum rise occurs.

Vacher (1974) observed that hydrographs of wells that penetrate the limestone reservoir seems to be composed of three superimposed fluctuations of different period:

- a) A seasonal oscillation with a period measured in months and a range of up to 25 cm, the local steric anomaly;
- b) An irregular fluctuation reflecting changes in atmospheric pressure, and with a variable period measurable in days
- c) A regular oscillation due to astronomical tides and composed largely of semi-diurnal and diurnal components.

Vacher concludes that the fluctuations in the water table are related to changes in the level of the surrounding ocean with no obvious effect due to unsteady recharge.

Tide generated waves of the water table experience different rates of damping in the lower permeability Southampton and Rocky Bay Formations of the Langton Aquifer than in the higher permeability Town Hill and Brighton Formations in the Brighton Aquifer due to the differences in hydraulic conductivity of the formations (Southampton and Rocky Bay Formations (Langton Aquifer) less permeable than the Town Hill and Brighton Formation rocks (Brighton Aquifer)). The tide generated wave is dampened at a greater rate per unit distance from the shoreline in Southampton and Rocky Bay rocks when compared to Town Hill and Brighton rocks.

For the Central Lens, where the Southampton and Rocky Bay Formation rocks of the Langton Aquifer are between the more or less east-west line of inland ponds and the

north coast, the damping is greater than in the Town Hill and Brighton Formation rocks (Brighton Aquifer) which are located between the inland ponds and the south coast.

For tidal fluctuations the amplitude of the pressure related water table fluctuations is less than that of the barometric fluctuations and the occurrence of the extremes is somewhat later than those of the barometric fluctuations. In addition, there appears to be a mechanism of selected removal of shorter period fluctuations reducing the 'noise' in the long term fluctuations thus making the signal of the fluctuations more obvious. It was apparent that the reduction in amplitude of the barometric fluctuations was considerably less than the reduction in amplitude of the shorter period oceanic tides (Vacher, 1974).

Vacher (1974) states that a water table map drawn from monthly average groundwater level elevations would give a statistically meaningful representation of a flow system for that particular month. This is because the longer period fluctuations are geographically concordant and their period is less than a month.

The configuration of the water table in the Central Lens has the following features:

- a) A general axial mound with flow both south and north to the shorelines on each side of the island. This axial divide is roughly parallel to the midline of the island but is closer to the north shore than the south shore.
- b) A steep sided valley on the water table surface in the vicinity of Foot of the Lane which likely indicates concentrated flow to the sea in this area
- c) A steep sided valley east of Mills Creek which indicates drainage into Mill Creek and the Pembroke Drainage Canal. However, Thomson, (1989) disputes these flows to the sea in c). Thomson states that, "It is unlikely that such outflows take place. The Canal, a shallow ditch dug in the 1800's to drain low-lying areas, runs over a now-reclaimed peat marsh and is not connected to the aquifer."
- d) A large saddle on the water table surface in the vicinity of the Devonshire Marsh West in the area of the Bermuda Waterworks flow galleries. The

saddle indicates convergent flow into the Devonshire Marsh area caused by the abstraction.

The overall maximum elevation of the water table (March, 1974) in the Central Lens is on the order of 0.30 m(1.0 ft.) to 0.37 m (1.2 ft.) on the east-west divide (Vacher, 1974). It is probable that the elevation is in reference to ordnance datum.

Marshes and Groundwater Dynamics

The fluctuation of the water level in the Devonshire Marsh (Vacher, 1974) which applies to all marshes, ponds and lakes in Bermuda is that there are two separate components affecting water levels: the precipitation component which causes an abrupt surface water level rise (which is the surface expression of the water table) followed by an exponential decline. The decline of the water level occurs because the water flows into the limestone reservoir along with a decline in the fresh water lens. The evapotranspiration component causes the water level to drop during the day with plants taking up the water and transpiring it in addition to direct evaporation from the water surface followed by the water level rising at night caused by influx from the limestone reservoir and/or rise of the fresh water lens.

Thomson (1989) disagrees with Vacher's point of view on the marshes. He maintains they are largely separated from the groundwater body because:

- 1) they are underlain by low permeability peat deposits to 15 m below Ordnance Datum (bOD) which act as a barrier to flow between the groundwater in the peat and groundwater in the fresh water lens
- 2) marsh and groundwater hydrographs behave differently even when a few metres apart. Groundwater in the lenses show semi-diurnal tidal effects while marsh water responds to daily marsh vegetation transpiration cycles
- 3) there is negligible recharge in the marshes except Pembroke Marsh East which is the landfill site and is unvegetated. Thomson says this is drained by the Pembroke Canal.

- 4) Geochemical studies (Simmons, 1985, 1987) indicate no migration of leachate from the landfill into the aquifer. He does, however, qualify this conclusion by saying that groundwater density may play an important role in this assessment and that the density of landfill leachate may result in a leachate plume which occurs deeper in the aquifer than the depth of the observations wells available for sampling (Simmons, 1987).

Detailed monitoring of the water level response in marshes and lakes along with monitoring water level response in the adjacent limestone aquifer would help in the understanding and clarifying the hydraulic behaviour of the marshes in relation to the freshwater lenses. The understanding of the following components of the water balance would be very useful:

- a) The quantity of water exchanged back and forth between the marsh (or pond or lake) and the surrounding limestone aquifer
- b) The time taken to restore hydrostatic balance after a sudden change in the elevation of the water table
- c) The evapotranspiration rate in areas where water is nearly always available to plants (potential evapotranspiration PE)
- d) Deeper monitoring of the aquifer underlying the landfill. Leachate plumes can be detected by geophysical methods and by installation of deep piezometers in boreholes.

Mangroves in Relation to Sea Level Rise and Salt Water Intrusion

Low island mangroves keep up with slow sea-level rise by peat accumulation. Holocene stratigraphic records show that they maintain the same pace of peat accumulation as sea-level rise at rates up to 9 cm/100 years. Tide gauge records from Bermuda since 1932 show sea-level rise at a rate of 28 cm/100 years. The largest mangrove area (6.26 acres) at Hungry Bay has for the last 2000 years been building peat at a rate of 8.5 to 10.6 cm/100 years. Retreat of the seaward edge has caused loss of 2.24 acres of mangroves,

commencing in the last few hundred years, with a second dieback between 1900 and 1947, and a third dieback in the last decade. The substrate elevation of the seaward margin of mangroves is below mean sea-level, the normal lower limit for mangroves. Present dieback shows problems of erosion indicating that the Bruun Rule of beach erosion with sea-level rise is also appropriate for mangrove swamps. Stratigraphy shows that before 4000 BP sea-level rose at a rate of 25 cm/100 years, from 4000 to 1000 years BP the rate of sea-level rise declined to 6 cm/100 years during which time mangroves established, and in the last 1000 years there was an increase to 14.3 cm/100 years, during which time the mangroves died back. This study indicates that low island mangroves will experience problems with the rates of sea-level rise predicted for the foreseeable future. (Glasspool, 2008)

Sea Level Rise and the Effect on the Fresh Water Lenses

Sea levels are rarely if ever static on the geological time scale. Stratigraphy in Bermuda shows that before 4000 years before present (BP) sea-level rose at a rate of 25 cm/100 years, from 4000 to 1000 years BP the rate of sea-level rise declined to 6 cm/100 years, and in the last 1000 years there was an increase to 14.3 cm/100 years. (Ellison, 1993) (Saintilan et al, unpublished)

Sea Level Rise (SLR) in Relation to Bermuda Ordnance Datum (OD)

The information on SLR was synthesized from literature sources, and specifically from the UWI study commissioned as part of this overall study – the MONA study (Clarke, L., Taylor, M., and Maitland, D, 2022). The purpose of this section is to correlate the local sea level around Bermuda with the elevation of the water table in the Central Lens.

Sea levels are rising relatively rapidly mainly due to human induced climate change caused by increasing rates of greenhouse gas generation and accumulation in the atmosphere since the beginning of the industrial revolution. The sum of the contributions to sea-level change from thermal expansion of the ocean, ice-mass loss and changes in terrestrial water storage is consistent with the trends and multidecadal variability in

observed sea level on both global and basin scales, which were reconstructed from tide-gauge records.

Ice-mass loss, predominantly from glaciers, has caused twice as much sea-level rise (SLR) since 1900 as has thermal expansion. Mass loss from glaciers and the Greenland Ice Sheet explains the high rates of global SLR during the 1940s, while a sharp increase in water impoundment by artificial reservoirs is the main cause of the lower-than-average rates of SLR during the 1970s. The acceleration in SLR since the 1970s is caused by the combination of thermal expansion of the ocean and increased ice-mass loss from Greenland. (Frederikse et al, 2020).

Between 1860 and 2010, a rise in global mean sea level (gmsl) of 245 mm has occurred. This is an average global SLR of 1.63 mm/yr. ([Church and White, 2011](#)). NASA gives the rate of sea level rise from 1900-2018 as 1.56 mm/yr which translates to a total rise in that period of 184 mm with an uncertainty of plus or minus 0.3 mm/yr. The rise since 1993 was 3.35 mm/yr which translates to 84 mm (1993-2018) with an uncertainty of plus or minus 0.47 mm/yr. (Frederikse et al, 2020, NASA Climate Change Portal).

Between 1860 and 1900, the sea level rose 50 mm, so in a comparable time to Church and White estimates (1860-2010), sea level rose 184 mm plus 50 mm=234 mm. Assuming the SLR of 3.35 mm/yr between 1993 -2018 is the same rate as between 2010 and 2018, the SLR estimate based on the Church and White calculation between 1860 and 2018 is 234 mm plus 26.8 mm=261 mm. The two estimates of SLR over the period 1860-2018 are within 11 mm. This SLR is consistent with the graph of msl vs OD.

Sea levels and the rate of sea level rise is variable across the globe. The NOAA website (<https://oceanservice.noaa.gov/>) shows that the SLR on the eastern margins of North America extending past Bermuda is higher than the global average.

Ellison (1993) quotes studies by Barnett (1984) and Pirazzoli (1986) with sea level rises computed from the tide gauge in Bermuda since 1932 as 24.0 cm/100 yr. and 28.0 cm/100 yr. respectively. This is 2.4 mm/yr-2.8 mm/yr. According to NOAA, SLR began rising at

a higher rate than previously in 1993 as discussed above. It is assumed that local sea level in Bermuda also saw an acceleration of local SLR. The MONA study calculated the annual mean sea level plot for the nearest relevant grid box to Bermuda Station (Latitude 32.373N and Longitude 64.703W) from the C3S data for the period of 1993-2020. The observed linear trend of sea level rise is approximately 3.84 ± 0.4 mm/year (Clarke, L., Taylor, M., and Maitland, D, 2022) The MONA study concluded: For Bermuda, there is good consensus across the two mapping tools examined about sea level rise. Though RCPs and SSPs are not directly comparable, by 2050, mean SLR is projected to 0.23m for RCP4.5 and 0.21m SSP2-4.5; while by 2100, mean SLR is projected to be 0.53m for RCP4.5 and 0.56 for SSP5-8.5. AR6 (IPCC 2022) suggests that if expert judgement on high impact ice-sheet processes and inputs from a model incorporating Marine Ice Cliff Instability are considered then by 2100, SLR may reach up to 1.46m for Bermuda according to SSP5-8.5. These projections are less than estimates of global mean sea level rise by 2100 which are 0.56m for SSP2-4.5 and 0.77m SSP5-8.5.

Table 19 from the MONA Study Showing Local Sea Level Projections at St. Georges, Bermuda

Year	Local Sea Level Rise (cm)			
	RCP	Median	Uncertainty Ranges	
			66%	90%
2030	2.6	13 [13]	7-19 [8-18]	2-24 [5-22]
	4.5	12	6-19	1-24
	8.5	12 [14]	5-20 [6-22]	0-26 [1-28]
2050	2.6	23 [26]	15-33 [17-37]	9-41 [10-49]
	4.5	23	14-34	7-43
	8.5	25 [32]	14-37 [20-46]	7-47 [11-61]
2100	2.6	48 [64]	27-73 [42-92]	14-100 [27-124]
	4.5	53	28-82	12-110
	8.5	65 [102]	34-102 [61-160]	14-136 [37-243]

Ordnance datum was set at a mean sea level (msl) of 0.000 m in 1963 from tide gauge records at the Bermuda Biological Station. (Johnson, 1984 cited in Ellison, 1993).

Glasspool 2008, gave msl as 0.21 m AOD. Plotting these values on a graph gives a 2022 msl of 0.26m AOD. The local sea level around Bermuda is rising approximately 4 mm/yr from 1993-2022.

The Central Lens Water Table and Sea Level Rise

As indicated above, Bermuda's fresh-water lenses float on the underlying saline groundwater due to the density differences between fresh and salt water. Sea water rise is translated throughout the subsurface of Bermuda through the highly permeable Walsingham Formation rocks with the result that a rise in sea levels is translated into a comparable rise of the fresh water lenses. The interface zone of mixing of fresh and saline water at the base of the lenses and the water table will rise at the same rate on average.

Data available for the analysis of the water table made available for this report included water table measurements in wells and the map of the March, 1974 water table in the Central Lens (Vacher 1974), the 1978 manuscript made available by Shaun Lavis from an unknown author, plus several spreadsheets that showed yearly average Central Lens water table elevations for the period 1975 – 1976 and monthly water table data for the Central Lens from 1988 to 1995. Average annual thickness of the freshwater lenses from the water table to the 3% mixing zone were also available for the period 1999-2020.

The water table data were used as a basis for judging the change in elevation of the water table between 1974 and 1994. The water table was plotted for the average water table elevations measured in March, 1994. The maximum water table elevation in the Central Lens in March 1994 was the Prospect Gym (PG or PRG) well with an elevation of 1.48 ft (0.45 m). This well in March 1974 had an average elevation of the water table as 1.15 ft (0.35 m). The difference is 0.1 m. Plots of the water table in the Central Lens in March 1974 and 1994 show approximately the same relative rise for water in wells in comparable areas.

The local rise in sea level between 1974 and 1994 is approximately 0.1 m which is the rise in the water table in that period. The mean average sea level rise from the Bermuda tide gauge is quite variable between the early 1970s and early 1990s. (see Ellison, (1993) Figure 2) It is recognized that comparing two water table configuration measurements of the Central Lens over 20 years does not prove water table rise is in concert with local SLR. Multiple months in 1974-1976 require analysis and then should be compared to multiple months in several years in the present (2022) and in the future. It is important to map the configuration of the water tables in the lenses as they rise under the influence of sea level rise to determine if and where the water tables intersect the ground surface and thus, increase the flow of fresh groundwater to the sea.

It is clear that a longer interval between water table representations is required to assess the effects of rising sea levels on the water table in the Central Lens. According to Vacher (1974), Section 4.3 and 4.5, the longer period fluctuations of the water table in the Central Lens are substantially less than a month. He concludes that the water table map drawn from monthly averages of elevations in wells gives a statistically meaningful representation of the flow system for that particular month. Therefore, comparing months that are 40 years or more apart should give a realistic indication of the amount of sea level and comparable groundwater level rise that has occurred over that period. It is suggested that this should be verified by additional calculations of the average monthly water table from 1995 to 2022 if monthly data for the wells can be located.

As detailed previously, fresh groundwater in the lenses underlying Bermuda constantly oscillate up and down in response to tidal effects, the local steric anomaly (rise due to expansion of water with temperature and salinity changes) and meso scale effects caused by the proximity of the Gulf Stream. To determine the maximum projected future SLR in coastal areas of Bermuda in relation to the topography in a given year, a common datum must be used. In addition, the effect of maximum spring tide, the local steric anomaly plus meso-scale effect must be added.

This steric anomaly occurs seasonally such that, in the early summer, an upper "mixed layer" of warm water develops in the ocean around Bermuda, with temperatures often exceeding 25°C by late summer and extending down to 100 m depth or more. Therefore from April to November the surface ocean waters around Bermuda undergo thermal expansion with a related sea level rise of about 0.125 m (Glasspool, 2008). This steric anomaly, combined with monthly spring tides, causes very high sea water levels typically observed as peaking in October (GlobalSecurity.org July, 2022, <https://www.globalsecurity.org/military/world/caribbean/bm-climate.htm>) A comparable drop in sea levels occurs around March each year for a total vertical range in the steric anomaly of 0.25 m.

The rise and fall of the sea level at the coast of Bermuda is translated inland and causes the fresh water lenses to rise and fall as well. Since the topography of Bermuda rises relatively steeply from the shoreline, the rise of the fresh water lenses are not likely to intercept the ground surface except for a limited area near the coast in the foreseeable future. Therefore the shape of the groundwater lenses in cross-section are predicted to stay the same assuming extraction and recharge remain constant. This is a recharge limited system as explained above rather than a topography limited system and the horizontal hydraulic gradient (and thus the groundwater flow to the sea) will remain the same in the future assuming the hydraulic conductivity of the aquifer is more or less the same above the existing water table as it is below the existing water table and the recharge remains the same.

In the coastal areas the sea level rise combined with the maximum tidal effect plus half the steric anomaly plus meso scale effects is currently (2022) calculated to have resulted in saline water some 1.49 m above OD intruding into the subsurface or 1.23 m above existing calculated sea level. Glasspool (2008) estimated sea level rise without including meso scale anomalies. In this study half the steric anomaly is used plus the meso scale effect since the rise in sea level will deposit salt within the pores of the rock or soil which will stay in situ for a period even after the sea levels decline in the annual cycle. This saline water will slowly drain by gravity or be slowly displaced by recharging infiltration

but at a much slower rate than the daily and seasonal effects controlling sea level rise and intrusion into the rock and soil matrix.

The effects of tidal damping diminish the range of oscillations of the water table moving inland from the coasts. Vacher (1974) shows that on the north shore of Bermuda and moving inland, the tidal oscillation in the Central Lens is reduced to 10 cm at 100-120 m from the north shore and reduced to 2 cm within 200 m from the north shore. The maximum tidal range at the coasts during spring tides is 1.2 m. This Central Lens north of the line of east-west trending inland ponds is underlain by the Langton Aquifer with its relatively low permeability rocks. The higher permeability Brighton Aquifer to the south has the 10 cm contour of tidal oscillation at approximately 500-600 m from the south shore, and the 2 cm contour at approximately 800 m from the south shore. Therefore, the effects of rising sea levels will be greater inland from the south shore in the Brighton Aquifer than on the north shore in the Langton Aquifer inland from the ocean.

Barometric effects on sea level occur every few days. For a drop in air pressure of 1 mb (0.1 Kpa) sea level rises 1 cm. Since barometric pressure does vary every few days it would be prudent to include a component of sea level rise due to varying atmospheric pressure. A value of 25 cm has been used.

Capillary effects of migrating salt into the vadose zone have not been included in the estimates of salinization. Further studies are required in different environments and soil types to determine the scope and extent of capillary effects.

Table 1 give the MONA projected sea level rises and ranges to be expected in the 21st century for RCP 4.5 and 8.5 around Bermuda(Clarke, L., Taylor, M., and Maitland, D, 2022)

Table 1 MONA Projected Sea Level Rises with RCPs

Year	RCP	Median Projected Sea Level Rise m	66% Uncertainty Range m
2030	4.5	0.12	0.06-0.19
2050	4.5	0.23	0.14-0.34
2100	4.5	0.53	0.28-0.82
2030	8.5	0.12	0.05-0.20
2050	8.5	0.25	0.14-0.37
2100	8.5	0.65	0.34-102.0

Notes: RCP Representative Concentration Pathway

With the projected sea level rise from the calculated 2022 sea level in relation to Bermuda Ordnance Datum, future projected sea level rises under RCP 4.5 are given with reference to this datum are given in Table 2.

Table 2 Projected Sea Level Rise and Elevation above Bermuda Ordnance Datum, RCP 4.5

Year	Years from Present	Projected Sea Level Rise (m) Extrapolated From Mona Data	Projected Sea Level above Present Level m above OD
2022	0		0.26
2042	20	0.18	0.44
2072	50	0.36	0.62
2122	100	0.66	0.92

Notes: OD Bermuda Ordnance Datum

The sea level rise for 2122 for both RCP 4.5 and 8.5 was calculated from graphing the MONA data plus OD and extrapolating to 2122. There is no allowance for the acceleration of sea level rise which may occur.

Table 3 shows projected sea level rise under RCP 8.5 in relation to the Bermuda Ordnance Datum.

Table 3 Projected Sea Level Rise and Elevation above Bermuda Ordnance Datum, RCP 8.5

Year	Years from Present	Projected Sea Level Rise (m)	Projected Sea Level above Present Level (m) above OD
2022	0		0.26
2042	20	0.18	0.44
2072	50	0.45	0.71
2122	100	0.85	1.1

Table 4 shows the expected sea level rise around Bermuda which includes tidal effects, the local steric anomaly and meso scale effects for RCP 4.5 and 8.5. This will also be the projected maximum rise of the groundwater lenses including the water table at the coasts. The tidal effect on groundwater lens rise will diminish fairly rapidly and progressively inland from the coasts.

Table 4 Projected Sea Level Rise around Bermuda plus Tidal, Steric and Meso Scale Effects, RCP 4.5 and 8.5 Equals Total Groundwater Lens Rise at the Coasts

Years From Present (2022)	RCP	Sea Level Rise Above OD m	Maximum Tidal Height m	Local Steric Anomaly m	Meso Scale Effects m	Barometric Pressure Effects m	Bermuda Subsidence Below 2022 Level m	Total Projected Groundwater Rise above OD m
0	4.5	0.26	0.6	0.125	0.25	0.25	0	1.49
20	4.5	0.44	0.6	0.125	0.25	0.25	0.018	1.68
50	4.5	0.62	0.6	0.125	0.25	0.25	0.045	1.89
100	4.5	0.92	0.6	0.125	0.25	0.25	0.09	2.24
0	8.5	0.26	0.6	0.125	0.25	0.25	0	1.49
20	8.5	0.44	0.6	0.125	0.25	0.25	0.018	1.68
50	8.5	0.71	0.6	0.125	0.25	0.25	0.045	1.98
100	8.5	1.10	0.6	0.125	0.25	0.25	0.09	2.42

The cumulative maximum sea level rise (therefore groundwater rise at the coasts) at any given time as a result of these effects will occur relatively infrequently. Spring tides occur twice each lunar month at new or full moons. Neap tides occur twice a month and occur when the sun and moon are 90 degrees from each other, at 1st and 3rd quarter. Barometric pressure effects vary daily or every few days and can be dramatic during relatively rare hurricanes which hit Bermuda. The local steric anomaly peaks in October each year at its maximum level of 12.5 cm and six months later it is at -12.5 cm. Meso scale effects can occur at any time around Bermuda and they emerge from instabilities of the strongly horizontally sheared motions of the Gulf Stream. These eddies often take

the form of well-defined rings extending to great depth and can last for weeks to over a year. (NOAA <https://oceanservice.noaa.gov/facts/eddy.html>).

In addition, the entire landmass of Bermuda is sinking at a rate of 0.9 mm/yr. which will add to apparent sea level rise of 9.9 cm after 100 years. Satellite GPS vertical motion velocity data published by the Jet Propulsion Laboratory in the US indicates that the island has been subsiding at the rate of 0.9 mm/year since 1993. These data have been derived from the vertical motion sensor positioned at the Bermuda Institute of Ocean Sciences. This subsidence will add to apparent sea level rise of 9.9 cm after 100 years. (Glasspool, 2008, JPL website <https://www.sonel.org/-JPL14-.html>)

This subsidence has been added to the total sea level rise in Table 4.

Table 5 give the total projected maximum groundwater lens rise at the inland ponds in the Central Lens area. Maximum tidal effects in these areas are diminished because of damping and the maximum rise due to tidal effects is approximately 2 cm. The exception to this is the area around and east of the Pembroke Canal where the maximum tidal effect will be 10 cm (Vacher, 1974).

Table 5 Maximum Central Lens Rise at Inland Ponds.

Years From Present (2022)	RCP	Sea Level Rise Above OD m	Maximum Tidal Height m	Local Steric Anomaly m	Meso Scale Effects m	Barometric Pressure Effects m	Bermuda Subsidence Below 2022 Level m	Total Projected Max Central Lens Rise in & around Inland Ponds, Above OD m
0	4.5	0.26	0.02	0.125	0.25	0.25	0	0.91
20	4.5	0.44	0.02	0.125	0.25	0.25	0.018	1.10
50	4.5	0.62	0.02	0.125	0.25	0.25	0.045	1.31
100	4.5	0.92	0.02	0.125	0.25	0.25	0.09	1.66
0	8.5	0.26	0.02	0.125	0.25	0.25	0	0.91
20	8.5	0.44	0.02	0.125	0.25	0.25	0.018	1.10
50	8.5	0.71	0.02	0.125	0.25	0.25	0.045	1.40
100	8.5	1.10	0.02	0.125	0.25	0.25	0.09	1.84

It is questionable whether the inland ponds (with the possible exception of Pembroke Marsh West) will become more saline as sea level rises. From the literature, it appears that the Central Lens underlies the NE-SW line of ponds and the lens will rise with rising sea levels. With the two interpretations of the degree of hydraulic connection between the ponds and the Central Lens groundwater, it is likely that the ponds will rise over the years and least as much as average sea level around Bermuda rises. If the hydraulic

connection is stronger, then some oceanic oscillations will be transmitted inland resulting in a higher water level in the ponds at various times than from sea level rise alone. The conclusion of this analysis is that the ponds in the Central Lens and the immediate surrounding area will not suffer from an increase in salinity in the foreseeable future. Monitoring of the ponds' water levels would be useful to ascertain the degree of hydraulic connection between the ponds and the Central Lens.

The saltwater ponds generally lie close to the south coasts. These are generally brackish as they lie in more permeable bedrock formations. Tidal effects are transmitted inland with less damping than along the north shore in the less permeable rocks.

The area at the west end of Pembroke Marsh West and towards the west coast from the marsh area to the Pembroke Canal will likely see an increase in salinization. Tidal effects of groundwater level rise will be strongest in the canal and rapidly diminish inland to about 2 cm in the Pembroke Marsh West. The other components of sea level rise will affect salinity levels in the groundwater around the Pembroke Canal and east possibly to the marsh.

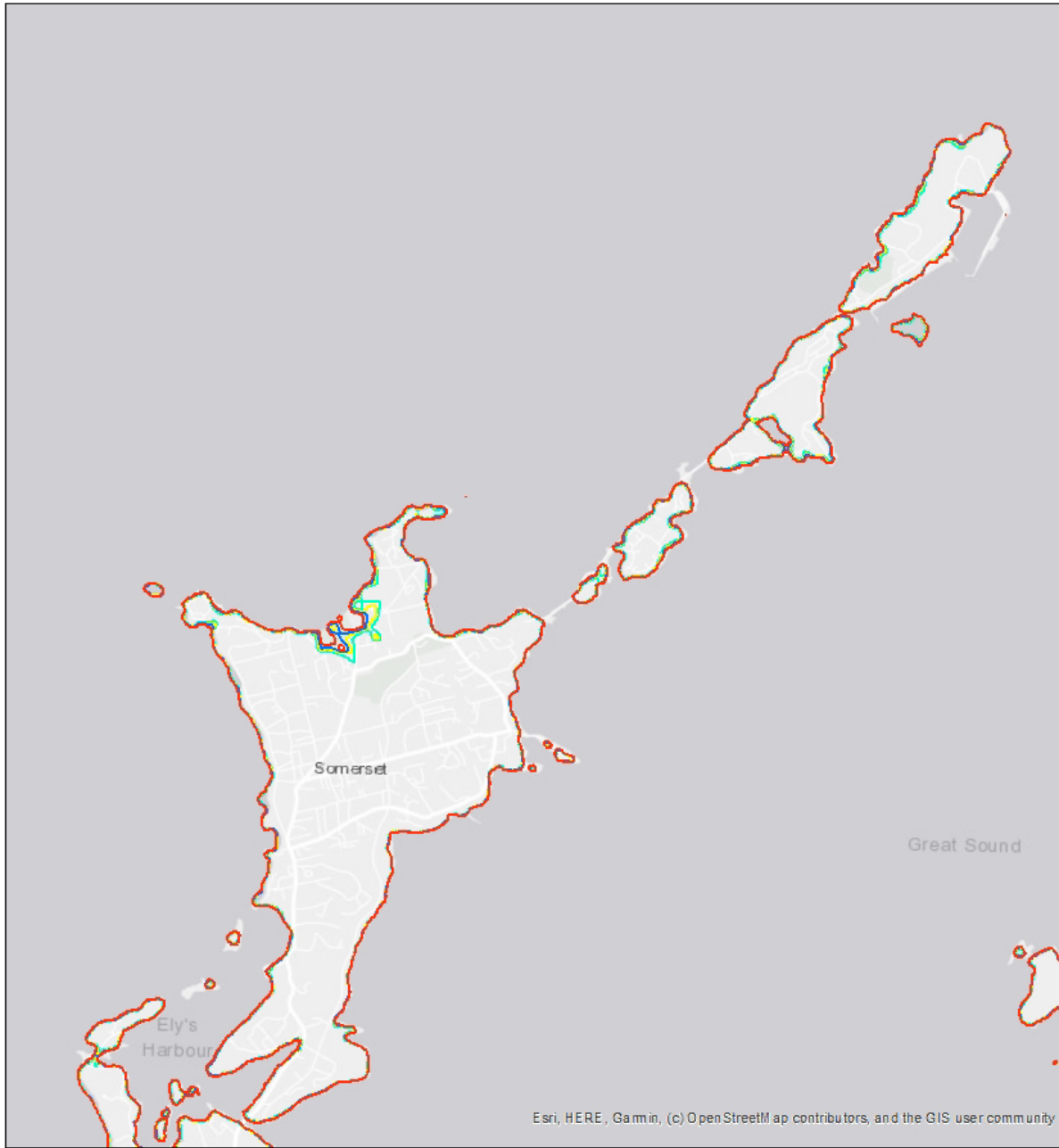
As explained above saline groundwater rising with oscillations of the ocean in areas just at the coast of Bermuda and for some distance inland will introduce saline conditions in rocks containing fresh water aquifers progressively higher in elevation as sea levels rise. Saline water will displace fresh or brackish water in the pores of the rocks of the Langton Aquifer and the pores and fractures and solution channels of the Brighton Aquifer with the greatest impact being at and near the coast. Even with the relatively infrequent occurrence of a spring tide with the passage of a low pressure area, with the October high steric anomaly and under the influence of a meso scale eddy, saline water will fill soil and rock pores to an elevation indicated on Table 4. With a decline in ocean levels (low tide, negative steric anomaly, high atmospheric pressure) some of this water will drain by gravity and the influence of recharging precipitation but the process is much slower than the water level rise. Chemical changes will occur relatively slowly and will involve cation exchange involving sodium, calcium and magnesium. This process is complicated by the

migration of the interface zone inland as sea levels rise and by the presence of the vadose zone above the oscillating water table where saline water could migrate as a result of chemical diffusion and dispersion processes. In addition, evapotranspiration could act as a pump to induce upward flow of saline or brackish water. Soil in agricultural areas near the coast may see a decline of production over the years depending on their elevation in relation to sea level.

Sea Level Rise and Associated Salt Water Intrusion and impacts on Land Use

The Government of Bermuda Digital Terrain Model (DTM) was used as the basis to produce maps showing land areas in Bermuda below the future maximum projected sea level (plus transient effects) elevation changes for two scenarios and three future points in time. The DTM works from the ordnance datum of 0 m elevation. Current mean sea level without oscillations detailed above was calculated in this study as 0.26 m above OD (2022).

Figure 1-12 show maximum projected groundwater rises (sea level plus transient effect rises) for present day, 20, 50 and 100 years under RCP 4.5 and 8.5.



Esri, HERE, Garmin, (c) OpenStreetMap contributors, and the GIS user community

BERMUDA - CLIMATE CHANGE STUDY

DOCKYARD RCP 4.5

LEGEND

- Present Groundwater Elevation 1.49 m Above OD
- Projected Groundwater Rise 1.68 m Above OD
- Projected Groundwater Rise 1.89 m Above OD
- Projected Groundwater Rise 2.24 m Above OD

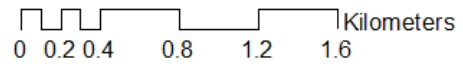
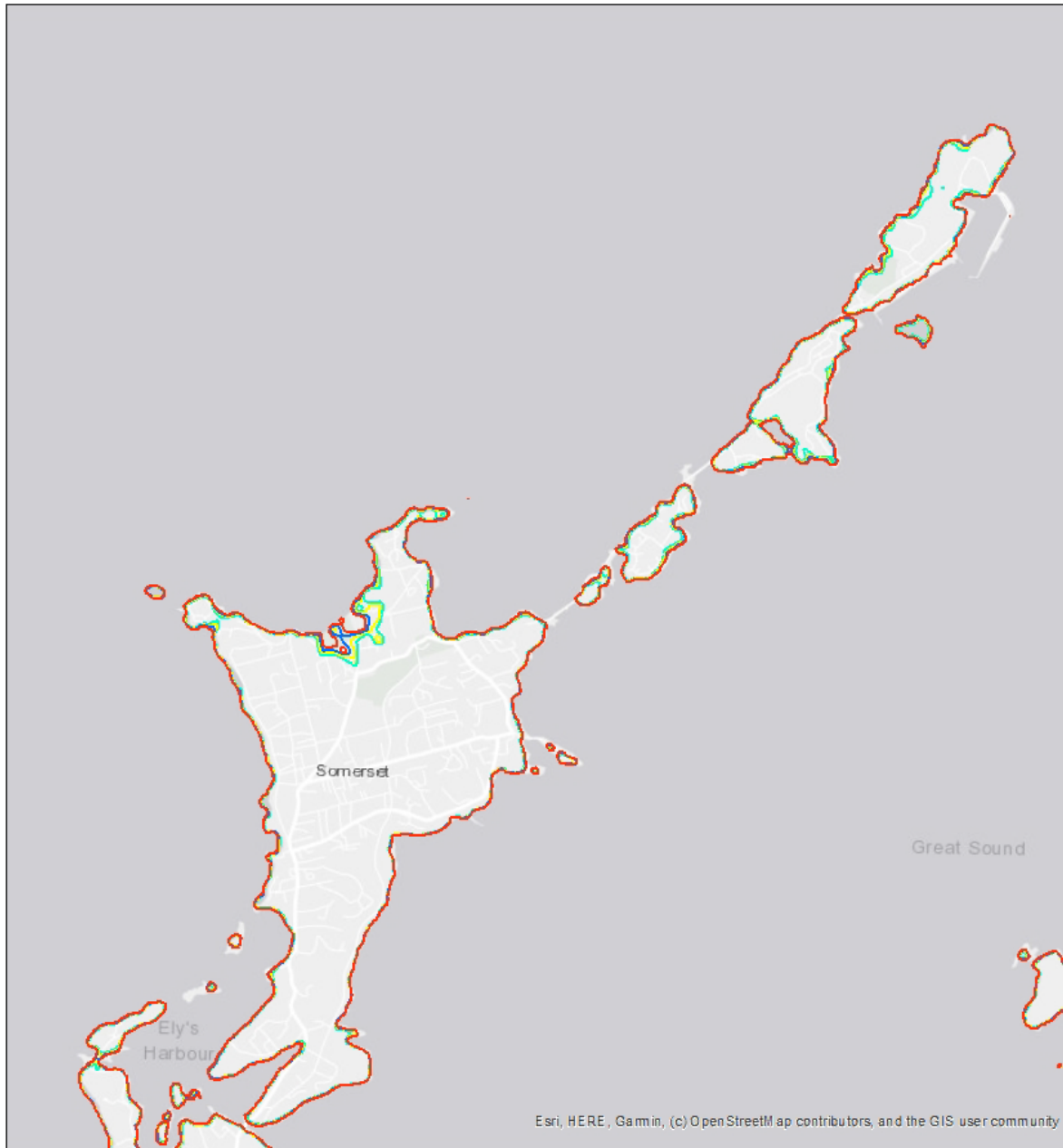


Figure 1 Predicted groundwater rise for the Dockyard area for RCP 4.5



Esri, HERE, Garmin, (c) OpenStreetMap contributors, and the GIS user community

BERMUDA - CLIMATE CHANGE STUDY

DOCKYARD RCP 8.5

LEGEND

- Present Groundwater Elevation 1.49 m Above OD
- Projected Groundwater Rise 1.68 m Above OD
- Projected Groundwater Rise 1.98 m Above OD
- Projected Groundwater Rise 2.42 m Above OD

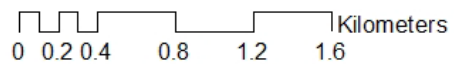
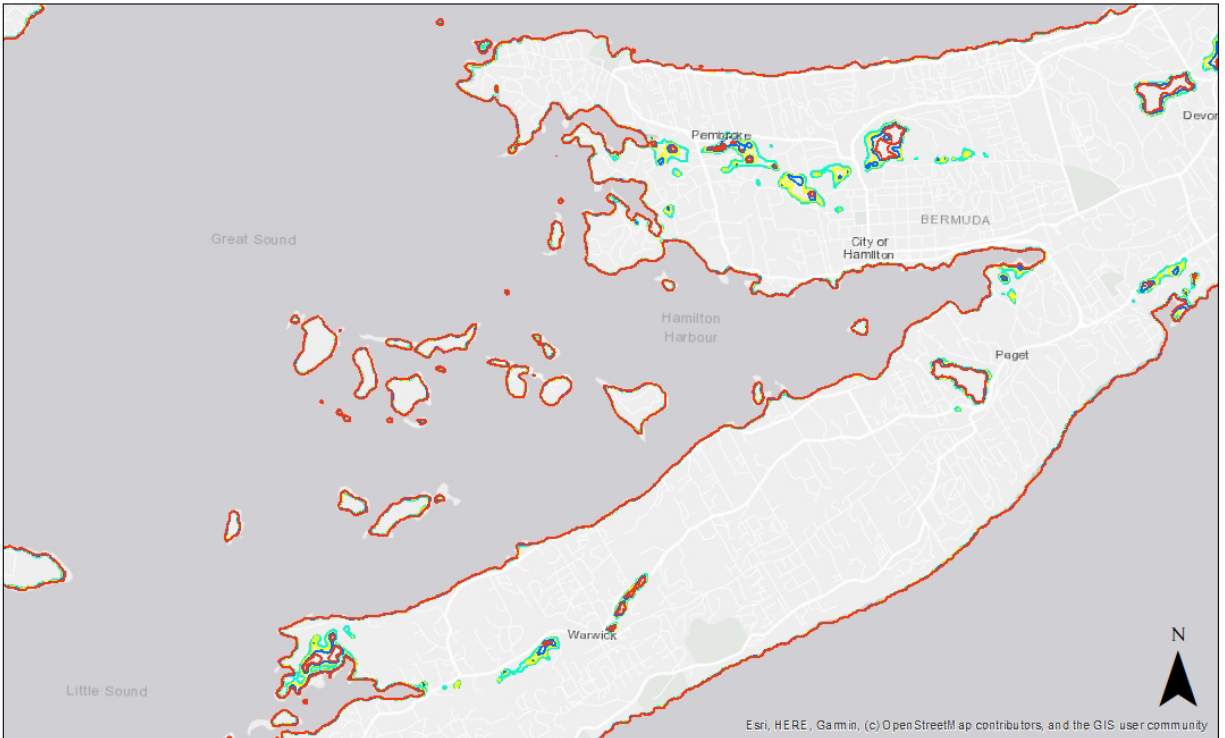


Figure 2 Predicted groundwater rise for the Dockyard area for RCP 8.5



BERMUDA - CLIMATE CHANGE STUDY
GREAT SOUND RCP 4.5

LEGEND

- Present Groundwater Elevation 1.49 m Above OD
- Projected Groundwater Rise 1.89 m Above OD
- Projected Groundwater Rise 1.68 m Above OD
- Projected Groundwater Rise 2.24 m Above OD

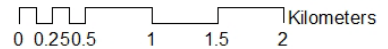
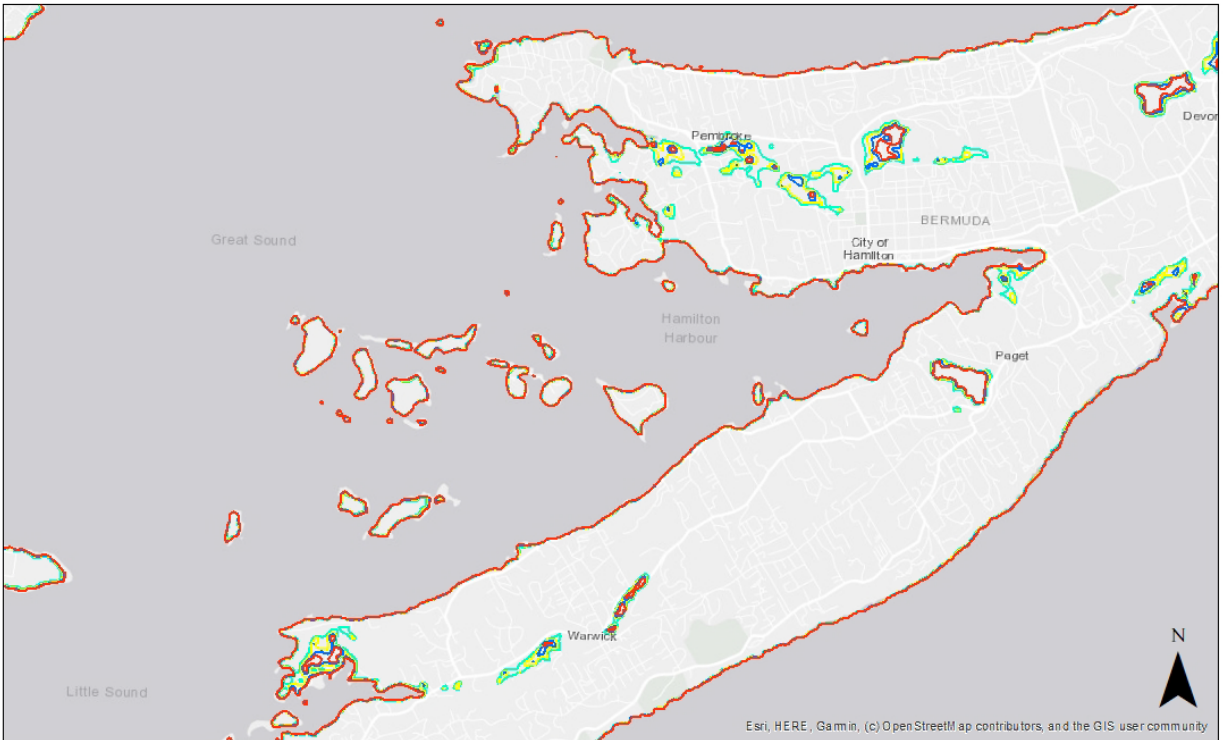


Figure 3 Predicted groundwater rise for the Great Sound area for RCP 4.5

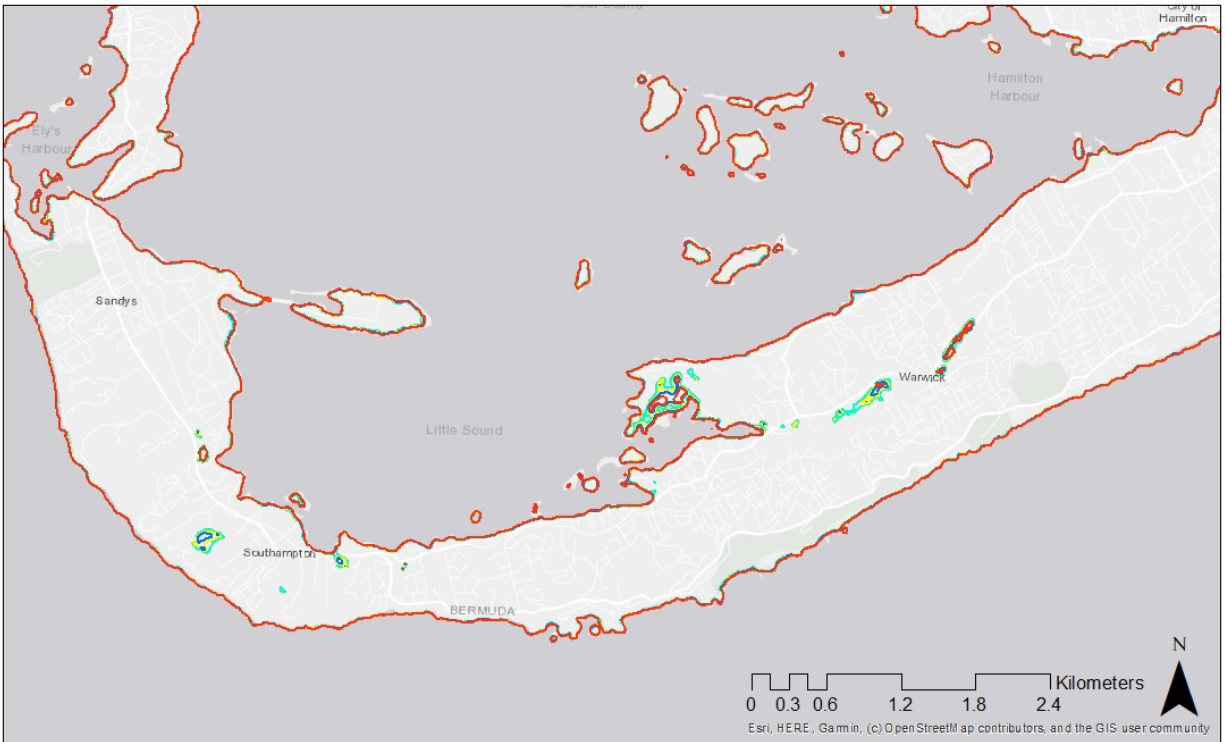


BERMUDA - CLIMATE CHANGE STUDY
GREAT SOUND RCP 8.5

LEGEND

- Present Groundwater Elevation 1.49 m Above OD
 - Projected Groundwater Rise 1.98 m Above OD
 - Projected Groundwater Rise 1.68 m Above OD
 - Projected Groundwater Rise 2.42 m Above OD
- 0 0.25 0.5 1 1.5 2 Kilometers

Figure 4 Predicted groundwater rise for the Great Sound area for RCP 8.5

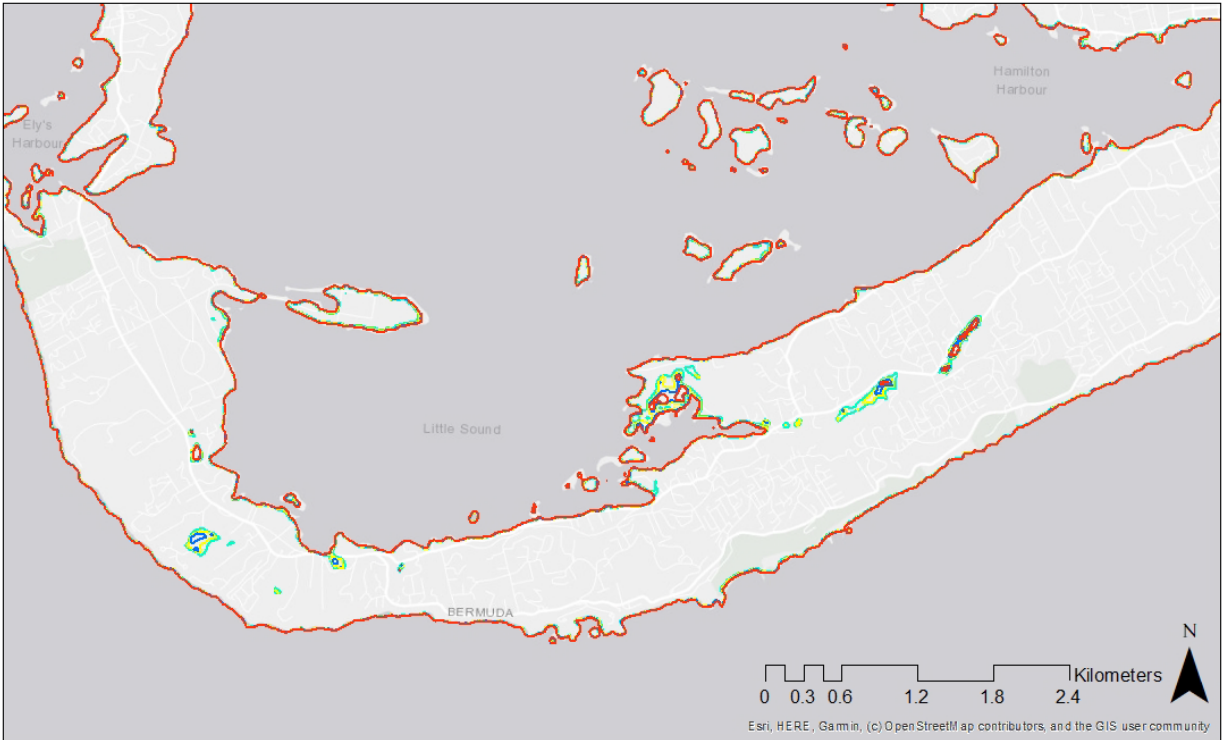


BERMUDA - CLIMATE CHANGE STUDY
SOUTH COAST BEACHES RCP 4.5

LEGEND

- Present Groundwater Elevation 1.49 m Above OD
- Projected Groundwater Rise 1.89 m Above OD
- Projected Groundwater Rise 1.68 m Above OD
- Projected Groundwater Rise 2.24 m Above OD

Figure 5 Predicted groundwater rise for south coast beaches for RCP 4.5



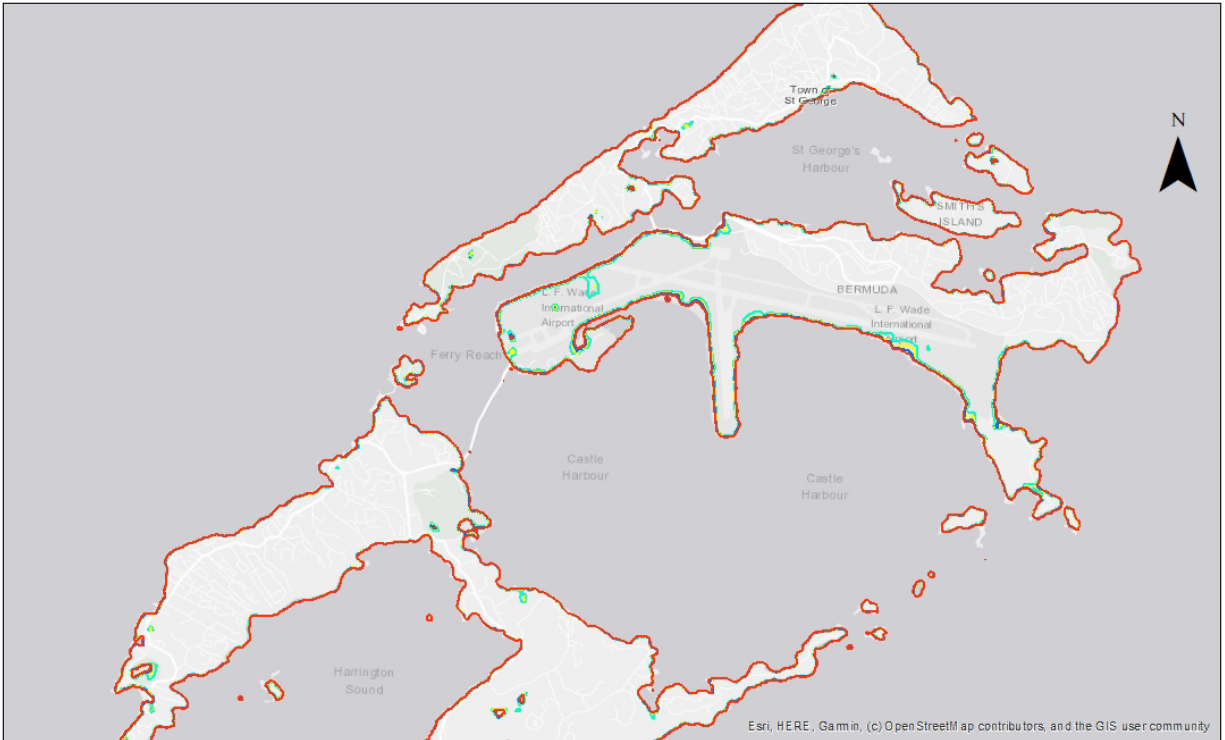
BERMUDA - CLIMATE CHANGE STUDY

SOUTH COAST BEACHES RCP 8.5

LEGEND

- Present Groundwater Elevation 1.49 m Above OD
- Projected Groundwater Rise 1.98 m Above OD
- Projected Groundwater Rise 1.68 m Above OD
- Projected Groundwater Rise 2.42 m Above OD

Figure 6 Predicted groundwater rise for south coast beaches for RCP 8.5



BERMUDA - CLIMATE CHANGE STUDY
ST. GEORGE'S AND CASTLE HARBOURS RCP 4.5

LEGEND

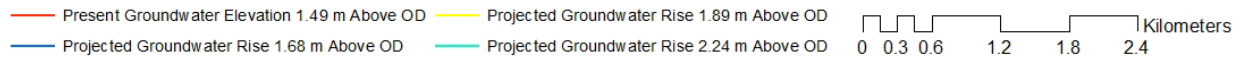
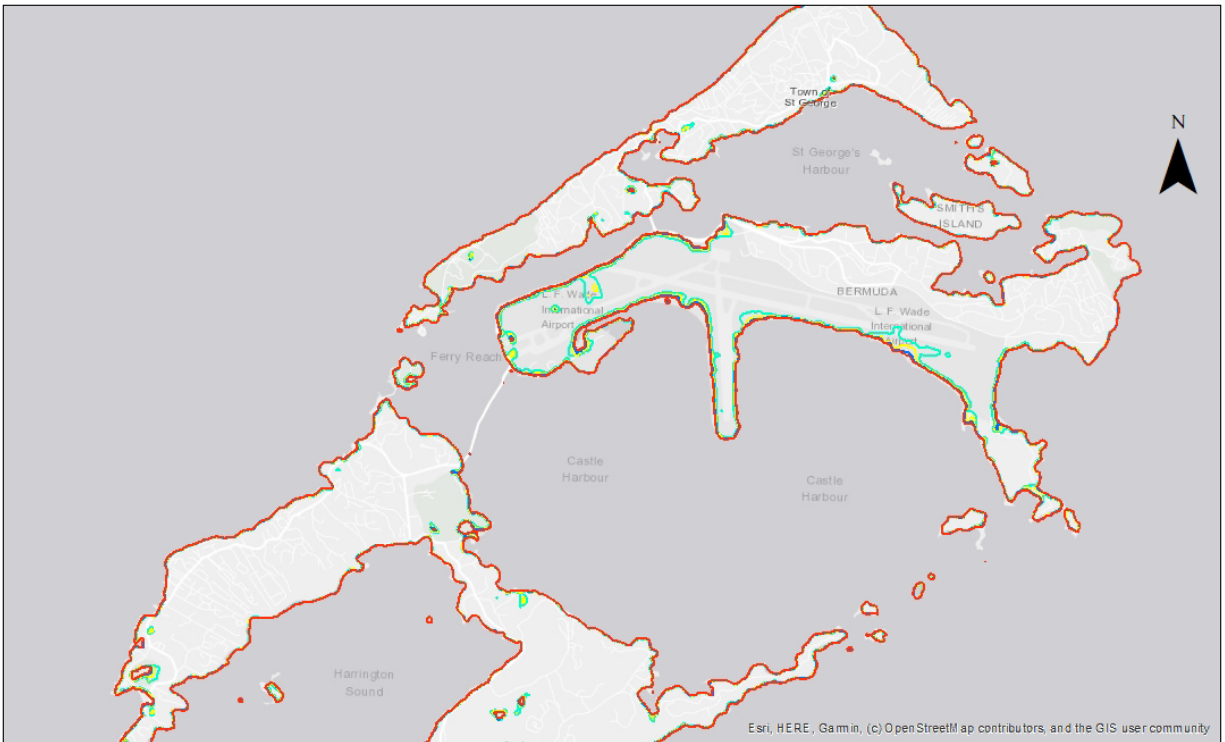


Figure 7 Predicted groundwater rise for St George's and Castle Harbour for RCP 4.5

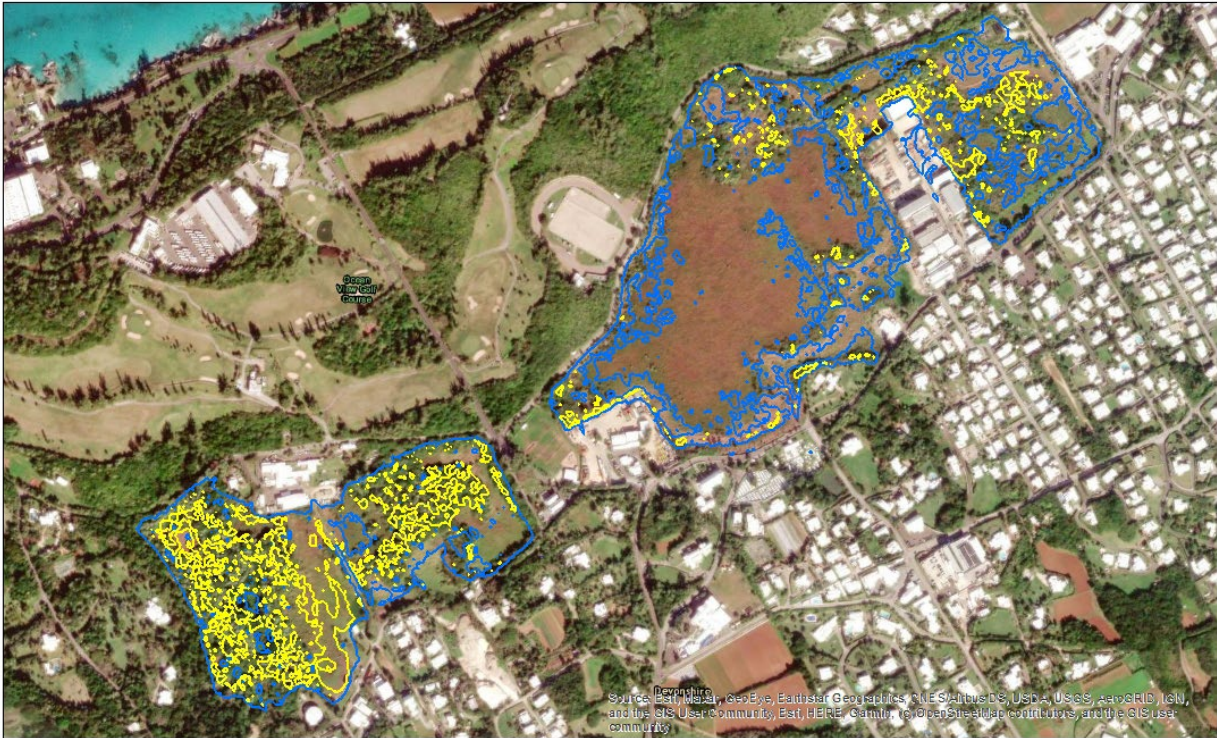


BERMUDA - CLIMATE CHANGE STUDY
ST. GEORGE'S AND CASTLE HARBOURS RCP 8.5

LEGEND

- Present Groundwater Elevation 1.49 m Above OD
 - Projected Groundwater Rise 1.68 m Above OD
 - Projected Groundwater Rise 1.98 m Above OD
 - Projected Groundwater Rise 2.42 m Above OD
- 0 0.3 0.6 1.2 1.8 2.4 Kilometers

Figure 8 Predicted groundwater rise for St George's and Castle Harbour for RCP 8.5



BERMUDA - CLIMATE CHANGE STUDY
DEVONSHIRE MARSH RCP 4.5

LEGEND

- Projected Maximum Central Lens Rise 1.31m
- Projected Maximum Central Lens Rise 1.66m

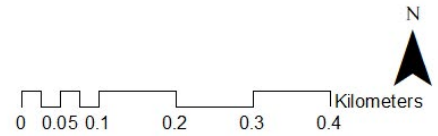
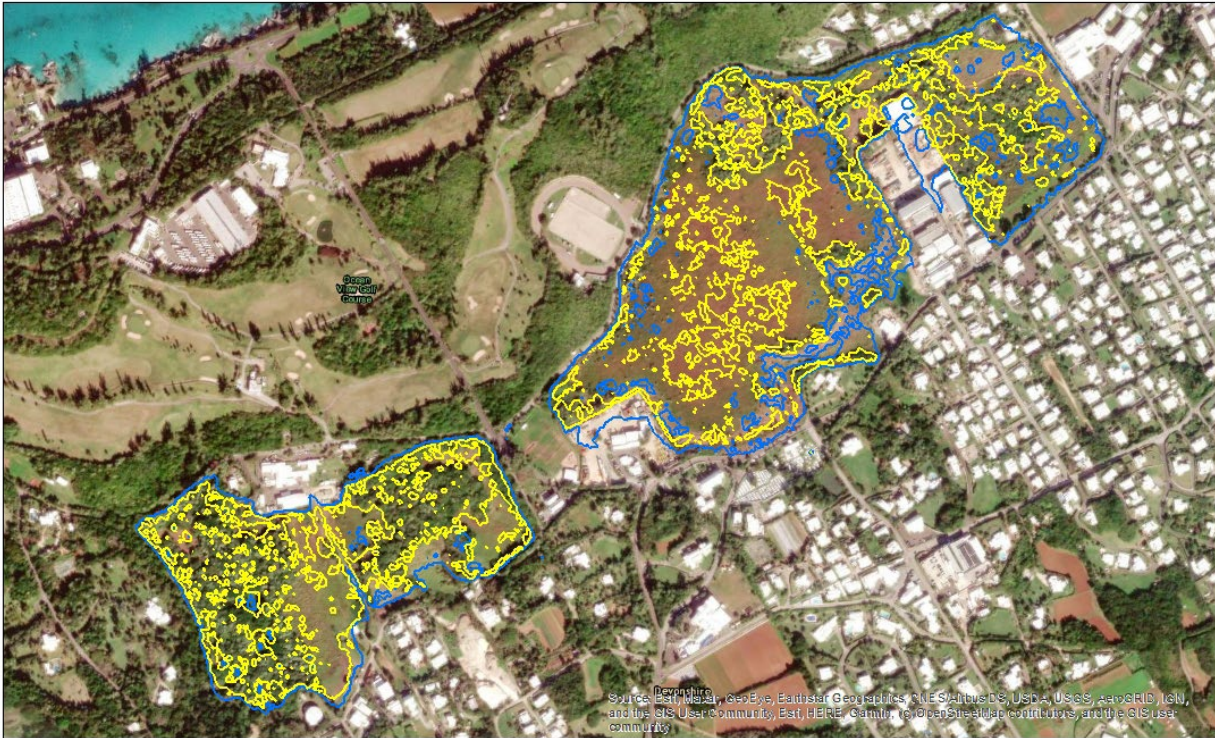




Figure 9 Predicted groundwater rise for Devonshire Marsh for RCP 4.5



BERMUDA - CLIMATE CHANGE STUDY
DEVONSHIRE MARSH RCP 8.5

LEGEND

-  Projected Maximum Central Lens Rise 1.40m
-  Projected Maximum Central Lens Rise 1.84m

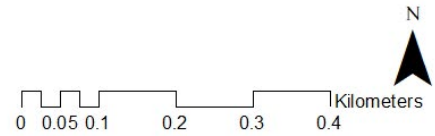


Figure 10 Predicted groundwater rise for Devonshire Marsh for RCP 8.5



BERMUDA - CLIMATE CHANGE STUDY
PEMBROKE MARSH RCP 4.5

LEGEND

- Projected Maximum Central Lens Rise 1.10m
- Projected Maximum Central Lens Rise 1.31m
- Projected Maximum Central Lens Rise 1.66m



Figure 11 Predicted groundwater rise for Pembroke Marsh for RCP 4.5



BERMUDA - CLIMATE CHANGE STUDY
PEMBROKE MARSH RCP 8.5

LEGEND

- Projected Maximum Central Lens Rise 1.10m
- Projected Maximum Central Lens Rise 1.40m
- Projected Maximum Central Lens Rise 1.84m

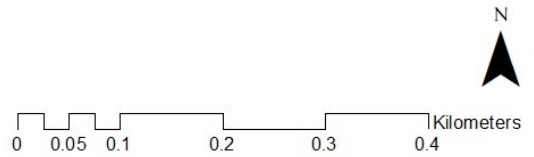


Figure 12 Predicted groundwater rise for Pembroke Marsh for RCP 8.5

References

- Vacher, H.L. Hearty, P.J. and Rowe, M.P., 1995, Stratigraphy of Bermuda: Nomenclature, concepts, and status of multiple systems of classifications. In: Curran, H.A. and White, B (Editors). *Terrestrial and Shallow Marine Geology of the Bahamas and Bermuda*. Geol. Soc. Am. Spec. Pap., 300: 271-294
- Rowe, M.P., 1981, The Central Lens of Bermuda: A Ghyben-Herzberg Lens in disequilibrium, M. Sc. Project, University College of London, London. p 108.
- Rowe, M.P., 1991. Bermuda. In: Falkland, A(Editor), *Hydrology and Water Resources of Small Islands: A Practical Guide*. UNESCO, Paris, pp 333-338
- Michael, Holly A., Russioniello, Christopher J. and Byron, Lindsay A., 2013, Global assessment of vulnerability to sea-level rise in topography-limited and recharge-limited coastal groundwater systems, *Water Resour. Res.*, 49, 2228-2240, doi:10.1002/wcwr.20212.
- [Adrian D. Werner, Craig T. Simmons](https://doi.org/10.1111/j.1745-6584.2008.00535.x), 2009, Impact of Sea-Level Rise on Sea Water Intrusion in Coastal Aquifers. Vol 47, No 2 –Groundwater-March-April 2009 (pages 197-204) <https://doi.org/10.1111/j.1745-6584.2008.00535.x>
- John A. Church • Neil J. White, (2011). *Sea-Level Rise from the Late 19th to the Early 21st Century*
Surv Geophys (2011) 32:585–602
DOI 10.1007/s10712-011-9119-1
- James A.M. Thomson (1989) , *Modeling Ground-Water Management Options for Small Limestone Islands: the Bermuda Example*
Vol 27, no 2 GROUND WATER MARCH-APRIL 1989
- Glasspool, Anne F. (Dec 2008). *The Impact of Climate Change on Bermuda*, The Bermuda National Trust, Hamilton, Bermuda, pp. 190
- Rowe, M. P., 1984, The fresh water “Central Lens” of Bermuda. *J. Hydrol.*, 73 (1984) 165-176, Elsevier Science Publishers B.V., Amsterdam
- Vacher, H.L., and Rowe, Mark P., 1997, *Geology and Hydrogeology of Bermuda*, in *Geology and Hydrogeology of Carbonate Islands*. *Developments in Sedimentology* 54, edited by H.L.Vacher and T. Quinn, Elsevier Science B.V.
- Vacher, H.L., 1988, Dupuit-Ghyben-Herzberg analysis of strip-island lenses. *Geol. Soc. Am. Bull.* 100: 580-591

Vacher, H.L., and Wallis, T. N., 1992, Comparative hydrogeology of fresh-water lenses of Bermuda and Great Exuma Island, Bahamas, *Ground Water*, 30: 15-20

Vacher, H.L., Rowe, M. P., and Garrett, P., 1989. The Geologic Map of Bermuda. Scale 1:25,000. Oxford Cartographers, London. Bermuda Gov. Ministry of Works and Engineering.

Vacher, H.L., 1978a. Hydrology of small oceanic islands-Influence of atmospheric pressure on the water table. *Ground Water*, 16:417-423

Vacher, H.L., and Quinn, T, Editors, 2004, *Geology and Hydrogeology of Small Carbonate Islands*, Developments in Sedimentology, Elsevier B.V. Amsterdam

[Frederikse](#) et al, 2020, The causes of sea-level rise since 1900, *Nature* v 584, pp 393-397.

Bermuda-Climate, website of GlobalSecurity.org.

<https://www.globalsecurity.org/military/world/caribbean/bm-climate.htm>

Sara Eeman Dynamics of rainwater lenses on upward seeping saline groundwater, 158 pages. PhD thesis, Wageningen University, Wageningen, NL (2017)

IPCC AR5 Fifth Assessment Report, 2014

Church et al, 2008, Revisiting the Earth's sea-level and energy budgets from 1961 to 2008, *Geophysical Research Letters*, Vol. 38, L18601, doi:10.1029/2011GL048794, 2011

Antonov, John I., Levitus, Sydney and Boyer, Timothy P., 2002, Steric sea level variations during 1957-1994: Importance of salinity, *Journal of Geophysical Research*, Vol. 107, NO. C12, 8013, doi:10.1029/2001jc000964, 2002

Uneke, L.A., Akpan, P.P, and Kormah, L.L., 2018, Effect of Salinity in Civil Engineering Concrete Basement, *international Journal of Engineering and Modern Technology* ISSN 2504-8856 Vol. 4 No. 2

Church, J.A., P.U. Clark, A. Cazenave, J.M. Gregory, S. Jevrejeva, A. Levermann, M.A. Merrifield, G.A. Milne, R.S. Nerem, P.D. Nunn, A.J. Payne, W.T. Pfeffer, D. Stammer and A.S. Unnikrishnan, 2013: Sea Level Change. In: *Climate Change 2013: The Physical Science Basis. Contribution of Working Group I to the Fifth Assessment Report of the Intergovernmental Panel on Climate Change* [Stocker, T.F., D. Qin, G.-K. Plattner, M. Tignor, S.K. Allen, J. Boschung, A. Nauels, Y. Xia, V. Bex and P.M. Midgley (eds.)]. Cambridge University Press, Cambridge, United Kingdom and New York, NY, USA.

- Bashir, R. and Chevez, E.P., Spatial and Seasonal Variations of Water and Salt Movement in the Vadose Zone at Salt-Impacted Sites, Department of Civil Engineering, Lassonde School of Engineering, York University, Toronto, ON M3J 1P3, Canada, Water 2018, 10(12), 1833, <https://doi.org/10.3390/w10121833>
- Zhao, X et al, 2019, Transport characteristics of salt ions in soil columns planted with Tamarix chinensis under different groundwater levels, PMC PubMeed Central, doi: 10.1371/journal.pone.0215138
- Spalding M, Mclvor A, Tonneijck FH, Tol S and van Eijk P (2014) Mangroves for coastal defence. Guidelines for coastal managers & policy makers. Published by Wetlands International and The Nature Conservancy. 42 p
- Chure et al. "Anthroponumbers.org: A Quantitative Database of Human Impacts on Planet Earth". Patterns (3), 2022. doi: [10.1016/j.patter.2022.100552](https://doi.org/10.1016/j.patter.2022.100552).
- Bergkamp, G., Orlando, B. and Burton, I. (2003). Change. Adaptation of Water Management to Climate Change. IUCN, Gland, Switzerland and Cambridge, UK. ix + 53 pp.
- Simmons, J.A.K., 1985. Hydrochemistry of the Pembroke dump, Bermuda, Part 1. Report to the Bermuda Government, 41 pp
- Simmons, J.A.K., 1987. Major and minor ion geochemistry of groundwaters from Bermuda, University of New Hampshire, Durham. Doctoral Dissertations. 1516. <https://scholars.unh.edu/dissertation/1516>
- Bretz, J. H., 1960. Bermuda: A Partially Drowned, Late Mature, Pleistocene Karst, GSA Bulletin (1960) 71 (12): 1729–1754.
[https://doi.org/10.1130/0016-7606\(1960\)71\[1729:BAPDLM\]2.0.CO;2](https://doi.org/10.1130/0016-7606(1960)71[1729:BAPDLM]2.0.CO;2)
- Conner, W, Noe, G, Lockaby, F.G., Krauss, K., 2012. The Effect of Increasing Salinity and Forest Mortality on Soil Nitrogen and Phosphorus Mineralization in Tidal Freshwater Forested Wetlands, USGS, DOI:10.1007/s10533-012-9805-1
- Tucholke, B.E., Vogt, P.R. et al., 1979. Initial Reports of the Deep Sea Drilling [Project 43. U.S. Gov.](#) Printing Office, Washington D.C., 1114 pp.
- Tucholke, B.E. and Mountain, G.S., 1986. Seismic stratigraphy, lithostratigraphy, and paleosedimentation patterns in the North American basin. In: M. Talwani. W. Hay and W.B.F. Ryan (Editors), Deep Drilling Results in the Atlantic Ocean: Continental Margins and Paleoenvironments, Maurice Ewing Ser., 3: 58-86.
- Simmons, J.A.K. and Lyons. B.W.. 1994. The ground water flux of nitrogen and phosphorus to Bermuda's coastal waters. Water Resour. Bull., 30: 983-991.

Ruhe, R.V., Cady, J.G., and Gomez, R.S., 1961. Paleosols of Bermuda, Geol. Soc. Am. Bull., 72:1121-1142

Richter, H., Aug 22, 2022, Circle of Blue Where Water Speaks, Fighting for Inches in the Southeast's Struggle with Salt.

Richter, H, August 2, 2022. Saltwater Intrusion, a "Slow Poison" to East Coast Drinking Water

in [Water News](#)/by [Hannah Richter](#)

<https://www.bbc.com/future/article/20220823-how-auckland-worlds-most-spongy-city-tackles-floods>

Brittany Trang et al, Low-temperature mineralization of perfluorocarboxylic acids, Science (2022). DOI:

[10.1126/science.abm8868](https://doi.org/10.1126/science.abm8868). www.science.org/doi/10.1126/science.abm8868

Shira Joudan et al, Taking the "F" out of forever chemicals, Science (2022). DOI: 10.1126/science.add1813

Government of Bermuda, Department of Planning, City of Hamilton Plan, 2015.

<https://planning.gov.bm/wp-content/uploads/2018/11/CityofHamiltonPlan2015.pdf>

[Haitjema HM](#), [Mitchell-Bruker S](#), 2005. Are water tables a subdued replica of the topography?

Ground Water, 01 Nov 2005, 43(6):781-786

DOI: [10.1111/j.1745-6584.2005.00090.x](https://doi.org/10.1111/j.1745-6584.2005.00090.x) PMID: 16323999

N. Saintilan et al, Thresholds of mangrove survival under rapid sea-level rise, Department of Earth and Environmental Sciences, Macquarie University, Australia.

Ellison, JC 1993 , 'Mangrove retreat with rising sea-level, Bermuda' , Estuarine Coastal and Shelf Science, vol. 37, no. 1 , pp. 75-87 , doi: [10.1006/ecss.1993.1042](https://doi.org/10.1006/ecss.1993.1042).

<https://thewaternetwork.com/article-FfV/prototype-toilet-that-is-safe-and-designed-for-household-use-vzrxLKhKfvA37SjrubtdNA>

[Neubauer](#), S.C. et al, 2009, [Global change and tidal freshwater wetlands: Scenarios and impacts](#)

[Virginia Commonwealth University](#)

J. Patrick Megonigal, Biogeochemistry of Tidal Freshwater Wetlands. In: Gerardo M. E. Perillo, Eric Wolanski, Donald R. Cahoon, Mark M. Brinson, editors, Coastal Wetlands: An Integrated Ecosystem Approach. Elsevier, 2009, p. 535. ISBN: 978-0-444-53103-2

Fisk, S.V., Feb 6, 2019, Gypsum as an Agricultural Product, Soil Science Society of America.

Jones, R., 2010, Environmental contamination associated with a marine landfill ('seafill') beside a coral reef, Marine Pollution Bulletin, vol 60, issue 11, Elsevier

Johnson, S. 1984. Relationship between Ordnance and Chart Datums. Memorandum 30/202, Public Works Department, Bermuda, 2 pp. (unpublished).

<https://www.bbc.com/future/article/20220823-how-auckland-worlds-most-spongy-city-tackles-floods>

Arup, Arup Global Sponge Cities Snapshot, Arup Website, www.Arup.com

www.Lystek.com, Recycling human waste to capture nutrients for agriculture

<https://www.bbc.com/future/article/20220830-the-new-science-of-recycling-human-poo>

PFAS: <https://thewaternetwork.com/rising-water-technologies/tech-news-post-TFp/6CrTA6SnmC3mvrBuvzzHw>

Brittany Trang et al, Low-temperature mineralization of perfluorocarboxylic acids, Science (2022). DOI:

[10.1126/science.abm8868](https://doi.org/10.1126/science.abm8868). www.science.org/doi/10.1126/science.abm8868

Shira Joudan et al, Taking the "F" out of forever chemicals, Science (2022). DOI: 10.1126/science.add1813

Liu, Z et al, 2022, Accelerated degradation of perfluorosulfonates and perfluorocarboxylates by UV/sulfite + [iodide](#): reaction mechanisms and system efficiencies," is published in Environmental Science & Technology, 2022, 56, 6, 3699-3709. <https://doi.org/10.1021/acs.est.1c07608>

NOAA website: <https://oceanservice.noaa.gov/>

Cousins, I. et al, 2022. Outside the Safe Operating Space of a New Planetary Boundary for Per- and Polyfluoroalkyl Substances (PFAS)

Environ. Sci. Technol. 2022, 56, 16, 11172–11179

Publication Date: August 2, 2022

<https://doi.org/10.1021/acs.est.2c02765>

Tigue, Kristoffer, Sept 27, 2022, Today's Climate - Hurricane Fiona Caught Communities Off Guard. Will Ian Follow Suit?

Inside Climate News, newsletters@insideclimatenews.org

International Biochar Initiative website <https://biochar-international.org/characterizationstandard>

Lehmann, J., 2007. Bio-energy in the black. *Frontiers. Ecol. Environ.* 5, 381–387.

Lehmann, J., Gaunt, J., Rondon, M., 2006. Biochar sequestration in terrestrial ecosystems. *Mit. Adapt. Strat. Glob. Change* 11, 403–427.

Hawken, Paul. *Drawdown 2017*. Penguin Publishing Group. New York, New York.

Simon, M, *A Poison Like no Other: How Microplastics Corrupted Our Bodies*. Oct 27, 2022, Island Press.

Clarke, L., Taylor, M., and Maitland, D., *Climate Profile and Projections for the Island of Bermuda*, Climate Studies Group MONA, The University of the West Indies, Mona Campus, Kingston 7, Jamaica, West Indies, May 31, 2022

Nisbet, C.T., Sarofim, A., 1972, Rates and Routes of Transport of PCBs in the Environment, *Environmental Health Perspectives*, Volume 1, <https://doi.org/10.1289/ehp.720121>

Gioia, R., Dachs, J., Nizzetto, L., Lohmann, R., Jones, K., 2013, Atmospheric Transport, Cycling and Dynamics of Polychlorinated Biphenyls (PCBs) from Source Regions to Remote Oceanic Areas, in McConnell et al., *Occurrence, Fate and Impact of Atmospheric Pollutants on Environmental and Human Health*, ACS Symposium Series, American Chemical Society: Washington, DC, 2013.

Panshin SY, Hites RA. Atmospheric concentrations of polychlorinated biphenyls in Bermuda. *Environmental science & technology*. 1994 Nov 1;28(12):2001-7.

Jet Propulsion Laboratory website showing vertical changes in landmass: https://www.sonel.org/IMG/txt/vertical_velocities_table_jpl14.txt

[International Institute for Sustainable Development \(IISD\)](https://www.iisd.org/focus-areas/climate). (<https://www.iisd.org/focus-areas/climate>).